The Formation and Evolution of the Central Arran Igneous Complex

Robert James Gooday

School of Earth and Ocean Sciences
Cardiff University

Submitted in partial fulfilment of the requirements for the degree of
Doctor of Philosophy

January 2019

“. . . quite dreary by the standards of Arran”

walkhighlands.co.uk on the central hills

Abstract

The Central Arran Igneous Complex – a system of intrusive and pyroclastic volcanic rocks – is one of the least understood onshore 'central complexes' of the British Palaeogene Igneous Province (BPIP). The BPIP is part of the wider North Atlantic Igneous Province, formed during opening of the North Atlantic Ocean and the arrival of the Iceland plume at the base of the lithosphere. Despite being known about for over a century, the magmatic and volcanic processes that formed the Central Arran Igneous Complex remain poorly understood.

The Central Arran Igneous Complex comprises a number of granitic and dioritic intrusions, a caldera-fill succession of pyroclastic and sedimentary rocks intruded by a dolerite sill, and a series of dykes ranging in composition from picrite to pitchstone. This study uses a combination of field mapping, whole-rock elemental geochemistry, radiogenic isotope geochemistry, and U-Pb zircon geochronology to determine how these units and their magmas formed, how they relate to one another, and their relationship with other igneous rocks throughout the BPIP.

Detailed study of the intra-caldera stratigraphy allows a prolonged volcanic history to be pieced together, with pyroclastic units separated by erosional surfaces indicating periods of volcanic quiescence and sedimentary processes. Following the initial period of caldera collapse, which was accompanied by highly explosive eruptions, volcanism was generally less explosive and formed abundant high-grade and lava-like ignimbrites.

The majority of magmas were derived from a mantle source compositionally transitional between N-MORB and the Iceland plume. Geochemical differences between the mafic units are derived from different degrees of melting, from different source regions. All magmas show some degree of crustal contamination by various units, and their isotope geochemistry can be used to constrain the poorly understood crustal architecture in the region.

U-Pb zircon geochronology shows that magmatism in central Arran took place over a very short space of time. The difference in interpreted $^{206}Pb/^{238}U$ ages between the oldest (Allt Ruadh Member ignimbrites; 58.92 ± 0.19 Ma) and the youngest (granitic Glenloig Hybrids; 58.71 ± 0.07 Ma) dated units is $\leqslant 470$ kyr.

DECLARATION

This work has not been submitted in substance for any other degree or award at this or any other university or place of learning, nor is being submitted concurrently in candidature for any degree or other award.

STATEMENT 1

This thesis is being submitted in partial fulfilment of the requirements for the degree of PhD.

STATEMENT 2

This thesis is the result of my own independent work/investigation, except where otherwise stated, and the thesis has not been edited by a third party beyond what is permitted by Cardiff University's Policy on the Use of Third Party Editors by Research Degree Students. Other sources are acknowledged by explicit references. The views expressed are my own.

STATEMENT 3

I hereby give consent for my thesis, if accepted, to be available online in the University's Open Access repository and for inter-library loan, and for the title and summary to be made available to outside organisations.

STATEMENT 4: PREVIOUSLY APPROVED BAR ON ACCESS

I hereby give consent for my thesis, if accepted, to be available online in the University's Open Access repository and for inter-library loans *after expiry of a bar on access previously approved by the Academic Standards and Quality Committee*

Signed _____ (candidate) Date _____

Acknowledgements

It seems ridiculous that mine is the only name on the front of this thesis. This PhD has relied heavily on the hard work, support, and advice of a huge number of people, and each one of them deserves a massive amount of credit. The biggest thanks should, of course, go to my three brilliant supervisors. Andrew Kerr has been a constant source of guidance, wisdom, and department gossip, and many a time has the geological world been put to rights in a petrology lab practical or over a curry. Davie Brown has taught me more about ignimbrites and field volcanology than any sensible person should ever know. And I will forever be amazed at Kathryn Goodenough's ability to work out an area's geological evolution from a few muddy outcrops, or read a rambling chapter draft and turn it into something resembling science with remarkable efficiency. I feel honoured to have been able to work with these people.

There is also a large number of people who, when I think about it, really did all of the actual work in this PhD. Thank you to Tony Oldroyd for excellent thin sections, Iain McDonald for whole-rock elemental data, Duncan Muir for guidance on the SEM, Ian Millar for radiogenic isotope data and zircon separation, and Dan Condon for U-Pb geochronology results. Without these people, this thesis would consist of a questionable map and some photos from the top of Ard Bheinn.

The PhD gang at Cardiff were the sole reason that I enjoyed my four years there as much as I did. Thank you especially to all residents of the Magma Chamber, the coffee room dwellers, and everyone whom I had the pleasure to face across the T-ball table.

A special mention should go to the Geology Twitter community. If it weren't for you... well, I probably would have been finished months ago. But you're the best group of nerds anyone could ask for.

Thank you to my awesome family, who have been constantly supportive, and who have nurtured and encouraged my curiosity about natural things for the last 27 years.

And of course, to Georgia. You're the best. Thank you for everything.

Table of contents

List of figures

List of tables

Chapter 1

Introduction

The hills of central Arran, western Scotland, are made up of a complex system of Palaeogene volcanic and intrusive rocks. This is one of the 'central complexes' of the British Palaeogene Igneous Province, and one of the least understood onshore examples.

There are two broad aims of this project:

1) To determine the geological structure and formation history of the Central Arran Igneous Complex, including the volcanic stratigraphy of the caldera-fill succession, and

2) To determine the geochemical nature and petrogenetic history of the magmas that formed the Central Arran Igneous Complex, and asses their relationship to other magmatic rocks on Arran and throughout the British Palaeogene Igneous Province.

1.1 The British Palaeogene Igneous Province

Magmatic rocks of Palaeogene age in the west of Scotland and elsewhere in the British Isles have been studied by geologists for over two hundred years. The foundation of our modern understanding of the British Palaeogene Igneous Province (BPIP) largely derives from the work undertaken during the production of the geological memoirs in the late nineteenth and early twentieth centuries. The BGS memoirs of Skye (Harker and Clough, 1904), the Small Isles (Harker and Barrow, 1908), Mull (Bailey et al., 1924), and Arran (Tyrell, 1928) discuss in incredible detail the magmatic lithologies, their genesis, and their relationships. Due in part to the sheer volume of work done on this well-exposed landscape in the early days of modern geology, the Scottish Hebrides became a standard to which volcanic systems throughout the world were compared. Indeed, ideas initially proposed in the Hebrides have become some of the most fundamental principles of igneous geology.

1.1.1 Pre-Palaeogene geology

The lava fields, dyke swarms, and central complexes of the BPIP are built upon and intrude all of the five crustal blocks that make up Scotland and the northern part of Ireland (Bluck et al., 1992). These are the Archaean-Palaeoproterozoic Hebridean Terrane, the Neoproterozoic Northern Highland Terrane, the Neoproterozoic-Lower Palaeozoic Grampian Terrane, and the Palaeozoic Midland Valley and Southern Upland terranes (Fig. 1.1).

The magmatic centres of St. Kilda, Skye, and Rùm were erupted through and emplaced into the Hebridean terrane, comprising the Archaean to Palaeoproterozoic Lewisian Gneiss, and its covering of Neoproterozoic Stoer Group and Torridon Group Sandstones. This area lies to the west of the Caledonian Moine Thrust Zone, and so can be considered the (largely) undeformed foreland to the Lower Palaeozoic Caledonian Orogeny (Park et al., 2002).

Across the Moine Thrust, in the Northern Highland terrane, magma on Ardnamurchan and Mull was erupted through basement made up of the Neoproterozoic Moine schists and gneisses. They were deformed in the Knoydartian Orogeny following emplacement of the West Highland granite gneiss at ~870 Ma (Strachan et al., 2002; Tanner and Evans, 2003), and again during the Lower Palaeozoic Caledonian Orogeny. Basement inliers and xenoliths show that the Moine rocks overlie a high-grade basement of Lewisian-like rocks (Park et al., 2002; Upton et al., 1998).

The Dalradian Supergroup also consists of passive margin sediments, but they are younger, with sedimentation in the latest Neoproterozic until possibly the Ordovician. A maximum age is given by pegmatites in the underlying Glen Banchor and Dava successions dated at ~806 Ma (Noble et al., 1996), units which have more in common with the Moine rocks. There is no evidence for Knoydartian metamorphism in the Dalradian, and there is also a lack of detrital Knoydartian zircons (Cawood et al., 2003), suggesting that the Dalradian and Moine Supergroups are not directly related. The basement to the Dalradian Supergroup in the south west of Scotland is thought to be made up of the Proterozoic gneisses that are exposed in the Rhinns of Islay, 80 km to the WNW of Arran. Similar lithologies are exposed on Colonsay and the Irish island of Inishtrahull, making up the Rhinns Complex (Daly et al., 1991; Marcantonio et al., 1988; Muir et al., 1994), which occupies the Islay block, as shown on Fig. 1.1.

Palaeogene igneous activity on the Grampian Terrane is largely confined to its bounding faults (Fig. 1.1). The Mull complex lies only a few kilometres to the north of the Great Glen Fault, and significant magmatic activity related to this system occurred on the Dalradian side; indeed, the Great Glen Fault itself appears to have

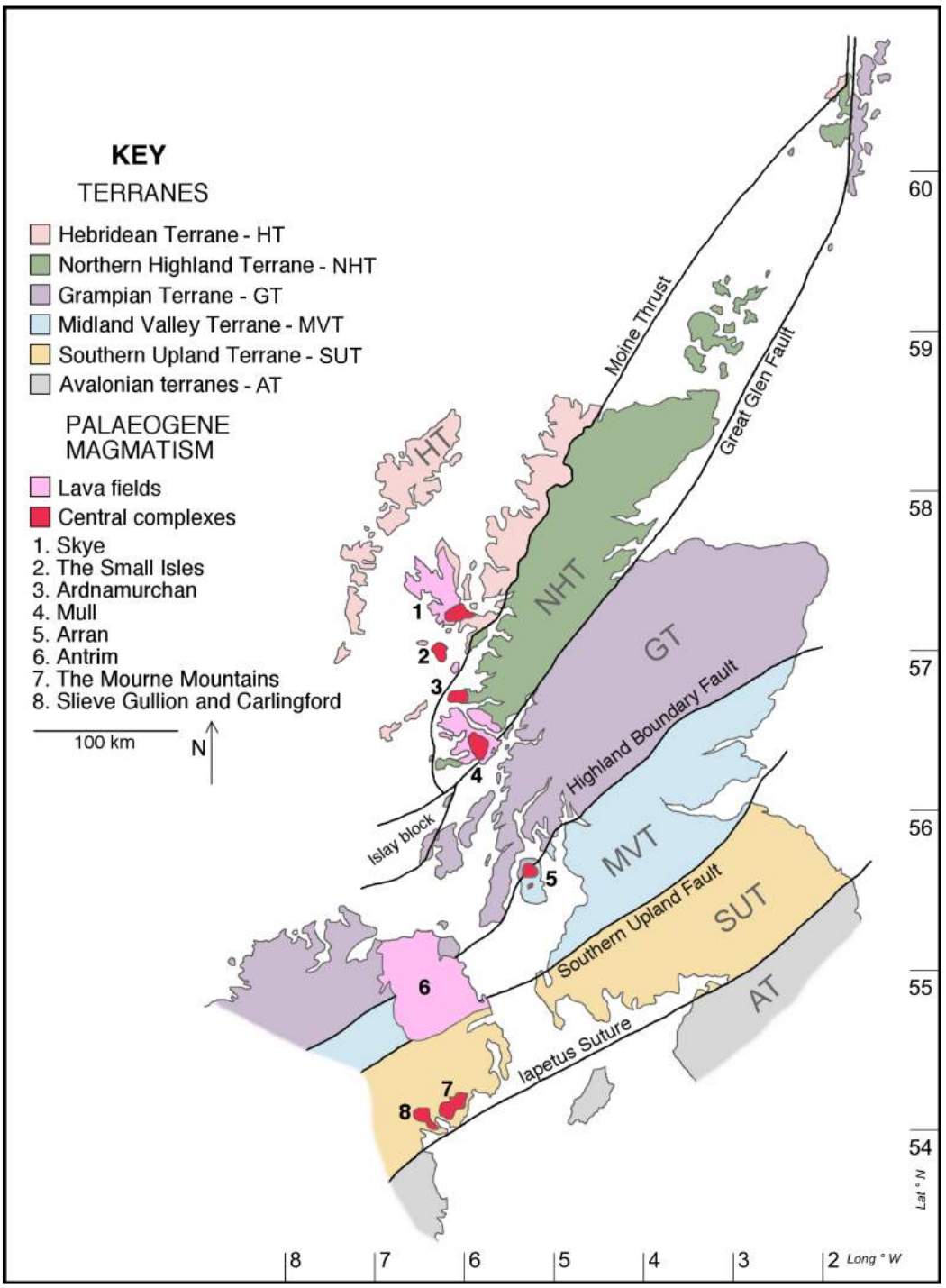

Fig. 1.1 – Map of the terranes which make up the northern part of the British Isles, showing the onshore lava fields and central complexes of the BPIP. Terrane map from Bluck et al. (1992). Palaeogene geology from Emeleus and Bell (2005) and Preston (2009).

been offset to the south by emplacement of the volcanic centre (Lee and Bailey, 1925). The North Arran Granite and much of the Antrim lava field appear to lie above the Highland Boundary Fault (known as the Fair Head-Clew Bay Line along its Irish extent) along the southern edge of the terrane.

The exposed rocks of the Midland Valley Terrane are Palaeozoic in age. Much of the outcrop is the Upper Palaeozoic cover that overlies Lower Palaeozoic units. Lower Palaeozoic units also include the Ordovician Highland Border Complex, juxtaposed against the Highland Boundary Fault. The Lower Palaeozoic lithologies represent sedimentary and volcanic rocks related to the shallowing and closure of the Iapetus Ocean, and provide a link between subduction-generated rocks to the south and the resultant metamorphism to the north (Bluck, 2002). Upper Palaeozoic sedimentation includes the Old and New Red Sandstones, with intervening Carboniferous strata. Palaeogene magmatism in the Midland Valley terrane largely comprises the central part of the Antrim lava field, as well as the central complex and dyke and sill swarms of Arran (Fig. 1.1).

The crystalline basement of the Midland Valley Terrane is not exposed. However, lower crustal xenoliths have been found in Permian and Carboniferous plugs and dykes across the Midland Valley, allowing petrological and geochemical analysis of this unexposed basement (Halliday et al., 1993).

The Southern Uplands Terrane is an accretionary wedge formed at the subduction zone that ultimately resulted in the final closure of Iapetus. The terrane consists of Ordovician and Silurian greywackes and siltstones, with the Ballantrae complex, thought to be a tectonically dissected Iapetean ophiolite along its northern margin (Oliver et al., 2002).

In Scotland, Palaeogene rocks in the Southern Uplands terrane are restricted to isolated members of the regional dyke swarm, which extends into the North Sea. However, Palaeogene rocks on the Northern Irish continuation of the Southern Uplands are more widespread. The Antrim lava field crosses the Southern Uplands Fault and continues to south of Lough Neagh. Further south are the central complexes of the Mourne Mountains, Slieve Gullion, and Carlingford (Fig. 1.1), the latter two on the border with the Republic of Ireland.

In the Mesozoic, extensional tectonics resulted in thinning of the crust in the area that would become the North Atlantic. Large normal faults developed in the Jurassic creating two large and several smaller sedimentary basins (Hudson and Trewin, 2002). The Sea of the Hebrides-Little Minch Trough is a large half-graben bounded to the west by the Minch Fault. The Inner Hebrides Trough is another large half-graben controlled by movement on the Skerryvore-Camasunary Fault. This basin translates south west into the Blackstones, Mailn, and Colonsay Basins -

grabens bounded by the Skerryvore and Colonsay Faults (Emeleus and Bell, 2005). The resulting Mesozoic sedimentary sequences largely crop out offshore, but can be seen as thinner successions representing the edges of the basins onshore, largely on Skye and Mull. The sediments were largely deposited in tropical shallow marine conditions.

It appears as though the central complexes of the Hebrides occur on the Mesozoic basement highs (not in the basins), at the point where these are intersected by the older Caledonian crustal lineaments (Emeleus, 1982). With the arrival of the Icelandic plume head at the base of the lithosphere, melt generated was channeled up through these faults and erupted where the crust was thinned and topographically high (Thompson and Gibson, 1991).

1.1.2 Magmatic activity

The BPIP itself is part of the North Atlantic Igneous Province (NAIP), a predominantly mafic Large Igneous Province that developed during the rifting of the North Atlantic Ocean in response to the arrival of the Iceland plume at the base of the lithosphere (e.g. Kent and Fitton, 2000; Storey et al., 2007; Thompson and Gibson, 1991). In the British Isles, the NAIP comprises the extensive lava fields of Skye, Eigg (one of the Small Isles), Mull, and Antrim (Emeleus and Bell, 2005), as well as localised intrusive and volcanic 'central complexes' (Fig. 1.1). Other Palaeogene remnants of the NAIP are preserved on Greenland, the Faroe Islands, and offshore (Saunders et al., 1997).

Following uplift caused by the arrival of the plume, magmatic activity in each volcanic area of the BPIP started with extrusion of a thick lava-pile through fissure eruptions, not unlike the volcanic landscape of present-day Iceland. These fissures are preserved as the NW–SE trending regional dyke swarm that cuts the underlying geology and the lava fields. From a combination of radiometric and palynological dating and field relationships, it is thought that eruption of the lava fields commenced 61–60 Ma (Chambers et al., 2005) in the Hebrides, and possibly prior to 62 Ma in Antrim (Ganerød et al., 2010). All magmatism preserved in the onshore BPIP was part of 'phase 1' (pre-sea floor spreading) of the NAIP (Saunders et al., 1997).

There are four lava fields recognised in the onshore BPIP (Bell and Williamson, 2002; Emeleus and Bell, 2005; Preston, 2009). The Antrim lava field is exposed over a large portion of Northern Ireland. The Eigg lava field is preserved on Eigg, Muck, and the south east part of Rùm. The Skye lava field is exposed on Skye, Canna, and in northern Rùm. The Mull lava field is also found on Ardnamurchan, and Morvern; it may connect to the Eigg lava field offshore (Fyfe, 1993). In addition to these

preserved lava fields, an Arran lava-pile was proposed to be preserved only as blocks which subsided or tumbled into the caldera of the central complex (King, 1954).

The lavas were generally erupted onto flat, low-lying land in a tropical climate, as shown by palynological and palaeontological studies (Emeleus and Bell, 2005). The lowermost flows occasionally erupted into lakes as shown by pillow lavas and hyaloclastites, or flowed over waterlogged sediments as shown by rootless cones, for example at Ardtun and Carsaig Bay on Mull. There is evidence that in places such as Mull, Skye, and Antrim, the first activity was eruption of basaltic scoria cones and pyroclastic tuffs (Emeleus and Bell, 2005; Ganerød et al., 2010). Topography was steep in places, indicated by presence of conglomerates interbedded with the lavas, and the onlap of lavas against underlying Moine or Torridonian rocks on Mull and Rùm, respectively (Bell and Williamson, 2002).

The lava-piles of the Hebrides reached thicknesses of 2 km, but may have been thicker in the deeper parts of the still-active half grabens, and were up to 5 km thick in the Faroes (Anderton, 2009; Emeleus and Bell, 2005). On Ben More on Mull, 966 m of continuous lava stratigraphy can be seen. Evidence from geographical relationships and zeolite assemblages in amygdales (which can be used to indicate metamorphic conditions, and therefore temperature and depth) show that there must have been around another 1 km of lava above this (Bailey et al., 1924; Walker, 1970). The bulk of the lavas are basalt and hawaiite sheet flows, generally less than 5 m thick. Higher in the stratigraphy more evolved lavas are encountered. These take the form of less laterally extensive flows of mugearite and trachyte (Kerr et al., 1999).

Emplacement of the central complexes involved localisation of magmatism and uplift of several hundred metres. The location of the volcanic centres is likely to have been controlled by Caledonian or other pre-Palaeogene crustal structures: Skye and Rùm on the Skerryvore-Camasunary Fault, Mull on the Great Glen Fault, and the North Arran Granite (NAG) and Arran central complex on or near the Highland Boundary Fault. The Northern Irish volcanic centres appear to lie close to the Navan-Silvermines Fault, the Irish continuation of the Iapetus Suture (Anderton, 2009; Bluck et al., 1992). There are known to be deep crustal structures in the offshore regions around St. Kilda; these could be faults providing a structural control on the position of the central complex (Bell and Williamson, 2002).

Magmatic activity at the central complexes took the form of various types of intrusions and, in most cases, surface volcanism, which was often explosive. Intrusive bodies include 1) coarse-grained mafic and ultramafic rocks such as the Cuillin gabbro of Skye and the layered peridotites and troctolites of Rùm, 2) intermediate and granitic rocks such as the heavily dissected granophyres on Mull and the NAG, 3) cone sheet swarms such as those on Mull and Ardnamurchan which can locally

make up almost 100% outcrop, 4) ring dykes such as the renowned Loch Bà felsite ring dyke on Mull, and 5) local basaltic dyke swarms, which may be radial around the central complexes (Emeleus and Bell, 2005). The focal point of activity can be identified as the central point of the cone sheets, radial dyke swarms, ring dykes, and other arcuate features. In this way, changes in the focal point of magmatic activity can be identified through time, such as on Mull, where the three magmatic centres get younger towards the north west (Bailey et al., 1924; Emeleus and Bell, 2005).

Although less common than mafic rocks, there is widespread evidence of extrusive silicic volcanism and explosive eruptions (Bell and Emeleus, 1988; Brown et al., 2009). Due in part to its historical importance and relative ease of accessibility, the BPIP has been the source of many developments in the global understanding of volcanological processes. Pyroclastic rocks are largely found within calderas (on Mull and Rùm, as well as Skye and Arran), often bound by arcuate faults and intrusions, originally interpreted as ring faults, ring dykes, and cone sheets.

Detailed studies of the pyroclastic successions on Skye and Rùm have revealed complex histories of caldera collapse in the BPIP (Brown et al., 2009; Troll et al., 2000), but exposures in these areas are limited due to later, cross-cutting layered intrusions. Recently, many silicic extrusive rocks in this province, previously described as lavas or shallow intrusions, have been re-interpreted as welded and rheomorphic lava-like ignimbrites, for example the rhyodacite sheets on Rùm (Holohan et al., 2009) and the Sgurr of Eigg Pitchstone (Brown and Bell, 2013).

Accompanying the injection of magma into the central complexes was a large degree of hydrothermal alteration. Fluid originated in the water-saturated upper crust (Taylor and Forester, 1971) and was heated to 400°C in zones up to 20 km around the central complexes. Temperatures in the centre of the system reached as high as 800°C. This alteration caused almost complete stripping of olivine and extensive alteration of amphiboles, pyroxenes, and biotite. Quartz, feldspar, and glass were also affected. Mineral veins containing chlorite, epidote, prehnite, and calcite were developed in the centres and extend into the country rocks (Emeleus and Bell, 2005).

Gravity studies of the Hebrides show steep-sided, highly positive anomalies below the centres of Mull, Skye, and Rùm. Smaller anomalies are seen under Ardnamurchan and central Arran (Fig. 1.2). This suggests that granitic rocks (low density) only occur in relatively thin sheets near the surface (Bott and Tantrigoda, 1987), and that the bulk of the volume of the volcanic centres consists of large bodies of basic and ultrabasic rocks (high density), such as gabbro and peridotite cumulates (Bott and Tantrigoda, 1987; Bott and Tuson, 1973).

Although most of the volcanic centres display some or all of these features, they each have a complex magmatic history, and different relative timing of events. They

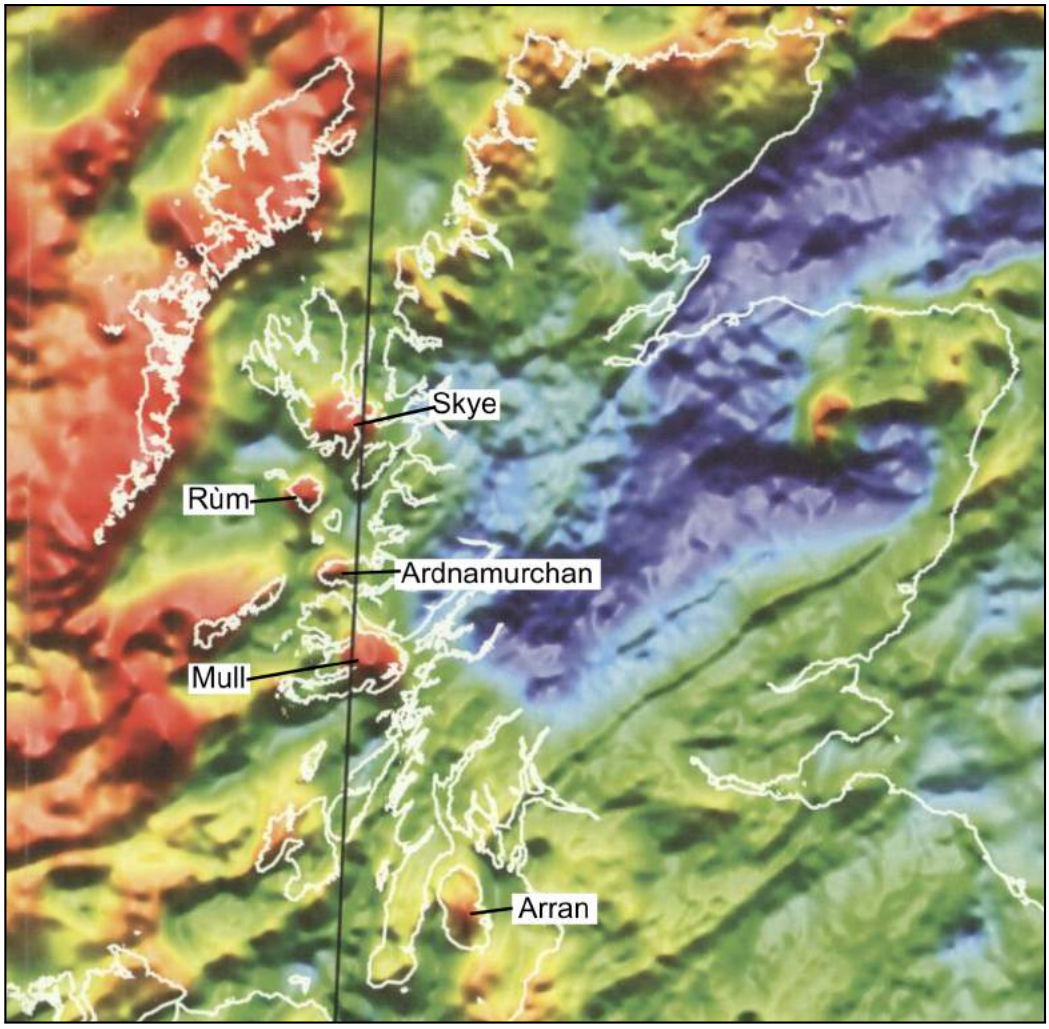

Fig. 1.2 – Bouguer (onshone) and Free-air (offshore) gravity anomaly over Scotland (BGS, 2007), showing the strong positive anomaly over the central complexes of the BPIP – blue = low, red = high.

also vary temporally across most of the life of the BPIP. Magmatism in the Rùm central complex occurred as early as 60.5 Ma (Chambers et al., 2005; Troll et al., 2008), and activity continued until 55 Ma on Skye and St. Kilda (Emeleus and Bell, 2005). In each centre, magmatic activity from early intrusion to unroofing could have been very rapid. On Rùm, the 60.0 Ma Canna Lava Formation sits on top of the subaerially eroded Western Granite, showing an age gap of as little as 500 ka (Emeleus and Troll, 2014). By 55 Ma, 'phase 2' magmatism had largely become focussed to the west of the British Isles and new ocean crust was formed along the northern extension of the Mid Atlantic Ridge (Saunders et al., 1997).

1.2 The geology of Arran

The island of Arran in the Firth of Clyde is often referred to as 'Scotland in miniature'. While this may be an insufferable and clichéd phrase, it is very geologically apt. The north is mountainous, and built on an ancient metamorphic basement. To the south of the Highland Boundary Fault (HBF) the landscape is lower and hilly, comprising Palaeozoic sedimentary geology. Systematic mapping by the BGS began in the latter part of the nineteenth century, carried out by Geike, Gunn, and Peach. This work was published as the Memoir for North Arran, Bute, the Cumbraes, and parts of Ayrshire and Kintyre (Gunn et al., 1903). The remainder of the island was mapped and the Arran Memoir was published 25 years later (Tyrell, 1928). Much of the information summarised here is from the British Geological Survey map of the solid geology of Arran (Fig. 1.3, BGS 1987).

1.2.1 Pre-Palaeogene geology

The oldest rocks are the Dalradian metamorphosed sands, gravels, silts, and muds of the Neoproterozoic-Cambrian Southern Highland Group (Stephenson et al., 2013), exposed around the NAG (Fig. 1.3). Sandstones of the Lower Devonian (Lower Old Red Sandstone) are separated from Dalradian rocks in the north east of the island by the Corloch Fault, a probable splay of the HBF. South of the NAG, however, the Dalradian schists and Devonian sandstones may be in unconformable contact (England, 1992). The trace of the HBF through Arran is not well constrained, but may be approximated as the contact between Dalradian and Devonian rocks around the south of the NAG (Tyrell, 1928; Young and Caldwell, 2012). Sandstones of the Upper Devonian (Upper Old Red Sandstone) are unconformable on Lower Devonian strata, showing Middle Devonian tectonism (Trewin and Thirlwall, 2002). Following the Devonian, a series of Carboniferous sedimentary units were deposited,

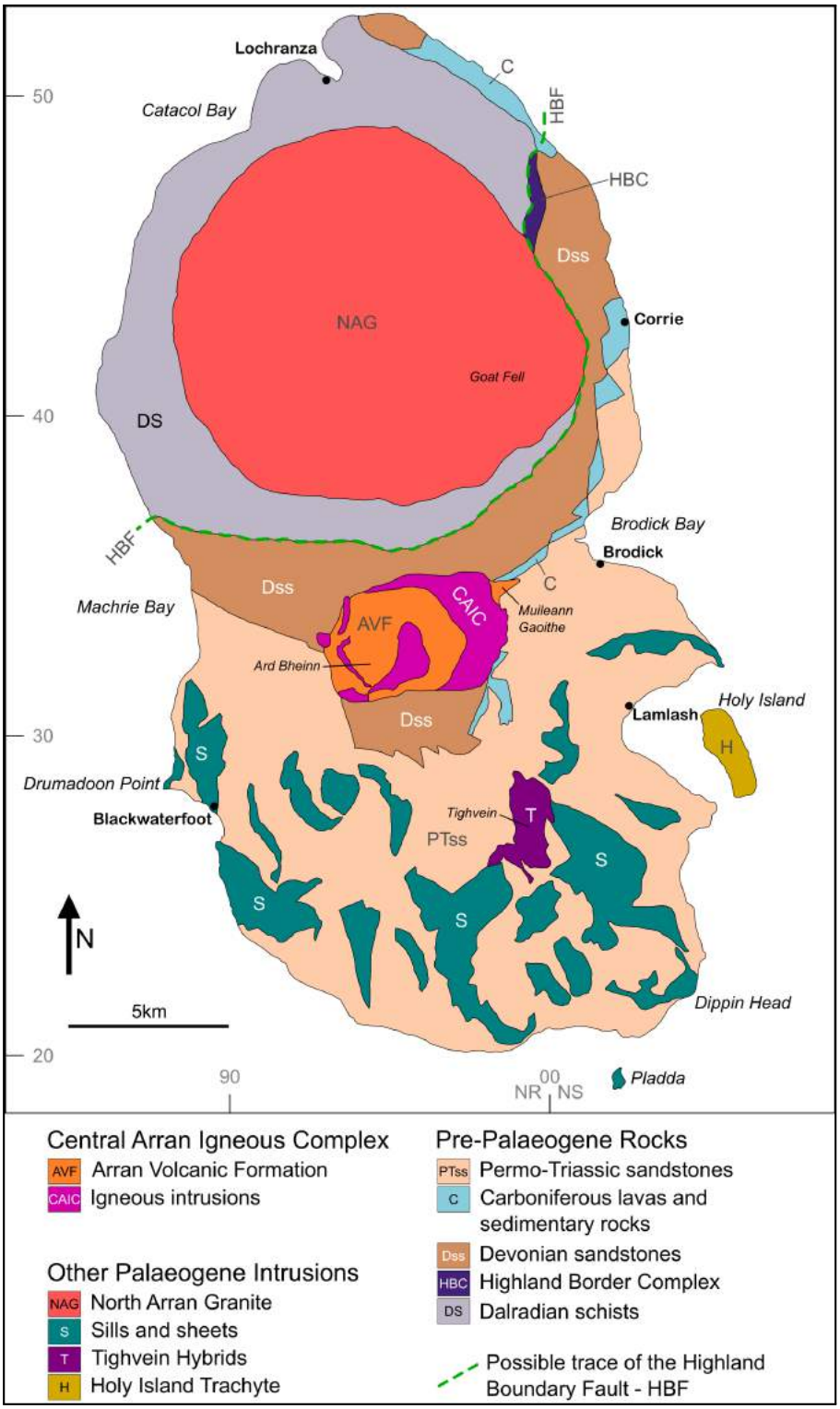

Fig. 1.3 – Simplified geological map of Arran. After BGS (1987)

showing a change in environment to tropical coal swamp conditions, with occasional transgression of a warm shallow sea. At the northern tip of the island these sandstones overlie Dalradian strata at the famous 'Hutton's Unconformity' locality. There was then a return to desert conditions as shown by the Permian and Triassic sandstones and mudstones (New Red Sandstone) that cover large parts of southern Arran. There must also have been at least a thin covering of Upper Triassic, Jurassic, and Cretaceous sediments, but these are now only preserved in blocks which have fallen or subsided into the Arran central complex.

There are various pre-Palaeogene igneous rocks interbedded with and intruding the sedimentary succession. Along the margin of the Dalradian outcrop in North Glen Sannox are the metabasalts, metagabbros, and black phyllites of the Ordovician Highland Border Complex (Fig. 1.3). Fossils, and the pillowed nature of the basalts, suggest an oceanic origin. The Lower Devonian volcanism seen in large areas of Scotland, (e.g. the Lorn Plateau Volcanic Formation) can also be found on Arran. This Devonian volcanism comprises andesite lavas, volcanic conglomerates, and a dolerite sill, all within the Lower Devonian sandstones south of the NAG. Carboniferous volcanism was widespread in the Midland Valley. On Arran, Carboniferous lavas are seen interbedded with the tropical marine sandstones, mudstones, and limestones along the Corrie shoreline.

1.2.2 Palaeogene magmatism

The Palaeogene magmatic rocks preserved on Arran are largely intrusive, with some pyroclastic rocks in the Arran central complex (renamed in this thesis, and Gooday et al. (2018) as the Central Arran Igneous Complex), and an outcrop of basaltic material previously interpreted as a megablock of lava. As well as the magmatic centres of the NAG and the Central Arran Igneous Complex (CAIC), there is a large sill swarm in the southern part of the island, and a dyke swarm that intrudes all units and is best observed intruding the Triassic sandstones along the south coast.

The most striking igneous feature of Arran is the large granite laccolith (Stevenson and Grove, 2014) which dominates the mountainous north of the island (Fig. 1.3). The NAG is suggested to have formed in two intrusive phases (England, 1992): firstly the coarse grained granite, and secondly the finer grained granite into the centre of the coarser unit. The petrology of both granites is similar, consisting of quartz, plagioclase (An_{20} – An_{10}), K-feldspar, and biotite. Apatite, allanite, zircon, and oxide minerals make up the accessory phases (England, 1992). Miarolitic cavities contain smoky quartz and amethyst, with rare blue beryl and topaz (MacDonald et al., 1983), along with REE-bearing fergusonite and gadolinite (Hyslop et al., 1999). The

coarse granite is petrologically and geochemically homogenous, showing it was all intruded as a single phase, and no post-emplacement fractionation took place (Dickin et al., 1981; England, 1992). The Rb, Sr, and Pb contents of the fine granite are thought to reflect late-stage fractionation of a magma similar in composition to the coarse granite (Dickin et al., 1981; Meighan, 1979).

Previous studies have shown that the NAG has an initial (59 Ma) $^{87}Sr/^{86}Sr$ value of 0.716, too low to be formed purely by melting of Dalradian or Permo-Triassic sandstones (Dickin et al., 1981). Although the Devonian sandstones and the Lewisian gneiss have similar $^{87}Sr/^{86}Sr$ values, England (1992) suggests that the magma was formed by fractional crystallisation, with some contamination, rather than by pure crustal melting. The magma was contaminated by crustal units with Nd isotopic values resembling exposed Dalradian units (Dickin, 1994). The granite has a thermal aureole, but it is remarkably narrow, often no wider than a few metres (Tyrell, 1928). The dry nature of this magmatism is shown by the lack of epidote, a ubiquitous mineral in the hydrothermal systems of Skye and Mull, and the high $\delta^{18}O$ values, which have not been depleted by interaction with meteoric water (Dickin et al., 1981).

The sills of southern Arran (Fig. 1.3) can be divided into three broad groups: I) silica-undersaturated olivine-analcime gabbros and dolerites (also termed 'teschenite'; 'crinanite' has more olivine and less analcime), II) quartz-dolerite, and III) quartz-porphyries, felsites, and pitchstones (MacDonald et al., 1983).

The first group is found in a ring around Lamlash Bay, and also in the cliffs at Dippin Head (Gibb and Henderson, 1978). Petrological similarity to the MPG and SMLS suggests that they are the earliest intrusive rocks on Arran, and could correlate with the basalt blocks in the CAIC (MacDonald et al., 1983). The Dippin Sill is at least 42 m thick, and formed by multiple injections from a stratified alkaline magma chamber, thus creating the observed differences in mineralogy within the intrusion (Gibb and Henderson, 1978). This type of intrusion contains multiple xenoliths of country rocks, and has led to contact metamorphism of the surrounding sedimentary rocks. Some of these intrusions transgress the Permo-Triassic stratigraphy, so should be referred to as alkaline sheets.

The quartz-dolerite sills crop out extensively in the south east of the island, but occur throughout southern Arran. They range in thickness from less than 1 m to 80 m, and some show a composite nature. They contain basaltic cognate xenoliths, but very few country rock xenoliths. The Tighvein complex in the south of the island consists of an augite diorite and quartz diorite intrusion, intruded and veined by microgranite and microgranophyre. Other intrusions associated with the Tighvein complex include rhyolite, pitchstone, and porphyritic basalt (Emeleus and Bell, 2005;

Herriot, 1975). The 8 m thick sill at Creag Dubh in Whiting Bay is curious in that it is a composite intrusion with a dolerite core and more silicic margins (Rogers and Gibson, 1977).

The final group of sills includes the quartz-porphyry Brown Head sill and the composite quartz-porphyry Drumadoon and Bennan Head sills. Numerous felsite and pitchstone sills and dykes, including the Corrygills dykes are also in this group. The intrusions of the Drumadoon Complex consist of a porphyritic rhyolite core with xenocrystic basaltic-andesite margins. The two magmas only interacted at shallow levels, and were contaminated by crustal material north of the HBF, indicating lateral transportation of magma at least several kilometres southwards (Meade et al., 2009). The same is true for many of the intrusions in the south of the island (excluding the CAIC), which have Nd isotopic values similar to the NAG, showing contamination by Dalradian crust (Dickin, 1994).

Dykes of this type (*i.e.*, quartz-porphyries, felsites, and pitchstones) intrude both of the previous types of sill, as well as the NAG and the granite of the CAIC (MacDonald et al., 1983). The only rocks unaffected by intrusion of felsites and pitchstones, and indeed the basic dyke swarm, are the felsite at Torr Righ Beag, north of Drumadoon, and the riebeckite-trachyte of Holy Island. These therefore are likely to be the youngest igneous units; however it is also possible that the Holy Island sheet is connected to the alkaline sheets of Lamlash Bay (Emeleus and Bell, 2005) or Ailsa Craig.

The majority of mafic dykes in the Arran dyke sward trend north north west. They are particularly prevalent on the eastern side of the NAG and along the south coast. As well as tholeiitic dolerite and basalt, members of the three types of sill/sheets on Arran are also present as dykes (MacDonald et al., 1983; Speight et al., 1982). Intrusion of the dykes was accommodated by at least 7.5% extension of the crust, perpendicular to the trend of the dyke swarm (Tyrell, 1928).

It is interesting to note that the positive Bouguer anomaly over Arran is centred on the CAIC (Fig. 1.4), and not the NAG (BGS, 2007). This implies that the central complex is accompanied at depth by some thickness of high-density mafic to ultramafic units, as is seen in the more deeply eroded centres of the BPIP, while the NAG lacks a deep root of denser cumulate rocks.

1.2.3 Previous Geochronology of the Arran Intrusions

The NAG was long assumed to be ‘lower Tertiary’, based on its similarity with other igneous rocks in Scotland and Northern Ireland (e.g. Tyrell, 1928). There, lavas had been dated by fossil assemblages preserved in inter-lava sedimentary horizons.

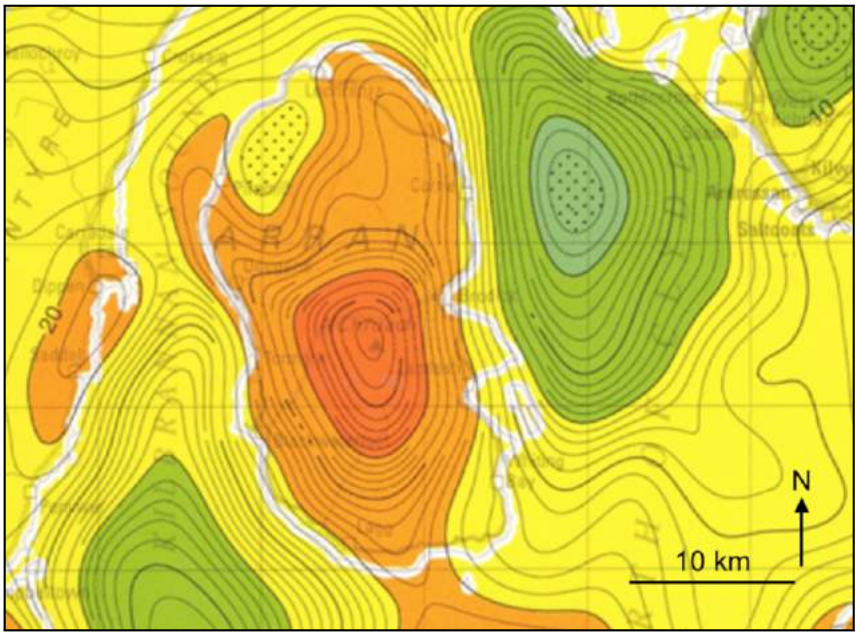

Fig. 1.4 – Bouguer gravity anomaly over Arran (BGS, 2007), showing the strong positive anomaly over the CAIC – green = low, orange = high.

The first analytical confirmation of a Palaeocene age came from Miller and Harland (1963), who used K-Ar dating to obtain ages of 65–55 Ma.

The work of the next few decades focussed more on magnetostratigraphy, with evidence that igneous activity took place over the magnetic sequence R-N-R (Hodgson et al., 1990). With the normal polarity rocks assigned to chron 26N, the timing of magmatic activity is restricted to a period from 61.6 Ma to 57.8 Ma (Harland et al., 1989; Hodgson et al., 1990). It is interesting to note that all quartz porphyries have normal polarity, while all felsites have reversed polarity. This suggests that all the quartz-porphyry intrusions are from the same episode of magmatism (Hodgson et al., 1990; Mussett et al., 1987, 1989).

The NAG was initially dated by K-Ar methods (Evans et al., 1973) at 58.8±0.6 Ma. This age was subsequently recalculated by Hodgson et al. (1990) to give 60.3±0.6 Ma. This agrees well with the 60.3±1.6 Ma Rb-Sr isochron age of Dickin et al. (1981). More recently however, a mean Ar-Ar age of 57.85±0.15 Ma has been obtained (Chambers, 2000).

The only age for the CAIC is a K-Ar age of the granite of 58.3±2.2 Ma (Evans et al., 1973). Aside from having a large error (±4.4 Ma if given to 2σ), this result was rejected by Hodgson et al. (1990), based on the acceptance criteria of Lanphere and Dalrymple (1978). The CAIC is thought to be younger than the NAG, as it cuts the doming structures formed by intrusion of the granite (King, 1954), although this requires geochronological confirmation.

Other published ages from Arran include the Drumadoon Complex with Ar-Ar ages of 58.5±0.8 Ma (Mussett et al., 1987) and 59.04±0.13 Ma and 59.16±0.17 Ma (Meade et al., 2009), and the Port na Feannaiche dykes with ages of 58.9±1.2 Ma and 58.8±2.3 Ma (Hodgson et al., 1990). The basaltic material in the CAIC, thought to be the last remaining fragment of the Arran lava-pile, was deemed too altered to be dated by Ar-Ar dating (Chambers, 2000).

1.3 Previous Work on the Central Arran Igneous Complex

The CAIC is ~5 km across west to east and 4 km south to north, lying half way between Brodick Bay and Machrie Bay, just south of the String Road (Figs 1.3, 1.5). It intrudes Devonian sandstones to the north and south and Permo-Triassic sandstones to the east and west.

The *"focus of great volcanic activity"* in central Arran was first mapped by William Gunn of the BGS at the end of the nineteenth century. It was noted that it was similar to other volcanic vents of the British Tertiary, but was *"exceptionally gigantic in its proportions"* (Gunn et al., 1901). He recognised that the complex was made up partly of fragmented explosive material and partly of intrusive granitic rocks. Gunn was also intrigued by the blocks of fossiliferous shale, marl, and sandstone within the CAIC which are not seen elsewhere on Arran. A block of marl and limestone in the Allt nan Dris yielded a Rhaetic age (204–200 Ma) determined from the presence of the bivalve *Avicula contorta*. The shale in Ballymichael Glen contained Liassic (200–175 Ma) fossils of *Ammonites angulatus* and *Gryphaea arcuata* (Fig. 1.6) (Gunn et al., 1901). A sedimentary stratigraphy of red marl, successively overlain by grey marl, dark shale, and limestone containing upper Triassic and lower Jurassic fossils, is consistent with sequences observed in Northern Ireland and South Wales. Limestone and chert blocks were assigned to the Upper Cretaceous, based on similarity with exposed units in Antrim (Gunn et al., 1901).

In the Arran Memoir, Tyrell (1928) described the area in detail (Fig. 1.5). He was also the first to use the term 'ring complex', noting that it was too complicated to be simply a 'volcanic vent', as Gunn et al. (1901) had described. The reasons he described it as *"a ring complex of the Mull type"* include the arcuate nature of outcrops, the recognition of large subsided blocks within the pyroclastic succession, and the hydrothermal alteration of the 'agglomerate' and early gabbros and felsites.

Although only the eastern part of the area had been mapped in detail, Tyrell proposed a history of the complex in the memoir. First, undersaturated basaltic lava

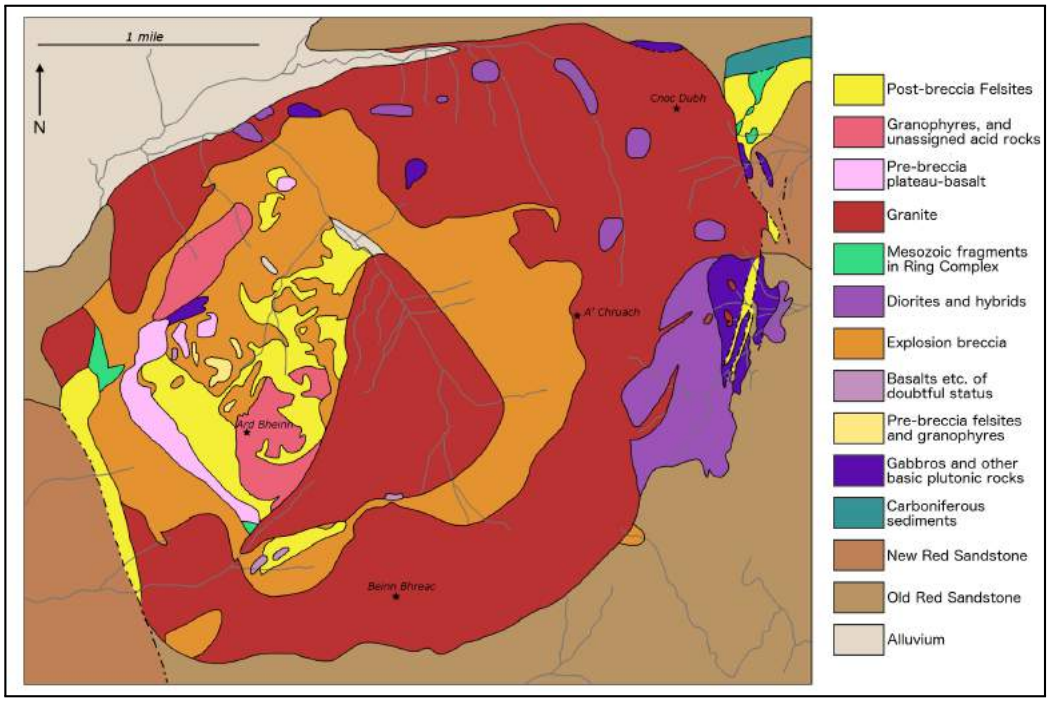

Fig. 1.5 – Geological map of the CAIC after the map produced in the Arran Memoir (Tyrell, 1928).

flows resembling those on Skye and Mull were erupted through Old Red Sandstone with a Mesozoic covering. At this time there was likely also doming and erosion. Intrusion of an over-saturated magma to form the gabbros in the east of the complex then occurred, followed by the emplacement of silicic intrusions. These include the ring granite, the central granite, and the felsite intrusions. The dioritic rocks are thought to result from interaction of the granite with the older gabbro. Explosive volcanism accompanied the silicic intrusions and caused the brecciation of all units, albeit more intense in some places than others. This magmatism occurred along arcuate fissures, and may have been accompanied by caldera subsidence at the surface. The final event was the injection of 'post-breccia' felsites and granophyres.

In the memoir, Tyrell (1928) also discusses the model of Gregory and Tyrell (1924). This 1924 model largely involves the intrusion of the central granite causing uplift of a dome, leading to erosion of the Old Red Sandstone, the Mesozoic cover, and the granite itself, along with minor silicic intrusions which invaded the granite at a similar time.

Although both Tyrell and Gregory highlight the drawbacks of using the term 'agglomerate', they disagreed on how these units should be described. Tyrell advocated 'explosion-breccia', and suggested that all of the fragmental rocks were formed by shattering during explosive eruption. Gregory, however, suggests that these units

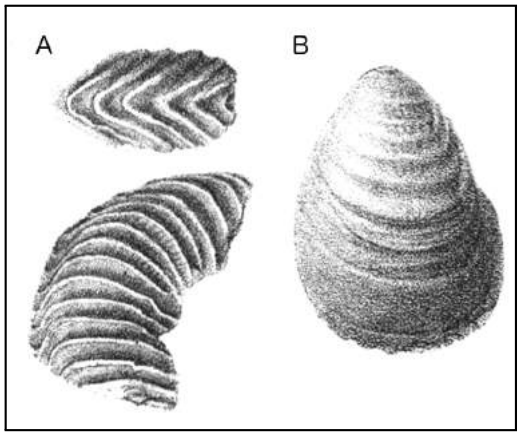

Fig. 1.6 – Diagrams of fossils used to assign a Liassic age to the block of shale in Ballymichael Glen. A) *Ammonites angulatus*. B) *Gryphaea arcuata* from Gunn et al. (1901).

comprise differing amounts of sedimentary conglomerates and breccias (including igneous clasts), intrusive breccias formed during injection of silicic magmas, and 'tuffs and agglomerates', *i.e.*, the products of explosive volcanic activity. With a modern take on caldera forming processes, it appears that Gregory's scenario is the most favourable.

It was in the Arran memoir that the location and geological features of the individual "Mesozoic fragments" in the complex were also described in detail. Tyrell also commented on all fossils found in the Rhaetic (Upper Triassic), Lias (Lower Jurassic), and Cretaceous blocks, as well as the relationships between sedimentary and igneous rocks in some fragments. It is also suggested in the memoir that the CAIC was younger than the NAG, based on the fact that it truncates country rocks which had previously been tilted by the emplacement of the granite to the north.

The most complete description of the interesting central area of the CAIC comes from Basil King's 1954 paper on the Ard Bheinn area in the north west of the complex (Fig. 1.7). This area contains the best exposure and the most varied lithologies.

1.3.1 King's interpretations

According to King (1954), the caldera was made up of pyroclastic and sedimentary rocks (referred to as 'agglomerates') intruded by later igneous units (Figs. 1.7, 1.8). The cauldron-like nature of the caldera was marked out by the arcuate form of the outer belt of agglomerate ('explosion breccia' in Figure 1.5), the large blocks of basalt and felsite in upper Allt Ruadh, the gabbro on Binnein na h-Uaimh, and the peripheral granite.

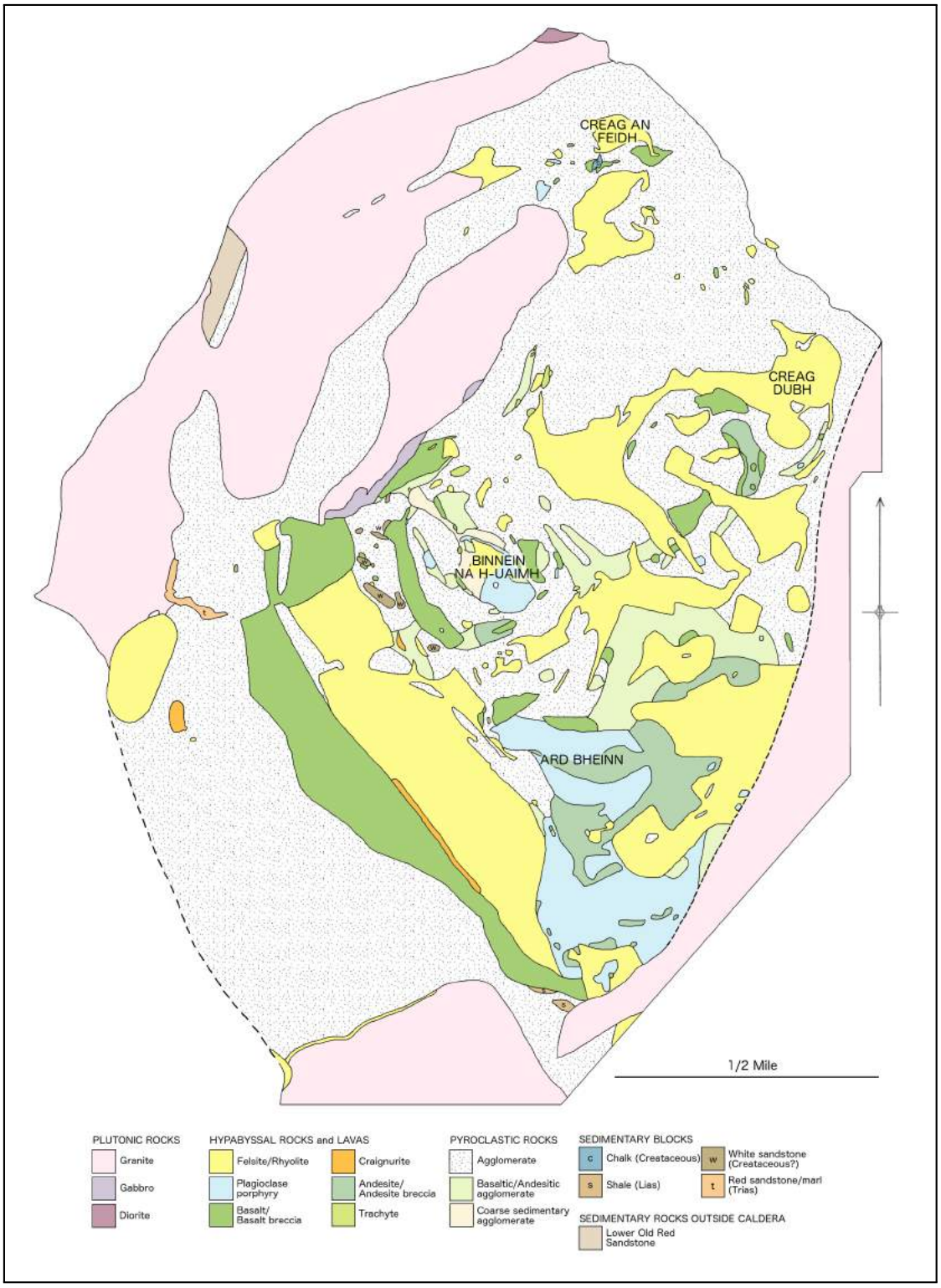

Fig. 1.7 – King's map of the Ard Bheinn area in the north west of the CAIC. (King, 1954)

Table 1.1 – The pre-subsidence stratigraphy of central Arran, according to King (1954).

Age	Lithology	Thickness
Tertiary	Basalt lavas	>100 m
Cretaceous	Limestone	a few m
	Sandstone	15 m?
Jurassic	Mudstones	15 m?
Triassic	Rhaetic shales	30 m
	Marls (sandstones?)	300 m
Permian	Sandstone	600 m
Carboniferous	Possible sediments and lavas	thin/missing
Devonian	Sandstone	>1 km

He determined that the clasts and blocks were largely derived from the pre-caldera stratigraphy, including Old Red Sandstone, Upper Triassic red marls, Early Jurassic mudstone (with some fossils), and Cretaceous chalk and limestone. In one block, basalt is seen intruding limestone, so King determined that the blocks of basalt must be Palaeogene in age.

From these blocks, King (1954) was able to reconstruct a pre-subsidence stratigraphy for central Arran (Table 1.1). The post-Triassic sedimentary cover has been entirely eroded away, unlike in the rest of the Hebrides where lava-piles and underlying Mesozoic sedimentary rocks are preserved. In the peripheral agglomerates, clasts of quartz, quartzite, and schist can be found in the 'sedimentary agglomerates' that ultimately derive from a Dalradian source. It is thought, however, that these were originally clasts in Devonian conglomerates prior to deposition in the caldera (King, 1954).

King noted that the matrix of the agglomerates is silicic, with sub angular quartz grains always present. All clasts are rounded, showing that the agglomerate was formed by what King believed was *"prolonged attrition in a vent"*, rather than by explosive brecciation.

The amount of subsidence of the caldera can be estimated in several places. At Dereneneach, the country rocks show the Devonian-Permian contact, while nearby, within the caldera, much younger Upper Triassic rocks are exposed. The difference in stratigraphic height shows subsidence on the order of 1 km. This is consistent with other examples from around the world, including Mull (Bailey et al., 1924). At the southern end of the basalt outcrop on the western slopes of Ard Bheinn, Palaeogene rocks are juxtaposed against Jurassic rocks, showing at least a small amount of further subsidence.

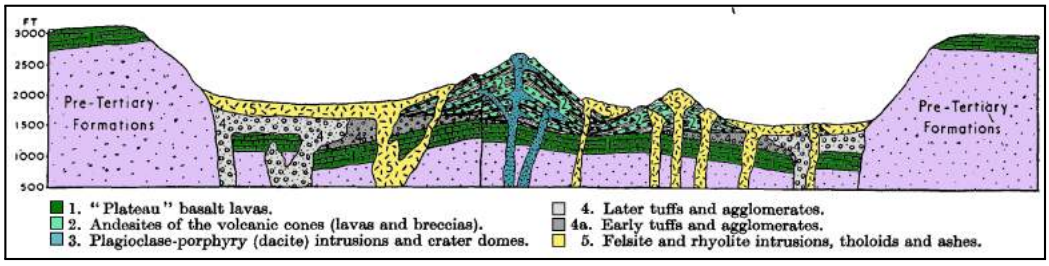

Fig. 1.8 – Schematic cross-section of the post-subsidence/pre-granite complex. The peak can be taken as roughly the summit of Ard Bheinn. From King (1954).

Post-collapse doming was assumed by King to have taken place in the centre of the caldera, as had been observed in the USA (Bucher, 1936). This was followed by caldera-scale radial and concentric fracturing.

From field evidence of the caldera and surrounding rocks, King proposed a structural history of the area. Initial pre-complex doming of the country rock was followed by cauldron subsidence, presumably accompanied by a large amount of explosive volcanism. There was then doming in the centre of the caldera, possibly connected to peripheral subsidence. Finally, renewed volcanism occurred at discreet centres on the floor of the caldera. There was possibly local doming at each of these new volcanic centres.

King (1954) proposed that four post-subsidence volcanic centres correspond roughly with the most elevated parts of the Ard Bheinn area: Ard Bheinn, Binnein na h-Uaimh, Creag Dubh, and Creag an Feidh (Figs. 1.7, 1.8). The first three all show gently dipping extrusive features, which are interpreted as volcanic superstructures.

It was suggested by King that the pre-volcanic floor of the caldera was basaltic. A suite of andesite lavas and breccias grade into one another, and together were termed 'andesite complexes'. 'Plagioclase-porphyries' (plagioclase-phyric dacites) were proposed to be shallowly intruded sheet-like and boss-like bodies. Rocks containing quartz and K-feldspar phenocrysts in a devitrified groundmass were termed 'rhyolites', 'felsites', or 'quartz-porphyries' based on texture and phenocryst content. They were interpreted as being later than the adjoining units, as they are arcuate in outcrop, and disrupt other arcuate structures (Fig. 1.7).

King (1954) identified four main outcrops of granite which intrude the volcanic rocks of the CAIC. These were the Creag Mhor granite, the lenticular Binnein na h-Uaimh granite, the peripheral granite, and the Glen Craigag granite in the centre of the complex (Fig. 1.7). This peripheral granite was considered a ring dyke, due to apparent evidence of steep contacts.

The Glenloig diorite was noted as being similar to other masses in the north and east of the complex, especially around the head of Glen Dubh. These rocks show

mineral characteristics of both gabbro and granite, so were suggested to be hybrid in origin (King, 1954).

1.4 Calderas

Calderas are the surface expressions of complex volcano-magmatic systems, with prolonged periods of unrest and eruption (Acocella et al., 2015; Nobile et al., 2017) punctuated by extensive periods of quiescence. Although much debated, caldera collapse is typically caused by the withdrawal of large volumes of magma from shallow magma chambers (Cashman and Giordano, 2014; Cole et al., 2005; Druitt and Sparks, 1984; Lipman, 1997), and subsidence of a coherent block of crust into the underpressurised chamber(s) (Acocella, 2007; Cole et al., 2005; Lipman, 1997; Mori and McKee, 1987), although collapse may also be triggered by overpressure within the chamber initiating fractures in the roof rocks (Gudmundsson, 1988, 1998). Caldera-forming eruptions are typically silicic and can deposit extensive sheets of ignimbrite both within and beyond the collapse caldera, together with widespread fall deposits, and even the circulation of ash globally (e.g. Hildreth and Fierstein, 2012; Newhall and Dzurisin, 1988; Self et al., 1984; Self and Rampino, 1981).

Understanding caldera-forming eruptions and syn-eruptive collapse mechanisms is notoriously difficult at both modern and ancient calderas. Monitoring unrest at active calderas using seismic and remote sensing methods is essential in forecasting volcanic activity, but understanding these relationships is complex. How much magma withdrawal is required to induce collapse and how does collapse vary (Geshi and Miyabuchi, 2016)? Furthermore, how many collapse events may occur in the lifecycle of a caldera (e.g. due to evacuation of multiple magma reservoirs), and how might the deposits of these different eruption and collapse events vary both temporally and spatially (proximal and distal)? Answering these questions at active calderas is challenging, as only the latest stages in the caldera's deposits and structures are preserved and access may be further obscured by water and sediments (Acocella, 2007).

Therefore, we can look to ancient and more recent but inactive calderas. There are numerous field studies of such calderas (see reviews by Cashman and Giordano, 2014; Cole et al., 2005) that attempt to resolve questions on caldera collapse and evolution, and these have been supported more recently by numerical and analogue modelling studies (e.g. Acocella, 2007; Geshi et al., 2012; Troll et al., 2002). However, ancient calderas can typically be obscured by resurgent intrusions and volcanic deposits, thoroughly disrupted by faults and hydrothermal alteration, and/or obscured by water

and later sediments. The level of erosion and preservation of the volcanic deposits and caldera-controlling structures can also represent a particular constraint to study. These constraints are particularly important with respect to the intra-caldera/proximal records of eruption, which are consequently less well studied than more distal, better preserved ignimbrite sheets (Smith and Kokelaar, 2013).

Therefore, it remains a challenge to volcanologists to identify ancient calderas where access and preservation allow for detailed field observations that can be used to elucidate caldera collapse and caldera-forming eruption processes. Given modern advances in physical volcanology (in particular pyroclastic density currents, the sedimentation of ignimbrites, and better understanding of lava-like ignimbrites; e.g. Branney et al., 2008; Branney and Kokelaar, 2002; Brown and Bell, 2013), it is essential to revisit localities that have not received recent attention.

1.5 General Structure of the CAIC

In this section, the results of mapping undertaken during this study will be introduced. The descriptions presented in this chapter are largely a result of fieldwork carried out on Arran between March 2015 and May 2017. The majority of mapping and sample collection was carried out by the author, with several days of input from supervisors Dr Davie Brown and Dr Kathryn Goodenough who provided ideas about possible structure and stratigraphy, and mode of emplacement of various lithologies.

Mapping and other digital data collection were carried out using Cardiff University Solid Earth Research Group's Panasonic CF-H2 Toughbook, running ArcGIS software and accompanying SIGMA mobile extension. Some sampling campaigns used a Garmin eTrex 10 GPS receiver and a notebook. Sampling was carried out with a hammer (by permission), with a chisel used to prise clasts from their host conglomerates. Every effort was made to minimise damage to exposures. A full list of samples and their locations is given in Appendix E1.

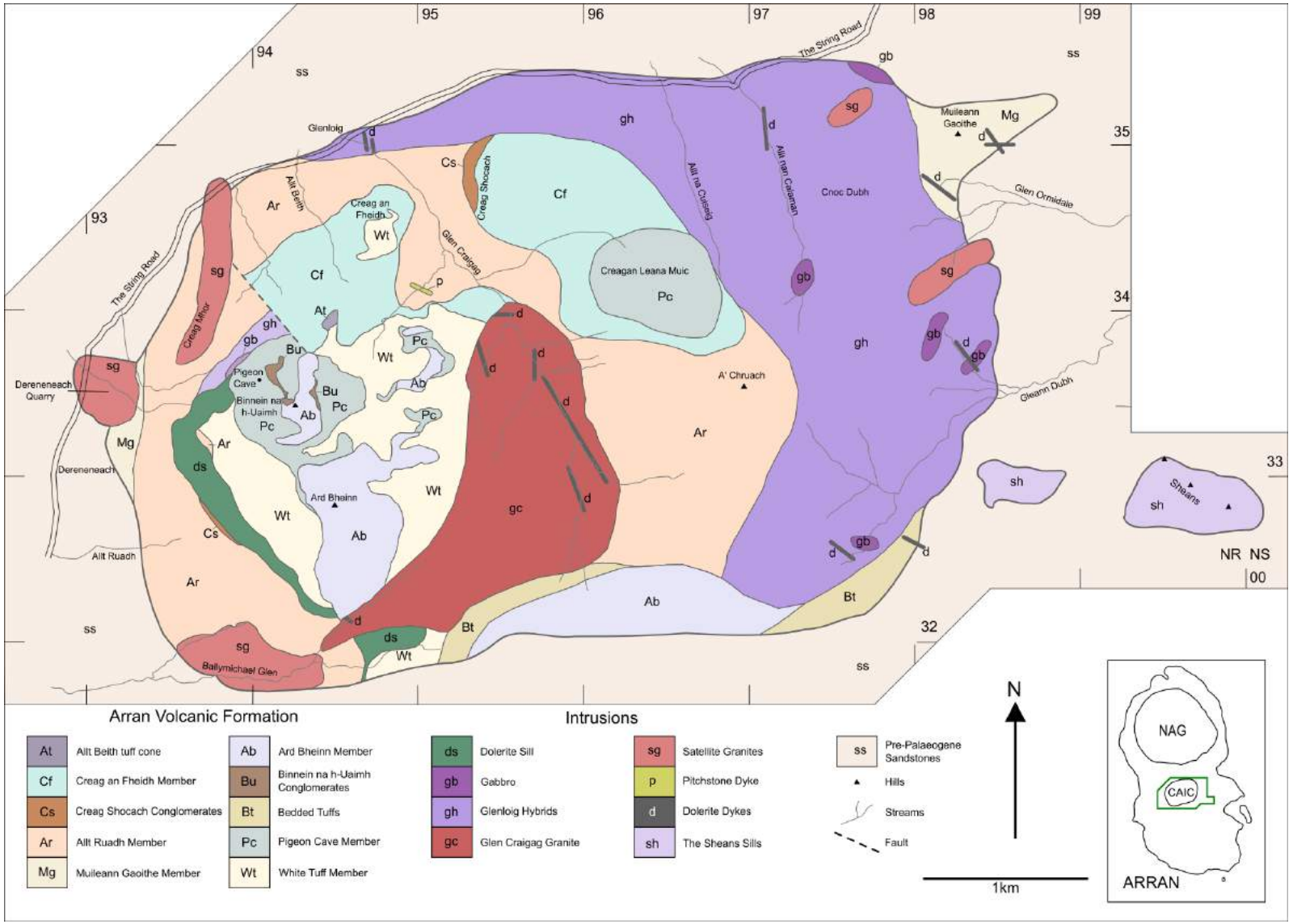

Fig. 1.9 – Geological map of the Central Arran Igneous Complex, from fieldwork undertaken in this study. This map is also given in Appendix E8 for easier electronic viewing.

The new geological map of the CAIC is show in Fig. 1.9. The east and north east of the complex are dominated by coarse-grained igneous rocks, including granites and intermediate amphibole-bearing dioritic rocks. Granites are also found as isolated bodies around the periphery of the western part of the complex, and in the upper parts of Glen Craigag and Ballymichael Glen in the centre of the complex.

The western two-thirds of the complex are dominated by pyroclastic rocks with minor sedimentary units (the Arran Volcanic Formation, see Chapter 3). There are several lines of evidence that the extent of these pyroclastic rocks defines the boundaries of a caldera. Firstly, the outcrop of pyroclastic rocks in this part of the complex (*i.e.*, not including the Muileann Gaoithe exposures) is roughly circular. Secondly, certain horizons within the caldera-fill succession are interpreted as collapse breccias. Lastly, Palaeogene ignimbrites are not found anywhere else on Arran or in the Firth of Clyde region. These deposits must have been aerially extensive at the time of deposition, and the fact that they are only preserved in the CAIC suggests they escaped a significant amount of post-Palaeogene erosion by occupying a depressed position within the crust. Additionally, the boundary between the Upper Devonian sandstones and conglomerates and Permo-Triassic sandstones and conglomerates is thought to crop out within metres of the CAIC ignimbrites (BGS, 1987). As the Permo-Triassic sandstones and conglomerates are known to be on the order of 1 km thick in the region, this shows that the (subaerially-deposited) CAIC ignimbrites must have experienced subsidence of at least this amount.

The caldera-bounding fault is not exposed, but is assumed to be roughly equal to the extent of pyroclastic rocks. This will be discussed in Section 3.3.

This map differs from those of Tyrell (1928) and King (1954) in a number of regards. Firstly, the 'ring intrusion' of granite has been reinterpreted as a series of isolated granite bodies, and a series of amphibole-bearing dioritic rocks intruded by rhyolites and microgranites (termed the Glenloig Hybrids). It is for this reason the term 'ring complex' has been dispensed with. Secondly, the large 1.5 km long outcrop of basalt on the western slopes of Ard Bheinn had previously been interpreted as a subsided megablock of a pre-caldera Palaeogene Arran lava-pile, similar to those seen extensively on Mull, Skye, and Antrim. However, due to mapping and petrology undertaken in this study, it has been reinterpreted as a dolerite sill that intrudes the pyroclastic rocks of the caldera-fill succession. Thirdly, the homogenous mass of 'explosion breccia' or 'agglomerate', disrupted by seemingly random outcrops of 'felsite' and rhyolite have together been reinterpreted as a stratigraphic succession of laterally extensive ignimbrite units which make up the intra-caldera succession.

A chronostratigraphic chart showing the interpreted age relationships between the volcanic and intrusive units of the CAIC and the North Arran Granite is shown

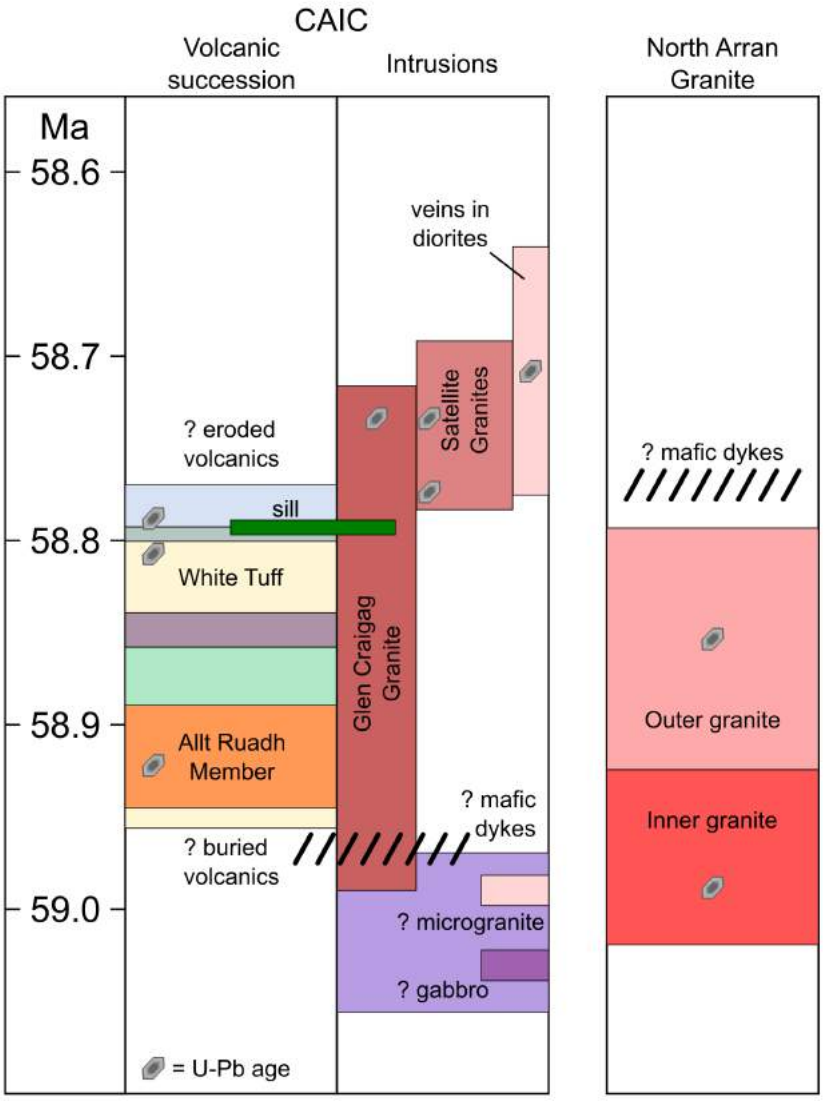

Fig. 1.10 – Chronostratigraphic chart showing the principal volcanic units and intrusions of the CAIC and the North Arran Granite

in Fig. 1.10. The U-Pb dates shown on the graph are from this study, and will be presented in Section 4.3.

Chapter 2

Petrography and Mineral Chemistry of Intrusive Rocks

In this chapter, the intrusive units that make up the Central Arran Igneous Complex (CAIC) are introduced. The focus of this chapter is field observations and petrography – the geochemistry of these units will be discussed in Chapter 4. The units outside the CAIC that were studied as part of this project will also be briefly discussed.

Coarse-grained intrusive rocks make up around half of the area of the CAIC (Fig. 1.9). These include several isolated granite bodies and a suite of intermediate-silicic intrusions with complex magma-interaction histories. There are also some minor gabbros. In addition to the coarse-grained intrusions, this section also discusses the suite of mafic dykes that cross-cut the complex. Rock names are based on the QAPF diagram of Le Maitre et al. (2002). A description of the methods used in energy-dispersive X-ray spectrometry (EDS) analysis is given in Appendix A, and full mineral chemistry results are given in Appendix E2.

2.1 Glenloig Hybrids

Tyrell (1928) and King (1954) noted and discussed the presence of *"dioritic rocks"* and *"rocks of hybrid aspect"* in several areas within the complex, notably underneath the road bridge at Glenloig (NR 946 350), and around the head of Gleann Dubh in the east of the complex (NR 98 33). Detailed mapping undertaken during this study suggests that these are both part of the same continuous unit that dominates the northern and eastern margins of the Central Arran Igneous Complex. The term 'hybrid' is retained, and is used loosely to reflect the complex and varying types of magma interaction that are observed in the exposures (Fig. 2.1).

The Glenloig Hybrids extend in a large crescent from several hundred metres west of Glenloig, east as far as Torr nan Dearc (NR 983 341), and south as far as Tir Dubh (NR 976 327; Fig. 1.9). Away from Glenloig bridge, they are best exposed on Tir Dubh and around the head of Gleann Dubh, as well as in the stream beds of the Allt na Cuiseig and the Allt nan Calaman. These outcrops are all interpreted to lie beyond the suggested caldera ring fault or faults, and therefore outside the caldera. A small outcrop of hybrid material is exposed inside the caldera (interpreted as an inlier) in the marshy ground between Pigeon Cave and Creag Mhor (Fig. 1.9). No contacts are exposed, although it appears to be surrounded on either side by pyroclastic units, and truncated at either end by a dolerite sill and an intra-caldera fault.

The Glenloig Hybrids are poorly exposed, and contacts with other units cannot be seen. However, in the stream bed at Glenloig two lines of evidence suggest that the Glenloig Hybrids pre-date volcanic activity. Firstly, the pyroclastic rocks of the Arran Volcanic Formation appear to lie on top of the hybrids. Secondly, the pyroclastic rocks do not show intrusion by the granitic veins which are prevalent throughout the Glenloig Hybrids in this area, and visible within several metres of the hybrid/pyroclastic contact. This suggests the intermediate hybrid rocks may have been intruded by granitic melt before exhumation and erosion, and subsequent deposition of the Arran Volcanic Formation.

Similar lithologies (*i.e.*, intermediate rocks intruded by, and mingled with, silicic magmas) are found on the Sheans (NR 998 328) - a trio of distinct summits above Brodick 2 km ESE of the head of Gleann Dubh, and on Tighvein (NR 997 274) - a remote moor-covered plateau 6.5 km SSE of A' Chruach (Section 2.7).

The rocks that comprise the Glenloig Hybrids vary greatly (Fig. 2.2). This variation occurs over different scales – changes occur from one exposure to the next, within the same exposure, and within several centimetres. It is not uncommon to observe three lithologically distinct domains within one sample.

At one extreme, exposures of amphibole microgranite contain small xenoliths of fine-grained amphibole bearing diorite (Fig. 2.2a). There are also common examples of relatively thick (5 cm) amphibole microgranite dykelets within a mafic/intermediate host, themselves containing rounded xenoliths of host material (Fig. 2.2b). Fig. 2.2c shows a sample from the exposure under Glenloig Bridge. It is a fine-grained intermediate unit intruded by a coarser unit which appears transitional between the mafic/intermediate host-rock and the granitic intrusions, possibly formed as a result of magma mixing. This unit contains xenoliths of a darker and finer grained lithology. The diorites containing coarser feldspars and amphiboles (Fig. 2.2d) are interpreted as a complete mixture between the dark mafic/intermediate

Fig. 2.1 – Granitic dykelets and vein networks in amphibole-rich quartz diorites on Tir Dhubh. Hammer for scale.

material and the granitic melt, such as seen at (7) in Fig. 2.2c and 10 in Fig. 2.2e. Some exposures are dominated by dark, fine grained dioritic material in contact with large amounts of this 'mixture', which grades into amphibole microgranite (Fig. 2.2e). The other textural end member of the Glenloig Hybrids is those exposures which are dominated by fine-grained dark dioritic rock, with very thin (<0.5 cm) veins of granitic material (Fig. 2.2f). These samples often show less mingling and mixing that the previously described types.

The samples collected from the stream beds at Glenloig (NR 946 350) all consist of amphibole-bearing quartz diorites and granodiorites with dykelets and vein networks of coarser amphibole microgranites. A third lithology, intermediate between these two, presumably formed by mingling, mixing, or both (Fig. 2.2c,e).

Creag nam Mult (NR 956 351) is an isolated exposure of hybrid lithologies 1 km east of Glenloig. It shows similar intermediate amphibole-bearing lithologies to the Glenloig exposures, and also a large exposure of a more 'typical' granite (*i.e.*, without amphibole as a primary mineral).

The exposures in the stream beds of the Allt na Cuiseig and the Allt nan Calaman show similar amphibole-bearing lithologies to Glenloig, but intruded to a much

greater extent by later granitic melt (Figs. 2.2b,f). The exposures on Cnoc Dubh, including those in the upper parts of the Allt nan Calaman, are also dominated by amphibole-bearing quartz diorites, intruded by xenolith-bearing granitic material (Fig. 2.2a).

The exposures in the south east of the complex, on Tir Dhubh (Fig. 2.1) and around the head of Gleann Dubh show all of the previously discussed lithologies (amphibole-rich quartz diorites, granodiorites, amphibole microgranites granophyre, and porphyritic rhyolite), with good examples of silicic material with enclaves of fine intermediate material.

The intra-caldera inlier contains all of the lithologies exposed in the main mass of the Glenloig Hybrids, *i.e.*, amphibole-bearing diorites and quartz diorites, and amphibole microgranite. These are both cut by a series of dykelets of amphibole-poor granite.

2.1.1 Petrography

The quartz diorites from the Glenloig exposures are largely made up of plagioclase laths (0.5-2 mm in length) and euhedral green-brown amphiboles up to 1 mm in length. Quartz and K-feldspar are also present, occasionally showing micrographic intergrowths (Fig. 2.3d). Opaque minerals are abundant, and amphibole crystals often form oikocrysts enclosing opaques and small plagioclase laths. Some of the larger opaques (0.5 mm) show skeletal morphologies. Small amounts of apatite are present in some samples, and ubiquitous chlorite and epidote show that the rocks have experienced some degree of greenschist facies hydrothermal alteration.

The amphibole microgranites from Glenloig largely comprise 0.5-1 mm quartz and K-feldspar crystals and 1 mm euhedral green-brown amphiboles. Larger (up to 2 mm) euhedral plagioclase and K-feldspar crystals show inclusion rims and sieve textures, and so may be antecrysts or xenocrysts. Euhedral opaques and apatites are abundant. Some samples are highly altered, showing almost complete replacement of amphiboles by chlorite. The contact between the amphibole quartz diorites and the amphibole microgranites at Glenloig is not sharp, but can be observed to within several millimetres in thin section. The morphology of the contact is irregular.

The Creag nam Mult fine-grained granite is made up of quartz and K-feldspar <1 mm in size, with rare micrographic intergrowths. Larger (up to 2 mm) euhedral K-feldspars and plagioclases are also present. Small green-brown amphiboles show evidence of extensive alteration, with many being almost completely replaced by chlorite. Sphene, zircon, and opaque minerals are present as accessory phases.

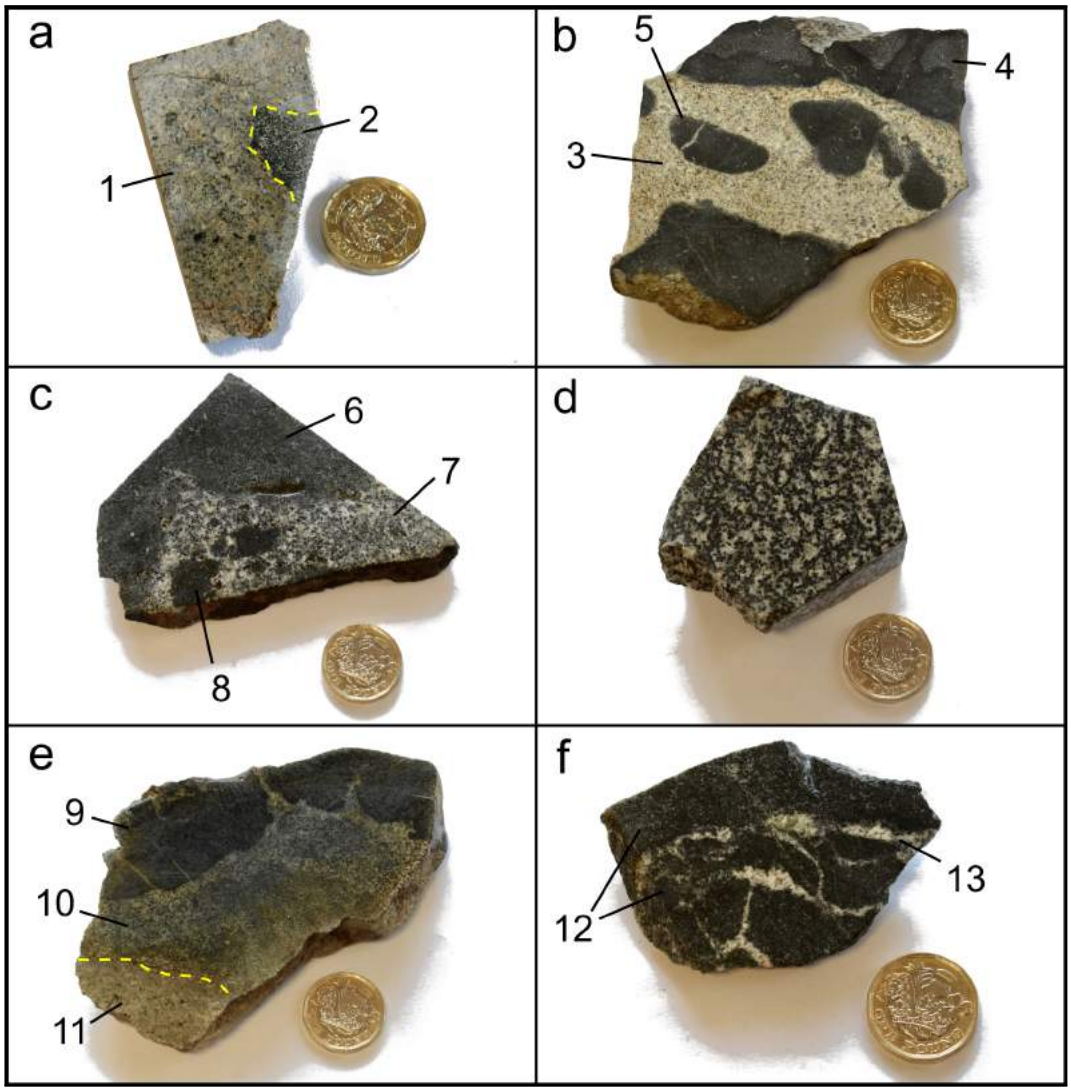

Fig. 2.2 – Photographs of samples of the Glenloig Hybrids. **a)** Photograph of sample BJG/15/342. (1) amphibole microgranite host. (2) Diorite xenolith. **b)** Photograph of sample BJG/15/321. (3) amphibole microgranite dyke. (4) Fine-grained mafic/intermediate host. (5) Rounded enclaves of host material. **c)** Photograph of sample BJG/15/103. (6) Fine-grained intermediate unit. (7) Coarser transitional unit. (8) Xenoliths of a darker lithology. **d)** Photograph of sample BJG/15/318, formed by mixing of the two magmas shown in (b). **e)** Photograph of a loose cobble found in Allt Beith. (9) Mafic/intermediate host. (10) Intermediate zone of mixing/mingling textures. (11) Amphibole microgranite. **f)** Photograph of sample BJG/15/324. (12) Fine-grained host. (13) Network of thin granitic veins.

Examples of samples from the Allt na Cuiseig and Allt nan Calaman exposures are shown in Fig. 2.3a, Fig. 2.4, and Fig. 2.5. Two of these samples were analysed by energy-dispersive X-ray spectroscopy (EDS), allowing mineral compositions to be determined. They contain amphibole quartz diorites, made up of 1 mm plagioclase (An_{32} – An_{56}; Figs. 2.7a, 2.4[1]) and amphibole crystals, with lesser quartz and K-feldspar, and opaque minerals and apatite as accessory phases (Fig. 2.3a - right). They occasionally contain larger (up to 5 mm) zoned euhedral plagioclases (cores An_{61} – An_{65}, rims An_{43} – An_{60}; Fig. 2.7a) that are highly sericictised and sieve-textured, suggesting they may be antecrysts/xenocrysts (Fig. 2.3b). Within 2 mm of the contact with the intruding granitic material, euhedral biotites and dark brown amphiboles (<200 μm) are found (Fig. 2.3a).

The granitic material in the Allt na Cuiseig and the Allt nan Calaman stream beds occurs as dykelets and net-veins intruding the diorites (Fig. 2.2b, 2.4). In places it contains angular xenoliths or rounded enclaves of the diorite. It largely comprises slightly coarser (2 mm) quartz and K-feldspar (Fig. 2.3a - left), rarely showing micrographic intergrowths. Plagioclase is also abundant as large (up to 1.5 mm) zoned (An_{20} – An_{33}; Figs. 2.7a, 2.4[2]) laths. Green-brown amphiboles appear similar to those found in the diorites, and are often highly altered, and may be completely replaced by chlorite. Hydrothermal alteration in some samples is shown by the presence of epidote, and more rarely calcite, filling void spaces (Fig. 2.5).

In the EDS element map of sample BJG/15/321 (Fig. 2.4), several domains of dioritic material can be seen. The zone on the left [3] is rich in amphibole but poor in Fe-oxides and calcic plagioclase. It appears to be disintegrating into the granite in its lower right end. In its top left corner it is rich in quartz and K-feldspar, again presumably related to interaction with the granite. The zone at the top of the image [4] is rich in calcic plagioclases [1], but poor in Fe-oxides. Its contact with the granite is similar to Fig. 2.3a. The zone on the lower right [5] is poor in calcic plagioclases, but rich in Fe-oxides. It is clearly rounded, and resembles the enclaves

Fig. 2.3 ***(facing page)*** – Photomicrographs of the Glenloig Hybrids. **a)** Sample BJG/15/321 showing amphibole-rich diorite (right) and intruding microgranite (left). K = K-feldspar, Q = quartz, P = plagioclase, B = biotite, A = brown amphibole. Plane polarised light. **b)** A coarser part of BJG/15/321, showing two plagioclase antecrysts. Crossed polars. **c)** Sample BJG/15/30, a porhyritic rhyolite. Q = quartz, F = altered feldspar, R = rhyolitic matrix. Plane polarised light. **d)** Sample BJG/15/318, a coarse-grained quartz diorite. Q = quartz, P = plagioclase, A = amphibole, mg = micrographic intergrowths of quartz and K-feldspar. Upper left - crossed polars, bottom right = plane polarised light.

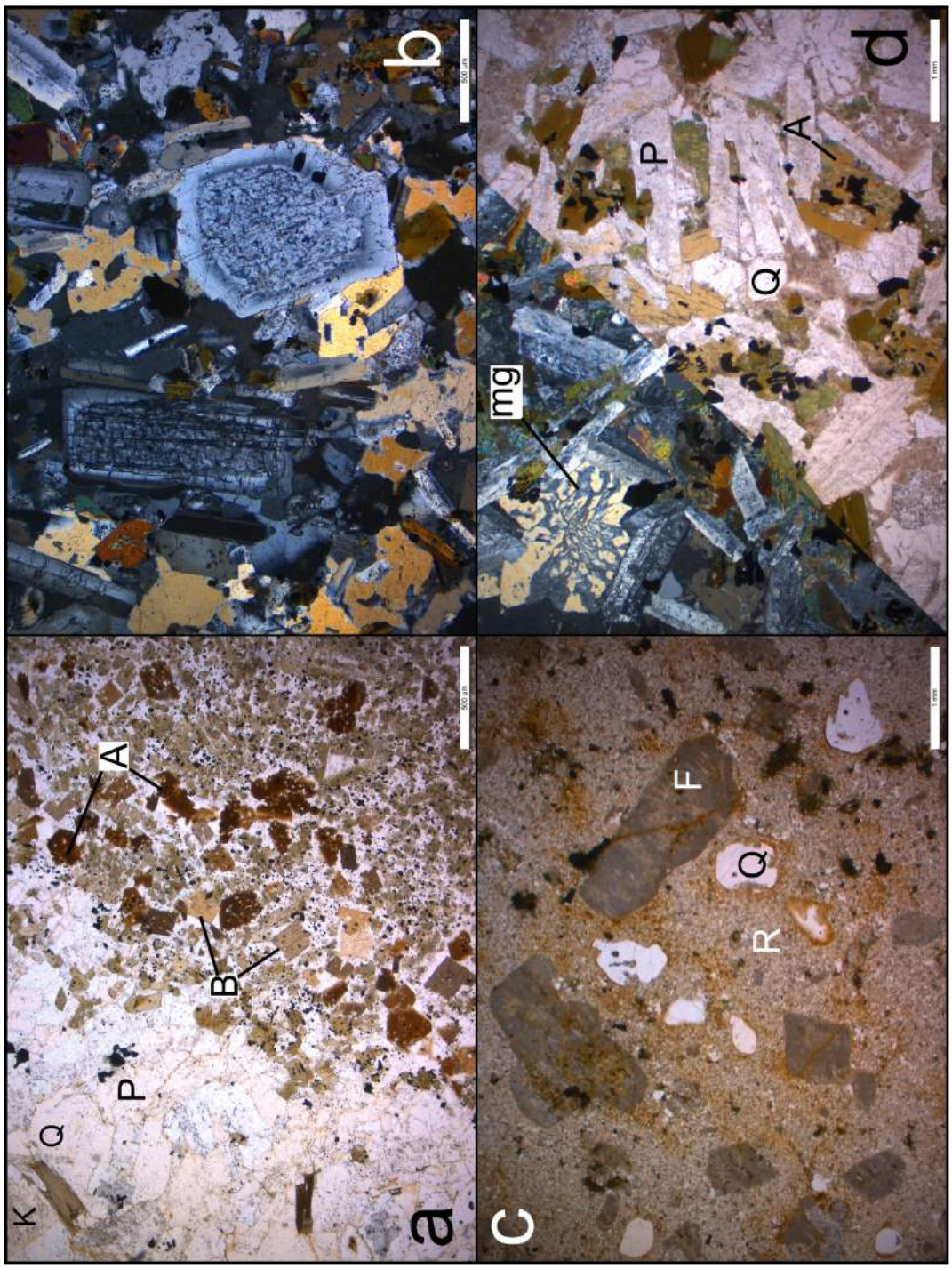
a
K
Q
P
A
B
b
c
F
Q
R
d
P
A
Q
mg

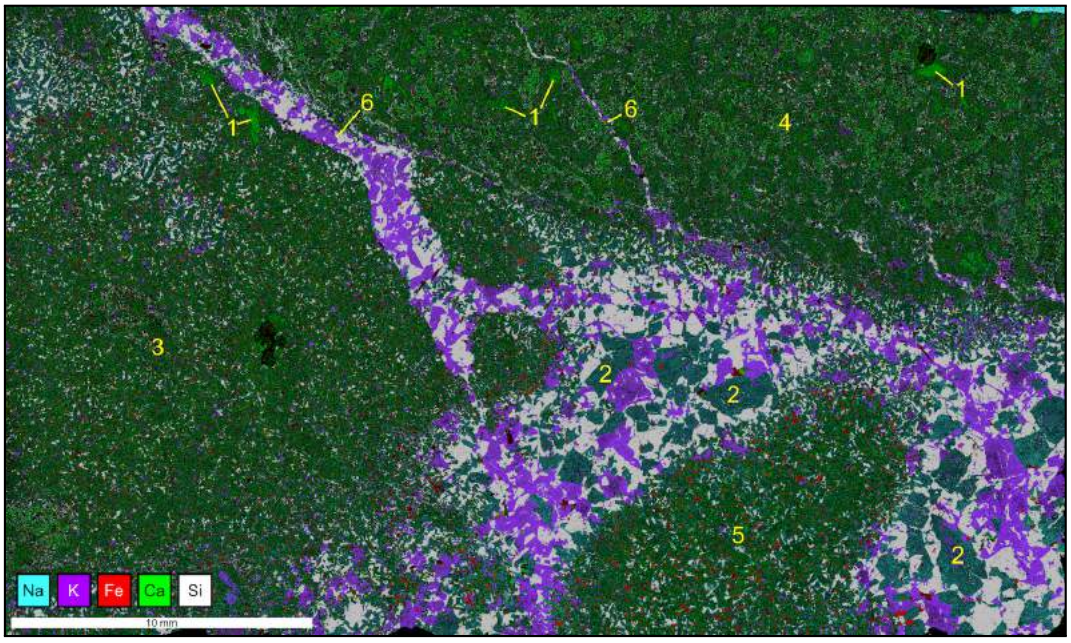

Fig. 2.4 – Major element EDS map of sample BJG/15/321, showing a granitic melt (purple and grey) intruding a dioritic host (dark green; see Fig. 2.2b). Using this element-based colour scheme, quartz is grey, K-feldspar is purple, amphibole is dark green, and iron oxides are red. Plagioclase varies in colour between light green calcic plagioclase in the diorite [1] and turquoise sodic plagioclase in the granite [2]. See text for descriptions of numbered zones.

in Fig. 2.2b. In places, the granitic melt shows clear intrusion into a brittle host, in the form of small veins with sharp boundaries [6].

The EDS element map of BJG/15/322 (Fig. 2.5) shows a fine dioritic unit [1] interacting, via a zone of intermediate composition [2] with a granitic melt [3]. It shows calcite and epidote in yellow – secondary products of hydrothermal alteration of the diorite. Large plagioclase crystals in the granite [4] show disequilibrium textures, so are presumably antecrysts/xenocrysts.

On Cnoc Dubh, the granitic material intruding as dykelets and net-veins is slightly different to the exposures to the north west. They are largely microgranophyres, with sub-millimetre quartz and K-feldspar displaying common micrographic intergrowths. Larger phenocrysts of plagioclase and perthitic K-feldspar can be up to 3 mm in length. These dykelets and net-veins contain minor amounts of amphibole and opaques, with zircon, epidote, and sphene making up the other accessory phases. Several of these granitic units contain rounded enclaves of the fine dioritic material, which do not have sharp outlines, suggesting they were (or became) partially fluid during entrainment within the granitic melt.

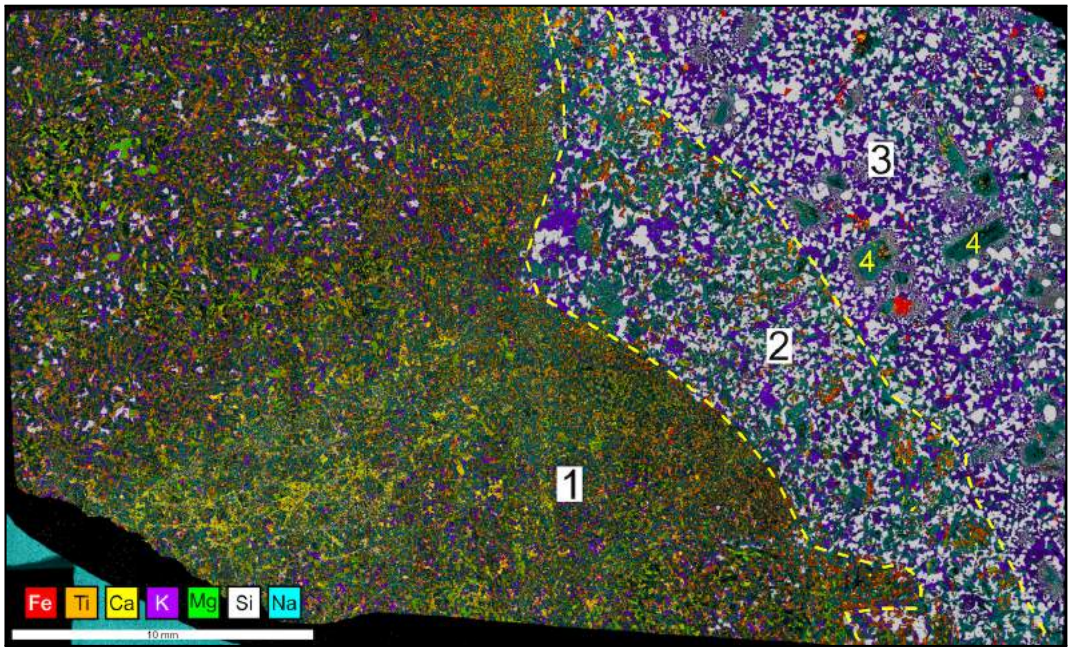

Fig. 2.5 – Major element EDS map of sample BJG/15/322. [1] fine dioritic unit , [2] zone of intermediate composition, [3] granitic melt, [4] plagioclase antecrysts/xenocrysts. Using this element-based colour scheme, quartz is grey, K-feldspar is purple, amphibole is bright green, sodic plagioclases are turquoise, iron oxides and iron sulphides are red, titanium oxides are orange, and calcite and epidote are yellow.

One exposure, in a stream bed between A' Chruach and Cnoc Dubh, shows a markedly different silicic lithology. This is a much finer rhyolite (Fig. 2.3c), with a groundmass of quartz and feldspar that could be devitrified glass. It contains phenocrysts of plagioclase and K-feldspar (up to 4 mm) which are very altered, and quartz crystals (up to 2 mm) which show highly resorbed textures. The phenocrysts often cluster together, along with opaques, as crystal clots. Abundant chlorite and epidote show that the rock has experienced significant hydrothermal alteration. Elongate patches of chlorite have often totally replaced original amphibole crystals.

One of the samples from Tir Dubh was also subjected to EDS analysis (Figs. 2.6, 2.7b). The EDS element map (Fig. 2.6) shows a fine intermediate enclave [1] sitting in a host granitic melt [2]. In places, the host is an intermediate hybrid [3] formed by disaggregation of the enclaves and mingling of the two magmas. The enclaves in the granitic material (Figs. 2.6[1] and 2.7b) contain plagioclases of highly varying compositions (An_{09} – An_{50}) and a range of alkali feldspars. The granitic host [2] contains plagioclases with compositions ranging from An_{03} – An_{13} as well as K-feldspars (Fig. 2.7). .

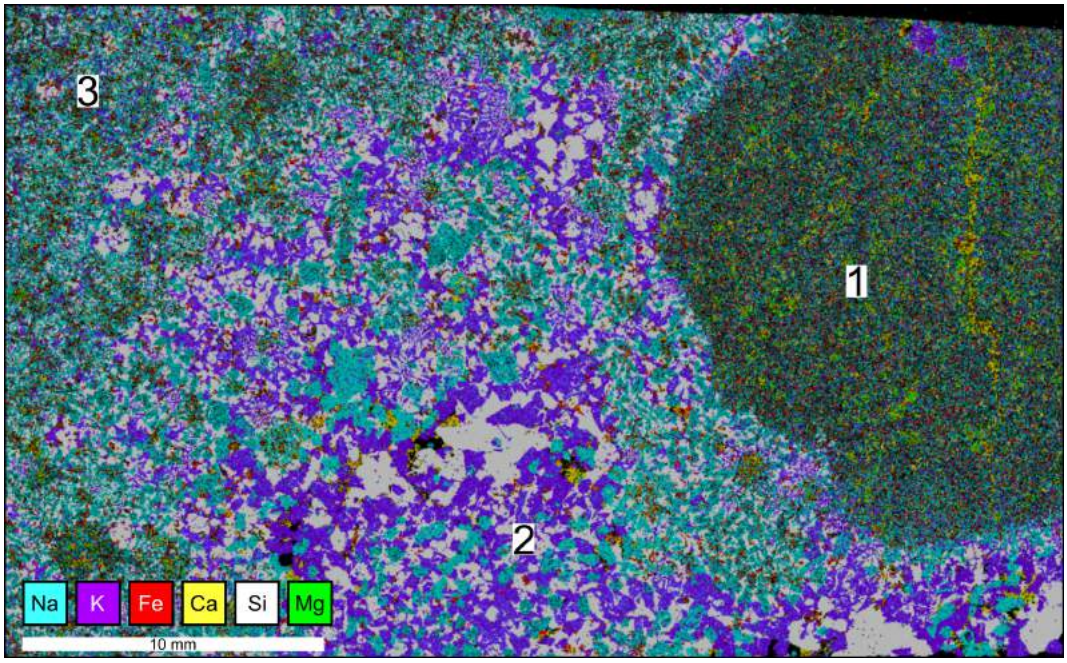

Fig. 2.6 – Major element EDS map of sample BJG/15/29. [1] intermediate enclave, [2] host granitic melt, [3] intermediate hybrid (3). Using this element-based colour scheme, quartz is grey, K-feldspar is purple, plagioclase is light blue, amphiboles are green, Fe-Ti oxides are red, and calcite and sphene are yellow.

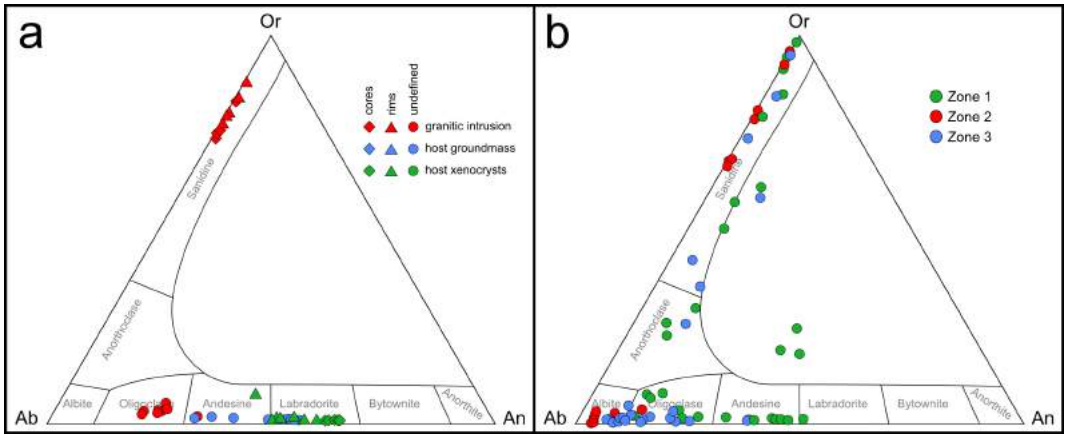

Fig. 2.7 – Ternary plots of EDS data from feldspar crystals in the Glenloig Hybrids. **a)** Feldspars in sample BJG/15/321, as shown in Fig. 2.4. **b)** Feldspars in sample BJG/15/29, as shown in Fig. 2.6.

All of the lithologies found in the intra-caldera inlier show evidence of recrystallisation, such as quartz crystal suturing and crystal triple-points. This could be due to thermal alteration during the volcanic phase of the caldera's evolution.

2.1.2 Summary

The Glenloig Hybrids are a series of intrusive rocks that crop out in the north and western parts of the complex, mostly in stream beds. They comprise a series of amphibole-bearing intermediate rocks of differing grain size, which have been intruded by, and mingled with, granitic melts. This forms a complex series of dykelets and net veins in the more intermediate host. On the hand-specimen and thin section scale, evidence for brittle intrusion, mingling, and mixing of intermediate and granitic magmas can be seen. The unit as a whole is so heterogenous and poorly exposed that all intermediate amphibole-bearing rocks and microgranites exposed in the northwestern part of the CAIC are assigned to the Glenloig Hybrids.

The intermediate rocks are diorites and quartz diorites, and finer grained equivalents. They contain plagioclase (andesine-labradorite), green-brown amphiboles and Fe-Ti oxides as major constituents, with or without quartz, K-feldspar, biotite, and plagioclase xenocrysts. The silicic rocks are microgranites and rhyolites, containing quartz, K-feldspar, and plagioclase (albite-oligoclase), with or without amphibole, biotite and Fe-Ti oxides.

2.2 Gabbros

There are at least six isolated gabbro bodies in the CAIC (Fig. 1.9). They are small and very poorly exposed, often only being visible in a few weathered or mossy outcrops. Five of these bodies lie within the main mass of the Glenloig Hybrids around Cnoc Dubh, Tir Dhubh, and the head of Gleann Dubh. One of these is seen only as one very weathered exposure next to the String Road in the far north east of the complex. The other is associated with the small inlier of Glenloig Hybrids within the caldera, ~400 m northwest of the summit of Binnein na h-Uaimh (Fig. 1.9).

No contacts between the gabbros and the dioritic host-material of the Glenloig Hybrids are exposed, so the relationship between the two is unknown. However, a rhyolitic dykelet (sample BJG/15/165 - petrographically similar to Fig. 2.3c) can be seen cutting one of the gabbro exposures on Tir Dhubh. This shows that there was at least one silicic intrusive event that occurred after the formation of the gabbros, but does not provide any information on the relative timings of the gabbro and the diorites and amphibole microgranites that make up the majority of the Glenloig

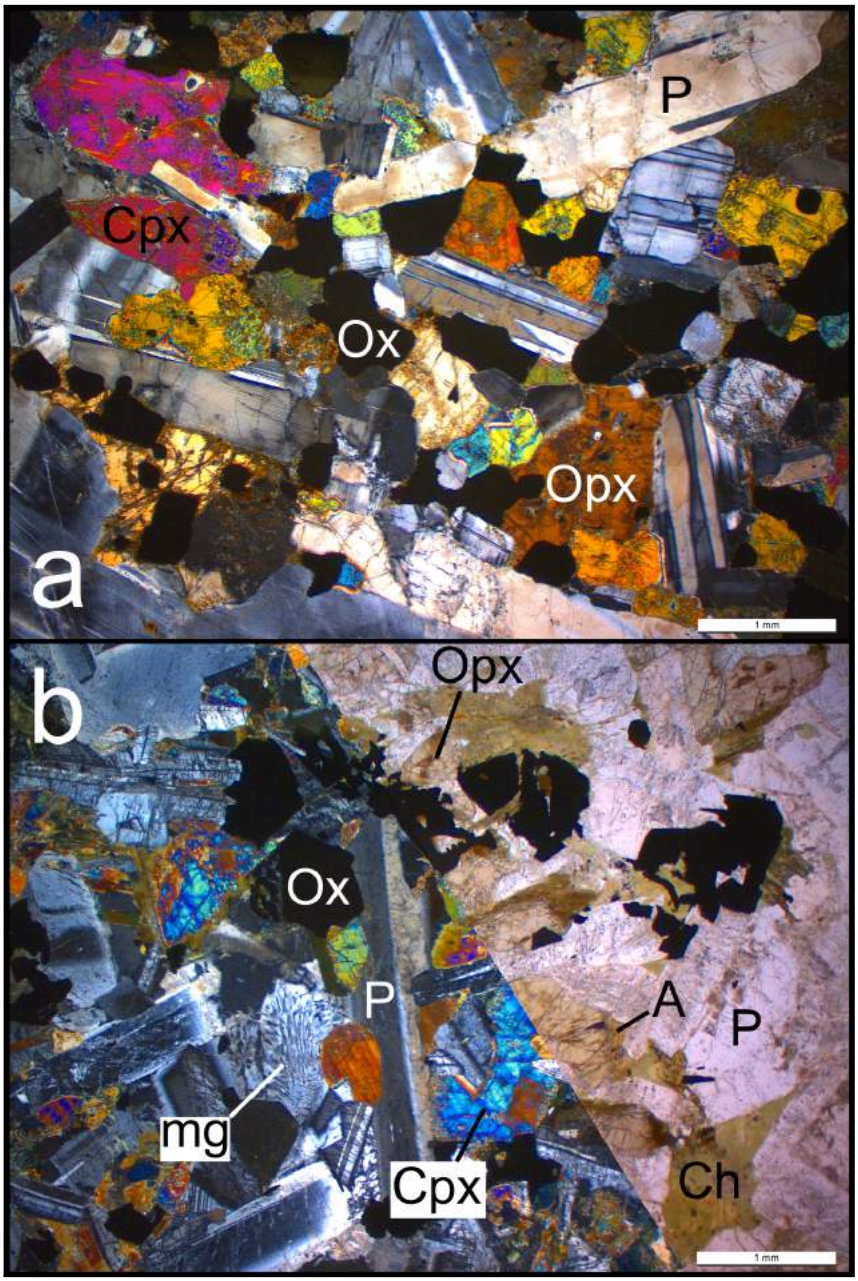

Fig. 2.8 – Photomicrographs of gabbros from the CAIC. **a)** Sample BJG/16/12 – the gabbro from the intra-caldera inlier. Cpx = clinopyroxene, P = plagioclase, Ox = Fe-Ti oxides, Opx = orthopyroxene. Crossed polars. **b)** Sample BJG/15/344 – gabbro from the Allt nan Calaman. Abbreviations as in a), with A = amphibole, Ch = chlorite, mg = micrographic intergrowths of quartz and feldspar. Left = crossed polars, right = plane polarised light.

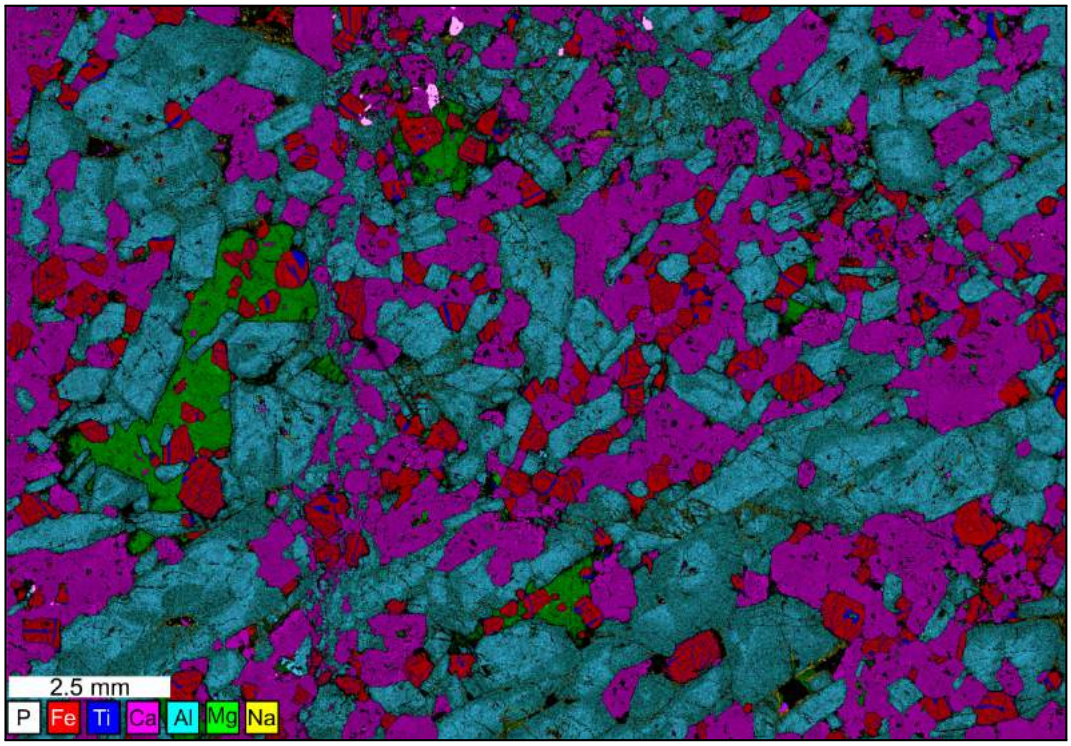

Fig. 2.9 – Major element EDS map of sample BJG/16/12 – also shown in Fig. 2.8a. Using this element-based colour scheme, clinopyroxene is magenta, orthopyroxene is green, plagioclase is turquoise, and apatite is pale pink. Fe-Ti oxides are shown in blue and red, with the magnetite host showing as red, and exsolved ilmenite lamellae showing as blue.

Hybrids. With regard to relationships in the intra-caldera inlier, King (1954) stated that the *"granite"* [here re-classified as the Glenloig Hybrids] was clearly younger than the gabbro. Such relationships were not observed during this study.

2.2.1 Petrography

The intra-caldera outcrop of gabbro contains plagioclase, clinopyroxene, orthopyroxene and opaque oxides, consistent with the descriptions of King (1954), who described *"plagioclase, augite, hypersthene and iron ores"*. This mineralogy is shown in samples collected during this study (Figs. 2.8a, 2.9). It was also noted by King (1954) that the plagioclase laths show alignment, *i.e*, the gabbro is foliated. This is particularly evident in the major element EDS map (Fig. 2.9). This element map shows that the plagioclase crystals have relatively calcic (light blue) euhedral cores (An_{52} – An_{56}; Fig. 2.10a), and relatively sodic (dark turquoise) overgrowth rims (An_{48} – An_{53}; Fig. 2.10a). This could suggest that the cores were original cumulate crystals, possibly along with the Fe-Ti oxides, deposition of which were

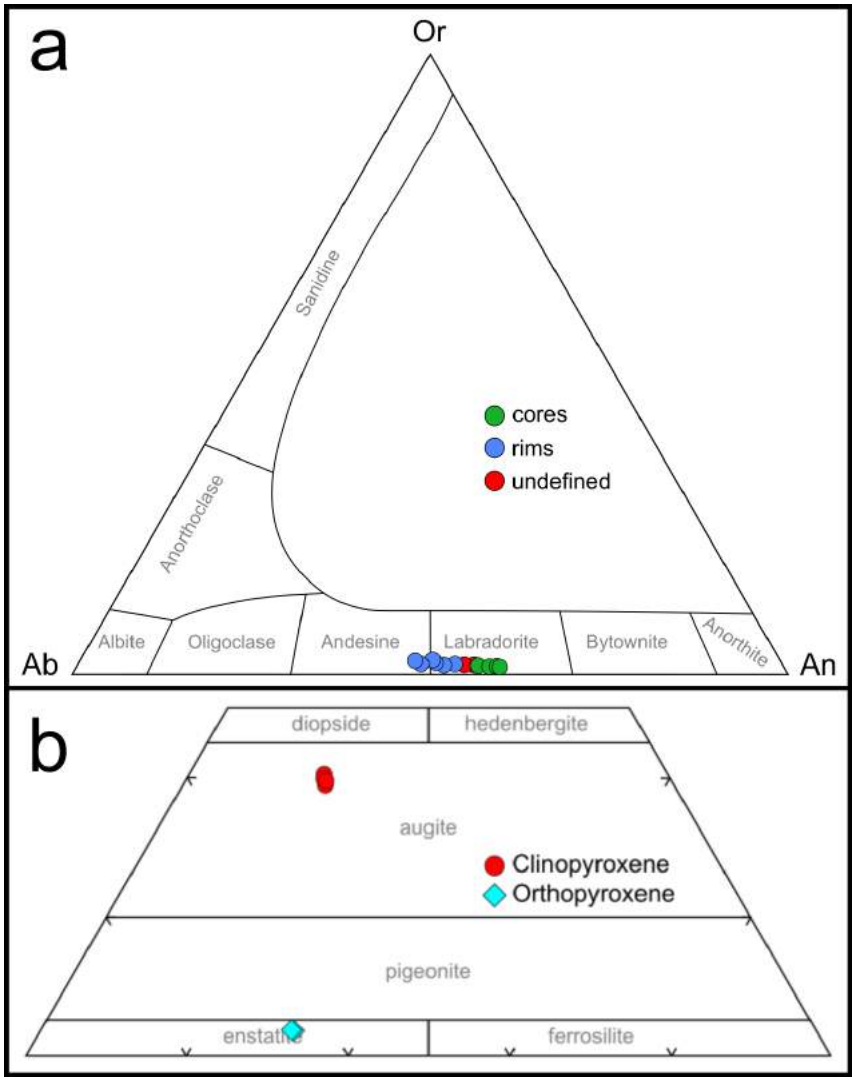

Fig. 2.10 – Ternary plots of EDS data from feldspars and pyroxenes in sample BJG/16/12, as shown in Fig. 2.9. **a)** Plagioclase data. **b)** Pyroxene data.

followed by crystallisation of interstitial pyroxenes and plagioclase overgrowths. These rims meet and coalesce, giving a partially adcumulate texture.

The orthopyroxene is much less abundant than clinopyroxene, but both form interstitial space-filling textures between euhedral plagioclase and Fe-Ti oxide crystals. The orthopyroxene is a clinoenstatite with a composition of En_{65}, while the clinopyroxene is an augite with compositions of En_{41} – En_{43} (Fig. 2.10b). The Fe-Ti oxides show excellent magnetite-ilmenite exsolution patterns in the major element map (red and blue, respectively, in Fig. 2.9). Apatite is an uncommon accessory mineral (light pink in Fig. 2.9).

All the other gabbros, exposed in the eastern parts of the complex, are petrographically similar to each other. They all contain abundant euhedral-to-subhedral zoned plagioclase laths up to 5 mm in length and euhedra-to-subhedral clinopyroxene (Fig. 2.8b). Some samples contain orthopyroxene. The pyroxenes are ubiquitously rimmed or completely replaced by amphibole, which in turn is almost entirely chloritised in the most highly-altered samples. Opaque minerals form large (up to 5 mm) skeletal crystals, and are often found as patches or aggregates of several crystals. A few samples contain small, space-filling patches of quartz and feldspar in micrographic intergrowths (Fig. 2.8b).

2.2.2 Summary

All gabbro found in the CAIC is found in small, poorly exposed bodies isolated from one another but associated with the Glenloig Hybrids. The gabbro found as an inlier within the ignimbrites of the Arran Volcanic Formation is a magnetite-plagioclase (andesine-labradorite) cumulate which also contains clinopyroxene (Mg-rich augite) and orthopyroxene (enstatite). The other gabbros, exposed in the east of the complex, comprise plagioclase, clinopyroxene, and Fe-Ti oxides, with or without orthopyroxene, quartz, and secondary amphibole and chlorite.

2.3 Glen Craigag Granite

The Glen Craigag Granite is exposed in a large crescent shape within the caldera, and is entirely surrounded by pyroclastic rocks (Fig. 1.9). The contact between the granite and pyroclastic units is only exposed in Ballymichael Glen, where a heavily weathered outcrop shows the ignimbrites of the Arran Volcanic Formation (AVF) overlying the granite. Due to the poor quality of the exposure, it is impossible to be sure whether it is a depositional, intrusive, or tectonic contact. Due to the increasingly fractured nature of the granite as the contact is approached, as well as

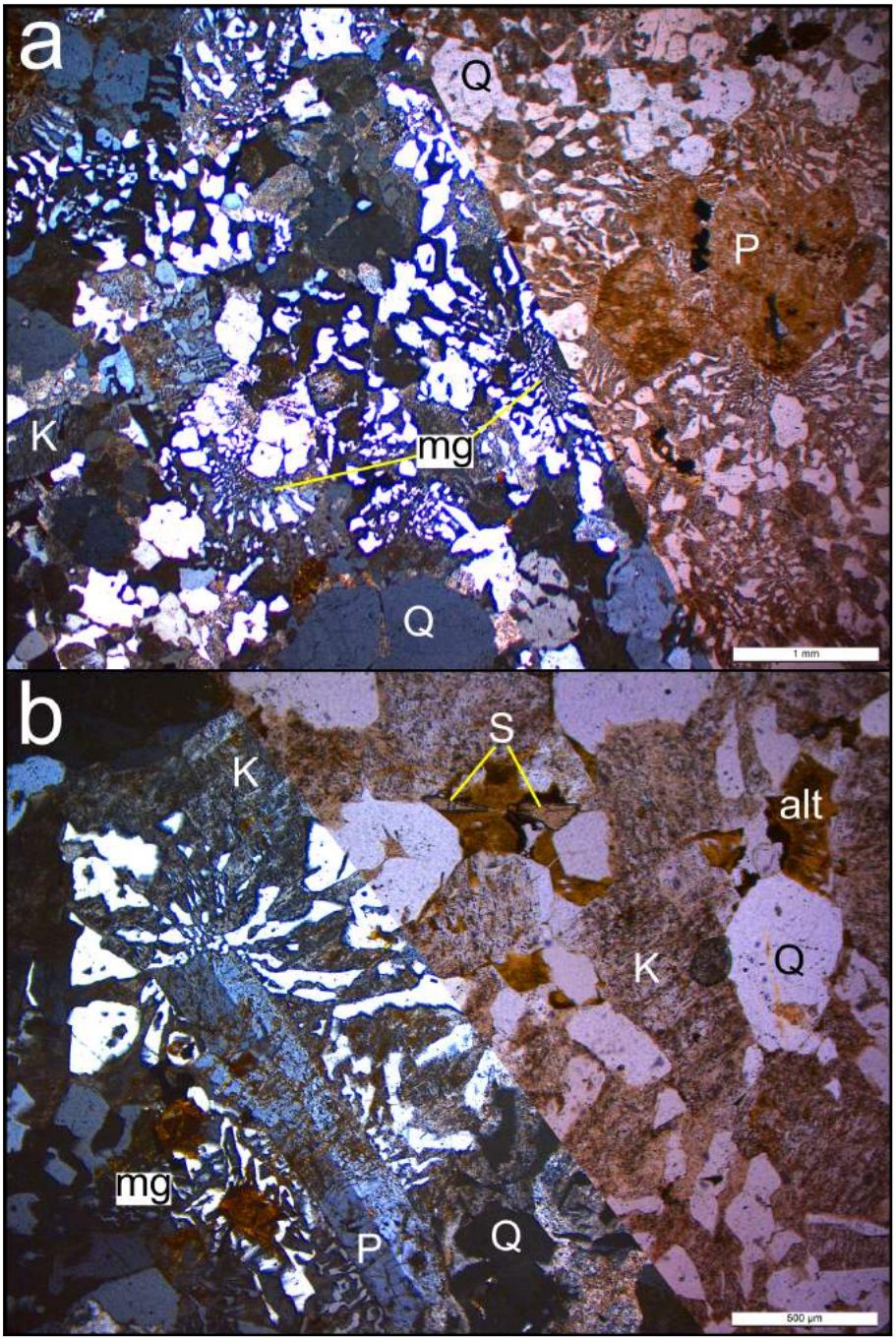

Fig. 2.11 – Photomicrographs of samples of the Glen Craigag Granite. **a)** Sample BJG/16/32, a granophyre from Glen Craigag. mg = micrographic intergrowths of quartz and K-feldspar. Q = quartz P = euhedral, heavily altered plagioclase. Accessory minerals comprise opaques, zircon, and sphene. Left = crossed polars, right = plane polarised light. **b)** Sample BJG/15/74 from Ballymichael Glen. Q = quartz, K = perthitic K-feldspar. mg = micrographic intergrowths of quartz and K-feldspar, P = plagioclase phenocrysts, alt = brown alteration products of mica or amphibole, S = sphene. Other accessory phases include opaques and zircon. Left = crossed polars, right = plane polarised light.

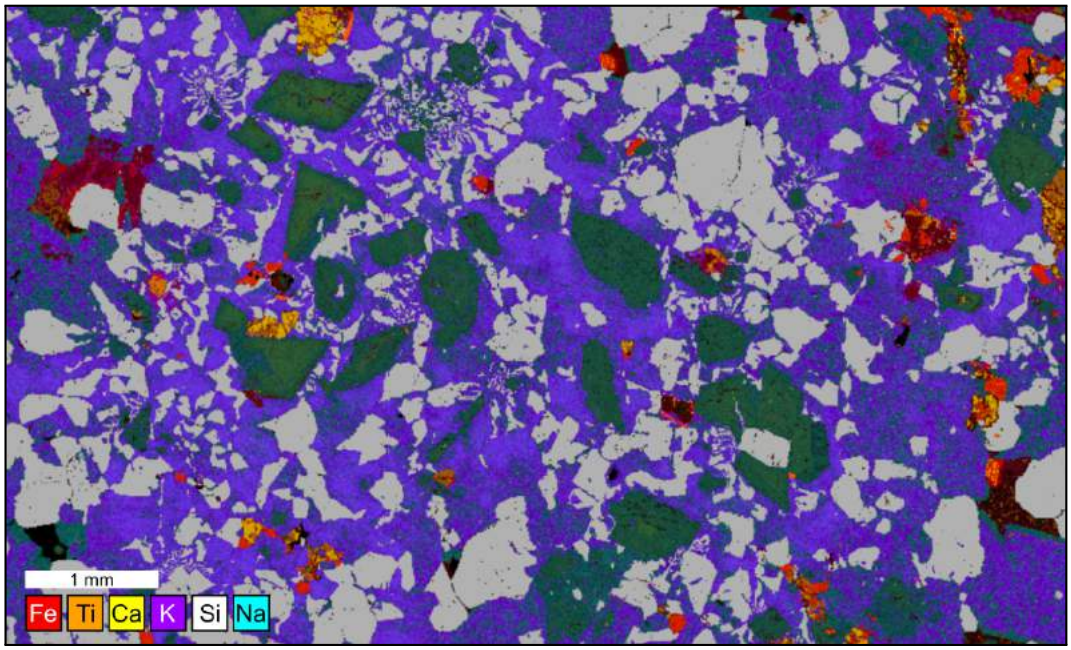

Fig. 2.12 – Major element EDS map of sample BJG/16/31. Using this element-based colour scheme, quartz is grey, K-feldspar is purple (albitic exsolution lamellae are turquoise), and plagioclase crystals have green calcic cores and turquoise sodic rims. Altered amphibole is dark red, while Fe-Ti oxides are bright orange-red. Yellow shows an altered phase containing largely Si, Ca, and Fe, which could have been clinopyroxene.

the horizontal and broadly planar nature of the contact, it is suggested that it is a depositional contact. This would make the Glen Craigag Granite older than the onset of volcanic activity at the CAIC (but see Section 4.3). Another reason to suggest that the granite is older than the AVF is the presence of several mafic dykes that intrude the granite. No such dykes are seen intruding the intra-caldera succession of the AVF, suggesting that a dyke-emplacement event occurred after formation of the Glen Craigag Granite, but before eruption of the AVF.

2.3.1 Petrography

All samples collected from the Glen Craigag Granite are highly altered, with sericitised feldspars, and complete alteration of primary amphiboles or micas. In some samples, more than half of the rock is formed of micrographic intergrowths of quartz and K-feldspar (Fig. 2.11a), meaning that parts of the unit are actually granophyres. These granophyres also contain larger quartz crystals, as well as heavily altered euhedral plagioclase crystals (Fig. 2.11a). Major Fe- and Mg-bearing phases seem to be absent. Zircon, sphene, and opaque minerals make up the accessory phases.

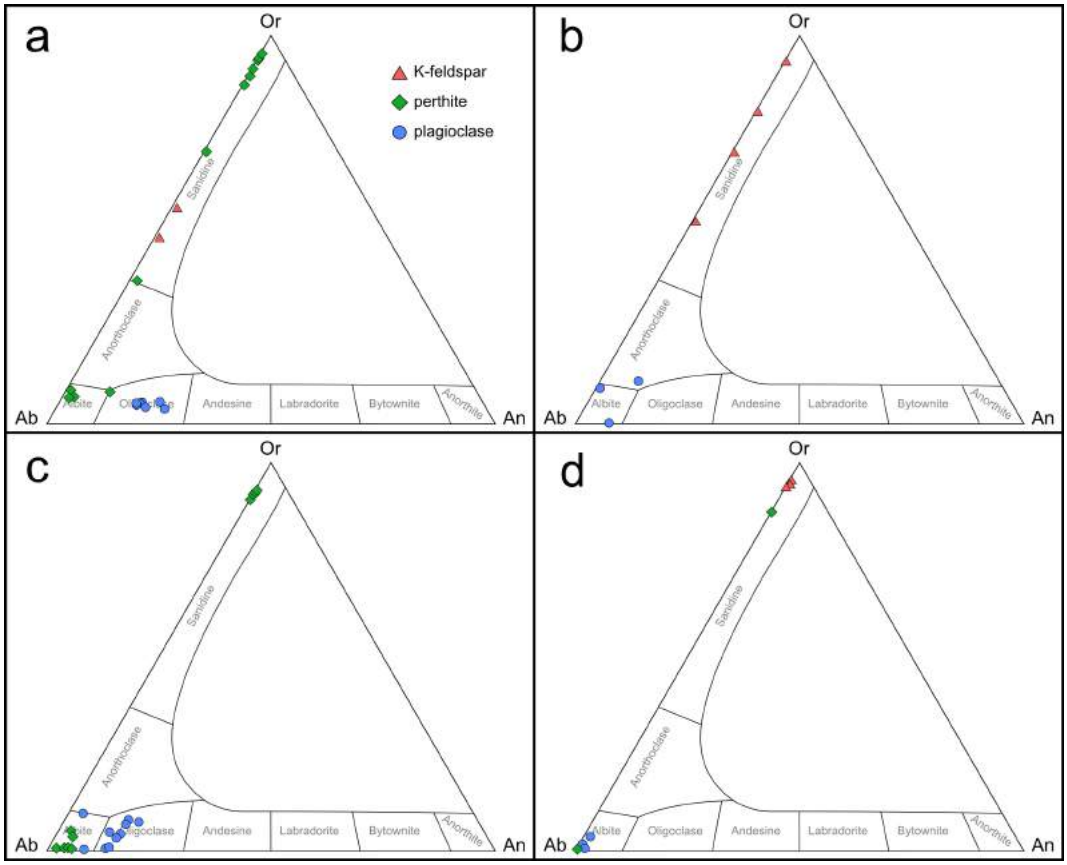

Fig. 2.13 – Ternary plots of EDS data from feldspars in the granites of the CAIC. Perthite is defined as any single crystal which contains distinct K-rich and Na-rich zones which can be distinguished in a back-scattered electron (BSE) image. **a)** Feldspars from sample BJG/16/31 of the Glen Craigag Granite, as shown in Fig. 2.12. **b)** Feldspars from sample BJG/15/328 of the Cnoc Dubh Granite, as shown in Fig. 2.15a. **c)** Feldspars from sample BJG/15/347 of the Creag Mhor Granite, as shown in Fig. 2.15b. **d)** Feldspars from sample BJG/15/335 of the Bridge Farm Granite, as shown in Fig. 2.15c.

Other samples have only minor amounts of micrographic quartz-K-feldspar intergrowths, often around large euhedral plagioclase laths (Fig. 2.11b). These plagioclases all show normal zoning, with relatively calcic cores and sodic rims (Fig. 2.12). The plagioclase crystals have compositions of $An_{17} - An_{25}$ (Fig. 2.13a). These samples also contain quartz and altered perthitic K-feldspar (Fig. 2.13a). There are also abundant brown alteration products, that EDS analysis suggests have chemistry similar to amphiboles (Fig. 2.12). Accessory phases include relatively large crystals of sphene (up to 200 μm; Fig. 2.11b), Fe-Ti oxides (Fig. 2.12), and zircon.

2.3.2 Summary

The Glen Craigag Granite crops out in the upper parts of Glen Craigag and Ballymichael Glen, in the centre of the CAIC. Many samples collected are actually granophyres, comprising quartz and K-feldspar in micrographic intergrowths. Other samples have these quartz–K-feldspar intergrowths only around large plagioclase phenocrysts. K-feldspars are often perthitic (distinct albite and orthoclase zones), while plagioclases are oligoclase. Sphene, Fe-Ti oxides, and zircon make up the accessory phases.

Fig. 2.14 ***(facing page)*** – Photomicrographs of samples from the Satellite Granites. Q = quartz, K = perthitic K-feldspar, P = plagioclase, E = epidote, Z = zircon, ox = Fe-Ti oxides, alt = alteration products of amphibole or mica, mg = micrographic intergrowths of quartz and K-feldspar. **a)** Sample BJG/16/26 of the Bridge Farm Granite. Top = crossed polars, bottom = plane polarised light. **b)** Sample BJG/16/20 of the Dereneneach Granite. Bottom left = plane polarized light, top right = crossed polars. **c)** Sample BJG/15/343 of the Torr nan Dearc Granite. Viewed between crossed polars. **d)** Sample BJG/15/328 of the Cnoc Dubh Granite. Bottom left = plane polarised light, top right = crossed polars.

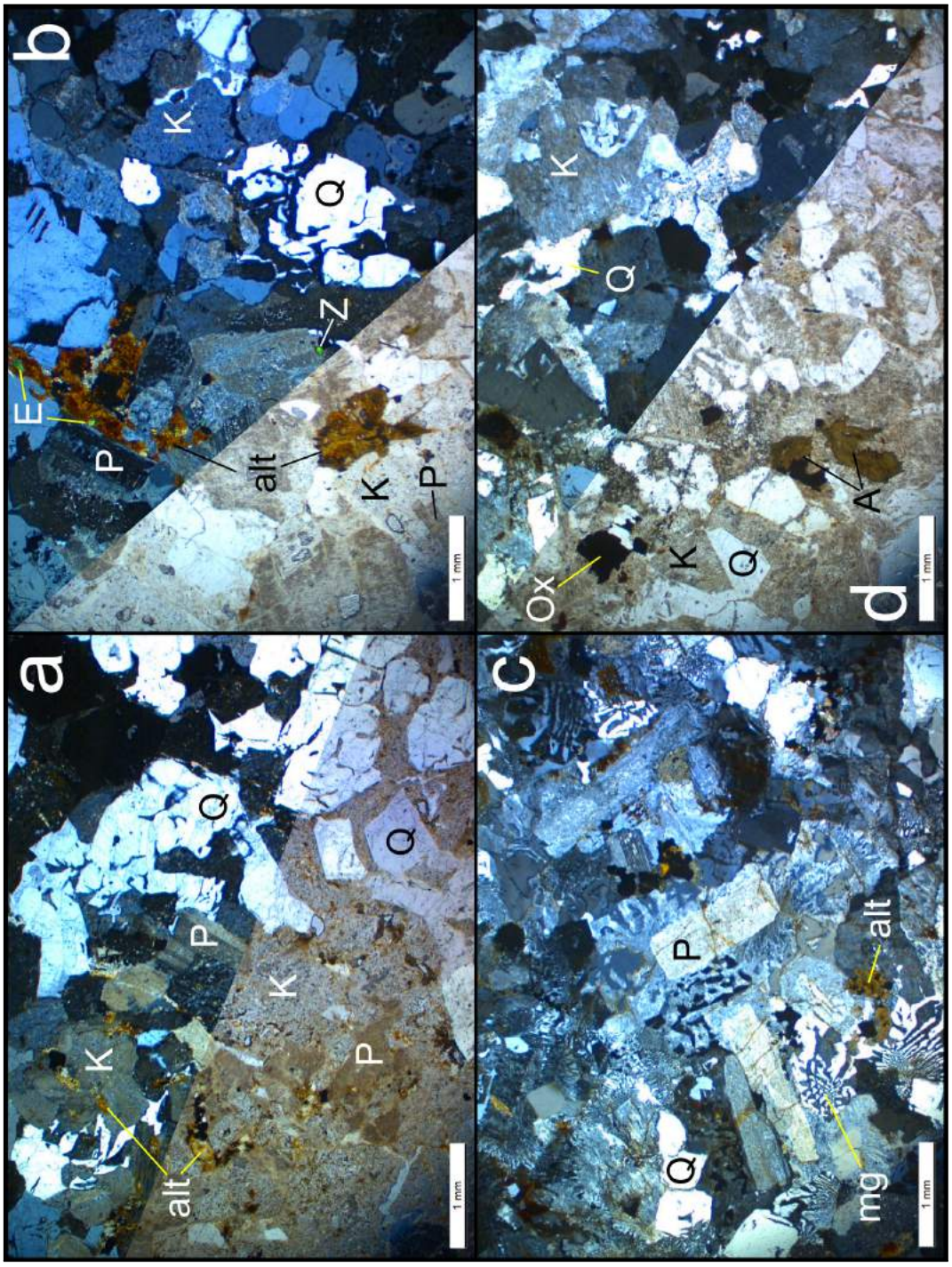
a
K
alt
P
Q
K
P
Q
1 mm
b
E
P
alt
Z
K
Q
K
P
1 mm
c
Q
P
alt
mg
1 mm
d
Ox
K
Q
A
Q
K
1 mm

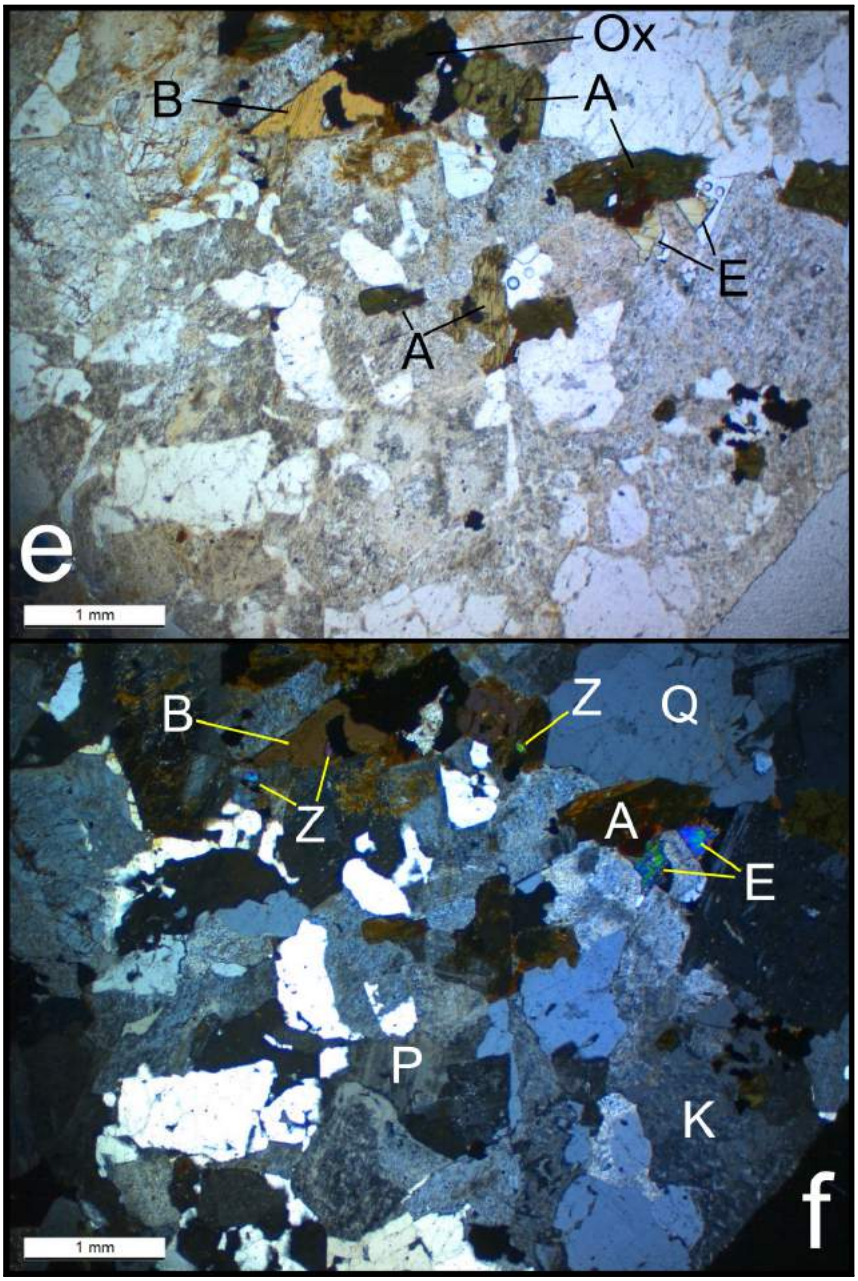

Figure 2.14 *cont.* – **e)** and **f)** Sample BJG/16/19 of the Creag Mhor Granite. Abbreviations as above, plus A = dark green-to-olive pleochroic amphibole and B = biotite. **e)** is viewed in plane polarised light, **f)** is viewed between crossed polars.

2.4 Satellite Granites

Five isolated granite bodies are exposed around the edge of the complex (Fig. 1.9), and are collectively termed the Satellite Granites. They appear unconnected at the surface, but are petrologically similar and all of a similar size.

The Bridge Farm Granite is exposed in Ballymichael Glen in the far south west of the complex, around 1 km west of Bridge Farm (NR 927 318). It is exposed extensively in the stream bed of the Ballymichael Burn, and one of the burn's tributaries follows the contact between the granite and the pyroclastic rocks of the AVF. This contact is vertical in places, and is highly irregular, suggesting fingering of the granite into the ignimbrites. This would indicate that intrusion of the Bridge Farm Granite post-dates volcanic activity.

The Dereneneach Granite is exposed in Dereneneach Quarry (NR 932 336), where it is quarried for aggregate. Despite the 100% exposure in the quarry itself, and good exposure in the Allt nan Dris, no contacts with surrounding lithological units are exposed.

The Creag Mhor Granite forms a prominent ridge above the String Road. The northernmost part of this granite is exposed in a road cut on the String Road itself. On Creag Mhor, the granite appears to take the form of a shallowly south-east-dipping sheet intruded into the ignimbrites of the AVF. Ignimbrites are exposed on the slopes below the granite (between Creag Mhor and the String Road) showing that the contact cannot be depositional. However, the actual contact is not exposed.

The Cnoc Dubh and Torr nan Dearc Granites are only known from a small number of isolated exposures that crop out on the flat heather moorland, so their geometry and relationships with other units are unknown.

2.4.1 Petrography

The Satellite Granites are all petrologically similar, being composed primarily of 1–2 mm quartz and perthitic K-feldspar with lesser euhedral-to-subhedral plagioclase

Fig. 2.15 ***(facing page)*** – Major element EDS maps of three samples from different bodies of the Satellite Granites. Using this element-based colour scheme, quartz is grey, K-feldspar is purple, plagioclase is green-turquoise, and amphiboles are orange. Dull red shows brown alteration minerals and some primary biotite. Fe oxides (bright red) and Fe-Ti oxides (bright orange) are the major accessory phases. Epidote is yellow. **a)** Sample BJG/15/328 from the Cnoc Dubh Granite. **b)** Sample BJG/15/347 from the Creag Mhor Granite. **c)** Sample BJG/15/335 from the Bridge Farm Granite.

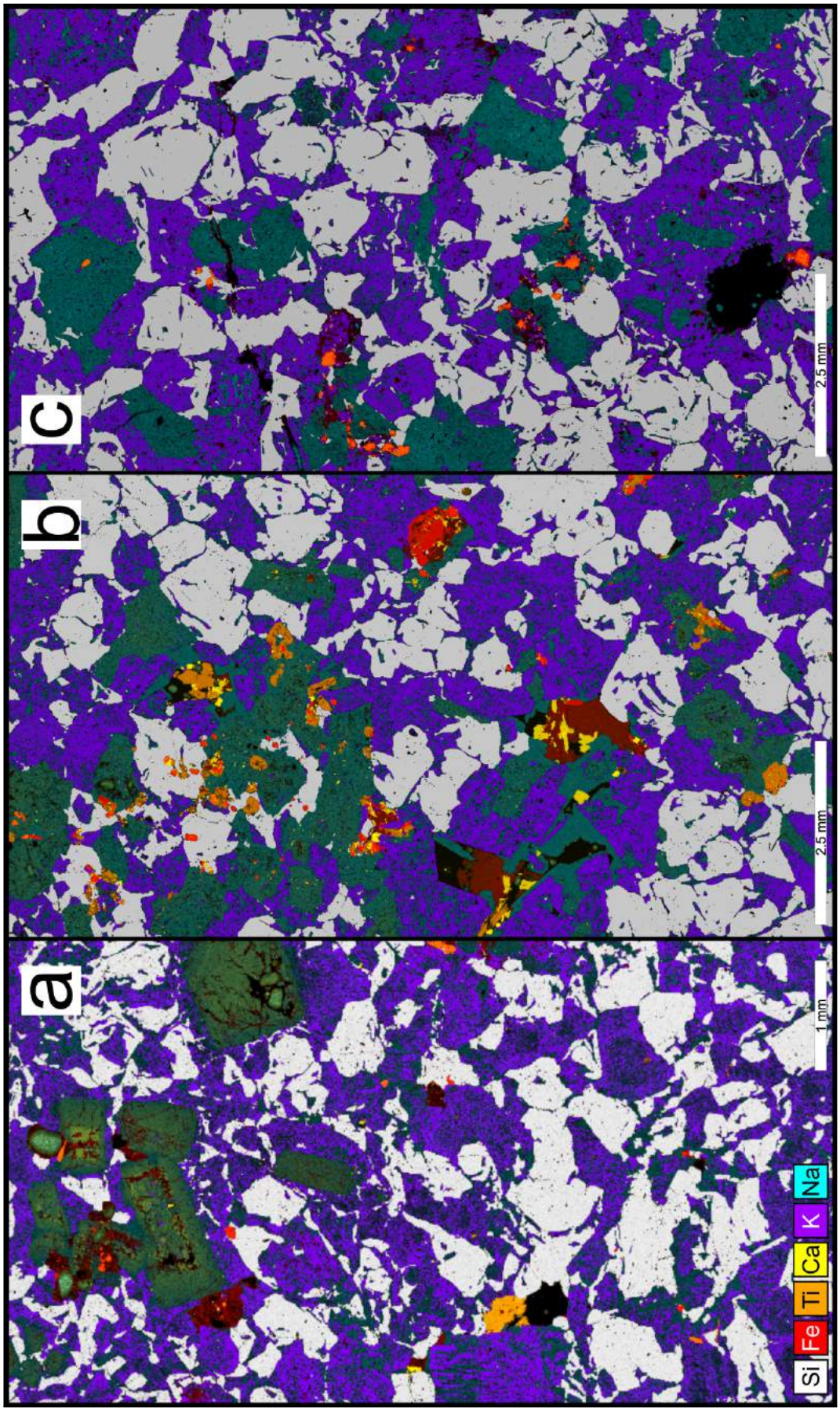
a
b
c
1 mm
2.5 mm
2.5 mm
Si
Fe
Ti
Ca
K
Na

(Figs. 2.14, 2.15). The Bridge Farm Granite (Figs. 2.14a) comprises quartz and perthitic K-feldspar in equal amounts, and slightly less plagioclase (albite; Fig. 2.13d) which are neither euhedral nor zoned. The quartz crystals all show vermicular intergrowth lamellae of K-feldspar (Fig. 2.15c). There are small amounts of alteration products, possibly replacing amphibole. The dominant accessory phase in this granite is Fe-Ti oxide

The Dereneneach Granite (Figs. 2.14b) comprises largely quartz and K-feldspar with lesser euhedral plagioclase. Again, the quartz and K-feldspar show vermicular intergrowths. This sample contains a relatively large amount of brown alteration products, often associated with epidote, showing hydrothermal alteration. Zircon is abundant.

The Torr nan Dearc Granite (Figs. 2.14c) comprises quartz and K-feldspar in micrographic intergrowths, with some euhedral quartz and plagioclase phenocrysts. Small amounts of brown alteration minerals presumably replace amphibole of biotite.

The Cnoc Dubh Granite (Figs. 2.14d) contains slightly more perthitic K-feldspar than quartz. Vermicular K-feldspar lamellae within the quartz crystals are present, but less common than in the Bridge Farm and Dereneneach Granites. Rare zoned plagioclases are albitic and euhedral (Figs. 2.13, 2.15a), showing sieve-textured cores and disequilibrium rims. Some amphibole that has escaped complete alteration is preserved. Fe-Ti oxides are larger and more abundant than the other samples.

The Creag Mhor Granite (Figs. 2.14e,f) is mostly made up of perthitic K-feldspar with lesser quartz and small amounts of anhedral plagioclase. The plagioclases are oligoclase in composition, while the Na-rich lamellae in the perthite are albite (Fig. 2.13c). Some of the small quartzes contain vermicular intergrowth lamellae of K-feldspar (Fig. 2.15b). Relatively fresh dark green-to-olive pleochroic amphibole is abundant. There is also a small amount of primary biotite. Fe-Ti oxides are often associated with the amphibole and biotite. Zircon and epidote are also present.

The quartz and K-feldspar in the Satellite Granites often show a distinctive intergrowth texture comprising small vermicular lamellae of K-feldspar within the quartz crystals. This can be seen clearly in Fig. 2.14a and the three major element EDS maps in Fig. 2.15. Where the plagioclase forms euhedral phenocrysts (Figs. 2.14c, 2.15a), they are normally zoned (relatively calcic cores with relatively sodic rims). Where the plagioclases are not euhedral, they are not zoned.

Most of the Satellite Granites have been altered to some extent, so any original amphibole or biotite has been replaced with brown alteration products (Fig. 2.14a,b,c). The freshest of the samples, however, contain both primary amphibole and biotite (Fig. 2.14d,e,f), neither of which are present in the Glen Craigag Granite samples. Opaque minerals comprise mostly Fe- and Fe-Ti oxides, with some small

needles of Ti-oxides. Zircon and epidote are abundant in all samples. Sphene is absent.

There are several petrological differences between the Glen Craigag Granite and the Satellite Granites: 1) The Glen Craigag Granite has micrographic intergrowths of quartz and K-feldspar typical of a granophyre. The Satellite Granites however display vermicular intergrowths of K-feldspar within quartz crystals. 2) The Glen Craigag Granite has abundant euhedral plagioclase laths. These are rare in the Satellite Granites. 3) The Satellite Granites contain more fresh and altered amphibole and biotite than the Glen Craigag Granite. 4) The Glen Craigag Granite contains abundant sphene, whereas sphene appears to be absent from the Satellite Granites.

2.4.2 Summary

The Satellite Granites form a series of small unconnected bodies of granite around the margins of the CAIC. They are primarily composed of quartz and perthitic K-feldspar, with a general lack of micrographic intergrowth between the two. They also contain generally euhedral plagioclase (albite to oligoclase), with some biotite and amphibole (which are often altered). Fe-Ti oxides, epidote, and zircon make up the accessory phases. The Satellite Granites do not contain visible sphene.

2.5 Dolerite Sill

Along the western slopes of Ard Bheinn and Binnein na h-Uaimh are some poor exposures of a purple-grey weathering fine-grained basaltic igneous rock. Similar exposures are found in the Allt nan Dris valley above Dereneneach Quarry and on the southern side of Ballymichael Glen. This unit was interpreted by both Tyrell (1928) and King (1954) as a megablock of plateau lava, and the only remaining fragment of a pre-caldera Arran lava field, such as those seen in Antrim and Mull. This suggestion was based on petrological similarity to the Hebridean lavas, and the 'arcuate' (*i.e.,* concentric around the caldera centre) form of the outcrop.

As a result of the detailed mapping and petrography undertaken in this study, this basaltic unit is now thought to be a sill that intruded the complex between two distinct pyroclastic units. The reasons for its interpretation as a sill rather than a plateau lava megablock or *in situ* lava flow are as follows: 1) It is found only as one continuous mass. If megablocks of a certain lithology are present in a caldera, they might be expected to be associated with small clasts of the same material, or megablocks of other lithologies. These are not seen. 2) It is largely concordant with stratigraphy, but one small fragment of the underlying unit (the Allt Ruadh Member,

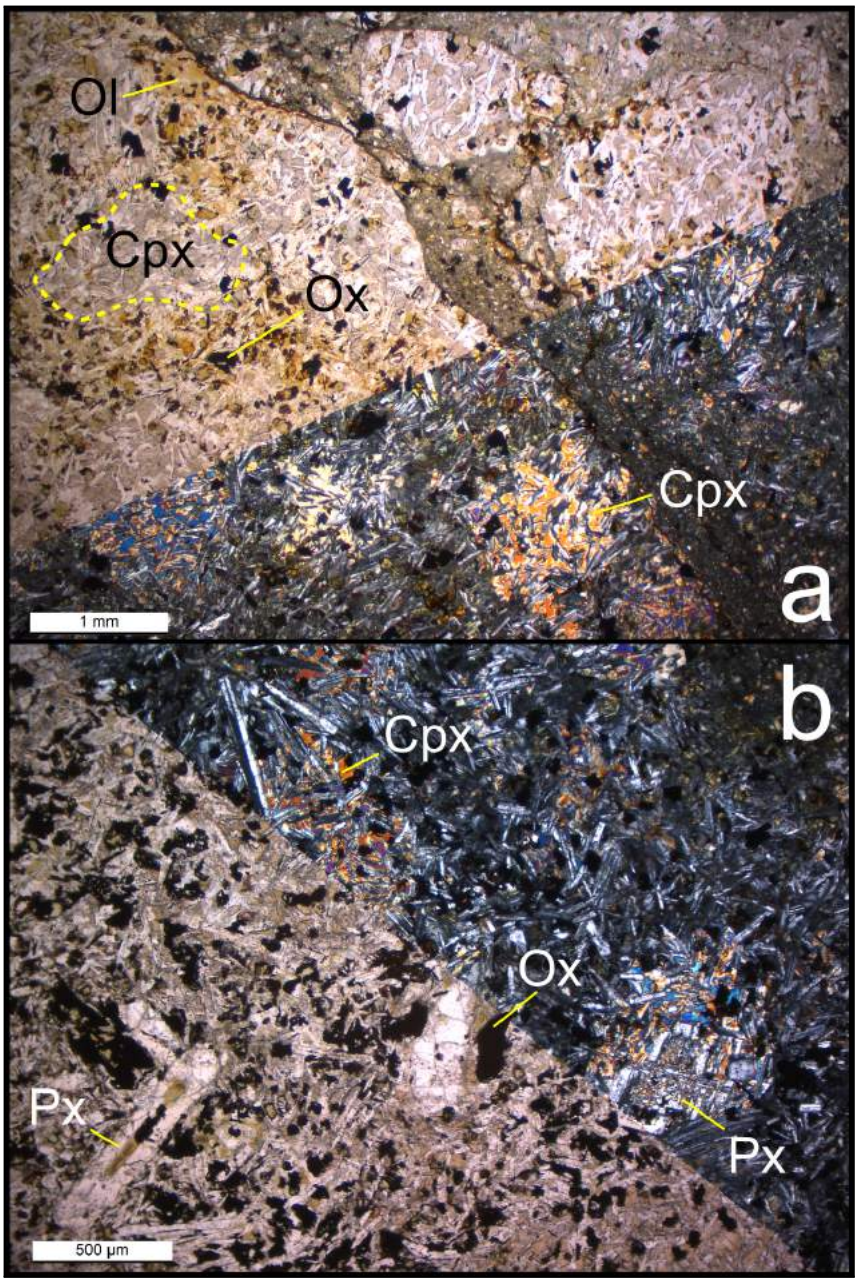

Fig. 2.16 – Photomicrographs of the dolerite sill that is exposed along the western side of Ard Bheinn. **a)** Sample BJG/15/57, brecciated clasts of dolerite in an ashy matrix. Cpx = clinopyroxene (the dashed line shows the outline of a single oikocryst), Ox = Fe-Ti oxides, Ol = alteration products after olivine. Top left = plane polarised light, bottom right = crossed polars. **b)** Sample BJG/16/11, a finer portion of the intrusion. Abbreviations as in a), plus Px = plagioclase xenocryst. Bottom left = plane polarised light, top right = crossed polars.

Section 3.1.2) is exposed above the sill around 500 m west of the summit of Binnein na h'Uaimh (NR 937 332; Fig. 1.9). 3) Small fingers of this material can be seen intruding the overlying unit (the White Tuff Member, Section 3.1.6). 4) The coarser grain size in places (more doleritic than basaltic) suggests emplacement as a shallow intrusion rather than a thin extrusive flow.

Some similar lithologies are found in other parts of the complex, but are not well exposed and are very spatially restricted (<20 m in diameter). These are particularly found around the north, east, and south sides of Binnein na h-Uaimh, and also on Creag an Fheidh and the southern slopes of Ard Bheinn. These are also interpreted as dolerite intrusions, but it is not possible to tell whether they are disjointed continuations of the main body of the sill, or separate intrusions entirely. Because these outcrops are small and do not show clear relationships with surrounding lithologies, they are not included in the geological map (Fig. 1.9).

In many of the exposures, especially near the margins of the sill, the rock is brecciated, and is made up of small fragments of altered dolerite in an ashy matrix (Figs 2.16a, 2.17). Given the poor nature of the exposures and the intense alteration, it is not clear what process caused this brecciation. However, the textures resemble those seen in peperites, formed when magma interacts with wet sediments. It is highly plausible that this occurred in the CAIC, if the sill was intruded before lithification of the un-welded ignimbrites in the AVF.

2.5.1 Petrography

The sill varies in grain size from a coarse ophitic dolerite (Fig. 2.16a) to a finer basalt (Fig. 2.16b). The outcrops with distinct clinopyroxene oikocrysts exceeding 1.5 mm in size were documented by King (1954) and described as *'ophimottled'* (after Bailey et al., 1924). These relatively large clinopyroxene crystals completely enclose much smaller plagioclase laths. The plagioclase laths have compositions of An_{41} – An_{73} (Fig. 2.18a,b), while the clinopyroxene oikocrysts have compositions of En_{39} – En_{46} (Fig. 2.18c). Fe-Ti oxides and olivine (now completely altered to iddingsite and other alteration products) occupy the interstitial spaces between these large oikocrysts, along with plagioclase.

The basalt from the margin of the intrusion, (Fig. 2.16b) shows a sub-ophitic texture with small plagioclase laths partially enclosed in sub-mm clinopyroxene crystals. No altered remnants of primary olivine are seen. This rock has much more abundant Fe-Ti oxides than the sample shown in Fig. 2.16a, and contains some larger (up to 1 mm) plagioclase xenocrysts or antecrysts, which can be tabular, lath-shaped, or anhedral, and have altered or sieve-textured cores

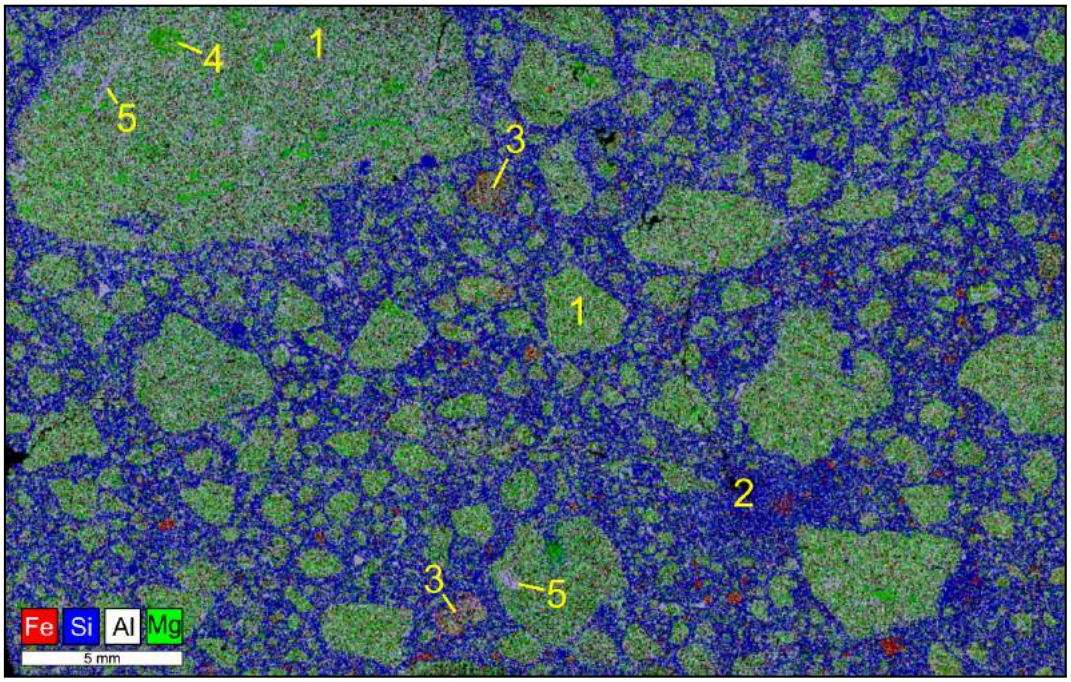

Fig. 2.17 – Major element EDS map of sample BJG/15/15, a brecciated dolerite. Using this element-based colour scheme, clinopyroxene is green, plagioclase is grey, Fe-Ti oxides are red, and quartz and silicic matrix material are blue. Doleritic clasts [1] are surrounded by a silicic matrix [2], with some clasts of more Fe-rich material [3]. In the dolerite, individual green clinopyroxene oikocrysts can be made out [4], and plagioclase xenocrysts or antecrysts appear as grey laths [5].

The brecciated (peperitic) nature of the dolerite is shown in Figs. 2.16a and 2.17. The matrix is silicic, as shown by the blue colour in the EDS element map (Fig. 2.17), suggesting that this material is derived from the ignimbrite units into which the sill was intruded. The matrix also contains crystals of quartz, Fe-Ti oxides, and occasional feldspars (An_{25} – An_{70}; Fig. 2.18a) and clinopyroxenes (En_{40} – En_{43}).

2.5.2 Summary

The dolerite sill intrudes the ignimbrites of the Arran Volcanic Formation, between the Allt Ruadh Member and the White Tuff Member. It is an ophitic dolerite, with small plagioclase (labradorite to bytownite) laths encased in larger (1 mm) clinopyroxene (Mg-rich augite) oikocrysts. It also contains Fe-Ti oxides, completely altered olivines, and occasional plagioclase xenocrysts. In many places, especially near the margins, the dolerite is brecciated, with dolerite clasts in an silicic matrix. This is interpreted as a peperitic texture related to intrusion into wet unconsolidated sediment.

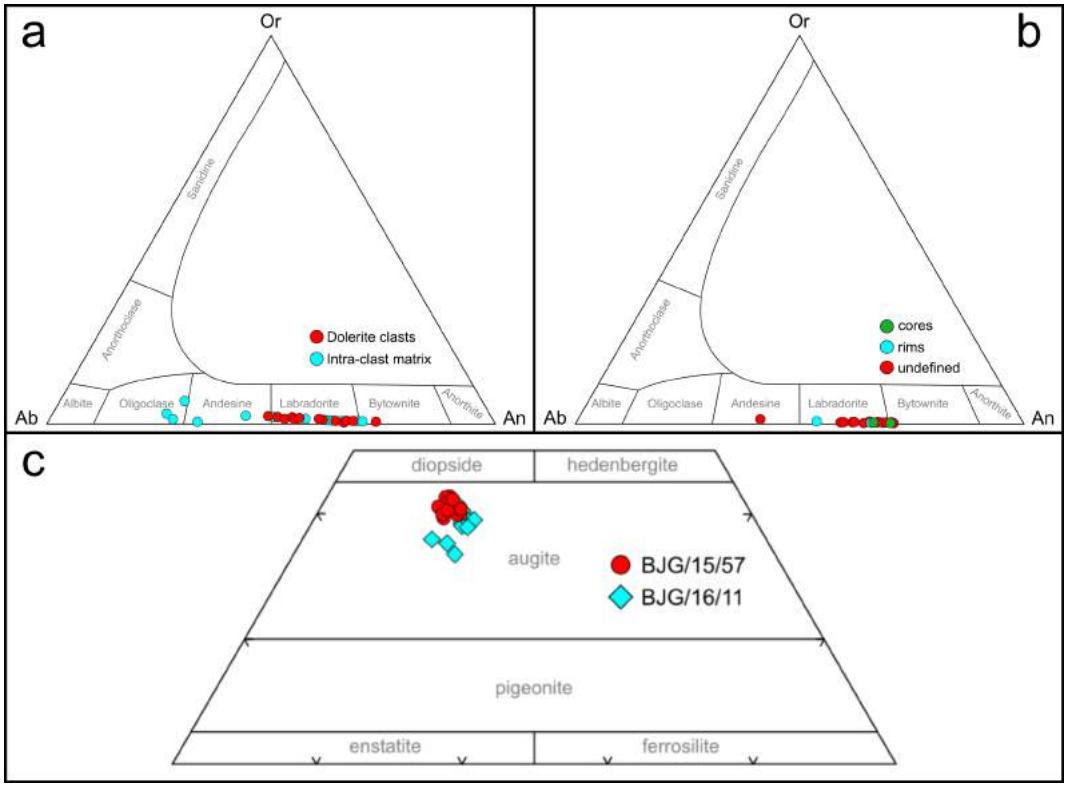

Fig. 2.18 – Ternary plots of EDS data from the dolerite sill. **a)** Feldspars in sample BJG/15/57, showing data for crystals in the dolerite clasts (similar to the green areas in Fig. 2.17) and the intra-clast matrix (similar to the blue areas in Fig. 2.17). **b)** Feldspars in sample BJG/16/11. **c)** Pyroxenes in both BJG/15/57 and BJG/16/11.

2.6 Dykes

In this section, the basaltic dykes that intrude the CAIC will be described, along with some basaltic dykes that intrude the North Arran Granite for comparison. Photographs of a selection of these dykes are shown in Fig. 2.19. The CAIC is also intruded by one picrite dyke and one pitchstone dyke, which are also described.

2.6.1 Basaltic Dykes Intruding the CAIC

The CAIC is cut by a suite of dolerite and basalt dykes, most of which strike generally NNW-SSE (Fig. 1.9). The majority intrude the Glen Craigag Granite and the Glenloig Hybrids, with a small number seen to be intruding the extra-caldera ignimbrites on the margins of the complex. None are observed intruding the intra-caldera Arran Volcanic Formation or the Satellite Granites.

The dykes range in thickness from less than 15 cm at Glenloig (Fig. 2.19a,b) to over 5 m in the Allt nan Calaman. All display columnar jointing on a scale proportional to the thickness.

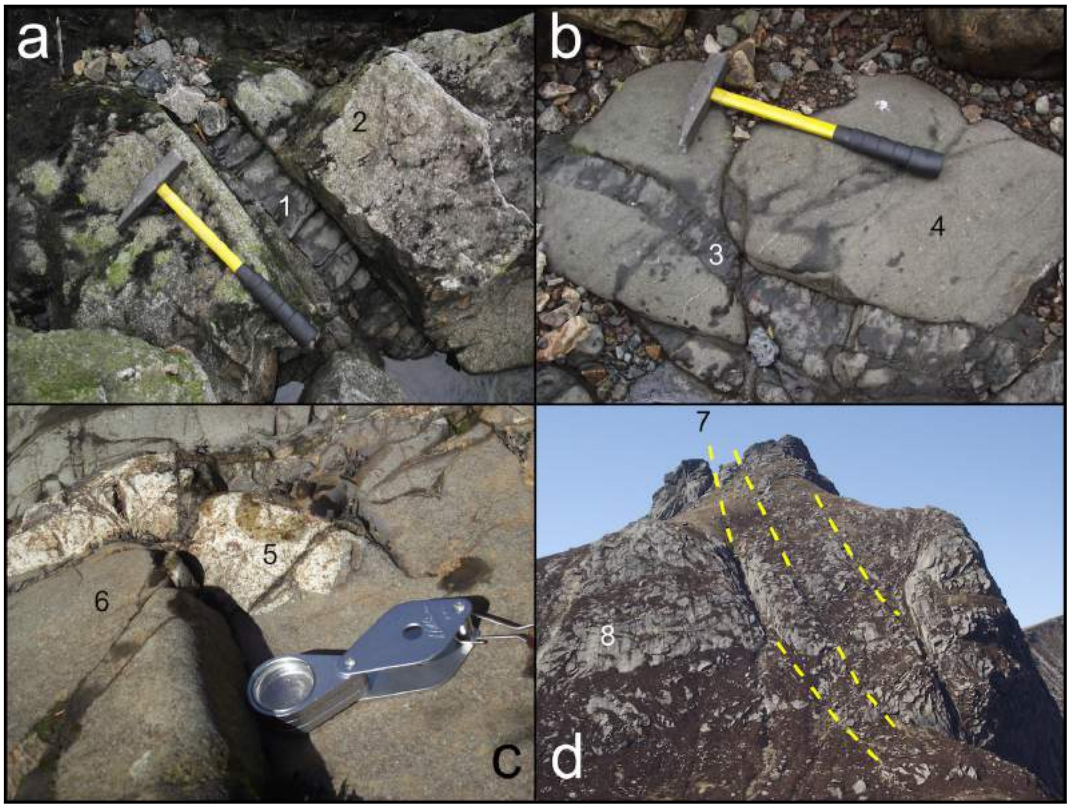

Fig. 2.19 – Photographs of dykes that intrude the Central Arran Igneous Complex and the North Arran Granite. **a)** Thin (<15 cm) basaltic dyke with columnar jointing [1] intruding the amphibole diorites of the Glenloig Hybrids [2] at Glenloig. **b)** Thin (<10 cm) basalt dykelet [3] intruding a much larger dolerite dyke [4] which itself intrudes the Glenloig Hybrids at Glenloig. **c)** Xenolithic dyke intruding the Glen Craigag Granite in Glen Craigag. The granite xenolith [5] caused chilling of the basalt host [6]. **d)** The eastern face of Cìr Mhòr in northern Arran. The scars in the rock face (7) show the locations of dolerite dykes intruding the North Arran Granite (8).

Petrography

The majority of the mafic dykes that intrude the CAIC are medium- to coarse-grained dolerites composed largely of plagioclase laths partly embedded in larger clinopyroxene oikocrysts (Figs. 2.20a,b, 2.21). There are no petrological differences between dolerite dykes that intrude the Glenloig Hybrids, the Glen Craigag Granite, and the AVF.

The groundmass plagioclase laths (An_{48} – An_{82}; Fig. 2.22a) show normal zoning, with relatively calcic cores and relatively sodic rims (Fig. 2.21). The clinopyroxenes (En_{36} – En_{46}; Fig. 2.22c) are also zoned, with relatively magnesium-rich cores and relatively iron-rich rims (Fig. 2.21).

Sample BJG/15/170 (Fig. 2.20a) is from a dolerite dyke that intrudes the extra-caldera lava-like ignimbrites of the Muileann Gaoithe Member on Torr Maol. It comprises a sub-ophitic groundmass of sub-mm plagioclase laths partly embedded in clinopyroxene oikocrysts up to 1 mm in size. Abundant patches of chlorite, and possibly other alteration minerals, may be replacing primary olivine. The other groundmass phases are Fe and Fe-Ti oxides. Some larger plagioclase antecrysts or xenocrysts are present, often with broken morphologies, disequilibrium textures, and rounded inclusion rims enclosed in re-growth rims.

Sample BJG/15/176 (Fig. 2.20b) is from a coarse dolerite that intrudes the Glenloig Hybrids at Glenloig. It comprises plagioclase laths and clinopyroxene oikocrysts up to 2 mm in size with a sub-ophitic texture. Oxide minerals are abundant. There are some small patches of alteration minerals that may indicate the previous presence of olivine. Plagioclase xenocrysts or antecrysts are abundant and can be over 10 mm long. They often contain rounded inclusion rims enclosed within re-growth rims

Sample BJG/15/175 (Fig. 2.20c) is from a basalt dyke that intrudes the Glenloig Hybrids at Glenloig. The groundmass is glassy with plagioclase microlites and

Fig. 2.20 ***(facing page)*** – Photomicrographs of samples of the dolerite and basalt dykes which intrude the CAIC. Cpx = clinopyroxene, P = plagioclase, Px = plagioclase antecryst/xenocryst, Ox = Fe-Ti oxides, Ol = olivine (totally replaced), ch = chlorite. **a)** Sample BJG/15/170, a dolerite that intrudes extra-caldera lava-like ignimbrites. Top left = crossed polars, bottom right = plane polarised light. **b)** Sample BJG/15/176, a coarse dolerite that intrudes the Glenloig Hybrids. Bottom left = plane polarised light, top right = crossed polars. **c)** Sample BJG/15/175, a basalt dyke that intrudes the Glenloig Hybrids. Bottom left = plane polarised light, top right = crossed polars. **d)** Sample BJG/15/155, a dolerite that intrudes the Glen Craigag Granite. Viewed in plane polarised light.

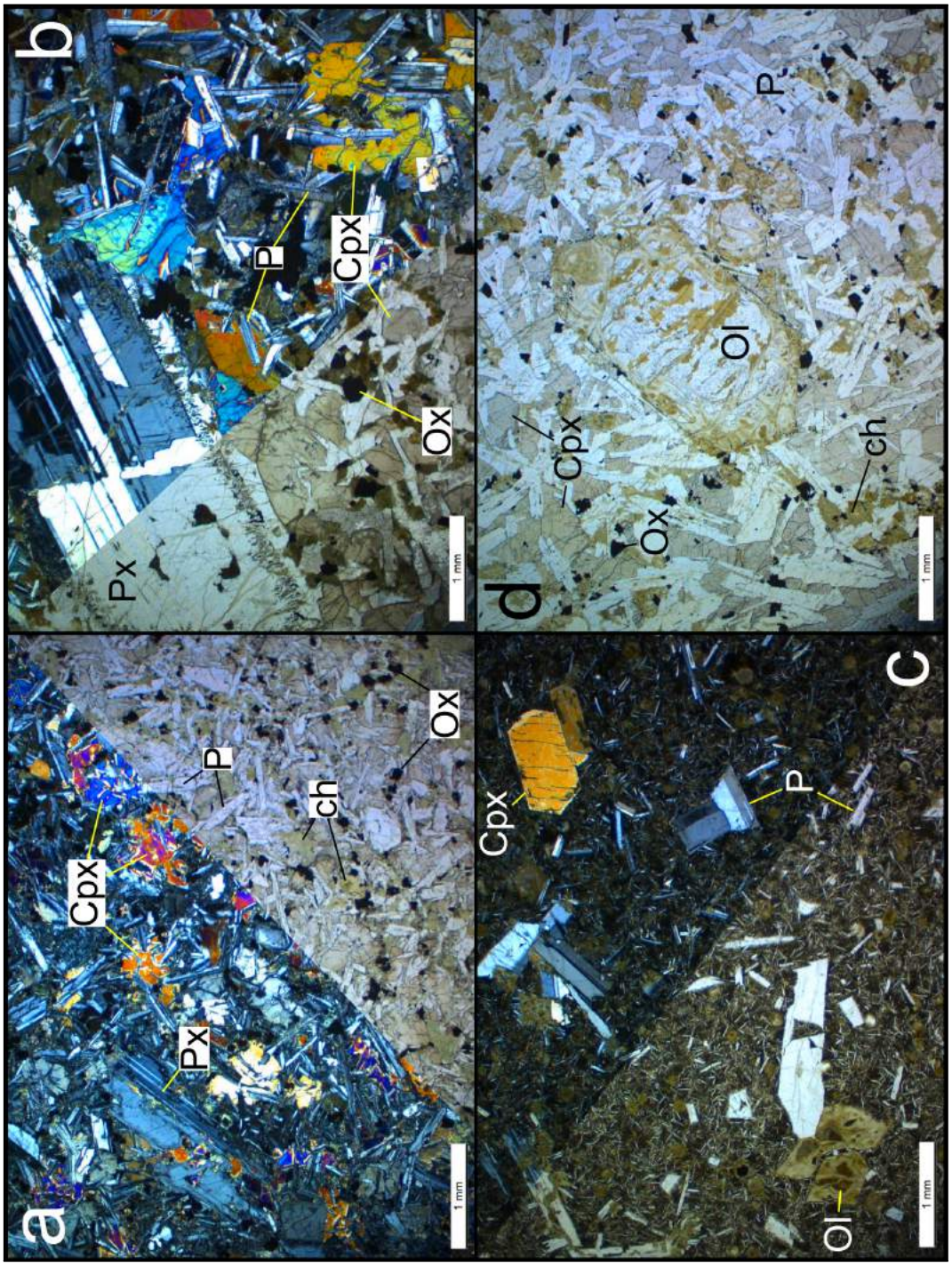
a
Px
Cpx
P
ch
Ox
1 mm
b
Px
P
Cpx
Ox
1 mm
c
Cpx
P
Ol
1 mm
d
Cpx
Ox
Ol
P
ch
1 mm

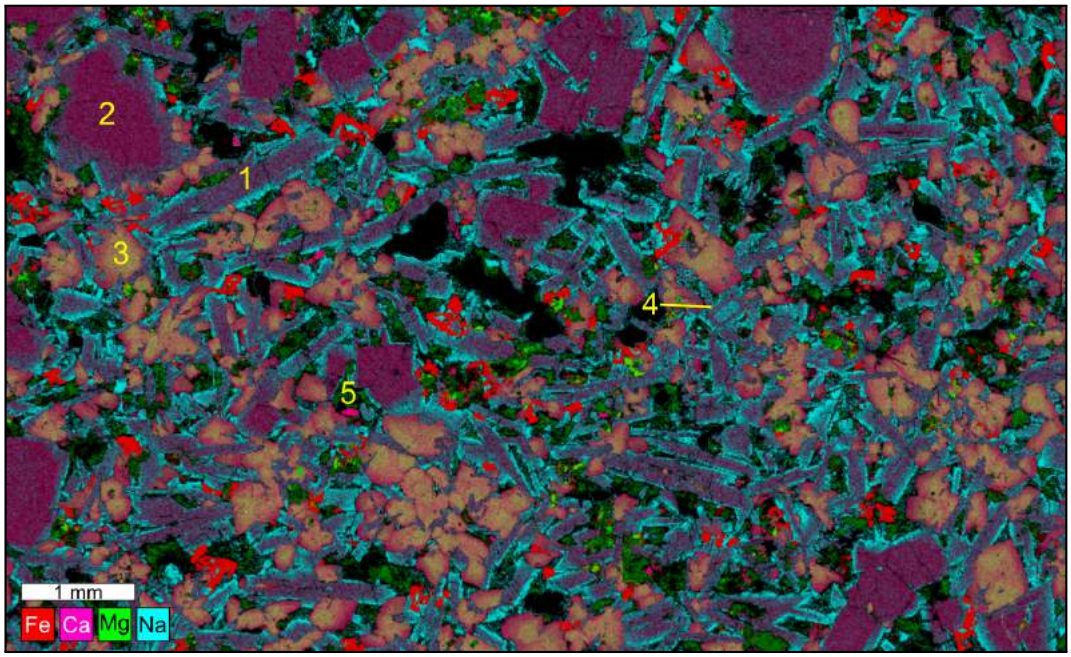

Fig. 2.21 – Major element EDS map of sample BJG/15/325, a dolerite dyke that intrudes the Glenloig Hybrids. Using this element-based colour scheme, calcic plagioclase is purple, sodic plagioclase is light blue, Mg-rich clinopyroxene is yellow, Fe-rich clinopyroxene is pink, Fe-Ti oxides are red, chlorite is green, and apatite is magenta. Plagioclase exists as elongate 1 mm laths [1], with larger (up to 2 mm) equant crystals [2]. Clinopyroxene is shown as [3]. One plagioclase crystal [4] shows a tabular morphology, a rounded sodic core, and a normally (calcic-to-sodic) zoned rim. Apatite is shown at [5].

patches of chlorite. Larger plagioclase crystals are euhedral and do not show disequilibrium textures so are presumably phenocrysts. There are also less abundant 1 mm clinopyroxene phenocrysts and sub-mm olivine phenocrysts which have completely altered to chlorite and other alteration minerals.

Only one dolerite has been sampled which contains olivine phenocrysts (Sample BJG/15/155; Fig. 2.20d). This is mineralogically similar to all of the other dolerites, including the presence of large plagioclase antecrysts with sieve-textured cores, but also contains large (up to 4 mm) completely altered euhedral olivines.

An EDS element map of sample BJG/15/325 is shown in Fig. 2.21. It is a dolerite dyke that intrudes the Glenloig Hybrids in the Allt nan Calaman. Two distinct morphologies of plagioclase can be identified. The volumetrically significant type comprises 1 mm long laths [1], with larger (up to 2 mm) equant crystals [2]. Both of these types show normal zoning, with relatively calcic cores and relatively sodic rims. The cores of the equant crystals are more calcic than the cores of the laths. Clinopyroxene crystals [3] show yellow relatively magnesium-rich cores, with

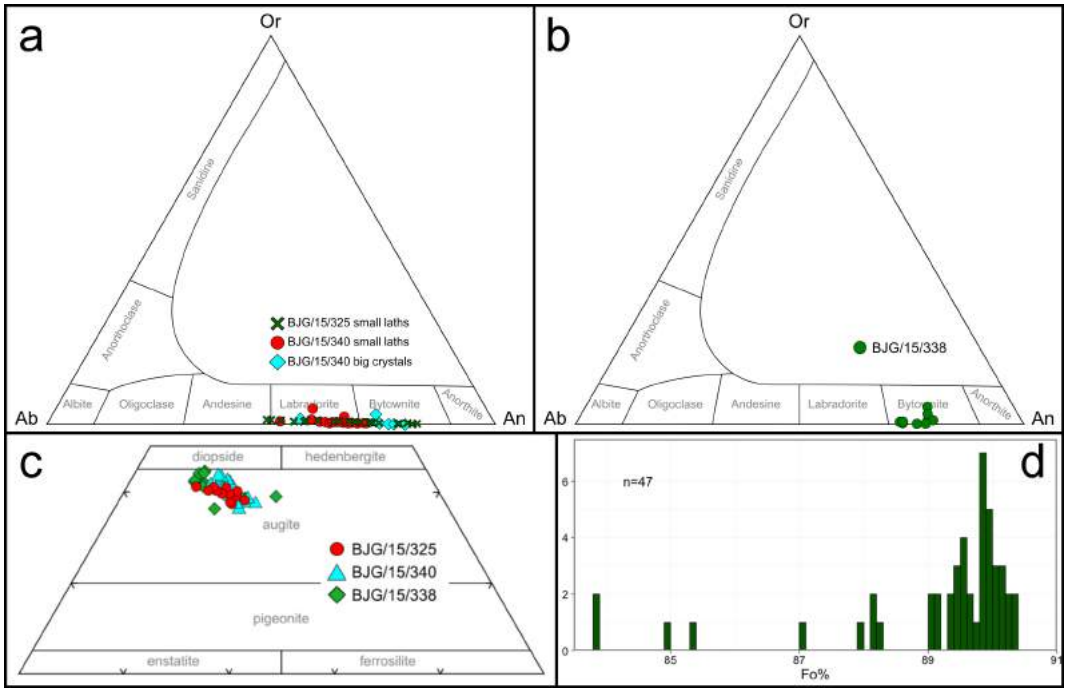

Fig. 2.22 – Geochemical plots of mineral data from the dolerite and picrite dykes in the CAIC. **a)** Ternary plot of feldspars from samples BJG/15/325 and BJG/15/340 - two of the dolerite dykes that intrude the CAIC, similar to those shown in Figs 2.20 and 2.21. **b)** Ternary plot of feldspars from sample BJG/15/338 - the picrite dyke that intrudes the Glen Craigag Granite, as shown in Fig. 2.26/ **c)** Ternary plot of pyroxenes from samples BJG/15/325 and BJG/15/340 (dolerite) and BJG/15/338 (picrite). **d)** Histogram of olivine Fo% in sample BJG/15/338, as shown in Figs 2.20c and 2.21.

zoning towards pink relatively iron-rich rims. One example, in the bottom right corner, shows sector zoning. Interstitial green material is chlorite, possibly replacing primary olivine. One plagioclase crystal [4] shows a tabular morphology, a rounded sodic core, and a normally (calcic-to-sodic) zoned rim. This crystal is presumably an antecryst or xenocryst.

Almost all of the dolerites contain plagioclase crystals larger than the euhedral groundmass laths (An_{56} – An_{80}; Fig. 2.22a). In a small number of cases, these are euhedral and do not show disequilibrium textures, suggesting that they are phenocrysts (Fig. 2.21). However, in the majority of examples, these plagioclases have broken morphologies, resorption (sieve) textures in the cores, and/or rounded inclusion rims enclosed within re-growth rims. (Fig. 2.20a,b). This suggests that they are xenocrysts derived from older country rocks or, more likely, antecrysts from elsewhere in the active magma system.

One basalt dyke intruding the Glen Craigag Granite (Sample BJG/15/153; Figs. 2.19c, 2.23a) contains xenoliths of granite, presumably sourced from the Glen

Craigag Granite itself. It comprises a very fine grained groundmass that is truly glassy at the contact. The crystals it contains are all plagioclase, mostly in the form of <0.5 mm long laths, but occasionally as large euhedral phenocrysts associated with the glassy contact. The granite xenolith comprises quartz and K-feldspar with minor alteration minerals and opaques. The xenolith is disaggregating around its edges.

2.6.2 Dykes intruding the North Arran Granite

The North Arran Granite is intruded by a large number of basalt and dolerite dykes (Fig. 2.19d). It is not the aim of this section to give a complete and comprehensive description of this suite of dykes, but some were sampled for geochemical comparison with CAIC dykes, and so shall briefly be described here. The NAG itself is described in section 2.7.

Petrography

These dykes are mostly dolerites, and these petrographically resemble the dolerite dykes from the CAIC. They display sub-ophitic textures with plagioclase laths partly embedded in clinopyroxene oikocrysts (Fig. 2.23d). As with the dolerites in the CAIC, it appears that the third major groundmass mineral was olivine, that has now been altered. However, in the NAG dykes, these olivines have been replaced by orange-brown iddingsite, rather than the light green patches of alteration minerals dominated by chlorite, as seen in Fig. 2.20. The NAG dykes also contain plagioclase xenocrysts or antecrysts, with sieve-textured cores, broken morphologies, and rounded inclusion rims enclosed within regrowth rims (Fig. 2.23d).

Fig. 2.23 ***(facing page)*** – Photomicrographs of dykes other than the CAIC basalts/dolerites. **a)** Sample BJG/15/153, the xenolithic dyke that intrudes the Glen Craigag Granite, shown in Fig. 2.19c. K = K-feldspar, Q = quartz, P = plagioclase, G = glassy margin of the basalt dyke, chilled against the xenolith. Viewed in plane polarised light. **b)** Sample BJG/15/104, a pitchstone dyke that intrudes the Arran Volcanic Formation. G = silicic glass, P = plagioclase, Cpx = clinopyroxene, Ox = Fe-Ti oxide. Left = crossed polars, right = plane polarise light. **c)** Sample BJG/15/338, an olivine-rich picrite dyke that intrudes the Glen Craigag Granite. Abbreviations as above, plus Ol = olivine. Opaque minerals include both Fe-Ti oxides, and chrome-spinel. Bottom left = plane polarised light, top right = crossed polars. **d)** Sample BJG/16/2, a dolerite intruding the North Arran Granite in Glen Rosa. Abbreviations as above, although all olivine has been replaced by red-brown iddingsite.

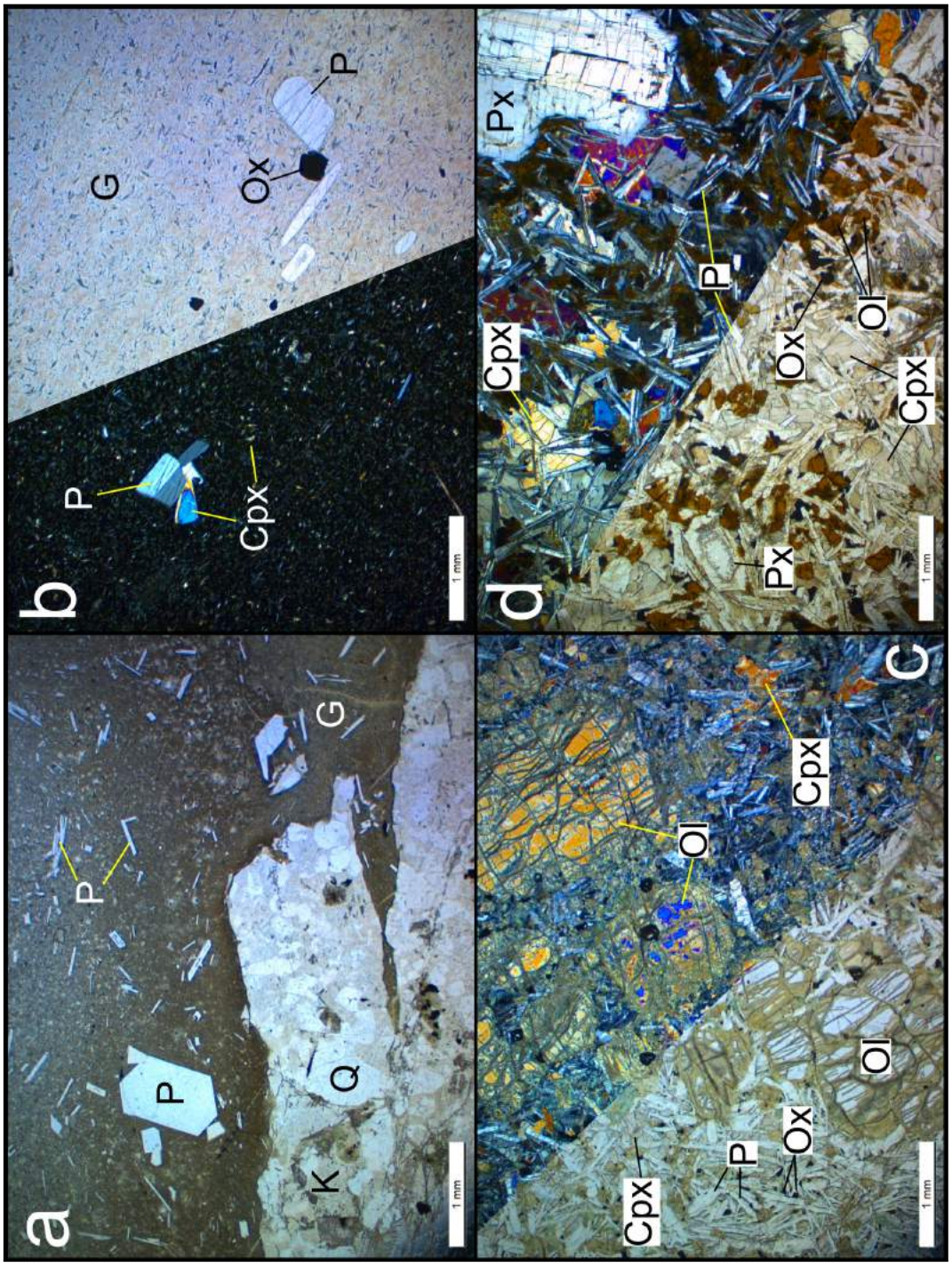
a
P
P
G
Q
K
1 mm
b
P
Cpx
G
Ox
P
1 mm
c
Cpx
Ol
Cpx
G
Cpx
P
Ox
Ol
1 mm
d
Px
Cpx
P
Ox
Ol
Px
Cpx
1 mm

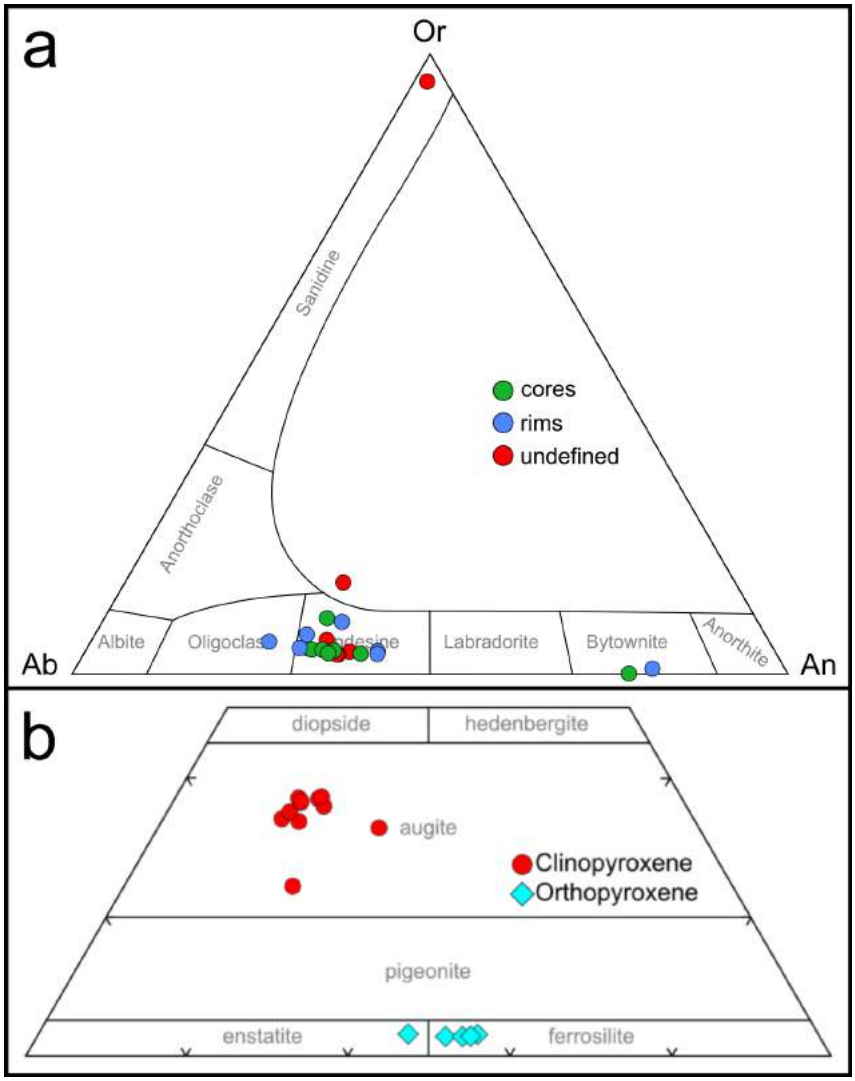

Fig. 2.24 – Ternary plots of EDS data from sample BJG/15/104 - the pitchstone dyke that intrudes the CAIC. **a)** Feldspar data. **b)** Pyroxene data.

2.6.3 Pitchstone dyke

The only dyke that intrudes the intra-caldera ignimbrites of the AVF is a black, glassy pitchstone (partly-hydrated silicic glass) dyke that strikes NW-SE. It displays flow-banding parallel to the margins of the dyke. This is the only example of this lithology seen anywhere in the CAIC. It is exposed in one of the tributaries to the Glen Craigag Burn where it flows down from Leana Cuil (NR 950 341). The exposure in the steep rocky stream is not excellent, but the dyke appears to be around 1 m wide.

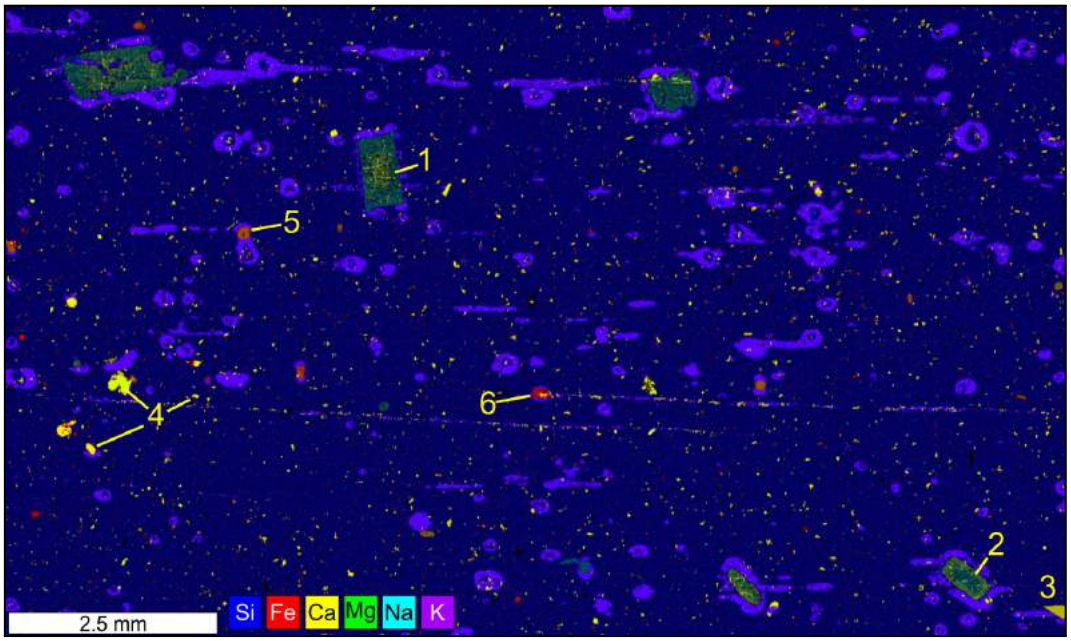

Fig. 2.25 – Major element EDS map of sample BJG/15/104, a pitchstone dyke that intrudes the AVF. Using this element-based colour scheme, the silicic groundmass glass is dark blue, and potassium-rich haloes in the glass around crystals are purple. Calcic plagioclase is dull yellow, while sodic plagioclase is green. Clinopyroxene is bright yellow, olivine is orange, and Fe oxides are bright red. See text for explanation of numbers.

Petrography

The groundmass of the pitchstone is a fresh, optically isotropic silicic glass (Figs 2.23b, 2.25). The majority of large crystals are euhedral-to-rounded plagioclases (largely An_{25} – An_{41}, with two measured examples of bytownite; Fig. 2.24a), which can be normally zoned [1], reverse zoned [2], or anorthitic [3] (Fig. 2.25). There are also occasional large clinopyroxene [4] crystals (En_{40} – En_{55}; Fig. 2.24b), orthopyroxene crystals (En_{42} – En_{51}; Fig. 2.24b), small rounded olivines [5] and Fe oxides [6] (Fig. 2.23b). Clinopyroxene in this rock also exists as tiny crystals within the groundmass glass, which can be seen as birefringent specks in Fig. 2.23b and as small yellow dots in Fig. 2.25.

2.6.4 Picrite dyke

In a steep tributary to the Allt Rollican in Ballymichael Glen are some poor, heavily weathered exposures of an olivine-rich dyke intruding the Glen Craigag Granite. Although the margins are largely obscured, it can be seen to strike NW-SE. This exposure is only several metres below where the ignimbrites of the AVF overlie the

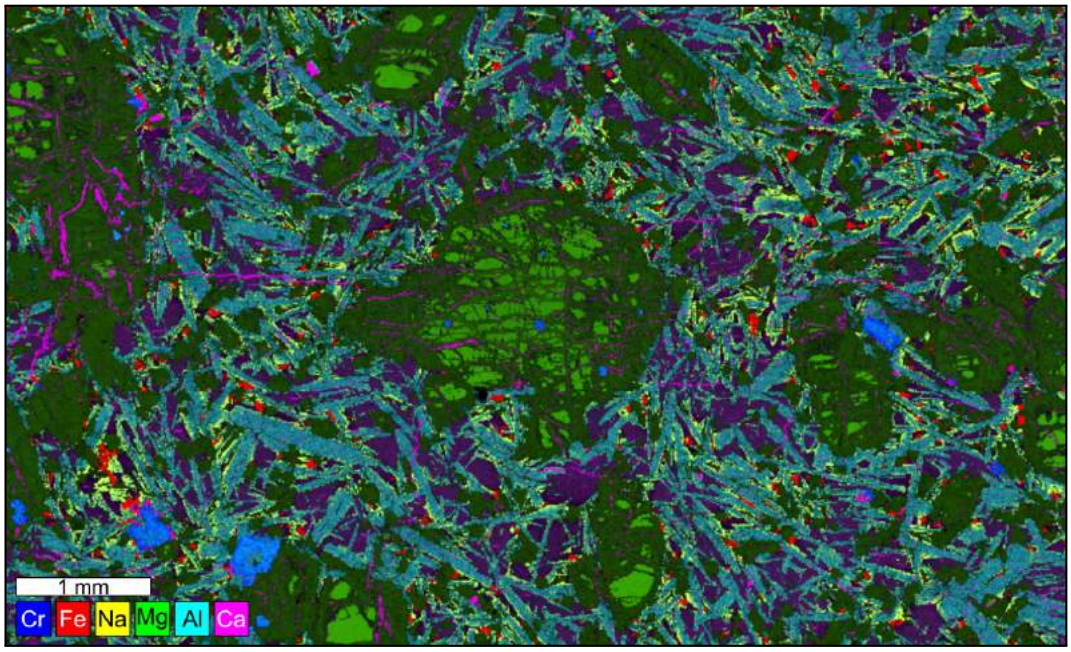

Fig. 2.26 – Major element EDS map of sample BJG/15/338, a picrite dyke that intrudes the Glen Craigag Granite in Ballymichael Glen. Using this element-based colour scheme, fresh olivine is bright green, while olivine-alteration products are shown in dark green. Plagioclases are turquoise with yellow albitic rims. Purple is interstitial clinopyroxene, red shows Fe-Ti oxides, and bright blue is chrome spinel. The pink streaks running through the rock are calcite veins.

Glen Craigag Granite, and the dyke cannot be seen intruding any pyroclastic rocks. This is an important piece of field evidence that suggests the dyke, and therefore the Glen Craigag Granite, are older than the pyroclastic rocks of the AVF.

Petrography

Petrographically, it is similar to the dolerite dykes the intrude the CAIC, with abundant 1 mm long plagioclase laths (An_{72} – An_{79}; Fig. 2.22a) partly embedded in larger clinopyroxene oikocrysts (En_{32} – En_{46}; Fig. 2.22c), both accompanied by small Fe-Ti oxides. The main petrological difference is the presence of large (rarely up to 10 mm) olivine crystals (Fo% 83.8–90.4; Fig. 2.22d), and chrome spinels (Figs 2.23c, 2.26). The olivines are mostly altered to chlorite and other alteration products around the margins and along internal cracks, but they are large enough that some fresh olivine is preserved. This is the only fresh olivine found anywhere in the CAIC. Chrome spinel is zoned, with relatively Cr-rich (darker blue) rims. This mineral is not observed anywhere else in the CAIC. The rock is intruded by thin (<100 µm) calcite veins. The composition of the olivines and their relationship to the host melt is discussed in Section 5.1.

2.6.5 Summary

The mafic dykes are basalts and dolerites between 15 cm and 5 m in thickness. Most are sub-ophitic to ophitic dolerites with small plagioclase (labradorite – bytownite) laths encased in larger clinopyroxene (Mg-rich augite) oikocrysts. The plagioclases and clinopyroxenes are zoned, with relatively Na-rich and Fe-rich rims, respectively. The dolerites contain plagioclase phenocrysts/xenocrysts and evidence for altered groundmass olivine. Some of the thinner dykes are basalt, with fine-grained groundmass and plagioclase microlites and phenocrysts. One basalt contains altered olivine and clinopyroxene phenocrysts.

The dykes intruding the North Arran Granite are petrographically similar to the mafic dykes intruding the CAIC. They are mostly ophitic dolerites with evidence of primary olivine.

A pitchstone dyke comprises fresh silicic glass and has a diverse crystal cargo, including plagioclase (andesine and bytownite), clinopyroxene (augite), orthopyroxene (ferrosilite), and Fe oxides. This is the only dyke intruding the caldera-fill succession of the Arran Volcanic Formation.

A picrite dyke intruding the Glen Craigag Granite contains a large amount of large weathered olivine crystals (mostly Fo_{89}–Fo_{90}). These crystals have retained the only fresh olivine seen in any rock in this study. The picrite also contains chrome spinel. The groundmass is a sub-ophitic dolerite with small plagioclase (bytownite) crystals partly encased in clinopyroxene (Mg-righ augite), as well as Fe oxides.

2.7 Other intrusive units on Arran

As well as the igneous rocks exposed within the Central Arran Igneous Complex, as part of this study intrusive rocks were sampled from other parts of Arran. A full study of the intrusive Palaeogene rocks on the island is beyond the scope of this PhD, but it was thought that some units would provide useful comparisons with various units within the CAIC. The North Arran Granite (Fig. 1.3) provides an obvious comparison with the granites of the CAIC. The mingled intrusions of the Sheans, just above the town of Brodick are in some ways similar to the hybrid rocks of the CAIC, and may be a discontinuous extension of the Glenloig Hybrids (Fig. 1.9). Further south on the island is the poorly exposed Tighvein Intrusion Complex (Fig. 1.3). The weathered rocks exposed here partly resemble the Glenloig Hybrids and the mingled rocks from the Sheans.

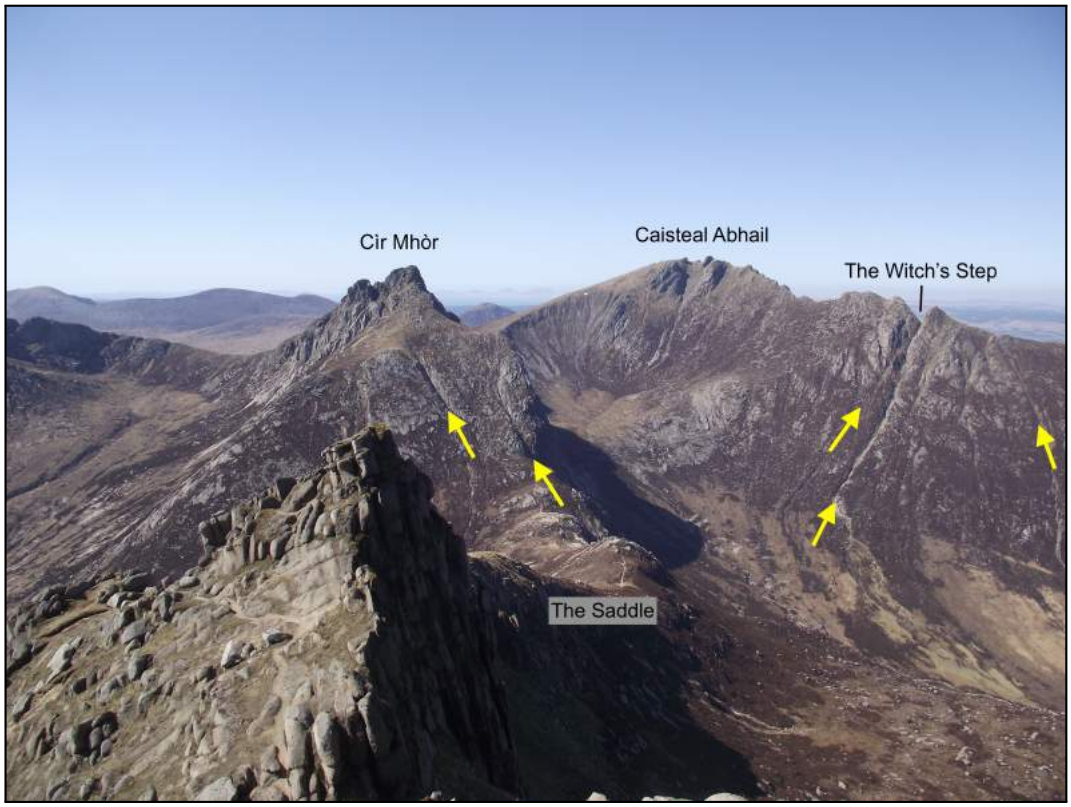

Fig. 2.27 – Photograph of the mountains of the North Arran Granite, looking north west across The Saddle from North Goat Fell. Several mafic dykes (yellow arrows) can be seen as scars in the landscape. These include the dykes on the eastern face of Cìr Mhòr (Fig. 2.19d), and the dyke that forms the Witch's Step, the large notch in the ridge that runs east from Caisteal Abhail.

2.7.1 The North Arran Granite

The North Arran Granite (NAG) dominates the geology of the north part of the island (Fig. 1.3), and makes up the rugged Corbetts (mountains with heights between 2,500 and 3,000 feet) of Goat Fell, Cìr Mhòr, Caisteal Abhail, and Beinn Tarsuinn. It takes the form of a laccolith that was intruded into the Dalradian Schists, and caused doming of the country rocks during inflation (Stevenson and Grove, 2014). Along most of its margins it has a steep intrusive contact with the schists and a finer chilled margin, although along its eastern edge it displays a faulted contact with the Devonian sandstones (BGS, 1987; Emeleus and Bell, 2005). Two mappable domains are identified in the NAG, and outer ring of coarse granite, and an inner finer granite. The inner granite is suggested to be younger; this is discussed in Section 4.3.

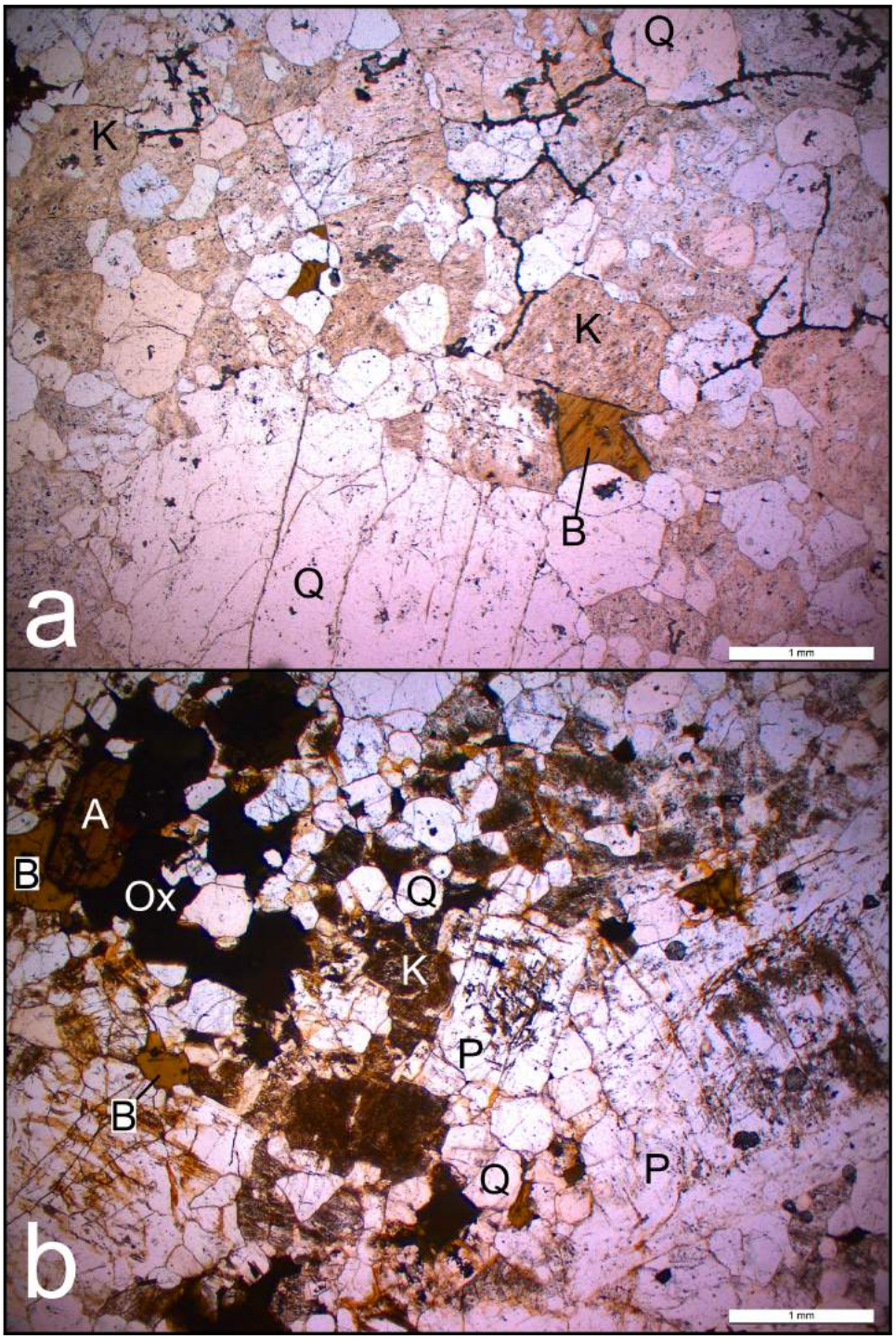

Fig. 2.28 – Photomicrographs of samples of the North Arran Granite. Q = quartz, K = K-feldspar, P = plagioclase, B = biotite, Ox = opaque oxide. A = allanite. **a)** Sample BJG/16/38, the inner 'fine unit'. Plane polarised light. **b)** Sample BJG/15/179, the 'coarse unit'. Plane polarised light.

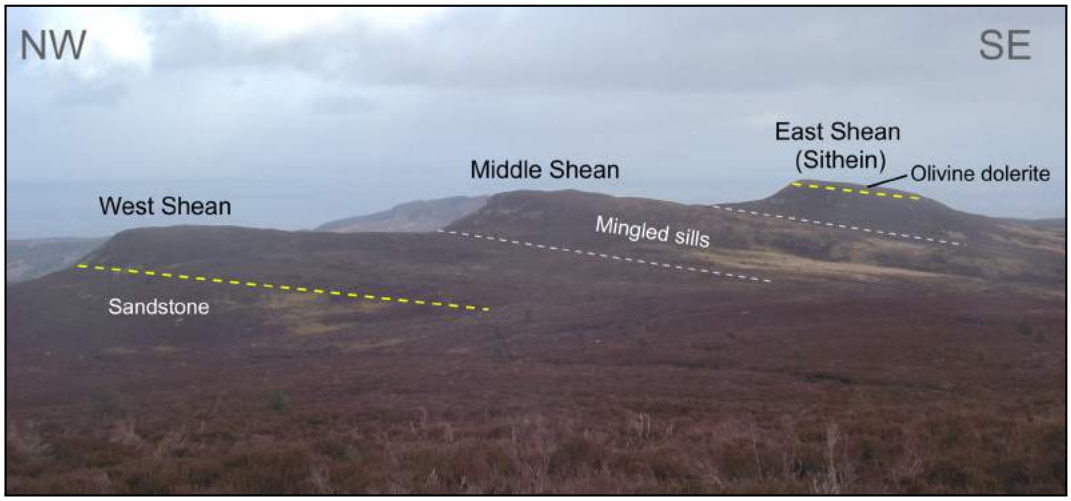

Fig. 2.29 – Photograph of the Sheans from the west.

Petrography

The petrology of the NAG has been described extensively in previous publications (Dickin et al., 1981; England, 1992; Hyslop et al., 1999), with which our observations from a limited number of samples agree. Both the coarse and fine units are biotite syenogranites (Fig. 2.28), with remarkably little mineralogical variation throughout the intrusion. Euhedral plagioclase phenocrysts are more abundant in the coarse unit (Fig. 2.28b). The accessory phases include Fe-Ti oxides, zircon, apatite, and allanite (England, 1992). Miarolitic and drusy cavities in the granite also contain mica, topaz, beryl, and REE-bearing fergusonite and gadolinite (Emeleus and Bell, 2005; Hyslop et al., 1999).

2.7.2 The Sheans

The ridge between Gleann Dubh and Benlister glen, to the east of the CAIC, is made up of three prominent summits known as The Sheans (Figs 1.9, 2.29. The majority of exposures on these summits show fine- to medium-grained intermediate rocks which display spectacular mingling textures with finer, more mafic enclaves. This lithology was described by Tyrell (1928) who interpreted these enclaves as basalt xenoliths, but their fluidal morphologies (Fig. 2.30a) suggest that a magma mingling origin is more likely. The summit of Sithein, or East Shean, is made up of dolerite which is intruded by a system of felsic dykelets and net-veins (most up to around 5 cm in width) similar to those seen throughout the Glenloig Hybrids.

The lower contact of the mingled intrusion with the underlying pre-Palaeogene sandstones can be followed below the West Shean (Fig. 2.29), and is sub-horizontal.

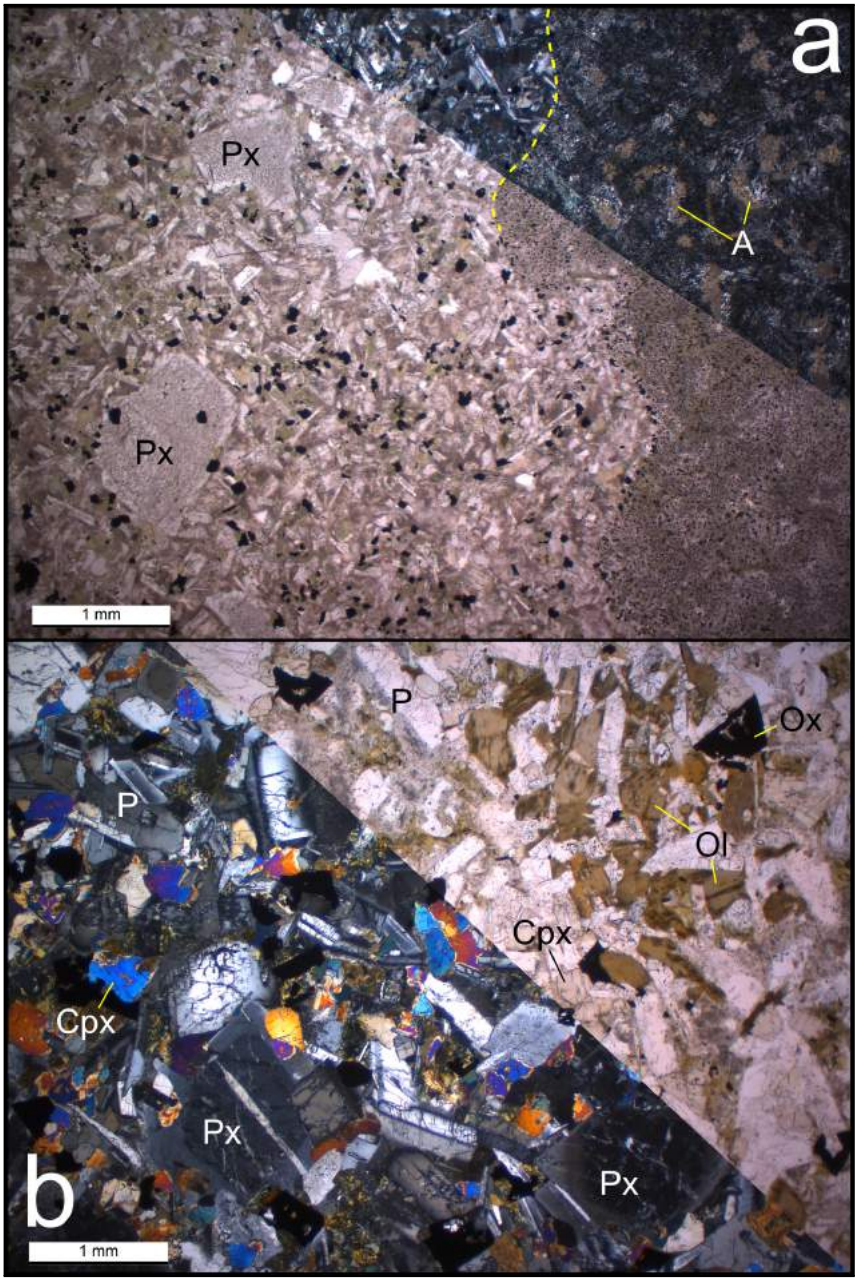

Fig. 2.30 – Photomicrographs of samples from the Sheans. **a)** Sample BJG/15/38 from the 'Middle Shean', comprising a dioritic host (left) with finer, more mafic material (right). Px = plagioclase xenocrysts, A = amphibole. Bottom left = plane polarised light, top right = crossed polars. **b)** Sample BJG/15/37, an olivine dolerite from the summit of Sithean, or the 'East Shean'. P = plagioclase, Cpx = clinopyroxene, Ol = olivine altered to chlorite and other products, Ox = Fe-Ti oxides, Px = plagioclase antecrysts/xenocrysts. Bottom left = crossed polars, top right = plane polarised light.

The upper contact with the olivine dolerite has a similar orientation. This suggests that the mingled intrusion is a sill. The general slope of the southern side of each summit (dashed grey lines in (Fig. 2.29)) suggests that the Sheans might be made up of three stacked sills, with the upper (Sithein) sill capped with dolerite.

Petrography

Sample BJG/15/38 (Fig. 2.30a) is from the 'Middle Shean'. It comprises a dioritic host that includes xenoliths and enclaves of a much finer, possibly more mafic, material. The contact between the two in this example (dashed line) is fluidal, and enriched in small opaque minerals. The coarser host is made up of sub-mm euhedral plagioclases and anhedral K-feldspars, along with abundant opaque minerals and possibly some heavily altered amphiboles. It hosts larger (over 1 mm) euhedral plagioclase xenocrysts with sieve-textured cores and overgrowth rims. The finer unit comprises feldspars, opaques, and completely altered amphiboles which can only be made out between crossed polars.

Sample BJG/15/37 (Fig. 2.30b) is a dolerite from the summit of Sithean, or the 'East Shean'. It is an fine-grained olivine dolerite comprising euhedral plagioclase laths, subhedral to anhedral clinopyroxenes, olivines which have been entirely altered to chlorite and other products, and Fe-Ti oxides. It also contains larger (>1 mm) plagioclase xenocrysts or antecrysts which show compositional zoning.

2.7.3 The Tighvein Intrusion Complex

Tighvein is a rather flat moorland summit around 5 km south of the Sheans. It is very poorly exposed, but the presence of intermediate, silicic, and mingled intrusions has been discussed by Tyrell (1928) and Herriot (1975). Samples were taken from the summit region and from the small crag Creag na h-Ennie which lies about a kilometre and a half north north east of the summit. The summit exposures show a medium- to coarse-grained, heavily weathered diorite, intruded by small dykes of silicic material (Fig. 2.31) similar to those seen on the East Shean or the Tir Dhubh exposures of the Glenloig Hybrids in the CAIC. The Creag na h-Ennie exposures show spectacularly mingled hybrid rocks with an intermediate host and highly abundant more mafic enclaves, much like the main body of the Sheans intrusion.

Petrography

The silicic intrusions visible in Fig. 2.31 are petrologically similar to the fine rhyolitic dykelets observed in several places intruding the Glenloig Hybrids (Fig. 2.3). Fig.

Fig. 2.31 – Photograph of the exposure at the Tighvein summit. It shows silicic dykelets (prominent) intruding a heavily altered dioritic host.

2.32a shows a fine rhyolitic groundmass made up of quartz, K-feldspar, and opaques, and larger crystals, usually found as glomerocrysts. These are mostly euhedral plagioclases with less abundant subhedral to anhedral clinopyroxenes. The euhedral shape and lack of disequilibrium textures in the plagioclases suggest that they may be phenocrysts.

The Creag na h-Ennie sample is a non-ophitic olivine dolerite (Fig. 2.32b) similar to that found on the summit of Sithein, but containing rounded enclaves of finer opaque-rich and amphibole-bearing material. The dolerite itself comprises <1 mm euhedral to subhedral plagioclase laths, small clinopyroxene and altered olivine crystals, and small but abundant opaque minerals. Larger plagioclases display disequilibrium features such as sieve-textured cores and so are presumably antecrysts or xenocrysts.

2.7.4 Summary

The North Arran Granite forms a large (13 km diameter) laccolith in the north of the island. It comprises biotite syenogranites or various grain sizes and textures.

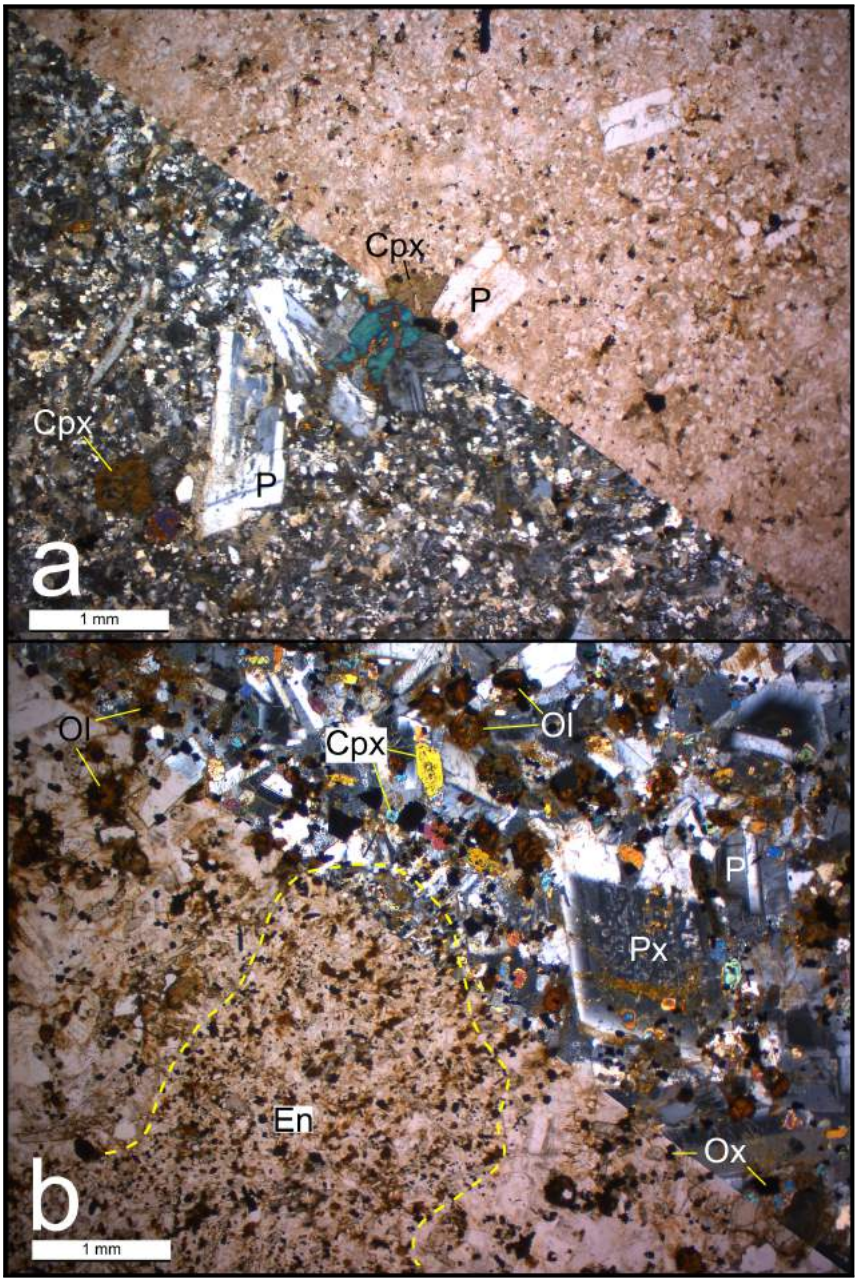

Fig. 2.32 – Photomicrographs of samples from the 'Tighvein Intrusion Complex'. **a)** Sample BJG/15/21 from a rhyolite dyke intruding on the summit of Tighvein. P = plagioclase, Cpx = clinopyroxene. Bottom left = crossed polars, top right = plane polarised light. **b)** Sample BJG/15/18, olivine dolerite from the Urie Loch area on Tighvein. En = enclave of finer grained intermediate material, P = plagioclase, Cpx = clinopyroxene, Ol = altered olivine, Px = plagioclase xenocryst, Ox = opaque oxides.

Accessory phases of Fe-Ti oxides, zircon, apatite, and allanite have been previously described.

The Sheans and Tighvein are poorly exposed moor-covered plateaus in the south of the island. They are made up of mafic and intermediate intrusive rocks intruded by felsic veins, much like the Glenloig Hybrids of the CAIC. Both contain non-ophitic olivine dolerites, amphibole diorites, and microgranites/rhyolites like those seen in dykelets in the Glenloig Hybrids.

2.8 Summary

The CAIC and surrounding areas contain a diverse variety of igneous rocks. Mafic rocks are largely restricted to basalt/ophitic dolerite dykes and one sill intruding the Arran Volcanic Formation. These all contain groundmass plagioclase, clinopyroxene, Fe-Ti oxides, and altered olivine, with phenocrysts/xenocrysts of plagioclase and rarely olivine. The only ultramafic rock is an olivine picrite dyke which, in addition to plagioclase, clinopyroxene, and Fe-Ti oxides also contains large olivines and Cr-spinels. The other mafic rocks are the poorly-exposed small gabbro bodies dotted around the complex. The most striking of these is a plagioclase-magnetite cumulate that also contains clinopyroxene and orthopyroxene.

Intermediate rocks are represented by the extensive and varied Glenloig Hybrids unit. This unit comprises a complex series of intermediate and silicic magmatic rocks, that show different degrees of intrusion, mingling, and mixing with one another. The intermediate examples all contain brown/green amphibole in addition to feldspars and opaque minerals, while the silicic examples are porphyritic rhyolites and microgranites.

A number of granite bodies are found within the CAIC. The Glen Craigag Granite in the centre of the complex appears to pre-date volcanic activity (depositional contact, and significant intrusion by mafic dykes, not seen in the ignimbrites), and comprises a granophyre containing quartz, K-feldspar, plagioclase, Fe-Ti oxides, zircon and sphene. The Satellite Granites around the margin of the complex show intrusive contacts with the ignimbrites, so must be younger, and also do not show evidence of intrusion by mafic dykes. They contain quartz and perthitic K-feldspar, with some plagioclase, Fe-Ti oxides, and zircon, but no sphene.

The other silicic intrusion in the CAIC is a glassy pitchstone dyke. It contains a large number of feldspar, pyroxene, and oxide xenocrysts.

The North Arran Granite to the north of the CAIC (across the trace of the Highland Boundary Fault) is a petrologically homogenous biotite bearing syenogranite.

The Sheans and Tighvein in the south of the island comprise complex series of intermediate and silicic intrusions, much like the Glenloig Hybrids.

Chapter 3

Volcanic Stratigraphy and Eruptive History

The data and interpretations presented in this chapter have been published in the Bulletin of Volcanology (Gooday et al., 2018).

The exposure on Ard Bheinn, Binnein na h-Uaimh, the western side of A' Chruach, and the lower parts of Glen Craigag are dominated by various pyroclastic rocks (Fig. 1.9). There are also some limited exposures of sedimentary rocks. As discussed, it is thought that the ellipsoidal extent of the main body of these pyroclastic rocks approximately defines the boundary of a caldera, meaning that these units are a caldera-fill succession. All of these intra-caldera pyroclastic and sedimentary units, as well as pyroclastic units that were deposited outside the caldera, are assigned to the Arran Volcanic Formation (AVF).

The Arran Volcanic Formation comprises a number of different mappable pyroclastic units (Fig. 3.1) which are interpreted as ignimbrites (*i.e.*, the deposits of pyroclastic density currents), separated by erosional unconformities and sedimentary horizons. They are best exposed in the western third of the complex (*i.e.*, west of Glen Craigag; Fig. 3.1), with good exposure on the high ground around Ard Bheinn and Binnein na h-Uaimh (Fig. 3.2). This is the area that King (1954) described in detail. Exposures of these rocks are found over an elevation change of more than 400 m (Fig. 3.2), giving the best estimate of total preserved thickness. Dips of units and other structural data are impossible to measure due to the lack of bedding seen at the scale of individual exposures. Where a sense of dip can be gleaned from following contacts, beds appear approximately horizontal. In one very poor, weathered exposure in Ballymichael Burn, pyroclastic rocks appear to lie on an eroded surface of the Glen Craigag Granite (Section 2.3). This is the only exposure

of a possible caldera floor, and in the rest of the complex it is impossible to say how deeply the caldera floor – presumably made up of pre-Palaeogene sedimentary rocks and CAIC intrusions – is buried. An unknown thickness of the Arran Volcanic Formation above the current level of exposure has been lost to erosion.

The pyroclastic rocks on Muileann Gaoithe record a thickness of over 130 m, and lie upon *in situ* Devonian Old Red Sandstone. The extra-caldera nature of the Muileann Gaoithe exposures is apparent, as they lie around 1.5 km from the proposed ring fault. This is not so apparent with the isolated exposures of ignimbrites in the south east of the complex, on Tir Dubh and Creagan Liatha. These are also in close association with *in situ* pre-Palaeogene sandstone country rocks, but due to the poor nature of the exposure in this flat, peaty part of the complex, it is impossible to determine a structural relationship between these ignimbrites and the caldera-fill succession or the ring fault. However, they are interpreted to be extra-caldera. The contact between the AVF and the Glenloig Hybrids at Glenloig is also not clear. The contact is not well exposed, but it appears as though the pyroclastic rocks overlie the hybrid rocks with a sub-horizontal contact, suggesting deposition on this surface. This could result from one of three situations, depending on the relative position of a possible caldera-bounding ring fault: 1) This exposure at Glenloig is inside the caldera and shows a caldera-floor comprising Glenloig Hybrids. 2) This exposure is outside the caldera and shows extra-caldera deposition of the ignimbrites. 3) There was little or no caldera subsidence in this part of the complex.

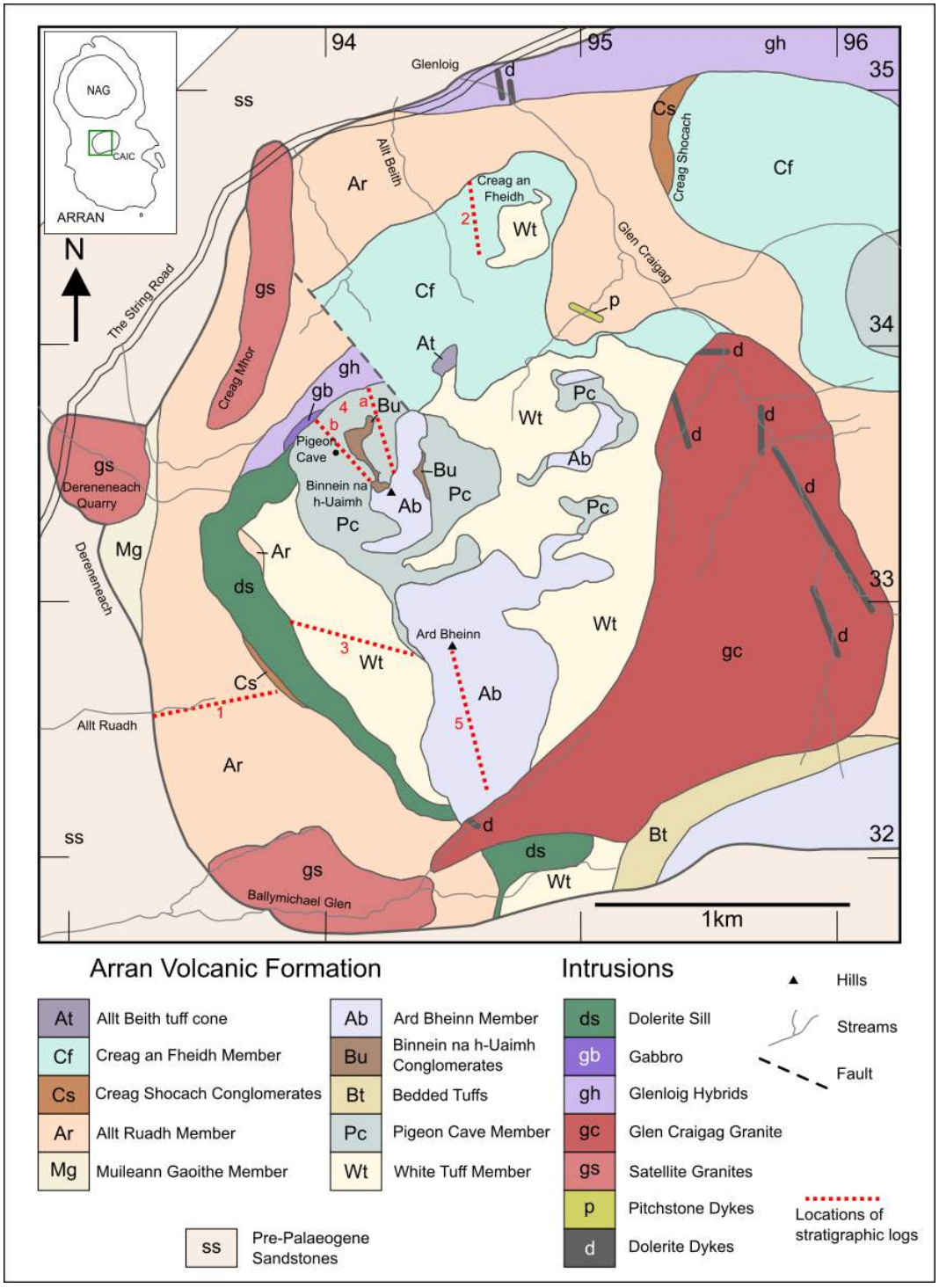

Fig. 3.1 – Geological map of the western half of the Central Arran Igneous Complex. Approximate locations of stratigraphic logs presented in this paper are shown in red. 1 = Allt Ruadh Member, 2 = Creag an Fheidh Member, 3 = White Tuff Member, 4 = Pigeon Cave Member, 5 = Ard Bheinn Member. The grid shows the 1 km eastings and northings of the British National Grid. Inset shows the location of the Central Arran Igneous Complex (CAIC) on Arran in relation to the North Arran Granite (NAG).

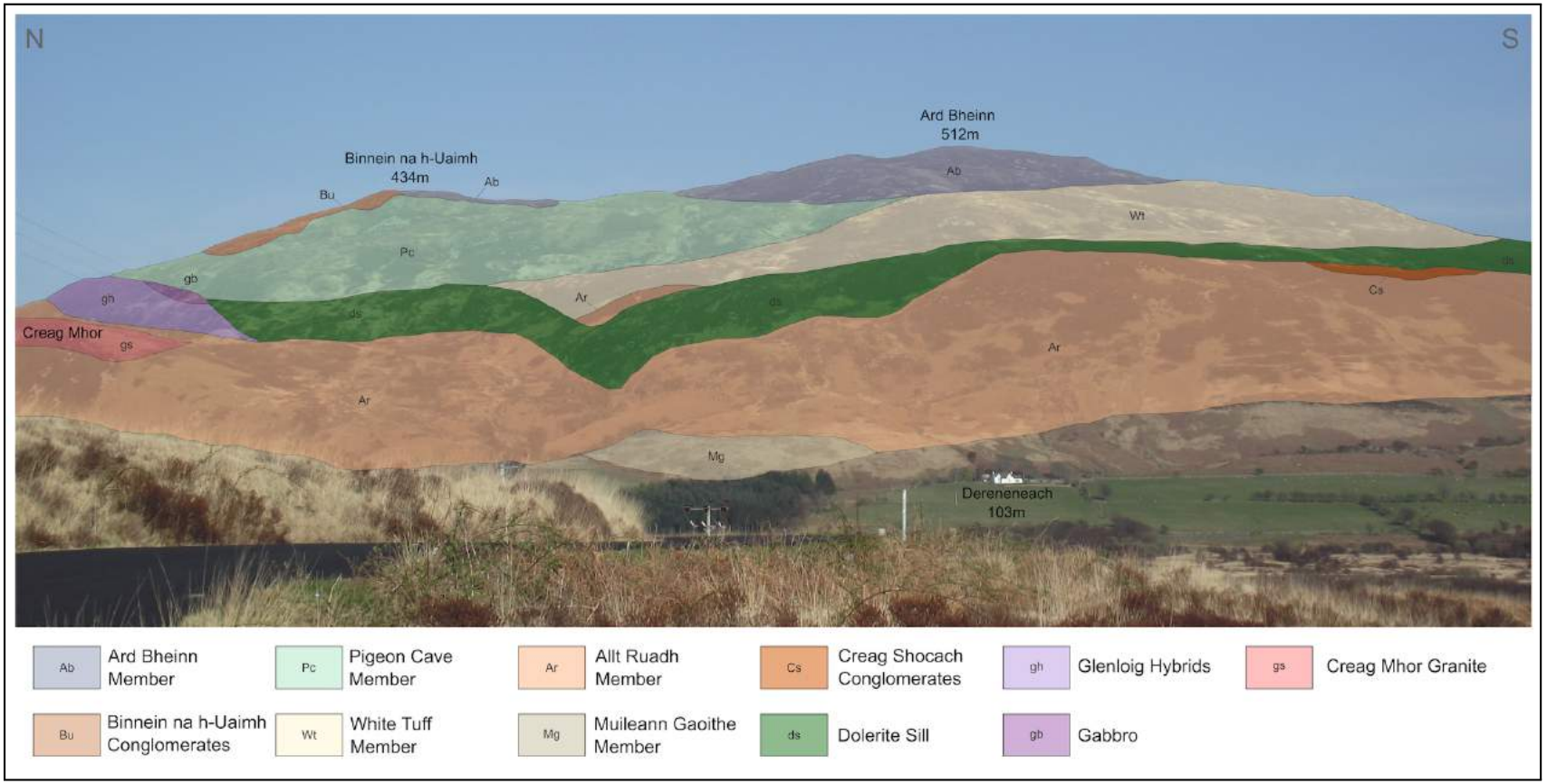

Fig. 3.2 – Overview of the hills Ard Bheinn and Binnein na h-Uaimh taken from the west. The coloured overlay shows the underlying geological units of the Arran Volcanic Formation. The uncoloured parts show areas underlain by the pre-caldera country rock. The summits of Ard Bheinn and Binnein na h-Uaimh are 670 m apart.

Table 3.1 – Explanation of ignimbrite lithofacies symbols used in this chapter, following the terminology of Branney and Kokelaar (2002).

Symbol	Meaning	Example lithofacies
m	massive	mT - massive tuff
s	stratified	sLT - stratified lapilli tuff
db	diffusely bedded	dbTcr - diffusely bedded crystal-rich tuff
L	lapilli	mLT - massive lapilli tuff
T	tuff	mT - massive tuff
Br	breccia	mBr - massive breccia
Ag	agglomerate	mLAg - massive lapilli agglomerate
l-l	lava-like	mTl-l - massive lava-like tuff
cr	crystal-rich	mTcr - massive crystal-rich tuff
v	vitrophyric	mTv - massive vitrophyric tuff
e	eutaxitic	mLTe - massive eutaxitic lapilli tuff

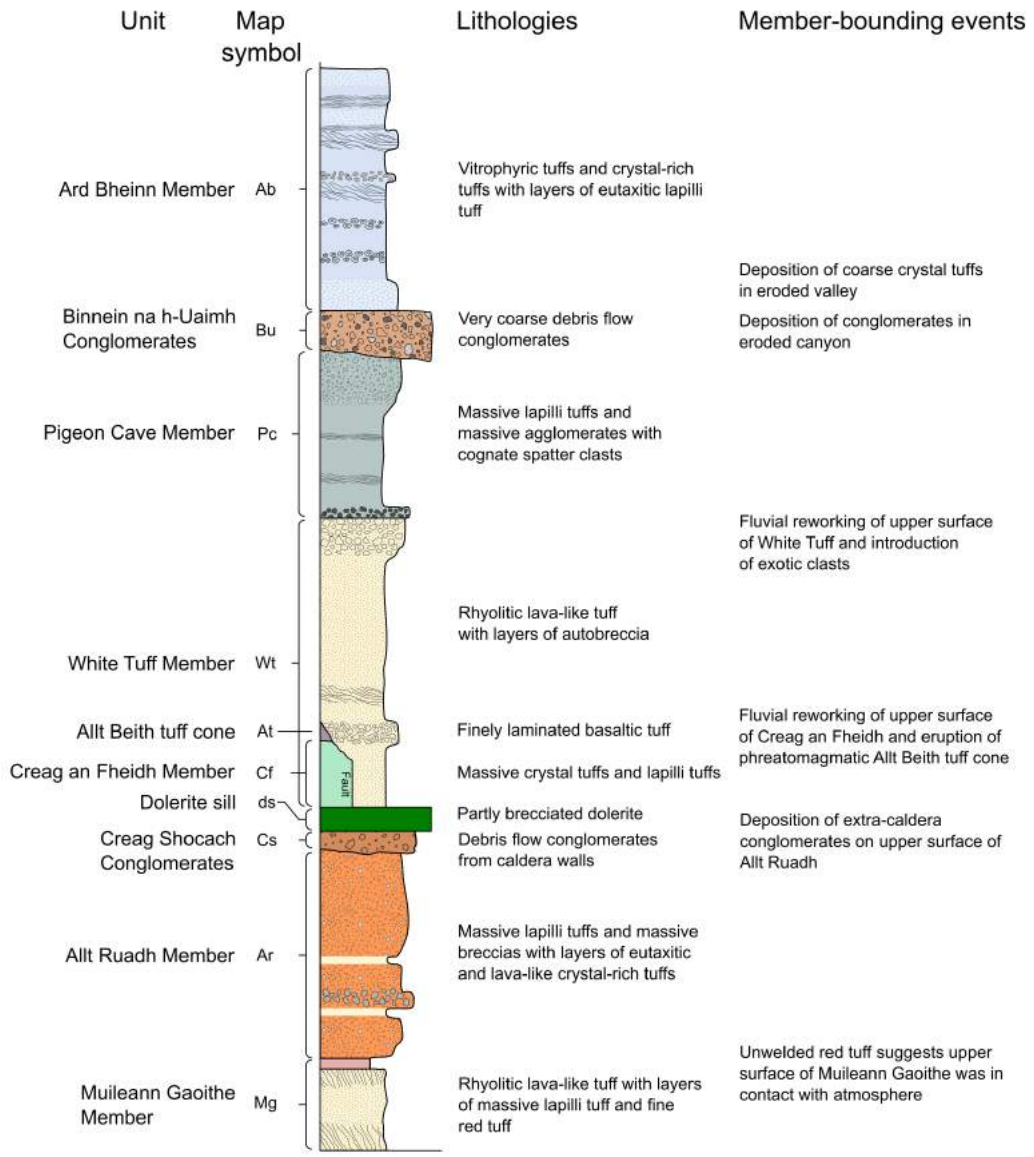

Fig. 3.3 – Generalised stratigraphic log of the Arran Volcanic Formation, showing the relationships between the pyroclastic and sedimentary units and major hiatus events. Vertical thicknesses are not to scale. Map symbols are consistent with those in Fig. 3.1.

3.1 Stratigraphy of the Arran Volcanic Formation

The general volcanic stratigraphy of the area is shown in Fig. 3.3. We assign the mappable pyroclastic units as individual members within the Arran Volcanic Formation, based on lithological variations between units, and the presence of mappable palaeotopographic surfaces. The general characteristics of each member (weathering colour, lithology, clast composition, etc.) are generally distinct enough to allow isolated exposures to be assigned to the appropriate unit. However, the upper surfaces of all members show evidence for fluvial reworking, erosion, deposition of sedimentary units, and/or prolonged contact with the atmosphere (Fig. 3.3), which all suggest volcanic hiatuses. Reddened units are tentatively used to identify either distinct members or intra-member eruptive/flow units whose surfaces have undergone prolonged exposure to the atmosphere (no features of true palaeosols such as rootlets or bioturbation were identified). Within members, deposition is assumed to be sustained with lithological differences reflecting variations in mass-flux and temperature during progressive aggradation of the ignimbrite (Branney and Kokelaar, 2002). Within certain members, cooling joints are used to identify distinct cooling units. The terminology used to describe the different lithofacies mapped here is given in Table 3.1 and follows the lithofacies code approach of Branney and Kokelaar (2002).

3.1.1 The Muileann Gaoithe Member

The Muileann Gaoithe Member is exposed in the cliffs on the southern side of Muileann Gaoithe [translation: *windmill*] ridge at the head of Glen Ormidale (Figs. 1.9, 3.4). Some small, isolated exposures near the farmhouse at Dereneneach (Fig. 3.1, 3.2) also belong to this unit. Its base is not seen, but at Muileann Gaoithe it seems to lie upon the Devonian and Permo-Triassic sandstones outside the caldera, which are exposed nearby.

A stratigraphic log up the south side of Muileann Gaoithe is shown in Fig. 3.5. The Muileann Gaoithe Member almost entirely comprises a white-weathering, homogeneous, glassy rhyolitic (77-79 wt.% SiO_2, Section 4.1.5) unit with abundant quartz, plagioclase, and K-feldspar crystals 0.5-2 mm in size (Fig. 3.6). Throughout the lower half and upper parts of the unit is a well-developed cm-scale flow fabric (Figs. 3.4, 3.5). This flow-banding is particularly striking at the base of the unit, where folds on the decimetre to metre-scale are preserved (Fig. 3.4). In the lower half of the unit, some layers and discontinuous lenses of non-glassy material containing lithic lapilli of sandstone and dolerite are interbedded with the glassy rhyolite.

Fine, thinly bedded, highly altered red material forms thin layers half-way up the Muileann Gaoithe section, as well as on the upper surfaces of the unit both at Muileann Gaoithe and Dereneneach.

Petrography

Fig. 3.6 shows photomicrographs of ignimbrites from the bottom, (Fig. 3.6a,b), middle (Fig. 3.6c), and top (Fig. 3.6d) of the Muileann Gaoithe Member. An EDS major element map of the flow-banded sample from the base of the unit is shown in Fig. 3.7.

The groundmass of the flow-banded lava-like ignimbrite contains continuous bands of lighter and darker material (Fig. 3.6a [1]). These bands are divided into relatively course, Si-rich layers up to 1 mm thick, and finer banded Si-poor layers (Figs. 3.6a, 3.7). These layers show chemically distinct Al and K-rich bands and relatively Na-rich bands. The crystal cargo is dominated by rounded to euhedral quartzes up to 1 mm in size. The other crystals are equal proportions of K-feldspar and Na-rich plagioclase (An_2 – An_9; Fig. 3.8). Small red minerals on the element map are Fe, Mg, Al rich amphiboles which resemble the chemistry of gedrite. The large purple object on the left edge of the element map that disrupts banding does not have the same chemistry as the K-feldspars, so may be a clast of a K-rich glass.

The dolerite-lapilli-bearing samples from near the base of the unit (Fig. 3.6b) do not show well developed flow banding, but have a similar rhyolitic glassy matrix, and the same quartz and feldspar crystal cargo. The dolerite itself comprises <500 µm euhedral laths of plagioclase in a matrix of chlorite and Fe-Ti oxides that presumably formed from the breakdown of olivine and pyroxene.

The central portion of the Member does not display any foliation at the outcrop scale (Fig. 3.5), and this is reflected in the thin section (Fig. 3.6c). The glassy rhyolitic matrix in this sample is homogenous and devitrified. K-feldspar crystals in this unit are up to 2 mm.

A sub-millimetre flow fabric texture can be seen in thin sections of the upper parts of the unit (Fig. 3.6d [2]). This fabric is defined by sub-millimetre to near-continuous bands and prolate rods that may have originated as vitroclastic shards or fiamme. As well as the quartz and feldspar crystals seen throughout the unit, these samples contain small lithic lapilli, including the partially recrystallised sandstone shown in Fig. 3.6.

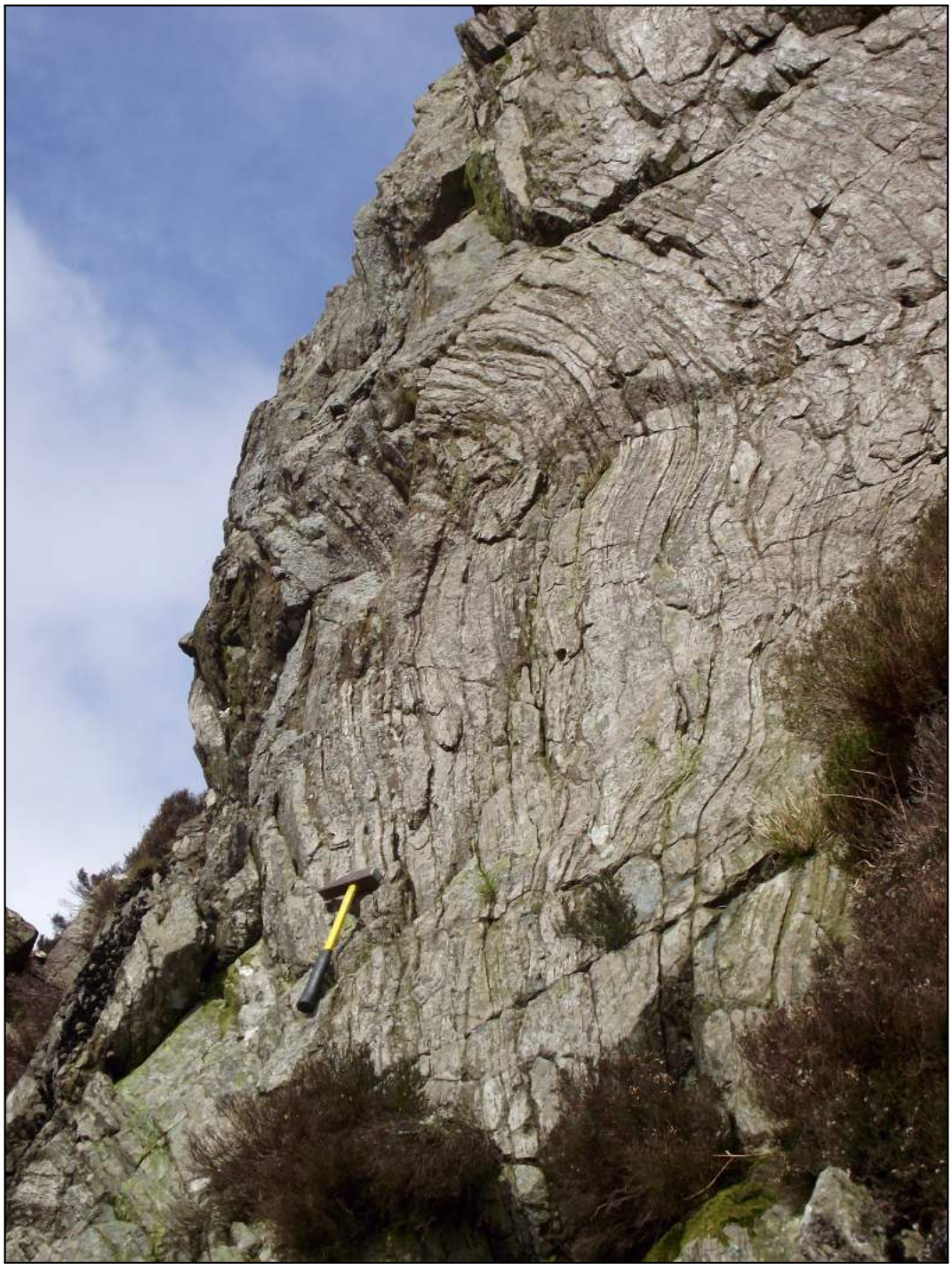

Fig. 3.4 – Photograph of folded flow banding in rhyolitic lava-like ignimbrites on the southern side of the Muileann Gaoithe ridge. NR 985 350, looking west.

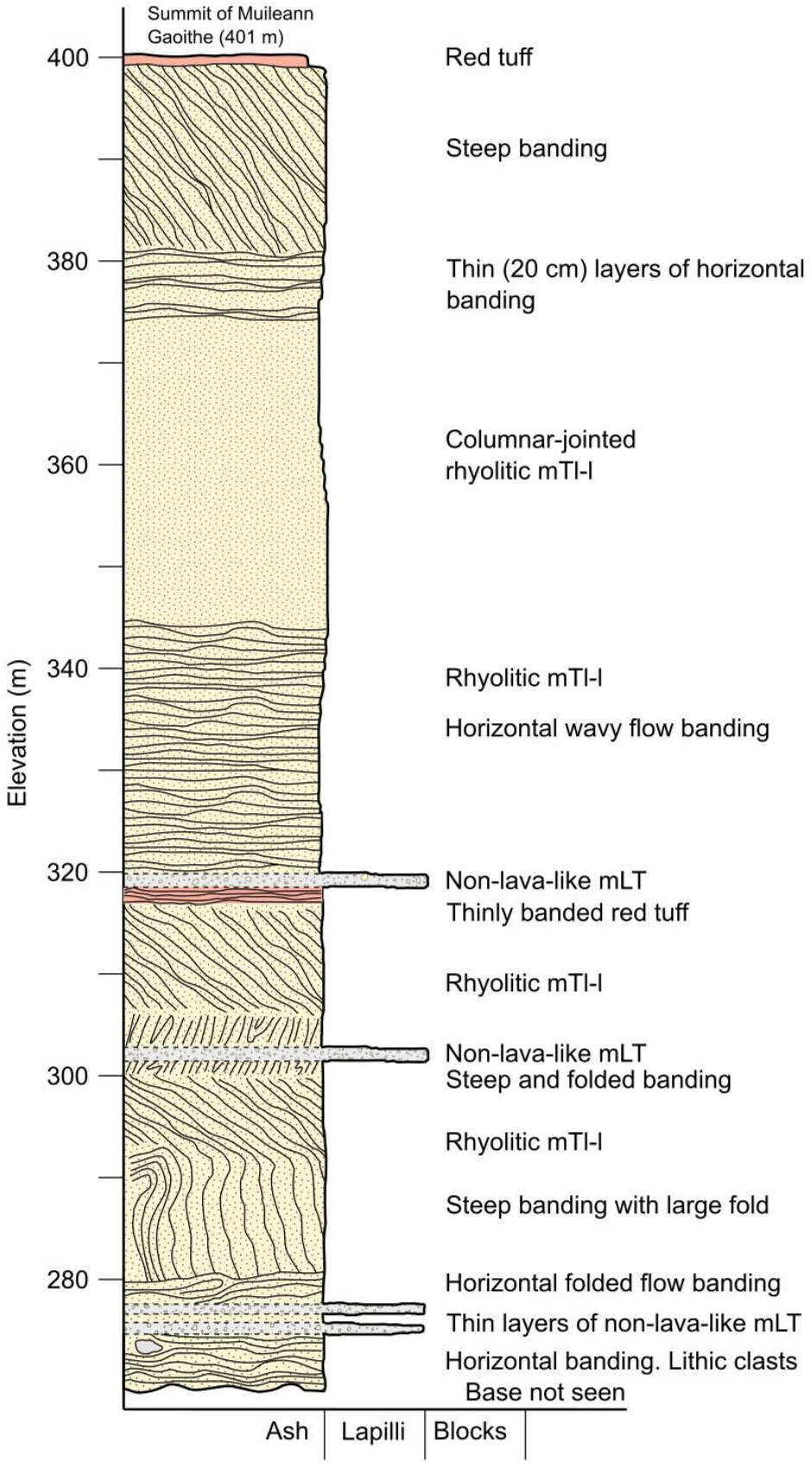

Fig. 3.5 – Stratigraphic log of the Muileann Gaoithe Member up the southern side of the Muileann Gaoithe ridge, from NR 985 350 to 984 350.

Interpretation

The Muileann Gaoithe Member is interpreted as an ignimbrite, due to the lack of visible upper/lower autobreccias, grading between different ignimbrite lithofacies, and the micro-scale parataxitic to lava-like texture. We here use 'parataxitic' to describe discontinuous bands and rods, indicating an ignimbrite grade higher than eutaxitic, but not as completely sheared as a fully lava-like texture, seen in Fig. 3.6d [2]. Because of the pervasive micro-scale flow fabric, and obliteration of glass-shard-pyroclasts (Fig. 3.6a,d), we suggest that the white-weathering rhyolitic portions of the unit should be classed as massive lava-like tuff (mTl-l). The non-lava-like clast-bearing layers are interpreted as lapilli tuffs. Although they form discrete, thin layers, they are internally structureless, so are therefore classed as massive lapilli tuffs (mLT). The fine, red-weathering material is very altered and poorly exposed, but these layers are interpreted as non-welded tuffs (T) that were exposed to the atmosphere for some time.

The microtextural features in the rhyolitic portion of this unit suggest that this is a very high-grade ignimbrite of 'Snake River type' (Andrews and Branney, 2011), indicating rapid deposition from a high temperature, (>900°C) high-mass-flux pyroclastic density current. These ignimbrites are thought to be formed by high-temperature, low-fountaining eruptions that do not entrain much atmospheric air, and therefore retain large amounts of heat (e.g. Branney et al., 1992).

The Muileann Gaoithe Member on Muileann Gaoithe (Fig. 3.5) is composed of two eruptive units, each capped by a layer of red tuff, representing the surface of the ignimbrite sheet in contact with the atmosphere prior to deposition of the next unit. The layers of lapilli tuff represent changes in flow-boundary conditions within the aggrading ignimbrite, which may reflect increased explosivity at the vent.

Fig. 3.6 ***(facing page)*** – Photomicrographs of ignimbrites from the Muileann Gaoithe Member. Q = quartz, F = feldspar. **a)** Sample BJG/17/1 from the base of the Muileann Gaoithe Member. The matrix displays continuous bands of glassy material defined by colour and texture [1]. plane-polarised light. **b)** Sample BJG/17/2 from just above the base of the Muileann Gaoithe Member. It contains rounded clasts of dolerite (dol). plane-polarised light. **c)** Sample BJG/17/23 from the central part of the Muileann Gaoithe Member. Bottom left = crossed polars, top right = plane-polarised light. **d)** Sample BJG/15/31 from the top of the Muileann Gaoithe Member. It contains rounded clasts of recrystallised sandstone (ss). The matrix displays non-continuous bands of glassy material defined by colour and texture [2]. Top left = crossed polars, bottom right = plane-polarised light.

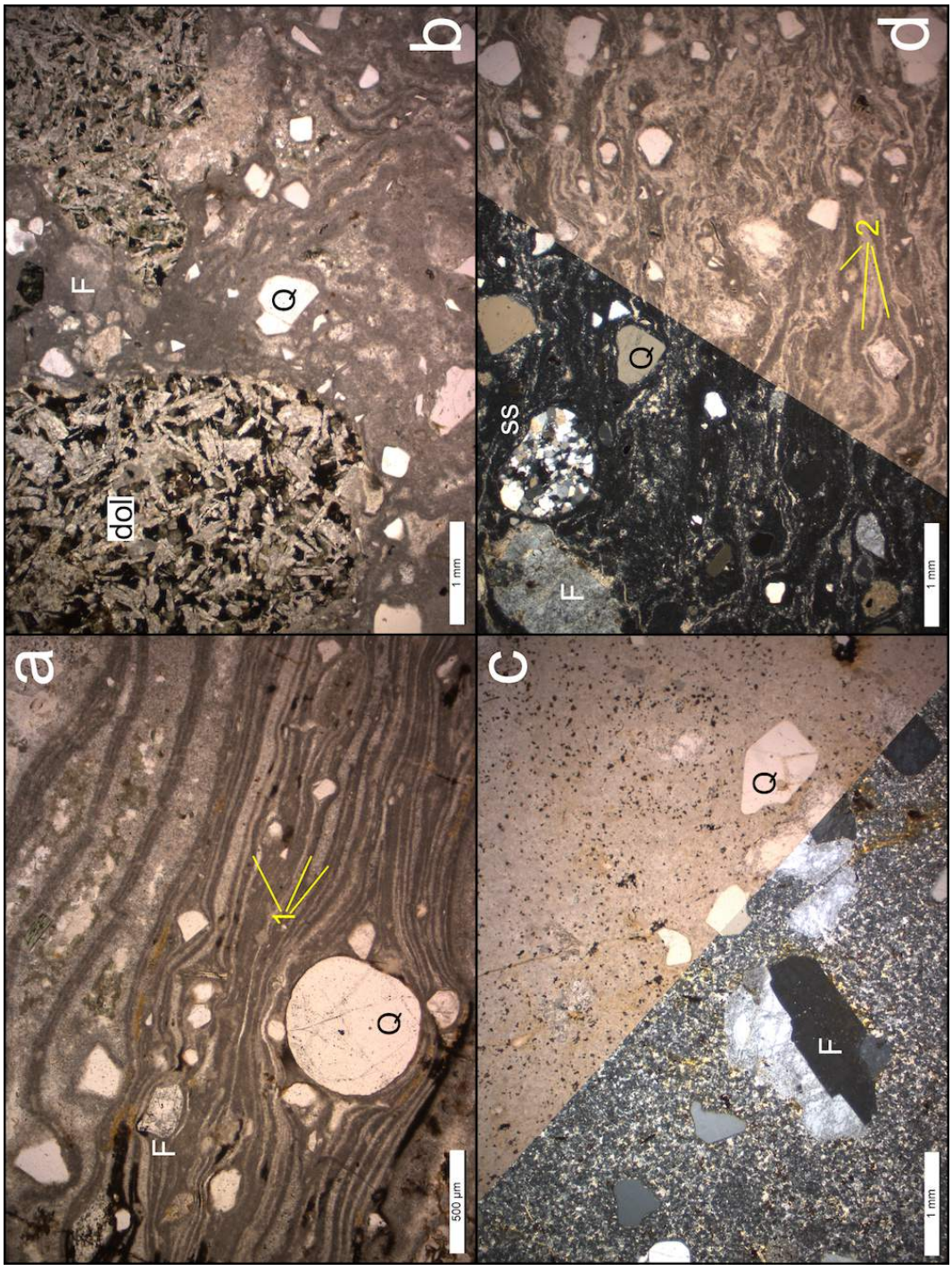
a
Q
F
500 µm
b
F
Q
dol
1 mm
c
Q
F
1 mm
d
2
Q
ss
F
1 mm

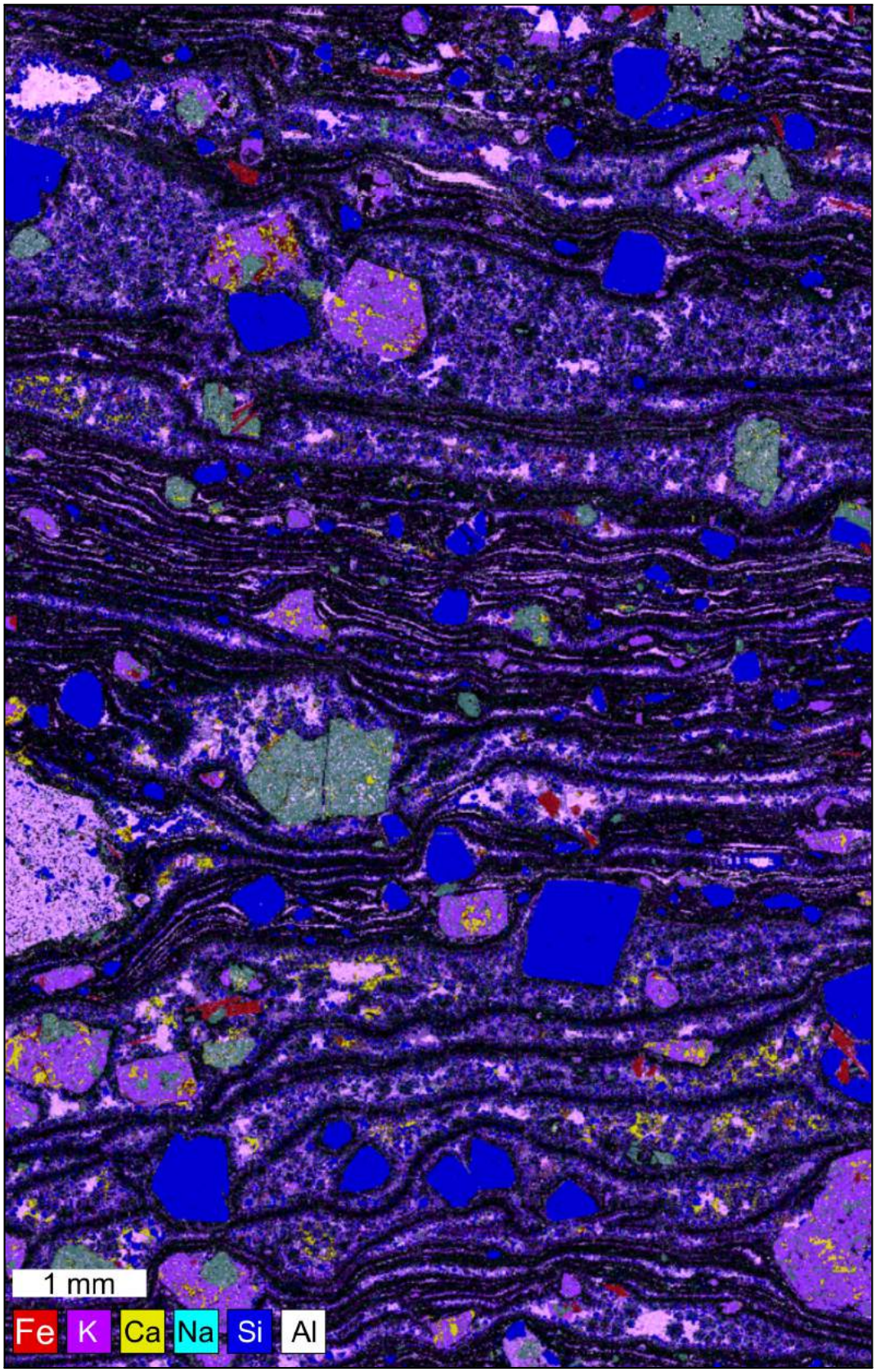

Fig. 3.7 – Major element EDS map of sample BJG/17/1, from the base of the Muileann Gaoithe Member. Using this element-based colour scheme, quartz is blue, K-feldspar is purple, and plagioclase is turquoise. Fe-Ti oxides are red.

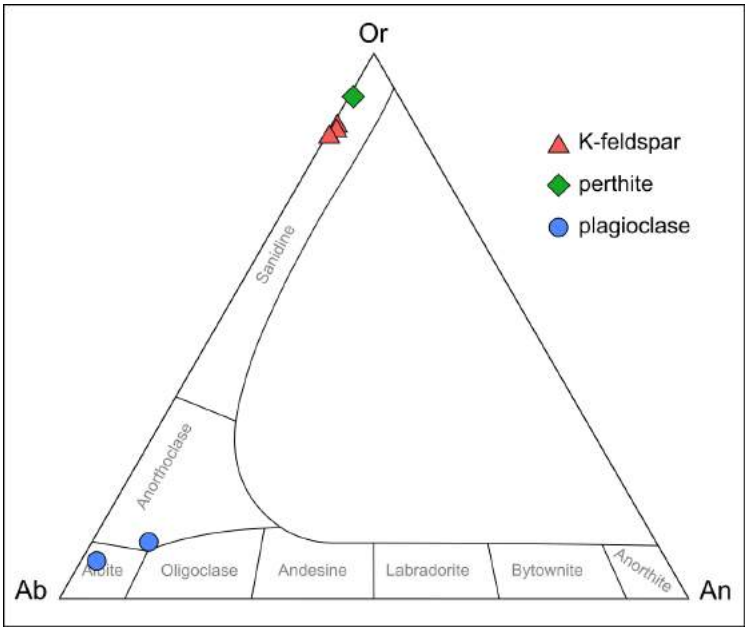

Fig. 3.8 – Ternary plots of EDS data from feldspar crystals in Sample BJG/17/1 from the Muileann Gaoithe Member.

3.1.2 The Allt Ruadh Member

The Allt Ruadh Member (Fig. 3.9) is the most extensive unit of the AVF at the current level of erosion (Fig. 3.1), and was possibly one of the most voluminous. Its type locality is the Allt Ruadh [translation: *red stream*, possibly after the orange-weathering ignimbrites exposed in its banks], a small stream in the south west of the complex, in which a near-complete vertical stratigraphy is exposed (Fig. 3.10). The Allt Ruadh Member also crops out in Ballymichael Glen, on the hillsides between Dereneneach and Creag Mhor, in the lower parts of Glen Craigag, and on the slopes of A' Chruach (Fig. 3.1). The lower contact of the Allt Ruadh Member is not seen, apart from a small stream exposure near Glenloig, where it overlies the Glenloig Hybrids. Near Dereneneach, the Allt Ruadh Member overlies the poorly exposed Muileann Gaoithe Member (Fig. 3.2), although the contact is not directly observed.

The Allt Ruadh Member (Fig. 3.10) comprises dominantly massive lapilli tuffs (mLT), with clasts of pre-Palaeogene sedimentary and metamorphic rocks, Palaeogene ignimbrites, and basaltic material (Figs. 3.9, 3.11). The majority of the mLT in the Allt Ruadh Member displays distinctive orange weathering (Fig. 3.9). In the Allt Ruadh section (Fig. 3.10), this coarse orange-weathering lithology makes up about half of the thickness of the unit. In other, less well-exposed areas, it comprises almost 100% of the exposure.

The size and lithology of the lithic lapilli changes both vertically and laterally across the complex, with blocks of ignimbrite over 600 mm in diameter found in the mLT in Glen Craigag. In places, these large blocks dominate the lithic clast population, meaning that the lithofacies in some places approaches massive breccia (mBr). Some thin layers of clast-poor ignimbrite are present. These glassy tuffs and eutaxitic quartz-feldspar crystal tuffs (Fig. 3.10) are only exposed in stream sections, so cannot be traced laterally.

Petrography

Fig. 3.11a–c and Fig. 3.12 show photomicrographs and an EDS major element map of typical Allt Ruadh mLT. A photomicrograph and EDS element map of the eutaxitic- to lava-like crystal tuff found in discrete layers within the Allt Ruadh Member are shown in Figs. 3.11d and 3.13, respectively.

The matrix of the all of the mLT is a brown glass that has been altered and devitrified. They all contain quartz and feldspar crystals, with the plagioclase crystals in sample BJG/15/3 having compositions of An_2 – An_{14} (Fig. 3.14a). The K-feldspar crystals also display a restricted range of compositions (Fig. 3.14a), suggesting that the crystals found within these mLTs are derived from the erupting magma rather than inherited from the eroding vent/substrate from which the lithic clasts were derived. The range of lithic lapilli is shown in Fig. 3.11a–c. Rhyolites and lava-like ignimbrites are shown as silicic, often flow-banded or spherulitic devitrified glasses. Basalt clasts are darker and fine grained, with a large number of small Fe-Ti oxide crystals. Fig. 3.11a shows a clast of basalt with <1 mm vesicles and amgydales. Dolerite clasts are similar to those seen in the Muileann Gaoithe ignimbrites, *i.e.*, <500 µm plagioclase laths with a groundmass of chlorite and opaque minerals. Many clasts of ignimbrite (not shown) are glassy, white, and contain abundant quartz and feldspar crystals, so presumably come from the underlying Muileann Gaoithe Member.

The layers of eutaxitic- to lava-like ignimbrites found as thin horizons between the mLTs (Figs. 3.11d, 3.13) have a glassy groundmass that displays some flow banding, which are shown on the EDS major element map (Fig. 3.13) as thin Si and K-rich and Si and K-poor bands. By far the most common crystal phase is plagioclase. This exists as euhedral laths as well as square and rounded anhedral crystals. These are albite in composition (An_3 – An_{10}; Fig. 3.14b). Quartz is less abundant and <1mm, and there is no K-feldspar. Minor amounts of sphene, amphibole, and Fe-Ti oxides are also present.

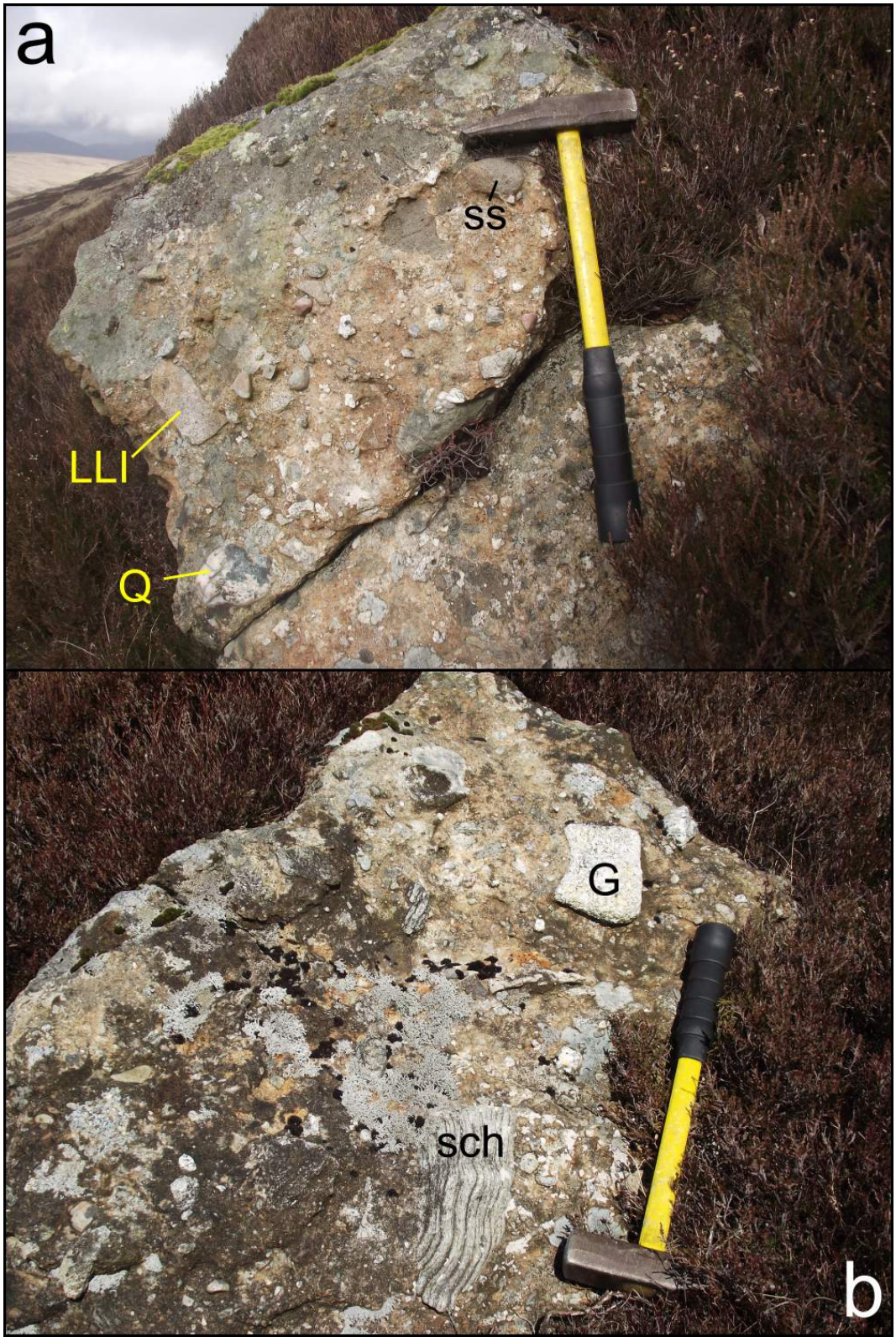

Fig. 3.9 – Photographs of typical orange-weathering mLT of the Allt Ruadh Member, containing a variety of lithic clasts. Q = quartzite, LLI = lava-like ignimbrite, ss = sandstone, G = granite, sch = schist.

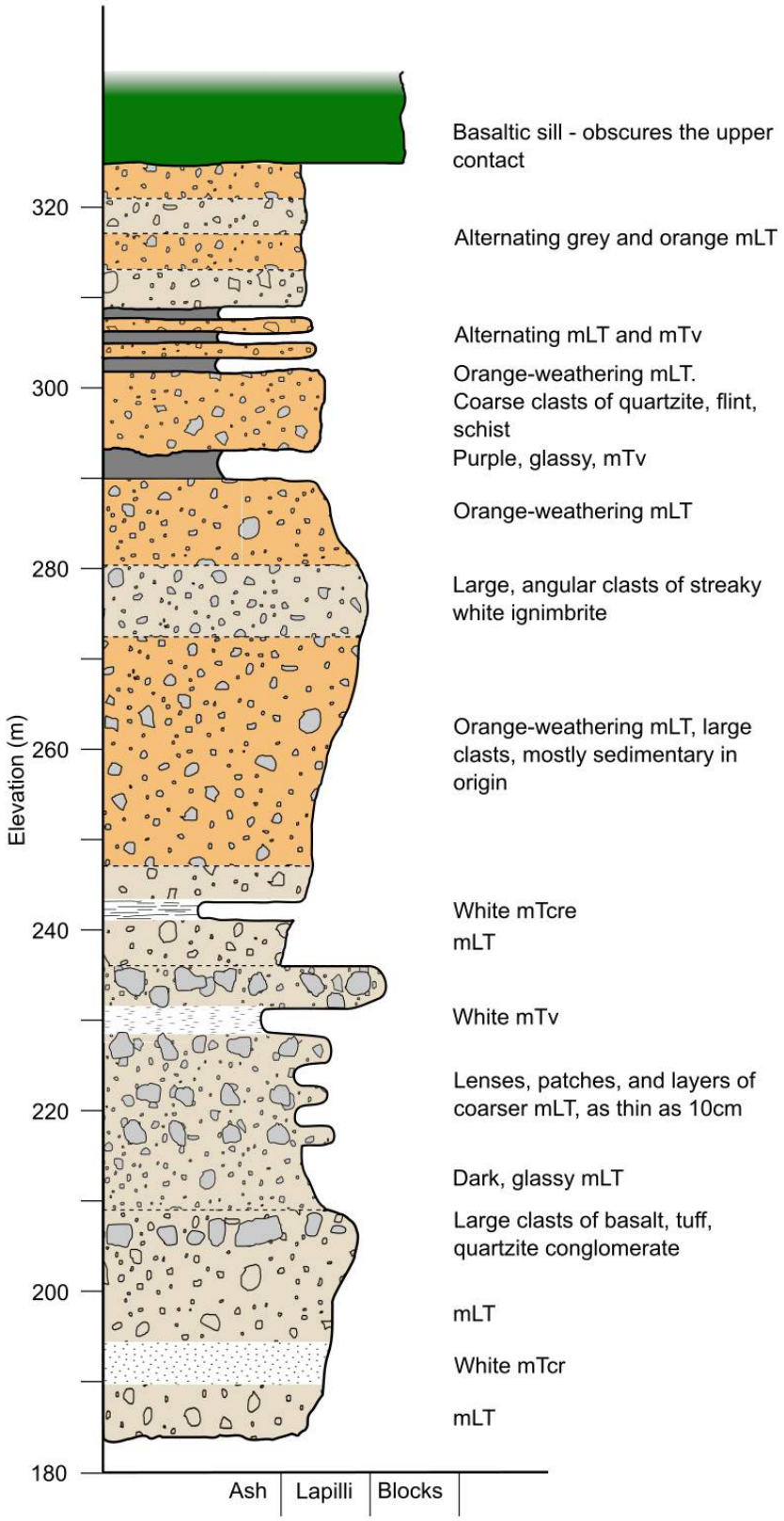

Fig. 3.10 – Stratigraphic log of the Allt Ruadh Member along the Allt Ruadh (log 1 on Fig. 3.1).

Interpretation

The Allt Ruadh Member is interpreted as representing a prolonged, highly explosive phase of volcanism in which there was a large volume of material ejected from the underlying magma chamber. This phase of volcanism is suggested to record deposition from a pyroclastic density current at a flow-boundary zone dominated by fluid-escape, with very little turbulent shear-induced tractional segregation (Branney and Kokelaar, 2002). These deposits are thought to record very highly explosive Plinian eruptions. The mBr observed in places within the member suggests occasional higher-energy conditions at the vent. Given the abundance of Muileann Gaoithe lava-like ignimbrite clasts within the mLT and mBr, the lithic clasts are interpreted as being sourced largely from erosion of the substrate by the pyroclastic density current.

The clast-free eutaxitic layers record phases of lower explosivity, in which accidental lithics and atmospheric air were not entrained, leading to higher temperatures within the aggrading pyroclastic density current. The thin, dark, glassy tuffs near the top of the Allt Ruadh section (Fig. 3.10) may be basal vitrophyres to the overlying packages of mLT. This would suggest pulses of eruption, rather than a single, sustained pyroclastic density current.

Clasts of granite

Several lithic clasts of granite have been observed in the Allt Ruadh mLTs (Fig. 3.9b). Two of these samples have been collected for petrographic and geochemical analysis. EDS major element maps for these samples are shown in Figs. 3.15 and 3.16. The first shows a typical two-feldspar muscovite granite. All K-feldspars are perthitc, with the smaller crystals showing patchy exsolution, and the larger crystals showing typical 'tiger-stripe' albite (An_1 – An_3; Fig. 3.14c) exsolution. Plagioclases (An_4 – An_{18}) all have relatively sodic rims (Fig. 3.15).

The EDS major element map of the other granite clast (Fig. 3.16) shows the edge of the clast and its contact with the host ignimbrite. In the far left of the image,

Fig. 3.11 ***(facing page)*** – Photomicrographs of ignimbrites from the Allt Ruadh Member. LLI = lava-like ignimbrite, B = Basalt, R = rhyolite, dol = dolerite, sch = schist. All shown in plane-polarised light. **a)** Sample BJG/15/3, a mLT from the lowest exposed part of the Allt Ruadh Member. Note the vesicular nature of the basalt clast. **b)** Sample BJG/15/6, a mLT from the middle of the unit. **c)** A different section of Sample BJG/15/6. **d)** Sample BJG/17/13, a lava-like tuff from the middle of the unit, containing abundant feldspar crystals.

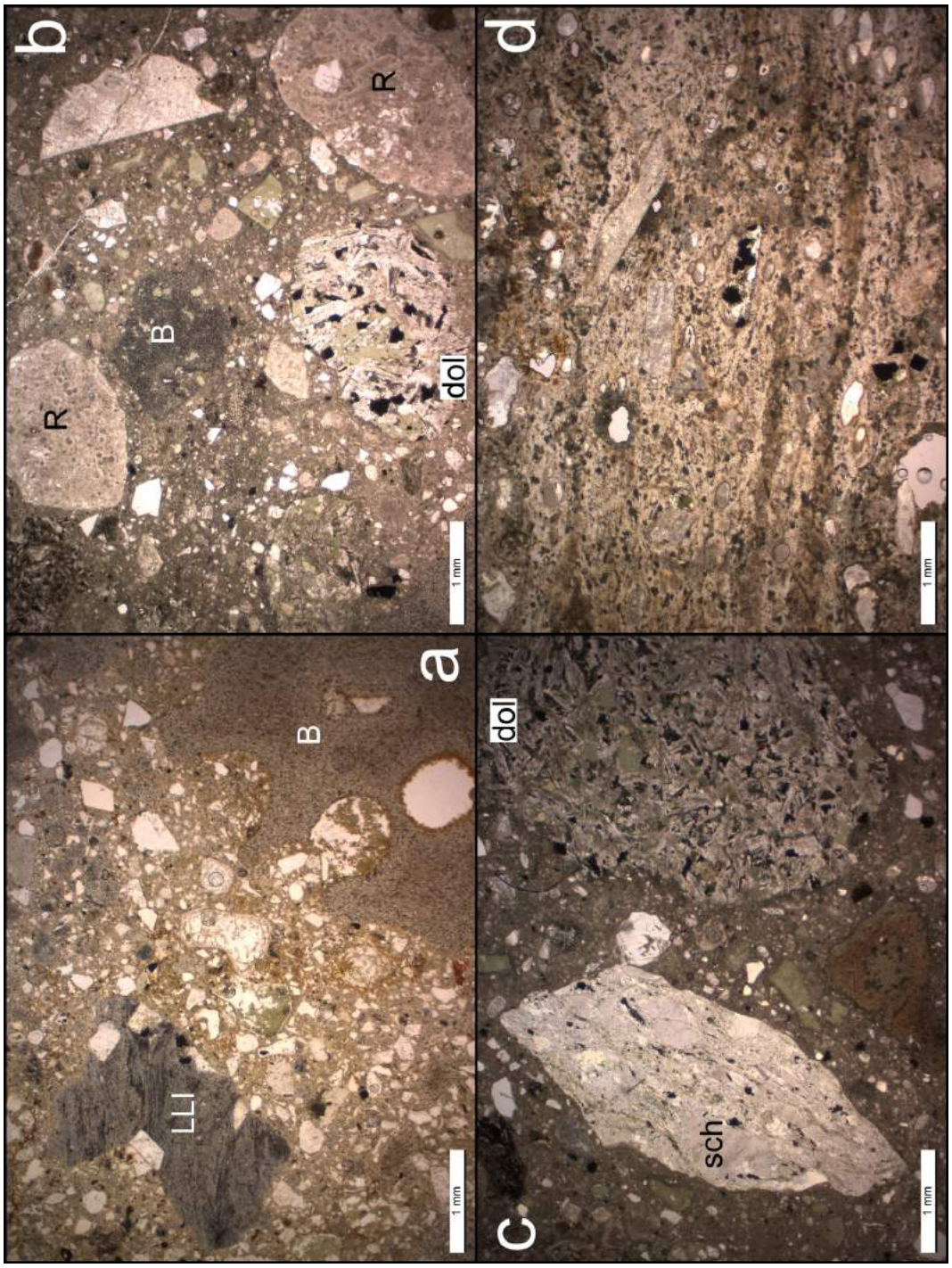
a
LLI
B
1 mm
b
R
B
dol
R
1 mm
c
dol
sch
1 mm
d
1 mm

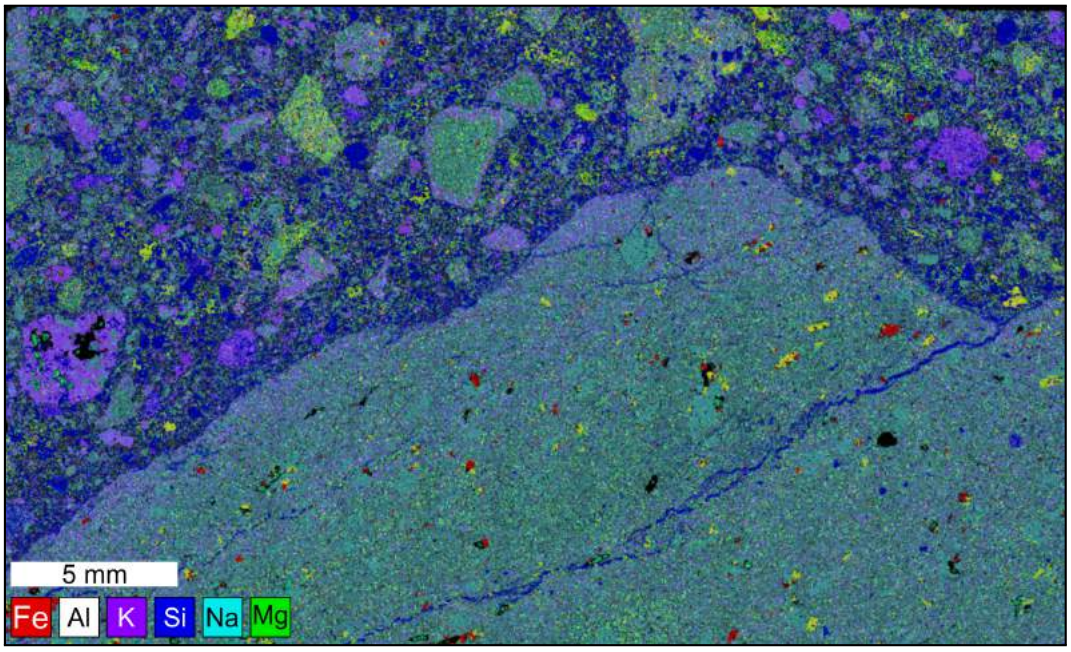

Fig. 3.12 – Major element EDS map of mLT sample BJG/15/3, showing a variety of lithic clasts in a silicic ashy matrix. Using this element-based colour scheme, quartz is blue, plagioclase is yellow, and Fe-Ti oxides are red. Mafic clasts are generally green due to high Mg, while more felsic clasts are purple.

the granite is petrographically similar to the other clast *i.e.*, a two-feldspar granites containing perthitic K-feldspar. However, close to the edge of the clast, the presence of K significantly decreases, leaving a plagiogranite (Fig. 3.16). This could be due to original lithological variation within the intrusion, but it could also be due to mobilisation and removal of K during weathering and alteration.

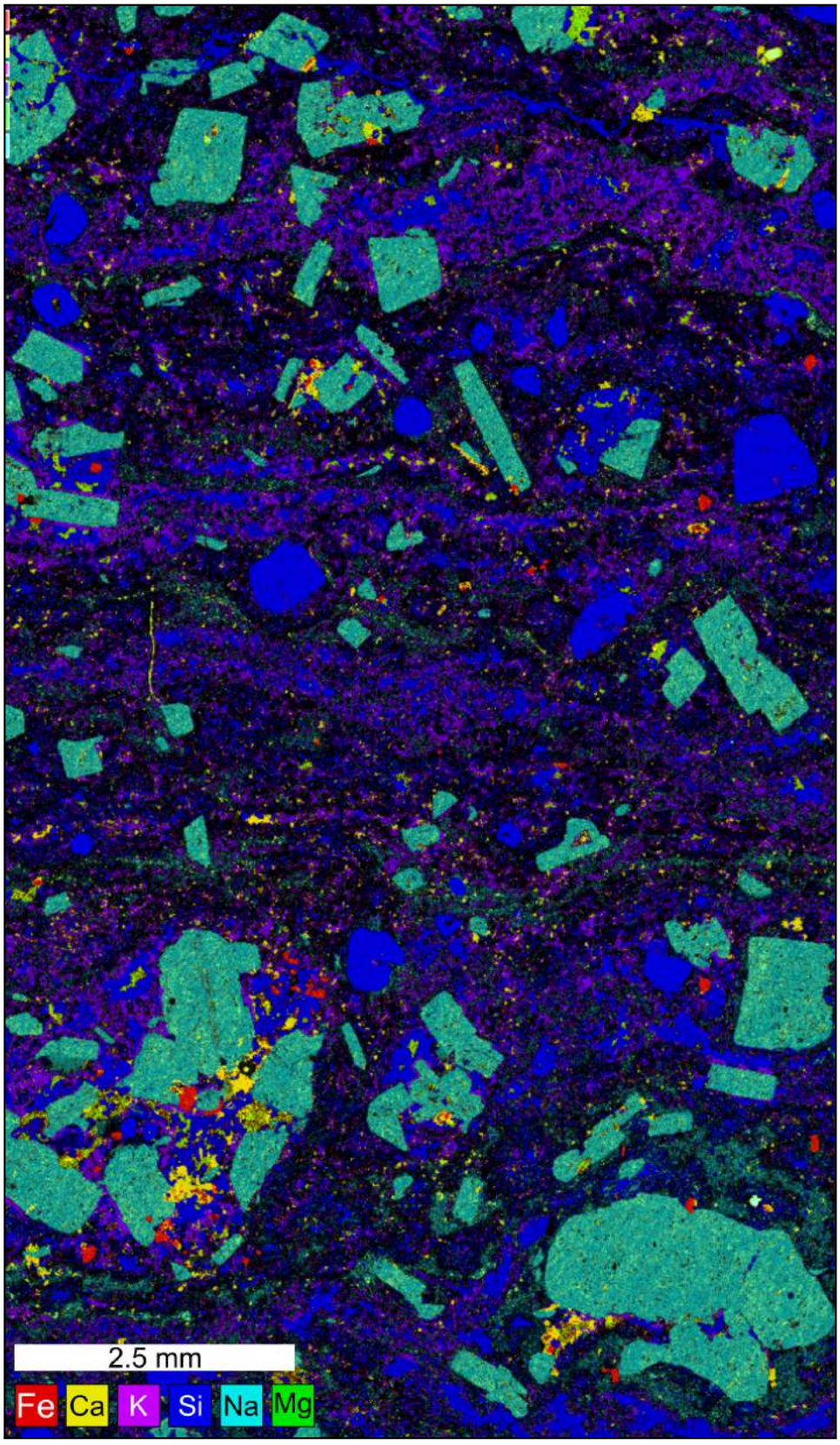

Fig. 3.13 – Major element EDS map of sample BJG/17/15, a crystal-rich lava-like ignimbrite from the Allt Ruadh Member. Using this element-based colour scheme, quartz is blue, plagioclase is turquoise, Fe-Ti oxides are red, and sphene is yellow.

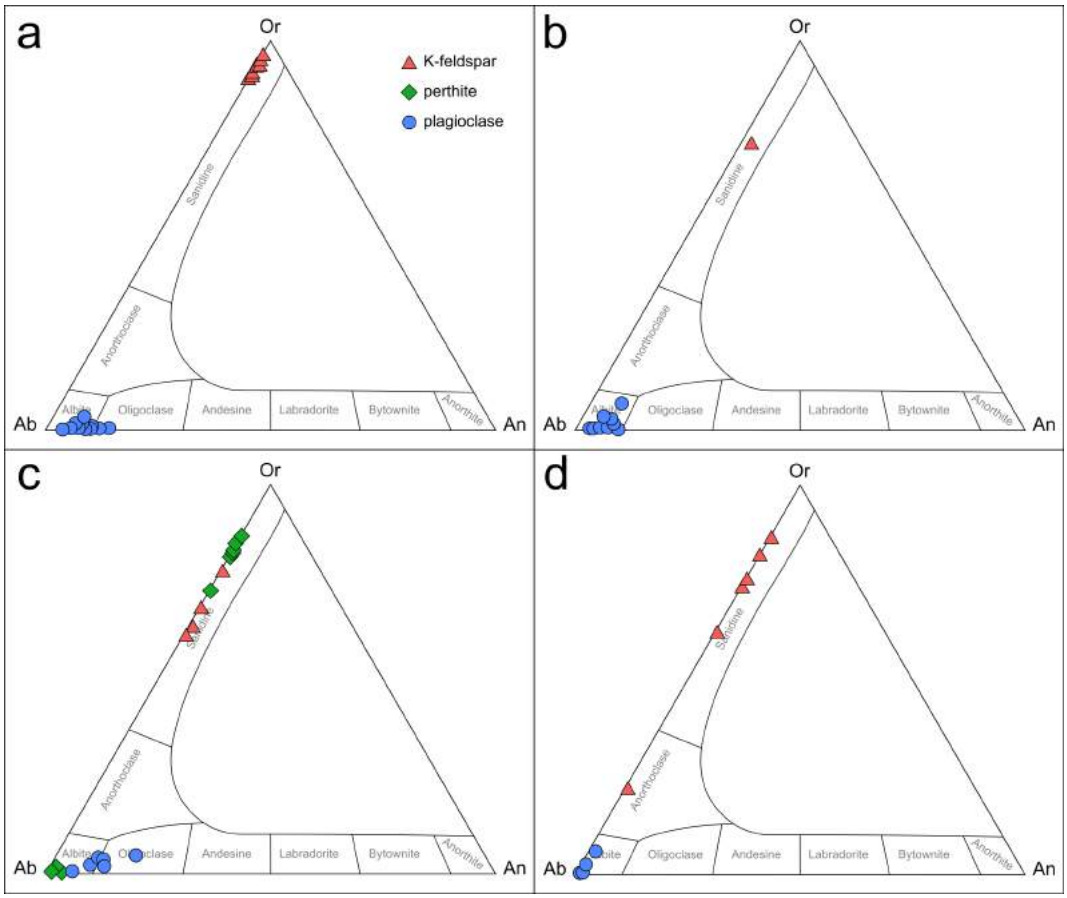

Fig. 3.14 – Ternary plots of EDS data from feldspar crystals in the Allt Ruadh Member. **a)** Feldspars from sample BJG/15/3, mLT at the base of the unit. **b)** Sample BJG/17/15, a crystal-rich lava like ignimbrite. **c)** Sample BJG/17/16, a clast of granite found in the Allt Ruadh Member mLT. **d)** Sample BJG/16/42, a clast of granite found in the Allt Ruadh Member mLT.

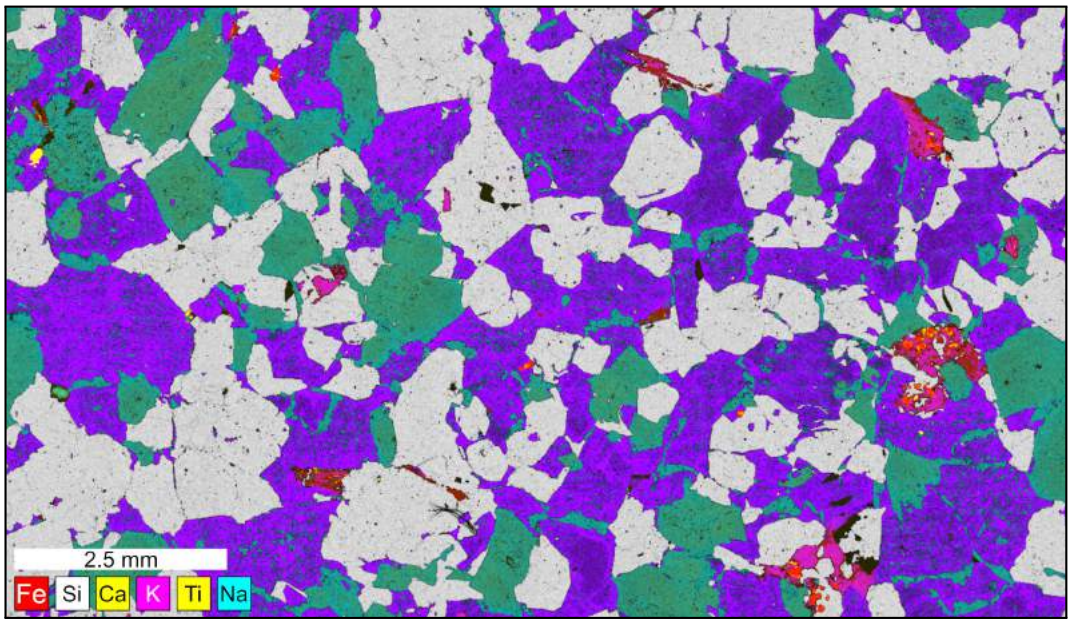

Fig. 3.15 – Major element EDS map of sample BJG/17/16, a clast of granite found in the Allt Ruadh Member mLT. Using this element-based colour scheme, quartz is grey, plagioclase is green, and perthitic K-feldspar is purple, with green sodic exsolution lamellae. Muscovite is magenta and chlorite is dark red. Fe oxides are red, Fe-Ti oxides are orange, and sphene is yellow.

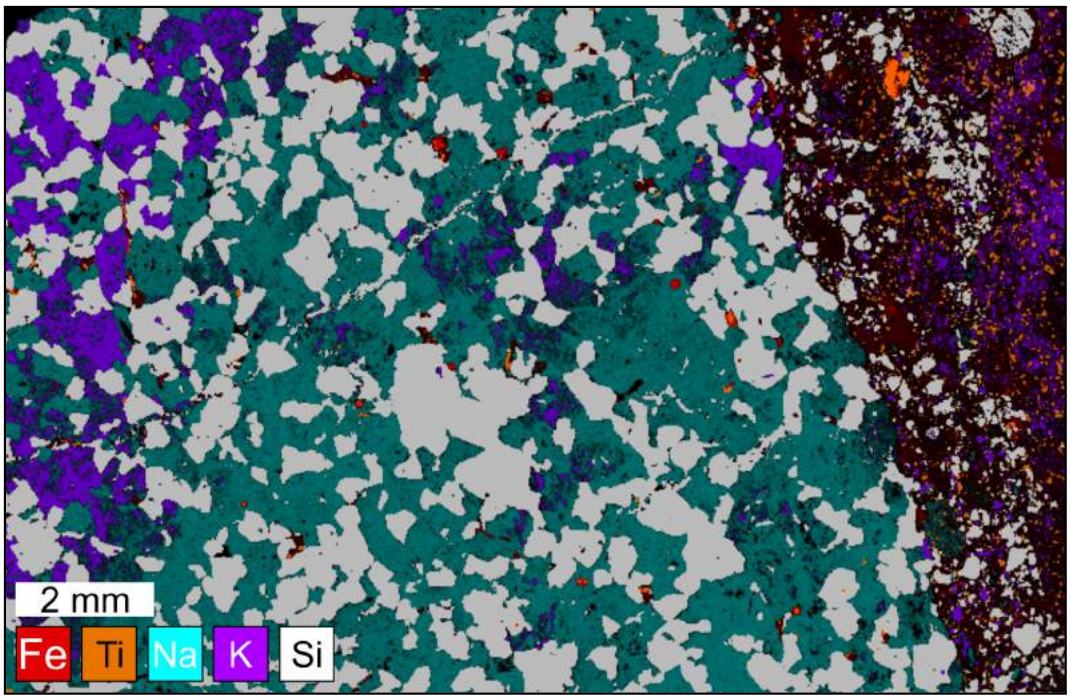

Fig. 3.16 – Major element EDS map of sample BJG/16/42, a clast of granite found in the Allt Ruadh Member mLT. Using this element-based colour scheme, quartz is grey, plagioclase is turquoise, K-feldspar is purple, Fe oxides are red, Fe-Ti oxides are orange, and Fe-rich amphibole is dull red. The fine-grained unit to the right is the host ignimbrite.

3.1.3 The Creag Shocach Conglomerates

Directly overlying the Allt Ruadh Member are some isolated outcrops of red sedimentary conglomerates and breccias (Fig. 3.3). These are found as a thin layer below the dolerite sill west of the Ard Bheinn summit (Fig. 3.2), and as the prominent crags of Creag Shocach [translation: *snout crag*] above Glenloig (Fig. 3.1). The Ard Bheinn outcrop is found at a lower elevation than some of the surrounding exposures of Allt Ruadh mLT (Fig. 3.2), suggesting deposition in low points on a highly topographical erosional surface. The clasts in these breccias and conglomerates are almost exclusively of the pre-Palaeogene lithologies exposed nearby (*i.e.*, medium- to coarse-grained red sandstones and quartzite conglomerates; Fig. 3.17). The matrix is mostly composed of fine- to medium-grained rounded quartz sand. The clasts in the Creag Shocach conglomerate (Fig. 3.17b) are larger (high proportion of cobbles) and generally rounder than those on Ard Bheinn (Fig. 3.17c). However, due to their similar stratigraphic position (overlying the Allt Ruadh Member) and similar matrix and clast lithologies, they are assigned to the same unit.

Interpretation

The Creag Shocach conglomerates are interpreted as representing erosion of Devonian and Permo-Triassic lithologies from topographic highs (possibly caldera walls) into the caldera by fluvial or mass wasting processes during the post-Allt Ruadh period of volcanic quiescence. The outcrops on Creag Shocach (Fig. 3.17a,b) are coarser, and have a massive, largely clast-supported structure. This could indicate that these exposures are proximal to the eroded source and were deposited as high energy debris flows. The Ard Bheinn exposures (Fig. 3.17c) are generally finer, matrix-supported, and show small channels and lenses of clast-free sandstones. This could indicate a more distal environment dominated by fluvial processes.

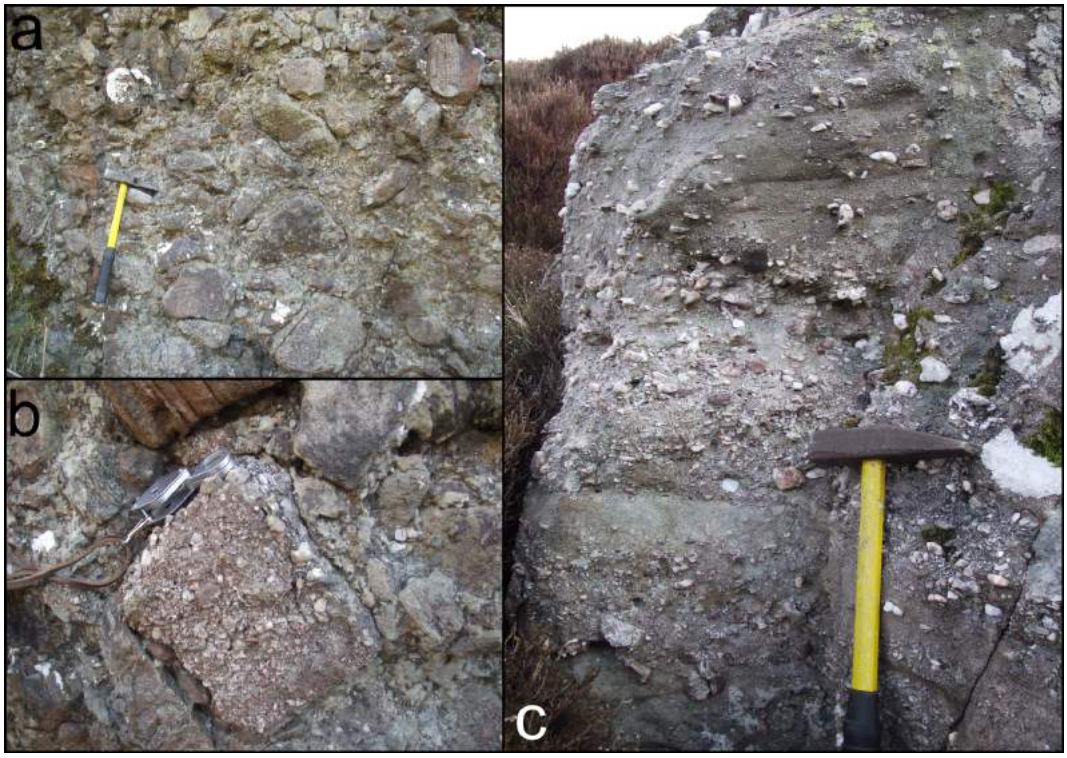

Fig. 3.17 – Photographs of the Creag Shocach Conglomerates. **a)** Very coarse conglomerates on Creag Shocach. **b)** Detail of a cobble of gritstone in the conglomerate on Creag Shocach. **c)** Sandstones and conglomerates on the western slopes of Ard Bheinn.

3.1.4 The Creag an Fheidh Member

The Creag an Fheidh [translation: *deer crag*] Member is named for a small line of crags 500 m south of Glenloig, where it is best exposed and can be traced almost vertically through its succession. The volcanic rocks belonging to this unit (Fig. 3.18) make up topographic shelves at ~300 m elevation, along both sides of Glen Craigag (Fig. 3.1). The Creag an Fheidh section exposes a vertical thickness of around 80 m (Fig. 3.19), from the contact with the underlying Allt Ruadh Member to the overlying White Tuff Member. At its western extent, the Creag an Fheidh Member is cut off by the same fault that truncates the intra-caldera outcrop of Glenloig Hybrids (Fig. 3.1).

The lower parts of this unit (which are only well-exposed on Creag an Fheidh, and may not be laterally extensive) are predominantly lithic-poor tuffs and crystal tuffs (mT and mTcr; Fig. 3.20). Some of the lithic- and crystal-poor glassy tuffs (mTv) display bedding-parallel flow fabrics (Fig. 3.19). Minor layers of mLT contain clasts of other ignimbrites, presumably from the underlying Muileann Gaoithe and Allt Ruadh members.

The upper part of the Creag an Fheidh Member consists of a coarse lapilli tuff (Figs. 3.18, 3.19) with abundant clasts of rhyolitic material which resemble the Muileann Gaoithe lava-like ignimbrites. Rounded clasts of sedimentary material are also present. In many places, the upper surface of this unit contains rounded clasts (pebbles and cobbles) of ignimbrite and quartzite.

Petrography

Photomicrographs of samples of the Creag an Fheidh ignimbrites are shown in Fig. 3.20, with an EDS major element map shown in Fig. 3.21. These ignimbrites contain abundant sub-mm quartz and sericitised feldspar crystals, with a lesser amount of lithic lapilli (Fig. 3.20a) and sub-lapilli lithic fragments (Fig. 3.20c,d) comprising dolerite, granite, sandstone, and other ignimbrites.

The matrix of some of these ignimbrites contain 1-2 mm long elongate glassy features (Fig. 3.20b [1]) that are interpreted as flattened pumice clasts or fiamme.

The major element map of sample BJG/15/90 (Fig. 3.21) shows the different mineral phases present as crystals in the Creag an Fheidh Member crystal-rich tuffs. The plagioclase crystals are oligoclases (An_{10} – An_{33}; Fig. 3.22). The pink crystals in the EDS map are amphiboles, and the matrix is rich in Si and K so is presumably rhyolitic.

Fig. 3.18 – Photograph of lapilli tuff (with conglomerate on upper surface) from the Creag an Fheidh Member.

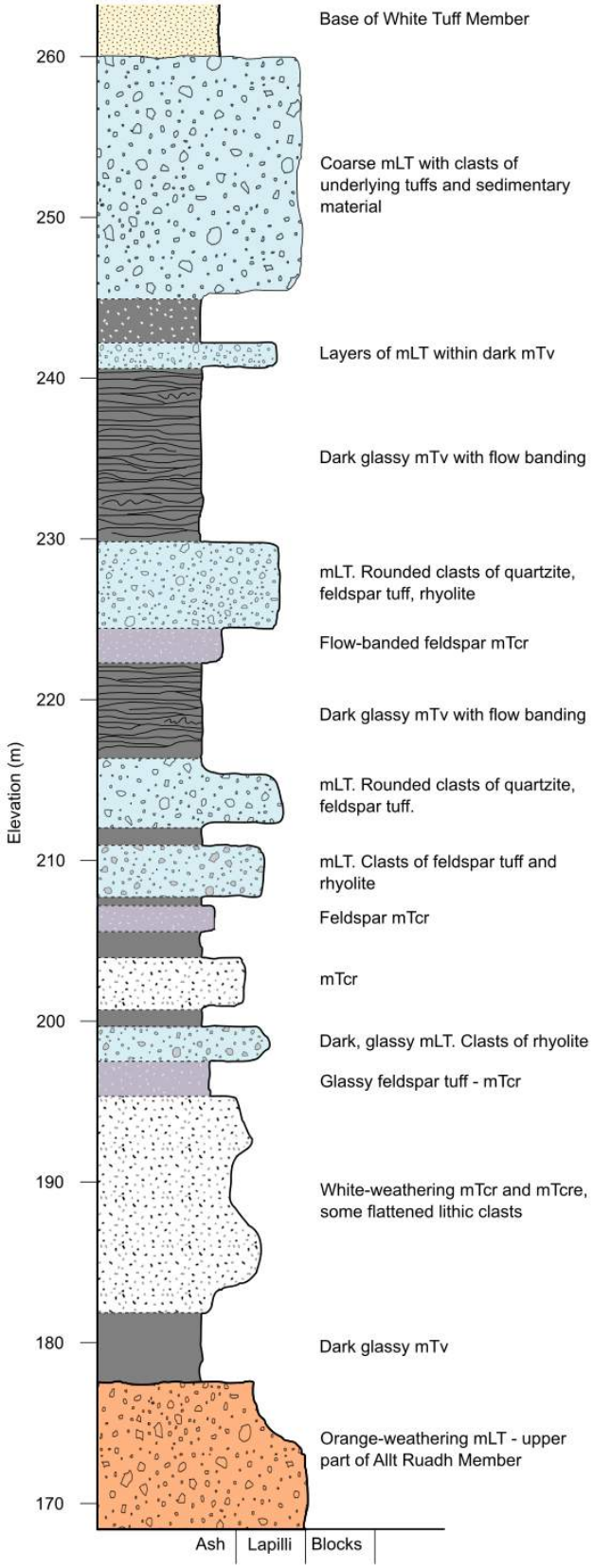

Fig. 3.19 – Stratigraphic log of the Creag an Fheidh Member along Creag an Fheidh (log 2 on Fig. 3.1).

Interpretation

The massive lapilli tuffs and clast-poor crystal tuffs (mLT and mTcr) record variably highly-explosive eruptions and deposition from a pyroclastic density current at a flow-boundary zone dominated by fluid-escape (Branney and Kokelaar, 2002). The varying degree of lithic clasts may reflect changes in explosivity at the vent or changes in erosive power across the substrate. The eutaxitic crystal tuffs and glassy tuffs displaying flow fabrics record lower explosivity, 'boil-over' pyroclastic fountaining, and higher temperatures within the pyroclastic density current. Some of the thin glassy units may be basal vitrophyres to their respective overlying ignimbrite packages.

The rounded cobbles of ignimbrite and quartzite on the upper surface of the Creag an Fheidh Member are thought to be the result of fluvial surface re-working and deposition on the exposed top of the ignimbrite. It is therefore inferred that surface water was present on top of the Creag an Fheidh Member in the period of volcanic quiescence before the eruption of the White Tuff Member.

Fig. 3.20 ***(facing page)*** – Photomicrographs of ignimbrites from the Creag an Fheidh Member. Q = quartz, F = feldspar, dol = dolerite, G = granite, ss = sandstone, LLI = lava-like ignimbrite. **a)** Sample BJG/15/102, a eutaxitic lapilli tuff. plane-polarised light. **b)** Another section of BJG/15/102, showing elongate features interpreted as fiamme [1]. Left = plane-polarised light, right = crossed polars. **c)** Sample BJG/15/133, a crystal-rich lapilli tuff. Left = plane-polarised light, right = crossed polars. **d)** Sample BJG/15/122, a clast- and crystal-rich lapilli tuff. plane-polarised light.

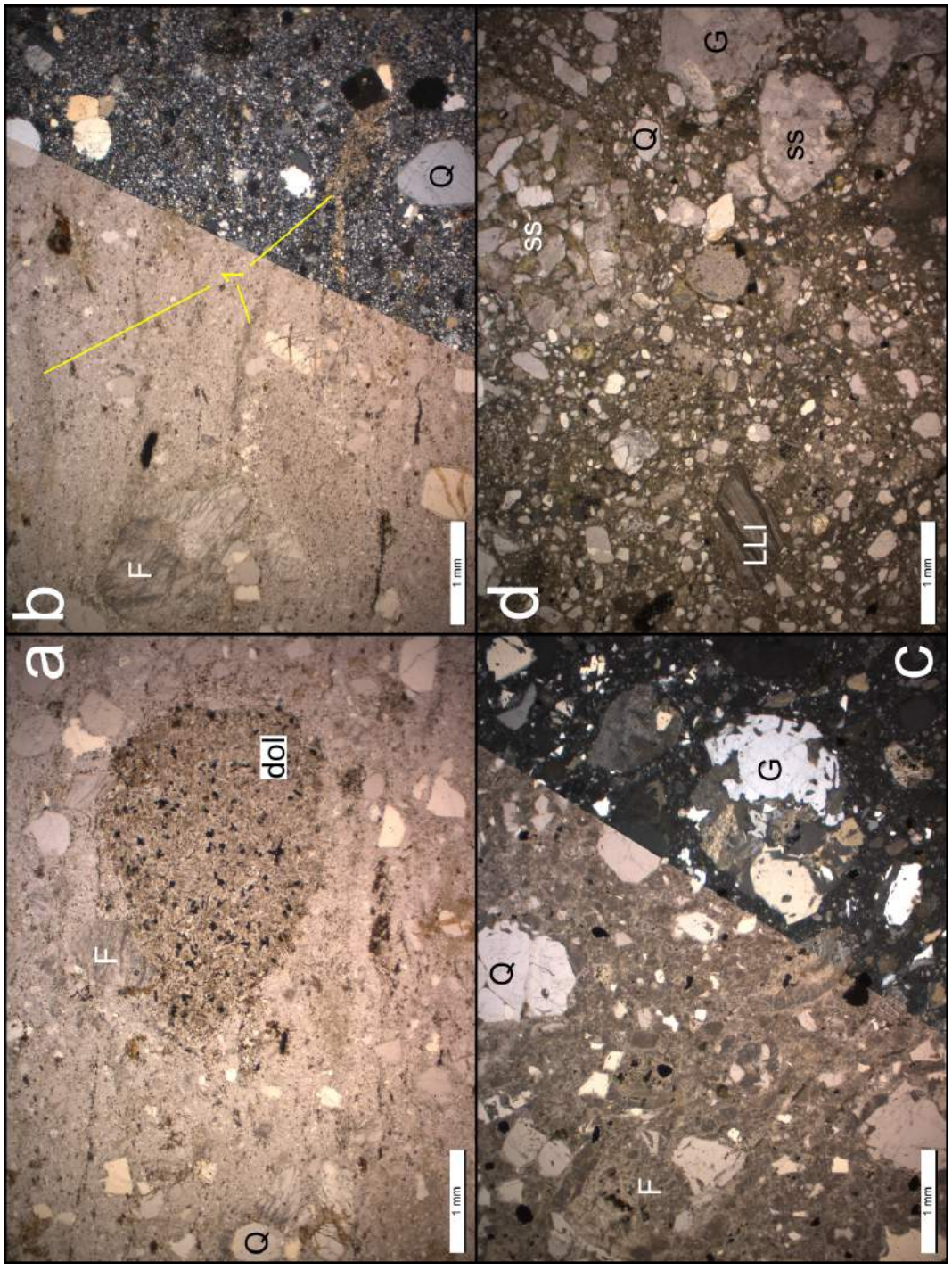
a
b
c
d
Q
F
dol
G
ss
LLI
1 mm

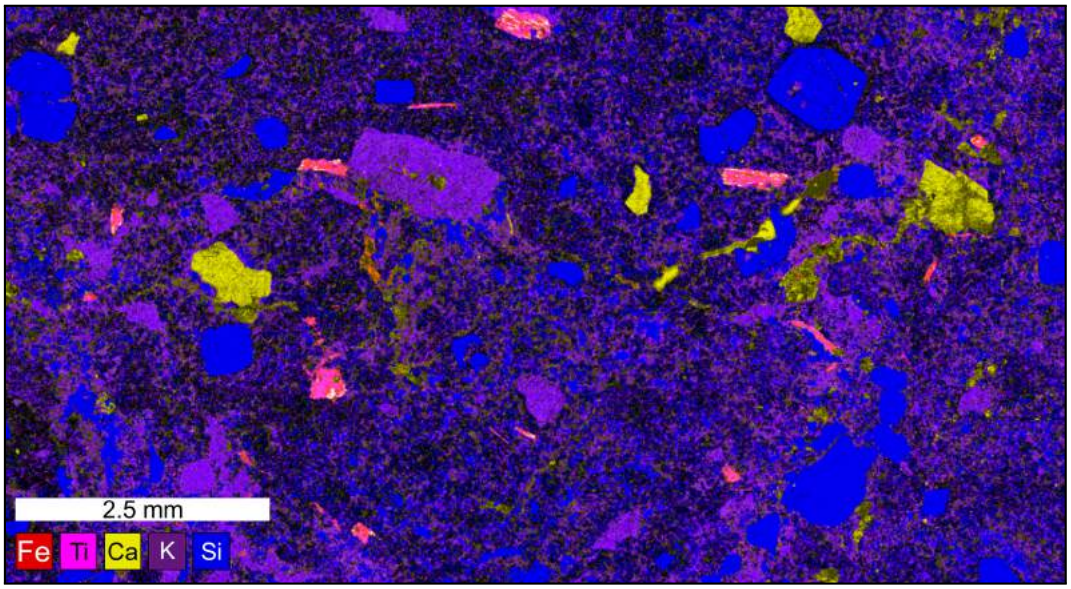

Fig. 3.21 – Major element EDS map of sample BJG/15/90, a crystal-rich tuff. Using this element-based colour scheme, quartz is blue, K-feldspar is purple, plagioclase is yellow, and amphibole is pink.

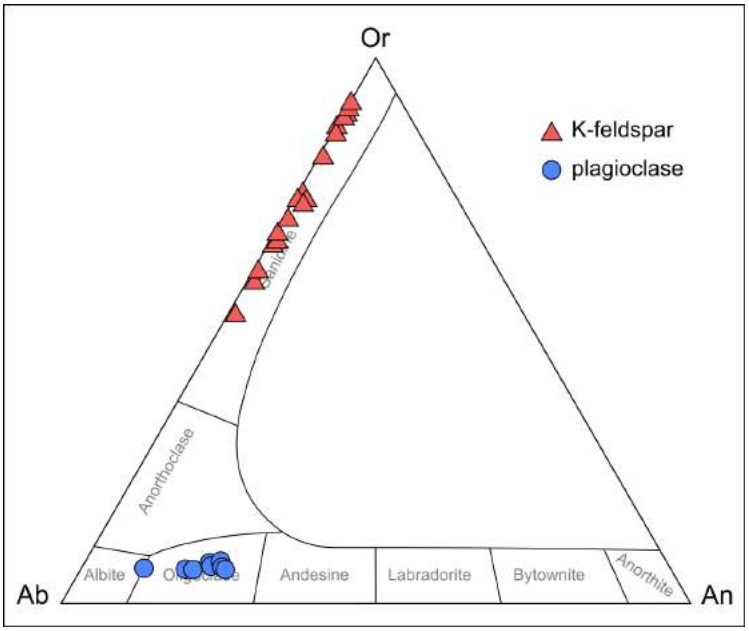

Fig. 3.22 – Ternary plots of EDS data from feldspar crystals in sample BJG/15/90 of the Creag an Fheidh Member.

3.1.5 The Allt Beith Tuff Cone

On the upper surface of the Creag an Fheidh Member, just south of the source of the Allt Beith [translation: *birch stream*], are several exposures of a very fine brown-grey thinly banded tuff (Figs. 3.1, 3.23). It shows both cross-stratified and planar bedding features on scales of <1 – 50 mm, with occasional graded bedding (Fig. 3.23). Unlike all other erupted products within the CAIC, it is basaltic-andesitic in composition (54.5 wt.% SiO_2; Section 4.1.5). The surrounding exposures are dominated by the conglomerates that make up the upper surface of the Creag an Fheidh ignimbrite.

Petrography

The majority of the Allt Beith exposure is so fine grained that minerals cannot be made out in thin section, but some fine layering can be seen (upper part of Fig. 3.24). The unit contains some layers and lenses of very fine quartz, feldspar, and oxide-rich tuff (Fig. 3.24 lower).

Interpretation

The Allt Beith exposures are interpreted as the remnants of a small basaltic phreatomagmatic tuff cone or ring. This interpretation is based on several features: 1) it is very fine grained, suggesting intense fragmentation, 2) phreatomagmatism can explain explosive mafic activity and the production of fine basaltic-andesitic ash, 3) its well developed stratification suggest deposition from a fully dilute pyroclastic density current at a traction dominated flow boundary zone (Branney and Kokelaar, 2002; Brown et al., 2007) and perhaps deposition in surface water, 4) it is surrounded by other deposits of fluvial facies, and 5) it is very localised, being seen nowhere else in the complex. It is proposed that between eruption of the silicic Creag an Fheidh and White Tuff Members, there was a small pulse of mafic magmatism that was erupted into a wet environment on the surface of the Creag an Fheidh ignimbrite, causing a relatively small phreatomagmatic event. Other such events are likely to have occurred at this stratigraphic level, but have now been buried or lost to erosion.

Fig. 3.23 – Photograph of finely laminated and cross laminated basaltic-andesitic tuff that makes up the Allt Beith tuff cone

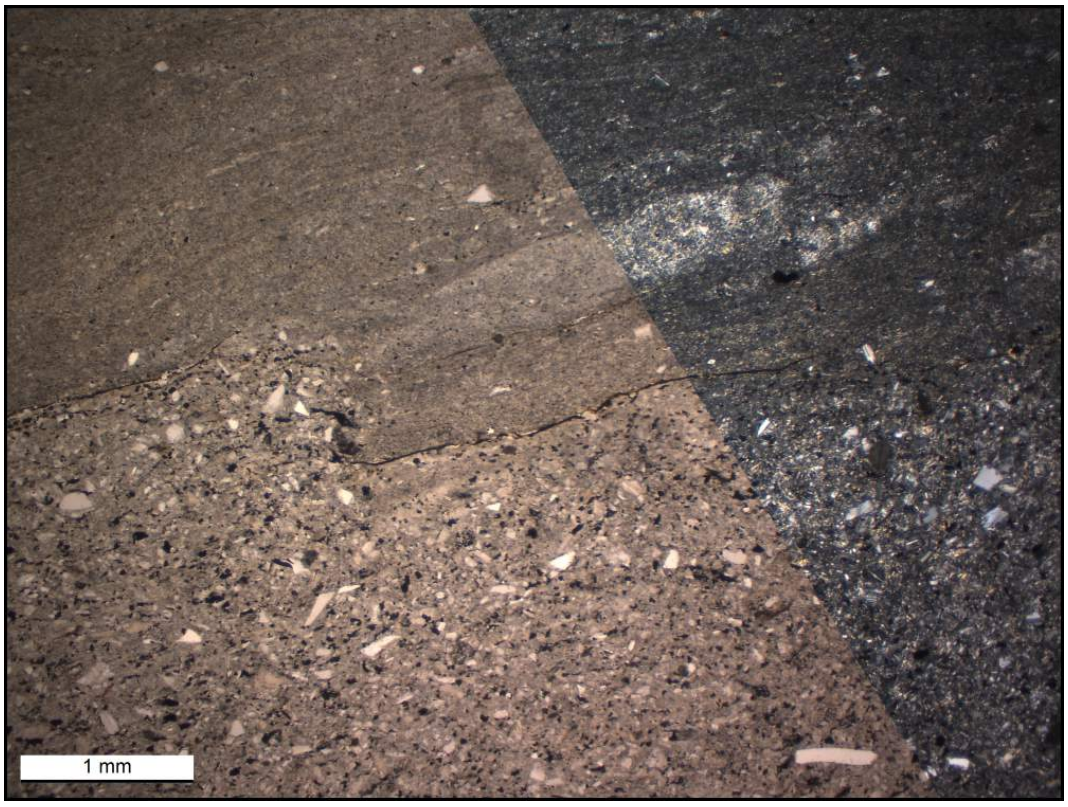

Fig. 3.24 – Photomicrograph of sample BJG/15/100, from the Allt Beith tuff cone. Left = plane-polarised light, right = crossed polars.

3.1.6 The White Tuff Member

The White Tuff is a very homogeneous, white-weathering rhyolitic lava-like ignimbrite (Fig. 3.25) that is mostly exposed in the Ard Bheinn area. It is best exposed in a string of crags to the southwest of the Ard Bheinn summit. It lies on top of the Allt Ruadh Member and Creag Shocach conglomerates to the west of Ard Bheinn (Fig. 3.2), on top of the Creag an Fheidh Member and Allt Beith tuff cone to the north, and on the Glen Craigag Granite to the east (Fig. 3.1). There are some small exposures in the Ballymichael Burn tributary 1 km south of the summit of Ard Bheinn. On the western side of Ard Bheinn, the preserved White Tuff is over 100 m thick (Fig. 3.2, 3.26). The lower contact is observed in some small exposures where it overlies the Creag an Fheidh Member. This contact has been mapped as a topographically uneven palaeo-surface in the area between Ard Bheinn and Glen Craigag (Fig. 3.1).

Most exposures of the White Tuff Member appear structureless, although in places a distinct meso-scale fabric can be seen (Figs. 3.25, 3.26). This is most often sub-horizontal planar banding, but in places it is chaotic. These fabrics are variably expressed as pervasive fractures tens of centimetres apart, or as fine mm-scale colour variations (Fig. 3.25b). Folding on the scale of tens of centimetres is uncommon, but observed in several places. In places within this unit, autobreccias with a similar petrology are found. The top of the unit comprises a localised conglomerate with rounded clasts of lava-like ignimbrite and quartzite (Fig. 3.26). The White Tuff Member is petrologically and geochemically homogeneous. It is rhyolitic throughout (76-77 wt.% SiO_2; Section 4.1.5), containing abundant plagioclase, K-feldspar, and smoky quartz crystals 1-5 mm in size.

Petrography

The White Tuff Member is very homogenous, with all samples containing a glassy to devitrified rhyolitic matrix, containing 0.5-2 mm feldspars and quartz crystals (Fig. 3.27). The larger quartz crystals are rounded and show resorption textures. Feldspar crystals can be euhedral laths (Fig. 3.27a) or anhedral rounded crystals (Fig. 3.27d). All samples contain small <1 mm needles of opaque oxides.

The groundmass of most samples from the White Tuff Member is homogenous and structureless. However, in certain samples (Figs. 3.27c,d, 3.28) a distinct banding can be seen, defined by continuous bands of different colour, texture, and composition.

The EDS major element maps of a banded (Fig. 3.28) and an unbanded crystal rich (Fig. 3.29) ignimbrite from the White Tuff Member show the rhyolitic Si and K

Fig. 3.25 – Photographs of the rhyolitic lava-like ignimbrites of the White Tuff Member. **a)** An exposure of the White Tuff ignimbrite showing steeply-dipping centimetre-to-decimetre scale fabric. Western Ard Bheinn, looking north. **b)** Finely-banded exposure showing sub-cm scale yellow, white, and grey bands.

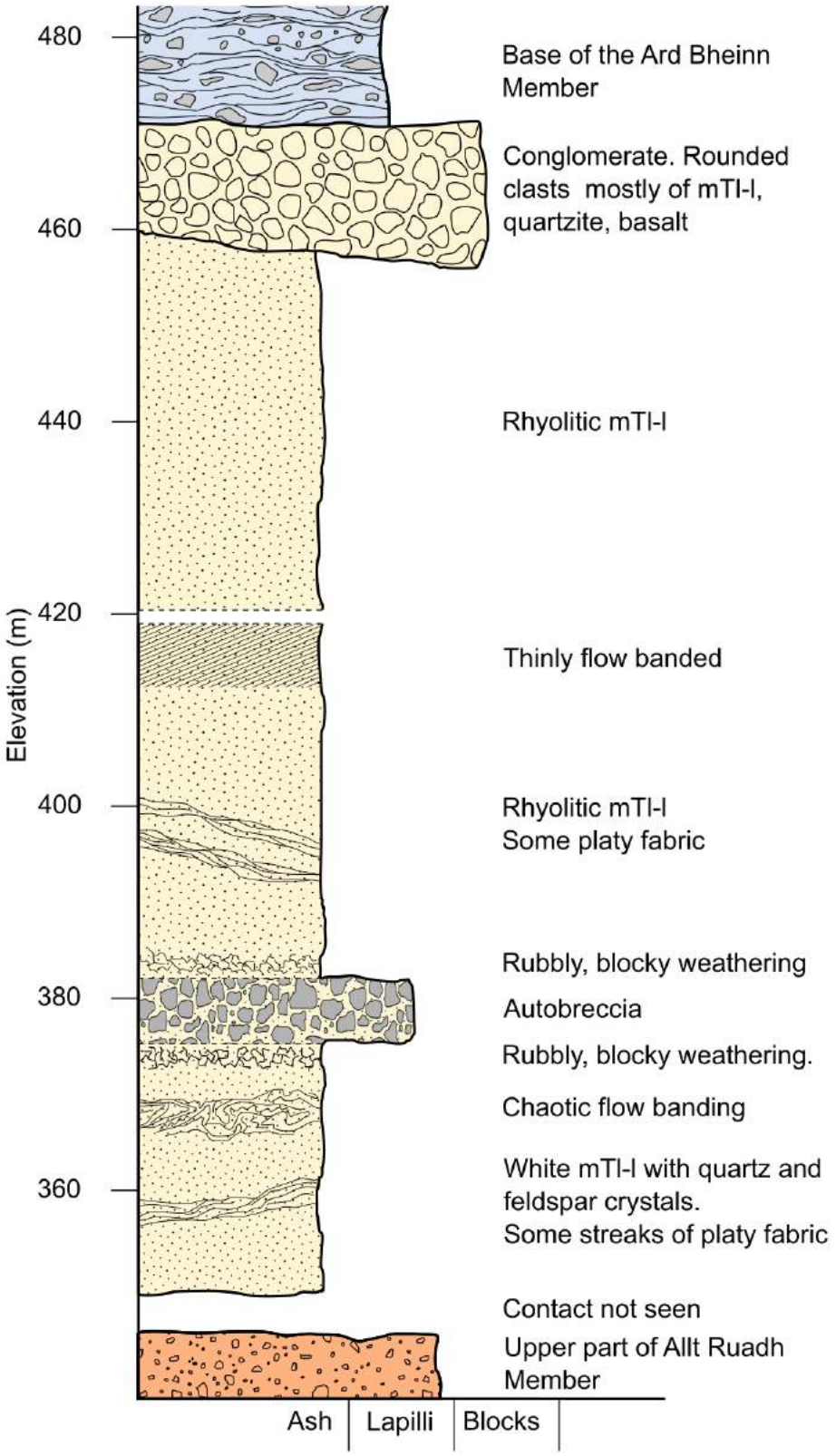

Fig. 3.26 – Stratigraphic log of the White Tuff Member Member on the western slops of Ard Bheinn (log 3 on Fig. 3.1).

rich matrix, and quartz and feldspar crystal cargoes. All K-feldspar crystals show thin Na-rich rims. The plagioclases (An_3 – An_{27}; Fig. 3.30) all have relatively Ca-rich (yellow) cores and Na-rich (green) rims. Fig. 3.28 shows the compositional variation between the distinct bands; Si and K rich bands tend to be coarser than the Si and K poor glass.

Interpretation

The stratigraphic conformity, and presence of internal stratigraphic variation, along with the presence of autobreccias and conglomerates show that this unit is undoubtedly extrusive. Due to the lack of basal and upper autobreccia, as well as the gradations between parts of the unit with different pervasive fabric characteristics (Fig. 3.26), the White Tuff Member is interpreted as a rhyolitic lava-like ignimbrite. This is further suggested by the lack of any visible individual pyroclasts (Fig. 3.27) which may have coalesced due to agglutination. These features suggest that, like the Muileann Gaoithe Member, this member is a very high-grade ignimbrite of 'Snake River type' (Andrews and Branney, 2011), suggesting rapid deposition from a high temperature, (>900°C) high-mass-flux pyroclastic density current. The localised conglomerates at the top of the member are interpreted as the result of fluvial surface re-working and deposition on the exposed top of the ignimbrite.

Fig. 3.27 ***(facing page)*** – Photomicrographs of lava-like ignimbrites from the White Tuff Member. Q = quartz, F = feldspar, ox = Fe-Ti oxides. **a)** Sample BJG/15/14, a crystal tuff with a homogenous matrix. Left = plane-polarised light, right = crossed polars. **b)** Another section of BJG/15/14, showing a large resorbed quartz crystal. Top = plane-polarised light, bottom = crossed polars. **c)** Sample BJG/17/18, a crystal tuff with a flow-banded matrix. plane-polarised light. **d)** Sample BJG/17/8, a crystal tuff with a flow-banded matrix. plane-polarised light.

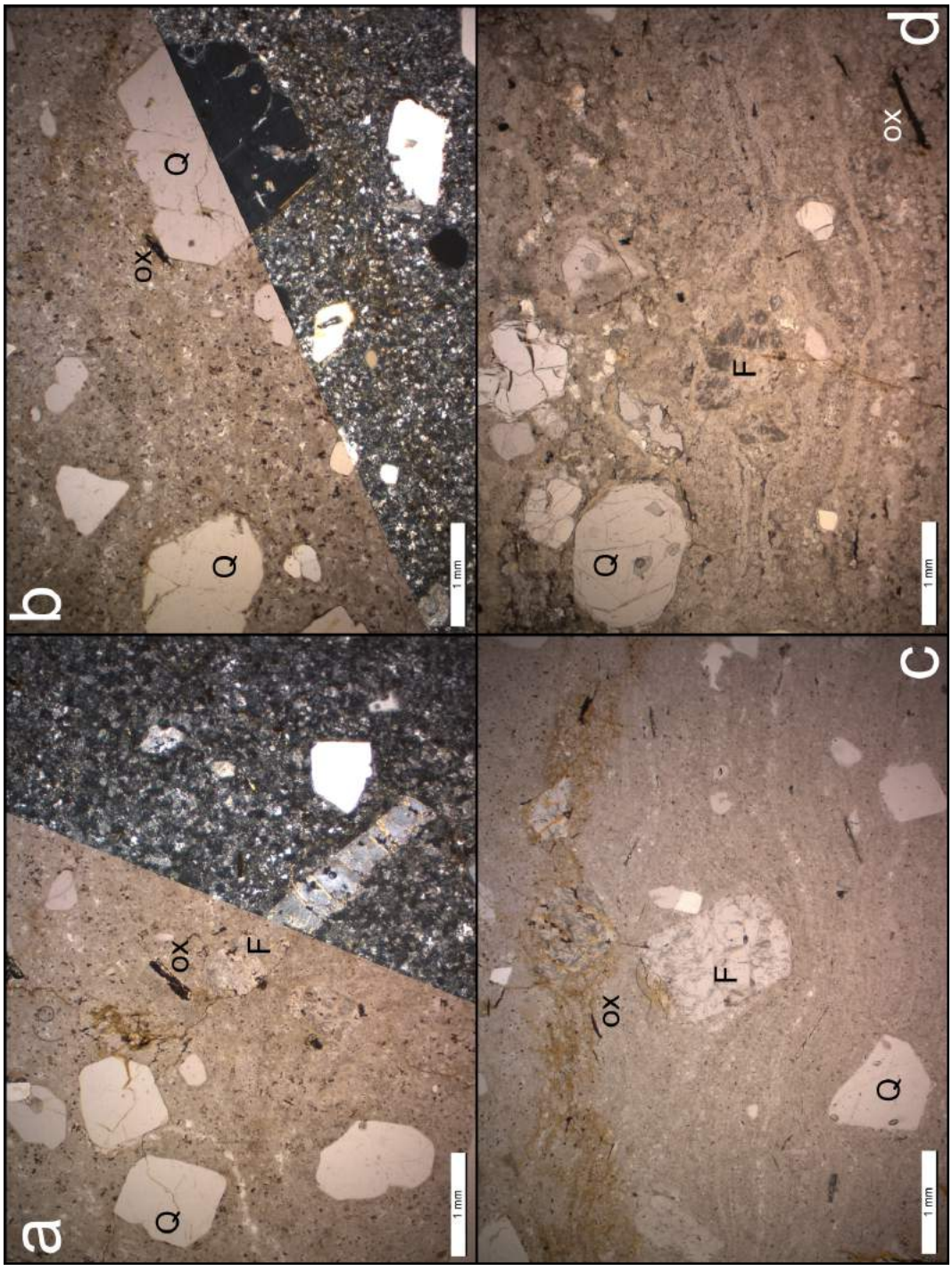
a
Q
ox
F
1 mm
b
Q
ox
Q
1 mm
c
ox
F
Q
1 mm
d
Q
F
ox
1 mm

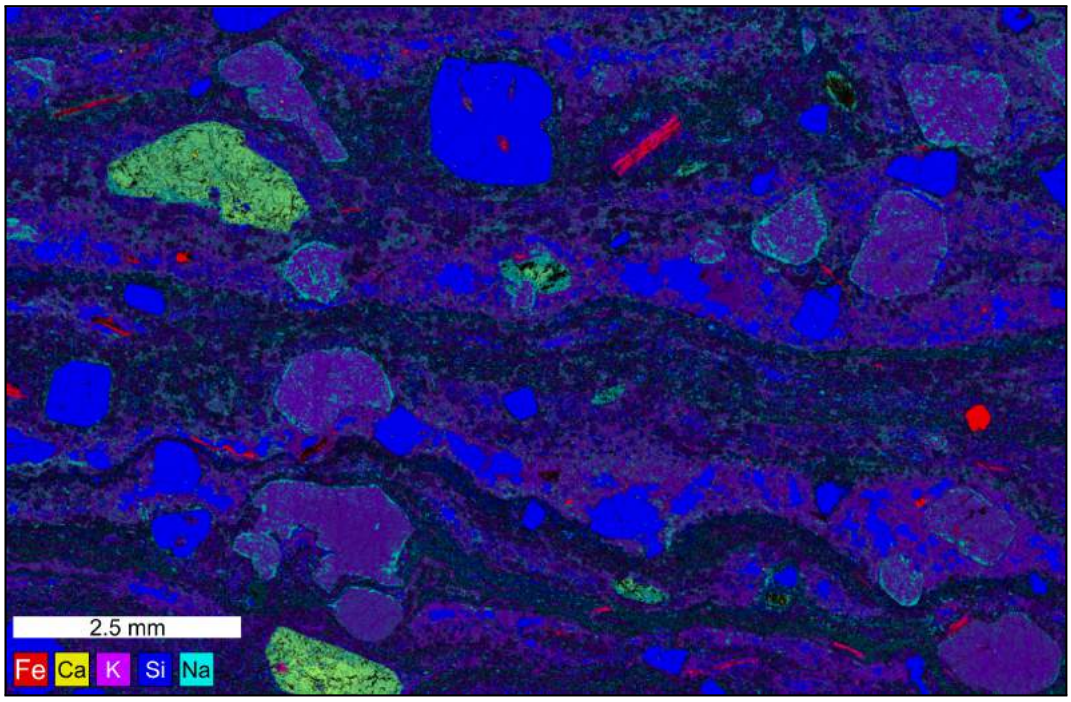

Fig. 3.28 – Major element EDS map of sample BJG/17/8, a lava-like ignimbrite. Using this element-based colour scheme, quartz is blue, K-feldspar is purple, plagioclase is bright green, and Fe-Ti oxides are red.

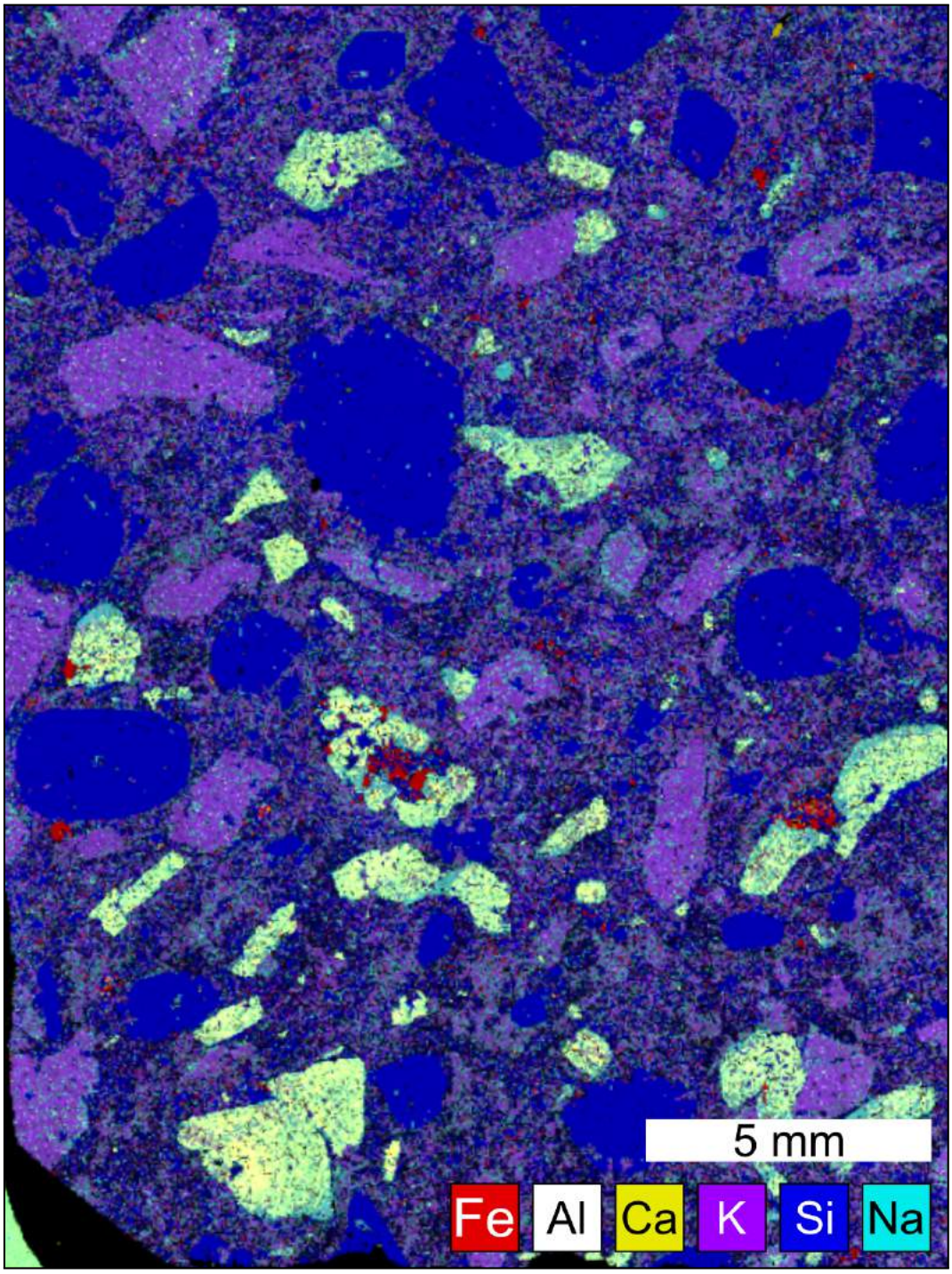

Fig. 3.29 – Major element EDS map of sample BJG/15/146, a crystal-rich lava-like ignimbrite. Using this element-based colour scheme, quartz is blue, K-feldspar is purple, plagioclase is pale yellow, and Fe-Ti oxides are red. A small yellow dot in the upper right corner is an apatite.

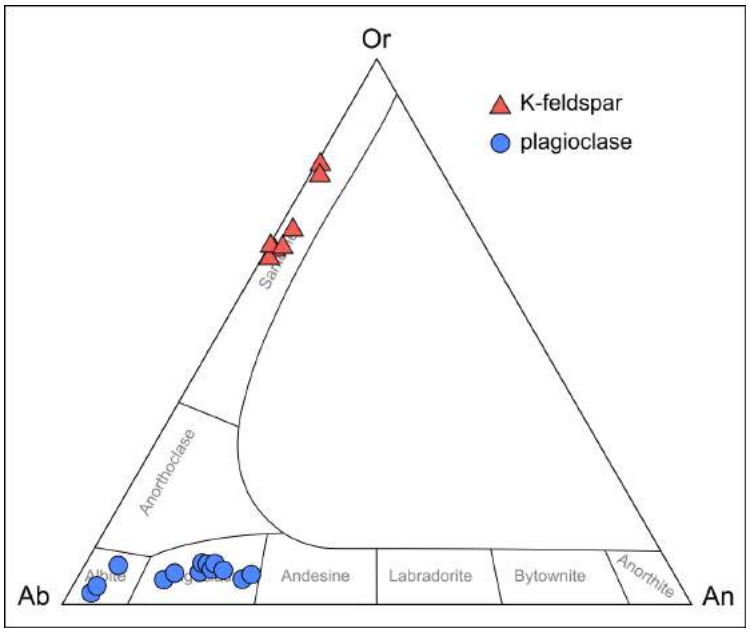

Fig. 3.30 – Ternary plots of EDS data from feldspar crystals in sample BJG/17/8 of the White Tuff Member.

3.1.7 The Pigeon Cave Member

The Pigeon Cave Member (Fig. 3.31) is exposed extensively on the western and eastern sides of Binnein na h-Uaimh (Fig. 3.2), and to a lesser extent along the ridge between Ard Bheinn and Creag Dubh, and on Creagan Leana Muic on the eastern side of Glen Craigag (Fig. 3.1). In the Ard Bheinn area it was deposited on the White Tuff Member. On Creagan Leana Muic, the Pigeon Cave Member was deposited on top of the Creag an Fheidh Member (Fig. 3.1). This suggests that the White Tuff was not deposited in this area, or was completely removed by erosion prior to eruption of the Pigeon Cave Member.

This member largely consists of massive lapilli tuffs and agglomerates (Fig. 3.32), most of which weather to a turquoise colour (Fig. 3.31). Agglomerates are here defined as ignimbrites which contain elongate bands and streaks of lava-like material in an otherwise non-lava-like matrix (Branney and Kokelaar, 2002). Lithic clasts within the ignimbrite consist of pre-Palaeogene country rocks (schist and sandstone) as well as presumably Palaeogene basalt and ignimbrite. Most layers within the unit contain abundant quartz crystals (Fig. 3.33). The basalt/dolerite breccias shown in Fig. 3.32 are interpreted as fingers of the dolerite sill that intruded below the White Tuff Member.

The Pigeon Cave Member contains several sedimentary units within it. The outcrop of 'chalk' at Pigeon Cave on Binnein na h-Uaimh (discussed by Tyrell (1928)) is overlain by the Pigeon Cave Member. Foraminifera fossils suggest a Cretaceous age for this chalk (Tyrell, 1928), and it has been previously interpreted as a subsided megablock (King, 1954; Tyrell, 1928). Some pink-white weathering sandstones are exposed several metres to the south of Pigeon Cave. These were also mentioned by Tyrell (1928), and King (1954) suggested these may also be Cretaceous due to similarities with sediments found on Mull and Morvern, and in Antrim. It is unclear whether these are part of the caldera floor, subsided megablocks, or have a Palaeogene intra-caldera origin.

Petrography

Photomicrographs of the varied tuffs of the Pigeon Cave Member are shown in Fig. 3.33. As well as showing abundant <1 mm quartz and feldspar crystals, Fig. 3.33a and b show sickle-shaped and wispy glassy features [1]. These are interpreted to be microscopic equivalents to the cognate spatter clasts shown in outcrop in Fig. 3.31.

Other samples are made up almost entirely of lithic clasts and crystals, with relatively little matrix glass (Fig. 3.33c,d). Lithic lapilli comprise dolerite and heavily altered rhyolite.

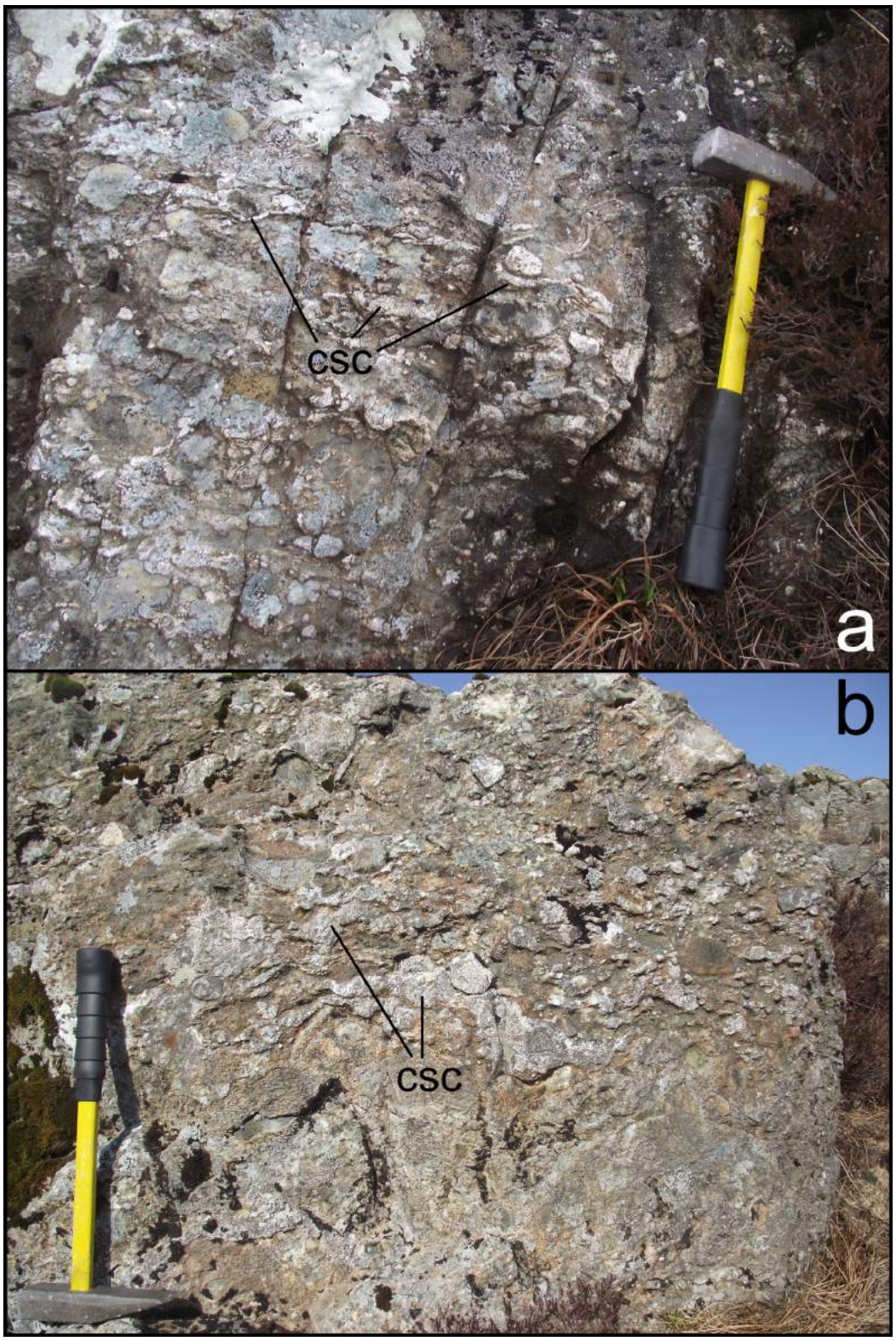

Fig. 3.31 – Photographs of massive agglomerates from the Pigeon Cave Member, showing lithic lapilli and elongate, flattened cognate spatter clasts (csc).

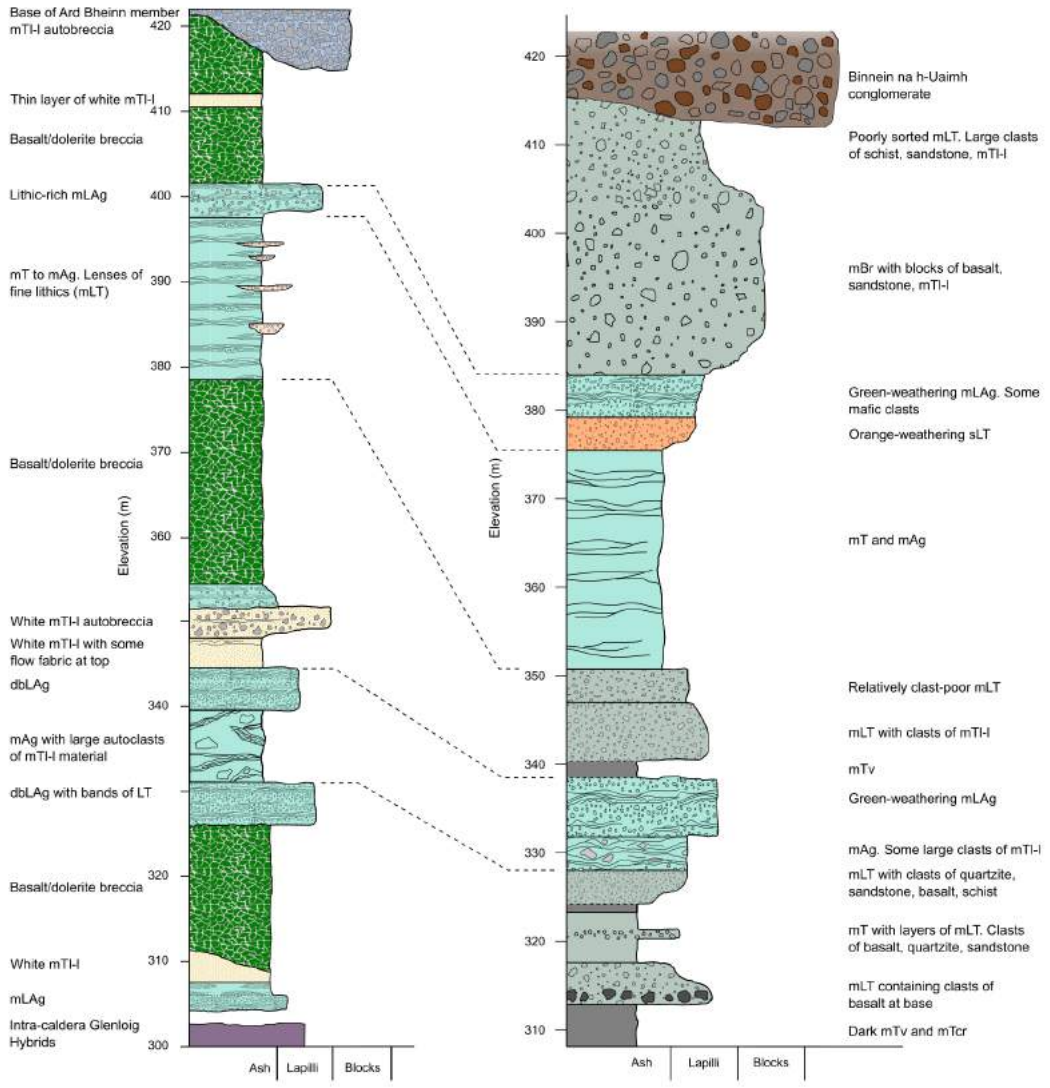

Fig. 3.32 – Stratigraphic logs of the Pigeon Cave Member up the northern side of Binnein na h-Uaimh, where it is intruded by brecciated fingers of the basalt/dolerite sill (left), and up the western side of Binnein na h-Uaimh, where it is not intruded by the sill. Dashed lines show possible lateral bed correlations (logs 4a and b in Fig. 3.1).

Interpretation

The presence of thin interbedded layers of lapilli-tuff, agglomerate, and lava-like and vitrophyric tuffs shows a highly dynamic and fluctuating deposition history. The mLT shows deposition from a pyroclastic density current at a flow-boundary zone dominated by fluid-escape, and with very little turbulent shear-induced tractional segregation (Branney and Kokelaar, 2002), while the true lava-like ignimbrites record high temperature deposition from a high-mass-flux pyroclastic density current. These differences would have been linked to processes at the vent, with highly explosive Plinian columns and low-fountaining boil-over eruptions, respectively.

The massive agglomerate lithofacies contains elongate ribbons of lava-like material, interpreted as forming as cognate spatter clasts at the vent, which are then entrained (and stretched) in the pyroclastic density current (Branney and Kokelaar, 2002). The lateral variation within this unit (shown by the differences between the logs in Fig. 3.32) could be explained by: 1) locally variable amounts of pumiceous matrix; and 2) topographic control of thickness and geographic distribution. These are two of the defining characteristics of the massive agglomerate lithofacies in Branney and Kokelaar (2002) (after Druitt et al., 1989; Mellors and Sparks, 1991). Branney and Kokelaar (2002) suggest that mAg has a similar mode of formation to mBr, with rapid deposition of cognate clasts (with or without lithic lapilli) from a pyroclastic density current rich in ash and dominated by fluid escape.

Fig. 3.33 ***(facing page)*** – Photomicrographs of ignimbrites from the Pigeon Cave Member. Q = quartz, F = feldspar, dol = dolerite, R = rhyolite. **a)** Sample BJG/15/49, a crystal-rich agglomerate showing wispy glassy features interpreted as rhyolitic cognate spatter clasts or fiamme [1]. plane-polarised light. **b)** The same section as a), but viewed between crossed polars. **c)** Another section of BJG/15/49, showing clasts of dolerite and more spatter clasts [1]. plane-polarised light. **d)** Sample BJG/15/149, a crystal-rich tuff containing clasts of rhyolite, with a dark glassy background. plane-polarised light.

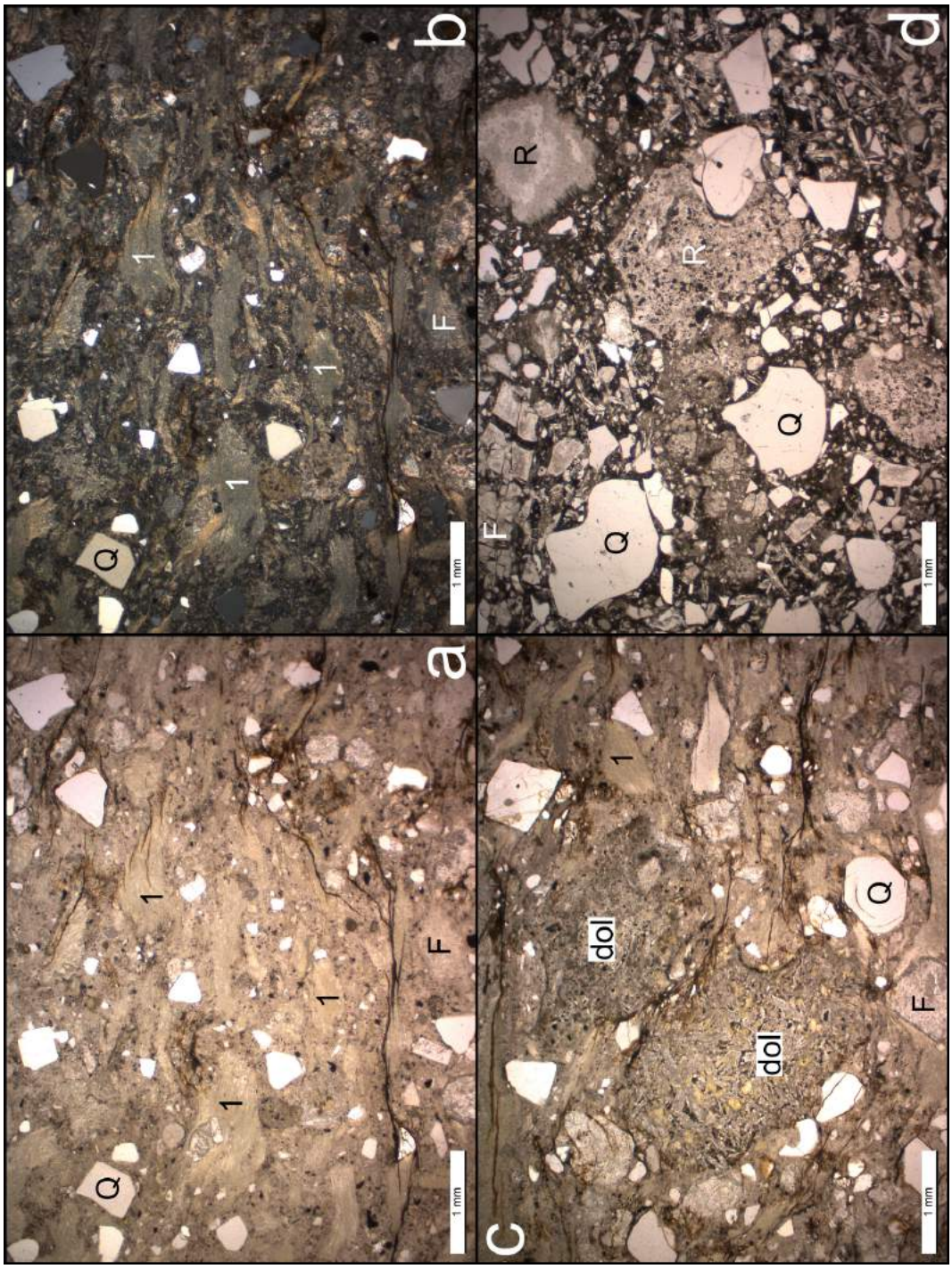
a
b
c
d
Q
F
R
dol
1
1 mm

3.1.8 The Binnein na h-Uaimh Conglomerates

The exposure on the north slopes on Binnein na h-Uaimh [translation: *hill of the cave*] is dominated by a very coarse clast-supported conglomerate (Fig. 3.1). This conglomerate (Fig. 3.34) forms an almost complete exposure from an elevation of 340 m, where it overlies the Pigeon Cave Member (Fig. 3.34d), to the summit of Binnein na h-Uaimh (430 m), where it is overlain by the basal breccias of the Ard Bheinn Member (Fig. 3.2). Clast size is mostly pebbles to large cobbles, with some boulders over 500 mm in length (Fig. 3.34b,c). The clasts are rounded to angular and mostly comprise country rock lithologies (*i.e.*, sandstone and schist). Some small, rounded pebbles of quartzite are unlike anything observed in the country rocks of central Arran, and may be inherited original clasts from the Devonian or Permo-Triassic conglomerates. The schists (such as the large boulders seen in Fig. 3.34b) resemble the Dalradian schists, which only crop out north of the Highland Boundary Fault, ~4 km to the north (Fig. 1.3). Similar schist clasts are found in the Devonian and Permo-Triassic conglomerates throughout Arran, but these are predominantly pebble-sized. There are no other comparable schists exposed south of the Highland Boundary Fault, suggesting that the Binnein na h-Uaimh conglomerates were sourced from the north.

The lower contact of the unit (Fig. 3.34d) can be traced for over 100 m up the slopes of Binnein na h-Uaimh (Fig. 3.2). This shows that the conglomerates were deposited on a highly uneven topographical surface.

Petrography of clasts

There are four main lithologies in the clasts of the Binnein na h-Uaimh conglomerates: 1) vein quartz, 2) quartz-rich schist and psammite, 3) mica-rich sandstone, and 4) quartzite. The vein quartz is shown in Fig. 3.34c. The foliated quartz-rich schist (Fig. 3.35a) and non-foliated mica psammite (Fig. 3.35b) are petrographically similar, containing a large amount of strained and partially recrystallised quartz, minor feldspar, and patches and streaks of very fine-grained mica. It is likely that these lithologies are derived from the same texturally heterogeneous source.

The mica-rich sandstone (Fig. 3.35c) is made up largely of <200 μm quartz and feldspar crystals, with elongate individual muscovite crystals up to 1 mm in length. The micas are aligned (bottom left to top right in Fig. 3.35c), giving the rock a foliated texture.

The quartzite (Fig. 3.35d) is coarser (crystals up to 1 mm). Almost the whole rock is made up of strained partially-recrystallised quartz crystals with sutured

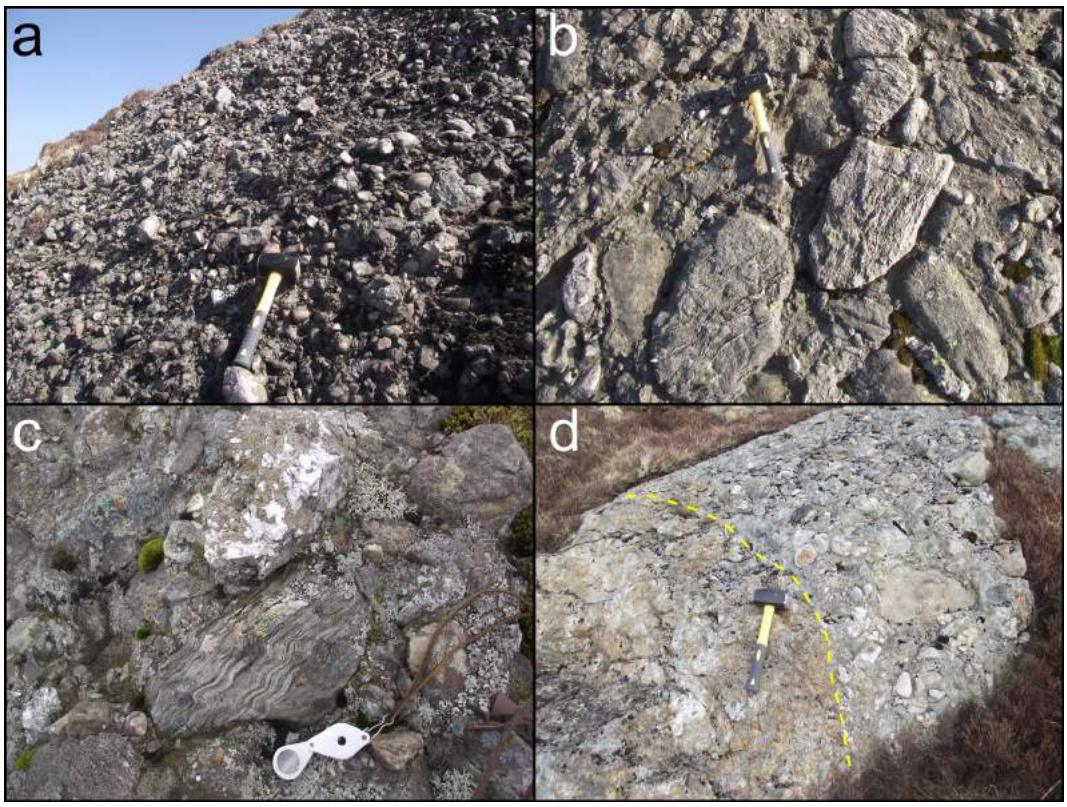

Fig. 3.34 – Photographs of the Binnein na h-Uaimh Conglomerates. **a)** Exposure dominated by very rounded quartzite pebbles. **b)** The coarsest part of the unit, including several boulders of schist. **c)** Cobbles of vein quartz (top) and crenulated schist (bottom). **d)** Contact (dashed line) between the Binnein na h-Uaimh conglomerates and the underlying Pigeon Cave Member (left).

edges. Minor amounts of mica and microcline feldspar are present. This lithology is interpreted as a partially recrystallised quartz sandstone.

All of these clast lithologies are found *in situ* elsewhere on Arran, and are also found as clasts within the conglomerates and breccias of the Devonian Old Red Sandstone and (less frequently) the Permian New Red Sandstone in various places across Arran.

Interpretation

It is proposed that the Binnein na h-Uaimh conglomerates were deposited from a debris flow in a canyon that was eroded into the upper surfaces of the Pigeon Cave Member. The steep canyon sides can be observed in several places along the exposure, with the conglomerates overlying the ignimbrites (Fig. 3.34d). There are no flow-direction indicators preserved in the conglomerates, but the canyon that they fill appears to slope steeply downhill from the summit of Binnein na h-Uaimh towards the north (Fig. 3.2). This would suggest that, in the absence of any later large-scale subsidence-related rotation, the flow was towards the north.

Fig. 3.35 ***(facing page)*** – Photomicrographs of the different lithologies found as clasts within the Binnein na h-Uaimh Conglomerates. Q = quartz, F = feldspar. **a)** Folded quartz-mica schist. Top left = plane-polarised light, bottom right = crossed polars. **b)** Non-foliated mica psammite. Note the sutured edges and undulose extinction of the quartz crystals. Viewed between crossed polars. **c)** Foliated mica-rich sandstone. Mica is shown by bright birefringence colours. Viewed between crossed polars. **d)** Quartzite containing minor mica and microcline feldspar. Viewed between crossed polars.

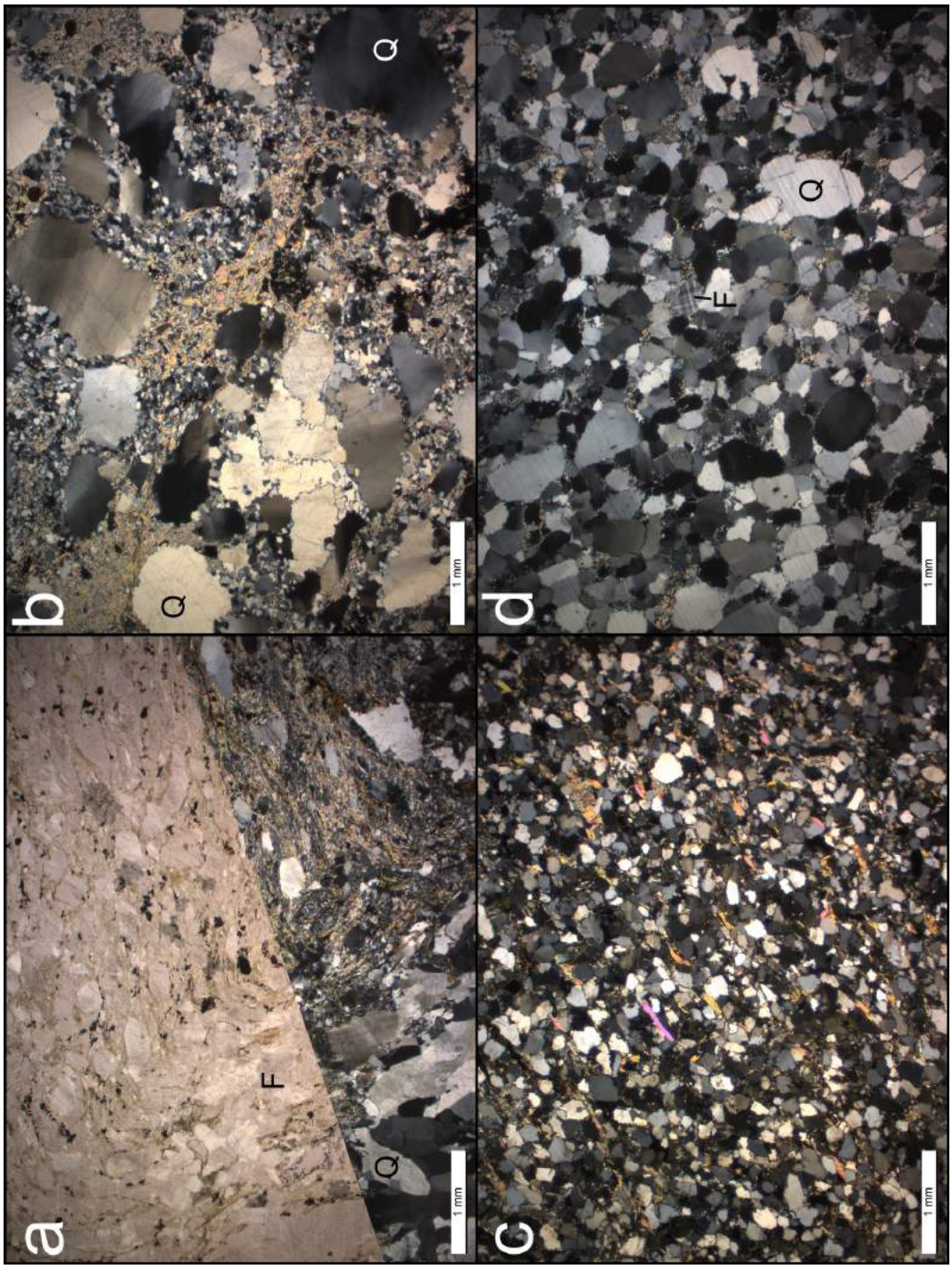
a
b
c
d
Q
F
1 mm

3.1.9 The Ard Bheinn Member

The youngest exposed unit of the AVF is the Ard Bheinn Member (Fig. 3.36). It is exposed extensively on the summits of Ard Bheinn [translation: *high peak*] and Binnein na h-Uaimh (Fig. 3.2), with some exposures to the south towards Ballymichael Glen, and to the north east towards Creag Dhubh (Fig. 3.1). There are also some isolated exposures in the boggy ground 2 km east south east of the Ard Bheinn summit (Fig. 3.1) which appear to belong to the same unit, although these exposures are isolated and local stratigraphy is impossible to discern.

On Binnein na h-Uaimh the Ard Bheinn Member can be seen directly overlying the Pigeon Cave Member and the Binnein na h-Uaimh conglomerates. On Ard Bheinn it overlies the Pigeon Cave and the White Tuff Members (Fig. 3.2). In Ballymichael Glen the Ard Bheinn Member appears to cut down into the White Tuff, the dolerite sill, the Glen Craigag Granite, and possibly even the Allt Ruadh Member (Fig. 3.1).

The Ard Bheinn Member is a heterogeneous dark grey unit (Fig. 3.37) which displays bedding-parallel and folded flow-fabrics in places. The base of the member varies between the several locations where it is observed. Near the summit of Binnein na h-Uaimh it is a coarse lapilli agglomerate (Fig. 3.36a), which overlies the Pigeon Cave Member and the Binnein na h-Uaimh conglomerates. In Ballymichael Glen, the lowest parts of the Ard Bheinn Member consist of stratified lava-like coarse crystal tuffs, with a very high content of quartz and feldspar crystals >5 mm in size (Fig. 3.38). These sTcrl-l appear to fill valleys on canyons which cut down into the underlying units.

The most complete section of the Ard Bheinn Member extends from the coarse crystal tuff in Ballymichael Glen, up the southern side of Ard Bheinn, to the summit (Fig. 3.37). The lower parts of this section, up to a topographic shelf at ~420 m, comprise a relatively homogeneous lithoidal brown unit (mTv), with crackly weathering, some irregular bands of lithophysae, and pervasive columnar jointing. An analysed sample of a similar lithology from Binnein na h-Uaimh is rhyolitic in composition (77 wt.% SiO_2, Section 4.1.5). Above this topographic shelf the ignimbrite becomes more clast-rich with layers of agglomerate, autobreccia, and lithic-poor tuffs. The lithoidal texture and lithophysae are still seen in places. Clasts are of varying sizes, but are almost exclusively composed of similar lithologies to the rest of the Ard Bheinn Member. One exposure, around 50 m south of the Ard Bheinn summit, displays eutaxitic texture, clasts of other lithologies, and streaky fiamme of mafic material (Fig. 3.36c,d). Around the summit, the top of the preserved part of the Ard

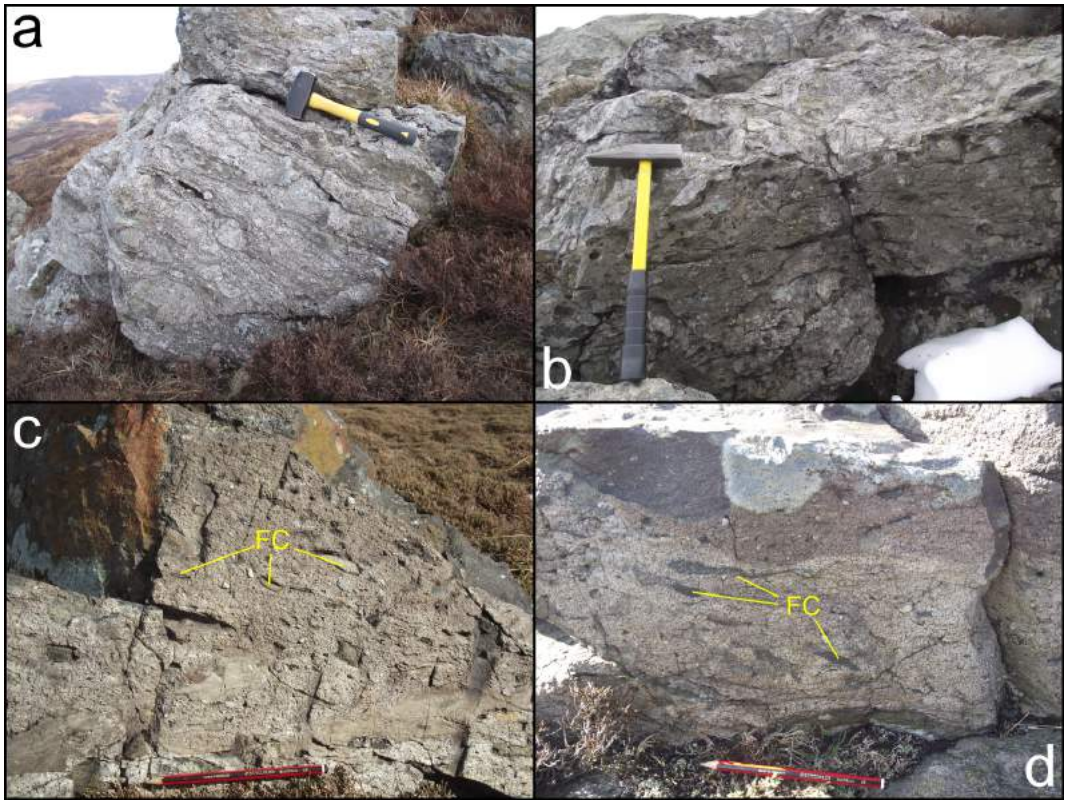

Fig. 3.36 – Photographs of ignimbrites of the Ard Bheinn Member. **a)** Massive lapilli agglomerate near the summit on Binnein na h-Uaimh, looking north showing lithic lapilli and elongate bands of rhyolite. **b)** Lighter lava-like ignimbrite overlying darker ignimbrite, near the Ard Bheinn summit. **c)** Eutaxitic tuff containing flattened clasts (FC), possibly fiamme. **d)** Another eutaxitic tuff showing flattened clasts (FC) of darker, possibly more mafic material.

Bheinn Member is dominated by fine purple-grey dacitic rock (68-70 wt.% SiO_2, Section 4.1.5) with abundant small plagioclase crystals (Fig. 3.38).

Petrography

Photomicrographs of Ard Bheinn Member ignimbrites are shown in Fig. 3.38. EDS major element maps are also shown for a coarse crystal-rich tuff (Fig. 3.39), the contact between two compositionally distinct layers in a eutaxitic tuff (Fig. 3.40), a dacitic feldspar tuff (Fig. 3.41), and a massive lapilli tuff (Fig. 3.42), all from the Ard Bheinn Member.

A glassy crystal rich ignimbrite typical of those seen in the lower part of the unit (Fig. 3.37) is shown in Fig. 3.38a. This shows 1-2 mm euhedral feldspars and larger resorbed quartzes in a homogenous rhyolitic matrix with some minor opaque oxides. This lithology is petrographically very similar to the unbanded ignimbrites

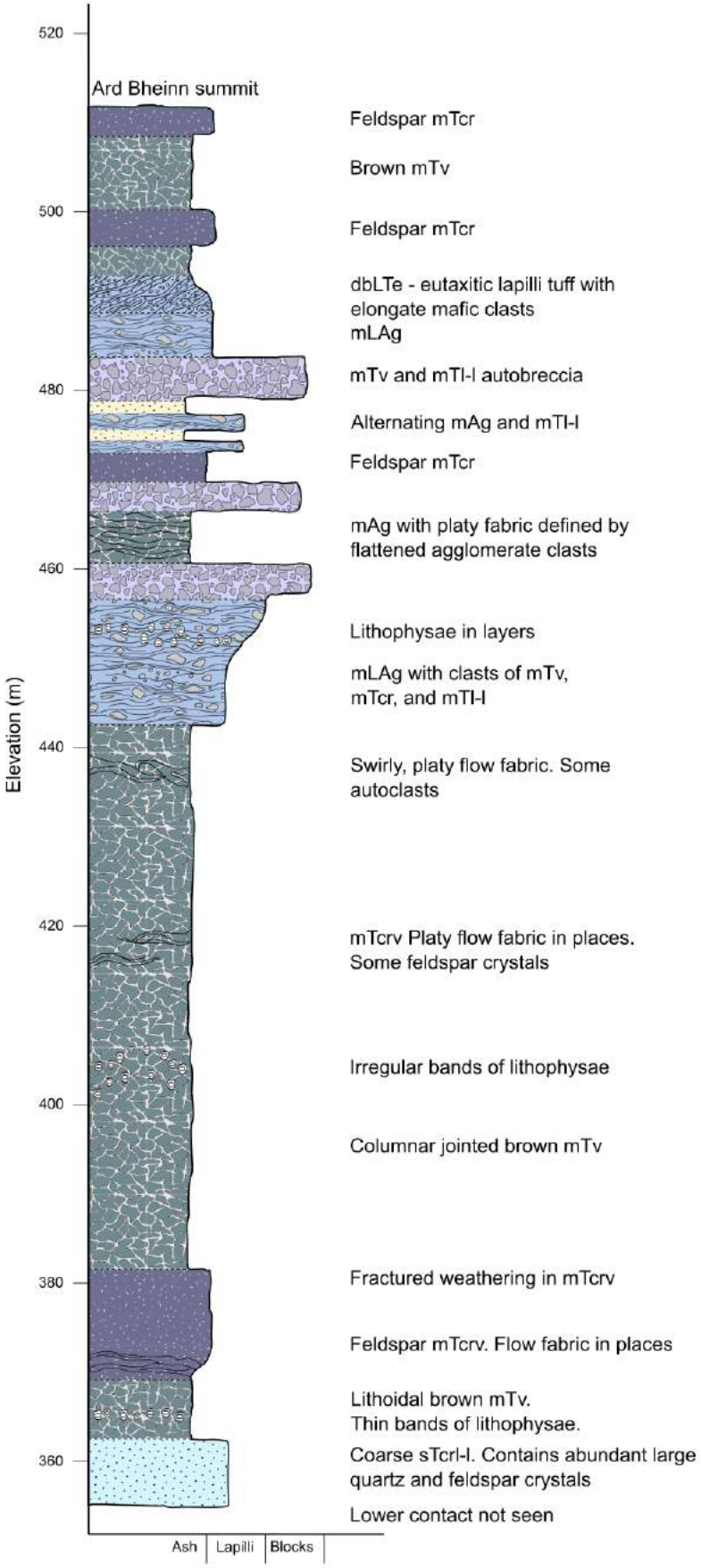

Fig. 3.37 – Stratigraphic log of the Ard Bheinn Member, up the southern slopes of Ard Bheinn (log 5 in Fig. 3.1).

from the White Tuff Member. An EDS major element map for a similar, but much coarser crystal tuff from the base of the Ard Bheinn Member (Fig. 3.39) shows quartz, plagioclase, and K-feldspar crystals up to 4 mm, with smaller Fe-Ti oxides. The plagioclases are all oligoclase (An_{17} – An_{27}; Fig. 3.43a), with one showing oscillatory zoning on the element map, with relatively Na-rich (green) and Ca-rich (pale yellow) zones.

A eutaxtic tuff with compositionally distinct layers is shown in Fig. 3.38b and Fig. 3.40. These images show a silicic eutaxitic tuff containing small (<1 mm) quartz and plagioclase (An_{17} – An_{44}; Fig. 3.43b) crystals, as well as Fe and Fe-Ti oxides, overlain by a darker, more Fe-rich layer containing much less quartz. The Fe-rich (red) streaks and lenses in the more silicic part in Fig. 3.40 could correspond to the the larger black flattened clasts seen in outcrop scale in Fig. 3.36c,d.

The summit area of Ard Bheinn is made up of dacitic and rhyolitic feldspar-rich glassy tuffs. This is the '*plagioclase porphyry*' described by King (1954). One example is shown in Fig. 3.38c, and as an EDS major element map in Fig. 3.41. This sample has a Si-poor glassy matrix, and the dominant crystal phase is relatively Ca-rich andesine-labradorite plagioclase (An_{42} – An_{53}; Fig. 3.43c). Small clinopyroxenes (Figs. 3.38c, 3.41) are mostly augites, with two examples showing distinctly Mg-cores and Fe-rich rims (Fig. 3.43d). Another plagioclase tuff is shown in Fig. 3.38d, with more rounded feldspar crystals, and large (>5 mm) basalt lapilli. The matrix of this sample is a rhyolitic glass, which has developed a distinct patchy devitrification texture.

Fig. 3.42 shows and EDS major element map for a massive lapilli tuff from the Ard Bheinn Member. It is very similar to mLT seen in other units, particularly the Allt Ruadh Member, with a silicic ashy matrix, quartz crystals, and a variety of angular lithic clasts, including a large (10 mm) dolerite clast.

Fig. 3.38 ***(facing page)*** – Photomicrographs of Ard Bheinn Member ignimbrites. Q = quartz, F = feldspar, B = basalt clasts, cpx = clinopyroxene. **a)** Sample BJG/15/146, a crystal-rich glassy ignimbrite. Bottom left = crossed polars, top right = plane-polarised light. **b)** Sample BJG/17/19, a rhyolitic crystal-rich ignimbrite overlain by a darker, more mafic, lithic-rich ignimbrite. Viewed in plane-polarised light. **c)** Sample BJG/15/78, a feldspar-rich ignimbrite from the summit of Ard Bheinn. Left = plane-polarised light, right = crossed polars. **d)** Sample BJG/15/134, a feldspar-rich ignimbrite with a devitrified glassy matrix. Left = plane-polarised light, right = crossed polars.

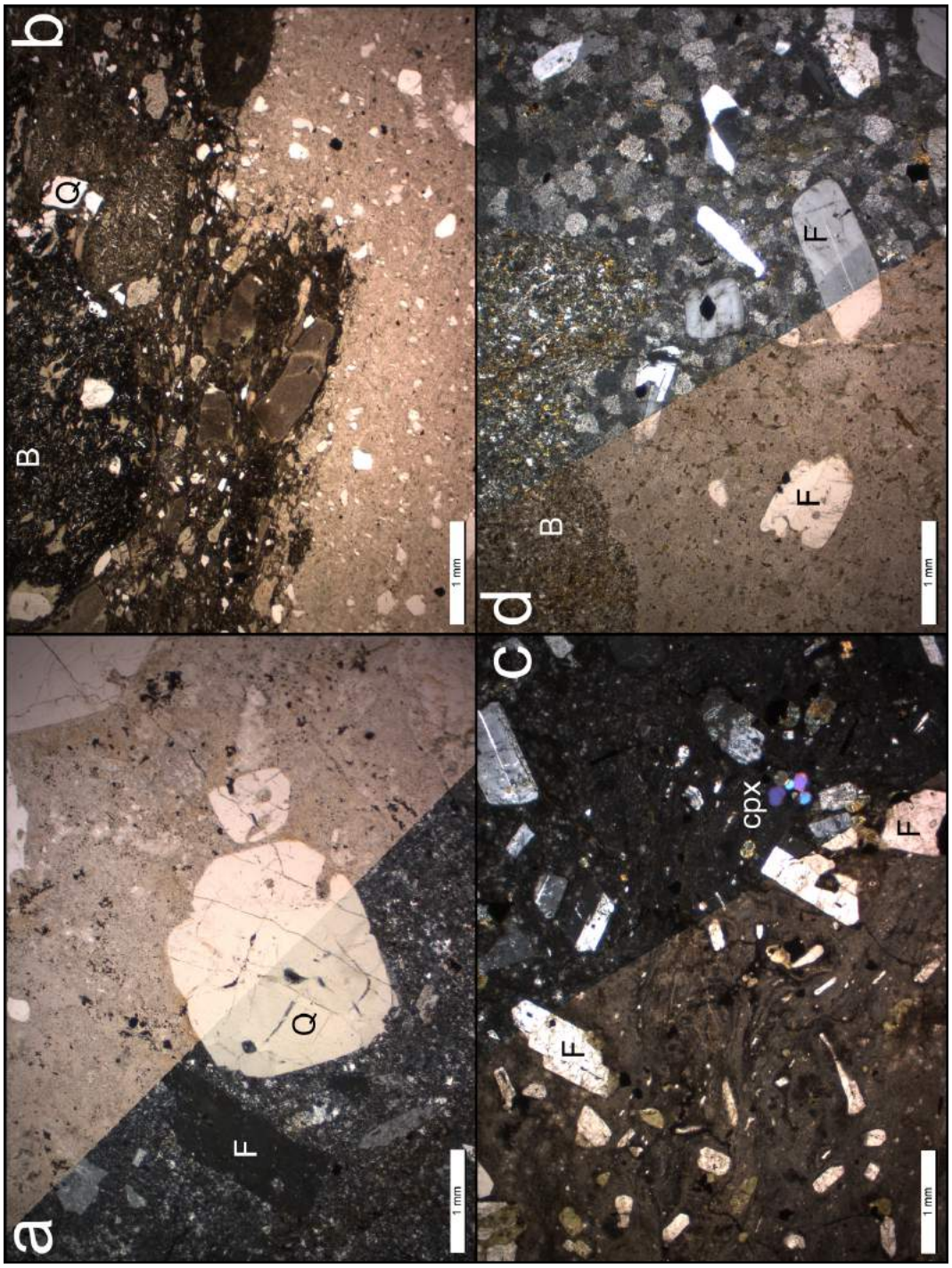
a
Q
F
1 mm
b
Q
B
1 mm
c
cpx
F
F
1 mm
d
F
F
B
1 mm

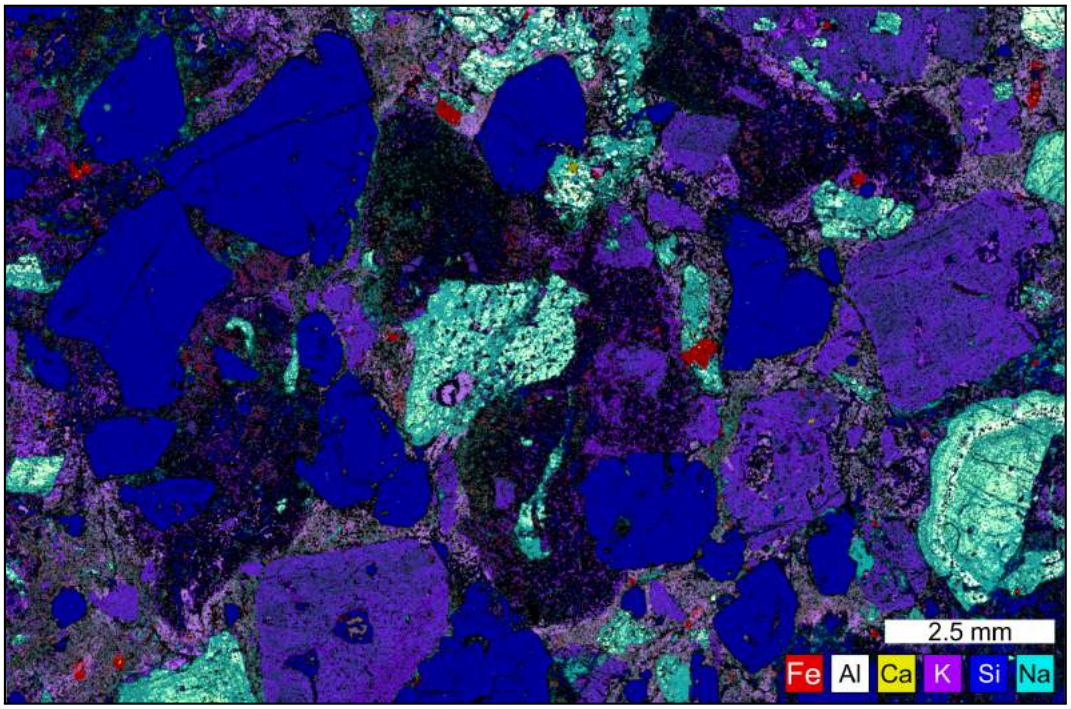

Fig. 3.39 – Major element EDS map of sample BJG/16/5, a crystal-rich tuff from the base of the Ard Bheinn Member. Using this element-based colour scheme, quartz is blue, K-feldspar is purple, plagioclase is pale green, and Fe-Ti oxides are red.

Interpretation

The Ard Bheinn Member is interpreted as a series of mostly lava-like ignimbrites, due to completely agglutinated pyroclasts (Fig. 3.38), pervasive flow-banding in parts, the presence of lithic clasts, and the gradations between units. In the section described in Fig. 3.37, the lower part of the unit, up to around 440 m, is thought to represent one single eruption event, with hot (>900°C) ash deposited from a pyroclastic density current at a relatively stable flow-boundary zone. The presence of columnar jointing throughout this lower section suggests it behaved as a single cooling unit.

The upper parts of the member (above 440 m, Fig. 3.37) were likely formed from a series of small pyroclastic fountaining eruptions of varying temperature, recording deposition at an unstable flow-boundary zone. The agglomerate in Fig. 3.36a contains elongate cognate spatter clasts and lithic lapilli (mTv, mTl-l, mTcr) that were deposited rapidly from a proximal pyroclastic density current.

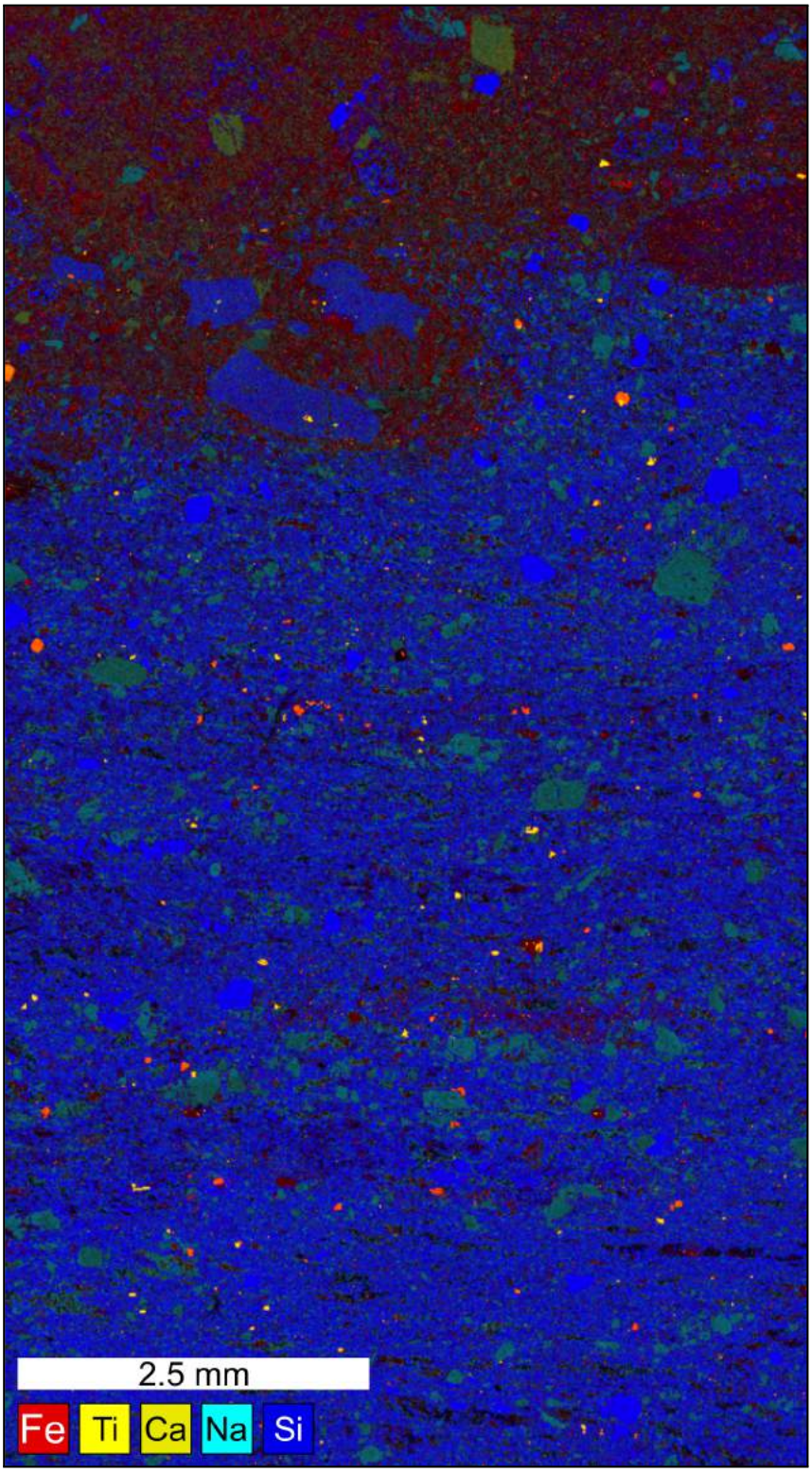

Fig. 3.40 – Major element EDS map of sample BJG/17/19, showing a silicic ignimbrite overlain by a more mafic (Fe-rich) one. Using this element-based colour scheme, quartz is blue, plagioclase is green, Fe oxides are red, and Fe-Ti oxides are orange.

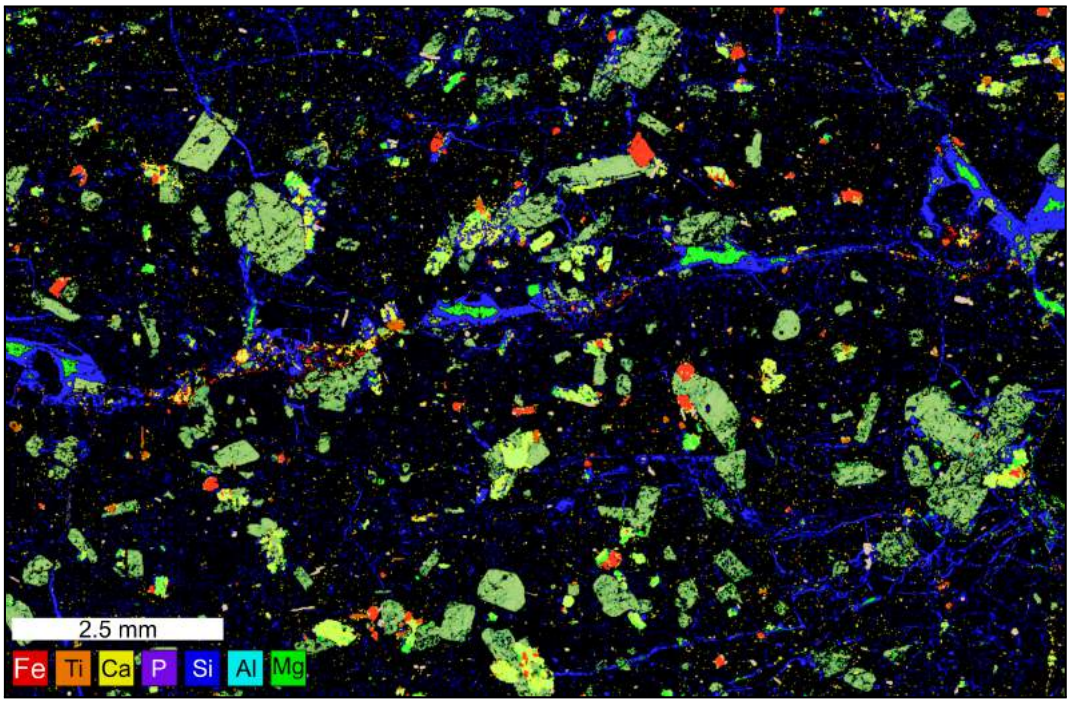

Fig. 3.41 – Major element EDS map of sample BJG/15/78, a feldspar-rich tuff from the summit of Ard Bheinn. Using this element-based colour scheme, plagioclase is pale green, clinopyroxene is yellowy-green, and Fe-Ti oxides are red.

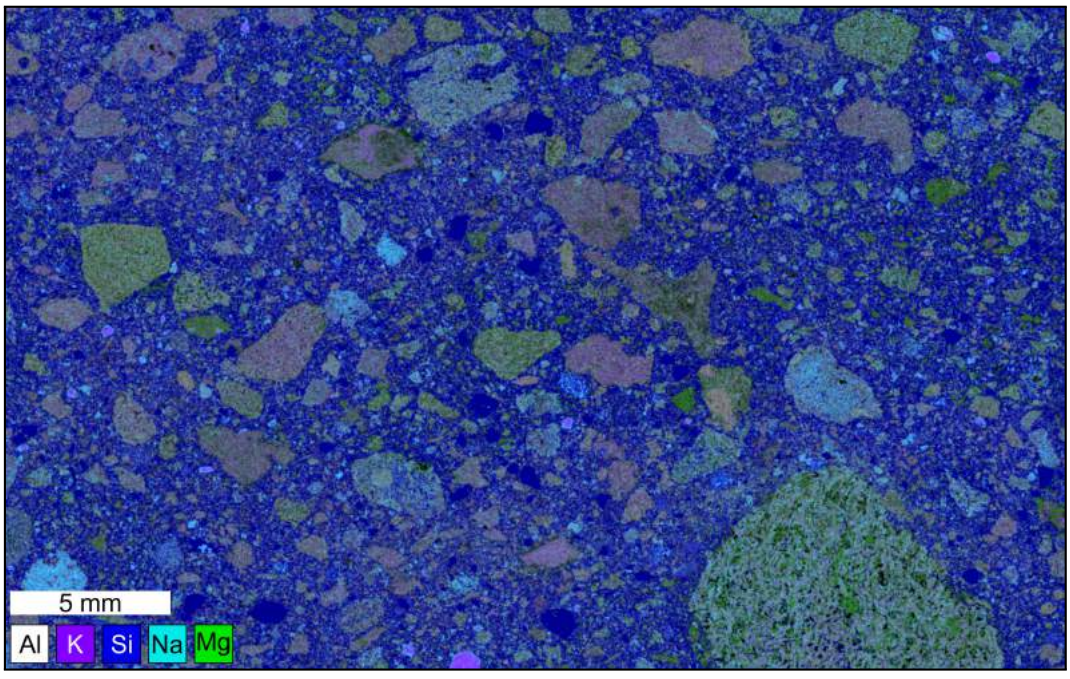

Fig. 3.42 – Major element EDS map of sample BJG/15/142, a massive lapilli tuff from the Ard Bheinn Member. Using this element-based colour scheme, quartz is dark blue, plagioclase is light blue, and a single K-feldspar crystal at the bottom of the map is purple. Mafic clasts are green.

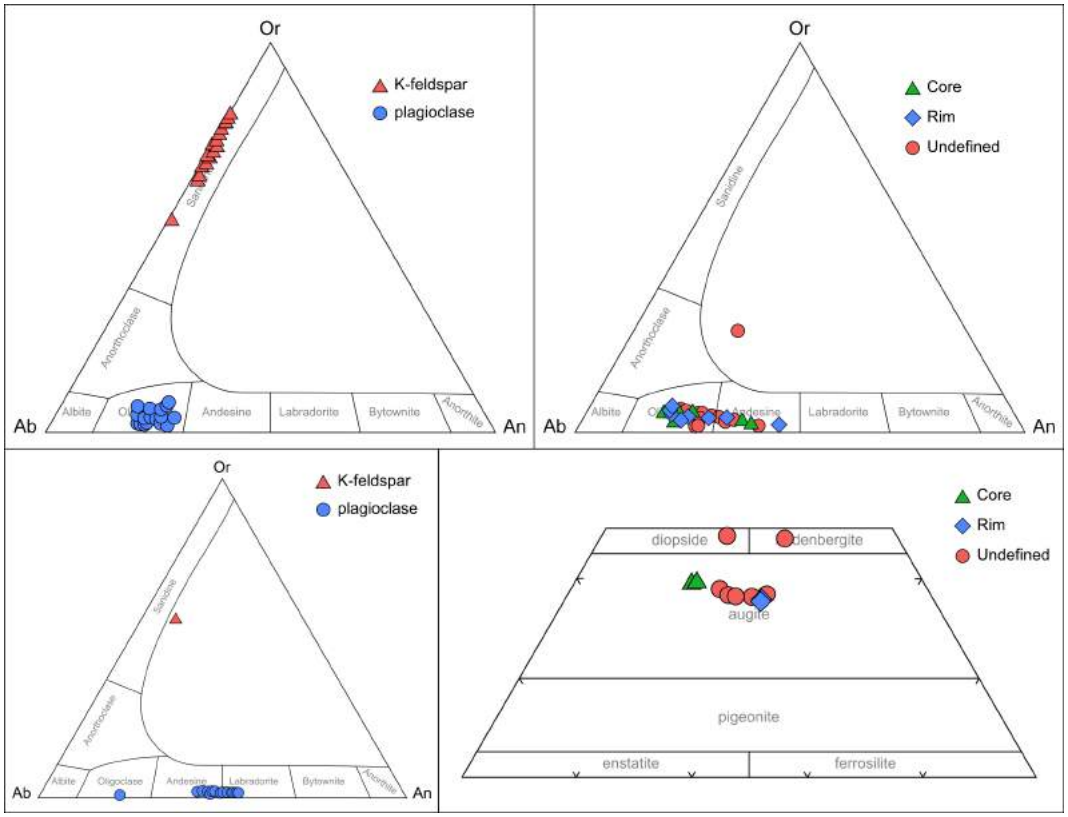

Fig. 3.43 – Ternary plots of EDS data from minerals in the Ard Bheinn Member. **a)** Feldspars in sample BJG/16/5, a coarse crystal tuff from the base of the Ard Bheinn Member. **b)** Feldspars in sample BJG/17/19, a eutaxitic ignimbrite near the Ard Bheinn summit. **c)** Feldspars in sample BJG/15/78, a plagioclase-rich tuff from the summit of Ard Bheinn. **d)** Pyroxenes in sample BJG/15/78.

3.1.10 The Banded Tuffs

Some isolated exposures around the upper parts of Ballymichael Glen and Gleann Dubh comprise ignimbrites that display flow banding on a variety of scales (Fig. 3.44). These are shown in Fig. 3.1. Due to their isolated nature, and poor exposure on flat, vegetated ground, it is impossible to discern their relationship with any other of the mapped units. For this reason, we make no attempt to determine their position within the stratigraphy of the AVF.

Petrography

Photomicrographs of the Banded Tuffs are shown in Fig. 3.45. Fig. 3.45a shows a glassy, banded rhyolite made up of compositionally and texturally distinct bands 0.1–1 mm in thickness. Unusually for ignimbrites in this Formation, it does not contain crystal fragments or lithic lapilli. Fig. 3.45b show a glassy crystal-rich tuff with very large (>5 mm) quartz and feldspar crystals, along with much smaller quartzes and opaque oxides.

An EDS major element map of this crystal rich tuff is shown in Fig. 3.46. This shows a Si and K-rich matrix, presumably rhyolitic glass. Large crystals are K-feldspar (purple) and plagioclase (turquoise-yellow). These are largely rounded and are up to 8 mm in length. The K-feldspars have a thin rim of Na-rich plagioclase. The plagioclases are slightly different from one another. The one in the top-centre is largely sodic with a thin Ca-rich rim. The one in the top right is largely Na-rich, but has irregular patches of Ca and K rich material. This may represent sieve-texturing. The one on the far right has no Ca-rich domains, but shows concentric K-rich zones that are poorly picked out by the low resolution map. The two fragments of plagioclase at the bottom of the image are largely Ca-rich, with thin Na-rich rims. Much smaller (up to 2mm) quartz crystals are rounded.

Fig. 3.44 – Photograph of an exposure of the Banded Tuffs on Tir Dhubh.

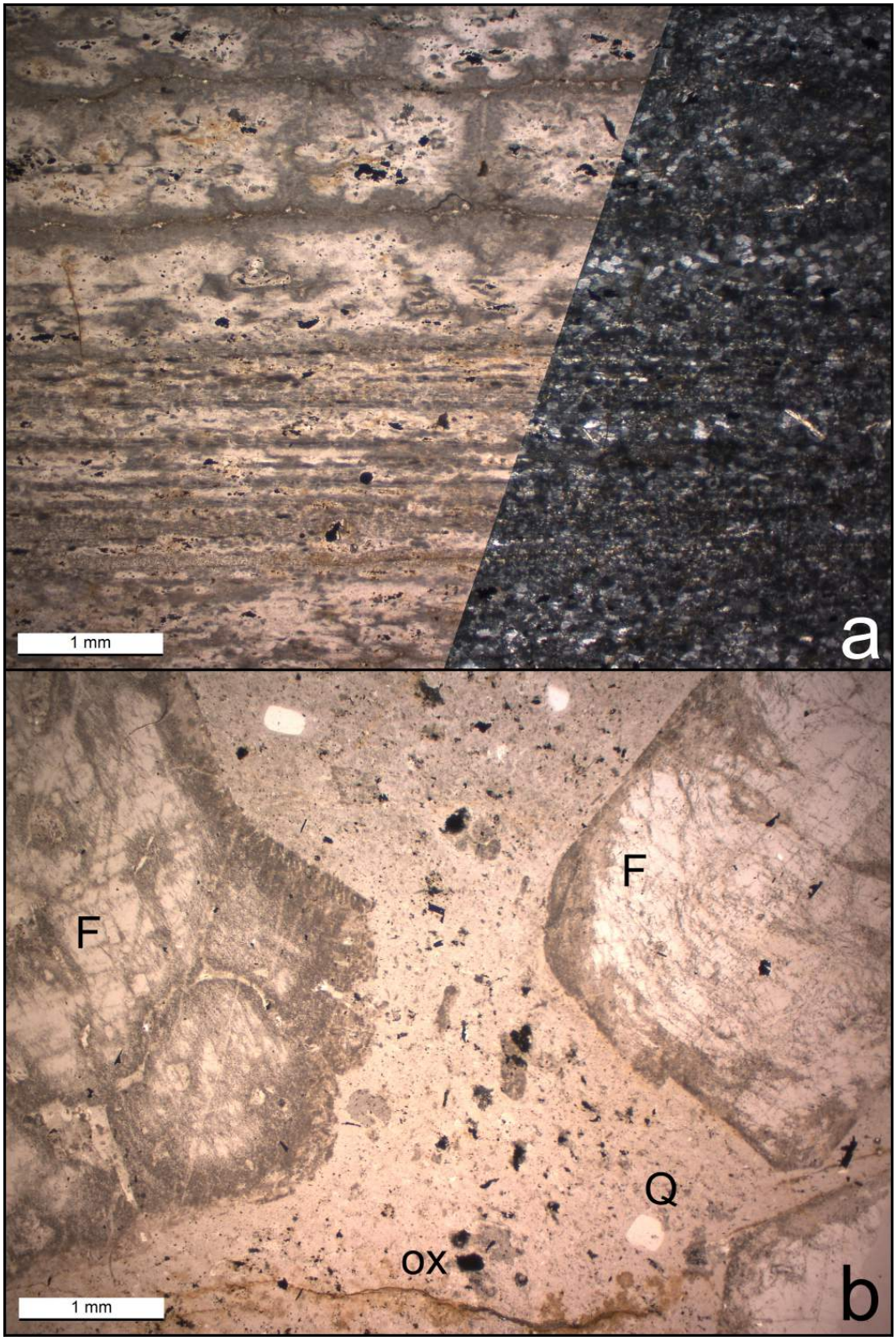

Fig. 3.45 – Photomicrographs of the Banded Tuffs. **a)** Sample BJG/15/163, a foliated, glassy, clast- and crystal-poor ignimbrite. Left = plane-polarised light, right = crossed polars. **b)** Sample BJG/15/159, a crystal rich tuff containing very large quartz (Q) and feldspar (F) crystals, as well as smaller Fe-Ti oxides (ox). Viewed in plane-polarised light.

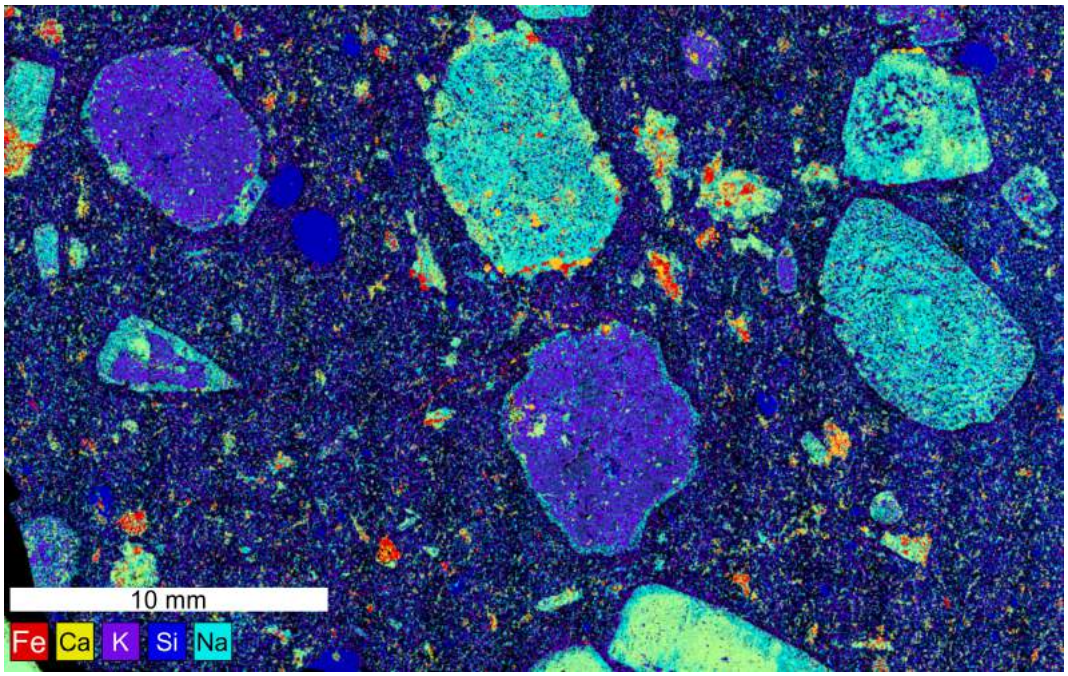

Fig. 3.46 – Major element EDS map of sample BJG/15/159, a coarse crystal-rich ignimbrite from the Banded Tuffs. Using this element-based colour scheme, quartz is blue, K-feldspar is purple, Ca-rich plagioclase is yellow, Na-rich plagioclase is turquoise, and Fe oxides are red. Orange minerals associated with the feldspars are epidote. Orange minerals in the groundmass are sphene.

3.2 Eruptive History

The first event for which evidence is preserved is the eruption of rhyolitic lava-like ignimbrites. These are preserved as the *in situ* Muileann Gaoithe Member ignimbrites on Muileann Gaoithe, where they overlie the pre-Palaeogene sandstones outside the caldera, and at Dereneneach where they underlie the Allt Ruadh Member ignimbrites. Ignimbrites from this phase of eruption are also found as clasts within the mLT of the Allt Ruadh Member and Creag an Fheidh Member. As the base of the Muileann Gaoithe Member is not seen within the caldera, it cannot be said whether this was the first stage of volcanism in the area. It is possible that it overlies the erupted products of earlier volcanism that are now buried.

Eruption of the Muileann Gaoithe Member was followed by a period of highly explosive eruptions to form the Allt Ruadh Member. These events are recorded as the blanket of mLT with minor lapilli-poor tuffs and lava-like ignimbrites that cover the entire area of the caldera (Fig. 3.1). The volume of material ejected from the magma chamber, as well as the inferred presence of steep caldera walls in the period following these eruptions, suggests that this phase of volcanism was accompanied by a significant period of caldera subsidence. No vents or volcanic edifices are preserved, although it is likely that these tuffs were erupted through vents related to the developing ring fault.

In the period after the eruption of the Allt Ruadh Member, significant transport of country-rock material into the topographically low caldera occurred. This is shown by the presence of the Creag Shocach conglomerates overlying the Allt Ruadh Member at Creag Shocach and on the west side of Ard Bheinn. In the Ard Bheinn exposures, interbedded sandstones and conglomerates (Fig. 3.17c) suggest fluvial processes, whereas the massive and highly unsorted nature of the conglomerates at Creag Shocach (Fig. 3.17a,b) suggest debris flows. It is proposed that these deposits represent rapidly collapsing steep caldera walls, created during the subsidence associated with eruption of the Allt Ruadh Member.

Overlying the Creag Shocach conglomerates and the Allt Ruadh Member in the east of the complex is the Creag an Fheidh Member. Because the Creag an Fheidh Member is only exposed in the east of the complex it is suggested that it was sourced from a localised vent or series of vents in the surrounding area. The crystal tuffs and lava-like ignimbrites of the Creag an Fheidh Member are truncated by the fault that runs from east of Binnein na h-Uaimh to west of Creag Mhor (Fig. 3.1). The time-relationship between the fault and the eruption of the Creag an Fheidh Member is unclear. However, the lack of any exposure of this unit west of the fault

suggests that it may already have been a fault scarp against which the Creag an Fheidh ignimbrites were deposited.

The presence of water on the surface of the Creag an Fheidh ignimbrites is inferred from the presence of conglomerates, and the phreatomagmatic Allt Beith tuff cone. There may have been a lake in the topographic low adjacent to the fault scarp that truncates the outcrop of the Creag an Fheidh Member, as this is the area in which the conglomerates and basaltic-andesitic tuffs are found.

The White Tuff Member was deposited on top of the Allt Ruadh Member in the west of the complex and the Creag an Fheidh Member in the east of the complex. The petrological and textural similarity of the White Tuff Member to the Muileann Gaoithe Member suggest very similar eruption styles, and geochemically similar magma sources. Due to the homogeneous and largely structureless nature of this large unit, it is thought that the White Tuff Member represents the deposits of a small number of large eruptive phases, presumably originating from the same magma chamber. Three eruption events are tentatively proposed, with unit tops represented by the autobreccia at 380 m elevation and the topographic shelf at 420 m elevation, as shown in Fig. 3.26.

The Cretaceous chalk found at Pigeon Cave is overlain by the Pigeon Cave Member ignimbrites, and so may have been transported to its current position immediately prior to ignimbrite deposition. The large size of this chalk block (at least 20 m long) and lack of other blocks of similar lithologies in the surrounding area suggest that it did not travel far. It could be a fragment of the caldera floor faulted relatively upwards as a horst during variable break-up of the floor, or it could have collapsed from a nearby caldera-wall fault scarp during caldera subsidence.

The Pigeon Cave Member tuffs and agglomerates were erupted onto the White Tuff Member. The dolerite sill was intruded after deposition of the Pigeon Cave Member ignimbrites, as it is seen to intrude them (Fig. 3.32). Given the brecciated nature of the intrusion, and the presence of peperitic textures around the margins, it is likely that the sill intruded at shallow levels into these ignimbrites, and possibly interacted with groundwater. Given that the Ard Bheinn Member appears to erode down into the sill (Fig. 3.1), it must have been erupted after the emplacement of the sill.

The upper surface of the Pigeon Cave Member was heavily eroded to create significant palaeo-topography, including at least one steep-sided canyon on the north face of Binnein na h-Uaimh. It was into these palaeo-canyons that the Binnein na h-Uaimh conglomerates were deposited. The source of these conglomerates is not clear, but the large size of clasts suggests that it was quite proximal, while the lack of AVF lithologies shows that it was outside the edge of the caldera.

The last phase of volcanism that is preserved within the AVF is the eruption of the Ard Bheinn Member. The coarse crystal tuffs at the base of the Ard Bheinn Member in Ballymichael Glen appear to fill a valley eroded into the White Tuff Member and the dolerite sill (Fig. 3.1). The highly heterogeneous nature of the upper parts of the Ard Bheinn Member (Fig. 3.37) suggests that it was either deposited from a highly unstable pyroclastic density current, or from many small eruptions.

An unknown thickness of the upper Ard Bheinn Member has been lost to erosion, and the total thickness of later AVF units that have been eroded away could total hundreds of metres.

3.3 Discussion of Caldera Structure

Given that the Arran Volcanic Formation comprises Palaeogene surface-deposited rocks juxtaposed against Devonian and Permo-Triassic rocks, it must occupy a caldera which has experienced at least some degree of downfaulting and must therefore possess at least one ring fault. Although this fault is not exposed, the complex meets the other criteria of Brown et al. (2009) for recognising a caldera in the British Palaeogene Igneous Province: (1) a collapse succession of breccias; and (2) evidence of subsidence (*i.e.*, displacement relative to country rocks).

A transect from the western edge of the caldera to the summit of Binnein na h-Uaimh is relatively well exposed, and no significant breaks or duplications in stratigraphy are seen. This suggests that there is only one ring fault, *i.e.*, at the contact between the Arran Volcanic Formation and the pre-Palaeogene sedimentary country rocks. Experimental studies and their comparison to real examples suggest that a caldera that displays one outward-dipping reverse ring fault is likely to have experienced subsidence in the range of 100 m to 1 km (Acocella, 2007).

One fault is identifiable within the caldera (Fig. 3.1), but there are doubtless others. The change in stratigraphy across this fault suggests the sense of movement was ‘down to the east’, but there is no way to determine the magnitude of displacement. This fault is radial to the caldera.

Given the presence of at least one radial fault, an element of piecemeal subsidence can be assumed (Moore and Kokelaar, 1998; Troll et al., 2002). However, there are no other places where the stratigraphy is noticeably disrupted at the scale of the available exposure, so this was clearly not a dominant collapse mechanism. There may also be an element of trapdoor subsidence (Lipman, 1997), as massive lapilli tuffs of the Allt Ruadh Member are exposed in the east of the complex at the same elevation as the summit of Ard Bheinn. This could suggest greater subsidence of

the caldera to the west, but could also be explained by lateral changes in deposit thicknesses (Brown and Bell, 2013) or amount of erosion. There is no evidence of consistently inward-dipping beds, or significant evidence of slumping, so funnel-like subsidence has not occurred (e.g. Miyakejima, Japan – Geshi et al., 2012). Given the broadly horizontal nature of the caldera-fill units and the lack of significant intra-caldera faulting, the closest-approximated end-member subsidence style (by the classification of Acocella, 2007; Lipman, 1997) is piston subsidence, in which a coherent caldera floor is bounded by one or more steeply-dipping ring faults. It is uncertain whether the Arran caldera ring fault is a simple outward-dipping reverse fault (Stage 2, Acocella, 2007) or an inward dipping normal fault with volcanic deposits masking the internal earlier ring fault (Stage 4, Acocella, 2007). However, the relatively simple stratigraphy and lack of disruption likely indicate an outward-dipping reverse fault, supporting rare field and seismic evidence from calderas such as Rabaul, Papua New Guinea (Mori and McKee, 1987; Saunders, 2001).

The upper two units described here – *i.e.*, the Binnein na h-Uaimh conglomerates and the Ard Bheinn Member – show some evidence of flow-directions towards the edges of the caldera. This suggests that at this stage in the caldera's history, there was a palaeo-topographic high roughly in the location of the current Ard Bheinn summit. It is tentatively suggested that this could be evidence for resurgent doming in the period following the main Allt Ruadh-related collapse event. Following Troll et al. (2002), doming may also explain the presence of the radial fault described above, and the northerly transport of Dalradian clasts within the caldera. Uplift associated with caldera resurgence has been linked to shallow magmatic intrusion of sills/dykes and laccoliths. This process has been identified through magnetotelluric imaging on the island of Ischia (Bay of Naples, Italy), where some 800 m of uplift, accompanied by volcanic activity, has occurred (Di Giuseppe et al., 2017).

3.4 Discussion of Proximal Ignimbrites

The majority of ignimbrites in the Arran Volcanic Formation are high grade (lava-like to welded) with rarer low grade, non-welded examples. These ignimbrites are indicative of high temperature, high mass-flux pyroclastic density currents generated from low fountaining columns that retained heat (Branney and Kokelaar, 2002). The lava-like ignimbrites typically display pervasive base-parallel flow banding, indicative of syn-depositional rheomorphism (Andrews and Branney, 2011). There are relatively few examples of post-depositional rheomorphism such as extensive domains of contorted flow banding and refolded folds (Andrews and Branney, 2011),

and a general absence of autobreccia. Together, this indicates there was little slumping, sliding, and ultimately brittle deformation of the cool(ing) ignimbrites (e.g. Andrews and Branney, 2011; Moore and Kokelaar, 1998).

The general lack of lithic-rich lapilli- and block-layers in the ignimbrites also provides information on caldera-scale processes. These types of breccias/lapilli-tuffs are commonly found in intra-caldera proximal ignimbrites and are typically linked to climactic subsidence events and associated caldera wall/floor destabilisation. Modern examples of such units include Ischia (75 ka, Brown et al., 2008) and Pantelleria (46 ka, Jordan et al., 2018) in Italy, and Tenerife (273 ka, Smith and Kokelaar, 2013). The absence of these units on Arran indicates that whilst subsidence clearly occurred, it was not always catastrophic and that explosive caldera-forming eruptions can occur without such 'tracers' of caldera collapse.

Overall, the general absence of slumping/sliding ignimbrites and the paucity of collapse-related lithic breccias, support a gradual piston-like collapse of the caldera, with only minimal disruption by faulting and/or later resurgence. In many respects, the Arran caldera is remarkable for its incremental but consistent collapse and the relative stability of the caldera floor.

3.5 Summary

A summary of the pyroclastic and sedimentary units of the Arran Volcanic Formation is given in Table 3.2. A full synthesis of the formation of the caldera is given in Chapter 6.

Table 3.2 – Descriptions and interpretations for the volcanic and sedimentary units that make up the Arran Volcanic Formation

Unit	Locations	Description	Interpretation
Muileann Gaoithe Member	Muileann Gaoithe in far NE of complex (extra-caldera). Dereneneach in the far W of the complex.	*Lithologies*: Massive rhyolite (77-79 wt.% SiO_2) tuff. Minor mLT and red weathered non-welded tuff. *Crystals and clasts*: Abundant quartz up to 2 mm. K-feldspar, plagioclase, Fe-Ti oxides. Clasts in mLT = sandstone, dolerite, rhyolite *Textures*: cm-scale flow banding in lower and upper parts. Sub-mm fabric defined by <1 mm to near-continuous elongate bands	Rhyolitic parataxitic to lava-like ignimbrite. Very high-grade ignimbrite of 'Snake River type' (Andrews and Branney, 2011). Rapid deposition from a high temperature, (>900°C) high-mass-flux pyroclastic density current from low fountaining eruption. mLT record pulses of higher explosivity. Red tuff (sT) represents upper surface of ignimbrite sheet in contact with atmosphere.
Allt Ruadh Member	Western slopes of Ard Bheinn. Lower Glen Craigag.	*Lithologies*: Orange- and grey-weathering mLT. Minor crystal-rich and glassy tuffs. *Crystals and clasts*: pre-Palaeogene schist, sandstone, quartzite. Palaeogene basalt, dolerite, occasional granite. Crystal tuffs contain feldspar and minor quartz *Textures*: mLT massive. Crystal tuffs are eutaxitic to lava-like.	Lithic-lapilli-rich non-welded ignimbrite deposited from a PDC at a flow-boundary zone dominated by fluid-escape, with very little turbulent shear-induced tractional segregation (Branney and Kokelaar, 2002). Highly explosive, caldera-forming eruptive phase. mTcr record phases of lower explosivity.
Creag Shocach Conglomerates	Western slope of Ard Bheinn. Creag Shocach above Glenloig.	*Lithologies*: Red conglomerates, breccias, and minor sandstones *Crystals and clasts*: Pre-Palaeogene medium- to coarse-grained red sandstones and quartzite conglomerates. Fine to medium sand matrix. *Textures*: Clast supported and matrix supported in different areas.	Erosion of Devonian and Permo-Triassic lithologies from steep caldera walls left by caldera subsidence related to eruption of the Allt Ruadh Member. Deposition – alluvial/fluvial.
Creag an Fheidh Member	Creag an Fheidh. E of Creag Shocach.	*Lithologies*: glassy mT, mTcr, and mLT *Crystals and clasts*: Crystals largely feldspar, with lesser quartz. Clasts in mLT of rhyolite and sedimentary rocks. Upper surface contains rounded pebbles and cobbles of rhyolite and quartzite. *Textures*: Some bedding-parallel flow-fabric in glassy units. Some mTcr are eutaxitic	Heterogeneous ignimbrites recording a range of eruptive styles. mLT and mTcr record variably highly-explosive eruptions and deposition from a PDC at a flow-boundary zone dominated by fluid-escape. Eutaxitic and glassy tuffs record higher emplacement temperatures. Rounded clasts evidence for fluvial reworking on upper surface of ignimbrite.
Allt Beith tuff cone	Near the head of the Allt Beith	*Lithologies*: Finely laminated basaltic-andesitic (54.5 wt.% SiO_2) tuff *Crystals and clasts*: None identified *Textures*: Planar bedding and cross-stratification. Some graded bedding.	Localised phreatomagmatic tuff cone – very fine grain size suggests intense fragmentation. Well-developed stratification suggests deposition from a fully dilute pyroclastic density current at a traction dominated flow boundary zone (Branney and Kokelaar 2002, Brown et al 2007).
White Tuff Member	Western slopes of Ard Bheinn. Plateau between Ard Bheinn and Glen Craigag.	*Lithologies*: Massive rhyolite (76-77 wt.% SiO_2) tuff with some autobreccia and conglomerate at top *Crystals and clasts*: Quartz and feldspar up to 2 mm. Upper conglomerate contains clasts of rhyolitic tuff, basalt, quartzite *Textures*: Largely massive with planar and chaotic flow banding in places	Rhyolitic lava-like ignimbrite. Very high-grade ignimbrite of 'Snake River type' (Andrews and Branney, 2011). Rapid deposition from a high temperature, (>900°C) high-mass-flux pyroclastic density current from low fountaining eruption. Autobreccia may record post-deposition slumping. Upper conglomerate evidence for fluvial reworking on upper surface of ignimbrite.

Table 3.2 cont.

Unit	Locations	Description	Interpretation
Pigeon Cave Member	Slopes of Binnein na h-Uaimh. E of Glen Craigag.	*Lithologies*: Turquoise-weathering mLT and mAg with minor glassy mT *Crystals and clasts*: Quartz and less abundant feldspar and Fe-Ti oxides. Clasts of pre-Palaeogene schist and sandstone and Palaeogene basalt and rhyolite. Lava-like cognate spatter clasts. *Textures*: Some bedding-parallel fabric in glassy units. Cognate spatter clasts are elongate ribbons.	Heterogeneous ignimbrites recording highly dynamic and fluctuating deposition history. mT and mLT formed as above. mAg formed from rapid deposition of cognate clasts (with lithic lapilli) from a pyroclastic density current rich in ash and dominated by fluid escape (Branney and Kokelaar, 2002).
Binnein na h-Uaimh conglomerates	Northern slopes of Binnein na h-Uaimh.	*Lithologies*: Very coarse conglomerate. *Crystals and clasts*: Pebbles to large cobbles of sandstone and schist (resemble local Dalradian units) and smaller pebbles of vein quartz and quartzite. *Textures*: Clast supported. No clast alignment.	Debris flow conglomerate recording mass wasting of surrounding landscape into caldera.
Ard Bheinn Member	Summits of Ard Bheinn and Binnein na h-Uaimh.	*Lithologies*: Dominated by glassy rhyolitic (77 wt.% SiO_2) mT and mTcr. Minor autobreccias, agglomerates, and lapilli tuff. Purple-grey units near top are dacitic (68-70 wt. % SiO_2) *Crystals and clasts*: Crystals in mTcr are primarily plagioclase. Coarse crystal tuff at base contains large resorbed quartz and less abundant feldspars. *Textures*: Largely vitrophyric with platy flow fabric in places. Agglomerates show distinct banding. Lapilli tuff near top is eutaxitic with fiamme of mafic material.	Mostly lava-like ignimbrites. Lower part of unit (to 440 m) is thought to represent one single eruption event, with hot (>900°C) ash deposited from a pyroclastic density current at a relatively stable flow-boundary zone. Continuous jointing throughout suggests one single cooling unit. Upper parts of the member (above 440 m) likely formed from a series of small pyroclastic fountaining eruptions of varying temperature, recording deposition at an unstable flow-boundary zone. Agglomerates deposited rapidly from a proximal pyroclastic density current.

Chapter 4

Geochemical and Geochronological Results

This chapter presents the results of whole-rock element geochemistry, whole-rock isotope geochemistry, and zircon U-Pb geochronology from the Central Arran Igneous Complex and other igneous rocks on Arran.

4.1 Whole-rock Element Geochemistry

Major element oxide concentrations (SiO_2, TiO_2, Al_2O_3, Fe_2O_3, MnO, MgO, CaO, Na_2O, K_2O, P_2O_5) and minor element concentrations (Sc, V, Cr, Co, Ni, Cu, Zn, Sr, Y, Zr, Ba) were measured with inductively coupled plasma optical emission spectrometry (ICP-OES).

Minor and trace element concentrations (V, Cr, Co, Ni, Cu, Zn, Ga, Ge, Rb, Sr, Y, Zr, Nb, Mo, Sn, Cs, Ba, La, Ce, Pr, Nd, Sm, Eu, Gd, Tb, Dy, Ho, Er, Tm, Yb, Lu, Hf, Ta, ^{208}Pb, ^{232}Th, ^{238}U) as well as TiO_2, MnO, and Fe_2O_3 concentrations, were measured by inductively coupled plasma mass spectrometry (ICP-MS). Full accounts of analytical procedures are given in Appendix A. Full major and trace element results are presented in Appendix E3, with accuracy and precision data given in Appendix E4.

Throughout this thesis the values presented for TiO_2, Sr, and Sc are from ICP-OES, and all other minor and trace elements are from ICP-MS. TiO_2 concentrations from ICP-OES are used for consistency with the other major elements. All minor element concentrations use data from the ICP-MS as this system is specifically designed for low-concentration measurements. Sr was the only element where ICP-OES data were more accurate when compared to international reference standards than the ICP-MS data. Sc was not analysed by ICP-MS.

Total iron was measured as Fe_2O_3 and are presented throughout this study as Fe_2O_3*. To convert to total FeO, a conversion factor is applied:

$$FeO^* = Fe_2O_3{}^* \times 0.8998$$

To estimate the absolute amounts of both Fe_2O_3 and FeO, the following equations are used:

$$FeO^{est.} = FeO^* \times 0.9$$

$$Fe_2O_3{}^{est.} = (FeO^* - FeO^{est.}) \times 1.11$$

Molar magnesium number (Mg#) is calculated from wt.% values using the following equation:

$$Mg\# = 100 \times \frac{(MgO/40.3)}{(MgO/40.3 + FeO/71.85)}$$

The samples analysed for whole-rock elemental geochemistry are as follows:

- A total of 18 mafic (basalt and dolerite) dykes which intrude the CAIC, along with a picrite dyke from Ballymichael Glen and a pitchstone dyke from Glen Craigag.
- Ten mafic dykes which intrude the North Arran Granite, for comparison with the CAIC dykes.
- A total of ten samples of the dolerite sill which intrudes the ignimbrites of the Arran Volcanic Formation.
- Seven samples from the various small isolated gabbro bodies associated with the Glenloig Hybrids.
- A total of 38 samples of the Glenloig Hybrids, along with four samples from the Sheans and five samples from Tighvein for comparison.
- Ten samples of the Glen Craigag Granite.
- A total 22 samples of the Satellite Granites. These comprise:
  - Eight from the Bridge Farm Granite.
  - Two from the Cnoc Dubh Granite.
  - Seven from the Creag Mhor Granite.

  - Three from the Dereneneach Granite.
  - Two from the Torr nan Dearc Granite.

- Eight samples of the North Arran Granite, for comparison with the CAIC granites.
- Two clasts of granite from the ignimbrites of the AVF, in order to assess geochemical similarities to any of the exposed *in situ* granites.
- Nine samples of ignimbrite. These were samples deemed to have near-magmatic compositions; this criterion ruled out the vast majority of ignimbrite samples collected which were full of inherited clasts or crystals. The nine analysed samples include two from the White Tuff Member, two from the Muileann Gaoithe Member, three from the Ard Bheinn Member, and one from the Allt Beith tuff cone.

4.1.1 Alteration and element mobility

The majority of igneous rocks in the Central Arran Igneous Complex display some degree of alteration (see Chapter 2). The mafic rocks all show evidence for the complete replacement of olivine by alteration minerals (other than a picrite dyke in Ballymichael Glen which retains relict fresh olivine), suggesting that volcanism-related hydrothermal activity – similar to the '*zone of pneumatolysis*' described by Bailey et al. (1924) on Mull – was an active process on Arran. Other than this, the basaltic rocks of central Arran are generally fresh, with fresh pyroxenes and feldspars.

The Glenloig Hybrids and gabbros contain chlorite and epidote, and some samples are so altered that they contain very little primary amphibole, and the feldspars are heavily sericitised.

The ignimbrites show varying degrees of alteration. The freshest contain unsericitised feldspars and textures in the glass can be very clearly seen (Sections 3.1.1, 3.1.6). The most heavily altered do not contain any original glass or ash textures, and instead have matrices of fine-grained alteration minerals, including sheet silicates and opaque minerals.

Care must be taken when studying elemental abundances in altered rocks, as certain elements can be susceptible to mobilisation. This group includes Ca, Mg, Na, K, Rb, Ba, Sr, Pb, and U (Pearce, 1996), and so while the abundances of these elements can be used to shed light on petrological processes, caution must be exercised. The elements that are generally immobile up to greenschist facies

conditions are Ti, Zr, Hf, Nb, Ta, Th, Al, and the REEs other than La (Pearce, 1996). Patterns in the abundances of these elements are therefore likely to be purely due to petrogenetic processes.

4.1.2 Major Elements

The major element geochemistry of the various units of the CAIC, as well as the North Arran Granite, the Sheans, and Tighvein are presented here. They are shown in the form of binary plots with a measure of magmatic evolution on the x-axis (Harker plots).

Mafic units

Representative major elements for the mafic (and ultramafic) dykes of the CAIC and NAG, as well as the dolerite sill and the gabbros, are plotted against SiO_2 (Fig. 4.1), MgO (Fig. 4.2; does not include picrite dyke), and Zr (Fig. 4.3), as these elements show trends related to magmatic evolution.

The CAIC dykes contain 46.5 – 53.5 wt.% SiO_2, 5.0 – 8.0 wt.% MgO, and Mg# 40.8 – 55.0. With increasing evolution (increasing SiO_2 and Zr and decreasing MgO), all major elements behave as expected with fractional crystallisation (decreasing MgO and Fe_2O_3*, and increasing Na_2O and K_2O).

The NAG dykes contain 46.6 – 60.0 wt.% SiO_2, 3.0 – 9.2 wt.% MgO, and Mg# 26.4 – 59.1. This is a greater range of composition than seen in the CAIC dykes, with the most evolved examples having andesitic compositions (Fig. 4.33). The most basic examples have higher MgO concentrations than any of the CAIC dykes (not including the picrite) suggesting they may be more primitive.

The samples from the dolerite sill that intrudes the CAIC contain 45.8 – 49.6 wt.% SiO_2, 7.3 – 9.2 wt.% MgO, and Mg# 48.1 – 57.0. This is a relatively limited range of composition, as would be expected for a single intrusion. The samples generally display similar major element compositions to the more basic NAG dykes. They are slightly more MgO-rich than the CAIC dykes. On the Zr diagrams they are generally indistinguishable from the main cloud of CAIC and NAG dykes.

The gabbros contain 44.2 – 53.2 wt.% SiO_2, 4.5 – 5.9 wt.% MgO, and Mg# 34.7 – 53.6. The outlier with high Fe_2O_3* and low SiO_2, Al_2O_3, Na_2O, and K_2O is sample BJG/16/12, the magnetite cumulate from the intra-caldera inlier. The rest of the gabbro samples form clusters on most major element plots (although sample BJG/15/164 has anomalously high Al_2O_3). They have more K_2O than all but the most evolved CAIC and NAG dykes.

The picrite dyke contains 43.6 wt.% SiO_2, 19.6 wt.% MgO, and a Mg# of 79.3. It is an outlier on all major element diagrams, as would be expected from a relatively primitive magma with accumulated olivine; in particular high MgO and low SiO_2, TiO_2, Na_2O, and K_2O.

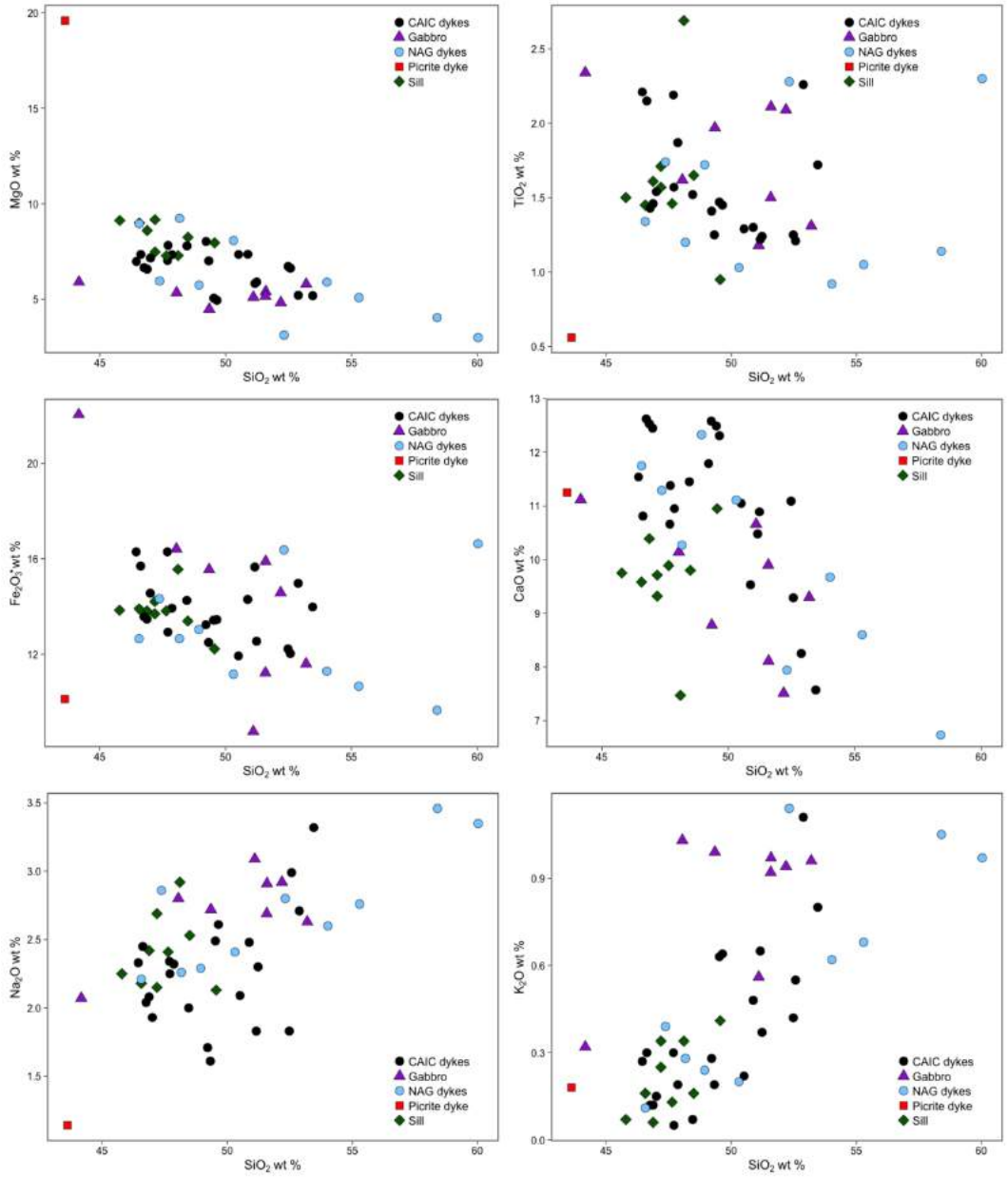

Fig. 4.1 – Representative major elements plotted against SiO_2 (Harker plots) for the dykes which intrude the CAIC and NAG, and the other mafic units.

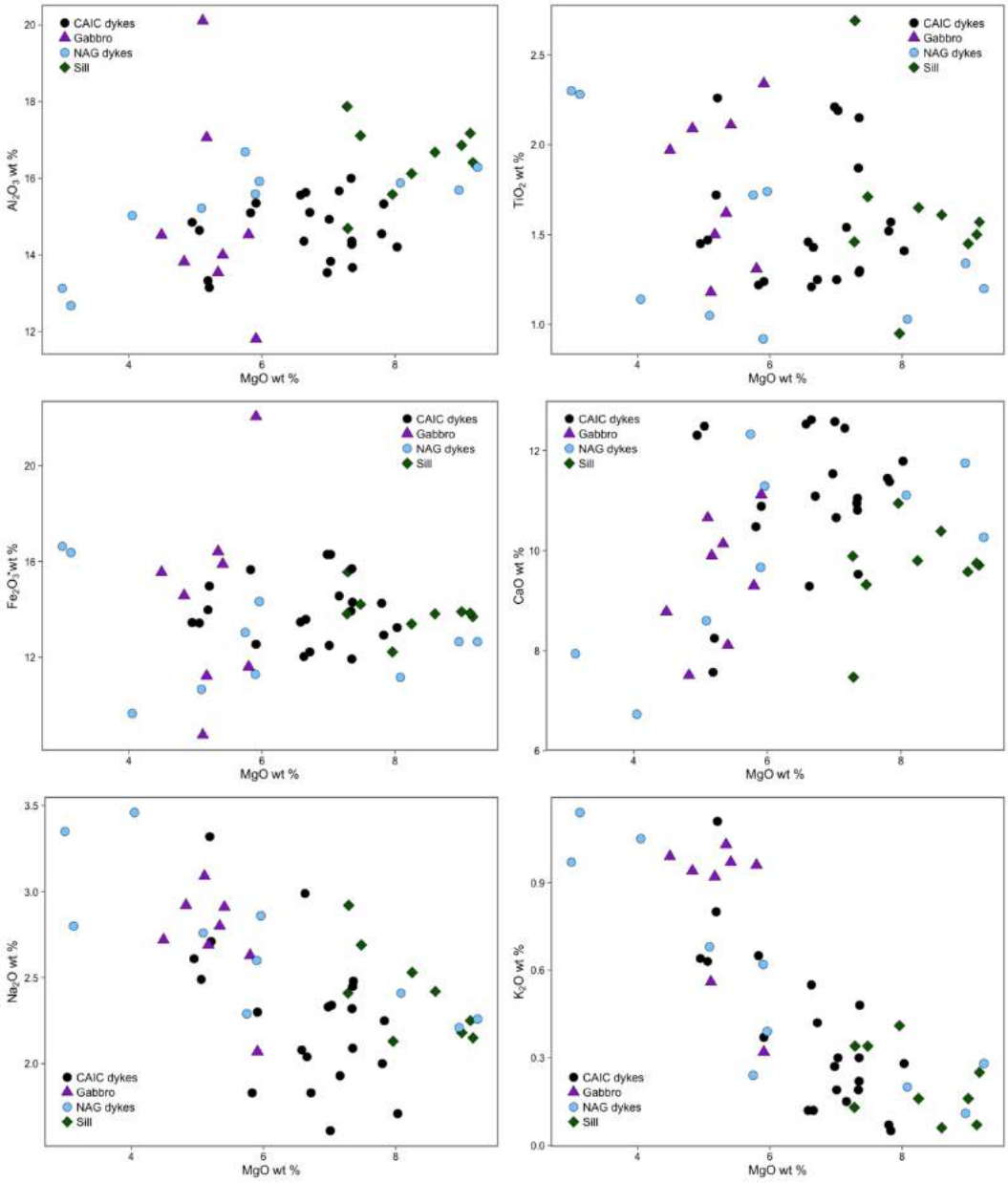

Fig. 4.2 – Representative major elements plotted against MgO for the dykes which intrude the CAIC and NAG, and the other mafic units. These figures do not include the picrite dyke, which would plot well to the right of the displayed range.

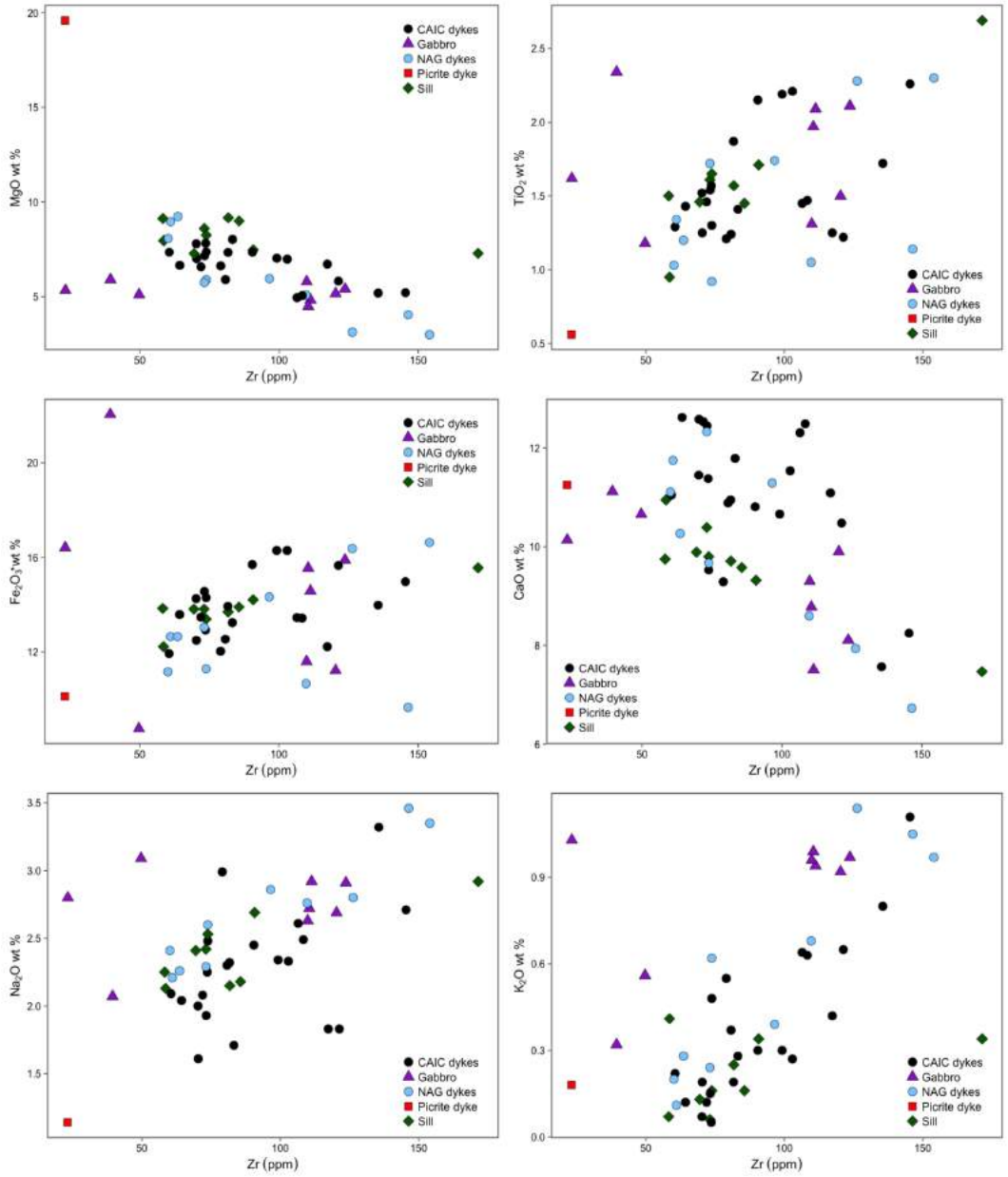

Fig. 4.3 – Representative major elements plotted against Zr for the dykes which intrude the CAIC and NAG, and the other mafic units.

Glenloig Hybrids and similar units

Representative major elements for the Glenloig Hybrids (including the intra-caldera hybrids), as well as samples from the Sheans and Tighvein, are plotted against SiO_2 (Fig. 4.4), MgO (Fig. 4.5), and Zr (Fig. 4.6).

The Glenloig Hybrids (including the intra-caldera hybrids) contain 52.9 – 82.3 wt.% SiO_2, 0.03 – 6.8 wt.% MgO (all but three are <4 wt.%), and Mg# 3.0 – 67.7. This large range of compositions reflects the range in lithologies (Fig. 4.38; Section 2.1). When plotted against SiO_2, most major elements display patterns consistent with evolution by fractional crystallisation. Some of the more evolved samples do not show this trend, and have higher CaO and lower Na_2O and K_2O. When plotted against MgO and Zr these trends are not as clear, but still generally present. On the SiO_2 and MgO diagrams, the intra-caldera hybrids plot within the main trend of the more evolved Glenloig Hybrids samples.

The Sheans samples contain 55.2 – 63.4 wt.% SiO_2, 3.4 – 4.0 wt.% MgO, and Mg# 34.8 – 46.9. These are consistent with the less-evolved Glenloig Hybrids samples, but on many of the major element diagrams they show significantly different trends (although this is based on a small number of samples). With increasing SiO_2 they show a trend of increasing TiO_2 and Fe_2O_3*, opposite to the trend of the Glenloig Hybrids. This suggests a different crystallisation history regarding Fe-Ti oxides (non-fractionation or accumulation). The Sheans samples also generally have higher Al_2O_3 and lower Na_2O and K_2O concentrations than the Glenloig Hybrids.

The Tighvein samples contain 63.7 – 75.3 wt.% SiO_2, 0.07 – 1.5 wt.% MgO, and Mg# 3.4 – 15.2. This is broadly consistent with the more evolved Glenloig Hybrids. Although they show the same trends as the Glenloig Hybrids (presumably related to fractional crystallisation) they have higher TiO_2 and Fe_2O_3* concentrations at intermediate SiO_2 and MgO compositions.

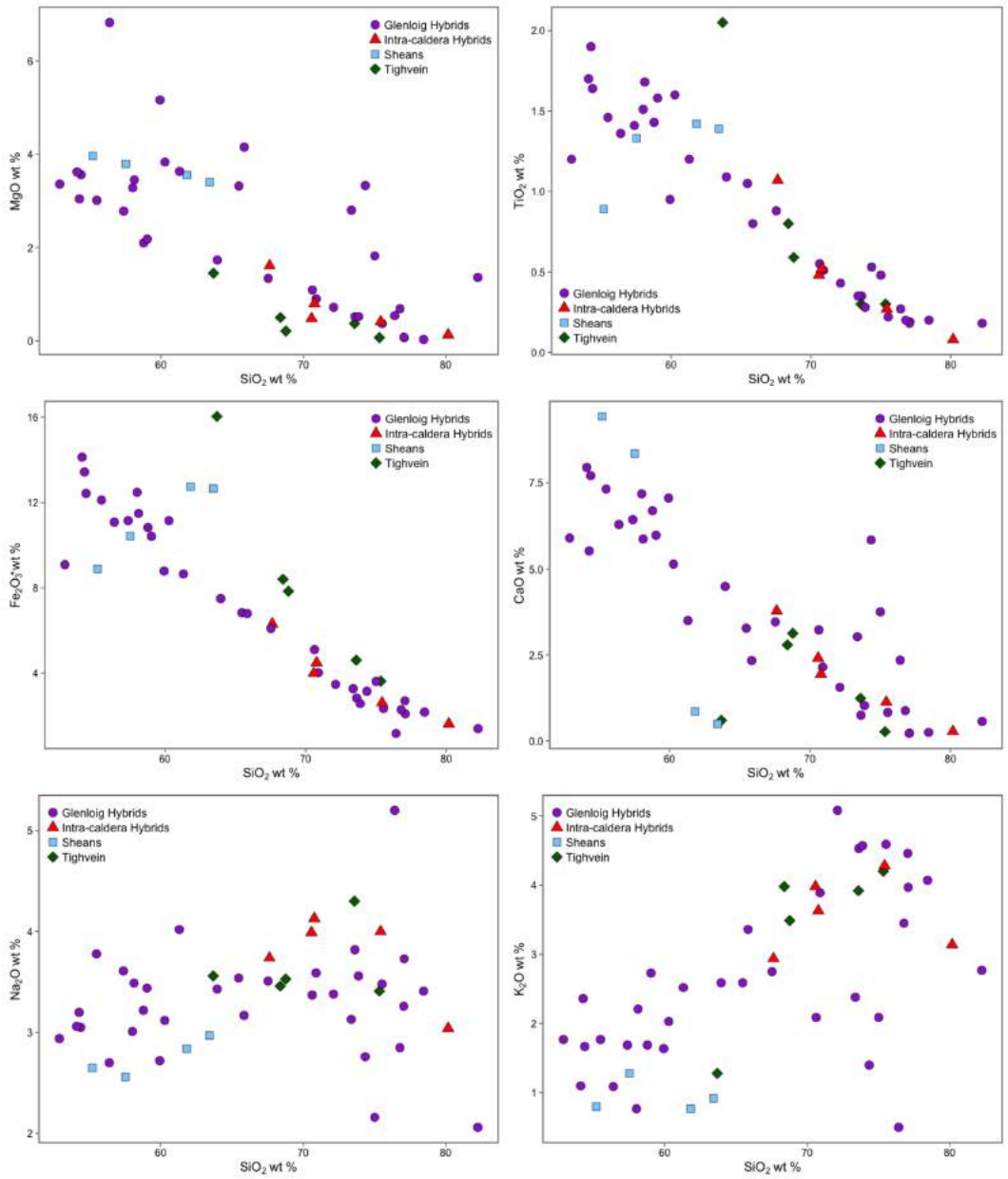

Fig. 4.4 – Representative major elements plotted against SiO_2 (Harker plots) for the hybrid rocks of the CAIC and similar units in the surrounding area.

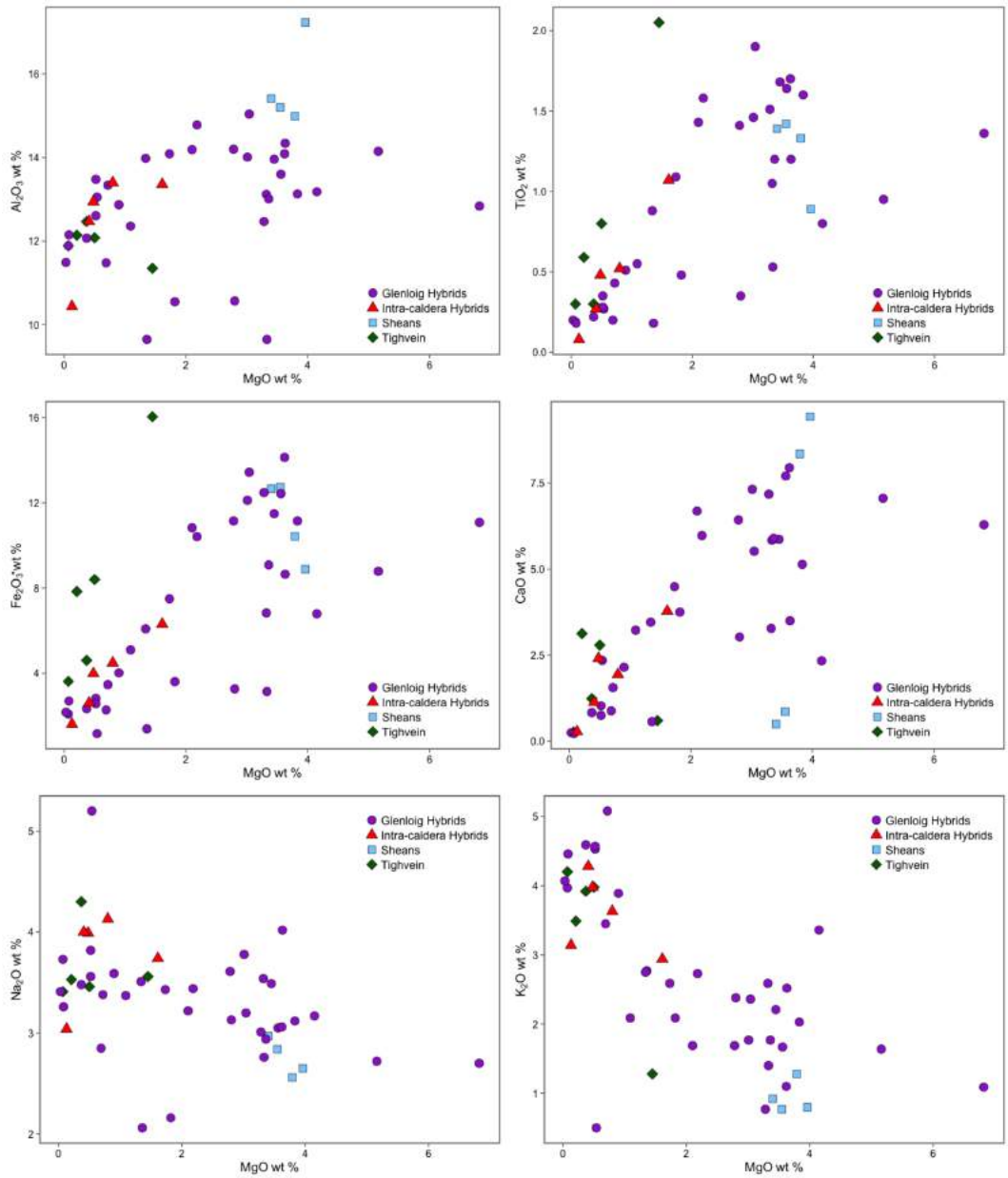

Fig. 4.5 – Representative major elements plotted against MgO for the hybrid rocks of the CAIC and similar units in the surrounding area.

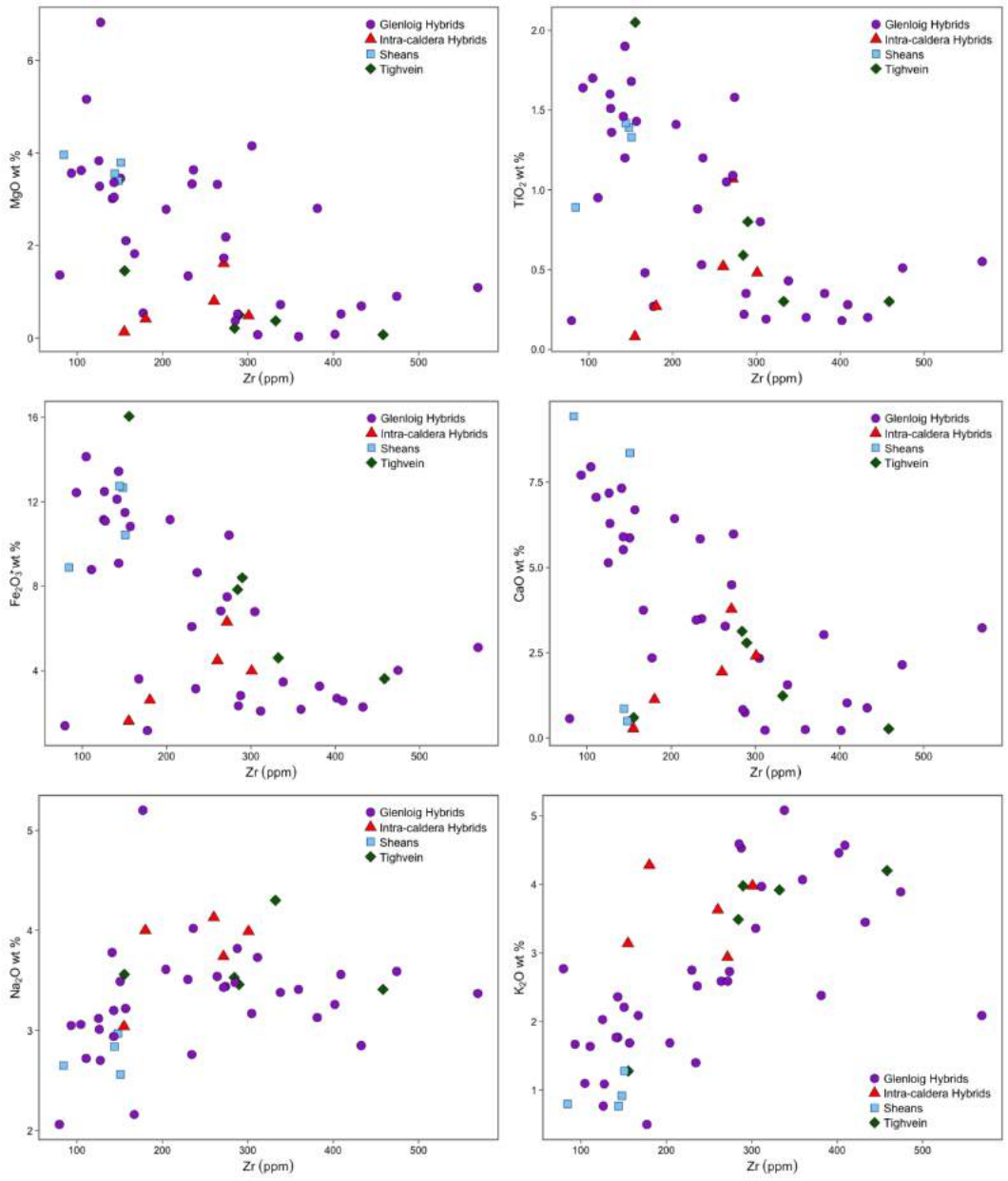

Fig. 4.6 – Representative major elements plotted against Zr for the hybrid rocks of the CAIC and similar units in the surrounding area.

Granites

Representative major elements for the Glen Craigag Granite and Satellite Granites from the CAIC, the North Arran Granite, and the granite clasts found within the ignimbrites of the AVF, are plotted against SiO_2 (Fig. 4.7), MgO (Fig. 4.8), and Zr (Fig. 4.9).

The Glen Craigag Granite contains 75.7 – 81.0 wt.% SiO_2, 2.0 – 3.6 wt.% Fe_2O_3*, and Mg# 2.8 – 30.4. Most major elements do not show significant evolution trends, except Fe_2O_3* which increases with decreasing MgO and increasing Zr.

The Satellite Granites contain 71.5 – 78.8 wt.% SiO_2, 1.8 – 6.9 wt.% Fe_2O_3*, and Mg# 3.0 – 33.7. There appear to be two groups based on MgO content, one with MgO < 0.25 wt.%, and one with MgO > 0.40 wt.%. The higher MgO group is significantly more MgO rich than the Glen Craigag Granite, while the lower MgO group is geochemically similar to the Glen Craigag Granite. The Satellite Granites generally have higher Fe_2O_3* and K_2O than the Glen Craigag Granite.

The North Arran Granite contains 76.4 – 78.6 wt.% SiO_2, 1.0 – 1.58 wt.% Fe_2O_3*, and Mg# 0.70 – 23.3. This SiO_2 content is similar to that of the Glen Craigag Granite and the more SiO_2-rich Satellite Granites. The most noticeable difference, in terms of major elements is that it has much lower TiO_2 and Fe_2O_3* than the other granites, presumably due to fractionation of Fe-Ti oxides.

The granite clasts found in the ignimbrites of the AVF contain 78.3 and 78.4 wt.% SiO_2, 1.05 and 1.4 wt.% Fe_2O_3*, and Mg# of 8.7 and 9.7. These samples have similar concentrations of most major elements to the North Arran Granite, notably in terms of low TiO_2 and Fe_2O_3*.

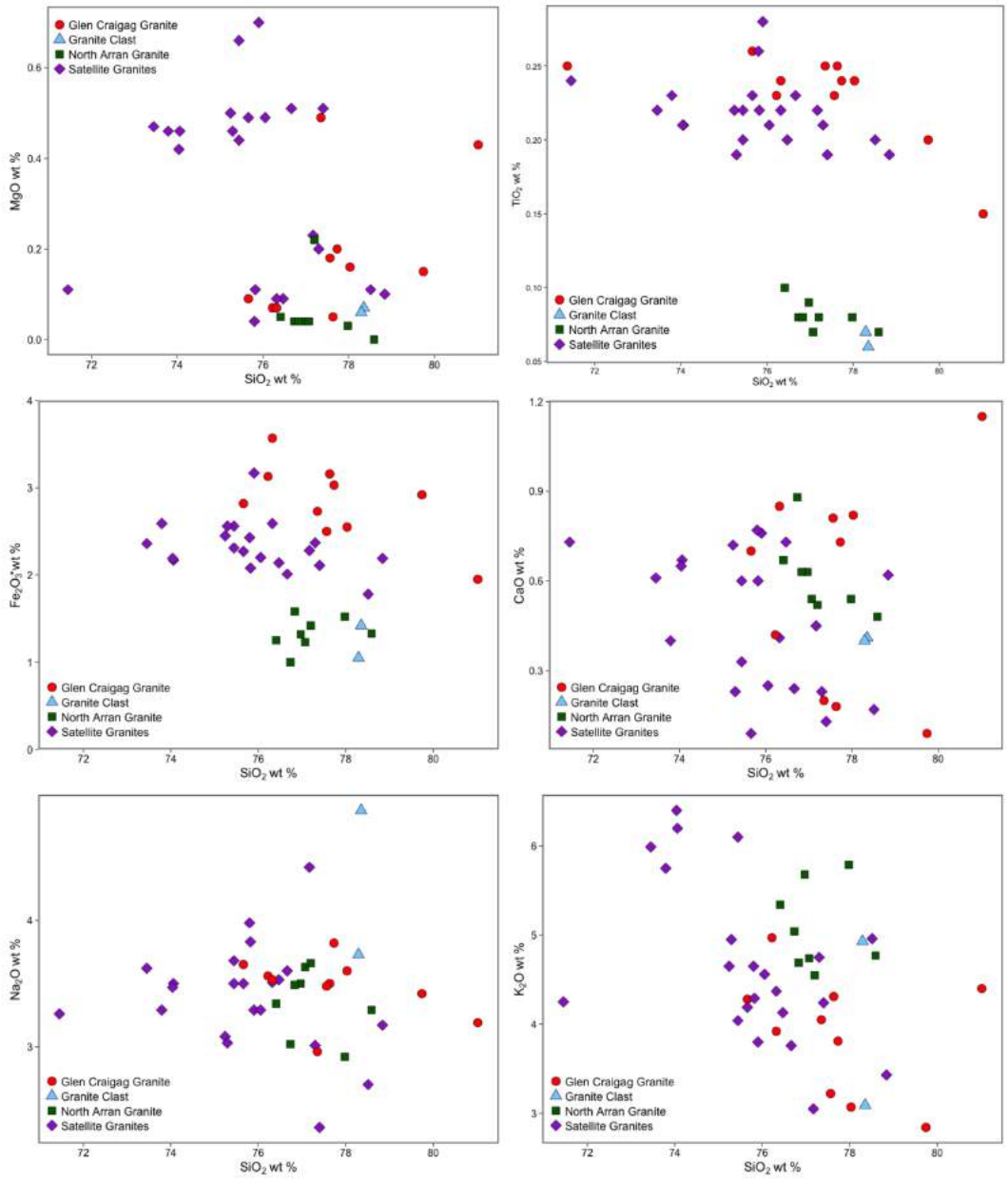

Fig. 4.7 – Representative major elements plotted against SiO_2 (Harker plots) for the granitic rocks of the CAIC and the NAG.

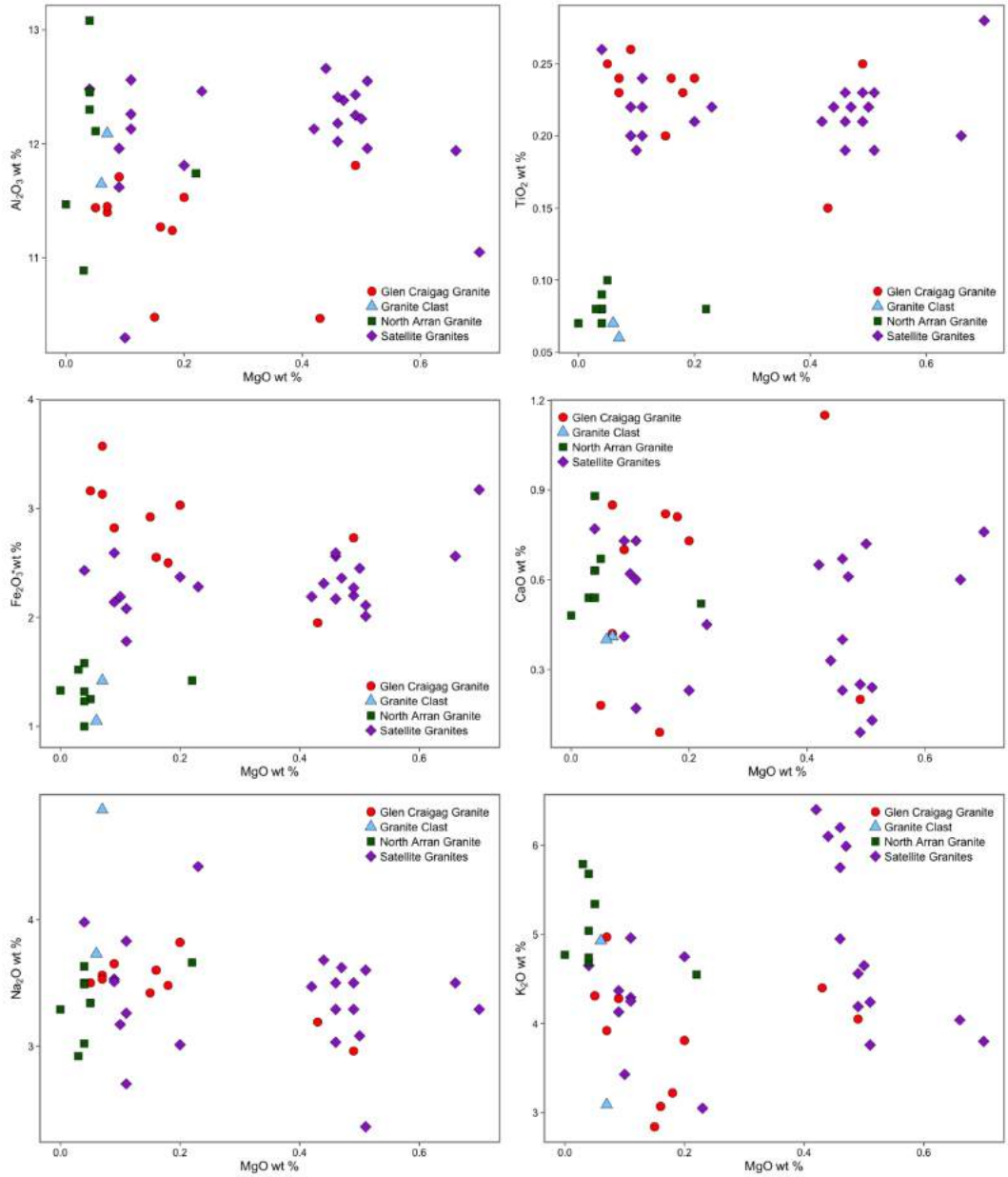

Fig. 4.8 – Representative major elements plotted against MgO for the granitic rocks of the CAIC and the NAG.

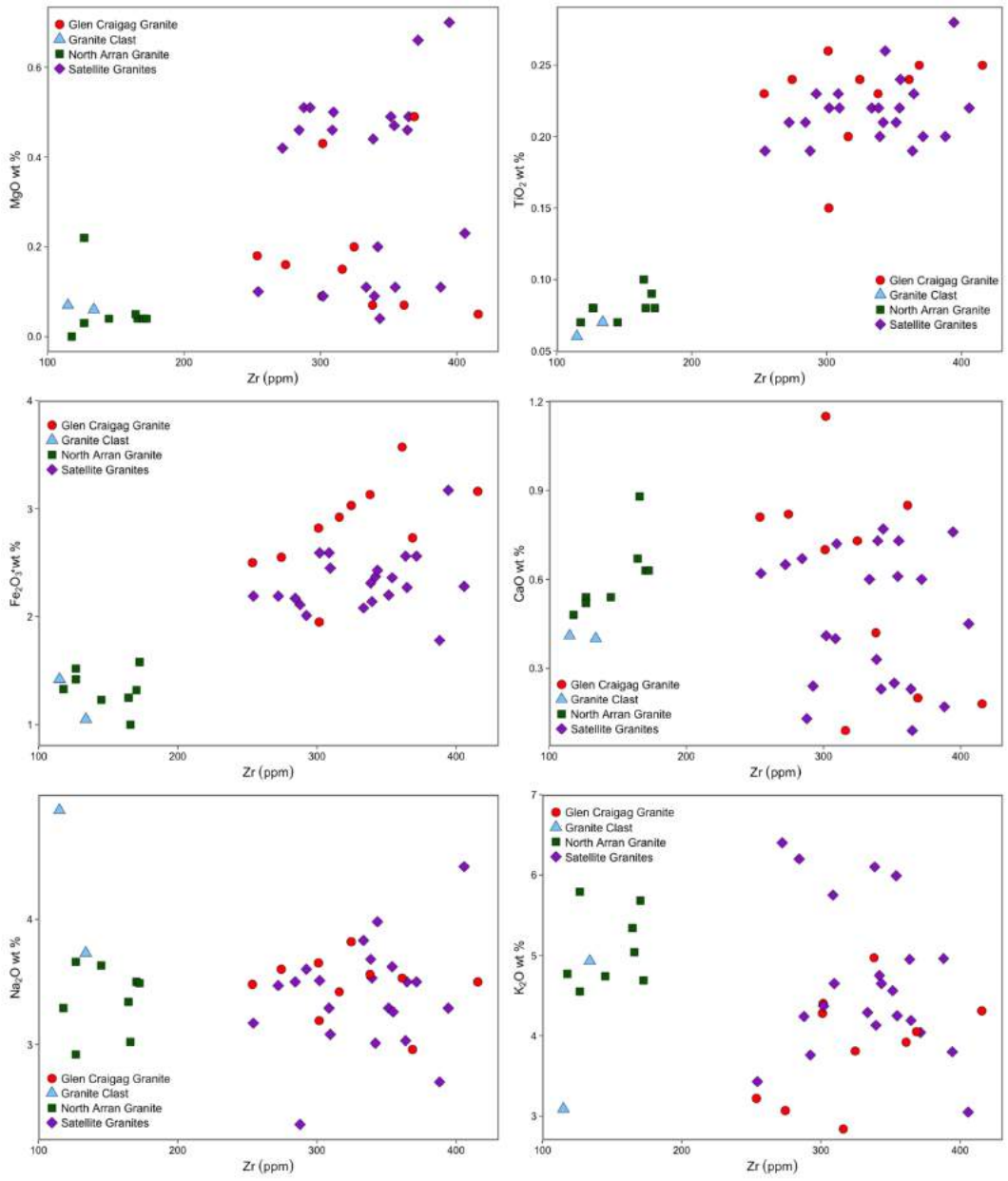

Fig. 4.9 – Representative major elements plotted against Zr for the granitic rocks of the CAIC and the NAG.

4.1.3 Trace Elements

In this section, the trace element composition of the various units of the CAIC, as well as the North Arran Granite, the Sheans, and Tighvein, are presented. Binary plots with a measure of magmatic evolution on the x-axis and primitive mantle normalised (Sun and McDonough, 1989) trace element variation diagrams (spider diagrams) are used to show the geochemical relationships between these units.

Mafic units

Representative trace elements for the mafic (and ultramafic) dykes of the CAIC and NAG, as well as the dolerite sill and the gabbros, are plotted against SiO_2 (Fig. 4.10), MgO (Fig. 4.11; does not include picrite dyke), and Zr (Fig. 4.12), as these elements show trends related to magmatic evolution. Primitive mantle normalised (Sun and McDonough, 1989) spider diagrams for the CAIC and NAG dykes are shown in Fig. 4.13, and for the sill, gabbros, and other dykes in Fig. 4.14.

The mafic dykes of both the CAIC and the NAG seem to comprise two geochemically distinct groups based on their incompatible trace element patterns (reflected in their REE patterns – see Section 4.1.4). One group shows a distinct depleted trend in the trace elements between La and Sm on the primitive mantle normalised spider diagram (Fig. 4.13), while the other group shows a flat to slightly enriched pattern among these elements. The first group are classified as the low La/Sm dykes. Although the other group do not have particularly high normalised La/Sm ratios, they are classified as the high La/Sm dykes for want of a better name, and to provide a clear distinction between the groups.

The CAIC dykes show increasing concentrations of Rb, Nb, and La with evolution (increasing SiO_2 and Zr and degreasing MgO). Y also shows this trend when plotted against MgO and Zr. Sr and Lu, which are more compatible in mafic crystallising assemblages (https://earthref.org/KDD/), do not show these evolution patterns (Figs. 4.10, 4.11, 4.12). The spider diagrams show that the low La/Sm CAIC dykes have depleted incompatible trace element patterns with minor enrichments in Ba and Sm (Fig. 4.13). The high La/Sm dykes have flatter incompatible trace element patters, and are highly enriched in Rb, Ba, Th, and U.

The NAG dykes show similar trace element trends to the CAIC dykes, but with much higher incompatible element concentrations at more evolved compositions. Much like the CAIC dykes, the low La/Sm NAG dykes have slightly depleted incompatible trace element profiles. Some display positive Sr anomalies. The high La/Sm NAG dykes are highly enriched in the most incompatible elements with flat more-compatible trace element profiles.

The dolerite sill has a smaller range of trace element compositions, as would be expected for a single intrusion. It does however display a large range of Sr, from 179 – 349 ppm. These Sr values show a steep negative trend when plotted against MgO. These samples show correlation between MgO and the trace elements Y, Nb, and La (Fig. 4.11). The trace element patterns are convex-up, with enriched Ba and depleted Th, U, Nb, and Ta. Most samples have low Rb, but in some Rb is enriched (Fig. 4.14).

The gabbros have a relatively limited range of compositions, not including sample BJG/16/12 which is a magnetite cumulate. In most cases they plot within the field of CAIC and NAG mafic dykes. Three of the samples, however, have lower Zr concentrations (<50 ppm; Fig. 4.12). The trace element profiles of the gabbros are generally enriched in incompatible elements, with negative Nb and Ta anomalies, and in the case of the three samples mentioned, Zr (Fig. 4.14).

The picrite dyke has very low incompatible trace element concentrations – lower than any of the mafic units of the CAIC or NAG (Figs. 4.10, 4.11, 4.12). It has a moderate Rb concentration (7.4 ppm) which is more than most of the basaltic CAIC and NAG dykes and the dolerite sill. The trace element diagram reflects these low concentrations, with relatively enriched Rb, Ba, and Sr, with highly enriched Th (Fig. 4.14).

The trace element pattern for the pitchstone dyke is also shown in Fig. 4.14. It has a highly enriched incompatible element profile, with moderate negative Nb, Sr, and Ti anomalies.

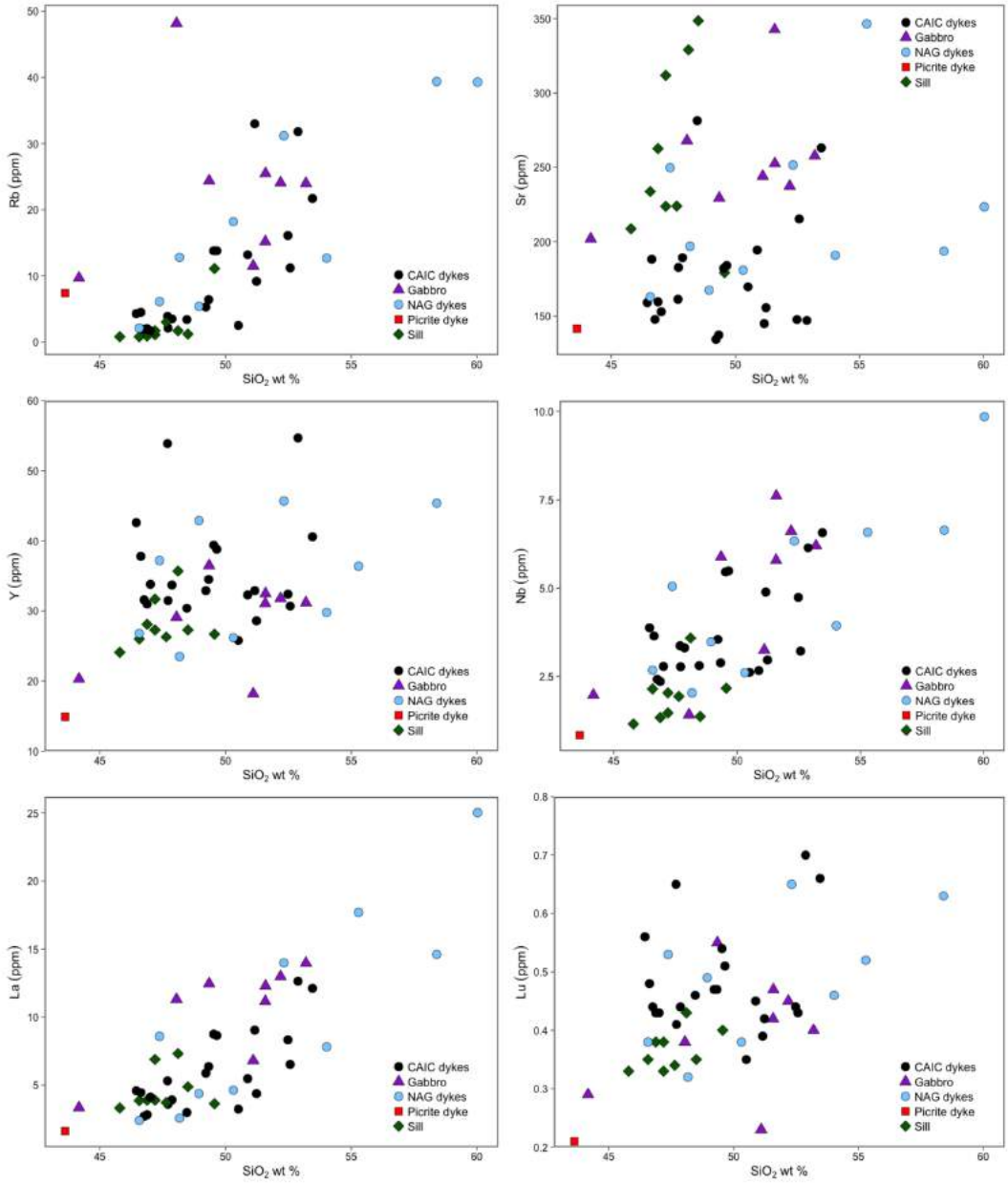

Fig. 4.10 – Representative trace elements plotted against SiO_2 for the dykes which intrude the CAIC and NAG, and the other mafic units.

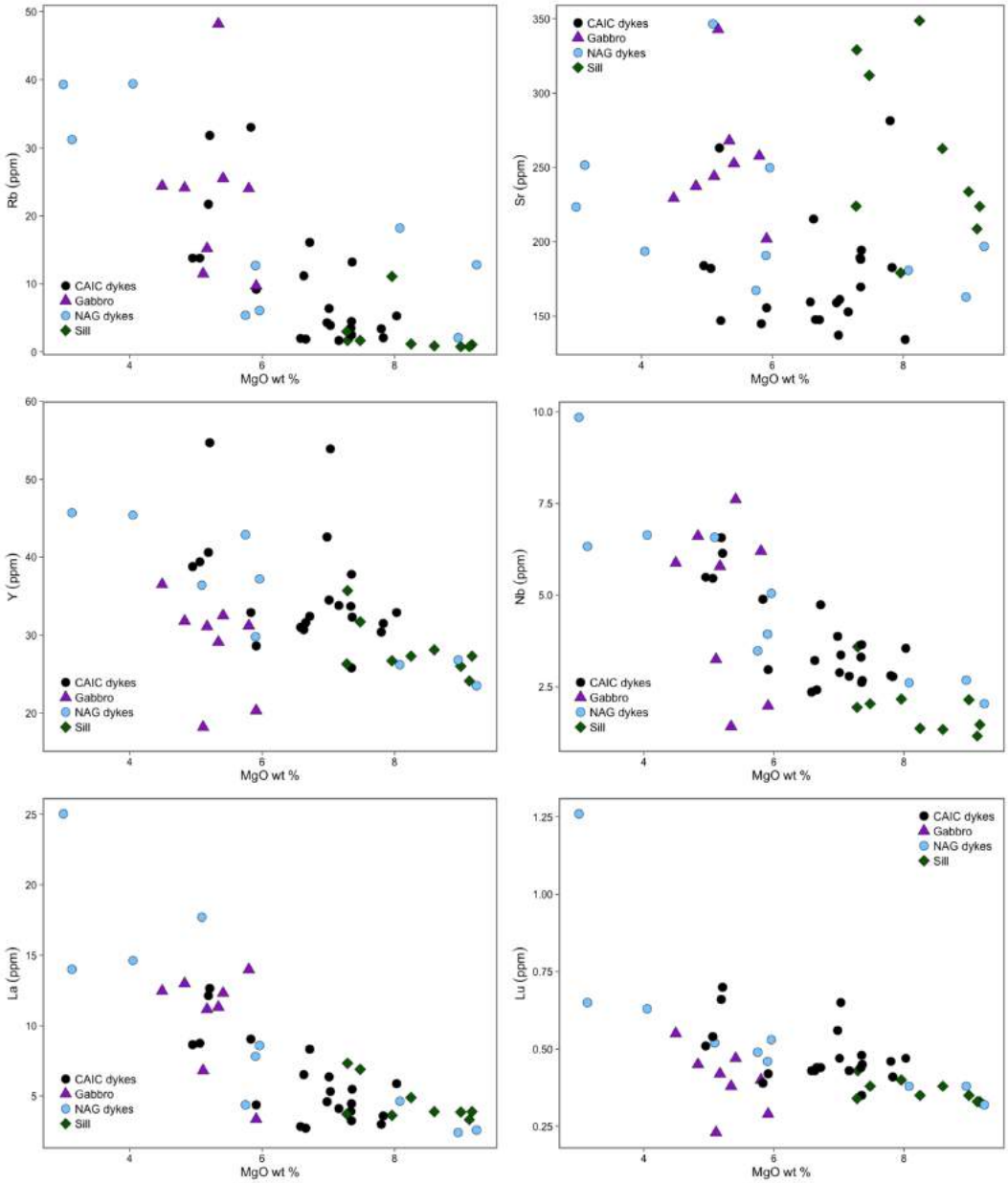

Fig. 4.11 – Representative trace elements plotted against MgO for the dykes which intrude the CAIC and NAG, and the other mafic units.

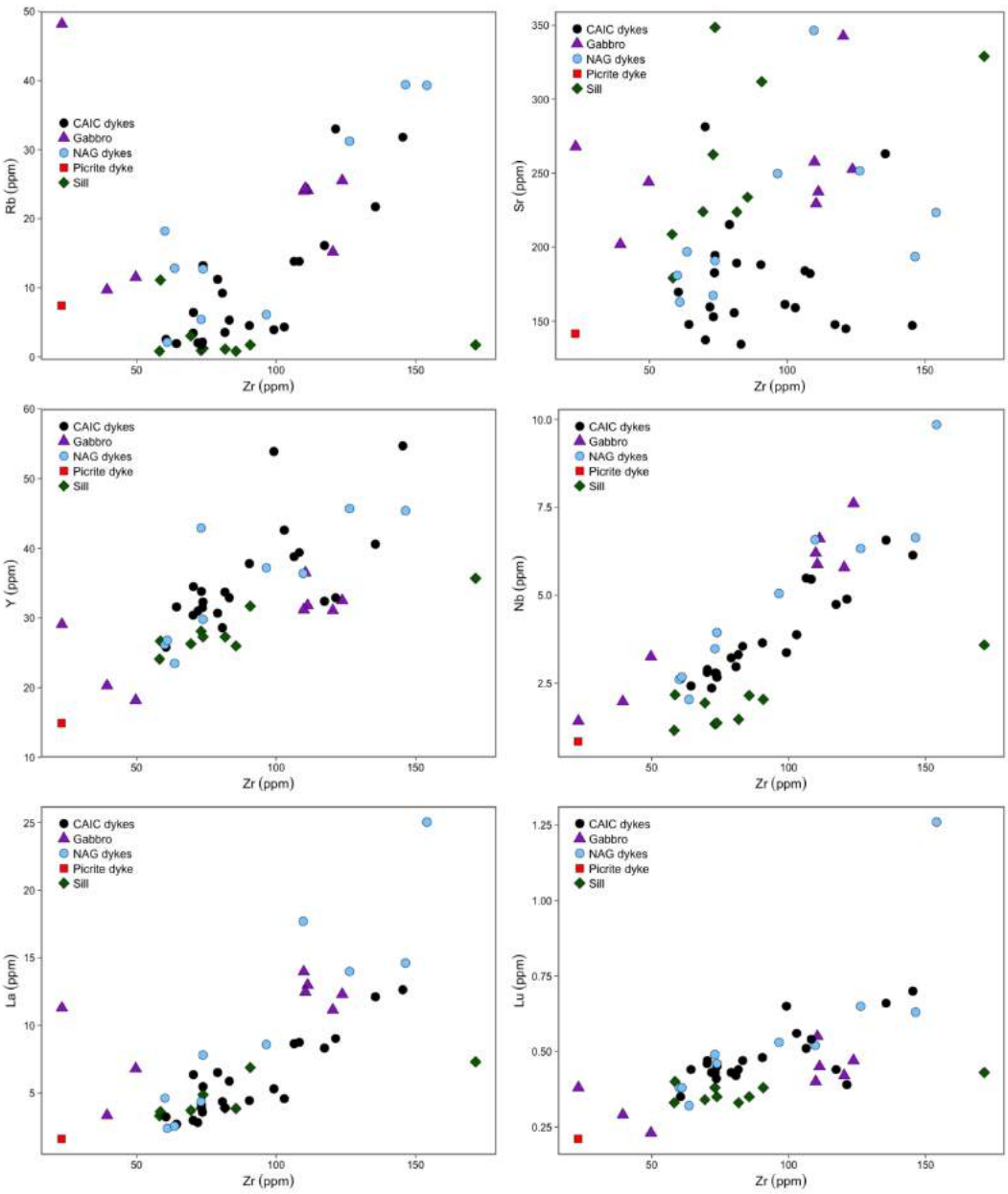

Fig. 4.12 – Representative trace elements plotted against Zr for the dykes which intrude the CAIC and NAG, and the other mafic units.

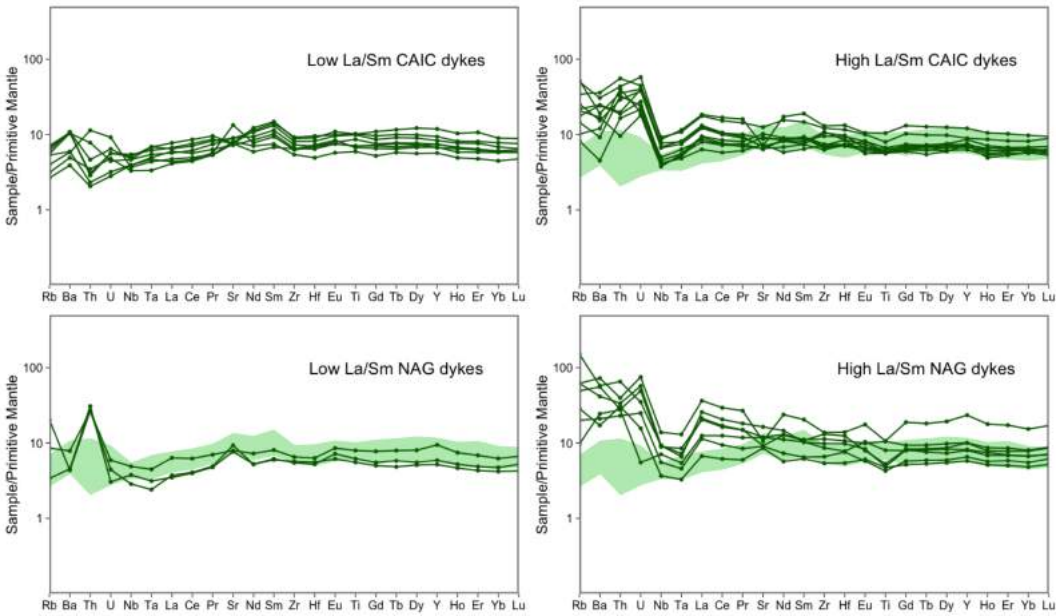

Fig. 4.13 – Primitive mantle normalised (Sun and McDonough, 1989) trace element diagrams for the mafic dykes that intrude the CAIC and the NAG. The coloured field shows the compositions of the low La/Sm CAIC dykes for comparison.

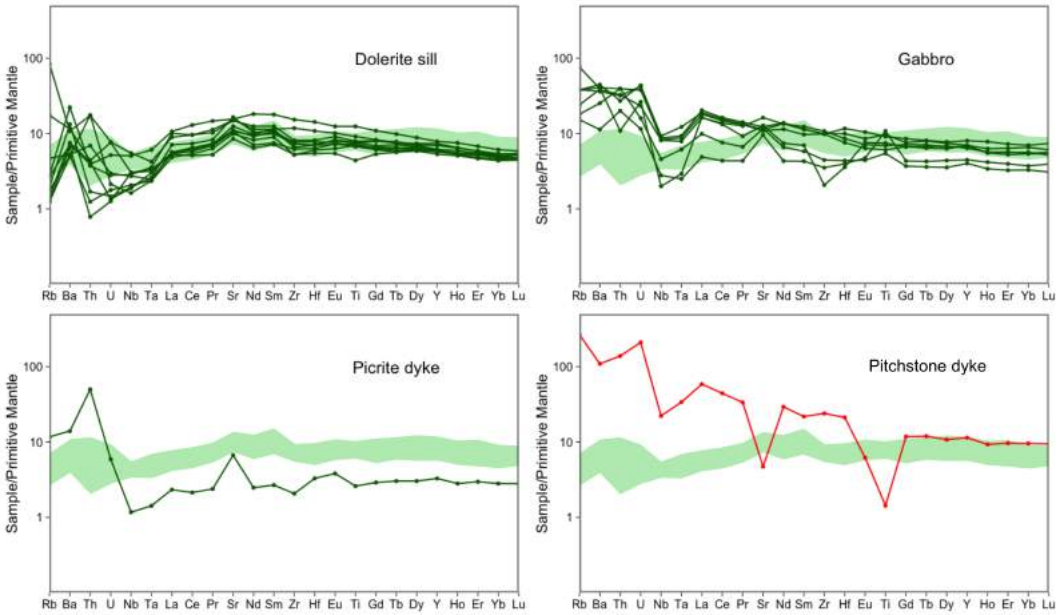

Fig. 4.14 – Primitive mantle normalised (Sun and McDonough, 1989) trace element diagrams for the dolerite sill which intrudes the ignimbrites of the AVF, the gabbros associated with the Glenloig Hybrids, the picrite dyke which intrudes the Glen Craigag Granite, and the pitchstone dyke which intrudes the ignimbrites of the AVF. The coloured field shows the compositions of the low La/Sm CAIC dykes for comparison.

Glenloig Hybrids and similar units

Representative trace elements for the Glenloig Hybrids (including the intra-caldera hybrids), as well as samples from the Sheans and Tighvein, are plotted against SiO_2 (Fig. 4.15), MgO (Fig. 4.16), and Zr (Fig. 4.17). Primitive mantle normalised (Sun and McDonough, 1989) spider diagrams for the Glenloig Hybrids, the Sheans, and Tighvein are shown in Fig. 4.18.

The Glenloig Hybrids (including the intra-caldera hybrids) generally show expected evolution-related trends (i.e., increasing incompatible element contents with increasing SiO_2 and Zr and decreasing MgO). However, some samples with high SiO_2 concentrations (>70 wt.%) and high Zr concentrations (>350 ppm) have low concentrations of incompatible elements (Rb, Y, Nb, La: Figs. 4.15, 4.16, 4.17). This, along with negative Ti anomalies, could be explained by sphene fractionation.

The intermediate Glenloig Hybrids (defined as all those with SiO_2<70 wt.%) have much more consistent primitive mantle normalised trace element patterns (Fig. 4.18) than the silicic (rhyolitic) Glenloig Hybrids (SiO_2>70 wt.%). The intermediate hybrids have generally incompatible element enriched trace element profiles with negative Nb, Ta, and Ti anomalies, with some showing a negative Sr anomaly. The silicic hybrids also have incompatible element enriched trace element profiles, with very pronounced negative Nb, Sr, and Ti anomalies. However, there is a large range in concentrations of all incompatible trace elements and individual profile shapes.

The Sheans samples have quite a restricted range of trace elements and largely plot in the field of the less evolved Glenloig Hybrids (Figs. 4.15 – 4.18). Some elements (Rb, La) show flatter evolution trends when plotted against SiO_2. The trace element patterns are slightly incompatible element enriched, with very slight negative Nb and Ti anomalies, very similar to the intermediate Glenloig Hybrids (Fig. 4.18).

The samples from Tighvein mostly have similar trace element concentrations to the more evolved Glenloig Hybrids, but with slightly higher Y, Nb, and Lu. The spider diagram (Fig. 4.18) shows trace element patterns similar to those of the silicic Glenloig Hybrids, with depleted Sr and Ti and slightly depleted Nb and Ta.

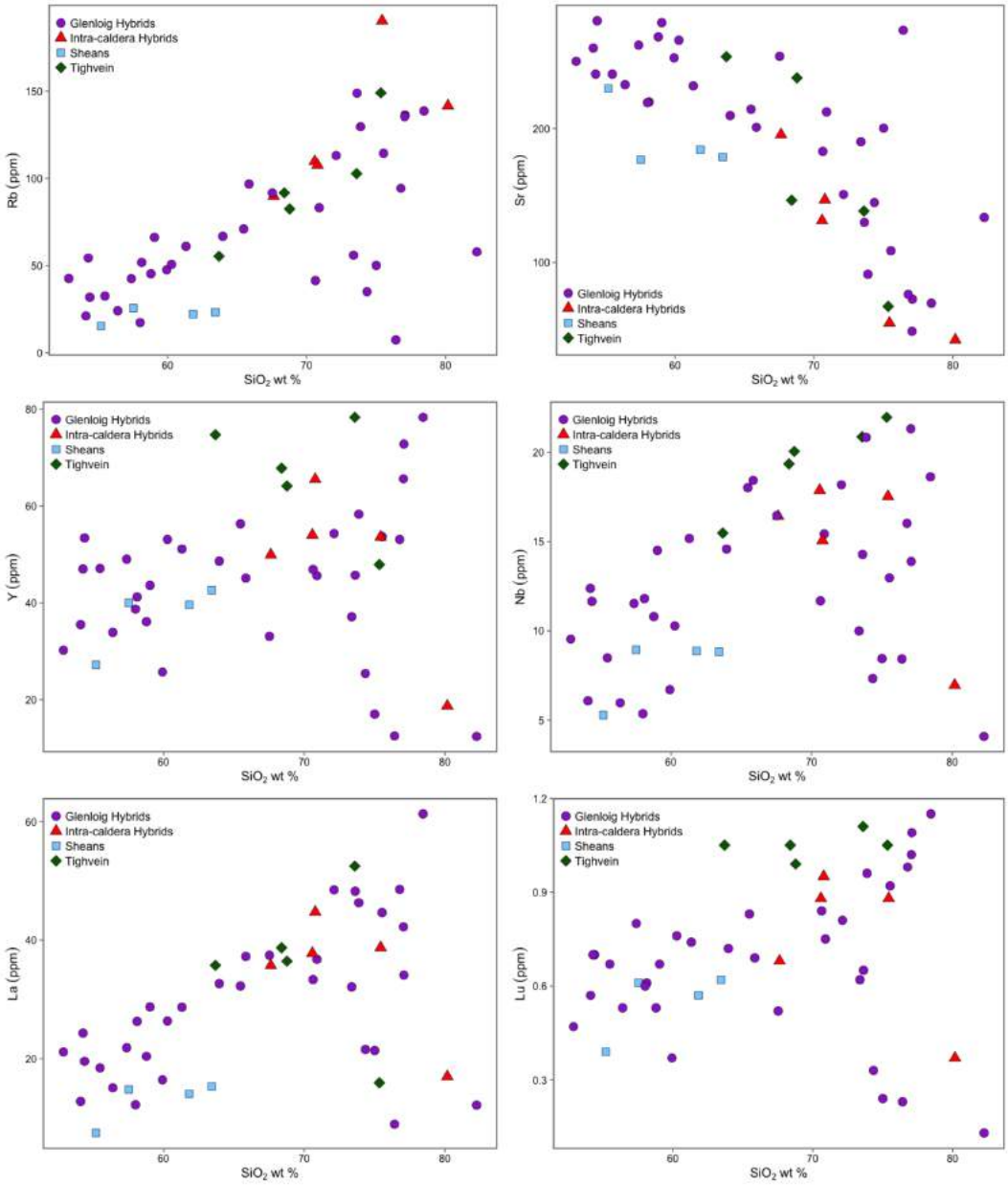

Fig. 4.15 – Representative trace elements plotted against SiO_2 for the hybrid rocks of the CAIC and similar units in the surrounding area.

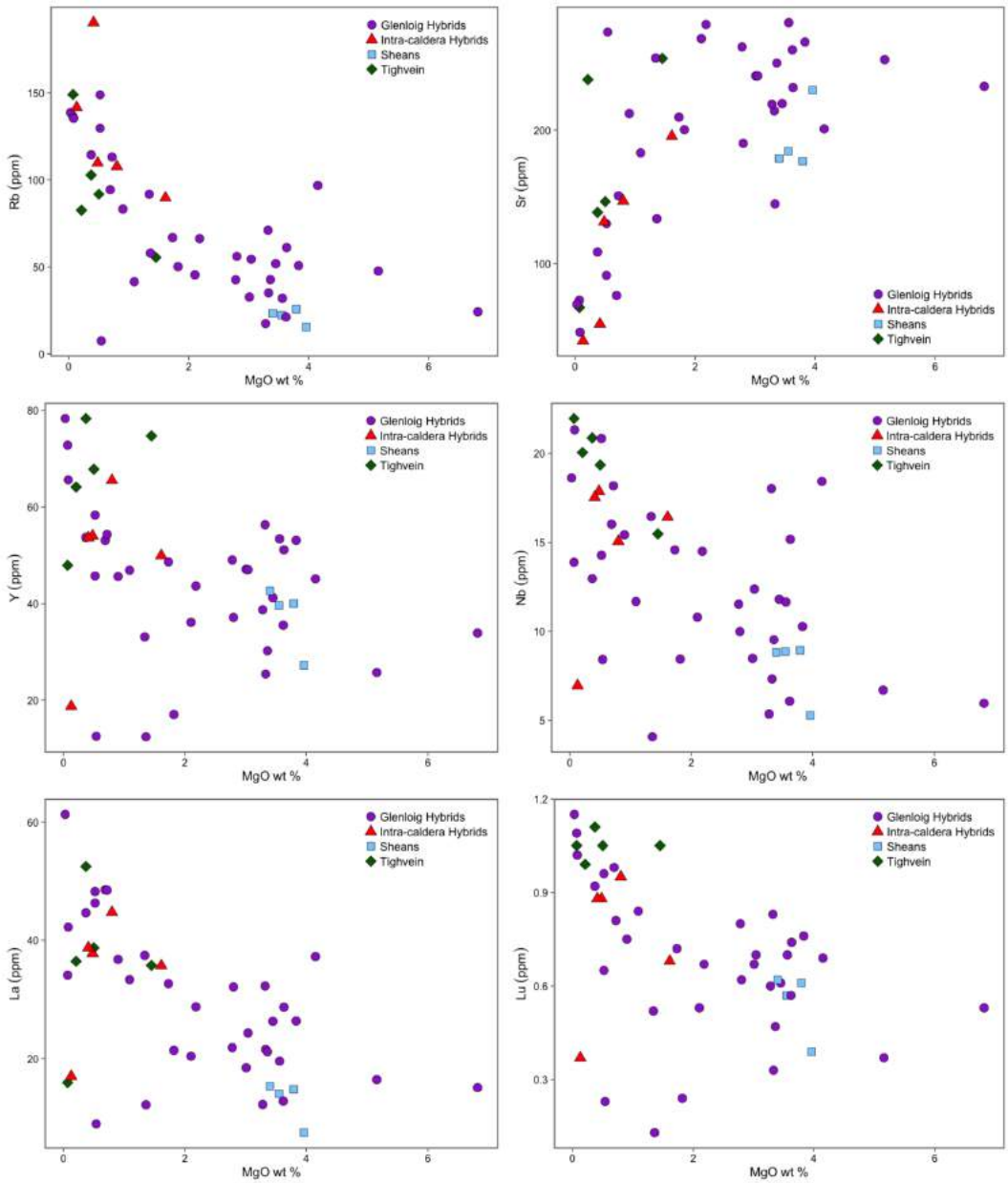

Fig. 4.16 – Representative trace elements plotted against MgO for the hybrid rocks of the CAIC and similar units in the surrounding area.

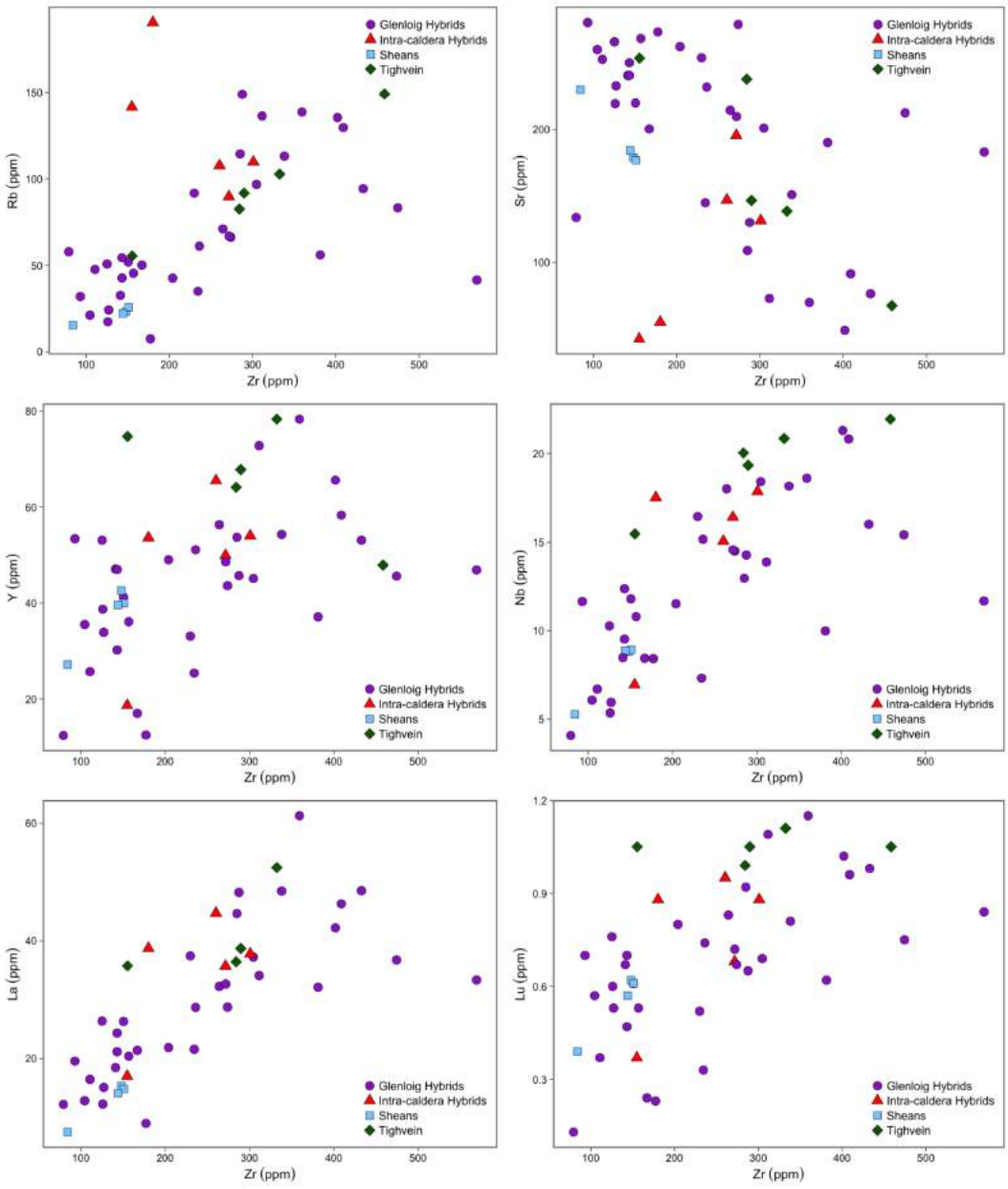

Fig. 4.17 – Representative trace elements plotted against Zr for the hybrid rocks of the CAIC and similar units in the surrounding area.

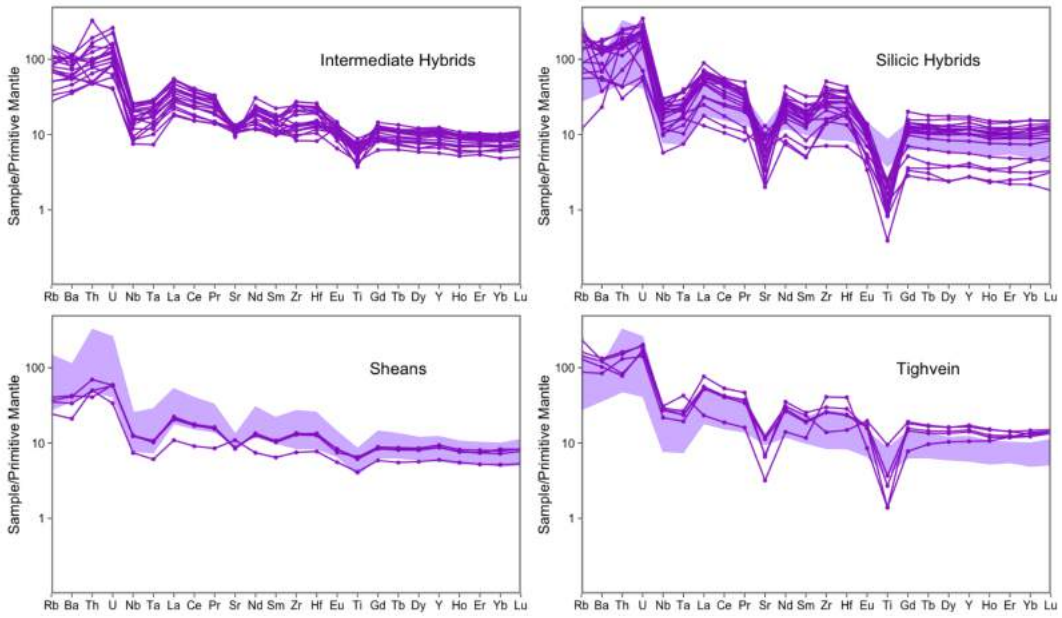

Fig. 4.18 – Primitive mantle normalised (Sun and McDonough, 1989) trace element diagrams for the intermediate and silicic rocks of the Glenloig Hybrids, the Sheans, and Tighvein. The coloured field shows the compositions of the intermediate Glenloig Hybrids for comparison.

Granites

Representative trace elements for the Glen Craigag Granite and Satellite Granites from the CAIC, the North Arran Granite, and the granite clasts found within the ignimbrites of the AVF, are plotted against SiO_2 (Fig. 4.19), MgO (Fig. 4.20), and Zr (Fig. 4.21). Primitive mantle normalised (Sun and McDonough, 1989) trace element diagrams for the Glenloig Hybrids, the Sheans, and Tighvein are shown in Fig. 4.22.

The Satellite Granites have relatively constant trace element concentrations, with only the REEs showing significant variation (Fig. 4.19, 4.20, 4.21). They have distinctly incompatible element enriched primitive mantle normalised trace element patterns (Fig. 4.22), with distinct negative Sr and Ti anomalies, and slight Nb and Ta depletions.

The Glen Craigag Granite has a relatively restricted range of most trace element compositions, with generally similar Rb, Ta, La, and Zr compositions to the Satellite Granites. However, they have generally higher Sr and Ba, and lower Lu. With the exception of a slight increase in Nb and Y with increasing Zr (Fig. 4.21), the samples do not show any clear trends. The spider diagrams show very pronounced depletions in Sr and Ti, with a moderate depletion in Nb and Ta.

The North Arran Granite has a significantly different trace element signature, most noticeably very low Zr concentrations (<175 ppm) compared to the Glen

Craigag and Satellite Granites (>250 ppm; Fig. 4.21). This is presumably due to the fractionation of zircon in the NAG. It also has generally lower Sr and Ba, and higher Rb, Nb, and Y. The spider diagrams show very extreme Sr, Ti, and Eu depletions, as well as a negative Ba anomaly and only a slight Nb anomaly.

The granite clasts from the AVF look geochemically similar to the NAG with regards to most elements (Figs. 4.19, 4.20, 4.21). They also have low Sr, Ba, La, and very low Zr, and high Ta and Nb. However, they have much lower Y concentrations than the NAG samples. The trace element profiles are similar to those of the NAG (Fig. 4.22), but with less pronounced Sr and Ba anomalies.

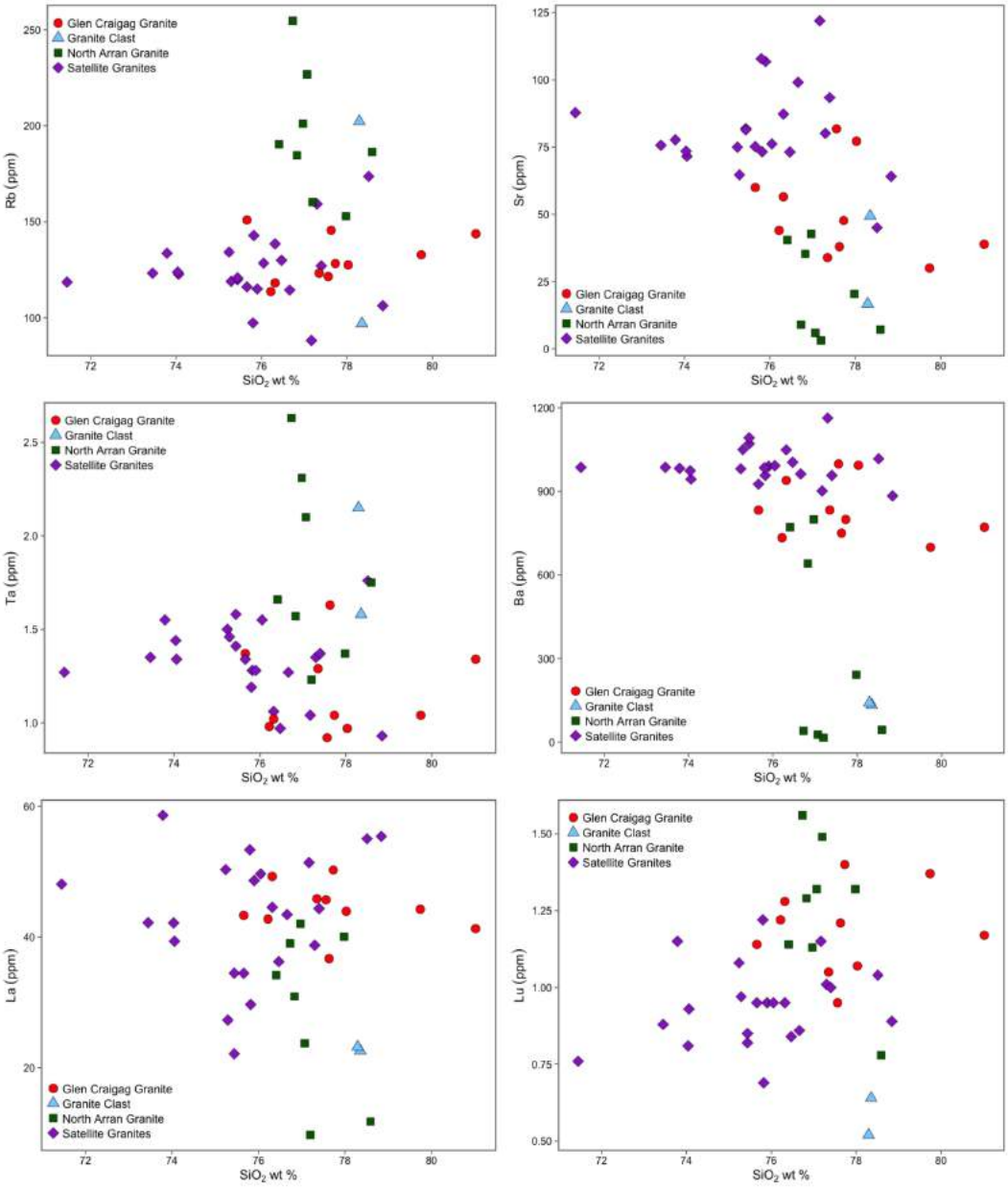

Fig. 4.19 – Representative trace elements plotted against SiO_2 for the granitic rocks of the CAIC and the NAG.

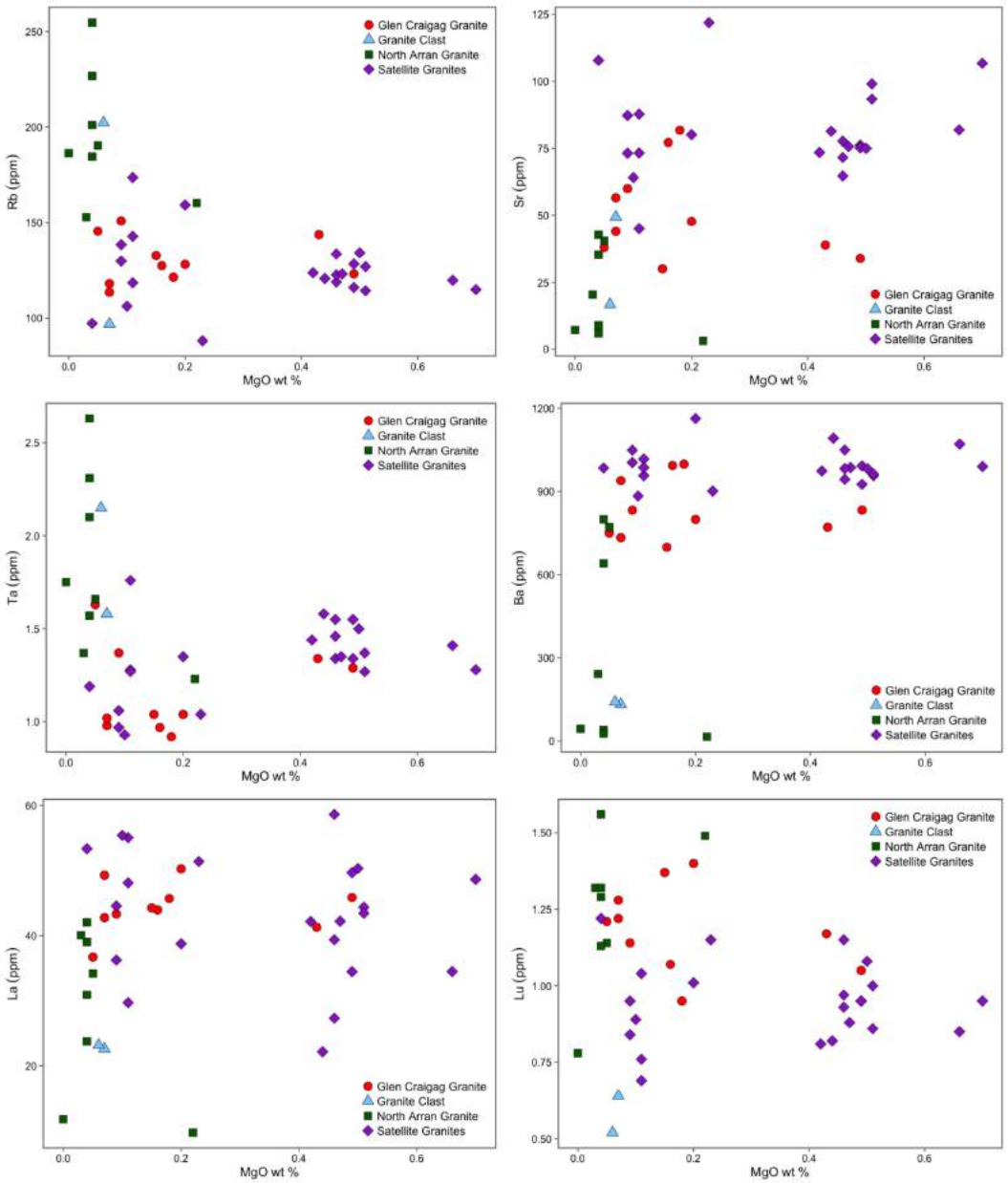

Fig. 4.20 – Representative trace elements plotted against MgO for the granitic rocks of the CAIC and the NAG.

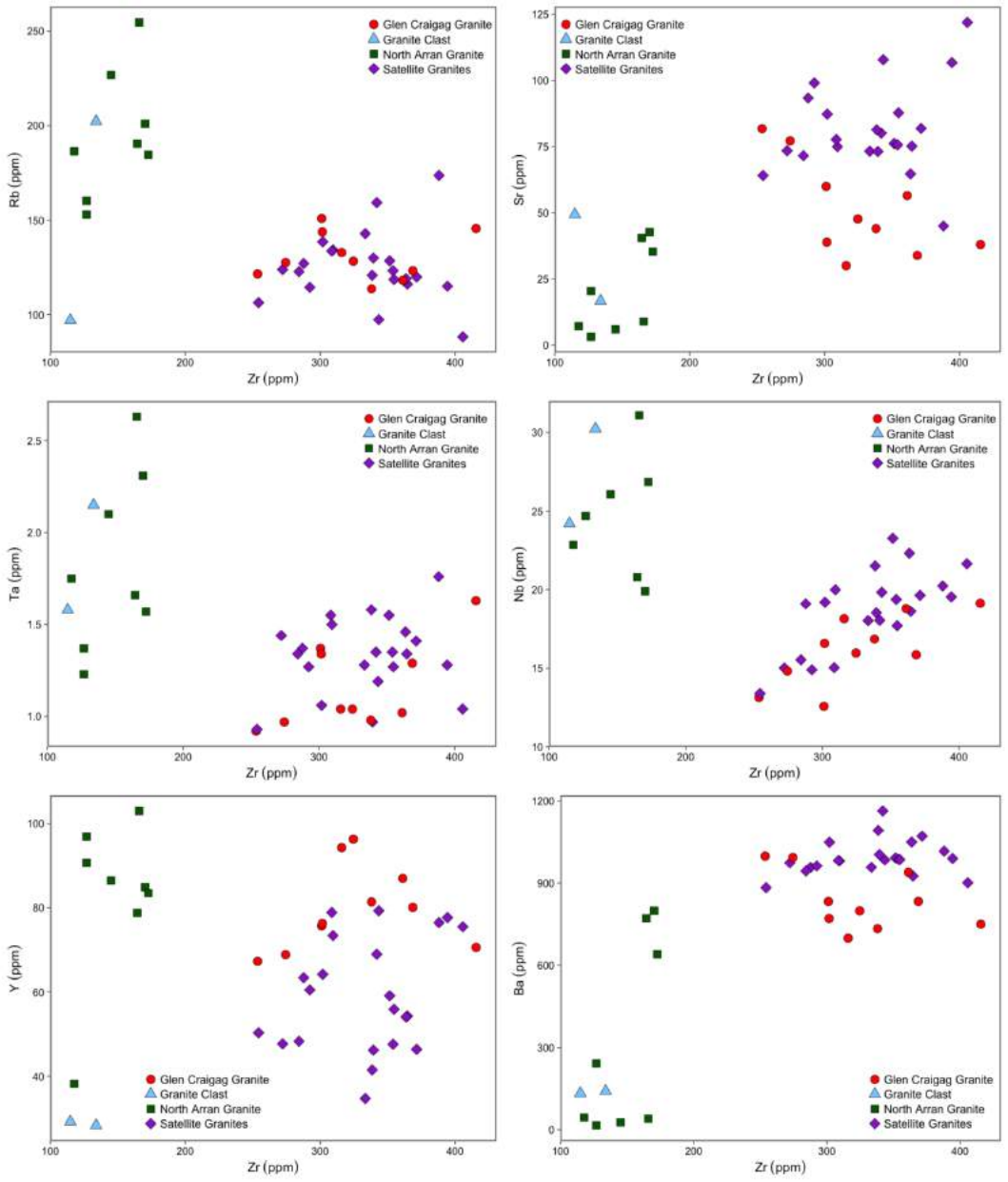

Fig. 4.21 – Representative trace elements plotted against Zr for the granitic rocks of the CAIC and the NAG.

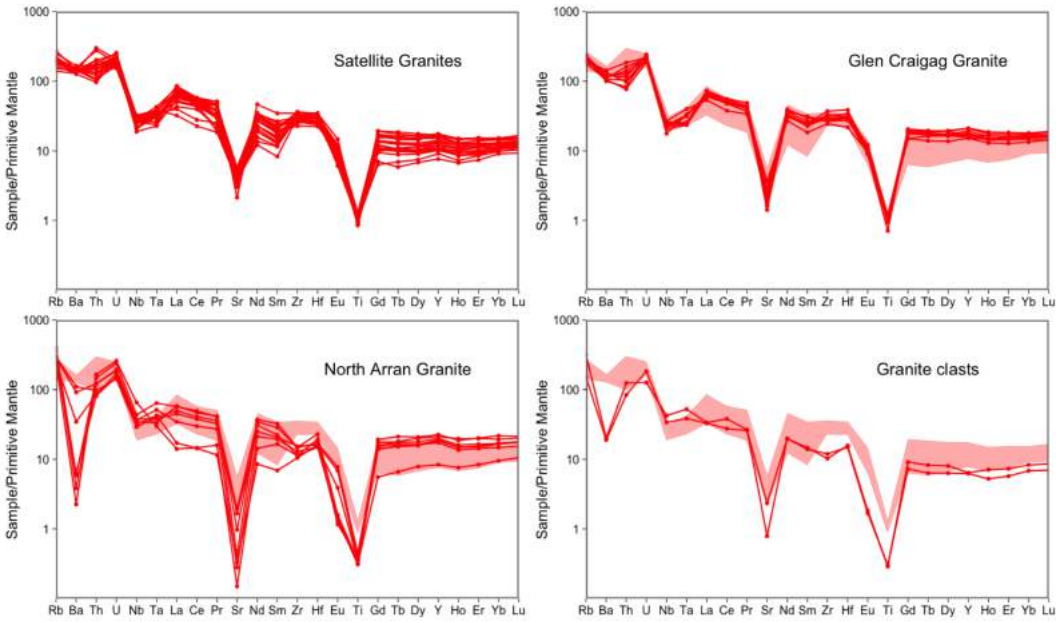

Fig. 4.22 – Primitive mantle normalised (Sun and McDonough, 1989) trace element diagrams for the granites of the CAIC, the NAG, and the granite clasts found in the ignimbrites of the CAIC. The coloured field shows the compositions of the Satellite Granites for comparison.

Ignimbrites

Primitive mantle normalised (Sun and McDonough, 1989) trace element diagrams for the Muileann Gaoithe and White Tuff rhyolitic lava-like ignimbrites are shown in Fig. 4.23. The profiles are very similar, although the White Tuff ignimbrites have slightly higher La and Ce, and lower Nb and Y. Both units display significant negative Ba, Sr, Eu, and Ti anomalies and high Rb concentrations.

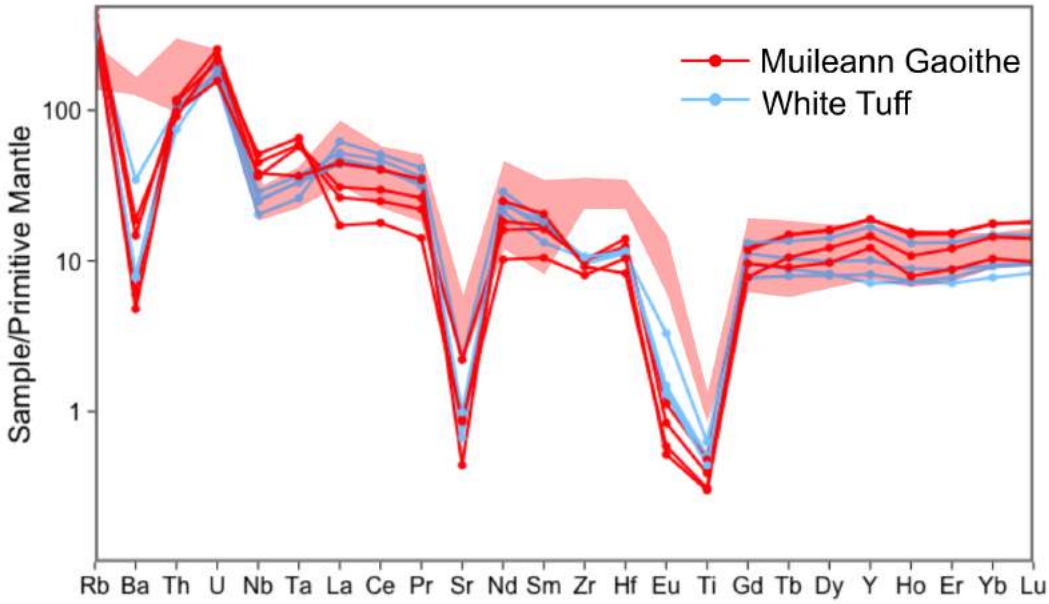

Fig. 4.23 – Primitive mantle normalised (Sun and McDonough, 1989) trace element diagrams for the rhyolitic lava-like ignimbrites of the AVF. The coloured field shows the compositions of the Satellite Granites for comparison.

4.1.4 Rare-earth Elements

In this section, the rare-earth geochemistry of the igneous rocks analysed in this study are presented. Chondrite normalised (McDonough and Sun, 1995) rare-earth element diagrams are used to show overall REE patterns, and the relationships between light rare-earth element (LREE) and heavy rare-earth element (HREE) are summarised by plotting chondrite normalised La/Sm against chondrite normalised Gd/Yb.

Mafic units

Chondrite normalised (McDonough and Sun, 1995) rare-earth element diagrams for the CAIC and NAG dykes are shown in Fig. 4.24, and for the sill, gabbros, and other dykes in Fig. 4.25. The light rare-earth element (LREE) patterns and heavy rare-earth element (HREE) patterns are summarised using La/Sm and Gd/Yb ratios in Fig. 4.26.

As mentioned in the previous section, the CAIC dykes fall into two distinct groups based on their LREE patterns. One group shows middle rare-earth element (MREE) enrichment, with $(La/Sm)n \leqslant 0.61$ and the other has flatter patterns with $(La/Sm)n \geqslant 0.86$. These are plotted separately on Fig. 4.24, and form separate clusters on Fig. 4.26. Both groups have flat to slightly depleted HREE patterns with

(Gd/Yb)n = 0.98–1.32. Most of the high La/Sm CAIC dykes display a slight negative Eu anomaly.

The dykes which intrude the NAG have also been divided into low and high La/Sm ratios (Fig. 4.24). They display higher (La/Sm)n ratios (up to 2.43) than the CAIC dykes (none higher than 1.59); Fig. 4.26, although these higher La/Sm values are associated with the more evolved compositions. The NAG dykes have similar HREE patterns to the CAIC dykes (chondrite normalised Gd/Yb = 1.02 – 1.22). They all display either very slight positive or very slight negative Eu anomalies.

The dolerite sill samples all show a distinct convex-up REE pattern (Fig. 4.25), with low (La/Sm)n of $\leqslant$0.8, and high (Gd/Yb)n of over 1.25 (except one sample with a flat HREE pattern; Fig. 4.26). The LREE patterns are similar to the low La/Sm groups of both CAIC and NAG dykes, but the HREE patterns are steeper than both.

The gabbros show a range of REE patterns, and a range of total REE abundances. They all have HREE-depleted patterns (Fig. 4.25), with higher La/Sm and Gd/Yb ratios than the CAIC and NAG dykes (Fig. 4.26).

The picrite dyke has low overall REE concentrations, and a flat to LREE-depleted profile (Fig. 4.25). It has (La/Sm)n=0.84 and (Gd/Yb)n=1.01 (Fig. 4.26). It has a small positive Eu anomaly which may indicate some plagioclase accumulation. In contrast, the pitchstone dyke has a large negative Eu anomaly, indicating plagioclase fractionation.

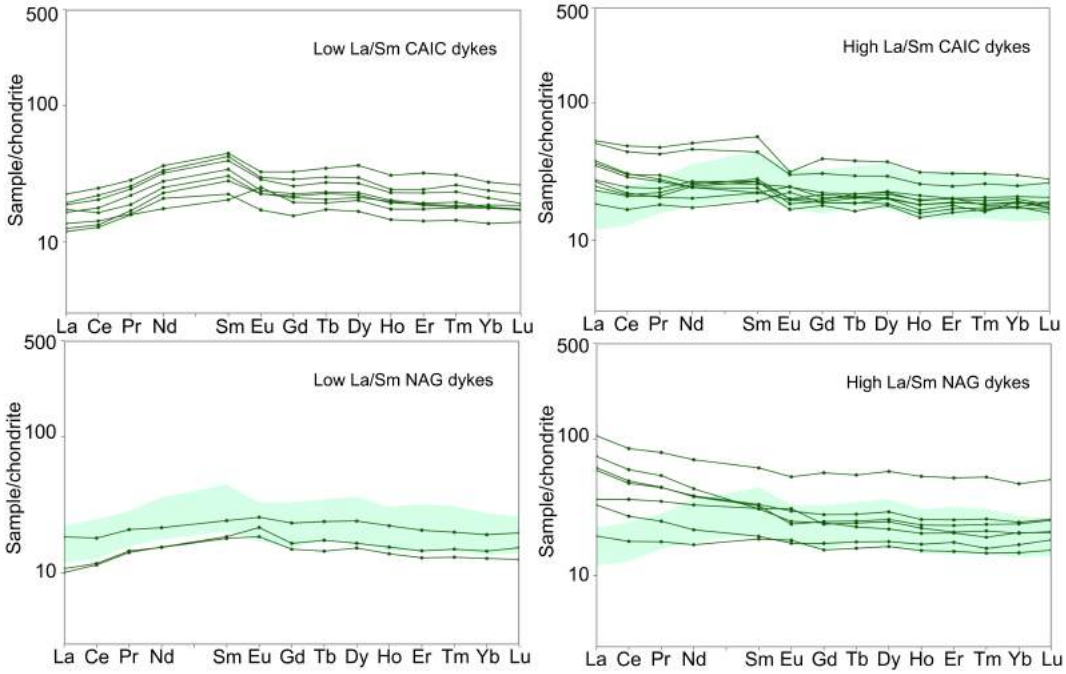

Fig. 4.24 – Chondrite normalised (McDonough and Sun, 1995) rare-earth element diagrams for the mafic dykes that intrude the CAIC and the NAG. The coloured fields show the compositions of the low La/Sm dykes for comparison.

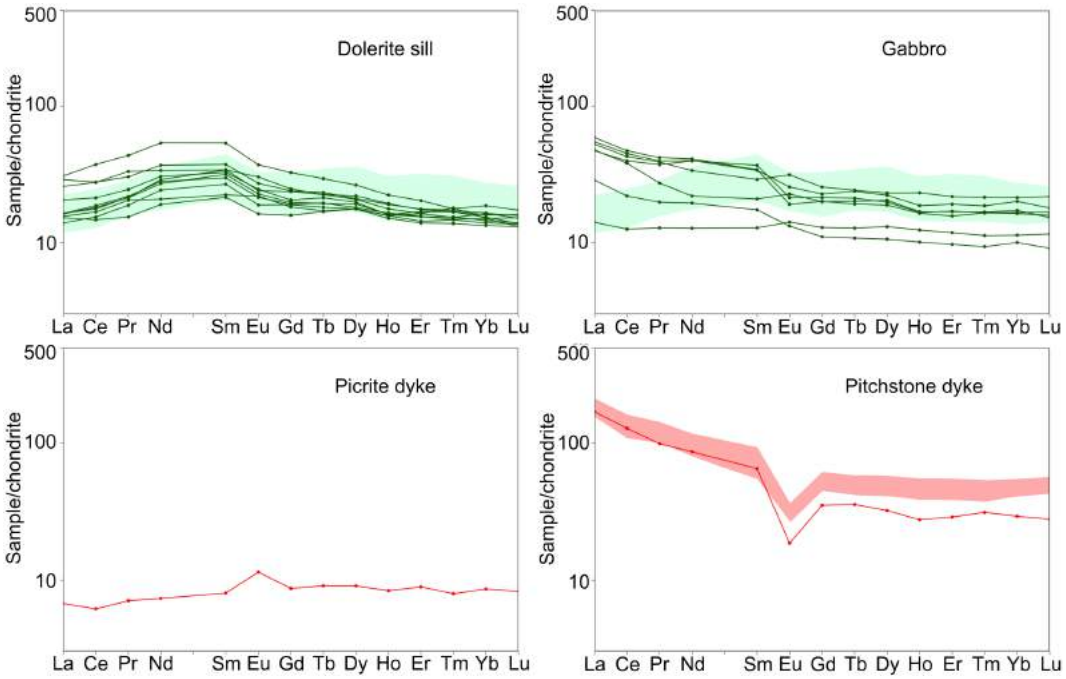

Fig. 4.25 – Chondrite normalised (McDonough and Sun, 1995) rare-earth element diagrams for the dolerite sill which intrudes the ignimbrites of the AVF, the gabbros associated with the Glenloig Hybrids, the picrite dyke which intrudes the Glen Craigag Granite, and the pitchstone dyke which intrudes the ignimbrites of the AVF. The green fields show the compositions of the low La/Sm dykes for comparison, and the pink field shows the compositions of the Glen Craigag Granite.

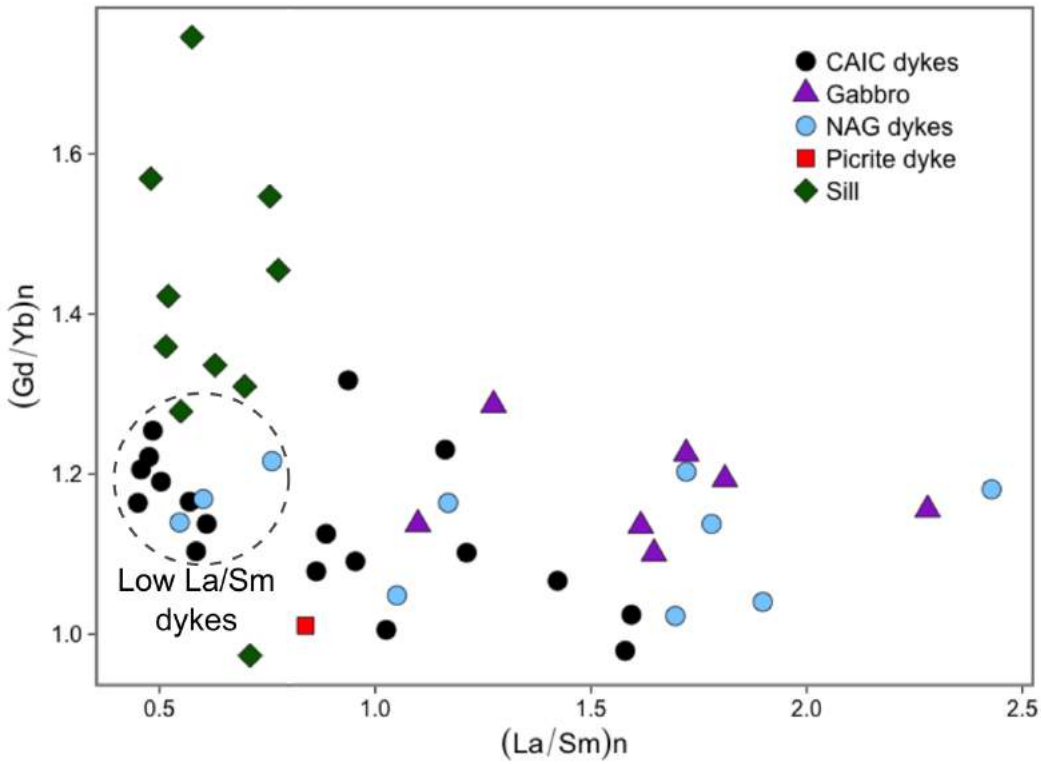

Fig. 4.26 – Chondrite normalised (McDonough and Sun, 1995) La/Sm and Gd/Yb ratios for the mafic units of the CAIC and the NAG.

Glenloig Hybrids and similar units

Chondrite normalised (McDonough and Sun, 1995) rare-earth element diagrams for the Glenloig Hybrids, the Sheans, and Tighvein are shown in Fig. 4.27. The light rare-earth element (LREE) patterns and heavy rare-earth element (HREE) patterns are summarised using La/Sm and Gd/Yb ratios in Fig. 4.28.

The intermediate Glenloig Hybrids have relatively consistent REE patterns, with enriched LREE and a concave-up profile. The steep LREE profile is shown by (La/Sm)n values of 1.54–3.28 (plus one anomalously high ratio of 4.55), with the consistently flat to slightly depleted HREE profile shown by (Gd/Yb)n values of 1.16–1.42 (Figs. 4.27, 4.28). Some samples have slight positive or negative Eu anomalies.

The silicic Glenloig Hybrids show a much greater range in REE concentrations and profiles. They generally have steeper LREE patterns than the intermediate hybrids (Fig. 4.27) with (La/Sm)n values of 1.91–4.00 (plus one anomalously high ratio of 4.70). The HREE concentrations vary greatly, and (Gd/Yb)n ratios range from 0.80–1.61 (Fig. 4.28). Some samples have a very pronounced negative Eu anomaly.

Three of the samples from the Sheans have almost identical REE concentrations and profiles, while the other has lower concentrations but a similar profile (Fig. 4.27). They have slightly enriched LREE profiles, with (La/Sm)n values of 1.63–2.03, and flat HREE profiles with (Gd/Yb)n values of 1.00–1.14 (Fig. 4.28).

Four of the Tighvein samples have consistent REE geochemistry. The outlier has similar HREE concentrations, but is much more depleted in LREE and middle rare-earth elements. In general, REE concentrations are greater than the Sheans. The profiles are all gently concave-up. They have moderately steep LREE patterns (normalised La/Sm values of 2.17–2.91), and slightly depleted HREE patterns (normalised Gd/Yb values of 1.17–1.42; Fig. 4.28).

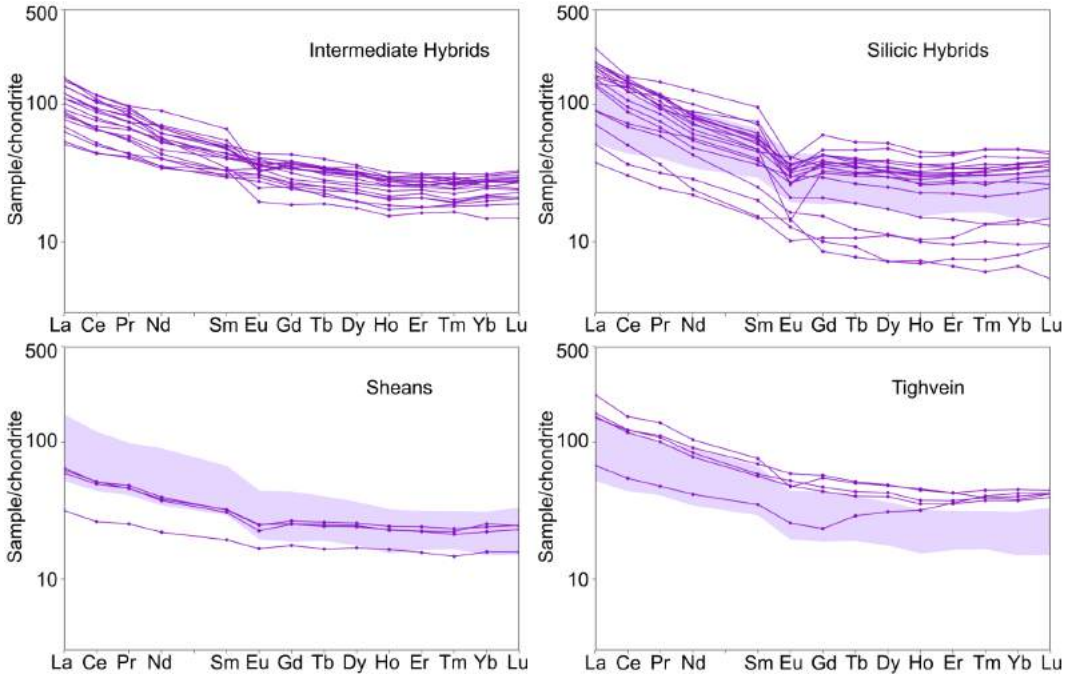

Fig. 4.27 – Chondrite normalised (McDonough and Sun, 1995) rare-earth element diagrams for the intermediate and silicic rocks of the Glenloig Hybrids, the Sheans, and Tighvein. The coloured fields show the compositions of the intermediate Glenloig Hybrids for comparison.

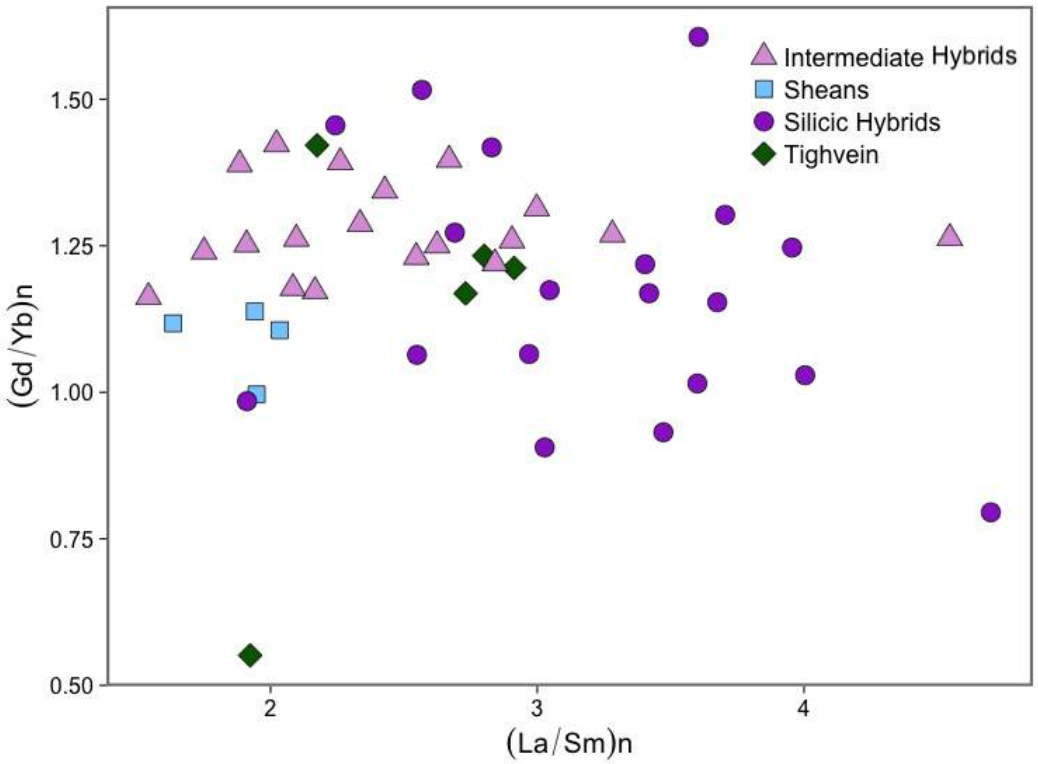

Fig. 4.28 – Chondrite normalised (McDonough and Sun, 1995) La/Sm and Gd/Yb ratios for the Glenloig Hybrids, the Sheans, and Tighvein.

Granites

Chondrite normalised (McDonough and Sun, 1995) rare-earth element diagrams for the granites of the CAIC, the NAG, and the clasts of granite found in the ignimbrites of the AVF are shown in Fig. 4.29. The light rare-earth element (LREE) patterns and heavy rare-earth element (HREE) patterns are summarised using La/Sm and Gd/Yb ratios in Fig. 4.30.

The Satellite Granites have a concave-up REE pattern, with enriched LREE profiles (Fig. 4.29), with most (La/Sm)n values $\geqslant$2.9 (Fig. 4.30). The HREE profiles are enriched to slightly depleted with (Gd/Yb)n values of 0.63–1.33. Negative Eu anomalies are present, but relatively slight.

The Glen Craigag Granite has a less pronounced concave-up REE pattern. Enriched LREE profiles are shown by (La/Sm)n values of 1.86–3.37 on Fig. 4.30. The HREE profiles are flat, with (Gd/Yb)n values of 0.90–1.24. Negative Eu anomalies are more consistent and pronounced than the Satellite Granites.

The North Arran Granite has slightly less enriched LREE patterns than the CAIC granites (Fig. 4.29), with (La/Sm)n values of 1.68–2.51, excluding the one sample with a depleted LREE slope and a (La/Sm)n value of 0.83. HREE patterns are flat to enriched, with (Gd/Yb)n values of 0.57–1.05 (Fig. 4.30). This unit displays extreme negative Eu anomalies.

The granite clasts found in the ignimbrites of the AVF have enriched LREE profiles and flat HREE profiles, with (La/Sm)n values of 2.16 and 2.33 and (Gd/Yb)n values of 1.04 and 1.08 (Figs. 4.29, 4.30). The Eu anomalies are very negative.

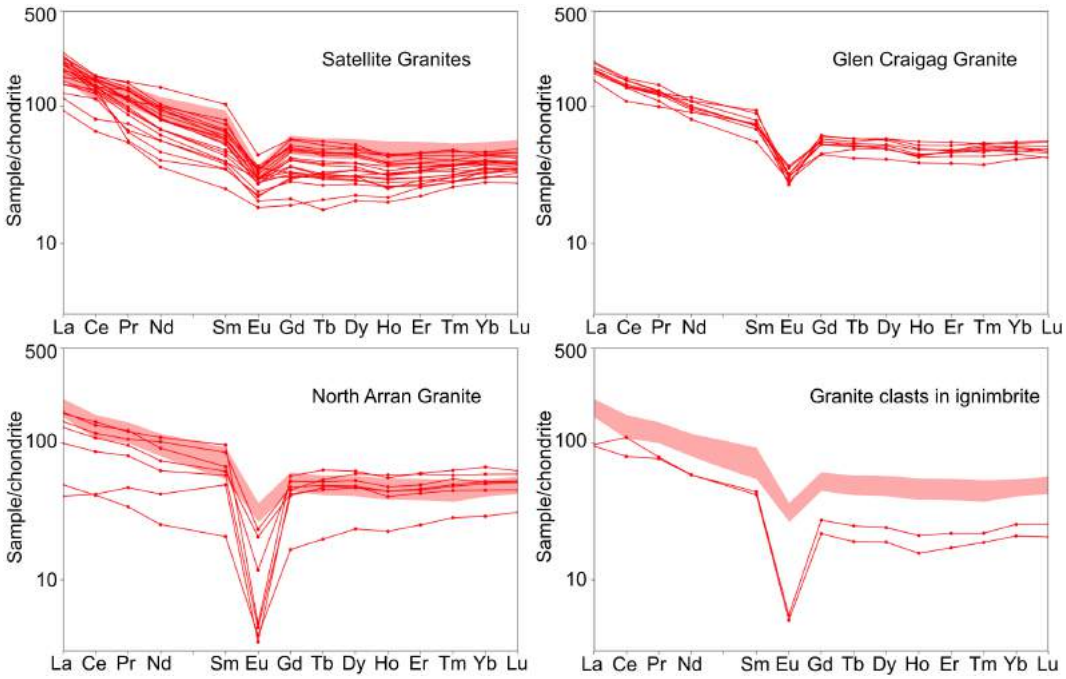

Fig. 4.29 – Chondrite normalised (McDonough and Sun, 1995) rare-earth element diagrams for the granites of the CAIC, the NAG, and the granite clasts found in the ignimbrites of the CAIC. The coloured fields show the compositions of the Glen Craigag Granite for comparison.

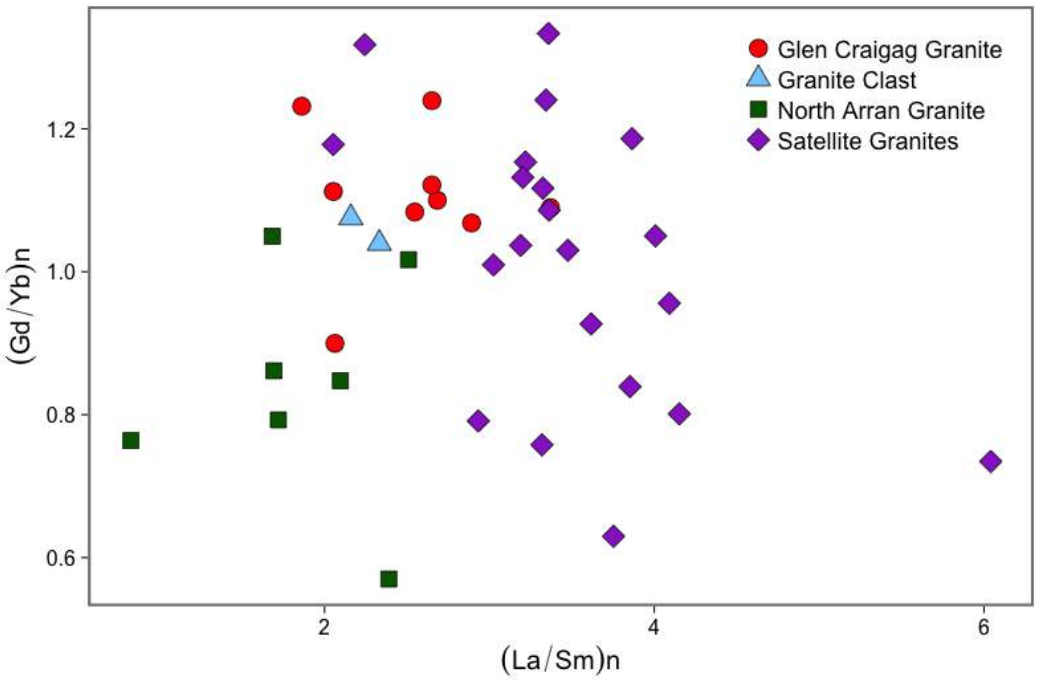

Fig. 4.30 – Chondrite normalised (McDonough and Sun, 1995) La/Sm and Gd/Yb ratios for the granites of the CAIC, the NAG, and the granite clasts found in the ignimbrites of the CAIC.

Ignimbrites

Chondrite normalised (McDonough and Sun, 1995) rare-earth element diagrams for the rhyolitic lava-like ignimbrites of the AVF are shown in Fig. 4.31. The light rare-earth element (LREE) patterns and heavy rare-earth element (HREE) patterns are summarised using La/Sm and Gd/Yb ratios in Fig. 4.32.

The Muileann Gaoithe rhyolites have slightly enriched LREE profiles with (La/Sm)n values of 1.56–2.10, and slightly enriched HREE profiles with (Gd/Yb)n values of 0.53–0.91. The negative Eu anomaly is very pronounced – even more so than the North Arran Granite.

The White Tuff Member rhyolites have more enriched LREE profiles than the Muileann Gaoithe rhyolites, with (La/Sm)n values of 2.37–3.46. They also have flatter HREE profiles, with (Gd/Yb)n values of 0.83–1.20 (Figs. 4.31, 4.32). The negative Eu anomaly is very pronounced, but not as extreme as the Muileann Gaoithe Member, as shown by higher normalised Eu values.

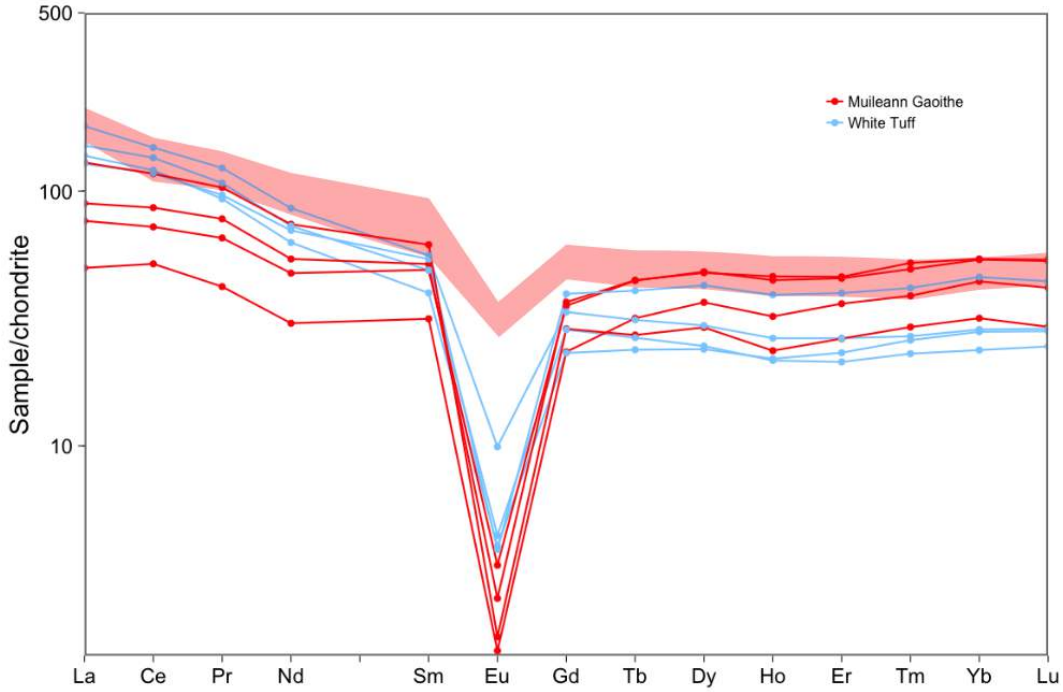

Fig. 4.31 – Chondrite normalised (McDonough and Sun, 1995) rare-earth element diagrams for the rhyolitic lava-like ignimbrites of the AVF. The coloured field shows the compositions of the Glen Craigag Granite for comparison.

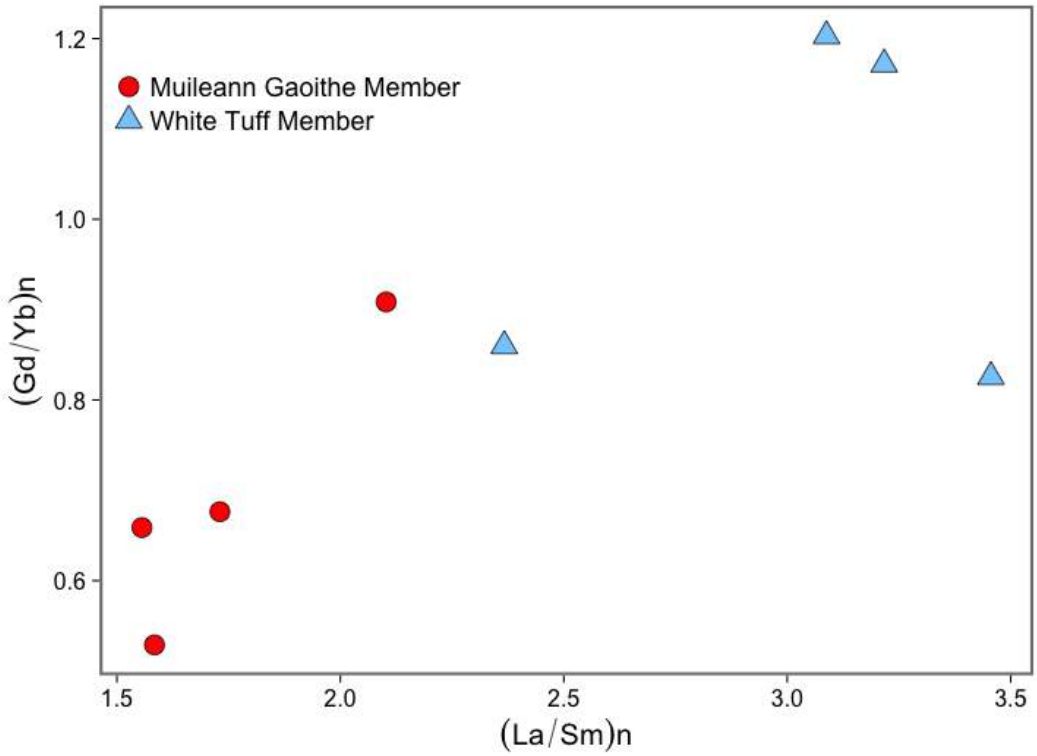

Fig. 4.32 – Chondrite normalised (McDonough and Sun, 1995) La/Sm and Gd/Yb ratios for the rhyolitic lava-like ignimbrites of the AVF.

4.1.5 Classification

The lithological names given in Chapter 2 are based largely on petrographic observations, including the use of the QAPF diagram (Le Maitre et al., 2002). It is useful, however, to classify rocks based on their whole-rock elemental composition. The most widely used method of doing this is by using a plot of Na_2O plus K_2O (total alkalis) vs. SiO_2. This total-alkali vs. silica (TAS) diagram contains classification fields for both volcanic (Le Bas et al., 1986) and plutonic (Cox et al., 1979) rocks. The alkalis can be susceptible remobilisation during alteration, so an alternative classification, using ratios of generally immobile trace elements – Nb/Y vs. Zr/Ti – is also used (Pearce, 1996).

Dykes

Geochemical classification of the dykes on the basis of major elements (TAS diagram; Figure 4.33) and trace element ratios (Nb/Y vs. Zr/Ti diagram; Figure 4.34) is broadly consistent. On the TAS diagram, the picrite dyke plots in the picro-basalt field – consistent with petrographic observations (Section 2.6.4). On the Nb/Y vs. Zr/Ti diagram it plots in the basalt field, as there is not a field for ultramafic rocks. The CAIC mafic dykes plot in the basalt and basaltic andesite fields on the TAS diagram and in the basalt field on the Nb/Y vs. Zr/Ti diagram (with one sample on the edge of the andesite/basaltic andesite field). The low La/Sm CAIC dykes are generally more mafic (lower SiO_2, total alkalis, Nb/Y, and Zr/Ti) than the high La/Sm CAIC dykes, suggesting that REE behaviour is at least partly controlled by evolution trends. The dykes which intrude the NAG have a greater range in composition, from basalt to andesite on the TAS diagram and basalt to andesite/basaltic andesite on the Nb/Y vs. Zr/Ti diagram. Again, the low La/Sm NAG dykes are generally more mafic than those with high La/Sm. The pitchstone plots as a rhyolite on the TAS diagram, and in the rhyolite/dacite field on the Nb/Y vs. Zr/Ti diagram, consistent with petrographic observations (Section 2.6.3). On the TAS diagram, all dykes show a clearly tholeiitic trend.

Dolerite sill and gabbros

Due to the plutonic nature of the gabbros, these are plotted on both the volcanic TAS diagram (Figure 4.35) and the plutonic TAS diagram (Figure 4.36), as well as the Nb/Y vs. Zr/Ti diagram (Figure 4.37).

The sill plots in the basalt field on the volcanic TAS diagram and the Nb/Y vs. Zr/Ti diagram, and in the gabbro field on the plutonic TAS diagram – consistent with

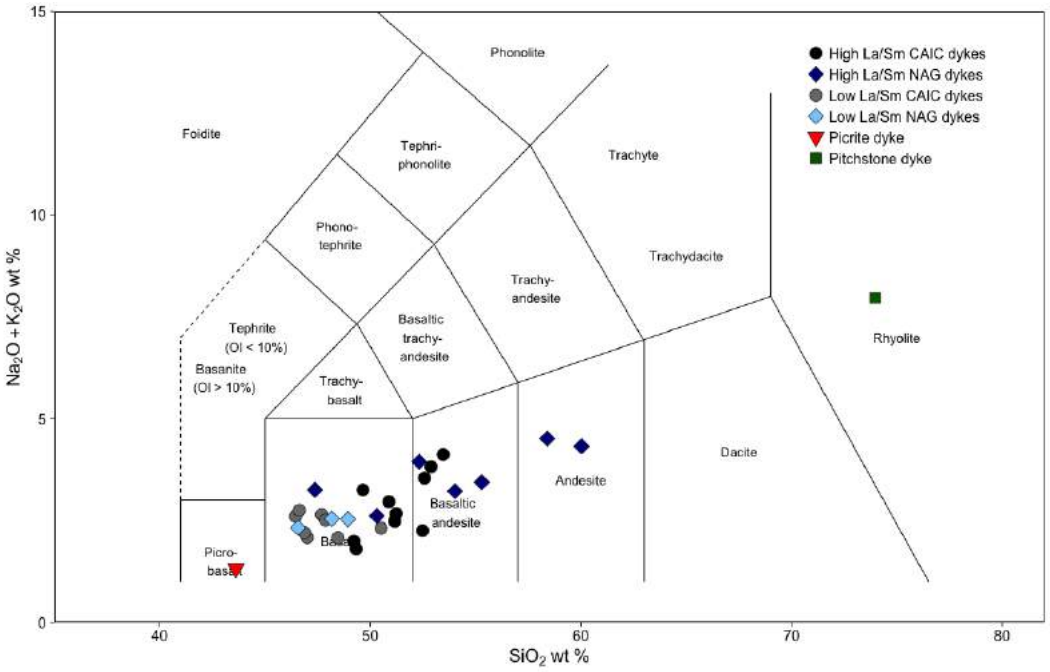

Fig. 4.33 – Total alkali vs. Silica diagram (Le Bas et al., 1986) for the dykes which intrude the CAIC and the NAG.

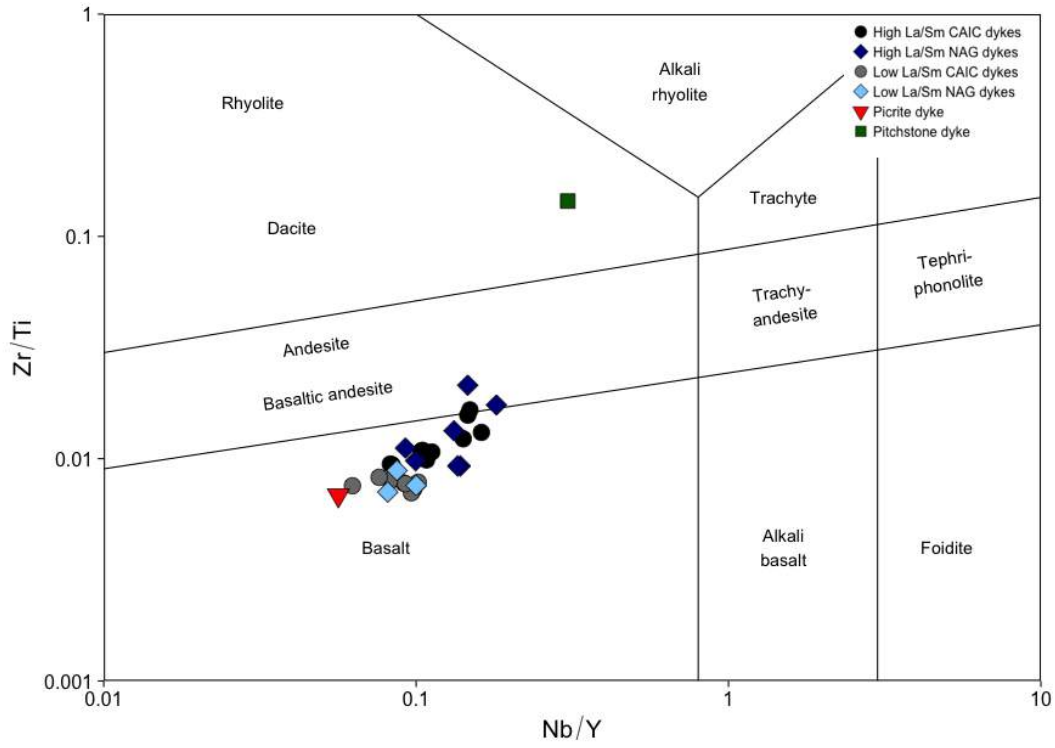

Fig. 4.34 – Nb/Y vs. Zr/Ti diagram (Pearce, 1996) for the dykes which intrude the CAIC and the NAG.

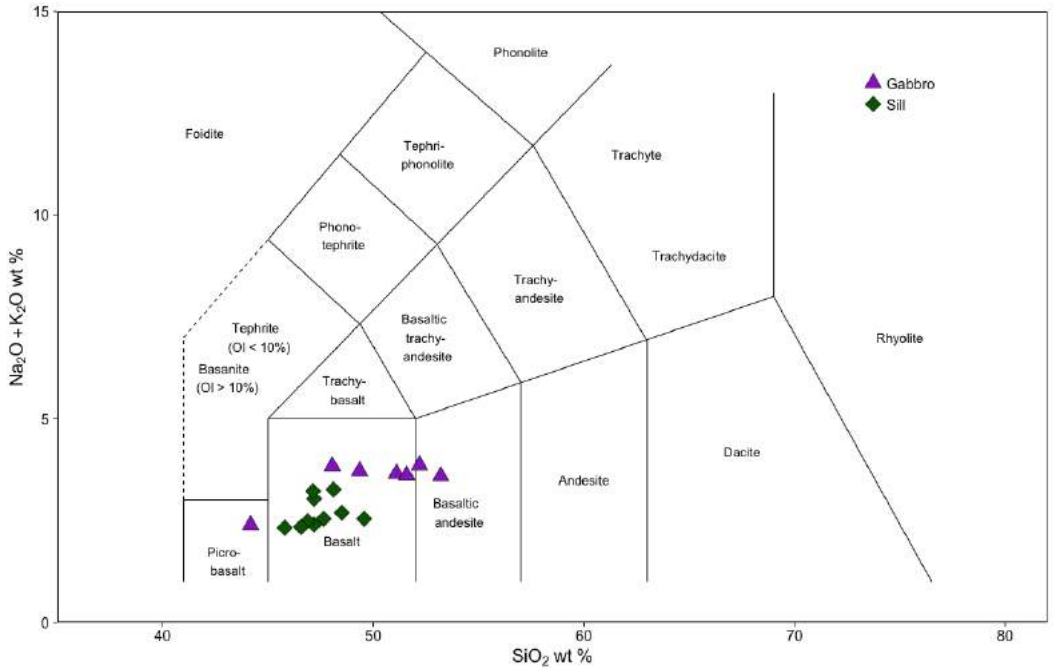

Fig. 4.35 – Total alkali vs. Silica diagram (Le Bas et al., 1986) for the dolerite sill which intrudes the ignimbrites of the AVF and the gabbroic intrusions associated with the Glenloig Hybrids

petrographic observations (Section 2.5). Most of the gabbros are generally more evolved than the sill (higher total alkalis and SiO_2), plotting in the basalt and basaltic andesite fields on the volcanic TAS diagram and the gabbro and diorite fields on the plutonic TAS diagram. The gabbro tends to have higher Nb/Y values than the sill, but still plots in the basalt field on the Nb/Y vs. Zr/Ti diagram. The outlier which plots in the picro-basalt field on the volcanic TAS diagram is sample BJG/16/12 – this is the magnetite cumulate shown in Figs 2.8 and 2.9. The sill and gabbros both show a tholeiitic trend. The only sample which plots above the tholeiitic-alkalic line in Fig. 4.36 is BJG/16/12, which does not have a magmatic composition.

Glenloig Hybrids and similar units

Many of the rocks included in this group are coarse grained, or at least have coarse grained equivalents in the CAIC, so they are plotted on both the volcanic TAS diagram (Figure 4.38) and the plutonic TAS diagram (Figure 4.39), as well as the Nb/Y vs. Zr/Ti diagram (Figure 4.40). In these diagrams, samples of the Glenloig Hybrids from the main continuous outcrop in the north and east of the complex (Fig. 1.9) are purple circles, while the samples from the intra-caldera inlier of hybrid rocks are shown as pink diamonds.

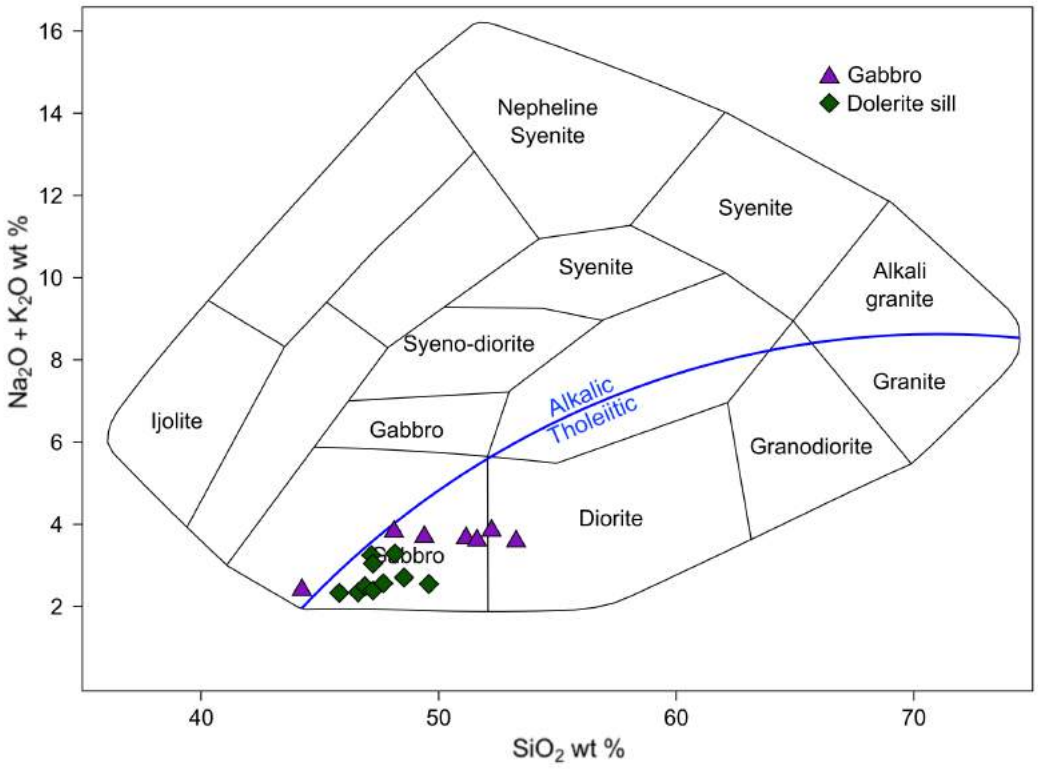

Fig. 4.36 – Plutonic total alkali vs. Silica diagram (Cox et al., 1979) for the dolerite sill which intrudes the ignimbrites of the AVF and the gabbroic intrusions associated with the Glenloig Hybrids

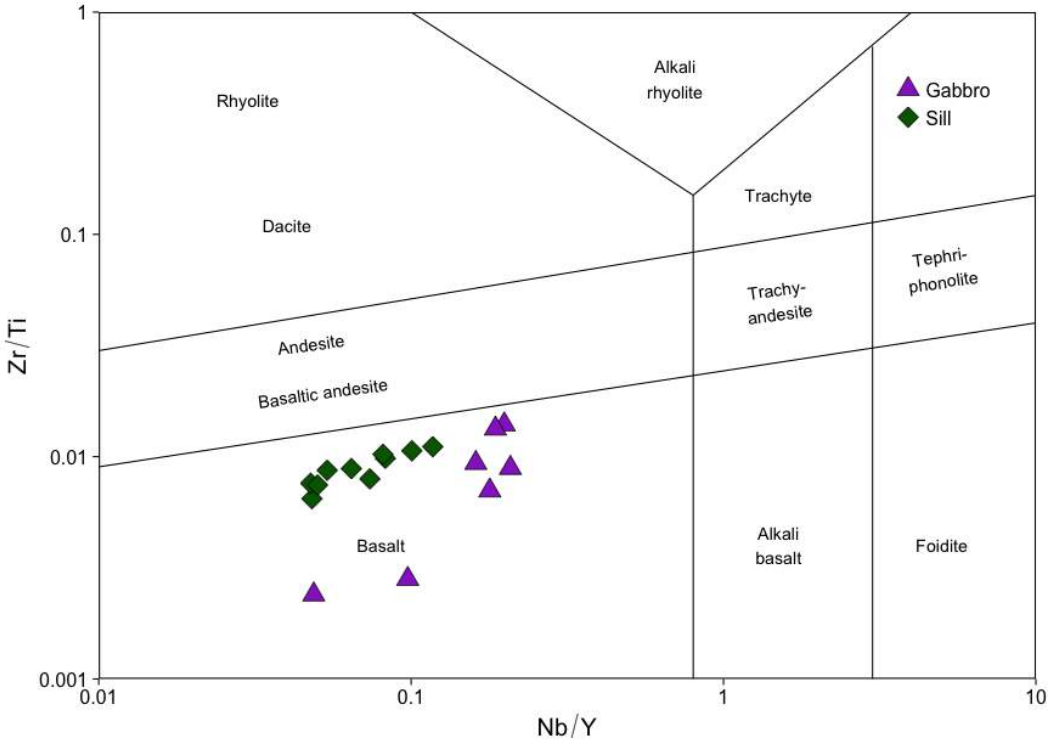

Fig. 4.37 – Nb/Y vs. Zr/Ti diagram (Pearce, 1996) for the dolerite sill which intrudes the ignimbrites of the AVF and the gabbroic intrusions associated with the Glenloig Hybrids

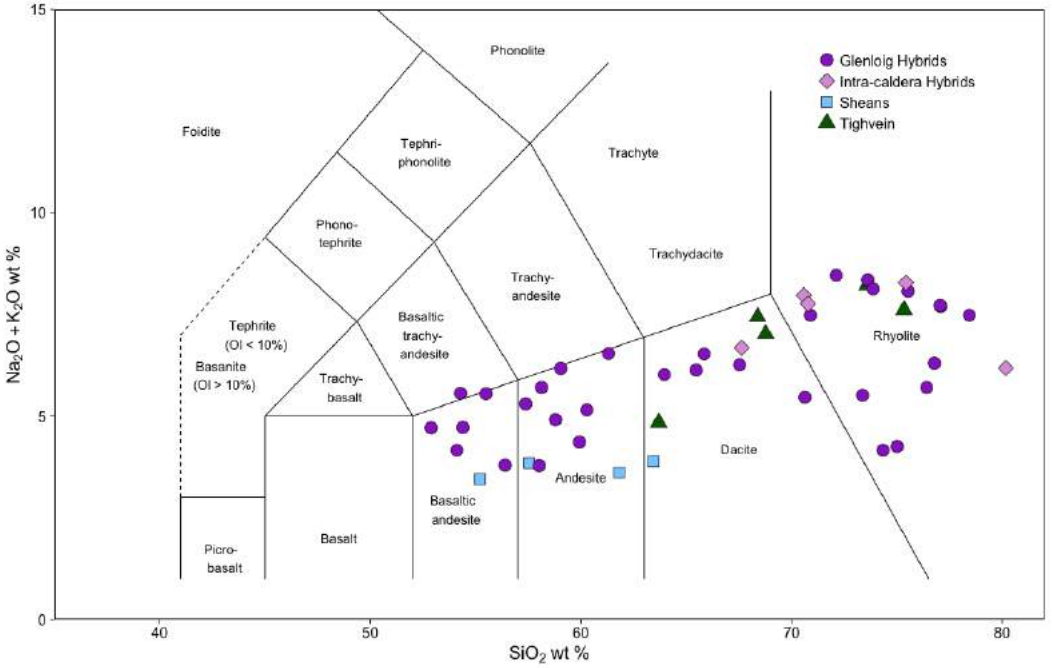

Fig. 4.38 – Total alkali vs. Silica diagram (Le Bas et al., 1986) for the hybrid rocks of the CAIC and similar units in the surrounding area.

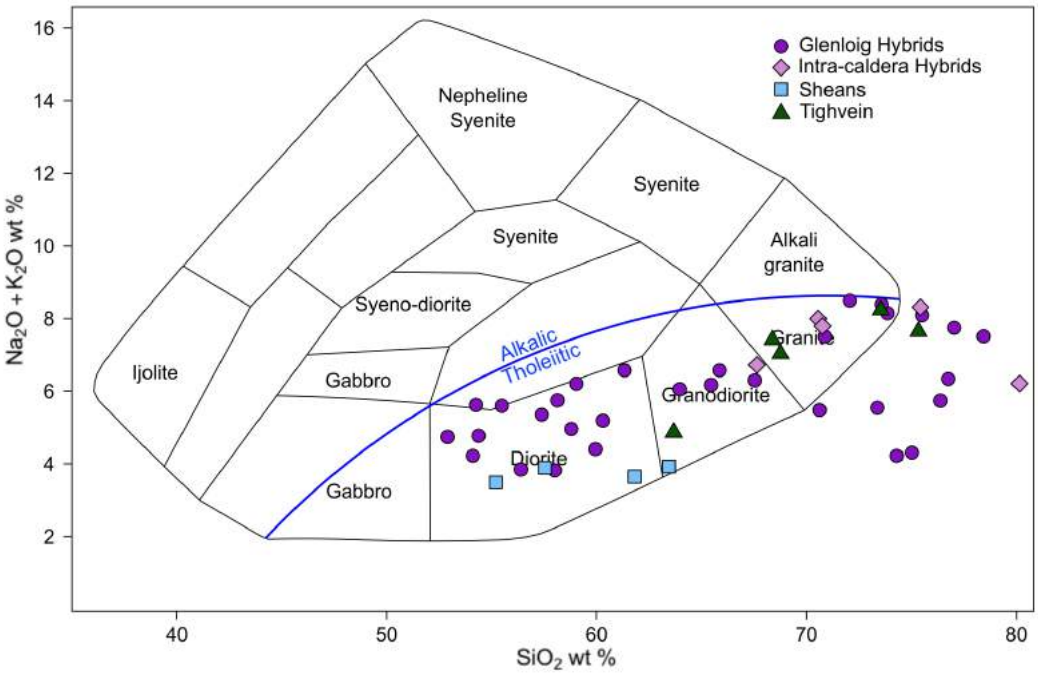

Fig. 4.39 – Plutonic total alkali vs. Silica diagram (Cox et al., 1979) for the hybrid rocks of the CAIC and similar units in the surrounding area.

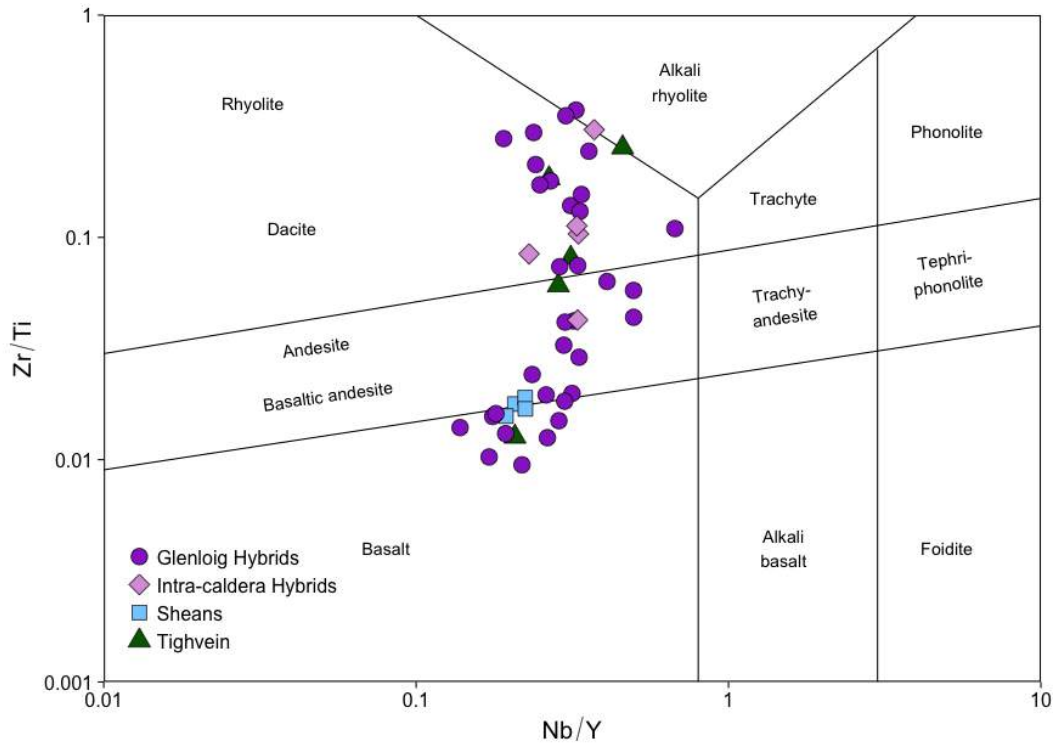

Fig. 4.40 – Nb/Y vs. Zr/Ti diagram (Pearce, 1996) for the hybrid rocks of the CAIC and similar units in the surrounding area.

The hybrid rocks of the CAIC and the surrounding area show a tholeiitic trend. Some have slightly more transitional compositions Fig. 4.40, but all plot below the tholeiitic-alkalic divide on Fig. 4.39. The hybrids exhibit the full range of compositions from basaltic andesite, through andesite and dacite, to rhyolite on the volcanic TAS diagram, and from diorite, through granodiorite, to granite and beyond on the plutonic TAS diagram. This suggests the presence of magma mixing, as well as the mingling described in Section 2.1. On the Nb/Y vs. Zr/Ti diagram (Fig. 4.38), they range from the basalt field, through the andesite/basaltic andesite field, to the rhyolite/dacite field. Some samples plot on the edge of the alkali rhyolite field. On the TAS diagrams, the Sheans samples occupy the less evolved part of the hybrid range, and display a flatter (lower total alkalis) trend than the Glenloig Hybrids. The Tighvein samples plot entirely within the range of the more evolved Glenloig Hybrids samples on both TAS diagrams and the Nb/Y vs. Zr/Ti diagram.

Granites

Due the coarse grained nature of granite, these samples are plotted on both volcanic (Fig. 4.41) and plutonic (Fig. 4.42) diagrams, as well as the Nb/Y vs. Zr/Ti diagram (Fig. 4.44). Fig. 4.43 shows a zoomed in version of the TAS diagram, so relationships can be seem more clearly. A TAS diagram with the different Satellite Granite intrusions plotted with different symbols is shown in Fig. 4.45.

All granites plot in the rhyolite field on the volcanic TAS diagram. On the plutonic TAS diagram, the majority of samples plot to the right of the marked fields, with some in the granite and alkali granite fields. The samples straddle the blue tholeiitic-alkalic line on Fig. 4.42. On the Nb/Y vs. Zr/Ti diagram the samples range from the rhyolite/dacite field to the alkali granite field. On the TAS diagrams, the ranges of the granites largely overlap and it is hard to distinguish them geochemically. This is easier on the Nb/Y vs. Zr/Ti diagram, where the different units display a spread of Nb/Y values, with the Glen Craigag plotting to the left (low Nb/Y), the Satellite Granites and North Arran Granite in the middle, and the granite clasts plotting to the right (high Nb/Y; Fig. 4.44). This suggests that the granite clasts are not sourced directly from any of the other units. The different Satellite Granites have overlapping compositional ranges and so cannot be distinguished on a TAS diagram (Fig. 4.45).

Ignimbrites

The analysed samples of ignimbrites from the Arran Volcanic Formation are plotted on the TAS diagram (Fig. 4.46) and the Nb/Y vs. Zr/Ti diagram (Fig. 4.47). On the

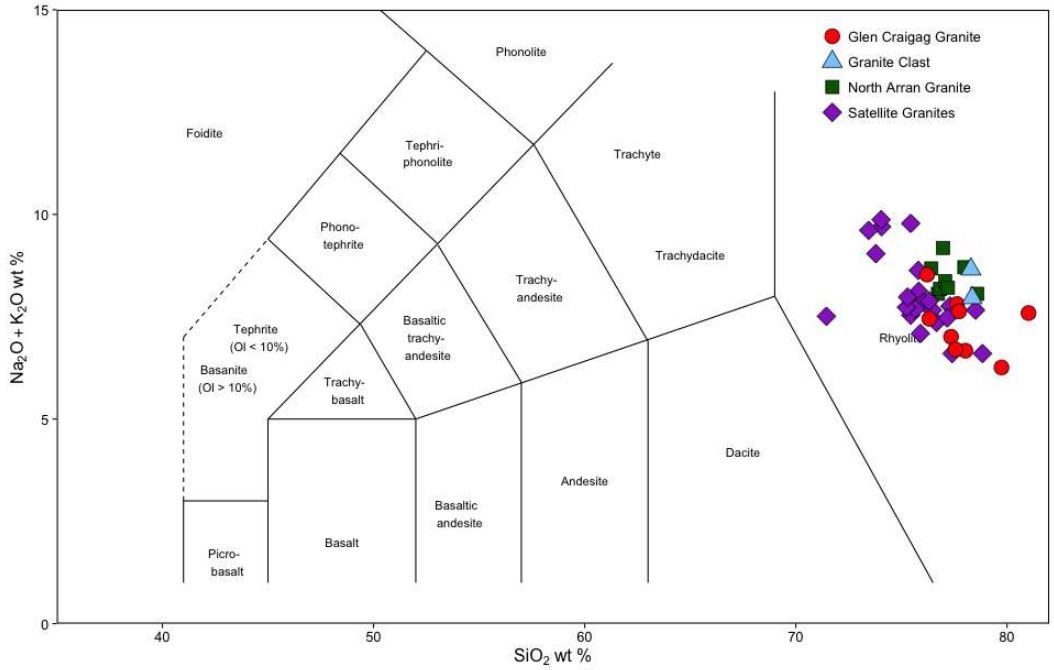

Fig. 4.41 – Total alkali vs. silica diagram (Le Bas et al., 1986) for the granitic rocks of the CAIC and the NAG.

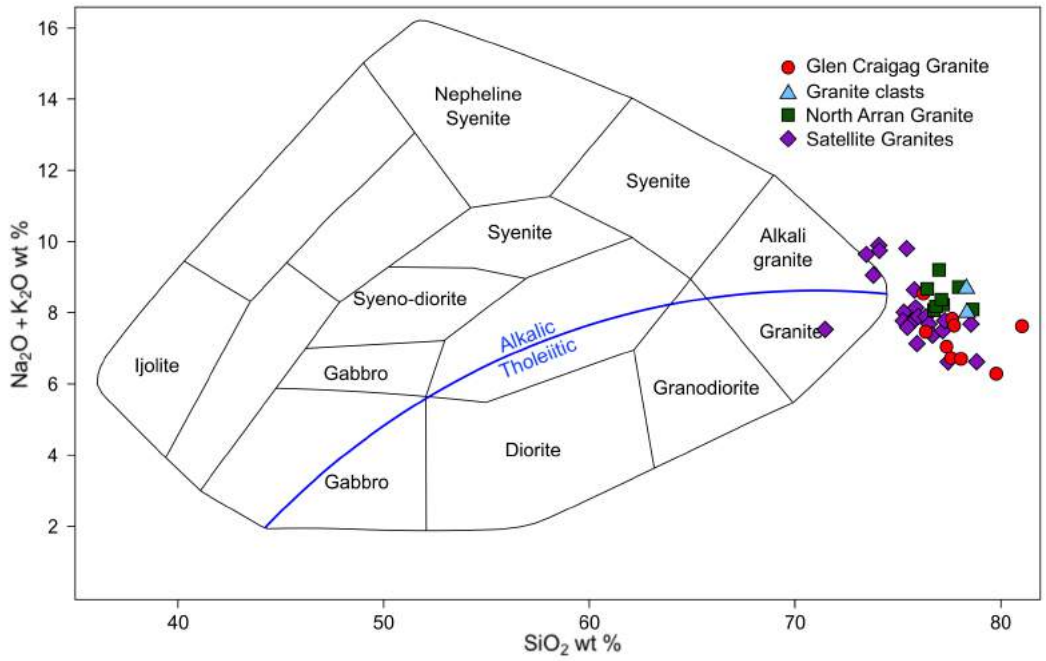

Fig. 4.42 – Plutonic total alkali vs. silica diagram (Cox et al., 1979) for the granitic rocks of the CAIC and the NAG.

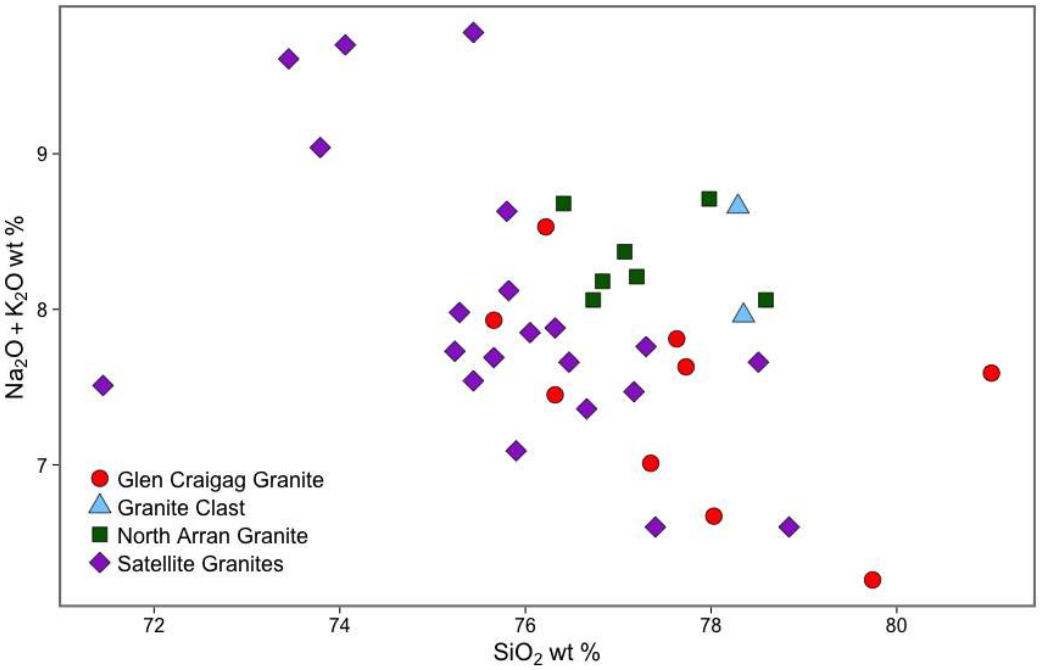

Fig. 4.43 – Zoomed total alkali vs. silica diagram for the granitic rocks of the CAIC and the NAG.

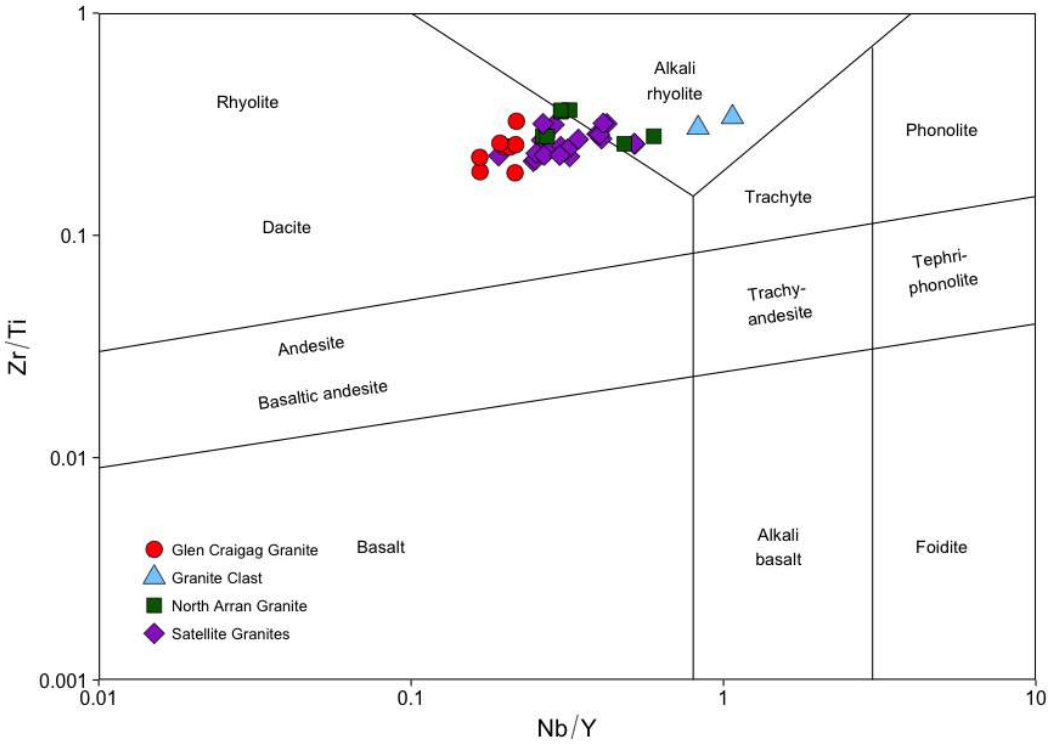

Fig. 4.44 – Nb/Y vs. Zr/Ti diagram (Pearce, 1996) for the granitic rocks of the CAIC and the NAG.

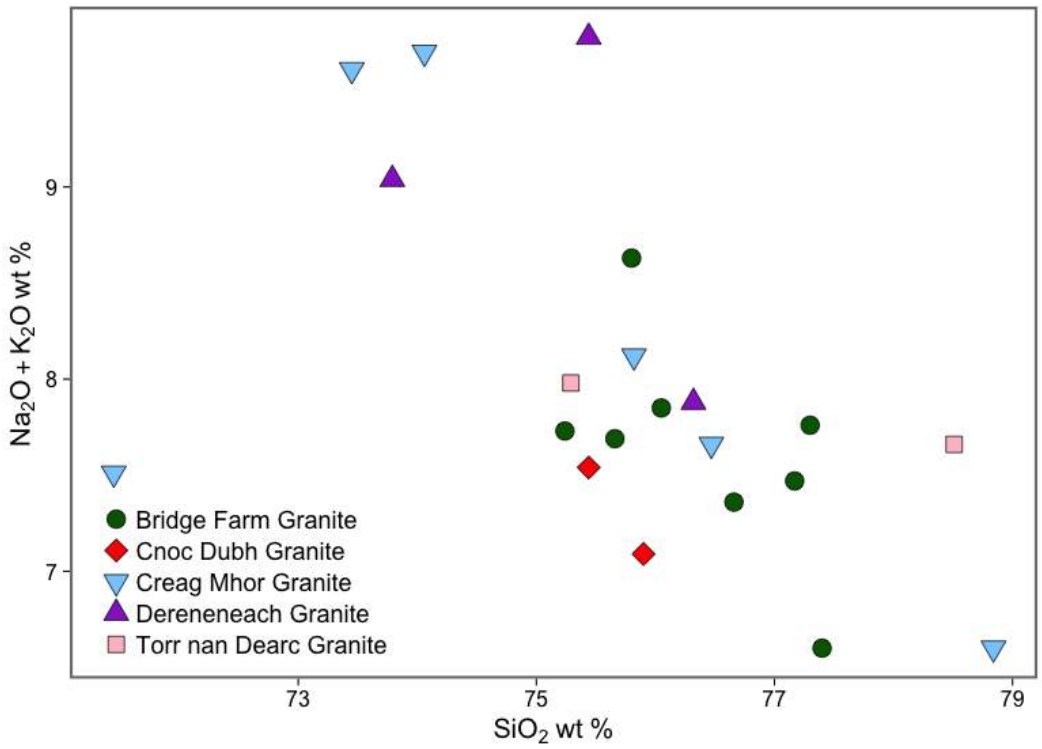

Fig. 4.45 – Total alkali vs. silica diagram for the Satellite Granites.

TAS diagram, the White Tuff Member and Muileann Gaoithe ignimbrites plot in the rhyolite field, consistent with petrographic observations (Sections 3.1.1, 3.1.6). On the Nb/Y vs. Zr/Ti diagram these units lie on the line between the rhyolite/dacite and alkali rhyolite fields, which is consistent with the TAS diagram. The Ard Bheinn Member ignimbrites plot in the dacite and rhyolite fields on the TAS diagram and the andesite/basaltic andesite and rhyolite/dacite fields on the Nb/Y vs. Zr/Ti diagram. On the TAS diagram, the Allt Beith tuff cone sample plots between the basaltic andesite and basaltic trachyandesite fields. However, on the Nb/Y vs. Zr/Ti diagram it plots in the rhyolite/dacite field. This is a significant discrepancy, and is presumably due to removal of Ti-rich phases, or accumulation or Zr-rich minerals.

4.1.6 Summary

The igneous rocks of the Central Arran Igneous Complex span the full range of tholeiitc compositions, from picro-basalt to granite, with all intermediate compositions represented by the more evolved dykes and the Glenloig Hybrids. The intermediate compositions in the dykes can be explained by fractional crystallisation (but see Section 5.3), while the intermediate Glenloig Hybrid samples are presumably formed

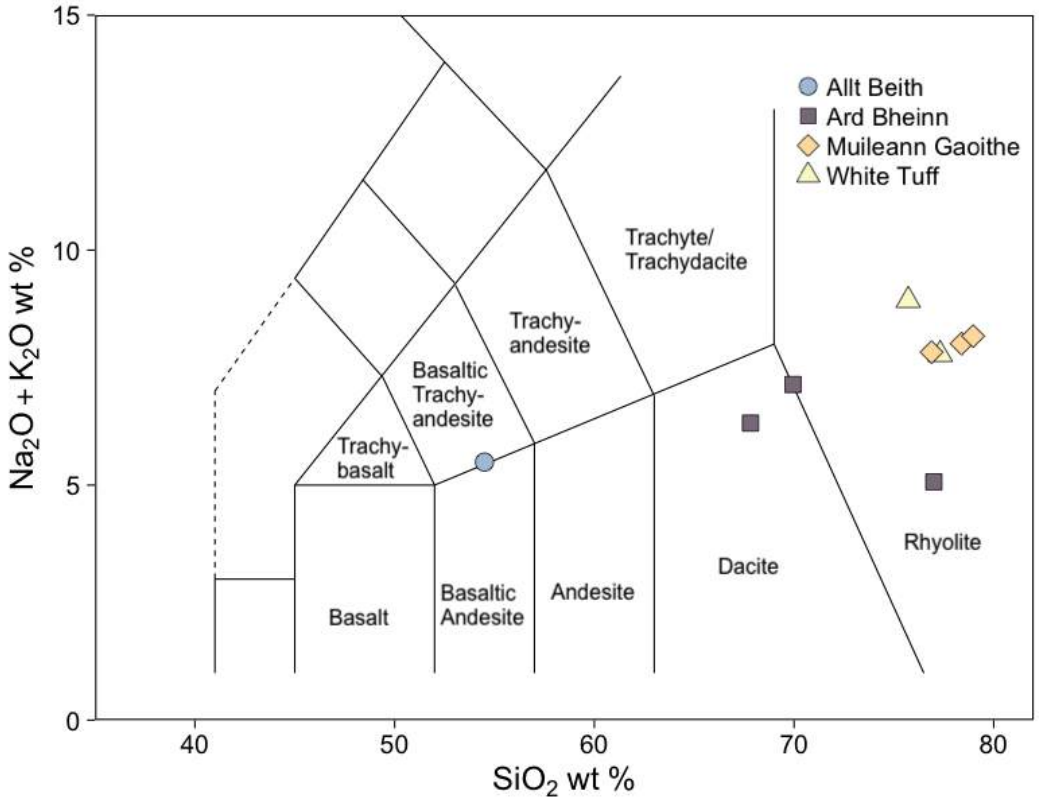

Fig. 4.46 – Total alkali vs. Silica diagram (Le Bas et al., 1986) for selected ignimbrites of the AVF.

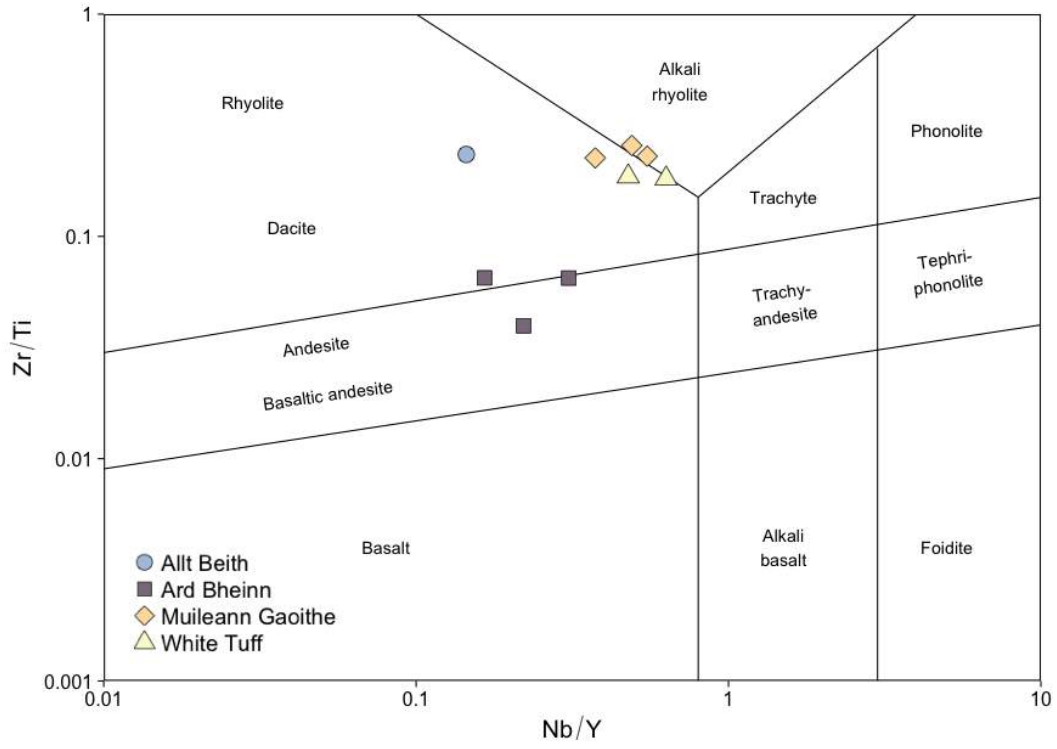

Fig. 4.47 – Nb/Y vs. Zr/Ti diagram (Pearce, 1996) for selected ignimbrites of the AVF.

by magma mixing, as suggested by the observed mingling on a range of scales in Section 2.1.

The mafic dykes that intrude the CAIC and the NAG define a tholeiitic trend, and have compositions ranging from basalt to andesite. All low La/Sm dykes are basaltic in composition. The olivine picrite dyke from the CAIC has a picro-basalt composition. They define major and trace element trends that would be expected with fractional crystallisation, *i.e.,* decreasing MgO, Fe_2O_3*, and CaO, and increasing Na_2O, K_2O, and incompatible elements with evolution. The low La/Sm dykes have incompatible element depleted trace element patterns, while those for the high La/Sm dykes are flatter, with significant enrichment of Rb, Ba, Th, and U. The Low La/Sm dykes (of both the CAIC and NAG) have LREE-depleted REE patterns, while the high La/Sm dykes have flat to LREE-enriched patterns.

The sill that intrudes the CAIC is basaltic and tholeiitic in composition. The samples have a restricted range of most major and trace elements, as would be expected from a single intrusion. However, the mobile incompatible elements (Rb, Ba, Th, U) show wide variations when plotted on the primitive mantle normalised spider diagram. The trace element pattern and REE pattern for the sill is distinctly convex-upwards, with depletion in both LREEs and HREEs, relative to Nd and Sm.

One sample of gabbro is a magnetite cumulate, and is very distinct from the other gabbros. This sample has a picro-basaltic composition. The rest have basaltic–basaltic andesitic tholeiitic compositions. They have a wide range of major and trace elements, reflecting differences in their mineralogy and degree of alteration. All of the gabbros have flat to incompatible element enriched trace element patterns, with high levels of Rb, Ba, Th, and U, and depletions of Nb and Ta.

The Glenloig Hybrids have a wide range of compositions from basaltic andesitic to rhyolitic on the volcanic TAS diagram (Le Bas et al., 1986), and from diorite to granite on the plutonic TAS diagram (Cox et al., 1979). Those that plot in the rhyolite field are classified as 'silicic Glenloig Hybrids' for the remainder of this thesis, while the rest are called 'intermediate Glenloig Hybrids'. Samples are tholeiitic, with some approaching transitional-alkaline. They show clear evolution trends in major and trace elements when plotted against SiO_2, with a small group showing low concentrations of incompatible elements at evolved compositions. The intermediate hybrids, although they have a wider range in major element compositions, have a more restricted range of trace element and REE patterns. They have concave-upwards REE profiles, with enrichment in LREEs and Rb, Ba, Th, and U, and moderate depletions on Nb, Ta, Sr, and Ti. The silicic hybrids have a much wider range of trace element and REE profiles, with significant negative Sr and Ti anomalies and highly varied Rb, Ba, and Th concentrations. The hybrid samples from the Sheans geochemically resemble the intermediate Glenloig Hybrids, while those from Tighvein are more similar to the silicic hybrids of the CAIC.

The granites are almost all tholeiitic, with some samples of the Satellite Granites (from Creag Mhor and Dereneneach) showing more alkaline compositions. The ranges of most major elements for the different granites overlap, but they do have distinctly different concentrations of Fe_2O_3*, with the Glen Craigag Granite having the highest concentration, and the North Arran Granite and the granite clasts having the lowest. The differences in trace element concentrations between the different granites are largely due to differing fractional crystallisation histories (see Section 5.3). The Satellite Granites have a distinctly concave-upwards REE pattern, whereas the Glen Craigag Granite and North Arran Granite have flatter HREE profiles with more enrichment in LREE. The granite clasts from the ignimbrites of the CAIC , as well as the rhyolitic lava-like ignimbrites, are geochemically similar to the the North Arran Granite, suggesting that they may share a common source.

4.2 Radiogenic Tracer Isotopes

Thirty-five samples of igneous intrusive rocks from the CAIC and the NAG were selected for Sr-Nd-Pb-Hf isotope analysis. These samples were chosen as a representative selection of the different magmas intruded in central Arran, and were selected for their relatively low levels of alteration. They include three samples of the dolerite sill, four mafic dykes from the CAIC, the picrite dyke from the CAIC, three samples of gabbro, seven of the Satellite Granites (at least one from each intrusion), four from the Glen Craigag Granite, nine of the Glenloig Hybrids (of varying composition), and four from the North Arran Granite. Sample preparation and analysis methods are given in Appendix A.

4.2.1 Age Correction and ε Notation

All radiogenic isotope ratios are age corrected to their initial values at 59 Ma using the following equations:

$$\frac{^{87}Sr}{^{86}Sr}(\text{initial}) = \frac{^{87}Sr}{^{86}Sr}(\text{measured}) - \frac{^{87}Rb}{^{86}Sr} \times (e^{\lambda t} - 1)$$

$$\frac{^{143}Nd}{^{144}Nd}(\text{initial}) = \frac{^{143}Nd}{^{144}Nd}(\text{measured}) - \frac{^{147}Sm}{^{144}Nd} \times (e^{\lambda t} - 1)$$

$$\frac{^{176}Hf}{^{177}Hf}(\text{initial}) = \frac{^{176}Hf}{^{177}Hf}(\text{measured}) - \frac{^{176}Lu}{^{177}Hf} \times (e^{\lambda t} - 1)$$

$$\frac{^{206}Pb}{^{204}Pb}(\text{initial}) = \frac{^{206}Pb}{^{204}Pb}(\text{measured}) - \frac{^{238}U}{^{204}Pb} \times (e^{\lambda t} - 1)$$

$$\frac{^{207}Pb}{^{204}Pb}(\text{initial}) = \frac{^{207}Pb}{^{204}Pb}(\text{measured}) - \frac{^{235}U}{^{204}Pb} \times (e^{\lambda t} - 1)$$

$$\frac{^{208}Pb}{^{204}Pb}(\text{initial}) = \frac{^{208}Pb}{^{204}Pb}(\text{measured}) - \frac{^{232}U}{^{204}Pb} \times (e^{\lambda t} - 1)$$

where λ is the decay constant shown in Table 4.1, and t is age in years, in this case 59,000,000. The measured isotope ratios and trace element data used in these calculations are shown in Appendix E5. The age-corrected Sr-Nd-Hf-Pb radiogenic isotope results are shown in Table 4.2.

To allow easier comparison of isotope ratios which are similar down to the fourth or fifth decimal place, epsilon (ε) notation is used for Sr, Nd, and Hf results. This

Table 4.1 – Decay constants of parent isotopes in the Sr-Nd-Hf-Pb systems studied in this thesis. Data from Hamilton et al. (1978); Sguigna et al. (1982); Steiger and Jager (1977).

Radioactive isotope	Decay constant (a^{-1})
^{87}Rb	1.42×10^{-11}
^{147}Sm	6.54×10^{-12}
^{176}Lu	1.93×10^{-11}
^{238}U	1.55×10^{-10}
^{235}U	9.85×10^{-10}
^{232}U	4.95×10^{-11}

is calculated by normalising the age-corrected isotope ratio to that of the chondrite uniform reservoir (CHUR).

$$\varepsilon Sr = \left(\frac{\frac{^{87}Sr}{^{86}Sr}(59)sample}{\frac{^{87}Sr}{^{86}Sr}(59)CHUR} - 1 \right) \times 10,000$$

$$\varepsilon Nd = \left(\frac{\frac{^{143}Nd}{^{144}Nd}(59)sample}{\frac{^{143}Nd}{^{144}Nd}(59)CHUR} - 1 \right) \times 10,000$$

$$\varepsilon Hf = \left(\frac{\frac{^{176}Hf}{^{177}Hf}(59)sample}{\frac{^{176}Hf}{^{177}Hf}(59)CHUR} - 1 \right) \times 10,000$$

Table 4.2 – Age-corrected (59 Ma) radiogenic isotope ratios.

Sample	Unit	$^{143}Nd/^{144}Nd$	εNd	$^{87}Sr/^{86}Sr$	εSr	$^{176}Hf/^{177}Hf$	εHf	$^{206}Pb/^{204}Pb$	$^{207}Pb/^{204}Pb$	$^{208}Pb/^{204}Pb$
BJG/15/54	Sill	0.51282	5.06	0.70391	-7.44	0.28313	13.86	17.423	15.397	37.246
BJG/15/7	Sill	0.51289	6.46	0.70410	-4.74	0.28315	14.54	17.501	15.401	37.393
BJG/15/58	Sill	0.51274	3.44	0.70454	1.53	0.28311	13.19	16.997	15.321	36.803
BJG/15/325	Dyke	0.51286	5.73	0.70353	-12.78	0.28312	13.71	18.622	15.494	38.443
BJG/15/340	Dyke	0.51261	0.93	0.70516	10.30	0.28317	15.54	18.618	15.496	38.635
BJG/15/154	Dyke	0.51295	7.63	0.70352	-13.00	0.28322	17.07	17.869	15.438	37.639
BJG/15/112	Dyke	0.51274	3.38	0.70449	0.83	0.28308	12.13	18.213	15.475	38.076
BJG/15/338	Picrite Dyke	0.51261	0.98	0.70457	1.94	0.28312	13.53	18.428	15.495	38.288
BJG/15/344	Gabbro			0.70587	20.48	0.28294	7.11	18.329	15.491	38.257
BJG/15/23	Gabbro	0.51241	-2.96	0.70623	25.53	0.28291	6.08	18.407	15.495	38.345
BJG/16/12	Gabbro	0.51254	-0.35	0.70641	28.07	0.28293	6.90	18.325	15.509	38.172
BJG/15/335	Satellite Granites	0.51233	-4.49	0.70927	68.75	0.28270	-1.29	18.627	15.505	38.653
BJG/16/26	Satellite Granites	0.51232	-4.72	0.70948	71.62	0.28268	-1.85	18.340	15.484	38.507
BJG/15/328	Satellite Granites	0.51232	-4.80	0.70851	57.90	0.28269	-1.50	18.770	15.508	38.747
BJG/16/18	Satellite Granites	0.51233	-4.61	0.70816	52.87	0.28269	-1.39	18.665	15.510	38.774
BJG/15/347	Satellite Granites	0.51232	-4.78	0.70795	49.91	0.28270	-1.26	18.913	15.516	38.787
BJG/15/349	Satellite Granites	0.51233	-4.62	0.70908	66.02	0.28270	-1.19	18.669	15.509	38.408
BJG/15/343	Satellite Granites	0.51227	-5.63	0.70845	57.08	0.28270	-1.10	18.763	15.516	38.774
BJG/16/44	Glen Craigag Granite	0.51230	-5.14	0.71048	85.84	0.28270	-1.35	18.185	15.462	38.196
BJG/16/31	Glen Craigag Granite	0.51226	-5.98	0.70875	61.34	0.28264	-3.23	18.276	15.474	38.193
BJG/15/111	Glen Craigag Granite	0.51231	-4.87	0.70829	54.76	0.28269	-1.73	18.328	15.477	38.285
BJG/15/74	Glen Craigag Granite	0.51226	-5.82	0.70934	69.66	0.28264	-3.19	18.360	15.476	38.233
BJG/15/324D	Glenloig Hybrids	0.51249	-1.42	0.70585	20.13	0.28280	2.49	18.562	15.516	38.536
BJG/15/321M	Glenloig Hybrids	0.51256	-0.02	0.70537	13.30	0.28295	7.75	18.327	15.495	38.229
BJG/15/127D	Glenloig Hybrids	0.51239	-3.28	0.70677	33.24	0.28278	1.72	18.566	15.507	38.537
BJG/15/306	Glenloig Hybrids	0.51251	-1.02	0.70587	20.42	0.28291	6.08	18.340	15.492	38.214
BJG/15/82	Glenloig Hybrids	0.51233	-4.56	0.70766	45.87	0.28275	0.71	18.679	15.504	38.695
BJG/15/27	Glenloig Hybrids	0.51233	-4.54	0.70755	44.24	0.28269	-1.61	18.610	15.501	38.614
BJG/15/127F	Glenloig Hybrids	0.51233	-4.51	0.70786	48.67	0.28270	-1.33	18.764	15.519	38.759
BJG/15/321F	Glenloig Hybrids	0.51234	-4.39	0.70622	25.34	0.28271	-0.85	18.454	15.500	38.388
BJG/15/324F	Glenloig Hybrids	0.51235	-4.06	0.70674	32.84			18.578	15.513	38.542
BJG/16/38	North Arran Granite	0.51206	-9.86	0.71702	178.71	0.28254	-6.71	17.876	15.451	38.018
BJG/15/178	North Arran Granite	0.51210	-8.96	0.72744	326.62	0.28250	-8.35	17.848	15.444	37.986
BJG/16/33	North Arran Granite	0.51206	-9.79	0.71878	203.65	0.28243	-10.66	17.809	15.445	37.995
BJG/15/179	North Arran Granite	0.51206	-9.85	0.71441	141.65	0.28248	-8.88	17.814	15.439	37.975

Bivariate plots of $^{87}Sr/^{86}Sr$ against other radiogenic isotope ratios are shown in Fig. 4.48, $^{143}Nd/^{144}Nd$ against other radiogenic isotope ratios are shown in Fig. 4.49, and $^{176}Hf/^{177}Hf$ and Pb isotope ratios are shown in Fig. 4.50. Coloured fields show the isotopic compositions of crustal units that could be the source of contamination for the Arran Magmas. The Midland Valley fields show mafic and silicic xenoliths of the unexposed Midland Valley basement, brought up in Permo-Carboniferous dykes and plugs (Halliday et al., 1993). The Dalradian field shows Proterozoic-Cambrian metasediments from Arran (Dickin, 1994; Dickin et al., 1981). The Devonian Sandstones unit is the Old Red Sandstone unit, also from Dickin et al. (1981). The field marked 'Islay' shows the compositions of the Proterozoic gneisses from the Rhinns Complex on Islay (Marcantonio et al., 1988). The Rhinns Complex is suggested to represent the basement to the Dalradian metasediments (Stephenson et al., 2013).

Average DMM (depleted MORB mantle) values are bounded by average enriched DMM and average depleted DMM values presented in Table 1 of Workman and Hart (2005). Iceland values are bounded by the highest and lowest values for $^{87}Sr/^{86}Sr$, $^{143}Nd/^{144}Nd$, and $^{176}Hf/^{177}Hf$ ratios presented in Kempton et al. (2000). Because this study showed a very large range in Pb isotopes, an 'Average Iceland' field has been determined for clarity when plotted on these graphs. Average Iceland values are bounded by the same $^{87}Sr/^{86}Sr$, $^{143}Nd/^{144}Nd$, and $^{176}Hf/^{177}Hf$ ratios, as well as the average $^{206}Pb/^{204}Pb$, $^{207}Pb/^{204}Pb$, and $^{208}Pb/^{204}Pb$ presented in Kempton et al. (2000). Average $^{206}Pb/^{204}Pb$ values are taken to be the mean value $\pm$ 0.1, average $^{207}Pb/^{204}Pb$ values are taken to be the mean value $\pm$ 0.01, and average $^{208}Pb/^{204}Pb$ values are taken to be the mean value $\pm$ 0.1.

4.2.2 Sr isotopes

The mafic units generally have lower (less radiogenic) $^{87}Sr/^{86}Sr$ values than the intermediate and silicic units (Fig 4.48). The mafic dykes of the CAIC have $^{87}Sr/^{86}Sr$ values of 0.70352 – 0.70516 (εSr -13.00 – 10.30). These values are only slightly higher than mantle values. The picrite dyke is at the upper end of this range, with $^{87}Sr/^{86}Sr$ of 0.70457 (εSr 1.94). The dolerite sill has similar but very restricted $^{87}Sr/^{86}Sr$ ratios of 0.70391 – 0.70454 (εSr -7.44 – 1.53).

The gabbros have higher $^{87}Sr/^{86}Sr$ ratios than the other mafic units, between 0.70587 and 0.70641 (εSr 20.48 – 28.07). This is entirely within the range of the intermediate Glenloig Hybrids, which have $^{87}Sr/^{86}Sr$ ratios of 0.70537 – 0.70766 (εSr 13.30 – 45.87). This range is higher than all of the mafic dykes, and the positive

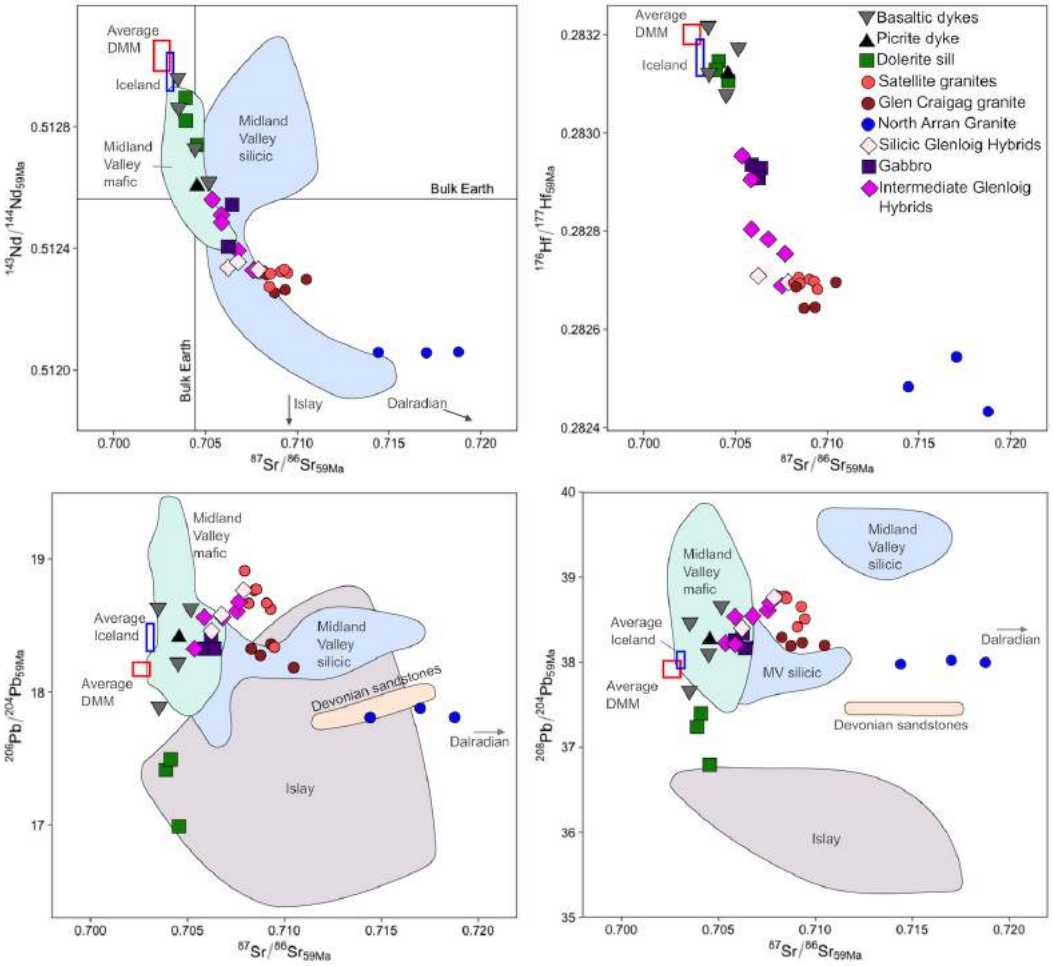

Fig. 4.48 – Plots of $^{87}Sr/^{86}Sr$ against other radiogenic isotope ratios (excluding the most radiogenic sample of the NAG for clarity).

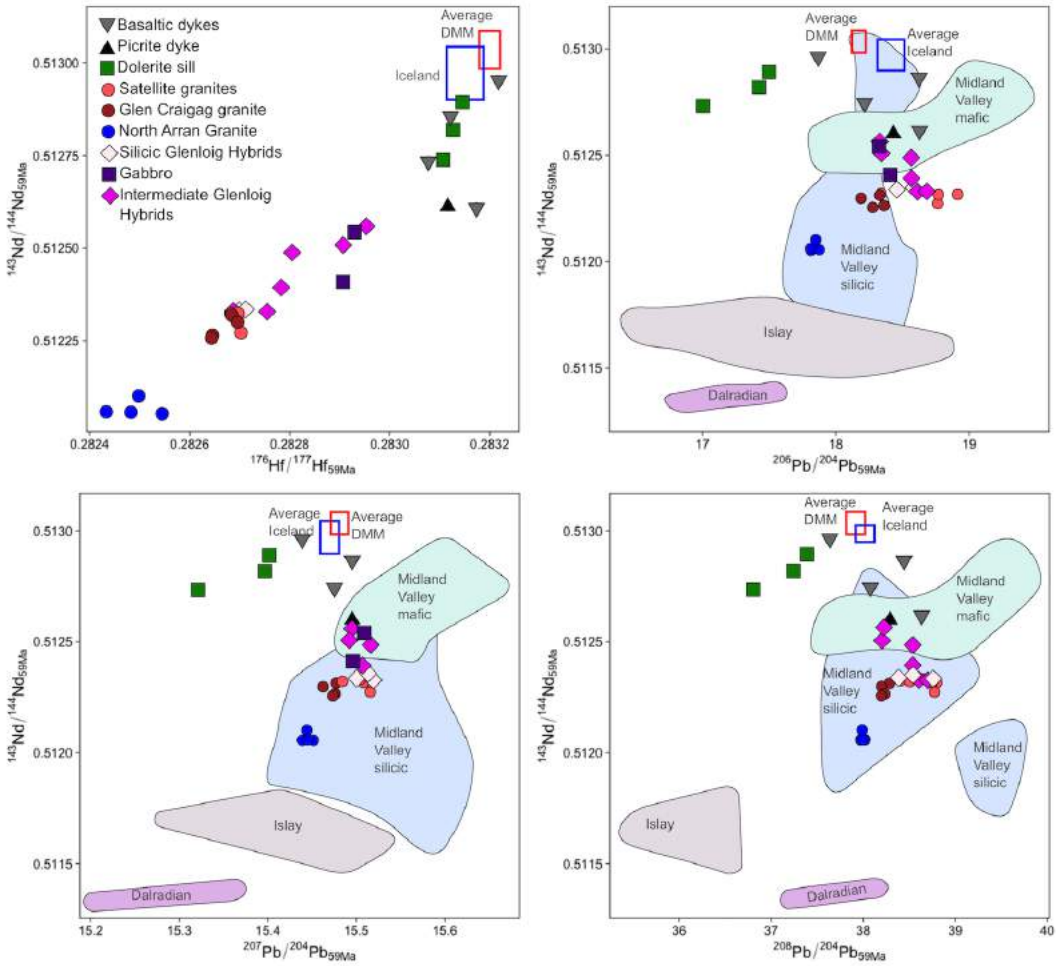

Fig. 4.49 – Plots of various radiogenic isotope ratios plotted against $^{143}Nd/^{144}Nd$.

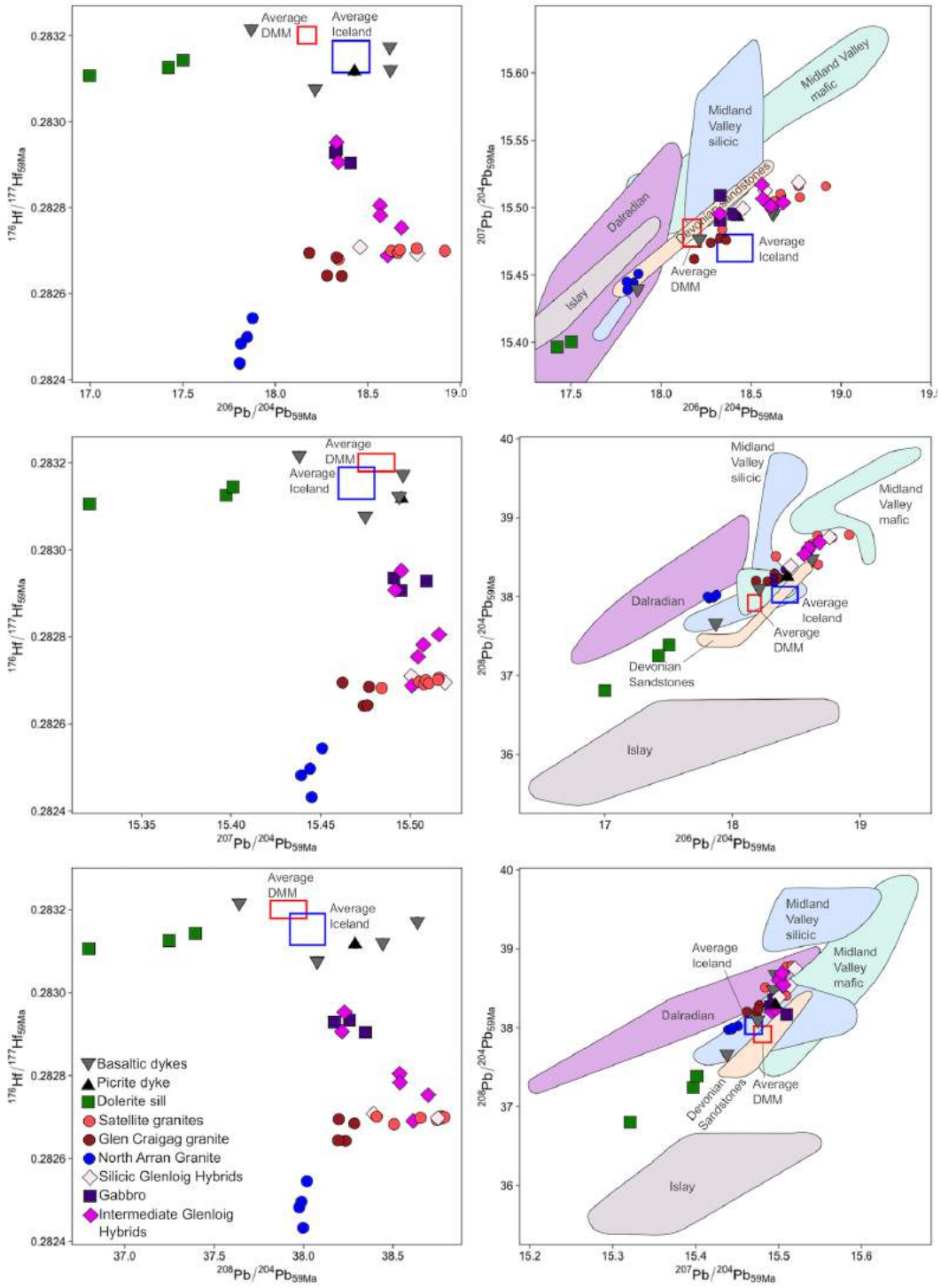

Fig. 4.50 – Plots of $^{176}Hf/^{177}Hf$, $^{206}Pb/^{204}Pb$, $^{207}Pb/^{204}Pb$, and $^{208}Pb/^{204}Pb$.

εSr values show that they are also more radiogenic than Bulk Earth. The silicic Glenloig Hybrids have a $^{87}Sr/^{86}Sr$ range of 0.70622 – 0.70786 (εSr 25.34 – 48.67).

The Satellite Granites generally have the lowest $^{87}Sr/^{86}Sr$ ratios of all the granites, at 0.70795 – 0.70948 (εSr 49.91 –71.62), although these are more radiogenic than the mafic and intermediate rocks, suggesting contamination by a high $^{87}Sr/^{86}Sr$ source. The Glen Craigag Granite has a $^{87}Sr/^{86}Sr$ range of 0.70829 – 0.71048 (εSr 54.76 – 85.84). The North Arran Granite has incredibly radiogenic Sr isotope ratios, with $^{87}Sr/^{86}Sr$ of 0.71441 – 0.72744 (εSr 141.65 – 326.62). This highest value has been omitted from Fig. 4.48 for clarity This is more radiogenic than the Midland Valley, Islay, and Devonian sandstone crustal units, suggesting contamination by a source with similar $^{87}Sr/^{86}Sr$ values to the Dalradian schists (Fig 4.48).

4.2.3 Nd isotopes

The mafic units generally have higher (more radiogenic) $^{143}Nd/^{144}Nd$ values than the intermediate and silicic units (Fig 4.49). The $^{143}Nd/^{144}Nd$ values of the mafic dykes range from 0.51261 – 0.51295 (εNd 0.93 – 7.63), only slightly lower than mantle values and above the Bulk Earth line on (Fig 4.48). The picrite dyke lies at the lower end of this range with $^{143}Nd/^{144}Nd$ of 0.51261 (εNd 0.98). The $^{143}Nd/^{144}Nd$ ratios for the dolerite sill lie within the range of values for the dykes, ranging from 0.51274 – 0.51289 (εNd 3.44 – 6.46).

Like the Sr isotopes, the $^{143}Nd/^{144}Nd$ ratios of the gabbros (0.51241 and 0.51254, εNd -2.96 – -0.35) plot within the range of values for the intermediate Glenloig Hybrids, which have $^{143}Nd/^{144}Nd$ ratios of 0.51233 – 0.51256 (εNd -4.56 – -0.02). The silicic Glenloig Hybrids have similar $^{143}Nd/^{144}Nd$ values of 0.51233 – 0.51235 (εNd -4.51 – -4.06).

The granites of the CAIC have similar Nd isotope ratios to the silicic Glenloig Hybrids. The Satellite Granites have $^{143}Nd/^{144}Nd$ values of 0.51227 – 0.51233 (εNd -5.63 – -4.49), while the Glen Craigag Granite has similar $^{143}Nd/^{144}Nd$ values of 0.51226 – 0.51231 (εNd -5.98 – -4.87). The North Arran Granite has extremely un-radiogenic $^{143}Nd/^{144}Nd$ values of 0.51206 – 0.51210 (εNd -9.86 – -8.96), again suggesting the input of a low $^{143}Nd/^{144}Nd$ source (Fig 4.49).

4.2.4 Hf isotopes

The Hf isotope ratios of these samples display a positive correlation with $^{143}Nd/^{144}Nd$ (Fig. 4.49). The relationship between the different units is therefore very similar.

There are no published Hf isotope data for the relevant crustal units, so these are omitted from graphs involving $^{176}Hf/^{177}Hf$ in Figs. 4.49 and 4.50.

The mafic dykes have $^{176}Hf/^{177}Hf$ values of 0.28308 – 0.28322 (εHf 12.13 – 17.07). The picrite dyke sits within this range with a $^{176}Hf/^{177}Hf$ value of 0.28312 (εHf 13.53). The dolerite sill also has Hf isotope ratios within the range of the dykes, with $^{176}Hf/^{177}Hf$ values of 0.28311 – 0.28315 (εHf 13.19 – 14.54).

The gabbros have $^{176}Hf/^{177}Hf$ values of 0.28291 – 0.28294 (εHf 6.08 – 7.11). This is in the upper range of the intermediate Glenloig Hybrids, which have $^{176}Hf/^{177}Hf$ values of 0.28269 – 0.28295 (εHf -1.61 – 7.75). The silicic hybrids have Hf isotope ratios at the lower end of the intermediate hybrids range, with $^{176}Hf/^{177}Hf$ values of 0.28270 and 0.28271 (εHf -1.33 and -0.85).

The Satellite Granites and the Glen Craigag Granite all have similar $^{176}Hf/^{177}Hf$ ratios. The Satellite Granites have values of 0.28268 – 0.28270 (εHf -1.85 – -1.10) while the Glen Craigag Granite has values of 0.28264 – 0.28270 (εHf -3.23 – -1.35). The North Arran Granite has low $^{176}Hf/^{177}Hf$ ratios of 0.28243 – 0.28254 (εHf -10.66 – -6.71).

4.2.5 Pb isotopes

The Pb isotope ratios show positive correlations with each other, but the relationship to other isotope systems and lithology are more complex Figs. 4.48, 4.49, 4.50.

The CAIC mafic dykes display more of a range in Pb isotope ratios than other isotope systems. They have $^{206}Pb/^{204}Pb$ values of 17.869 – 18.622, $^{207}Pb/^{204}$ Pb values of 15.438 – 15.496, and $^{208}Pb/^{204}Pb$ values of 37.639 – 38.635. Their arrangement around the mantle values on most plots suggests contamination by different sources with varying Pb isotope chemistry. The picrite dyke has Pb isotope values within this range, with a $^{206}Pb/^{204}Pb$ value of 18.428, a $^{207}Pb/^{204}Pb$ value of 15.495, and a $^{208}Pb/^{204}Pb$ value of 38.288. The samples from the dolerite sill are so un-radiogenic that they plot as obvious outliers on all diagrams featuring Pb isotopes on one of the axes. They have $^{206}Pb/^{204}Pb$ values of 16.997 – 17.501, $^{207}Pb/^{204}Pb$ values of 15.321 – 15.401, and $^{208}Pb/^{204}Pb$ values of 36.803 – 37.393. This suggests contamination by a distinct low-radiogenic Pb source, such as the Rhinns of Islay.

The gabbros have $^{206}Pb/^{204}Pb$ values of 18.325 – 18.407, $^{207}Pb/^{204}Pb$ values of 15.491 – 15.509, and $^{208}Pb/^{204}Pb$ values of 38.172 – 38.345. These ranges generally overlap with the Pb isotope ratios of the intermediate Glenloig Hybrids, which have $^{206}Pb/^{204}Pb$ values of 18.327 – 18.679, $^{207}Pb/^{204}Pb$ values of 15.492 – 15.516, and $^{208}Pb/^{204}Pb$ values of 38.214 – 38.695. The silicic Glenloig Hybrids also plot within this range, but have generally more radiogenic Pb isotope ratios than the gabbros,

with $^{206}Pb/^{204}Pb$ values of 18.454 – 18.764, $^{207}Pb/^{204}Pb$ values of 15.500 – 15.519, and $^{208}Pb/^{204}Pb$ values of 38.388 – 38.759.

The Glen Craigag Granite has moderately radiogenic Pb isotope ratios, and plots close to the Iceland and DMM fields on Pb-Pb plots, with $^{206}Pb/^{204}Pb$ values of 18.185 – 18.360, $^{207}Pb/^{204}Pb$ values of 15.462 – 15.477, and $^{208}Pb/^{204}Pb$ values of 38.193 – 38.285. The Satellite Granites have the most radiogenic Pb isotope ratios of any of the analysed units, with $^{206}Pb/^{204}Pb$ values of 18.340 – 18.913, $^{207}Pb/^{204}Pb$ values of 15.484 – 15.516, and $^{208}Pb/^{204}Pb$ values of 38.408 – 38.787. This suggests contamination to a different degree, or by a different source, than the Glen Craigag Granite. The North Arran Granite has much less radiogenic Pb isotope ratios than the other granites with $^{206}Pb/^{204}Pb$ values of 17.809 – 17.876, $^{207}Pb/^{204}Pb$ values of 15.439 – 15.451, and $^{208}Pb/^{204}Pb$ values of 37.975 – 38.018.

4.2.6 Summary

In terms of Sr, Nd, and Hf isotopes, the mafic rocks of the CAIC are significantly less contaminated that the intermediate and silicic rocks, *i.e.,* they plot closer to mantle values. The exception to this is the Pb isotope values of the dolerite sill that intrudes the CAIC (and possibly one mafic dyke with similar isotopic compositions). This sill has very unradiogenic Pb isotope values, suggesting contamination by a low radiogenic Pb source. The most fitting candidate seems to be the Rhinns Complex of Islay (see Section 5.4.2).

The Glenloig hybrids have moderately contaminated concentrations of all isotopes, with the granites (and the North Arran Granite in particular) having the least mantle-like isotopic compositions. This general trend suggests increasing crustal contamination with magmatic evolution. Although the Satellite Granites and the Glen Craigag Granites have similar Sr, Nd, and Hf compositions, they have distinctly different Pb isotope values, suggesting different contamination histories. The North Arran Granite has distinctly higher radiogenic Sr and lower radiogenic Nd and Hf that all other units, suggesting significant contamination by source resembling the Dalradian schists (see Section 5.4.2).

There is a remarkable correlation between $^{143}Nd/^{144}Nd$ and $^{176}Hf/^{177}Hf$ isotopes for the samples analysed, suggesting that these two systems behaved in a similar way during evolution and contamination of these magmas.

4.3 U-Pb Zircon Geochronology

Nine samples are selected for U-Pb dating of zircon crystals by isotope-dilution thermal ionization mass spectrometry (ID-TIMS, full account of analytical methods is given in Appendix A). These include three ignimbrite samples (one each from the Allt Ruadh Member, the White Tuff Member, and the Ard Bheinn Member), two samples from the Satellite Granites (one each from the Bridge Farm Granite and the Creag Mhor Granite), one from the Glen Craigag Granite, one from a granitic vein cutting the Glenloig Hybrids, and two from the North Arran Granite (one each from the inner granite and the outer 'coarse' granite).

In this section, the interpreted $^{206}Pb/^{238}U$ ages will be presented, along with $^{207}Pb/^{235}U$ vs. $^{206}Pb/^{238}U$ Concordia plots (Wetherill, 1956) showing the results from each analysed crystal. The full ID-TIMS results are presented in Appendix E6.

Cathodoluminescence (CL) images of representative zircon crystals from each sample are also presented. Brightness and contrast were adjusted for each image individually to improve clarity, so cannot be used to compare trace element concentrations between crystals. Due to the practicalities of removing sub-100 µm zircons from epoxy, these are not the crystals that were analysed for U and Pb isotopes, but give an idea of the characteristics of the zircon populations separated from each sample.

4.3.1 Ignimbrites

Allt Ruadh Member

BJG/15/3 is a sample of a massive lapilli tuff from the Allt Ruadh Member of the Arran Volcanic Formation (Section 3.1.2). CL images of zircon crystals separated from sample BJG/15/3 are shown in Fig. 4.51. This shows that the majority of crystals are cracked, or are broken fragments of larger crystals, as may be expected from zircons which have been involved in highly explosive volcanic eruptions. Many of these zircons show strongly resorbed cores and/or inclusions or pores in the centre of the crystals. Oscillatory zoning is the dominant texture in the outer parts of the crystals, with most showing several resorption surfaces.

Analyses of zircons from BJG/15/3 are shown on the Concordia plot in Fig. 4.52. They yield (^{230}Th corrected) $^{206}Pb/^{238}U$ dates that range between 58.65 and 59.26 Ma (n = 6) with 2σ uncertainties on the order of 0.07 to 0.23 Myr. These dates are statistically distinguishable from one another.

There are two possible interpretations of these data. The two youngest analyses give a weighted mean (^{230}Th corrected) $^{206}Pb/^{238}U$ date of 58.669 $\pm$ 0.052 Ma

(MSWD = 0.13, n = 2) which could be interpreted as representing a single age population and thus a significant interpreted geological (weighted mean) age. However, an alternative interpretation is that the two youngest dates reflect minor Pb-loss and that the next oldest coherent population is significant, and these yield weighted mean (^{230}Th corrected) ^{206}Pb/^{238}U date of 58.92 $\pm$ 0.19 Ma (MSWD = 2.6, n = 4). This older value is taken as the interpreted age on the basis of comparison with the overlying units. The White Tuff Member ignimbrite clearly stratigraphically overlies the Allt Ruadh Member, so choosing the younger age for the BJG/15/3 zircons would not agree with stratigraphic relationships. This date of 58.92 $\pm$ 0.19 Ma provides a constraint on the eruption of the Allt Ruadh Member ignimbrites.

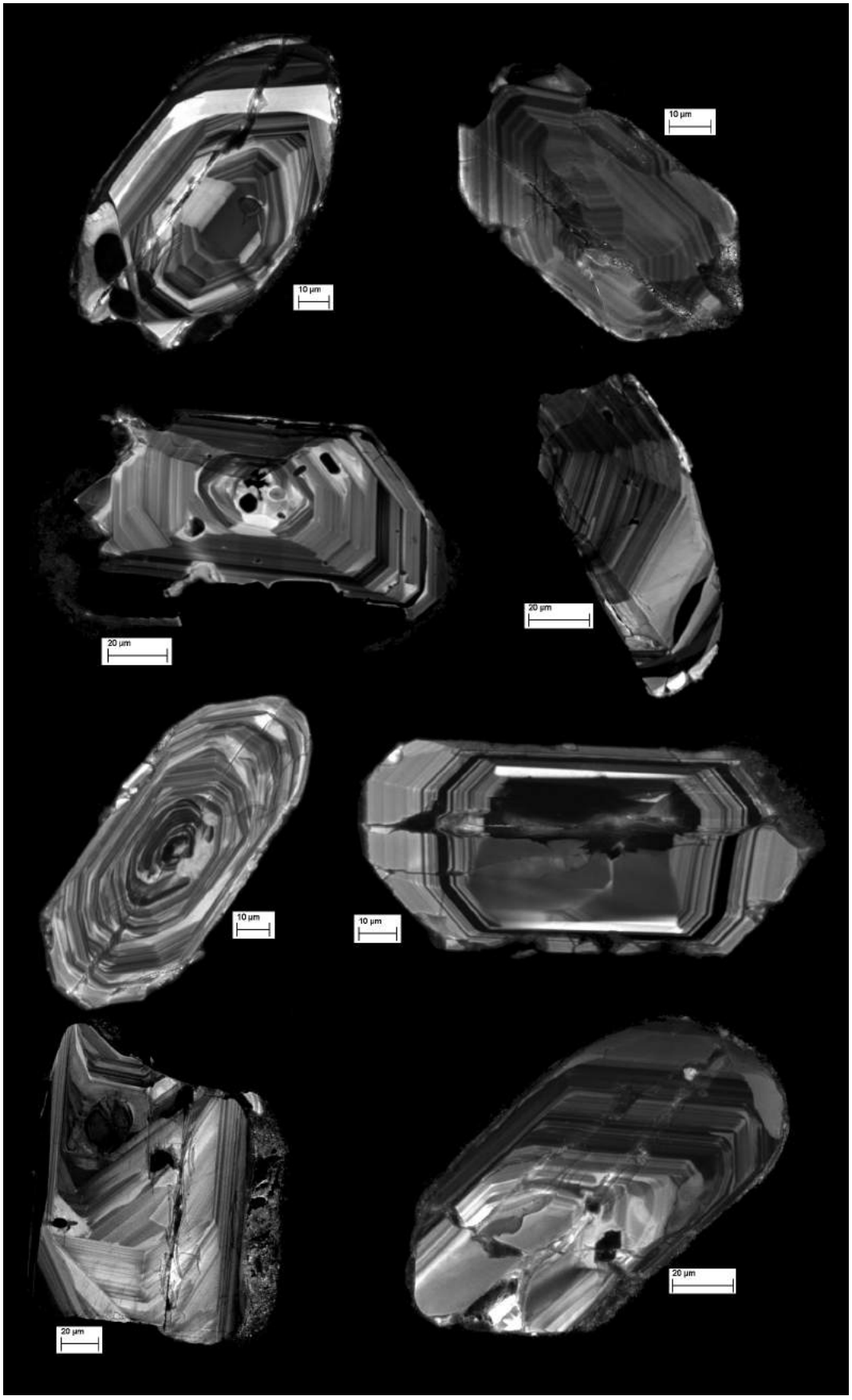

Fig. 4.51 – CL images for selected zircons from sample BJG/15/3, a massive lapilli tuff from the Allt Ruadh Member of the Arran Volcanic Formation.

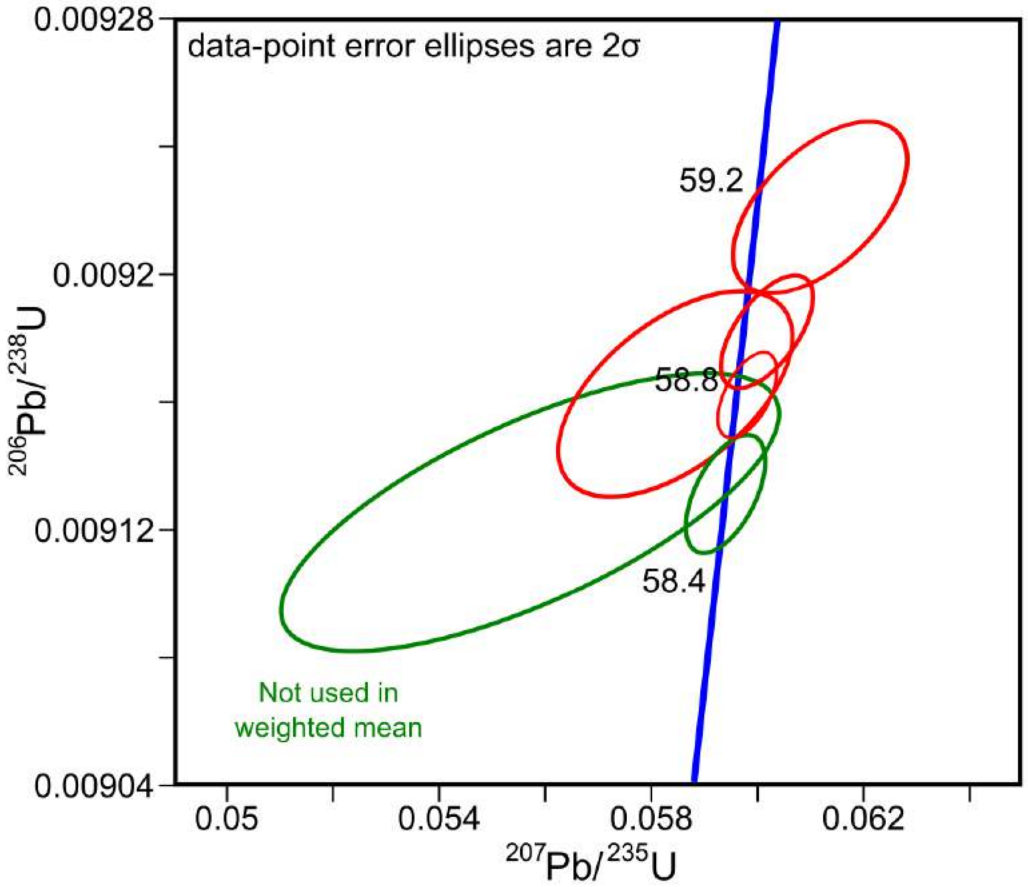

Fig. 4.52 – Concordia plot of the analysed zircons from BJG/15/3.

White Tuff Member

BJG/15/14 is a sample of a rhyolitic lava-like ignimbrite from the White Tuff Member of the Arran Volcanic Formation (Section 3.1.6). CL images of zircon crystals separated from sample BJG/15/14 are shown in Fig. 4.53. Many of the crystals contain anhedral heavily resorbed inherited cores. These are surrounded by homogenous, resorbed, or oscillatory zoned euhedral rims. All crystals show evidence of resorption during crystal growth.

Analyses of zircons from BJG/15/14 are shown on the Concordia plot in Fig. 4.54. They yield concordant (^{230}Th corrected) ^{206}Pb/^{238}U dates that range between 58.81 and 59.86 Ma (n = 4) with 2σ uncertainties on the order of 0.07 Myr, with one discordant ^{206}Pb/^{238}U date of 67.03 Ma with 2σ=0.18 Ma. These dates are statistically distinguishable from one another, and the youngest date of 58.81 $\pm$ 0.06 Ma is interpreted as the best approximation for the (maximum) age of this sample. This date of 58.81 $\pm$ 0.06 Ma therefore provides a constraint on the eruption of the White Tuff Member lava-like ignimbrites.

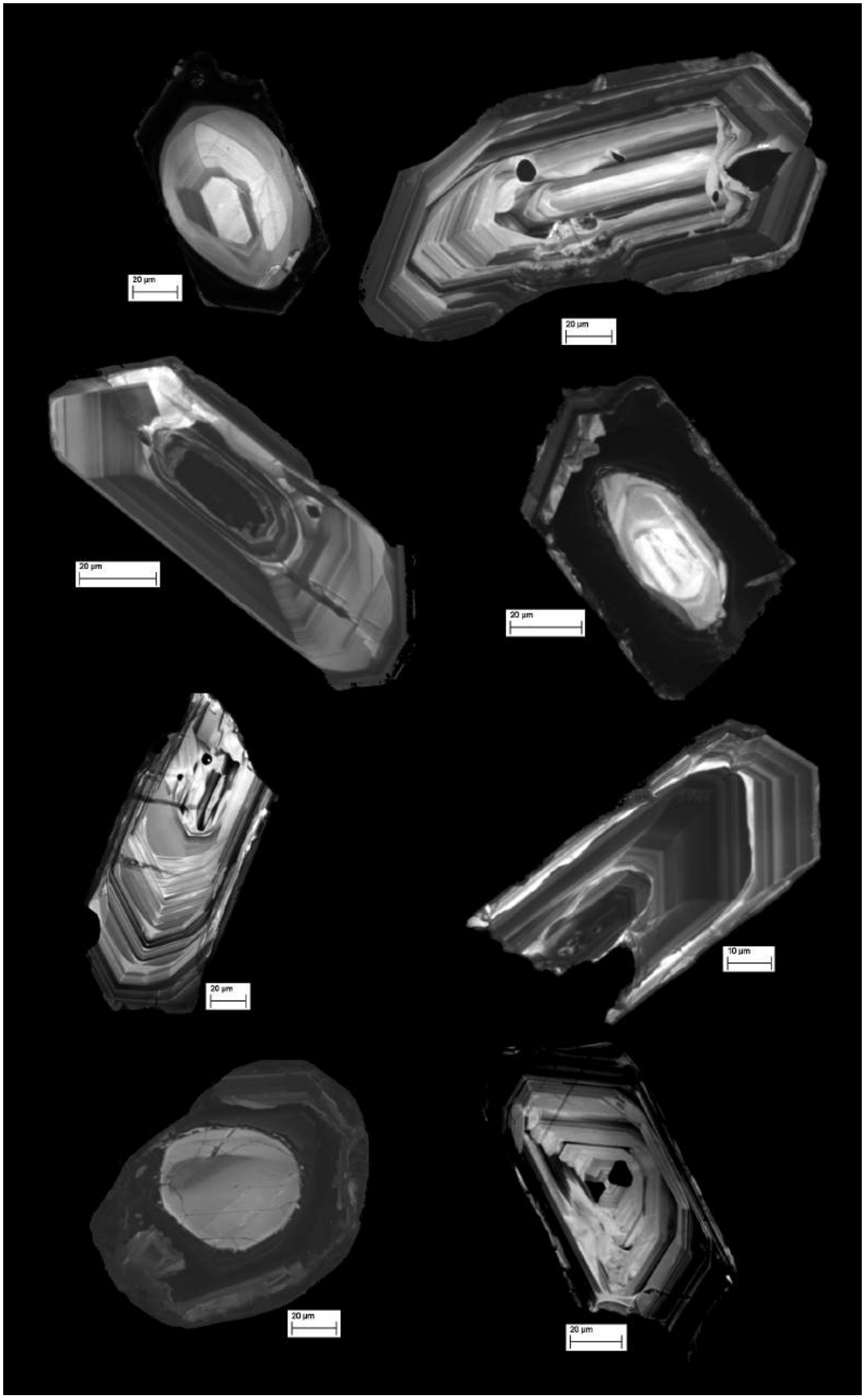

Fig. 4.53 – CL images for selected zircons from sample BJG/15/14, a rhyolitic lava-like ignimbrite from the White Tuff Member of the Arran Volcanic Formation.

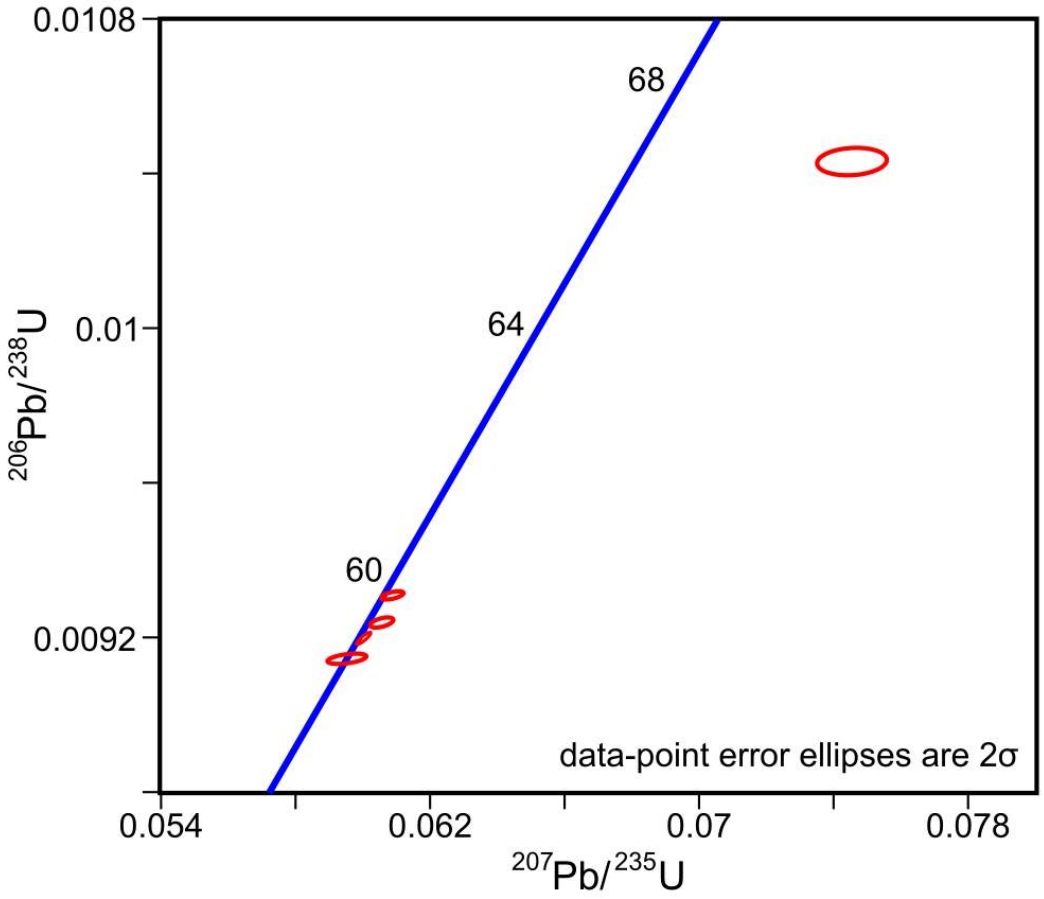

Fig. 4.54 – Concordia plot of the analysed zircons from BJG/15/14.

Ard Bheinn Member

BJG/15/142 is a sample of a vitrophyric lapilli tuff from the Ard Bheinn Member of the Arran Volcanic Formation (Section 3.1.9). CL images of zircon crystals separated from sample BJG/15/142 are shown in Fig. 4.55. The zircons in this unit are have highly variable shapes and internal morphologies. Homogenous and resorbed cores are common, with low-contrast oscillatory zoning around the rims of most crystals. Many crystals are cracked, again consistent with experiencing explosive volcanic eruptions.

Analyses of zircons from BJG/15/142 are shown on the Concordia plot in Fig. 4.56. They yield concordant (^{230}Th corrected) ^{206}Pb/^{238}U dates that range between 58.76 and 59.34 Ma (n = 5) with 2σ uncertainties on the order of 0.07 to 0.12 Myr. These dates, excluding the oldest one, which is interpreted represent an older xenocrystic component, are statistically indistinguishable from one another.

These four youngest analyses give a weighted mean (^{230}Th corrected) ^{206}Pb/^{238}U date of 58.791 $\pm$ 0.037 Ma (MSWD = 0.51, n = 4), are interpreted as representing a single age population and thus a significant interpreted geological (weighted mean) age. This date of 58.79 $\pm$ 0.037 Ma therefore provides a constraint on the eruption of the Ard Bheinn Member. This is consistent with stratigraphy, as the Ard Bheinn Member clearly overlies the White Tuff Member.

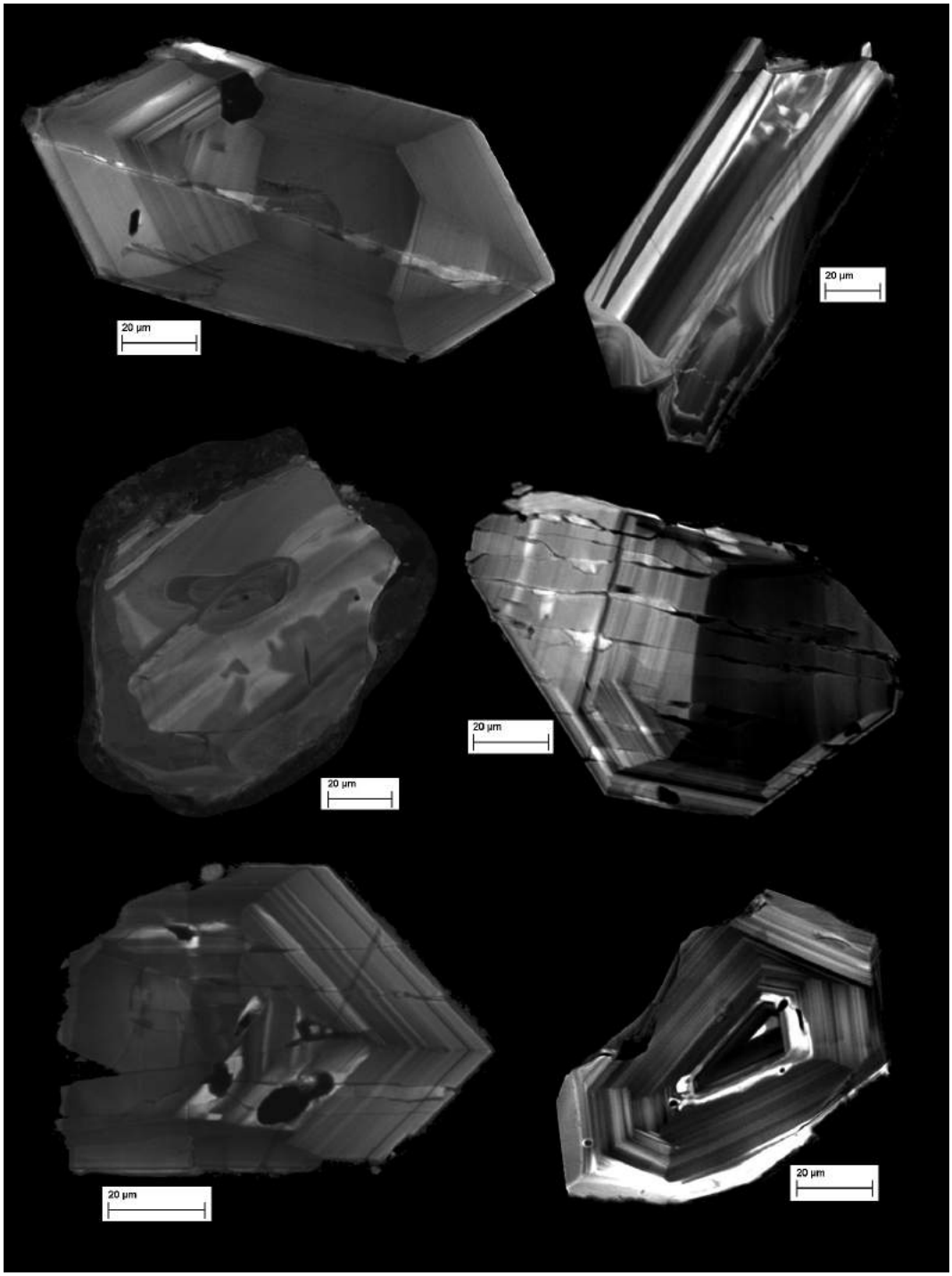

Fig. 4.55 – CL images for selected zircons from sample BJG/15/142, a vitrophyric lapilli tuff from the Ard Bheinn Member of the Arran Volcanic Formation.

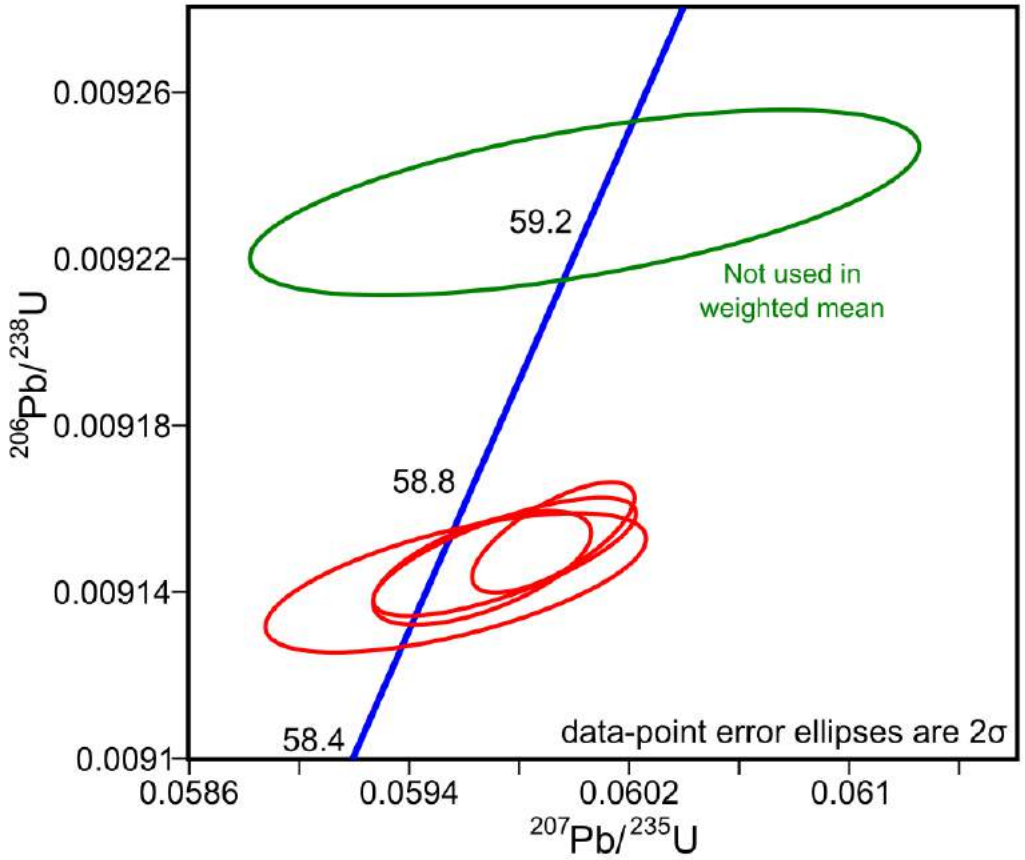

Fig. 4.56 – Concordia plot of the analysed zircons from BJG/15/142.

4.3.2 CAIC Intrusions

Bridge Farm Granite

BJG/16/26 is a sample of the Bridge Farm Granite, one of the Satellite Granites (Section 2.4). CL images of zircon crystals separated from sample BJG/16/26 are shown in Fig. 4.57. All zircons are euhedral with well-developed oscillatory zoning and without inherited resorbed cores, although some show resorption surfaces in the outer parts of the crystals. They are all proposed to have formed from crystallisation in the Bridge Farm Granite magma.

Analyses of zircons from BJG/16/26 are shown on the Concordia plot in Fig. 4.58. They yield (^{230}Th corrected) ^{206}Pb/^{238}U dates that range between 58.68 and 58.96 Ma (n = 5) with 2σ uncertainties on the order of 0.05 to 0.11 Myr. These dates, excluding the oldest which is interpreted represent an older xenocrystic component, are statistically indistinguishable from one another.

These dates yield a weighted mean (^{230}Th corrected) ^{206}Pb/^{238}U date of 58.78 $\pm$ 0.11 Ma (MSWD = 2.6, n = 4). These zircons have been taken to represent a single age population, suggesting that this weighted mean age of 58.78 $\pm$ 0.11 Ma reflects the sample age and therefore provides a constraint on intrusion of the Bridge Farm Granite.

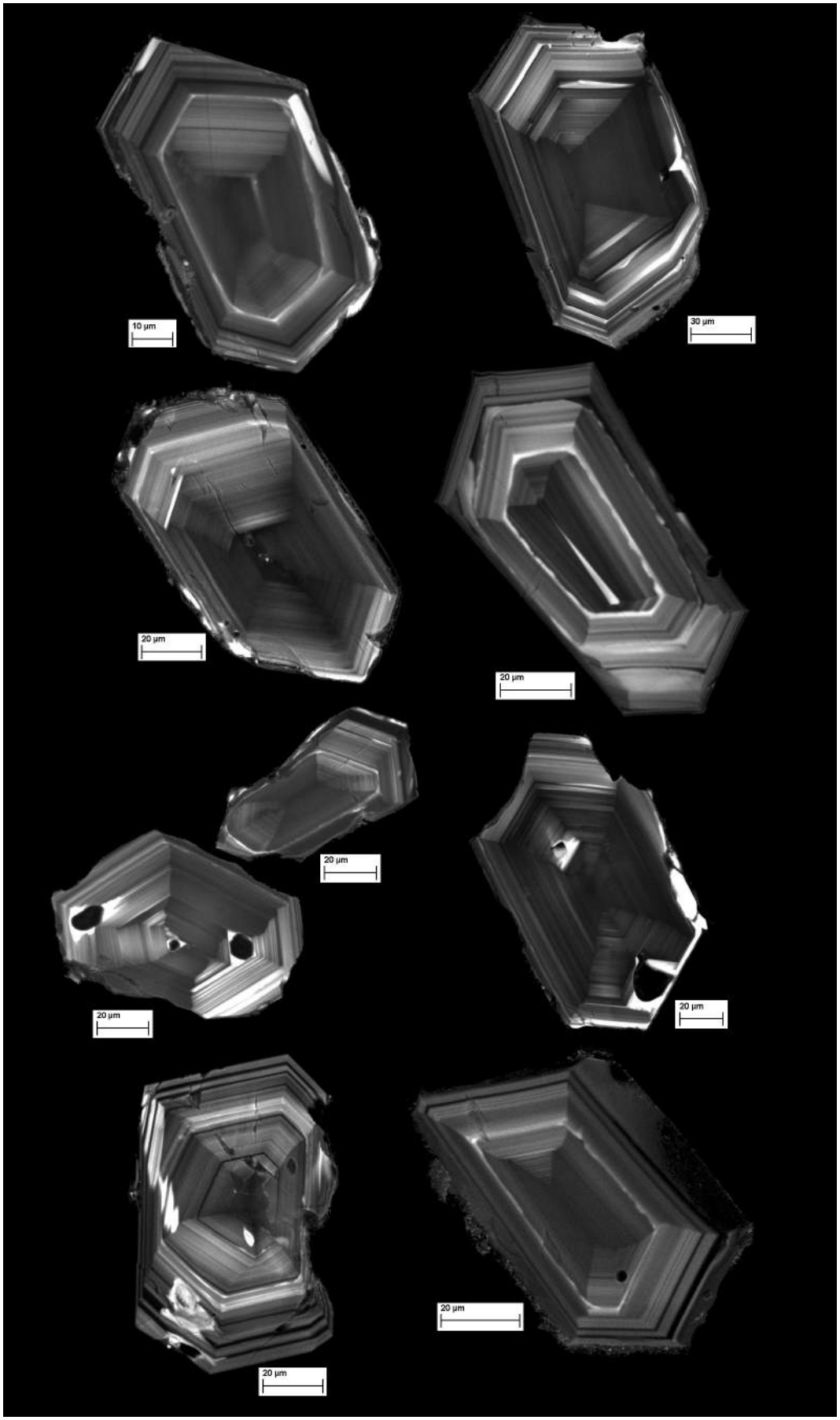

Fig. 4.57 – CL images for selected zircons from sample BJG/16/26 from the Bridge Farm Granite, one of the Satellite Granites.

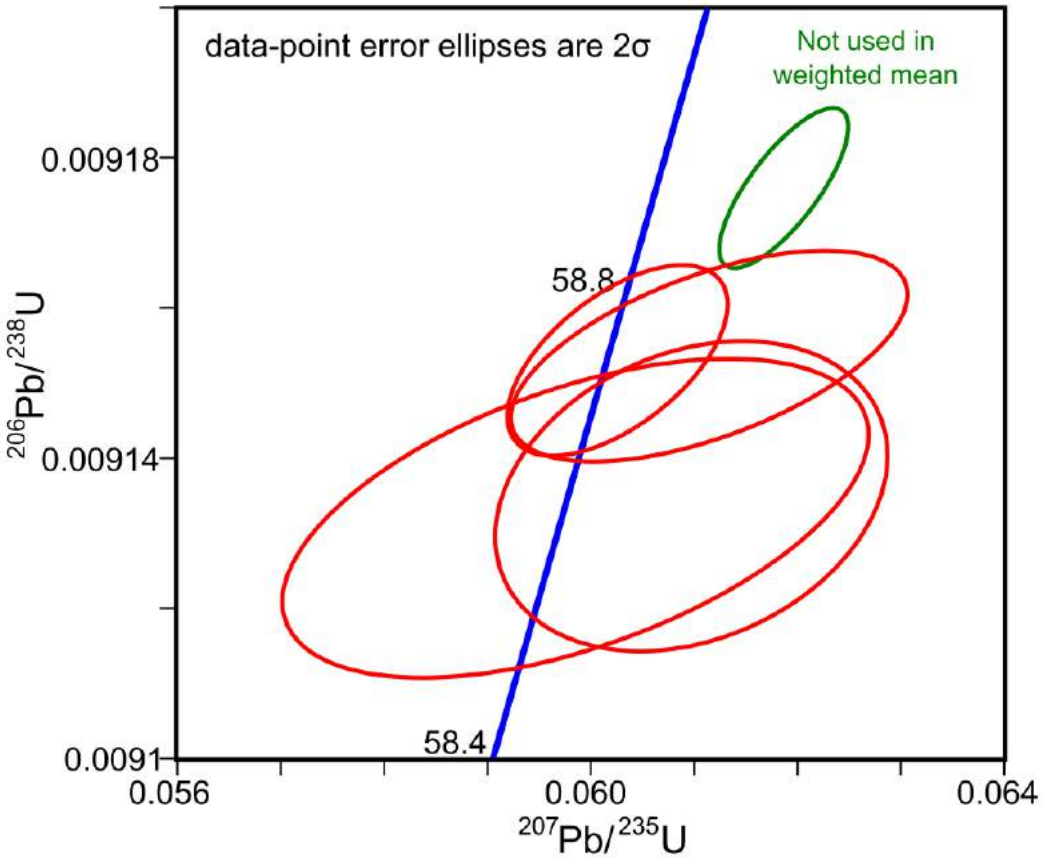

Fig. 4.58 – Concordia plot of the analysed zircons from BJG/16/26.

Creag Mhor Granite

BJG/15/347 is a sample of the Bridge Farm Granite, one of the Satellite Granites (Section 2.4). CL images of zircon crystals separated from sample BJG/15/347 are shown in Fig. 4.59. The zircons are all euhedral (stubby to elongate) with oscillatory zoning in the outer parts of the crystals. Some have resorbed cores which also display oscillatory zoning. Those that do not, have homogenous dark (in the CL images) centres. Many have small inclusions/pores.

Analyses of zircons from BJG/15/347 are shown on the Concordia plot in Fig. 4.60. They yield concordant (^{230}Th corrected) ^{206}Pb/^{238}U dates that range between 58.69 and 58.78 Ma (n = 4) with 2σ uncertainties on the order of 0.05 Myr, and are statistically indistinguishable from one another.

These zircons are interpreted as representing a single age population and yield a weighted mean (^{230}Th corrected) ^{206}Pb/^{238}U date of 58.740 $\pm$ 0.058 Ma (MSWD = 1.8, n = 4), suggesting that this weighted mean age reflects the sample age. This date of 58.74 $\pm$ 0.06 Ma therefore provides a constraint on intrusion of the Creag Mhor Granite.

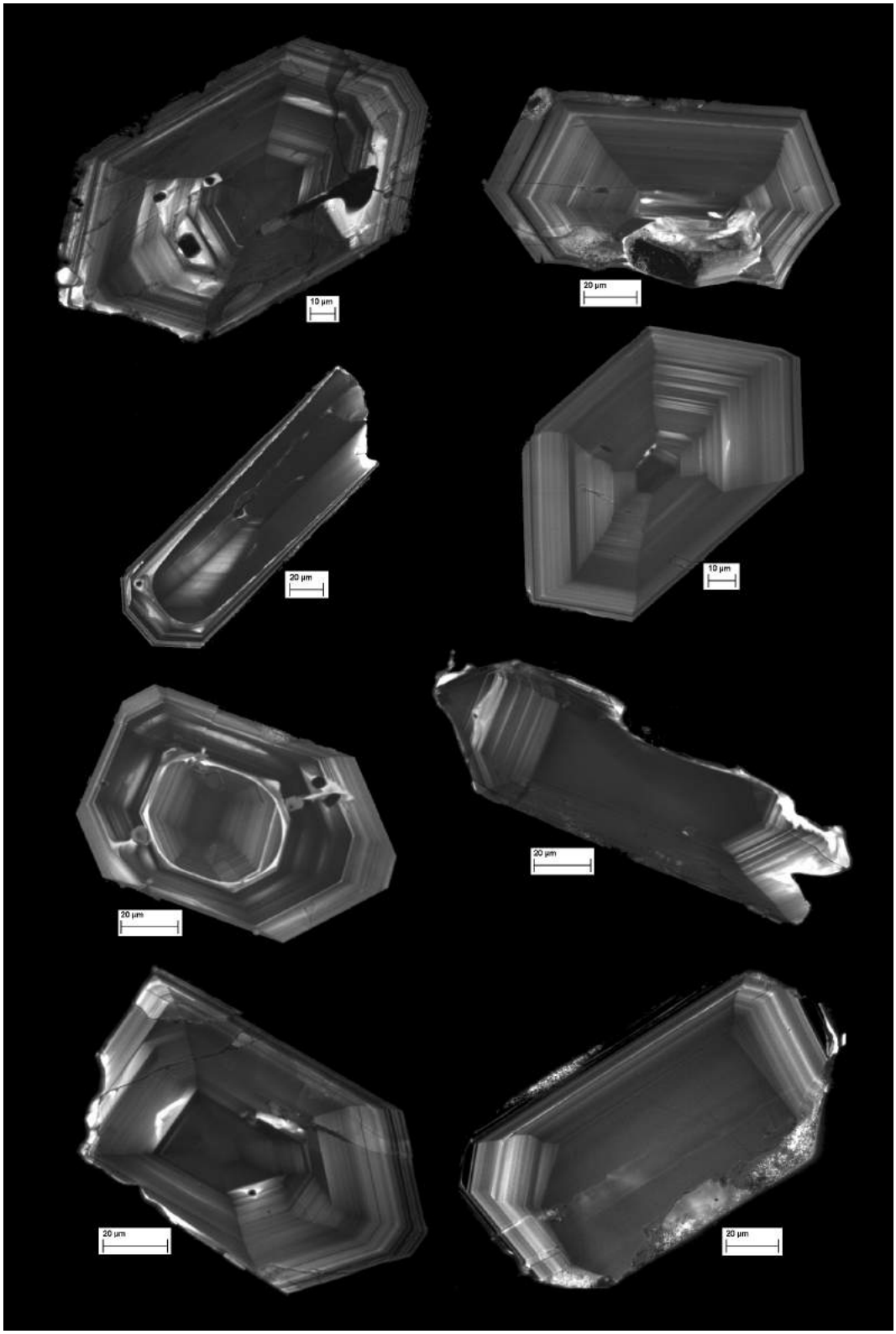

Fig. 4.59 – CL images for selected zircons from sample BJG/15/347 from the Creag Mhor Granite, one of the Satellite Granites.

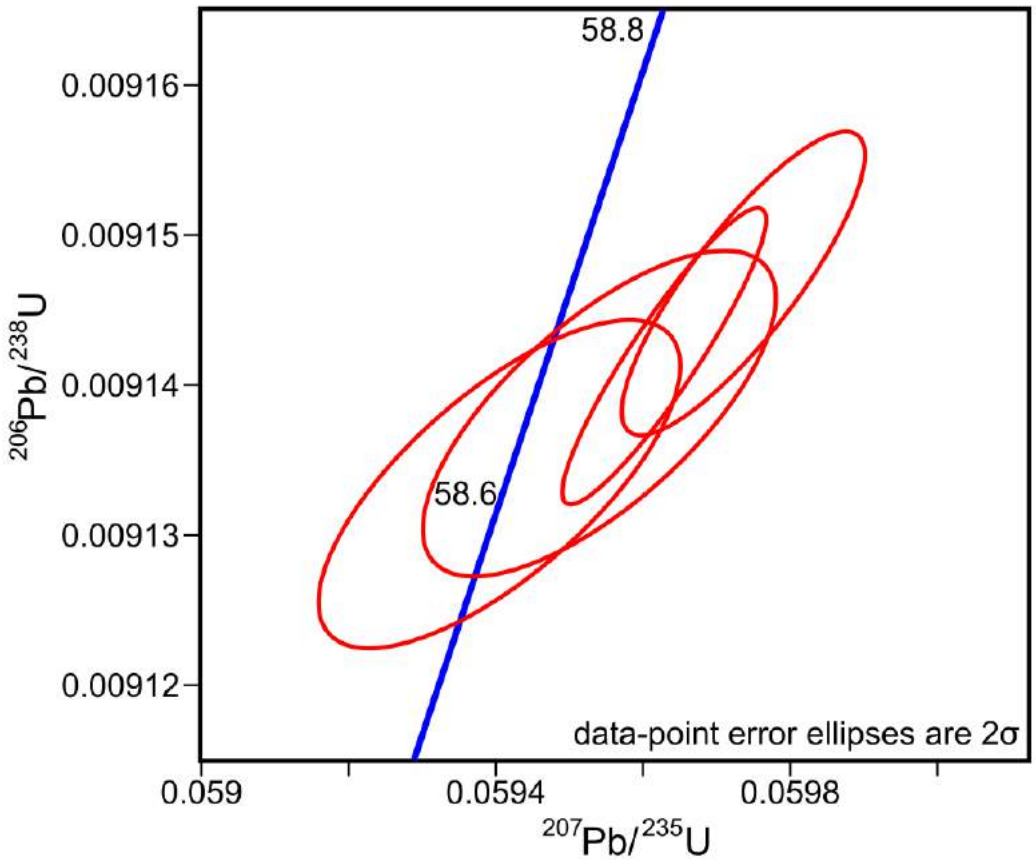

Fig. 4.60 – Concordia plot of the analysed zircons from BJG/15/347.

Glen Craigag Granite

BJG/16/44 is a sample of a the Glen Craigag Granite (Section 2.3). CL images of zircon crystals separated from sample BJG/16/44 are shown in Fig. 4.61. The zircons are all euhedral, but many have cracks and inclusions/pores. There is a lack of inherited or resorbed cores, but most have homogenous dark (in CL) centres. Oscillatory and sector zoning are common throughout the crystals.

Analyses of zircons from BJG/16/44 are shown on the Concordia plot in Fig. 4.62. They yield (^{230}Th corrected) ^{206}Pb/^{238}U dates that range between 58.69 and 60.15 Ma (n = 8) with 2σ uncertainties on the order of 0.06 to 0.2 Myr. These dates, excluding the oldest two which are interpreted represent an older xenocrystic component, are statistically indistinguishable from one another.

These zircons are interpreted as representing a single age population and yield a weighted mean (^{230}Th corrected) ^{206}Pb/^{238}U date of 58.740 $\pm$ 0.059 Ma (MSWD = 1.7, n = 6). This can be taken to represent the intrusion age of the Glen Craigag Granite.

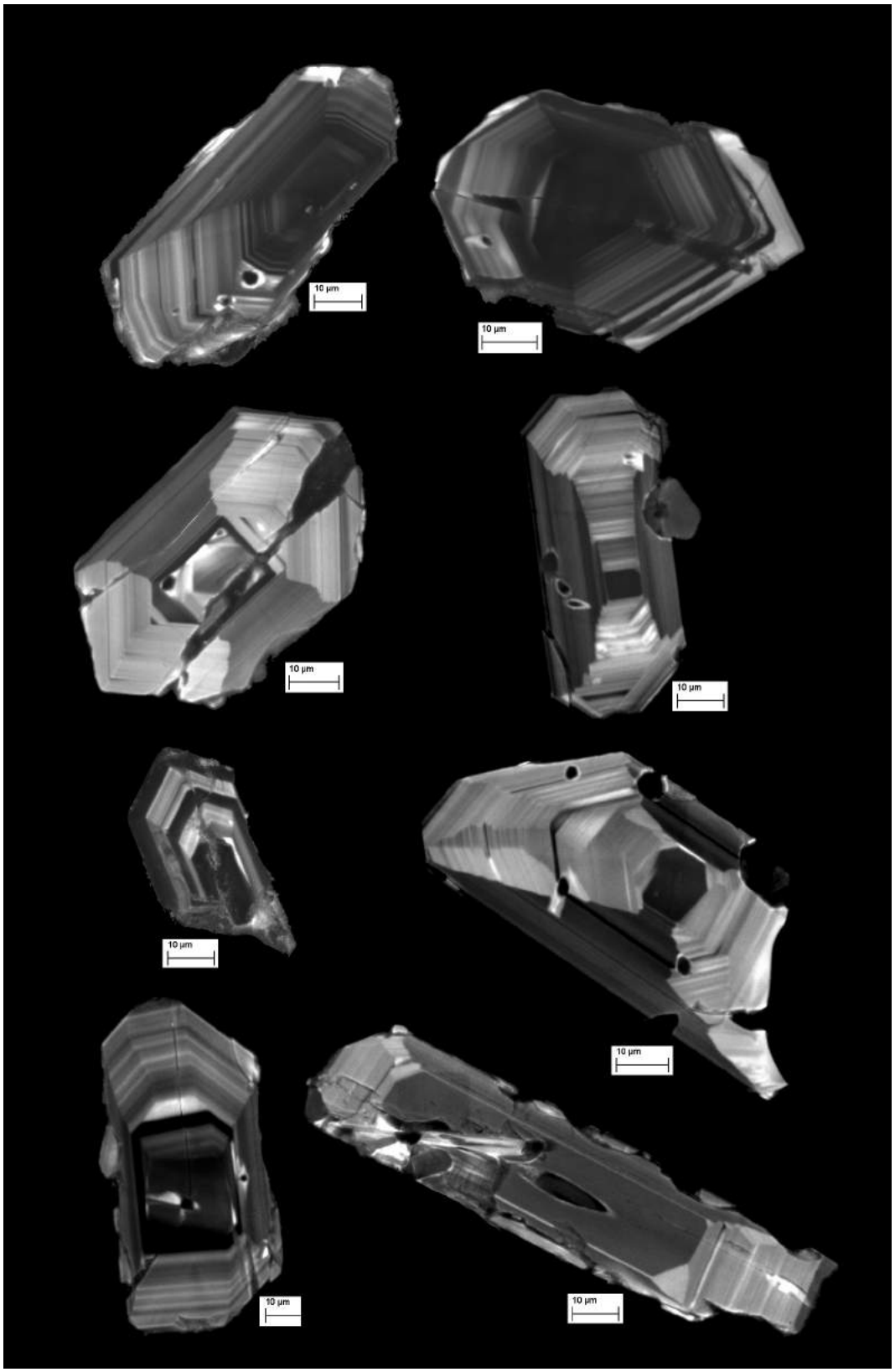

Fig. 4.61 – CL images for selected zircons from sample BJG/16/44 from the Glen Craigag Granite.

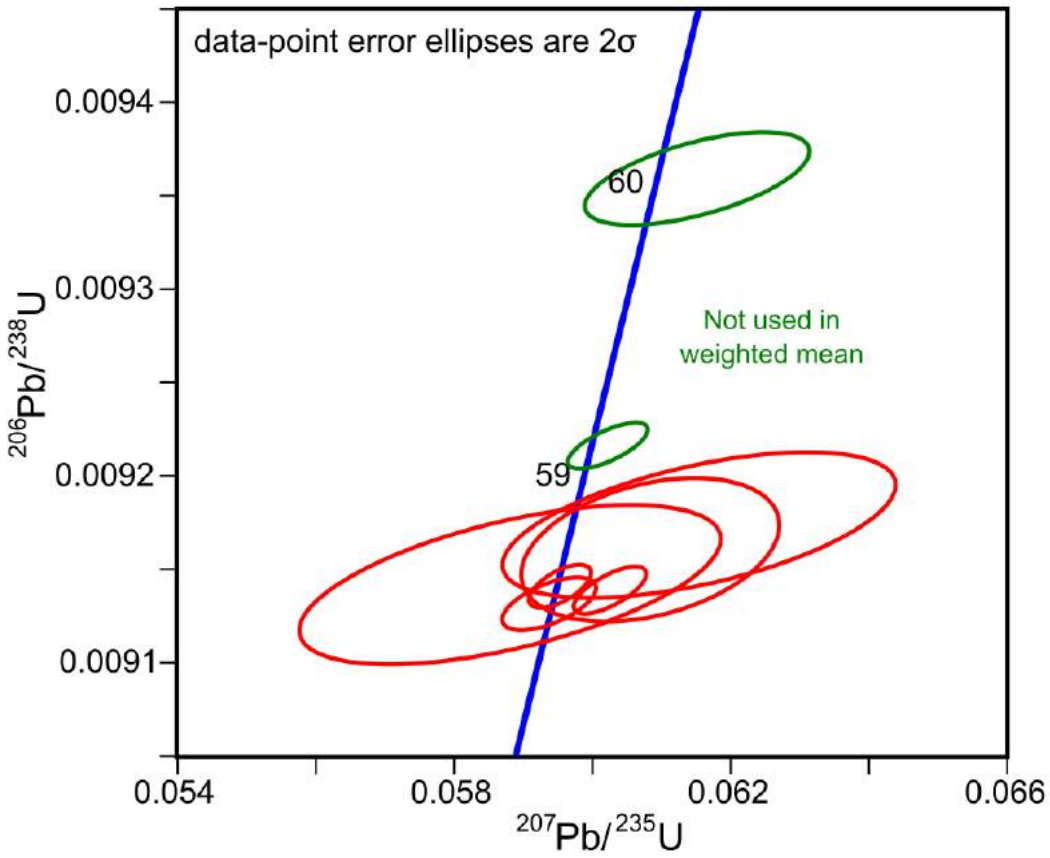

Fig. 4.62 – Concordia plot of the analysed zircons from BJG/16/44.

Glenloig Hybrids

BJG/15/345 is a sample of a granitic vein that intrudes the Glenloig Hybrids (Section 2.1). CL images of zircon crystals separated from sample BJG/15/345 are shown in Fig. 4.63. The zircons are all euhedral, and largely free from cracks and inclusions. They all have relatively dark (on CL images) centres, with outer parts dominated by oscillatory zoning. Most show some evidence for resorption surfaces.

Analyses of zircons from BJG/15/345 are shown on the Concordia plot in Fig. 4.64. They yield (^{230}Th corrected) ^{206}Pb/^{238}U dates that range between 58.63 and 58.76 Ma (n = 5) with 2σ uncertainties on the order of 0.05 to 0.08 Myr, and are statistically distinguishable from one another.

The dates yield a weighted mean (^{230}Th corrected) ^{206}Pb/^{238}U date of 58.709 $\pm$ 0.069 Ma (MSWD = 1.8, n = 5). These zircons are interpreted as representing a single age population, suggesting that this interpreted geological (weighted mean) age reflects the sample age. This date of 58.71 $\pm$ 0.07 Ma therefore provides a constraint on intrusion of the Granite veins in the Glenloig Hybrids, and therefore the Glenloig Hybrids themselves.

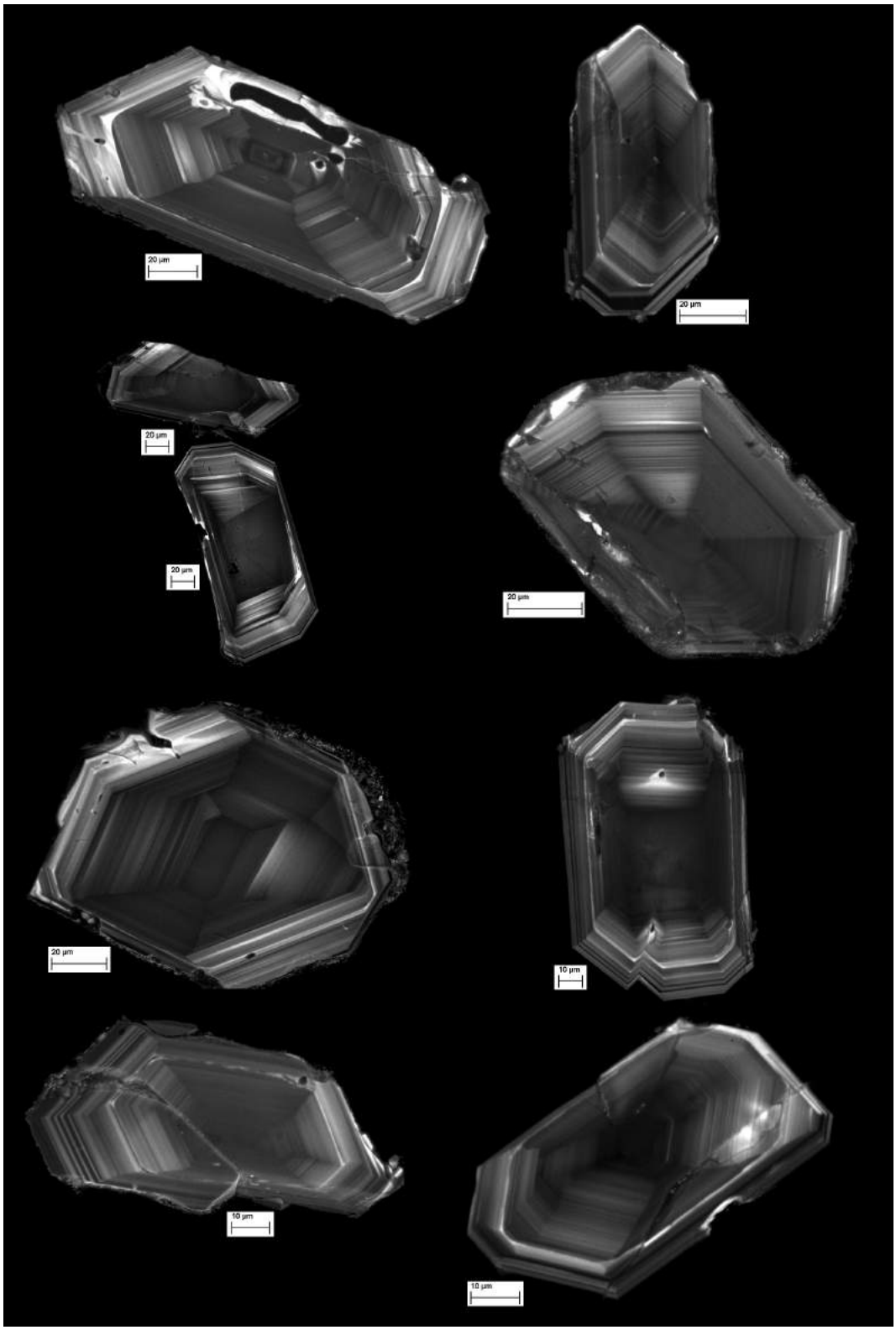

Fig. 4.63 – CL images for selected zircons from sample BJG/15/345 from a granitic vein intruding the Glenloig Hybrids.

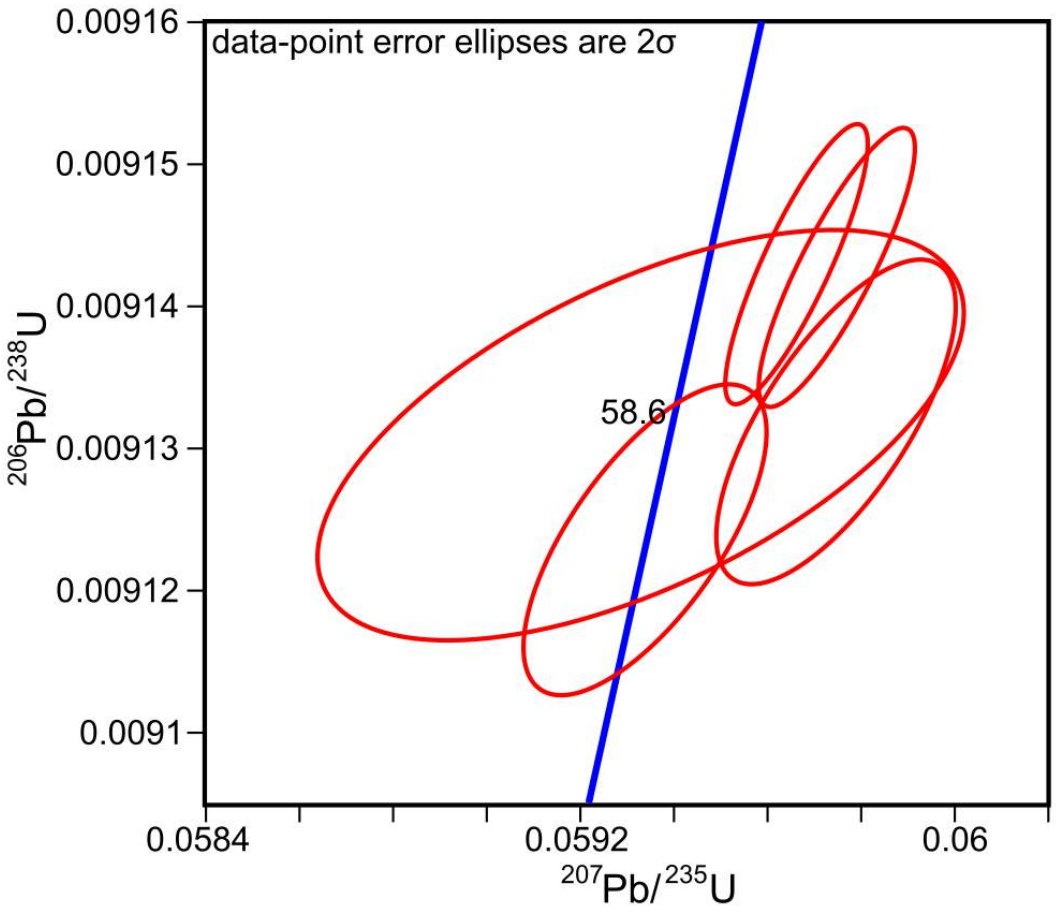

Fig. 4.64 – Concordia plot of the analysed zircons from BJG/15/345.

4.3.3 North Arran Granite

Inner Granite

BJG/15/178 is a sample of the North Arran Granite (Section 2.7), from the finer inner part of the intrusion. CL images of zircon crystals separated from sample BJG/15/178 are shown in Fig. 4.65. The zircons are largely euhedral, or fragments of larger euhedral crystals. Most have homogenous or highly resorbed cores, with oscillatory zoning and resorption surfaces common in the outer parts of the crystals.

Analyses of zircons from BJG/15/178 are shown on the Concordia plot in Fig. 4.66. They yield (^{230}Th corrected) ^{206}Pb/^{238}U dates that range between 58.92 and 59.27 Ma (n = 6) with 2σ uncertainties on the order of 0.06 Myr. These dates, excluding the oldest one which is interpreted as an older xenocrystic component, are statistically indistinguishable from one another.

These zircons represent a single age population and yield a weighted mean (^{230}Th corrected) ^{206}Pb/^{238}U date of 58.978 $\pm$ 0.064 Ma (MSWD = 3.4, n = 5), that is interpreted as the sample age. This date of 58.98 $\pm$ 0.06 Ma therefore provides a constraint on intrusion of the inner part of the North Arran Granite.

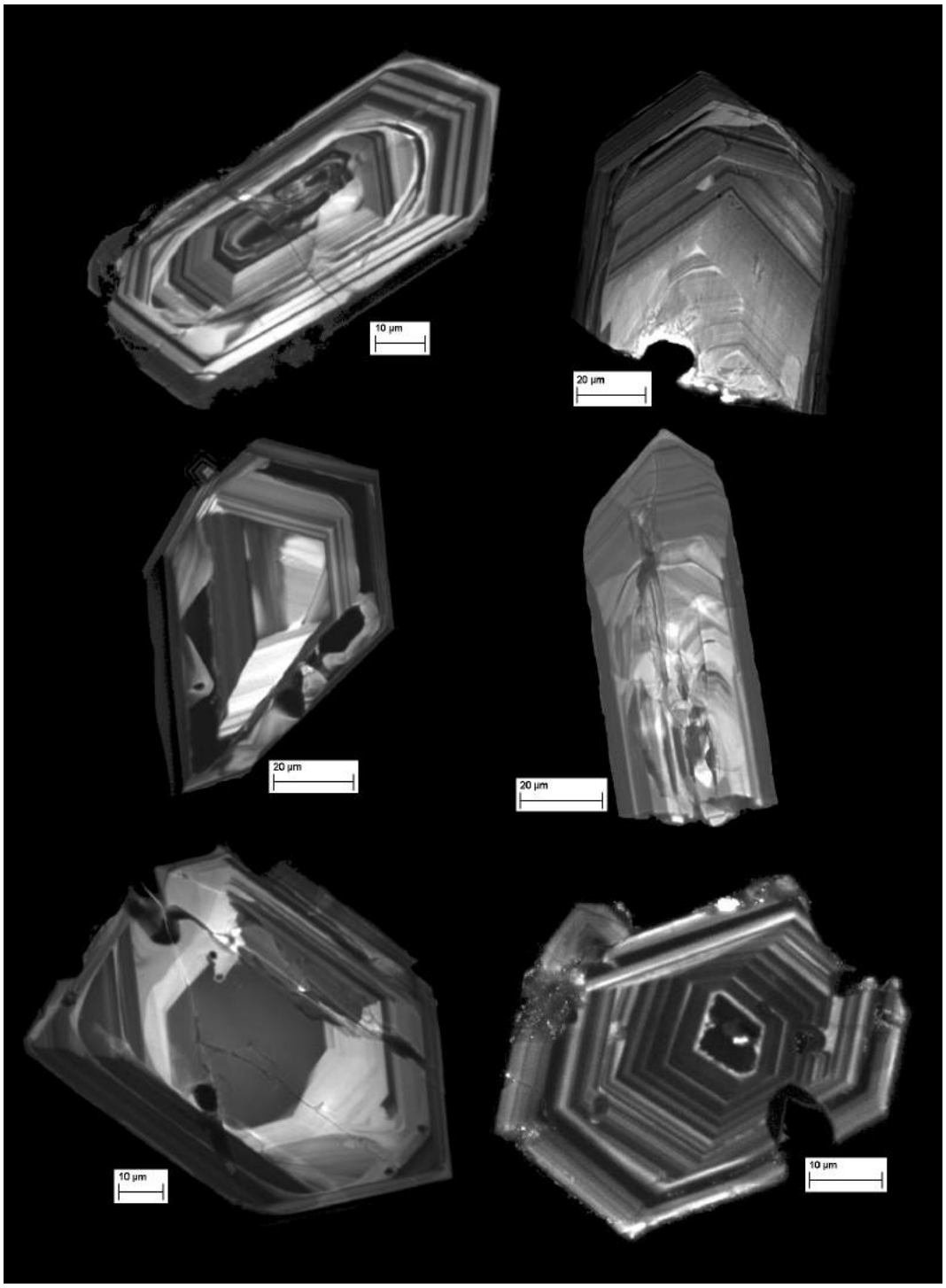

Fig. 4.65 – CL images for selected zircons from sample BJG/15/178 from the inner unit of the North Arran Granite.

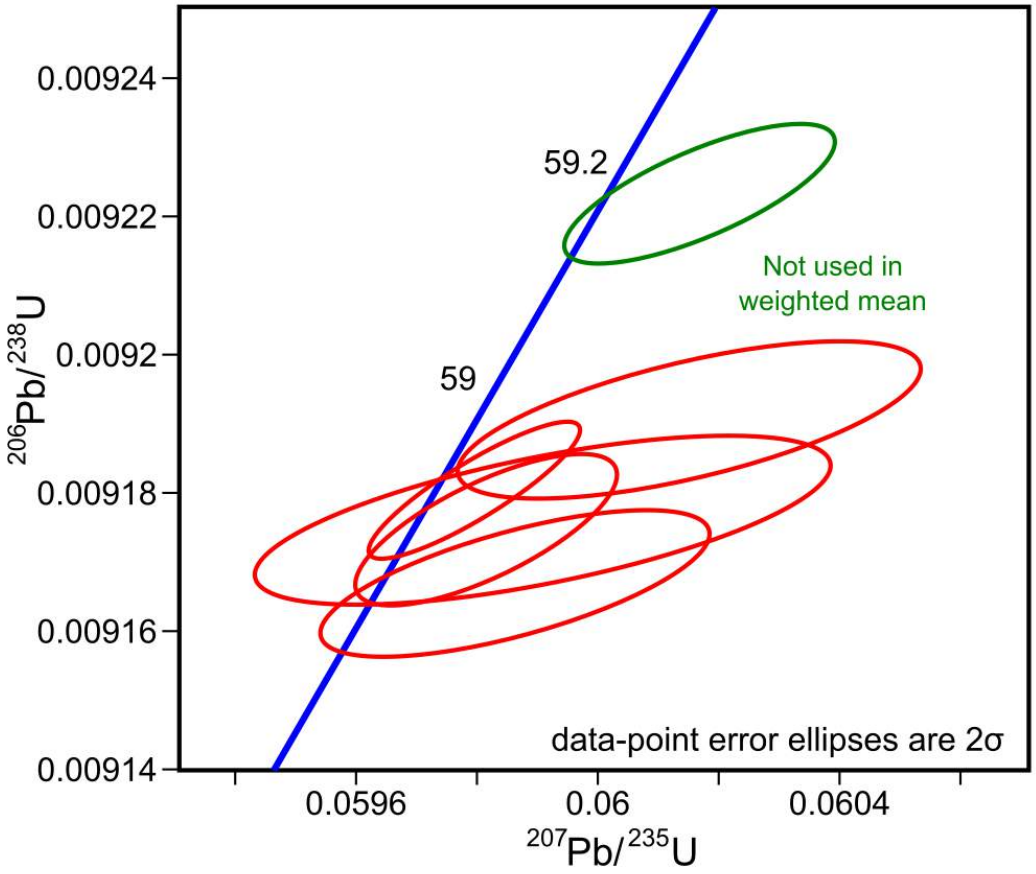

Fig. 4.66 – Concordia plot of the analysed zircons from BJG/15/178.

Coarse Outer Granite

BJG/15/179 is a sample of the North Arran Granite (Section 2.7), from the coarse outer part of the intrusion. CL images of zircon crystals separated from sample BJG/15/179 are shown in Fig. 4.67. The zircons are euhedral and elongate, and significantly larger than those from the other units discussed in this section. Most have highly resorbed cores with a large number of inclusions/pores. All display oscillatory zoning and resorption surfaces, with some showing resorption textures in the rims.

Analyses of zircons from BJG/15/179 are shown on the Concordia plot in Fig. 4.68. They yield (^{230}Th corrected) ^{206}Pb/^{238}U dates that range between 58.82 and 59.33 Ma (n = 5) with 2σ uncertainties on the order of 0.06 to 0.20 Myr. These dates, excluding the oldest one which is interpreted as an older xenocrystic component, are statistically indistinguishable from one another.

These dates yield a weighted mean (^{230}Th corrected) ^{206}Pb/^{238}U date of 58.86 $\pm$ 0.07 Ma (MSWD = 1.7, n = 4). We interpret that these zircon represent a single age population and that this interpreted geological (weighted mean) age reflects the sample age. This date of 58.86 $\pm$ 0.07 Ma therefore provides a constraint on intrusion of the outer part of the North Arran Granite.

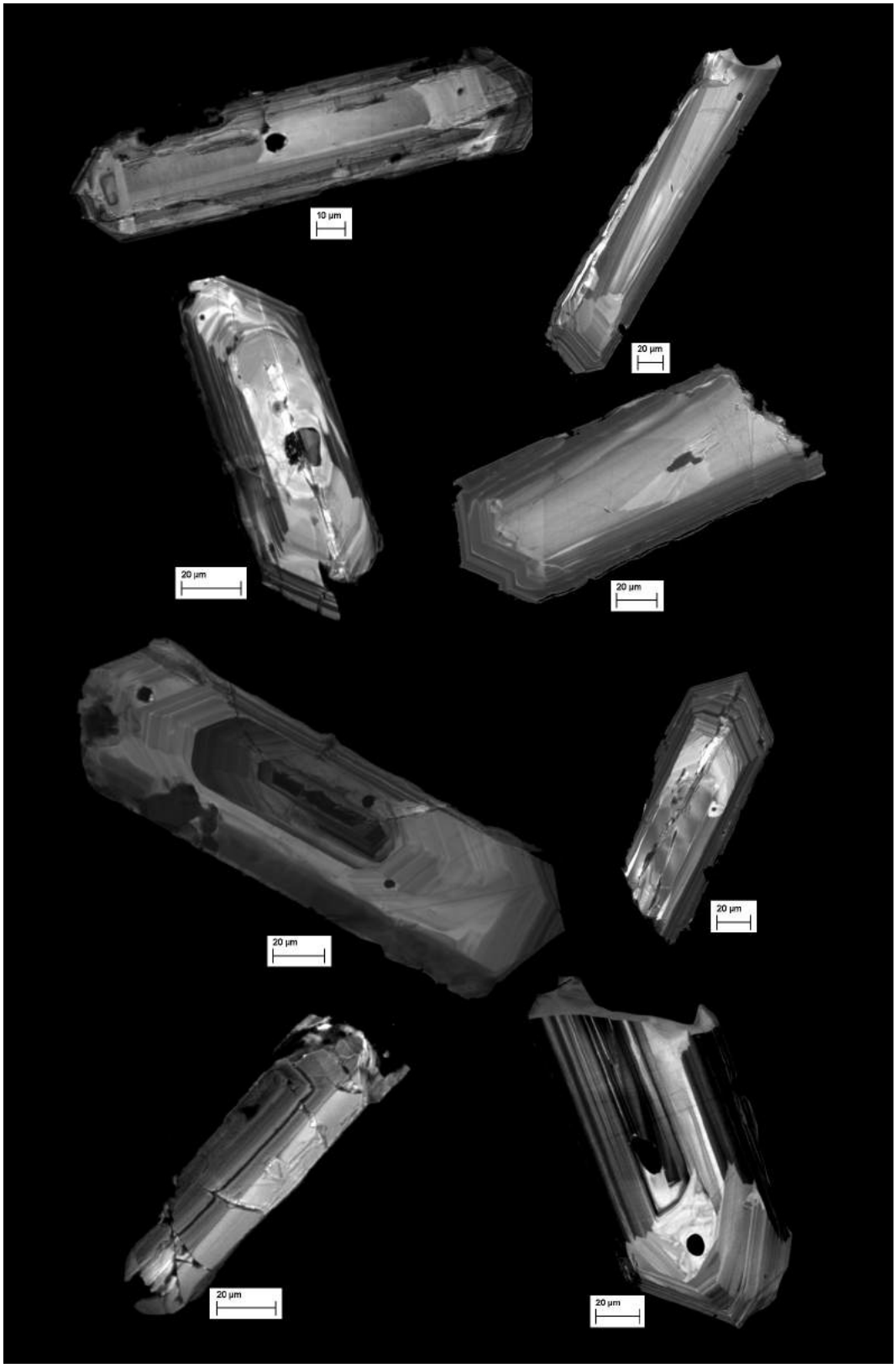

Fig. 4.67 – CL images for selected zircons from sample BJG/15/179 from the outer 'coarse' unit of the North Arran Granite.

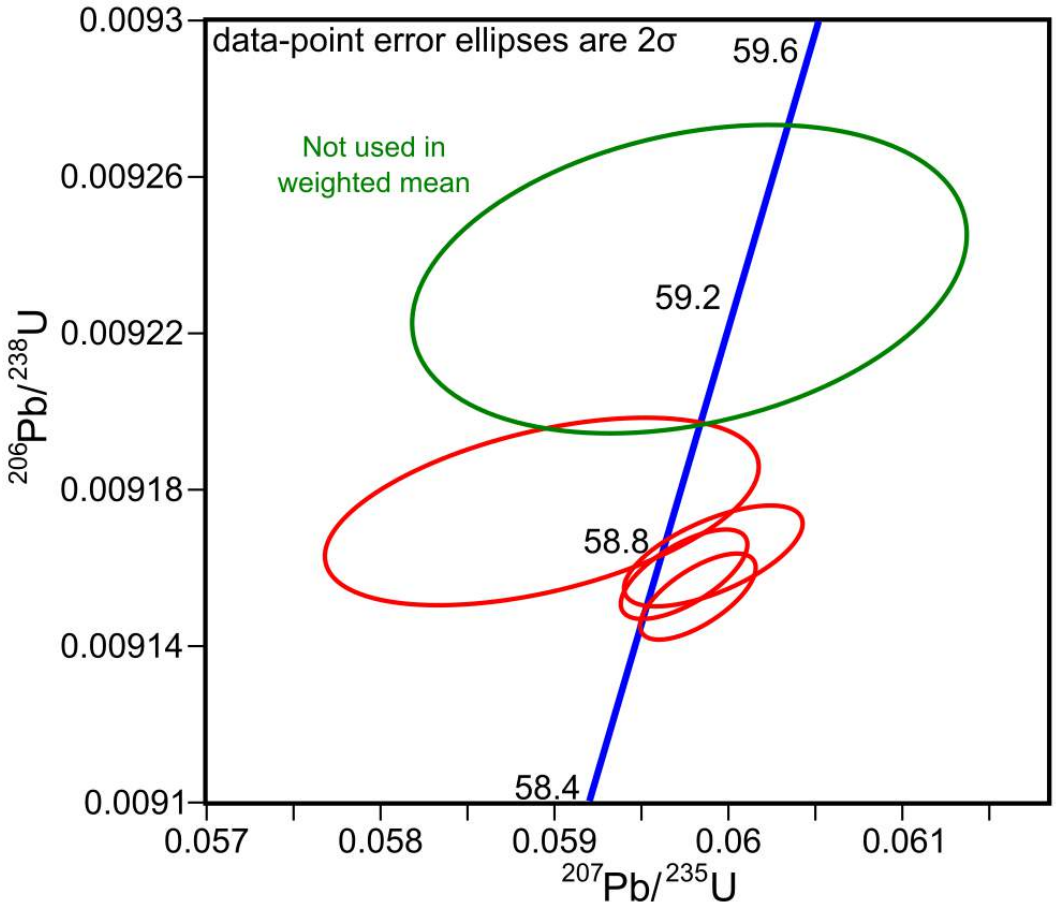

Fig. 4.68 – Concordia plot of the analysed zircons from BJG/15/179.

4.3.4 Summary

Interpreted $^{206}Pb/^{238}U$ ages for each sample are summarised in Table 4.3, and shown to $\pm 2\sigma$ in Fig. 4.69. The most important conclusion is that all of these dates are very similar, with all silicic magmatism at the CAIC and the North Arran Granite taking place within a window of 470 kyr. This is very rapid for a system involving several phases of granitic intrusion as well as a protracted history of silicic volcanism.

The oldest unit is the North Arran Granite, although its interpreted ages overlap with the ignimbrites of the Arran Volcanic Formation. The Satellite Granites and Glen Craigag Granite have interpreted emplacement ages that are indistinguishable from each other, with the granitic vein in the Glenloig Hybrids being the youngest analysed unit. This however does not give an age for the intermediate rocks of the Glenloig Hybrids, which field relations suggest are older than the ignimbrites of the AVF.

The conclusion that the Glen Craigag Granite is younger than the ignimbrites of the AVF is at odds with the interpretation gleaned from field relationships, although these are very poorly exposed and not conclusive.

Table 4.3 – Interpreted $^{206}Pb/^{238}U$ ages for certain units of the Central Arran Igneous Complex, as well as the North Arran Granite.

Sample	Unit	Interpreted $^{206}Pb/^{238}U$ age (Ma)	$\pm 2\sigma$
BJG/15/3	Allt Ruadh ignimbrite	58.92	0.19
BJG/15/14	White Tuff ignimbrite	58.81	0.06
BJG/15/142	Ard Bheinn ignimbrite	58.79	0.04
BJG/15/178	North Arran Granite (inner)	58.98	0.06
BJG/15/179	North Arran Granite (outer)	58.86	0.07
BJG/15/345	Granitic vein in Glenloig Hybrids	58.71	0.07
BJG/15/347	Creag Mhor Granite	58.74	0.06
BJG/16/26	Bridge Farm Granite	58.78	0.11
BJG/16/44	Glen Craigag Granite	58.74	0.06

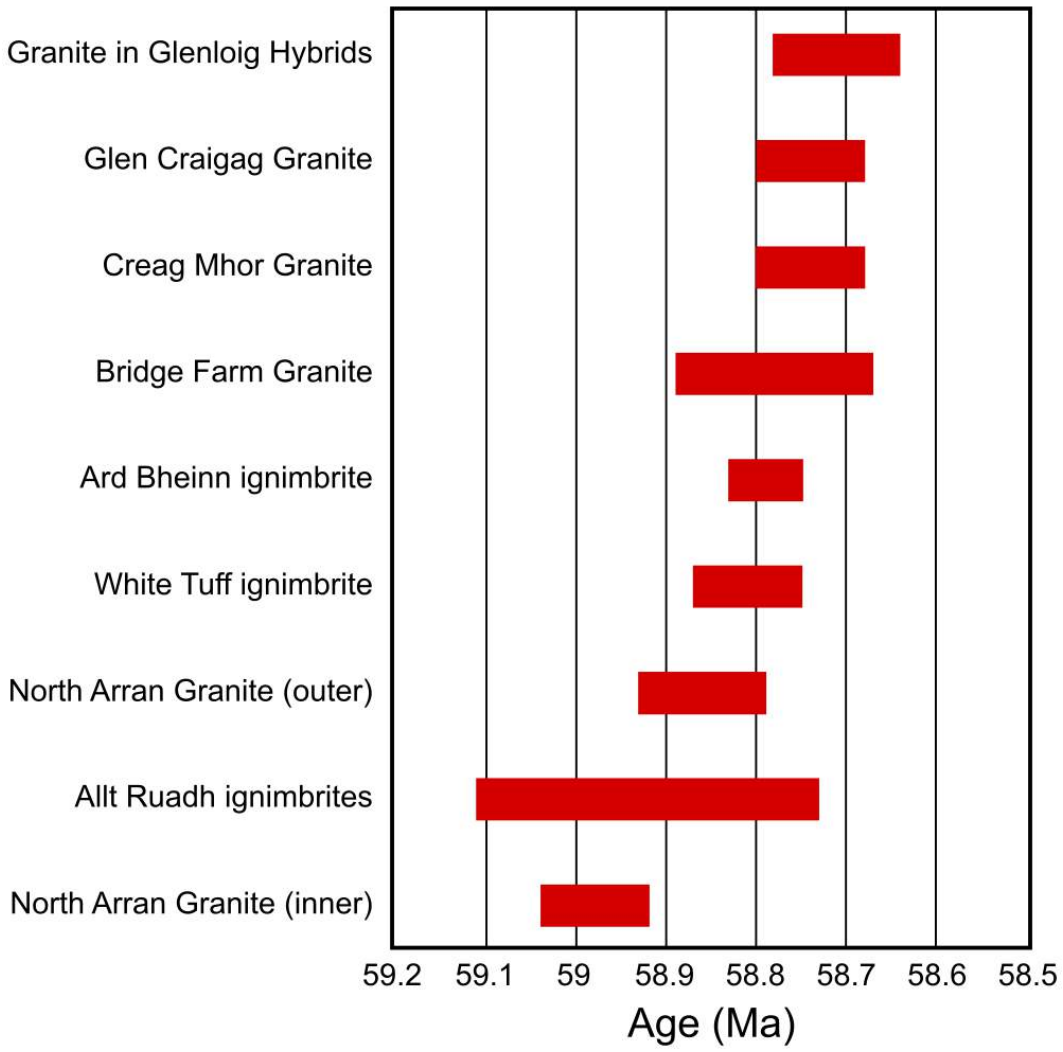

Fig. 4.69 – Plot of interpreted $^{206}Pb/^{238}U$ ages $\pm 2\sigma$ for the units analysed in this study.

Chapter 5

Magmas and Petrogenesis

Prior to this study, the relationship of the Central Arran Igneous Complex to the other central complexes of the BPIP was poorly understood, in terms of both physical and geochemical processes. This chapter draws on the geochemical data presented in the previous chapter to develop a model for the petrogenesis of the magmas that formed the different units of the CAIC, as well as the North Arran Granite.

The first section will consider the possible primary magma composition. The next section will look at the melting processes that could have formed the mafic magmas found throughout the CAIC, and the role of fractional crystallisation in the generation of these magmas, as well as the silicic magmas, will be discussed. Trace element and isotopic data will allow for a discussion of crustal contamination in the genesis of the magmas. Finally, the geochemistry of the samples analysed in this study will be compared to magmas throughout the BPIP, for which petrogenetic models have already been proposed.

5.1 Primary magma composition

The closest approximation to parental magma composition is most likely to be found in mafic dykes and sills within the complex. However, the majority of the mafic dykes which intrude the CAIC and North Arran Granite, as well as the dolerite sill which intrudes the AVF, have MgO concentrations between 3.0 and 9.3 wt.% and magnesium numbers (Mg#) between 26.3 and 59.14, suggesting that these are not primary magmatic compositions, and have all undergone some degree of fractional crystallisation.

The picrite dyke that intrudes the Glen Craigag Granite in Ballymichael Glen (sample BJG/15/338) has the highest MgO concentration and Mg# of any rock in the CAIC, with MgO 19.59 wt.%, and Mg# = 79.32. It is therefore likely to represent

the closest approximation of the composition of parental melts in the complex. In order to be able to use the whole-rock composition of this picrite as a possible parental magma composition, it is important to ensure that the abundant olivines are in equilibrium with the whole-rock composition. The Rhodes diagram (Putirka, 2008; Rhodes et al., 1979) graphically shows the relationship between the Mg# of the whole-rock and the forsterite content (Fo) of the olivine crystals (Fig. 5.1). Olivines that plot on the curved line are in equilibrium with the host rock. The equilibrium curve is dictated by the Fe-Mg exchange coefficient ($K_{\mathrm{D}}(\mathrm{Fe\text{-}Mg})^{ol\text{-}l}$), which Roeder and Emslie (1970) determined to be $K_{\mathrm{D}} = 0.30 \pm 0.03$ (dashed lines show the ± 0.03 error bars).

The purple symbols in Fig. 5.1 show the measured Fo content of olivines from sample BJG/15/338. Forsterite content ranges from 83.8 to 90.4. The fact that all of these values plot to the right of the equilibrium line indicates that this rock contains accumulated olivine, *i.e.*, the olivines are not in equilibrium with the melt, and the bulk composition of this rock cannot be used as a proxy for the primitive magmas in the CAIC system.

Table 5.1 shows the results of mathematically removing increments of the highest Fo olivine from the composition of the whole-rock values. These calculated liquid compositions are plotted on Fig 5.1 (blue circles). The calculated composition after removal of 15% of the olivine lies on the equilibrium line, so it can be concluded that BJG/15/338 represents a primary magma with ~15% accumulated olivine crystals. The calculated composition for this primary magma is shown in the 15% ol column in Table 5.1. This calculated primary magma has a SiO_2 content of 44.25 wt %, a MgO concentration of 14.41 wt %, and a Mg# of 73.91.

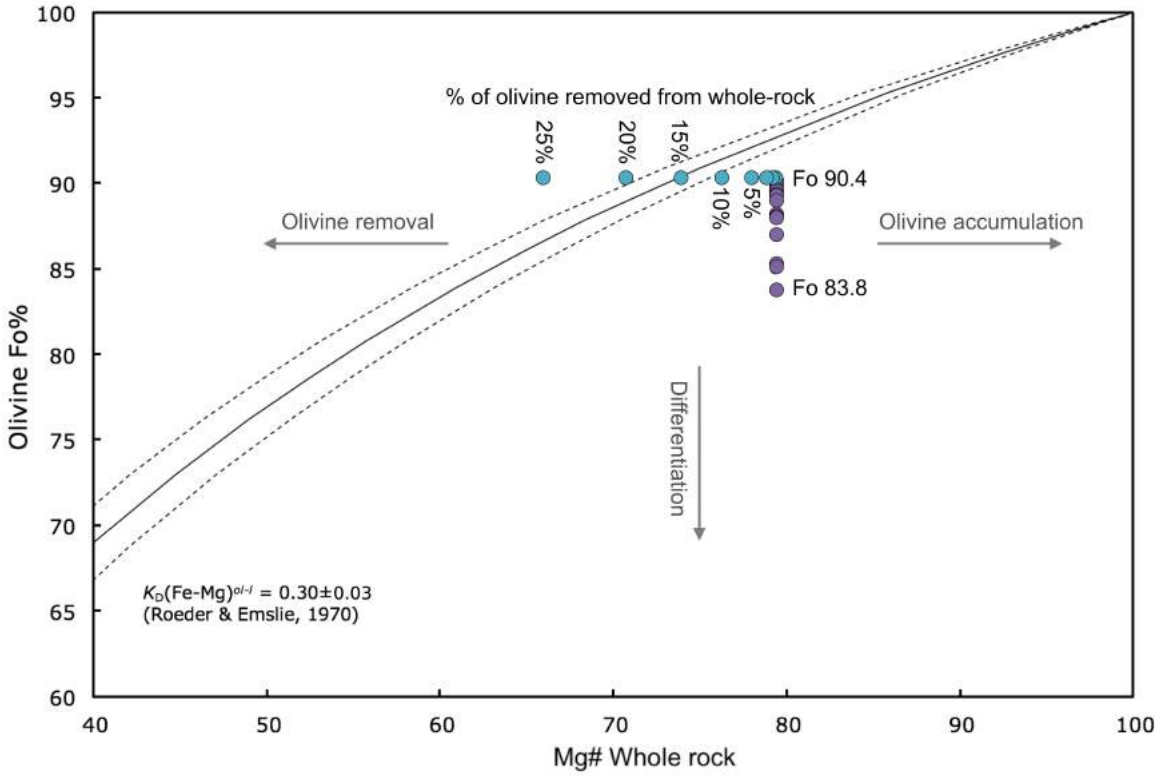

Fig. 5.1 – Rhodes diagram (Putirka, 2008; Rhodes et al., 1979) showing measured forsterite (Fo) contents of olivine crystals from sample BJG/15/338 (purple) and calculated magnesium number (Mg#) of the host rock after incremental removal of olivine with the composition of the highest measured Fo crystal.

Table 5.1 – Calculated whole-rock major element compositions (wt.%) after removal of incremental amounts of olivine from BJG/15/338

	Whole-rock	Olivine	0.1% ol	0.5% ol	1% ol	2% ol
SiO_2	43.65	40.22	43.65	43.67	43.68	43.72
TiO_2	0.56	0.00	0.56	0.57	0.57	0.58
Al_2O_3	13.44	0.15	13.45	13.50	13.57	13.71
FeO	9.11	9.33	9.11	9.11	9.11	9.10
MnO	0.19	0.15	0.19	0.19	0.19	0.19
MgO	19.60	49.01	19.57	19.46	19.31	19.00
CaO	11.26	0.35	11.27	11.32	11.37	11.48
Na_2O	1.14	0.00	1.14	1.14	1.15	1.16
K_2O	0.18	0.00	0.18	0.18	0.19	0.19
P_2O_5	0.08	0.00	0.08	0.08	0.08	0.08
Total	99.21	99.21	99.21	99.21	99.21	99.21
Mg#	79.32	90.36	79.30	79.20	79.08	78.82

	5% ol	10 % ol	**15% ol**	20% ol	25% ol
SiO_2	43.83	44.03	**44.25**	44.51	44.79
TiO_2	0.59	0.63	**0.66**	0.70	0.75
Al_2O_3	14.13	14.91	**15.78**	16.76	17.86
FeO	9.10	9.09	**9.07**	9.05	9.04
MnO	0.19	0.19	**0.19**	0.20	0.20
MgO	18.06	16.34	**14.41**	12.25	9.80
CaO	11.84	12.47	**13.19**	13.99	14.90
Na_2O	1.20	1.27	**1.34**	1.42	1.52
K_2O	0.19	0.20	**0.22**	0.23	0.24
P_2O_5	0.08	0.08	**0.09**	0.09	0.10
Total	99.21	99.21	**99.21**	99.21	99.21
Mg#	77.97	76.22	**73.91**	70.69	65.91

5.2 Mantle Melting

By comparing LREE and HREE ratios of relatively unaltered basaltic rocks, it is possible to make deductions about the mineralogy (and therefore depth) of the melting mantle source region (Ellam, 1992), due to the fact that the presence of garnet in the source generally leads to HREE depletion in the melt (e.g. Hole et al., 2015). A key conclusion of such studies in the Hebrides is that the melting mantle source region shallowed through time during development of the Mull lava succession. This has been ascribed to progressive lithospheric thinning during magmatism (Kerr, 1994, 1995), although regional estimates of crustal stretching and the thermodynamic feasibility of thermal lithospheric erosion do not adequately explain the amount of thinning required – see discussion in Kerr et al. (1999).

In central Arran, all basaltic rocks are intrusive, and in the absence of relative (lava-stratigraphic) or absolute (radiometric or palynological) ages no inferences can be made about changes in mantle source regions *through time*, but these melting environments can still be discussed.

It is also possible, using immobile incompatible trace element ratios to approximate the relative input of plume mantle material and MORB mantle material in these melting regions (Fitton et al., 1997).

5.2.1 Mantle Melting Modelling

The non-modal equilibrium melting model is thought to produce the best approximation of a real-world magma that forms from melting in a column over a range of depths (Plank and Langmuir, 1992), and is used in preference to the less realistic modal melting model. The non-modal equilibrium melting equation is

$$C_{\mathrm{L}} = \frac{C_{\mathrm{S}}}{F + D - FP}$$

where C_L is the concentration of an element in the liquid, C_S is the concentration of that element in the melting solid source, and F is the degree of melting.

D is the bulk distribution coefficient between the solid mineral phases and the liquid:

$$D = \Sigma K_{\mathrm{d}}1 \cdot X1 + K_{\mathrm{d}}2 \cdot X2 + ...$$

where K_d1 is the distribution coefficient between mineral 1 and the liquid, and X1 is the proportion of mineral 1 in the melting solid source.

P is the bulk melting coefficient:

$$P = \Sigma K_{\mathrm{d}}1 \cdot p1 + K_{\mathrm{d}}2 \cdot p2 + ...$$

where $K_{\mathrm{d}}1$ is the distribution coefficient between mineral 1 and the liquid, and p1 is the melting proportion of mineral 1.

Modal mineralogy, melting proportions, and melting equations used in the non-modal equilibrium melting model in this study are from Kostopoulos and James (1992), while distribution coefficients are from McKenzie and O'Nions (1991).

Figs. 5.3 – 5.7 show the results of modelling non-modal equilibrium melting of an incompatible-element-depleted (relative to bulk Earth) asthenospheric mantle, with a range of mineralogies to approximate different depths. The La/Nd and Gd/Lu ratios are dependent on the amount of garnet in the melting source, as the compatibilities of REEs in garnet (with respect to basaltic melt) increase with atomic number (*i.e.*, the lanthanide contraction), so that the partition coefficients of these elements go in the order La<Nd<Gd<Lu (Green et al., 2000). Depleted HREE values therefore reflect the presence of garnet in the source, causing samples to plot at high levels on the (Gd/Lu)n axis in Figs. 5.3, 5.6, and 5.7. The incompatible nature of LREEs in both garnet lherzolite and spinel lherzolite mean that small degree melts have the highest (La/Nd)n ratios and La concentrations, which are then lowered by 'dilution' of the other incompatible elements with higher degrees of melting. High degree melts therefore plot to the left of the melting model graphs (Figs. 5.3, 5.6, 5.7). The models represent melting of a garnet lherzolite source (>95 km depth), a spinel lherzolite source (<85 km depth), and a 50:50 mixture of the two to approximate a transitional garnet – spinel lherzolite source (85–95 km depth) (Watson, 1993).

The effects of crustal contamination, alteration, and mineral accumulation

Many of the mafic samples analysed in this study are likely to show some degree of contamination, especially since no basaltic dykes have MgO > 8.0 wt.% and no samples from the dolerite sill intruding the CAIC have MgO > 9.2 wt.%. On the other hand, Kerr et al. (1995) found that lavas on Mull with MgO < 8 wt.% seemed the least contaminated.

The analysed Arran data have been filtered to remove any samples with Ba/Zr > 2, which has been used as a criterion for a sample being relatively uncontaminated by crustal material (Kent and Fitton, 2000). However, Ba belongs to the group of elements that are susceptible to mobilisation during alteration (Pearce, 1996) as discussed in Section 4.1.1. It is therefore important to determine to what extent Ba has been mobilised in these mafic rocks. This can be done by plotting Ba concentration against a generally immobile incompatible element. Fig. 5.2a shows a

good correlation in most groups between Ba and Nb, suggesting limited mobility of Ba during alteration. The exception is the dolerite sill which which shows significant scatter, possibly indicating mobility. The same is true when plotted against Zr, another generally immobile incompatible element (Fig. 5.2b). These plots suggest that Ba has been mobilised to a minor degree in all units other than the sill, in which case alteration may have been significant.

Another element that can be used to show crustal contamination, but is generally less mobile, is Th. Th/Zr (a possible control for crustal contamination) is plotted against Ba/Zr (the control used in this section) in Fig. 5.2c. This plot shows that while the majority of samples pass the Ba/Zr $\leqslant$ 2 filter, some of these have high Th/Zr and so may indeed have experienced significant crustal contamination. Fig. 5.2d shows that some samples with Ba/Zr $\leqslant$ 2 (and therefore included in melting modelling) have relatively high loss on ignition (LOI) values, and therefore may have been significantly altered.

Many of the samples included in these models have elevated Th/Zr rations (>0.03), particularly the low La/Sm dykes that intrude the North Arran Granite, and some of the high La/Sm dykes from the CAIC. It is possible that these samples have experienced some crustal contamination that was not controlled for by the Ba/Zr filter.

Another control on the amount of contamination is the isotopic signature of analysed samples. Crustal contamination generally leads to elevated $^{87}Sr/^{86}Sr$ and lowered $^{143}Nd/^{144}Nd$ relative to mantle source values. The CAIC dykes analysed for radiogenic isotope ratios in this study all have $\varepsilon Sr < 10.3$ and $\varepsilon Nd > 0.9$ and the analysed CAIC sill samples all have $\varepsilon Sr < 1.6$ and $\varepsilon Nd > 3.4$ (Fig. 4.48) showing that all of these samples are fairly uncontaminated compared to the most primitive samples in the BPIP (e.g. the M9 picrite from Rùm which has εSr = -23.1 and εNd = 11.08 (Meyer et al., 2009; Upton et al., 2002)). Samples that have been analysed for isotopes are shown by orange circles in Figs. 5.3 and 5.7.

Contamination can increase La concentration and the La/Nd ratio (Kerr, 1995; Meyer et al., 2009), thus moving points further to the right on graphs where (La/Nd)n or La (ppm) make up the x-axis. This could lead to an underestimation of degree of melting in samples that have experience crustal contamination. Crustal contamination by various sources will be discussed in detail in Section 5.4.

Many of the samples included in the modelling are known, from petrographic study (Chapter 2), to have experienced some accumulation of olivine (picrite dyke) or plagioclase (most basaltic dykes), which could affect the outcome of the models. Neither olivine nor plagioclase that have crystallised from basaltic melts are likely to contain significant levels of REE (other than Eu; https://earthref.org/KDD/).

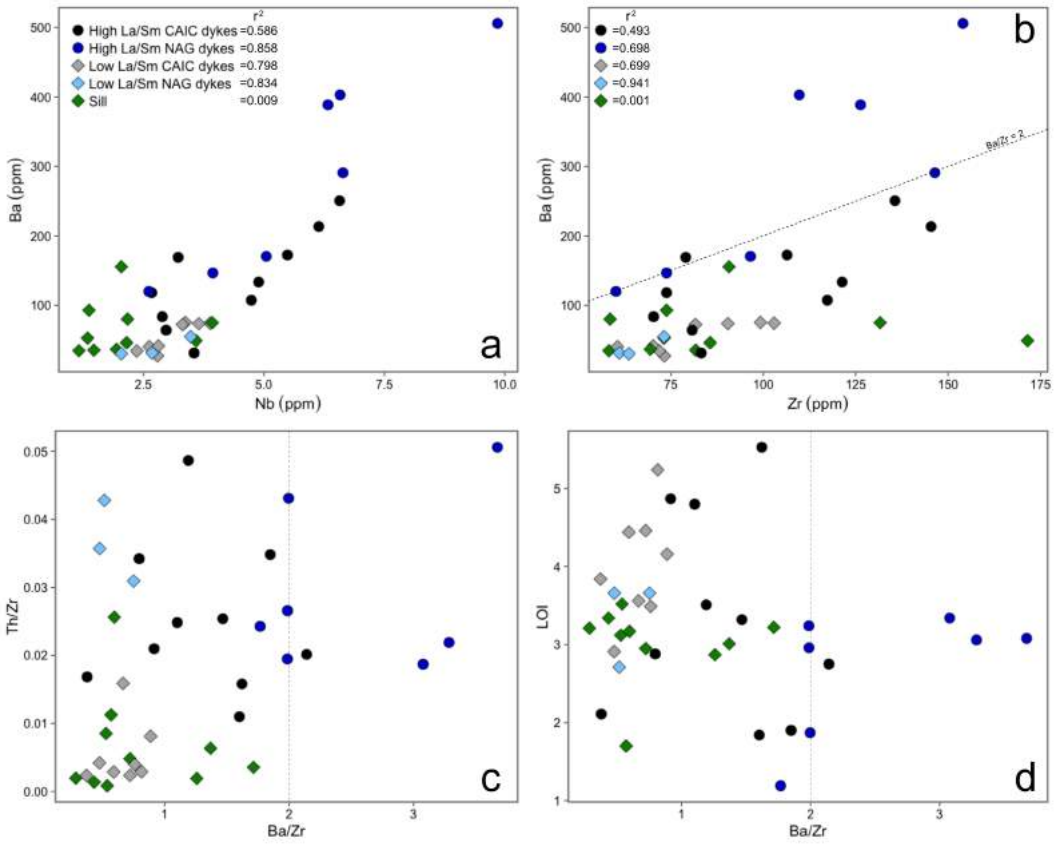

Fig. 5.2 – Binary plots showing the effect of alteration on Ba. (a) Nb vs. Ba showing a good correlation, indicating a low degree of alteration. (b) Zr vs. Ba showing correlation within the groups. The dashed line shows Ba/Zr, the ratio used to control for crustal contamination in the mantle melting models. (c) Ba/Zr plotted against Th/Zr, an alternative control for crustal contamination. (d) Ba/Zr vs. loss on ignition (LOI), with the poor correlation suggesting that some samples with low Ba/Zr values may have been significantly altered.

Therefore, accumulation of these minerals is unlikely to affect ratio:ratio plots, but may have the effect of moving points to the left on plots where La concentration is shown on the x-axis.

In summary, using Ba/Zr $\leqslant 2$ is a suitable test for excessive crustal contamination, as most units have not experienced significant mobilisation of Ba during alteration, other than the dolerite sill that intrudes the CAIC. However, many samples that pass the filter have relatively high LOI values, and so may have experienced significant general alteration. Using Th/Zr as a filter for crustal contamination instead of Ba/Zr would have yielded similar results, but some samples which passed the Ba/Zr $\leqslant$ 2 would be excluded. Crustal contamination could lead to an underestimation of degree of melting in the model, but mineral accumulation of olivine and plagioclase is unlikely to have a significant effect.

CAIC dykes

The basaltic (and picrite) dykes from the CAIC are shown in relation to the non-modal batch melting model in Fig. 5.3. On Fig. 5.3a, showing (La/Nd)n vs. (Gd/Lu)n, the low La/Sm dykes cluster around the convergence point of the three melting models, but on Fig. 5.3b, showing La (ppm) vs (Gd/Lu)n they form a clear trend, which lies between the spinel lherzolite and transition zone models. The (Gd/Lu)n ratios are slightly more elevated than would be expected for high-degree melting of a spinel lherzolite source, suggesting a deeper melt source region. Then again, the (La/Nd)n ratio and La concentration are too high to be consistent with high-degree melting of a garnet-bearing lherzolite source. It therefore seems that the magma that makes up these dykes were formed from relatively high degree (5–10%) melting of a spinel lherzolite source, possibly with a small amount of garnet in the melting column.

The full chondrite-normalised (McDonough and Sun, 1995) REE profile for sample BJG/15/154 is shown in Fig. 5.4, along with modelled melts formed from varying degrees of melting of a depleted spinel lherzolite source using the same equations. This is the only sample of a low La/Sm dyke from the CAIC which has been analysed for isotopes. With an εSr value of -13.00 and an εNd value of 7.63, it is clear that this magma has experienced minimal crustal contamination. Its REE profile closely matches that of a modelled melt formed from 8% melting of a depleted spinel lherzolite (Fig. 5.4), albeit with higher overall REE concentrations.

The high La/Sm dykes clearly lie along the spinel lherzolite melting curve in Fig. 5.3. Given the controls for crustal contamination mentioned above, significant amounts of contamination of low La/Sm-like magmas can be ruled out as the only source of this trend. It is therefore likely that the magmas belonging to this group formed by low-degree melting (up to around 4%) of a spinel lherzolite source at depths shallower than 85 km. The least contaminated high La/Sm CAIC dyke which has been analysed for isotopes is sample BJG/15/325, which has an εSr value of -12.78 and an εNd value of 5.73. The chondrite normalised REE profile for this sample is shown in Fig. 5.5, along with model melts sourced from a depleted spinel lherzolite source. This shows that the characteristically flat REE profile can be formed from around 1% melting of spinel lherzolite (but with lower overall REE concentrations than the model).

The picrite dyke also lies on the spinel lherzolite melting model, but the two models in Fig. 5.3 suggest different degrees of melting. The low La concentration is consistent with overall low REE concentrations in this sample (Section 4.1.4), and may be due to dilution of the magma by accumulated olivine (which does not contain REE). It is therefore suggested that the normalised La/Nd ratio provides a

better insight into melting conditions, and so it is likely that this magma formed from around 2% melting of a spinel lherzolite source at depths shallower than 85 km.

North Arran Granite dykes

The basaltic dykes that intrude the North Arran Granite are shown in relation to the melting model in Fig. 5.6. As none of these samples were analysed for radiogenic isotopes, the Ba/Zr $\leqslant$ 2 filter is the only control for contamination. It is possible that some of these samples are relatively contaminated, especially given that their MgO concentration can be as low as 4 wt.%.

With this in mind it appears that these dykes show the same general results as for the CAIC dykes. The low La/Sm dykes appear to have formed from higher degree (5–10%) melting of a spinel lherzolite source, possibly with small amounts of garnet given their slightly elevated (Gd/Lu)n ratios. The high La/Sm dykes formed from smaller-degree ($\leqslant$4%) melting of a spinel lherzolite source at shallow depths (less than 85 km).

CAIC sill

The dolerite sill that intrudes the CAIC is shown in relation to the melting model in Fig. 5.7. The circled samples have been shown to be fairly uncontaminated on the basis of Sr and Nd isotope ratios. All samples of this sill analysed in this study have Ba/Zr < 2.

The main cluster, which includes the isotopically analysed samples, lies at around 10% melting of a garnet-spinel lherzolite source on Fig. 5.7a, and 5–8% melting of a spinel to garnet-spinel lherzolite source on Fig. 5.7b. It is possible that the samples with higher (La/Nd)n and higher La concentrations than this cluster indicate a shallower melting source, but it also possible that these samples have been moved right on the graph by minor post-melt generation contamination.

The least contaminated sample of the dolerite sill that has been analysed for isotopes is sample BJG/15/7. It has an εSr value of -4.74 and an εNd value of 6.46. Because Fig. 5.7 does not show clearly whether the magma formed from a garnet lherzolite or transitional garnet-spinel lherzolite source, models of both are plotted alongside the complete chondrite normalised REE profile for sample BJG/15/7 in Fig. 5.8. A relatively good fit is produced from 7% melting of a garnet lherzolite source, but an even closer match is found with 5% melting of a transitional garnet-spinel lherzolite source.

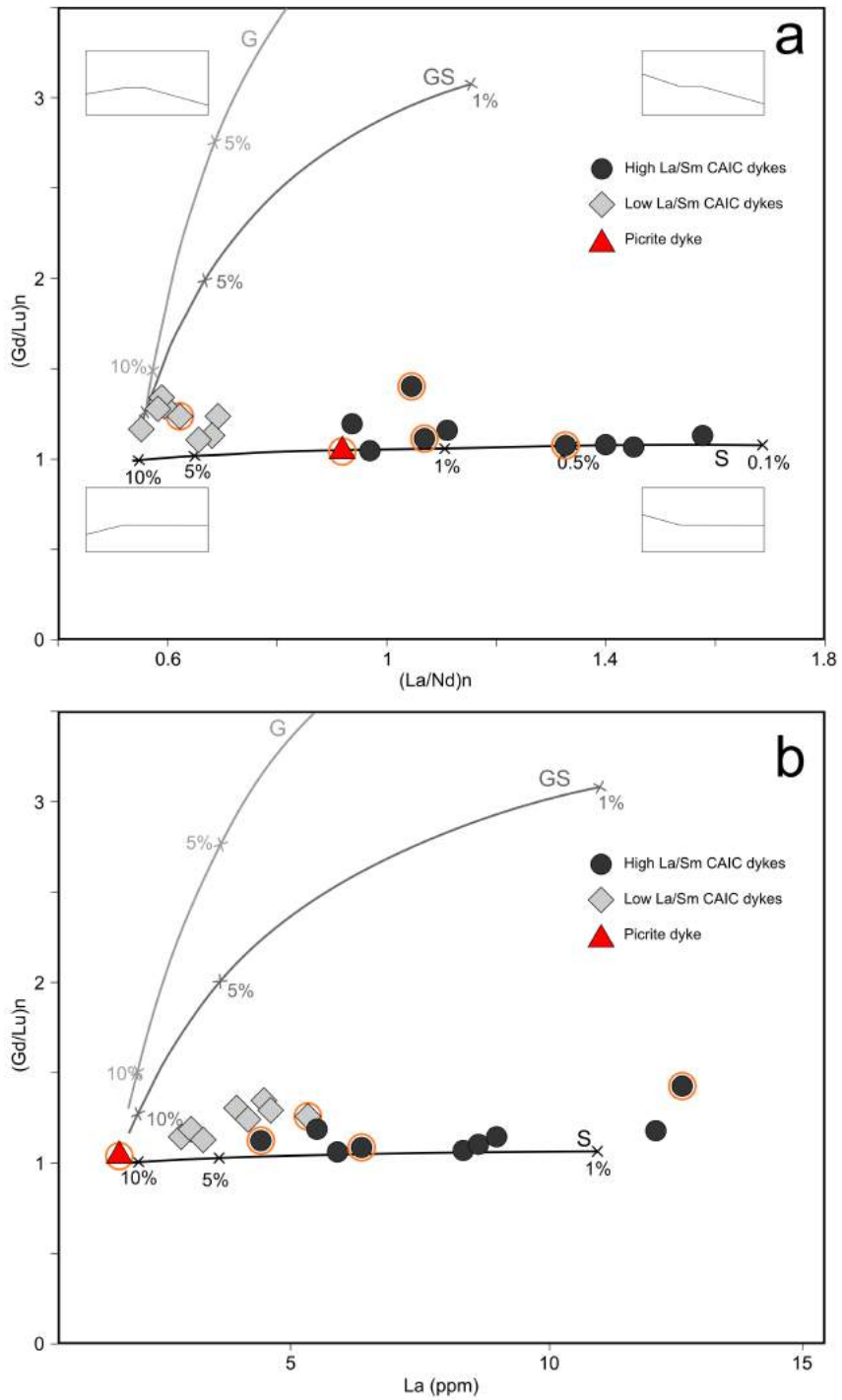

Fig. 5.3 – Chondrite-normalised (McDonough and Sun, 1995) Gd/Lu plotted vs. normalised La/Nd **(a)** and La concentration **(b)** for the mafic dykes of the CAIC (filtered to remove samples with Ba/Zr > 2). Circled points are those for which we have radiogenic isotope data. Lines show modelled magmas produced from varying degrees of non-modal batch melting of a depleted garnet lherzolite (G), a depleted spinel lherzolite (S), and a 50:50 mixture of depleted garnet and spinel lherzolite (GS). Crosses show the amount of partial melting. Insets show example chondrite-normalised REE plots for the different areas of **(a)**.

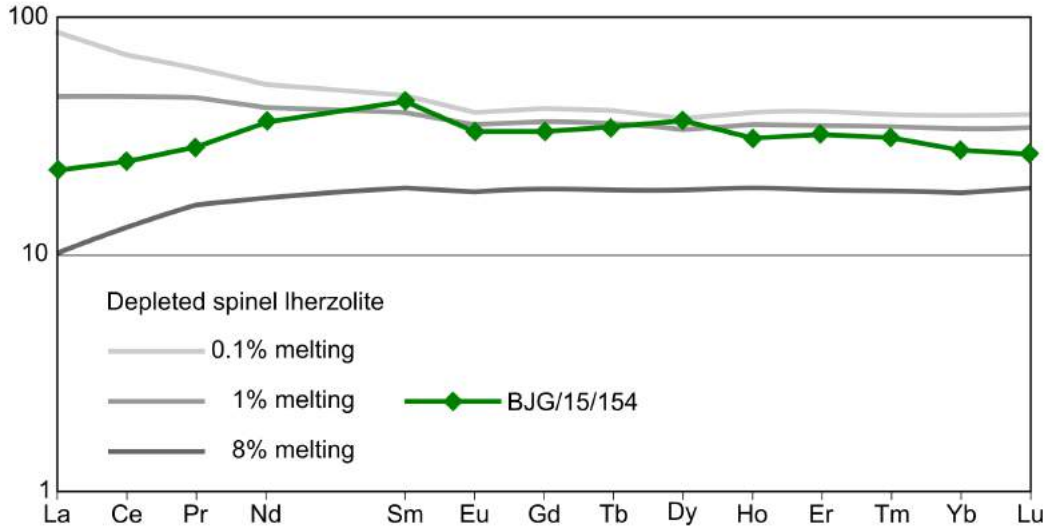

Fig. 5.4 – Chondrite-normalised (McDonough and Sun, 1995) REE diagram for an uncontaminated low La/Sm CAIC dyke, as well as model REE profiles formed by different degrees of non-modal equilibrium melting of a depleted spinel lherzolite source (Kostopoulos and James, 1992).

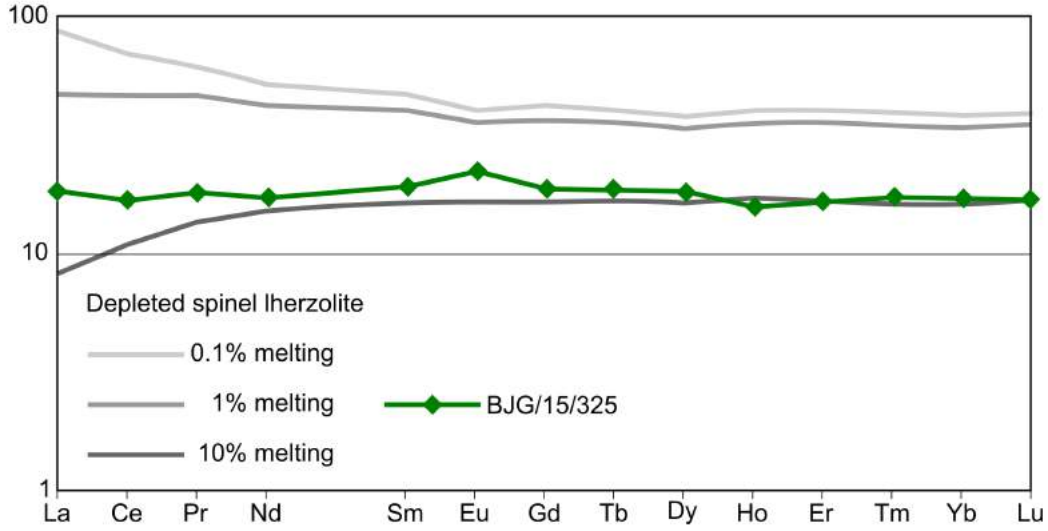

Fig. 5.5 – Chondrite-normalised (McDonough and Sun, 1995) REE diagram for an uncontaminated high La/Sm CAIC dyke, as well as model REE profiles formed by different degrees of non-modal equilibrium melting of a depleted spinel lherzolite source (Kostopoulos and James, 1992).

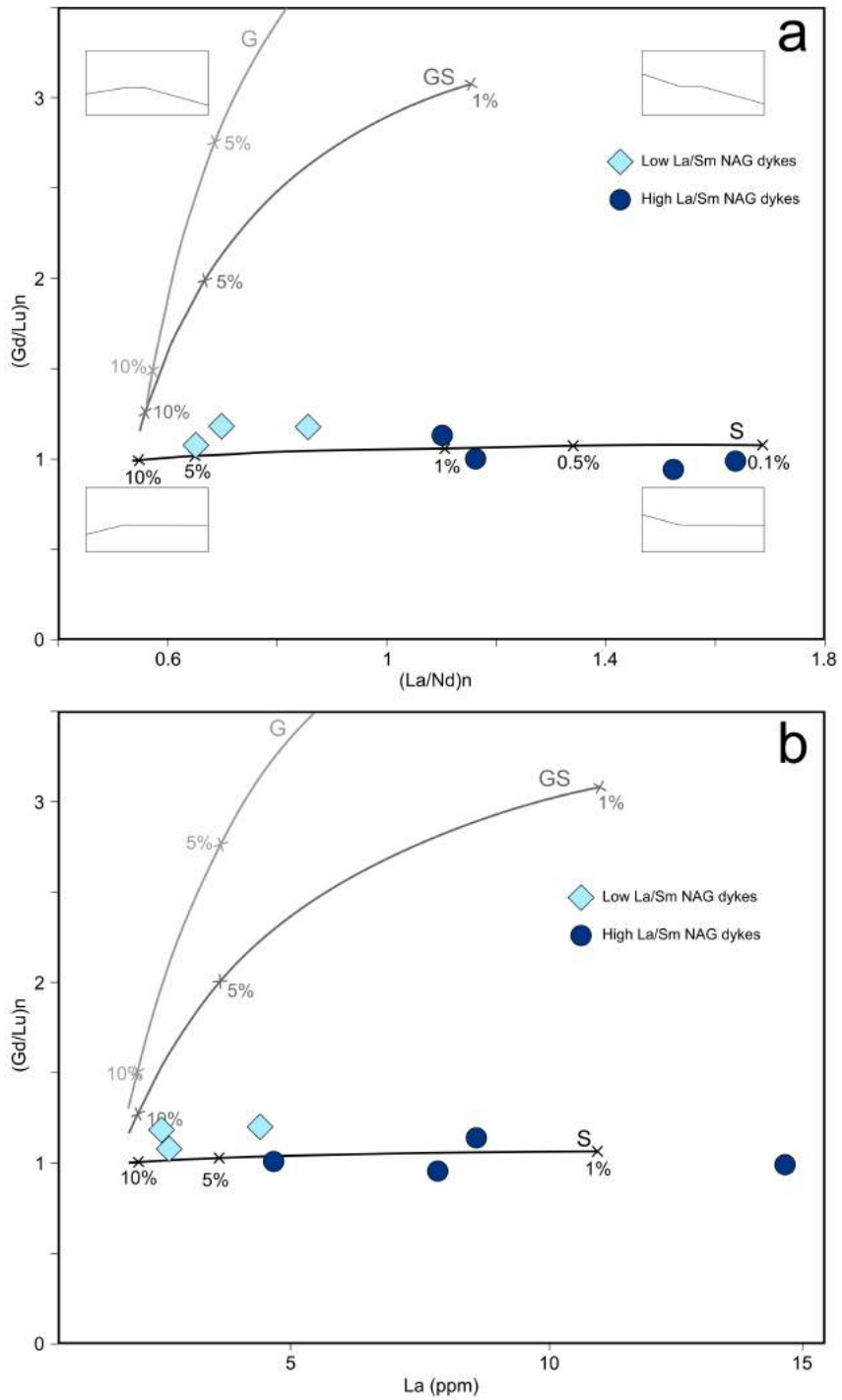

Fig. 5.6 – Chondrite-normalised (McDonough and Sun, 1995) Gd/Lu plotted vs. normalised La/Nd **(a)** and La concentration **(b)** for the mafic dykes that intrude the North Arran Granite (filtered to remove samples with Ba/Zr > 2). Lines show modelled magmas produced from varying degrees of non-modal batch melting of a depleted garnet lherzolite (G), a depleted spinel lherzolite (S), and a 50:50 mixture of depleted garnet and spinel lherzolite (GS). Crosses show the amount of partial melting. Insets show example chondrite-normalised REE plots for the different areas of **(a)**.

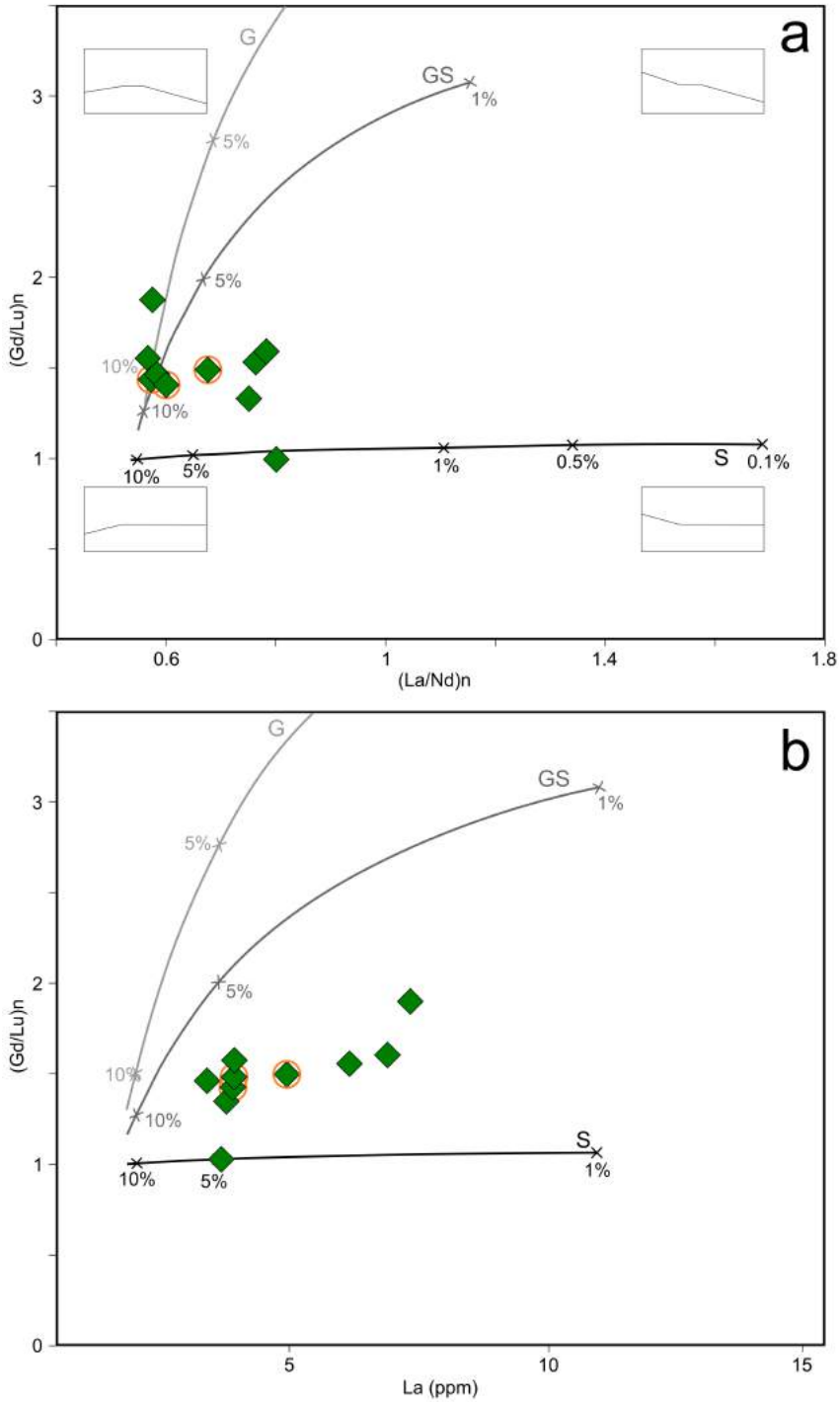

Fig. 5.7 – Chondrite-normalised (McDonough and Sun, 1995) Gd/Lu plotted vs. normalised La/Nd **(a)** and La concentration **(b)** for the dolerite sill that intrudes the ignimbrites of the CAIC (no samples have Ba/Zr > 2). Circled points are those for which we have radiogenic isotope data. Lines show modelled magmas produced from varying degrees of non-modal batch melting of a depleted garnet lherzolite (G), a depleted spinel lherzolite (S), and a 50:50 mixture of depleted garnet and spinel lherzolite (GS). Crosses show the amount of partial melting. Insets show example chondrite-normalised REE plots for the different areas of **(a)**.

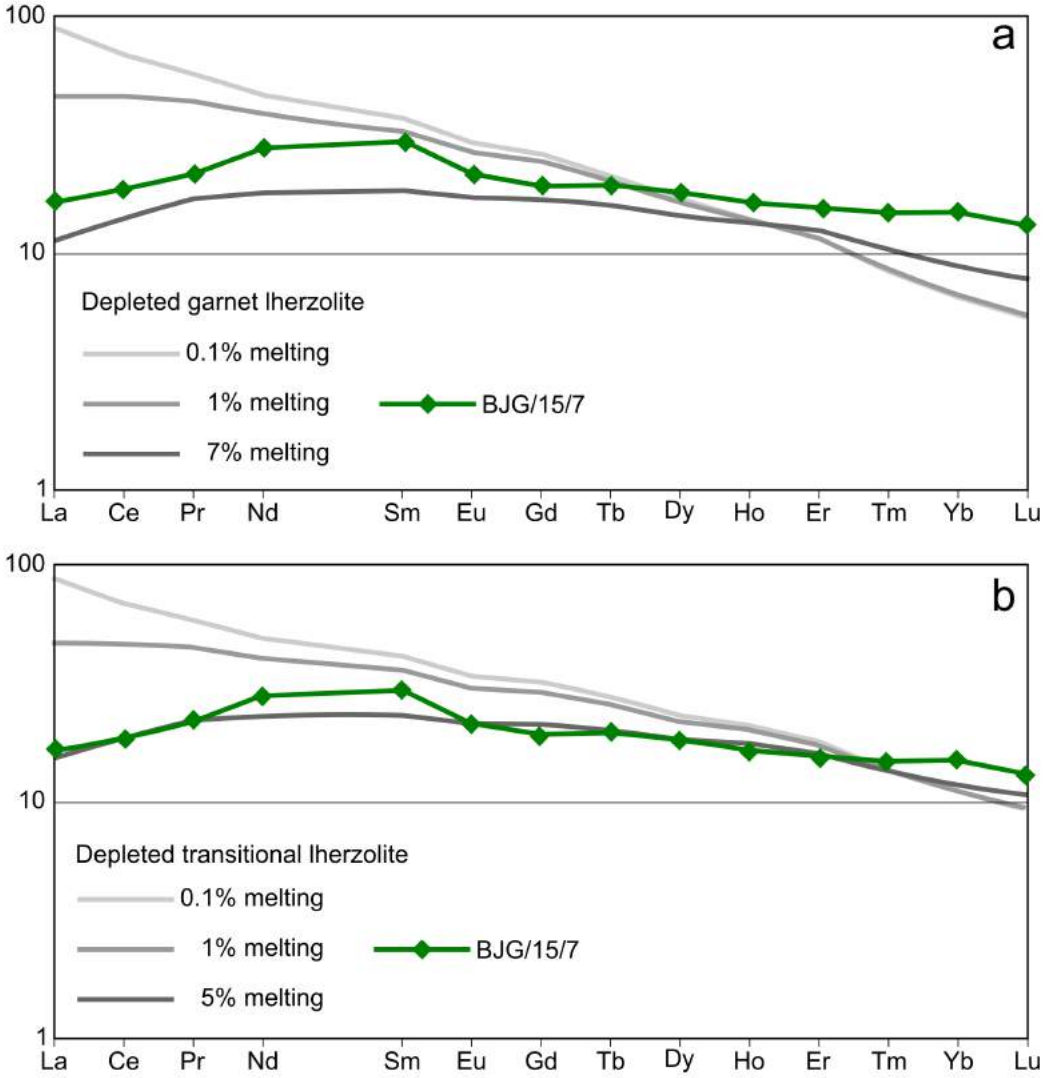

Fig. 5.8 – Chondrite-normalised (McDonough and Sun, 1995) REE diagrams for uncontaminated samples of the dolerite sill that intrudes the CAIC, as well as model REE profiles formed by different degrees of non-modal equilibrium melting of a depleted garnet lherzolite source **(a)** and a depleted transitional garnet-spinel lherzolite source **(b)** (Kostopoulos and James, 1992).

Summary

Simple melting models are just that – simple, and models. The non-modal equilibrium melting model is built on a great many assumptions, not least the geodynamic mechanics of melting in the mantle, and the composition of the solid melting source. These considerations are discussed in Kostopoulos and James (1992).

With these assumptions and caveats in mind, *possible* melting environments for the rocks analysed in this study can be proposed.

The picrite is formed by low-degree (2%) melting of a spinel lherzolite source; increased degrees of melting (up to 4%) of that source produced high La/Sm dykes and then eventually (at around 5-10% melting) lower La/Sm dykes. The dolerite sill, however, shows evidence of a different source altogether, being formed from 5–8% melting of a transitional garnet-spinel lherzolite source.

5.2.2 Assessing Plume vs. MORB Sources

Fitton et al. (1997) showed that the input of the Iceland Plume, relative to an N-MORB source, for North Atlantic Igneous Province basalts could be shown by plotting Zr/Y vs. Nb/Y. Icelandic basalts lie above the line

$$log(Nb/Y) = 1.92log(Zr/Y) - 1.74$$

while N-MORB basalts lie below this line. On Fig. 5.9 the majority of previously published Hebridean samples belonging to the M1, M2, and M3 magma types (Kent and Fitton, 2000; Kerr et al., 1999) plot below the line, suggesting a dominantly N-MORB source for the majority of basaltic rocks in the BPIP. The basaltic dykes from the CAIC and North Arran Granite, as well as the gabbros of the CAIC, plot in a linear array along this line, and within the fields of the M2 and M3 Hebridean magma types. This suggests a source which has sub-equal input from both N-MORB and Iceland Plume components, that presumably also provided the M2 and M3-type magmas. All samples of the dolerite sill plot well below this line, showing that they have an N-MORB source with little or no input from the Iceland Plume.

Crustal units that could be the source of contamination will always lie below the lower limit of the Icelandic Array (Kent and Fitton, 2000), so could have the effect of dragging affected samples to the right of the diagram (Fitton et al., 1997). Crustal contamination cannot cause data points to cross the line from N-MORB-like to Iceland-like. This could explain the horizontal spread of data in the sill, gabbros, and high La/Sm dykes. However, Kent and Fitton (2000) propose that mafic rocks from the BPIP that have Ba/Zr $\leqslant 2$ reflect only mantle sources in terms of plume

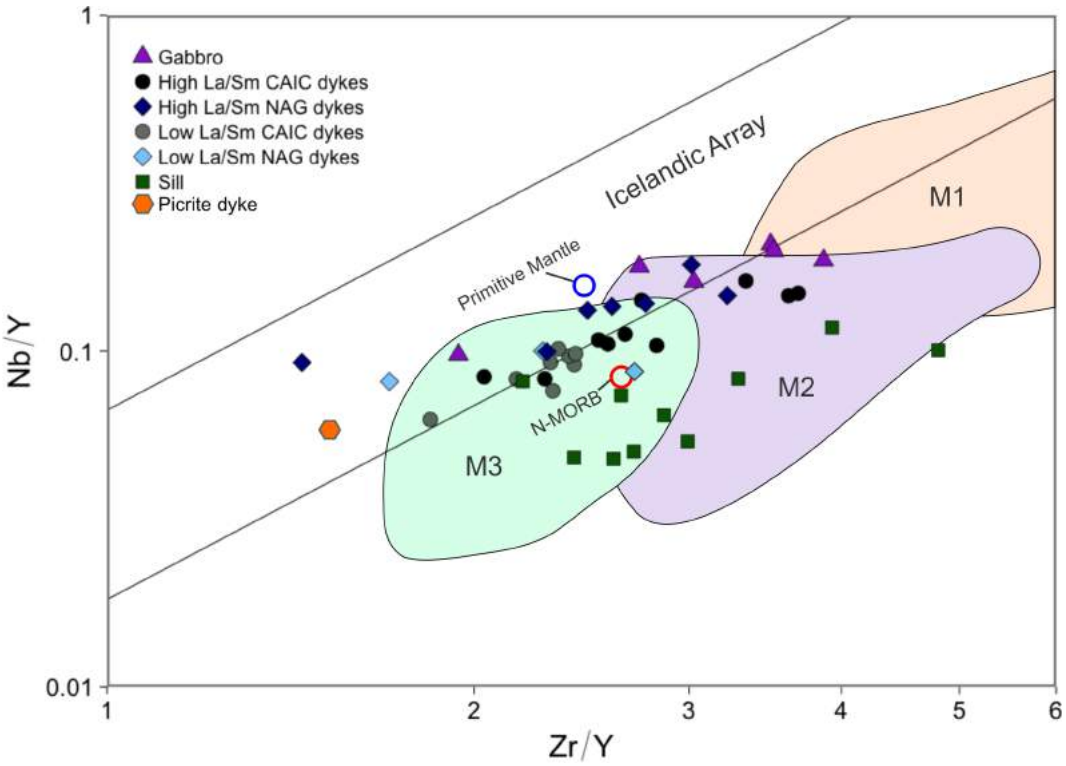

Fig. 5.9 – Plot of Zr/Y vs. Nb/Y with lines showing the upper and lower boundaries of the array of Icelandic basalts. N-MORB-derived samples form a parallel array below the lower boundary (Fitton et al., 1997). Also shown are the fields for the three Hebridean magma types from Kent and Fitton (2000), as well as samples from this study.

vs. MORB on the Zr/Y vs. Nb/Y diagram. The gabbros and the high La/Sm dykes include samples that fail this test, so contamination is a likely source of the variation in these units.

Kent and Fitton (2000) showed that the input of 'Icelandic' (plume) material relative to N-MORB in the melting regime below the western British Isles increased and then decreased through time during formation of the British Palaeogene Igneous Province. This could suggest that the array of dolerite sill samples along the lower part of the Zr/Y vs. Nb/Y graph (Fig. 5.9) is controlled by the age of the intrusion. Field relationships and radiometric ages show that it is possible that the dolerite sill is the youngest mafic unit analysed in this study. The magma that makes up the sill could therefore have formed from mantle melting during the waning stage of Icelandic plume input.

5.3 Fractional Crystallisation

In this section, the role of fractional crystallisation in the petrogenesis and evolution of the Arran magmas will be assessed. Fractional crystallisation modelling is used to determine whether the mafic magmas of the CAIC (and dykes intruding the North Arran Granite) could be a result of fractional crystallisation of picritic primary magmas. It is also used to discuss whether fractional crystallisation can explain the spread of data within groups in the mafic units. Trace element concentrations are used to assess the role of fractional crystallisation in the generation of granitic magmas.

5.3.1 Fractional Crystallisation Modelling of Mafic Melts

Major element fractional crystallisation modelling was carried out using the Petrolog (Version 3) modelling software of Danyushevsky and Plechov (2011). Magmas were modelled from a range of starting compositions at two different initial pressures, and allowing crystallisation of various mineral assemblages. All models were run under anhydrous conditions, using the quartz-fayalite-magnetite (QFM) oxygen buffer, and were stopped when the melt reached 4 wt.% MgO.

For each starting composition, three involving purely fractional crystallisation models were run with different parameters:

- Fractional crystallisation of olivine at 1 kbar.
- Fractional crystallisation of olivine, plagioclase, and magnetite at 1 kbar.
- Fractional crystallisation of olivine, plagioclase, and magnetite at 5 kbar.

and another two models were run in which 80% of certain minerals were fractionated, while the other 20% were retained in the melt (equilibrium crystallisation):

- Fractional crystallisation of olivine and magnetite, with 80% fractional crystallisation of plagioclase, at 1 kbar.
- Fractional crystallisation of magnetite, with 80% fractional crystallisation of olivine and 80% fractional crystallisation of plagioclase, at 1 kbar.

The pressures of 1 kbar and 5 kbar were selected to show the effects of changing pressure in relation to the effects from other starting parameters. The starting compositions used in the models are shown in Table 5.2.

Table 5.2 – Major element compositions of the starting points used in the fractional crystallisation modelling (wt. %).

	calculated Arran picritic magma	Rùm picrite M9	BJG/15/174	ARA-5
SiO_2	44.24	42.45	46.63	48.17
TiO_2	0.66	0.54	2.15	1.20
Al_2O_3	15.78	5.94	14.28	16.29
$Fe_2O_3^{est.}$	1.01	1.08	1.57	1.26
$FeO^{est.}$	8.16	8.78	12.72	10.24
MnO	0.19	0.16	0.33	0.18
MgO	14.40	34.61	7.35	9.24
CaO	13.19	4.56	10.81	10.27
Na_2O	1.34	0.80	2.45	2.26
K_2O	0.22	0.08	0.30	0.28
P_2O_5	0.09	0.03	0.17	0.11

Fractional crystallisation from picritic melts

Two picritic melts were used as the starting composition for the model, to assess whether the mafic Arran rocks were derived from primitive mantle melts. The first is a melt with the composition of the calculated picrite, produced by removal of 15% of olivine from picrite sample BJG/15/338 (Section 5.1), which is thought to represent the primary magma that formed the picrite dyke intruding the CAIC. The second is a melt with the composition of picrite M9 from a dyke on Rùm, which has been proposed to be one of the closest approximations to a primary mantle melt in the BPIP (Upton et al., 2002).

The results of modelling using the calculated Arran picritic magma as a starting composition are shown in Figs. 5.10 and 5.11. The different models provide variously good matches to the analysed data from the mafic dykes (Fig. 5.10). When plotted against MgO, the models provide a good fit for TiO_2, FeO, and Al_2O_3, a moderate fit for SiO_2 and Na_2O, and do not fit the CaO data. It is the models that include the crystallisation of olivine+plagioclase+magnetite that provide the best fits. This is to be expected from the petrography, as all of the mafic dykes include plagioclase phenocrysts and magnetite crystals, while some contain relict olivine phenocrysts (Section 2.6). None of the mafic dykes in the CAIC or the North Arran Granite contain clinopyroxene phenocrysts. It should be noted that the effect of pressure is negligible when compared to the variation produced by other starting parameters.

On the plots for MgO vs. TiO_2 and FeO, it appears that a model involving 100% fractional crystallisation of ol+plag+mgt produces the best fit for the low La/Sm dykes, while the ol+plag(80% fractional crystallisation)+mgt model provides the best fit for the high La/Sm dykes. This could explain the apparent geochemical differences between these two groups. As the high La/Sm dykes do not lie further

along fractional crystallisation trends than the low La/Sm dykes, the hypothesis that that they are merely more fractionated magmas can be rejected.

The fact that all models predict higher CaO and lower Na_2O than the observed data suggests fractionation of a high-CaO low-Na_2O phase. An obvious candidate is clinopyroxene, although very few of the mafic dykes analysed in this study contain clinopyroxene phenocrysts, and none are observed in the dolerite sill. This is consistent with the paucity of clinopyroxene phenocrysts in basaltic rocks throughout the BPIP (e.g. Bailey et al., 1924; Kerr, 1993; Thompson et al., 1972). Apatite crystallisation may also have played a role. This over-estimation of CaO concentrations by fractional crystallisation models was also noted by Kerr (1993) who suggested that clinopyroxene had fractionated at high pressures to suppress the CaO (and Sc and V) in the melt. To explain both the geochemical evidence for clinopyroxene fractionation, and the physical lack of clinopyroxene phenocrysts in the rocks on Skye, Thompson et al. (1980) proposed that the magmas had spent time at shallow depths in the crust during their ascent, allowing time for high-pressure minerals to dissolve, and low-pressure assemblages to crystallise. This would cause any clinopyroxenes that crystallised at high pressures to be removed, while the melt retained the geochemical signature of their fractionation (Thompson et al., 1980). It is proposed that the Arran magmas underwent a similar process, leading to the discrepancy between the models and the analysed data with respect to CaO and Na_2O.

The different models provide variously good fits to the analysed data from the dolerite sill (Fig. 5.11). When plotted against MgO, the models provide a good fit for TiO_2, FeO, and Al_2O_3, a moderate fit for SiO_2, and do not fit the CaO or Na_2O data. Much like with the dykes, it is the models that include the crystallisation of olivine+plagioclase+magnetite that provide the best fit. The majority of samples are best explained by the ol+plag(80%)+mgt model.

The isotopic composition of the sill (lower radiogenic Nd and higher radiogenic Sr than the dykes - Section 4.2) suggest that this magma was subjected to greater degrees of crustal contamination (this will be discussed further in Section 5.4.2), so fractional crystallisation of a primary melt cannot be the only petrogenetic process at work.

The results of modelling using the M9 picrite from Rùm as a starting composition are shown in Figs. 5.12 and 5.13. It should be noted that the ol(80%)+plag(80%)+mgt model could not run to completion, *i.e.*, it could not produce a melt with MgO of 4 wt.%. The models are able to explain at least some of the mafic dyke compositions with respect to all major elements (Fig. 5.12). However, these models still do not full explain the spread of data with regard to FeO, CaO, and Na_2O.

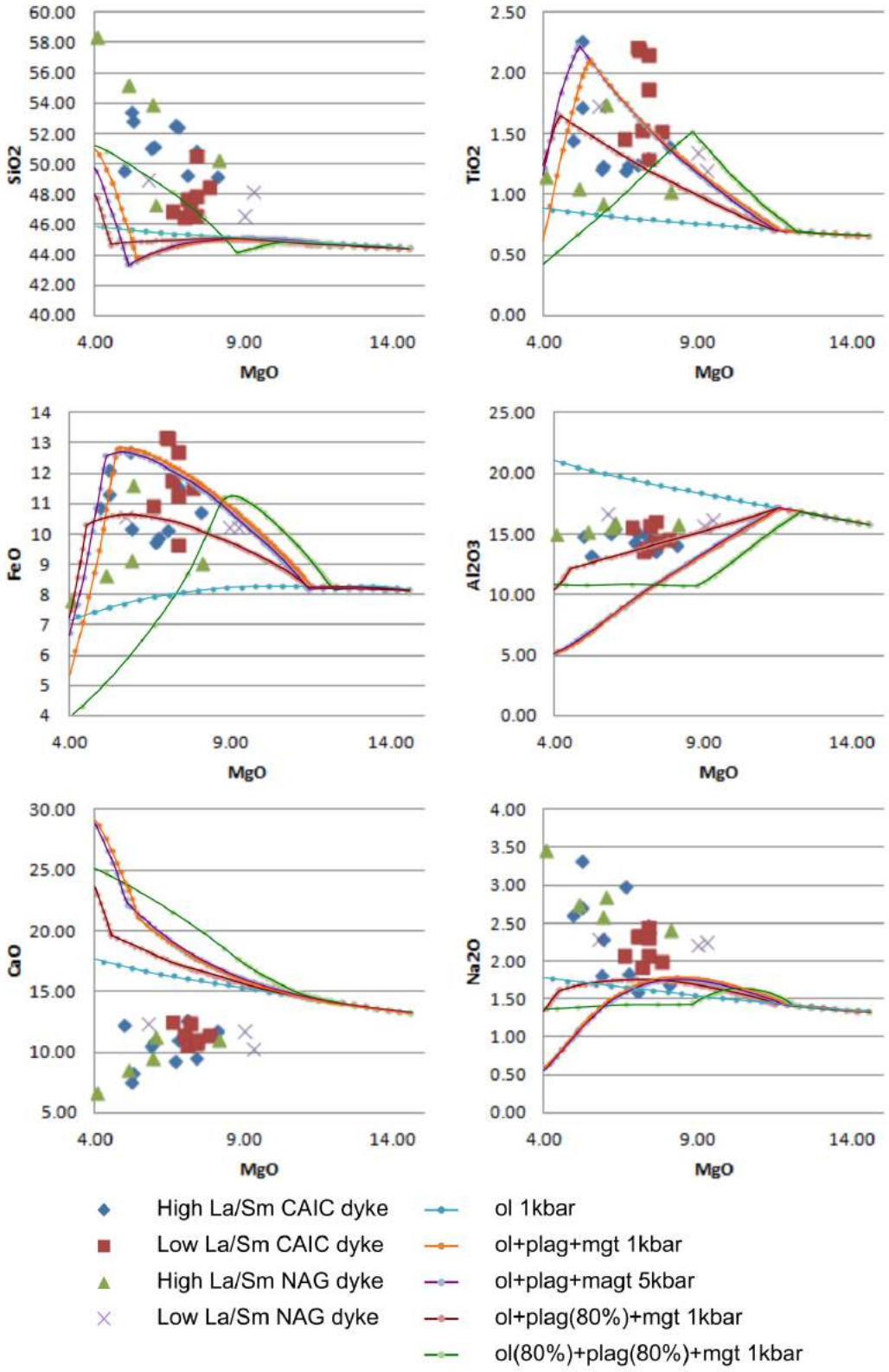

Fig. 5.10 – Major element bivariate plots showing the compositions of the mafic dykes of the CAIC and the North Arran Granite, with lines showing the modelled results of fractional crystallisation of the calculated Arran picritic magma composition.

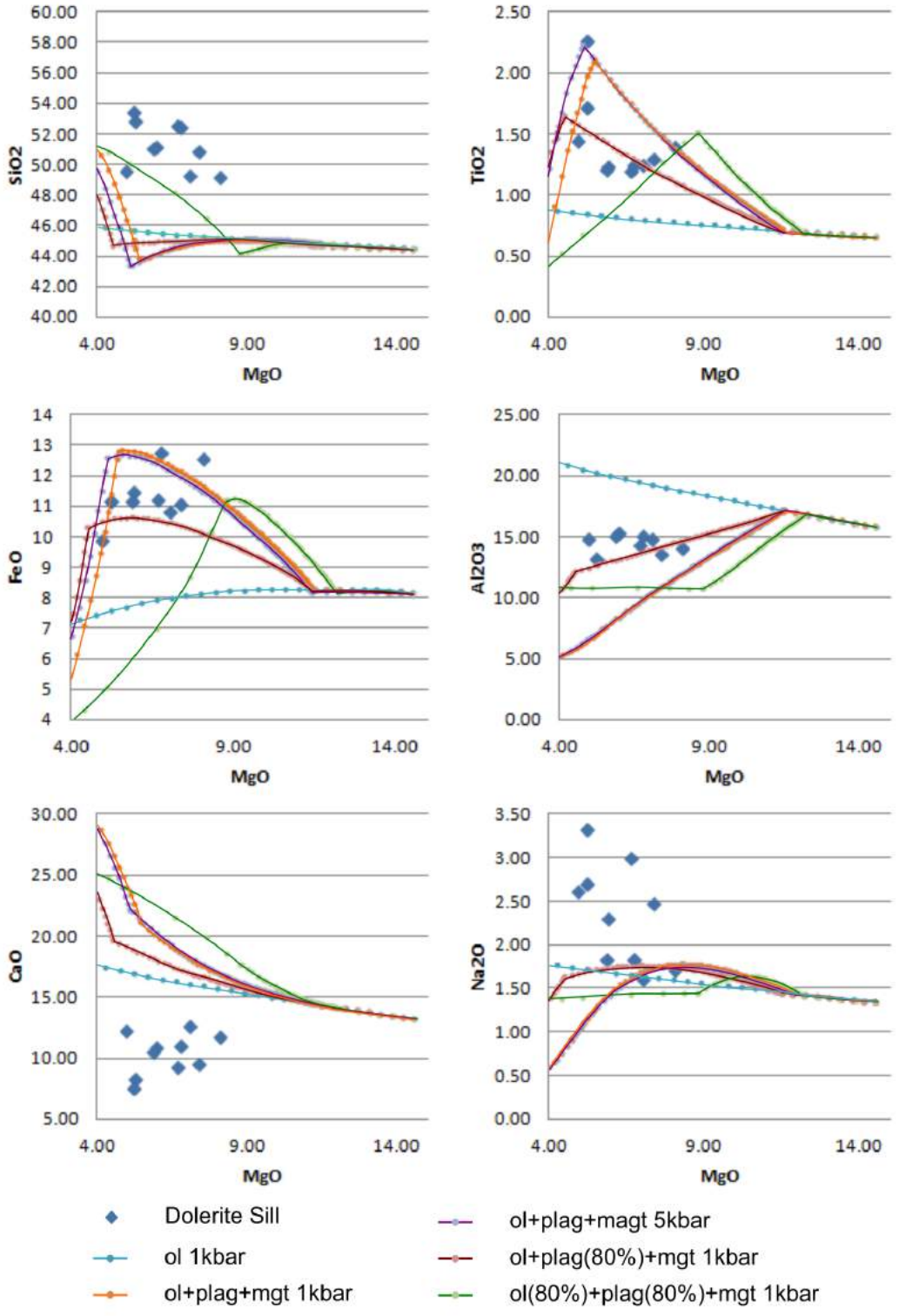

Fig. 5.11 – Major element bivariate plots showing the compositions of the CAIC dolerite sill samples, with lines showing the modelled results of fractional crystallisation of the calculated Arran picritic magma composition.

Unlike the models that start with the calculated Arran picritic magma, the M9 models show that 100% fractional crystallisation of only olivine can provide a reasonable fit to the mafic dyke data. However, petrography suggests that plagioclase and magnetite must have played at least some role in fractional crystallisation (Section 2.6). Of the models including fractionation of these minerals, the ol+plag(80%)+mgt model seems to provide the best match with the data, but this is not as good as the olivine-only model. Again, the fact that no models adequately explain the spread of CaO values suggest fractional crystallisation of clinopyroxene crystals that are not preserved as phenocrysts, possibly due to being dissolved at low pressures (Kerr, 1993; Thompson et al., 1980).

The fractional crystallisation of only olivine from picrite M9 can partly explain the range of certain elements in the dolerite sill that intrudes the CAIC (Fig. 5.13). None of the models explain the spread of SiO_2, CaO, or Na_2O data. Again, it is not surprising that the data cannot be fully explained by fractional crystallisation of a picritic melt, as the isotopic data show that this magma has been contaminated with crustal material.

Variation within groups

To assess whether the geochemical variation observed in the mafic dykes and dolerite sill are due to fractional crystallisation, models were run using the most primitive dykes from the CAIC and the North Arran Granite as starting compositions. The most primitive mafic dyke from the CAIC, in terms of SiO_2 and incompatible elements, is the one from which sample BJG/15/174 was collected. The most primitive dyke that intrudes the North Arran Granite based on SiO_2, MgO, and incompatible elements, is represented by sample ARA-5. Both belong to the low La/Sm group of dykes.

The results of modelling starting from the composition of sample BJG/15/174, along with the compositions of the mafic dykes and the dolerite sill, are shown in Figs. 5.14 and 5.15. These models do not adequately fit the spread of data between the mafic dykes and dolerite sill with regard to most elements.

When dyke ARA-5 from the North Arran Granite is used as the starting composition for the fractional crystallisation models, the spread of data of both the mafic dykes of the CAIC and the North Arran Granite, as well as the dolerite sill, can be adequately explained (Figs. 5.16, 5.17). No single model provides the best fit to the mafic dyke data with regard to all elements (Fig. 5.16), so while it can be reasonably assumed that fractional crystallisation is a possible source of geochemical variation among the dykes, it is hard to draw precise conclusions regarding minerals, pressure, and the amount of fractionation compared to equilibrium crystallisation. On the plots

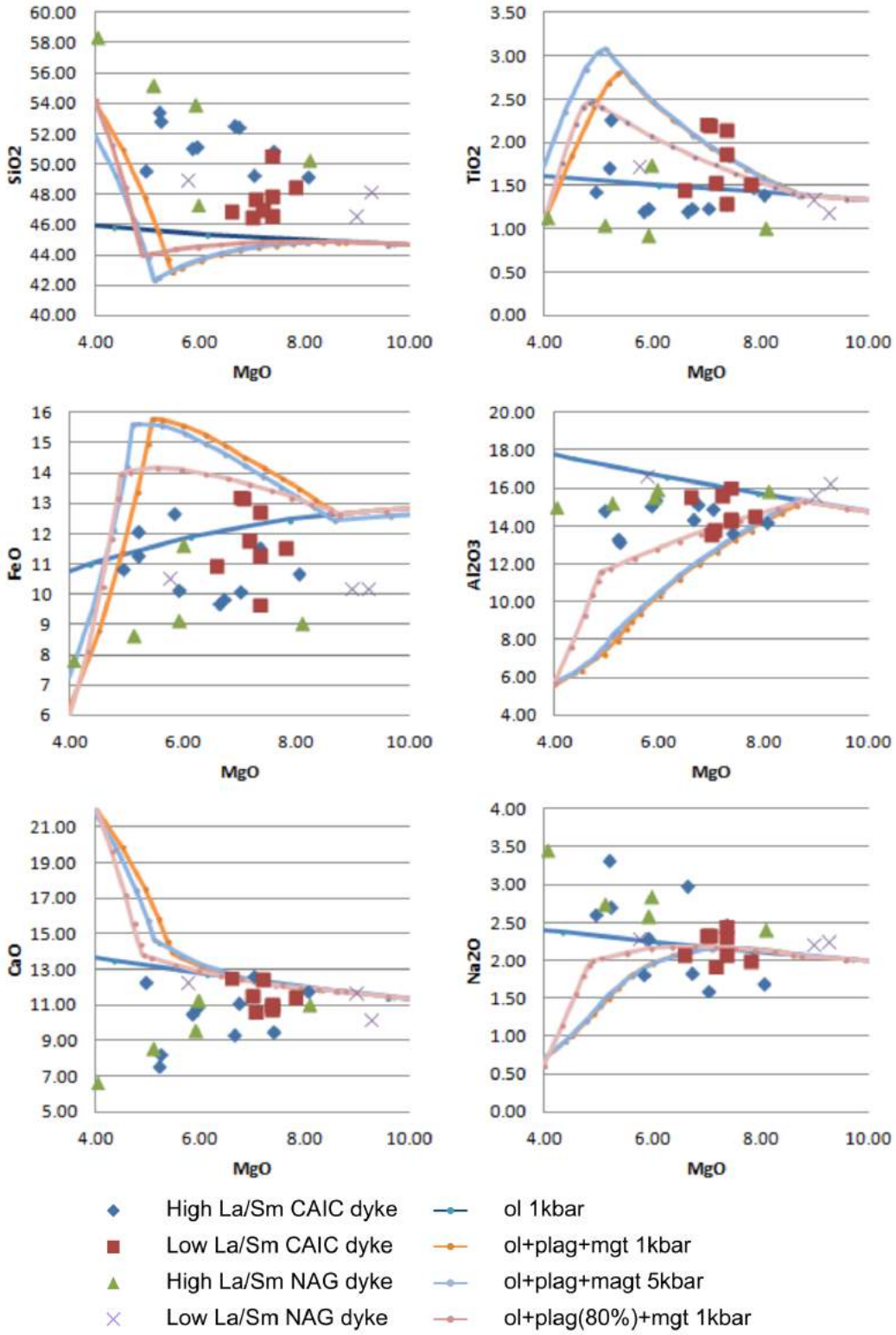

Fig. 5.12 – Major element bivariate plots showing the compositions of the mafic dykes of the CAIC and the North Arran Granite, with lines showing the modelled results of fractional crystallisation of the M9 picrite from Rùm (Upton et al., 2002).

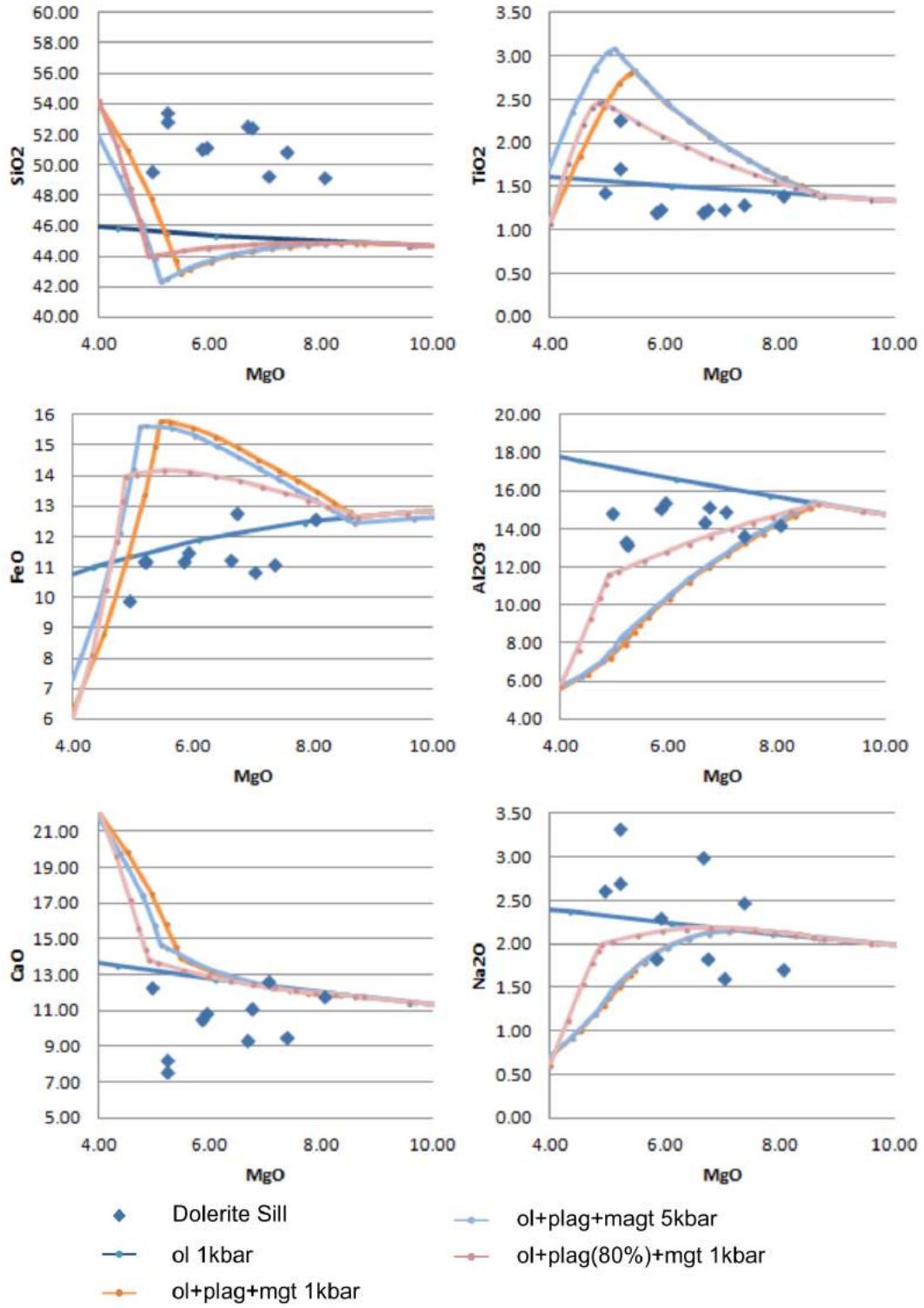

Fig. 5.13 – Major element bivariate plots showing the compositions of the CAIC dolerite sill samples, with lines showing the modelled results of fractional crystallisation of the M9 picrite from Rùm (Upton et al., 2002).

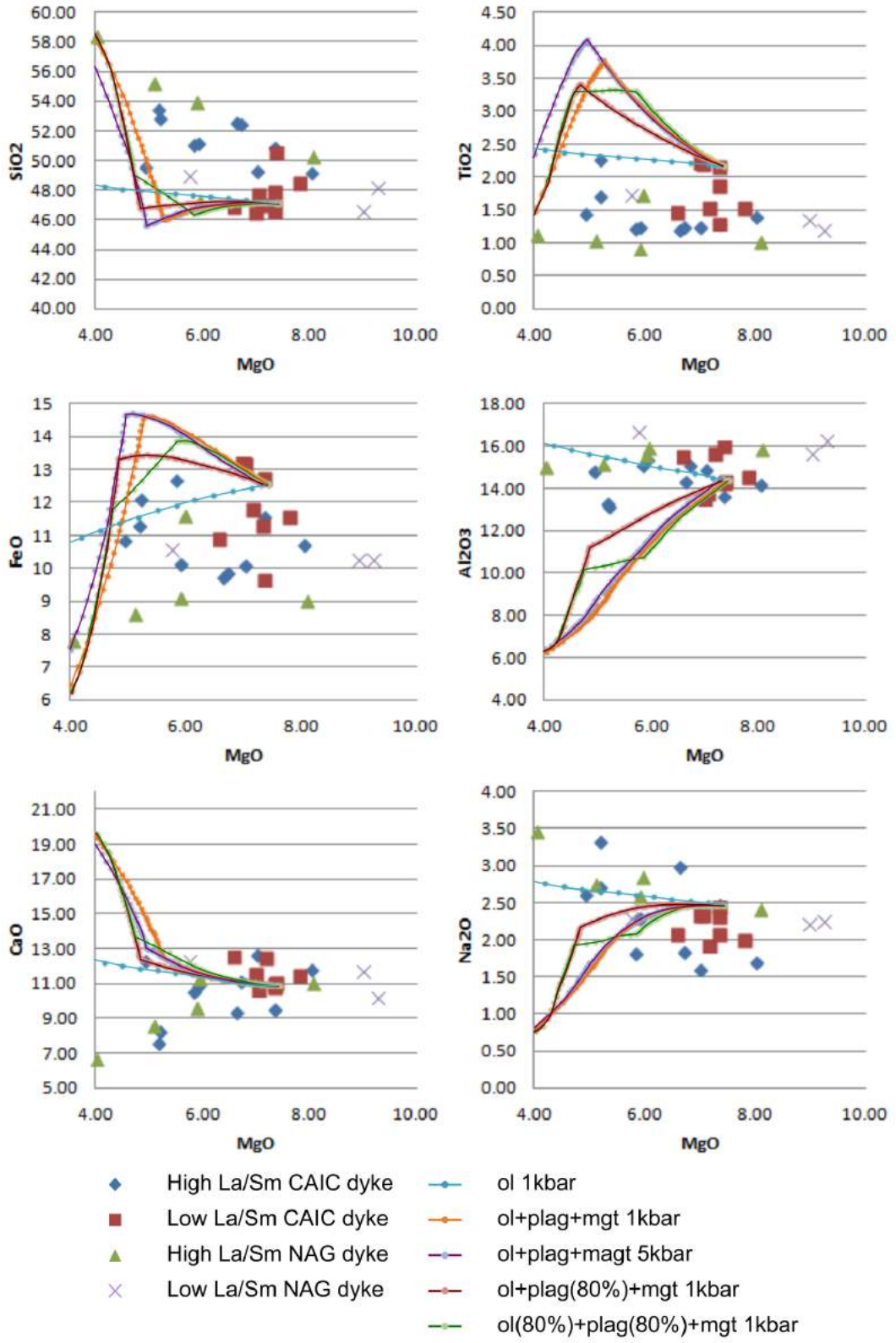

Fig. 5.14 – Major element bivariate plots showing the compositions of the mafic dykes of the CAIC and the North Arran Granite, with lines showing the modelled results of fractional crystallisation of the most primitive mafic dyke in the CAIC (sample BJG/15/174).

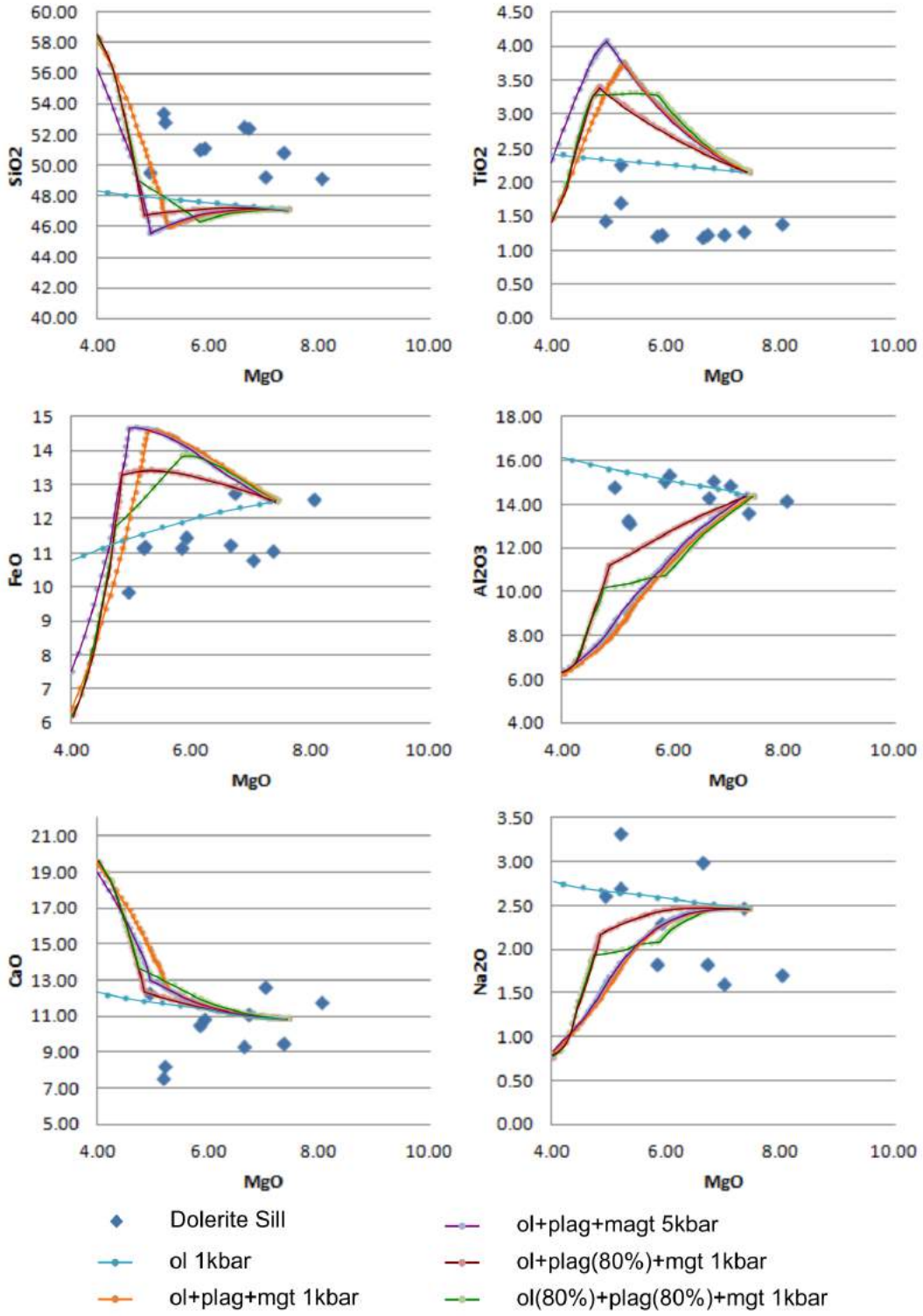

Fig. 5.15 – Major element bivariate plots showing the compositions of the CAIC dolerite sill samples, with lines showing the modelled results of fractional crystallisation of the most primitive mafic dyke in the CAIC (sample BJG/15/174).

of MgO vs. TiO_2, FeO, and Na_2O, it appears that the model in which only olivine is fractionating provides to best fit to the trend shown in the high La/Sm dykes.

Again, there is not a model which clearly fits the spread in dolerite sill data better than any of the others (Fig. 5.17). It can therefore be concluded that the sill magma could have formed from fractionation of a magma with the major element geochemistry of sampleARA-5, conclusions cannot be drawn regarding fractionating minerals, pressure, or the amount of fractional (as opposed to equilibrium) crystallisation.

Summary

Fractional crystallisation modelling shows that the magmas that were intruded as the mafic dykes in the CAIC and the North Arran Granite, and the dolerite dyke in the CAIC could have been formed from fractional crystallisation of a primary picritic melt. The models suggest that the magma that formed the mafic dykes could have formed from fractional crystallisation of olivine, plagioclase, and magnetite from a primary picritic magma. However, none of the models involving fractionation of these minerals explain the variations of all major elements. The models are particularly poor at producing the measured CaO and Na_2O concentrations. This is likely to reflect fractionation of plagioclase with a different composition to that in the model, or a different mineral entirely.

The parental magma was broadly similar in composition to the calculated Arran picritic magma (modelled by removing 15% olivine from sample BJG/15/338) or the M9 picrite from Rùm (Upton et al., 2002). The models suggest that olivine, or plagioclase, or both may not have experienced pure fractional crystallisation, and some of these minerals may have stayed in and equilibrated with the melt. These models agree with petrographic observations (the presence of plagioclase phenocrysts, magnetite, and occasional relict olivine phenocrysts). Given that isotopic data show that the majority of dykes are relatively uncontaminated, it's possible that fractional crystallisation from a primary melt is the dominant process in the petrogenesis of these magmas.

The models suggest that the dolerite sill in the CAIC may have been formed from the fractional crystallisation of olivine, magnetite, and plagioclase from a picrite with a composition similar to that of the calculated Arran picritic magma, or from fractional crystallisation of only olivine from a magma similar to the M9 Rùm picrite. As this magma is known to be contaminated by some amount of crustal material, fractional crystallisation of primary melt cannot be the only processes that formed the sill magma.

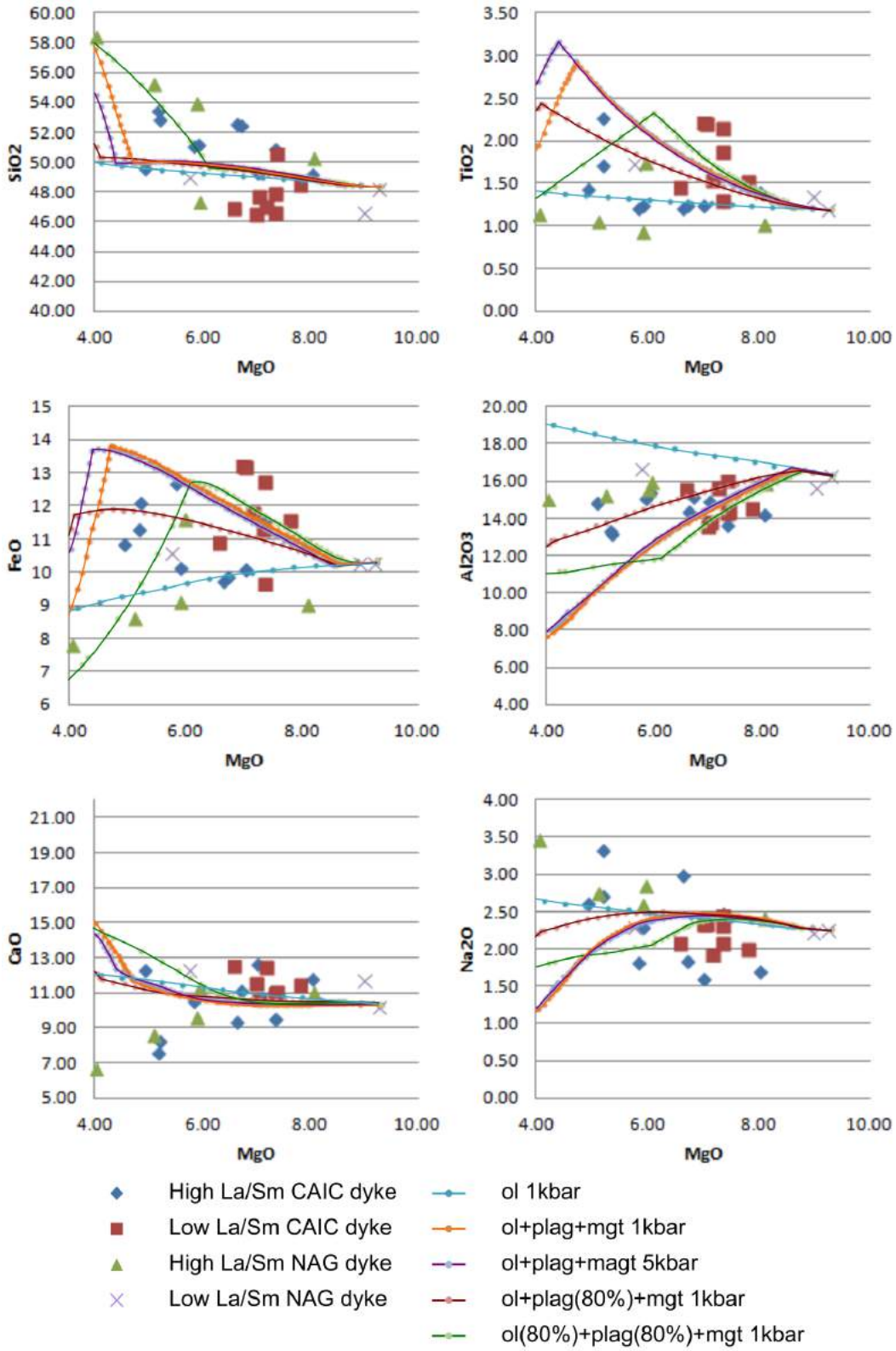

Fig. 5.16 – Major element bivariate plots showing the compositions of the mafic dykes of the CAIC and the North Arran Granite, with lines showing the modelled results of fractional crystallisation of the most primitive mafic dyke that intrudes the North Arran Granite (sample ARA-5).

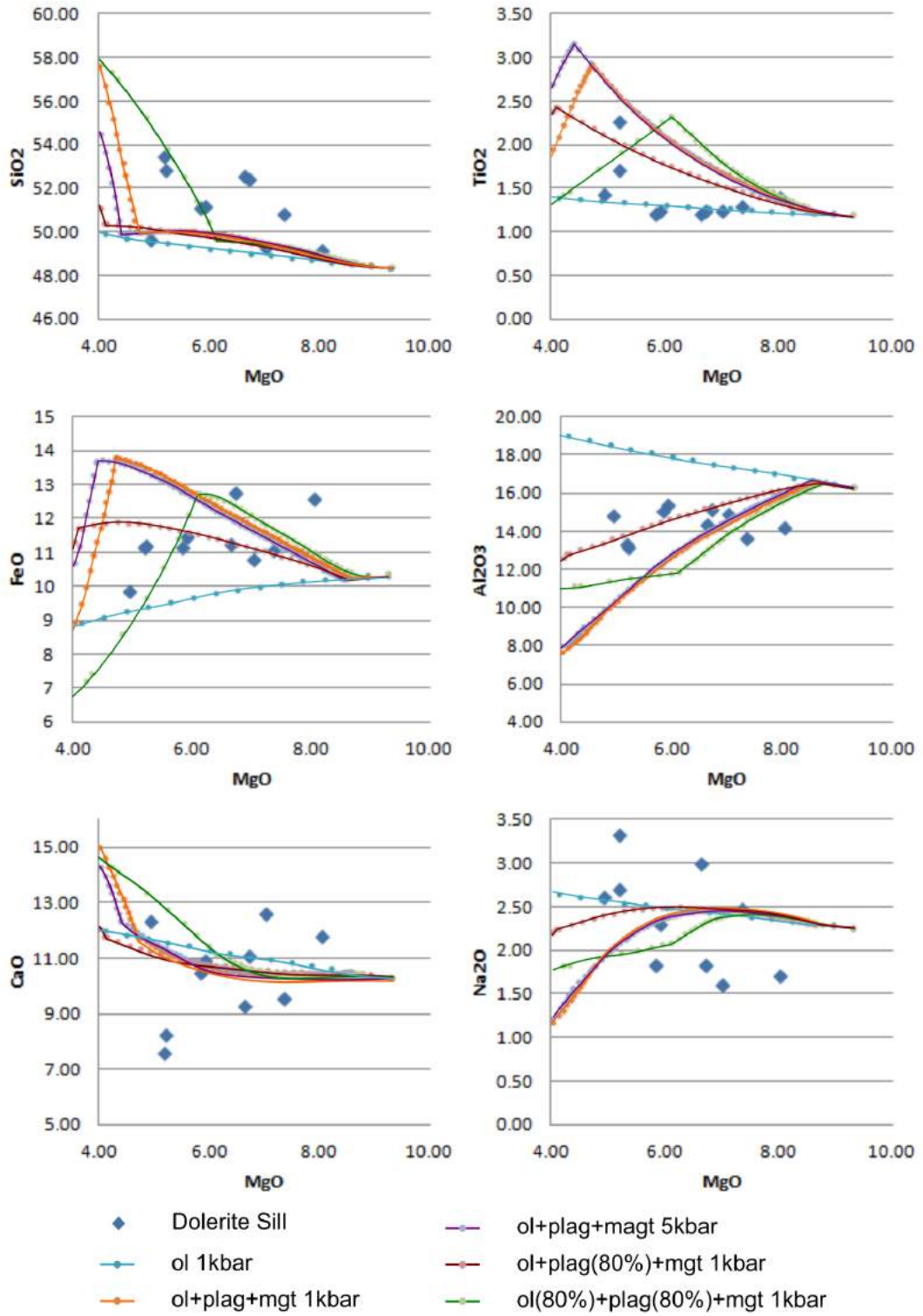

Fig. 5.17 – Major element bivariate plots showing the compositions of the CAIC dolerite sill samples, with lines showing the modelled results of fractional crystallisation of the most primitive mafic dyke that intrudes the North Arran Granite (sample ARA-5).

The modelling also suggests that fractional crystallisation of a magma with the composition of sample ARA-5 can account for the variation in major element geochemistry among the mafic dykes and the dolerite sill. This fractionation involved olivine±plagioclase±magnetite, but the pressure and amount of fractional crystallisation (as opposed to equilibrium crystallisation) cannot be determined.

5.3.2 Fractional Crystallisation in the Generation of Granitic Magmas

The fractionation of certain minerals during the evolution of granitic magmas can be assessed by studying certain trace elements. Depletion of elements which are only compatible in certain phases (compared to granitic melt) with progressive evolution suggests fractionation of that mineral. This section will look at depletions in Eu, Zr, Ba, and P_2O_5 in the silicic rocks of the CAIC and the North Arran Granite.

Eu anomalies

The chondrite-normalised REE diagrams for the silicic rocks analysed in this study presented in Section 4.1.4 show variable negative Eu anomalies (Figs. 4.27, 4.29, 4.31). Eu is more compatible in plagioclase (and to an extent, K-feldspar) than other REEs with respect to granitic magma (https://earthref.org/KDD/), so negative Eu anomalies can indicate plagioclase fractionation.

Eu anomalies (Eu/Eu^*) can be quantified by comparing the chondrite normalised Eu value with the value predicted from chondrite normalised Sm and Gd values:

$$Eu/Eu^* = Eu_n/\left(\frac{Sm_n + Gd_n}{2}\right)$$

meaning that 'positive' Eu anomalies have $Eu/Eu^*>1$ and 'negative' Eu anomalies have $Eu/Eu^*<1$.

Eu/Eu^* values for the silicic rocks analysed in this study are plotted against Nb, SiO_2, and Zr in Fig. 5.18. The majority of the silicic Glenloig Hybrids and Satellite Granites have minor negative Eu anomalies, with Eu/Eu^* between 0.5 and 1. The Glen Craigag Granite and the pitchstone dyke that intrudes the CAIC have moderate negative Eu anomalies, with Eu/Eu^* around 0.3 – 0.6. The group with the lowest Eu anomalies includes the North Arran Granite, the granite clasts found in the ignimbrites of the CAIC, and the rhyolitic lava-like ignimbrites of the CAIC, which largely have $Eu/Eu^* < 0.3$ (Fig. 5.18).

These data suggest that this latter group (North Arran Granite, granite clasts, lava-like ignimbrites) formed from magmas that fractionated significant amounts of

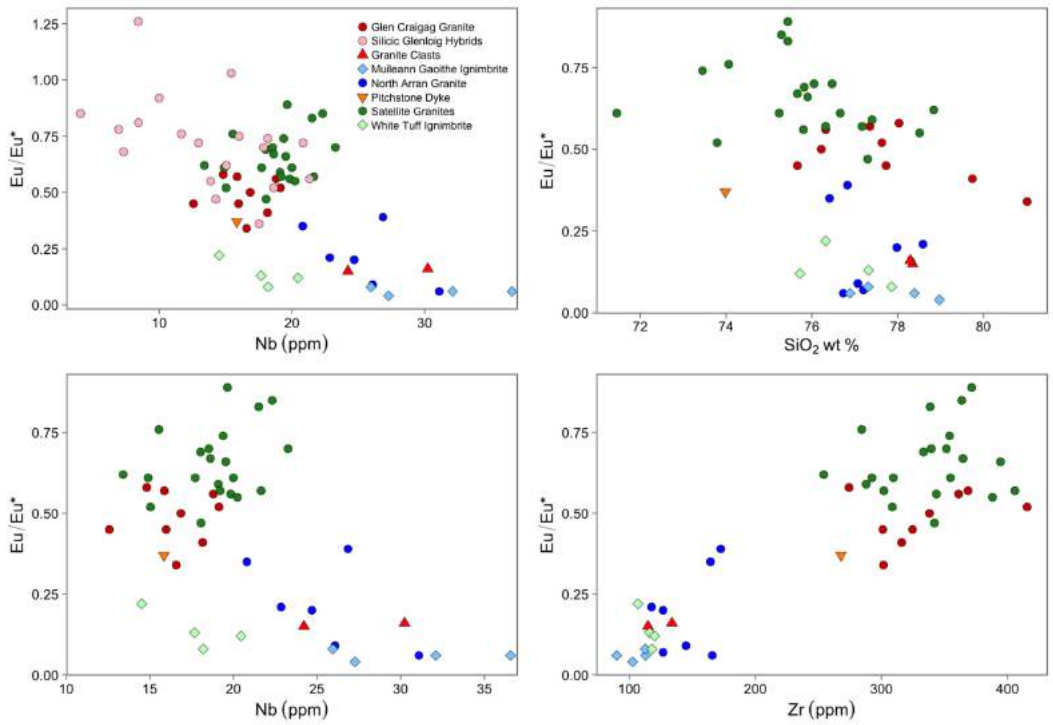

Fig. 5.18 – Binary plots of Nb, Zr, and SiO_2 (as measures of fractionation) against Eu/Eu* for the silicic rocks from the CAIC, as well as the North Arran Granite (the second Nb vs. Eu/Eu* plot omits the silicic Glenloig Hybrids to better display patterns in the other data).

plagioclase±K-feldspar during their evolution. The Glen Craigag granite and the pitchstone dyke also show evidence of fractionation of feldspars with evolution. The Satellite Granites and the silicic Glenloig Hybrids have Eu compositions that suggest that fractionation of plagioclase (±K-feldspar) played less of a role in the magmatic evolution of these units towards granitic compositions.

Zr, Ba, TiO_2, and P_2O_5

Zr, Ba, Ti, and P are compatible in certain minerals that crystallise from granitic melts; Zr in zircon, Ba in K-feldspar, Ti in Fe-Ti oxides, and P in apatite (https://earthref.org/KDD/). The evolution trends (plotted against Nd and SiO_2) of these elements in the silicic rocks analysed in this study are shown in Fig. 5.19.

The Nb vs. Zr plot shows a clear trend of increasing Zr with magmatic evolution (increasing Nb) among the silicic Glenloig Hybrids, the Glen Craigag Granite, the Satellite Granites, and the pitchstone dyke. This trend is seen less clearly in the SiO_2 vs. Zr plot. A second trend is shown by the North Arran Granite, the granite clasts found in the ignimbrites of the CAIC, and the rhyolitic lava-like ignimbrites of

the CAIC. These units are as evolved, or more so, than the other granites (equal or greater Nb and SiO_2 concentrations), but define a flat array of very low Zr values. This is clear evidence for the fractionation of zircon in the evolving granitic melt. Watson (1979) determined that the saturation level of zircon depends strongly on molar $(Na_2O + K_20)/Al_2O_3$, a measure of peralkalinity. More peralkaline granitic liquids retain Zr to higher concentrations before zircon fractionates. This is a possible geochemical reason for the low Zr contents in only certain units. However, when Zr is plotted against $(Na_2O + K_20)/Al_2O_3$, there is no correlation, suggesting other factors must determine the fractionation of zircon in the granitic melts (Fig. 5.20).

It should be noted that these low-Zr units also make up the group that have the greatest negative Eu anomalies (Fig. 5.18). This suggests fractionation of both zircon and plagioclase in these melts, to a greater extent than any of the other units. (Although Eu is moderately compatible in zircon, it is no more compatible than Sm or Gd (https://earthref.org/KDD/), so zircon fractionation cannot produce a negative Eu anomaly.)

The patterns seen in the Zr plots are also seen in the Ba plots (Fig. 5.19), *i.e.*, Ba increases with fractionation in the silicic Glenloig Hybrids, CAIC granites, and pitchstone dyke, and forms a flat array at low values in the low-Zr group (North Arran Granite, the granite clasts, and the rhyolitic lava-like ignimbrites). This shows that these magmas, as well as fractionating plagioclase and zircon, also fractionated K-feldspar during their evolution.

The low-Zr group also cluster on the TiO_2 diagrams, with concentrations around 0.1 wt.% or lower (Fig. 5.19). These units therefore must also have fractionated Fe-Ti oxides during evolution. The Glen Craigag and Satellite Granites have similar TiO_2 levels, with the Satellite Granites possibly defining a trend below that of the Glen Craigag granite. The CAIC pitchstone dyke has the highest TiO_2. Petrography suggests that it accumulated Fe-Ti oxides at some stage in its evolution.

The North Arran Granite and the Glen Craigag Granite are the units with the lowest P_2O_5 concentrations, suggesting that fractional crystallisation of apatite played a significant role in their evolution (Fig. 5.19).

Summary

The silicic Glenloig Hybrids and the Satellite Granites have minor negative Eu anomalies, suggesting relatively little fractional crystallisation of feldspars during evolution of the melt. This indicates that their petrogenesis involved processes other than simple fractional crystallisation of mafic magmas. The Zr and Ba concentrations

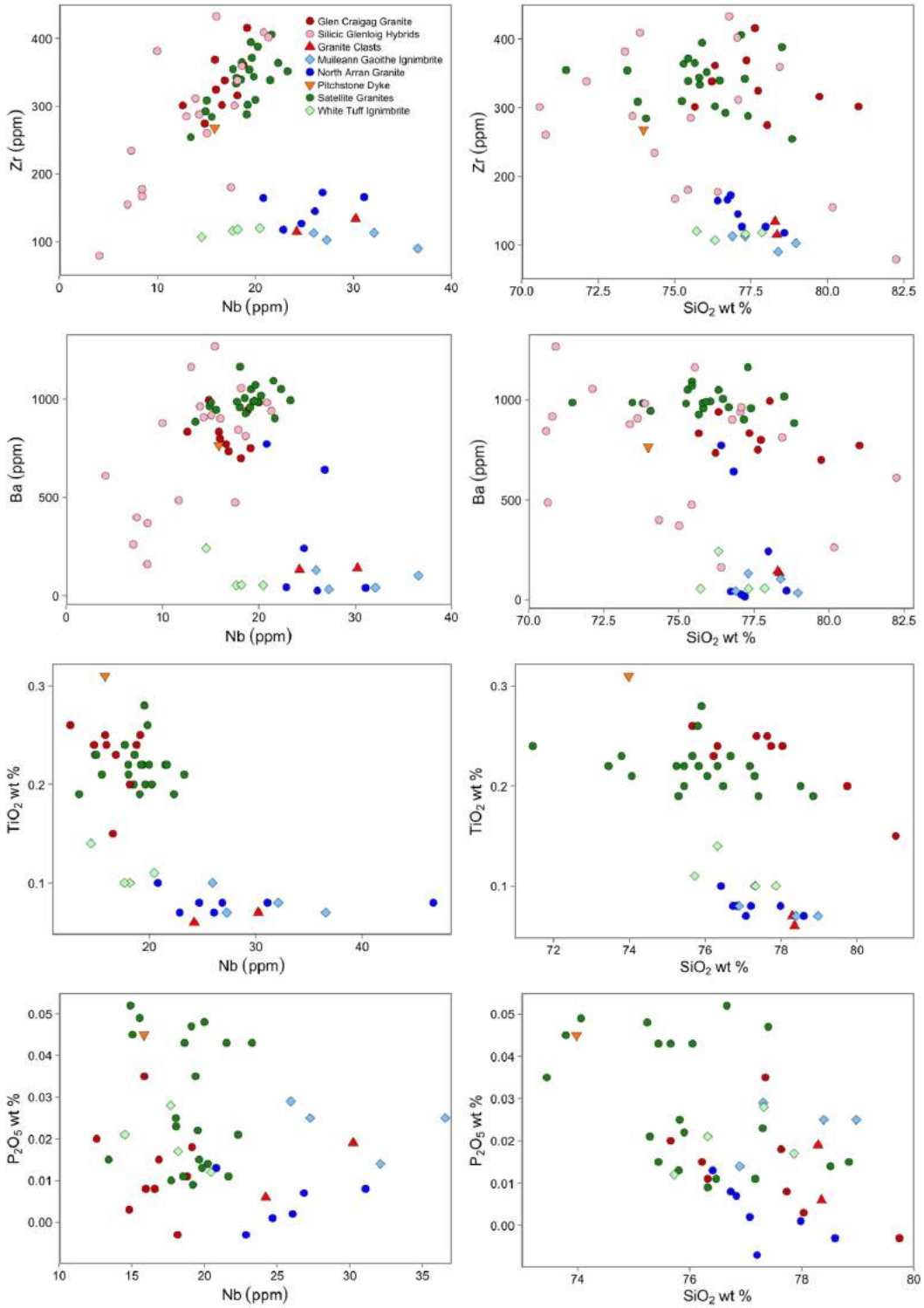

Fig. 5.19 – Binary plots of Nb and SiO_2 against Zr, Ba, TiO_2, and P_2O_5 for the silicic rocks from the CAIC, as well as the North Arran Granite.

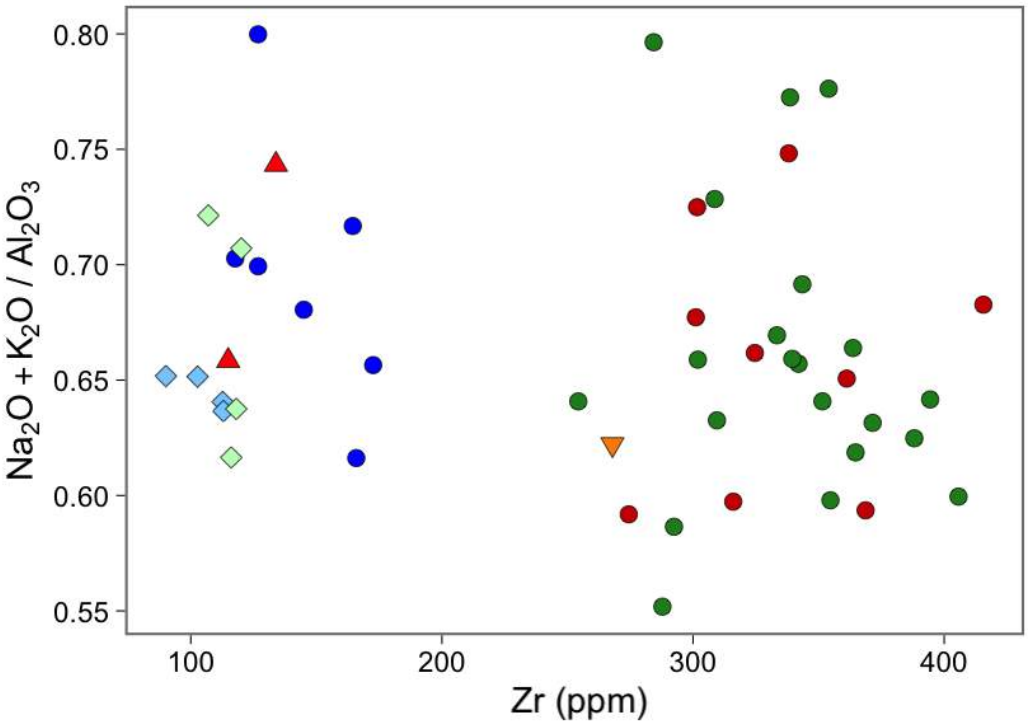

Fig. 5.20 – Binary plot of Zr against $(Na_2O + K_20)/Al_2O_3$ to determine whether peralkilinity is the primary control on zircon fractionation (sec. Watson, 1979). Symbols as Fig. 5.19

of these units also increase with increasing magmatic evolution, showing that zircon and K-feldspar did not significantly fractionate either.

The Glen Craigag Granite and the pitchstone dyke that intrudes the CAIC have moderate Eu anomalies, suggesting that fractionation of plagioclase was a significant process in the evolution of these melts. They also have Zr and Ba concentrations that suggest zircon and K-feldspar were not fractionated. The main difference between these two intrusions is P_2O_5. The Glen Craigag Granite has amongst the lowest P_2O_5 concentrations of all the silicic units analysed, suggesting the fractional crystallisation of apatite. The pitchstone dyke has a much higher P_2O_5 concentration, suggesting apatite was not fractionated to the same extent.

The North Arran Granite, the granite clasts found in the ignimbrites of the CAIC, and the two rhyolitic lava-like ignimbrite members of the CAIC (Muileann Gaoithe and the White Tuff) belong to a group defined by large negative Eu anomalies, and low Zr and Ba concentrations. This suggests that these rocks were formed from magmas in which plagioclase, zircon, and K-feldspar were fractionated to a significant degree. The P_2O_5 concentrations suggest that the North Arran Granite magma fractionated apatite, while the granite clasts and the lava-like ignimbrites may have fractionated small amounts of apatite.

It appears from these fractional crystallisation histories that the rhyolitic lava-like ignimbrites of the CAIC show more affinity with the North Arran Granite than the granites of the CAIC. The same is true of the granite clasts found in the massive lapilli tuffs of the CAIC.

5.4 Crustal Contamination

The magmas that were intruded into the shallow crust on Arran ascended through a significant thickness of continental crust from the location of melting in the asthenospheric mantle. The interaction of these magmas with the crustal units through which they passed can be studied geochemically, and can be used to answer two broad questions: what was the role of crustal assimilation in the petrogenesis of these magmas, and what can their contaminants tell us about their path through the crust and the structure and composition of the crust in the region?

The continental crustal architecture of this region is complex in three dimensions (Fig. 1.1). The Highland Boundary Fault is known to cross Arran at depth, and the crustal terranes on either side (the Grampian Terrane to the north and the Midland Valley Terrane to the south) are not homogenous and are thought to be, at least to an extent, vertically stratified. By comparing geochemistry and modelling the

interactions between these geochemically distinct crustal units and mantle-derived melts, we can assess which units the magmas were contaminated by, and where in the crust they spent time during ascent.

The Grampian Terrane to the north of the Highland Boundary Fault is largely made up of the Dalradian schists at the surface in the Clyde region. Isotopic data for the Dalradian rocks on Arran is presented in Dickin et al. (1981) and Dickin (1994). For trace element data, the Dalradian-derived leucogranites (partial melts) of Johnson et al. (2003) are used as the closest approximation of Dalradian melts that could be contributing to the compositions of the Arran magmas. It should be noted that this is the only partial melt source that will be discussed, as no geochemical data exist for partial melts of the other crustal units.

The basement to the Dalradian Supergroup is thought to be represented by the Proterozoic gneissic rocks of the Islay Block (Fig. 1.1), exposed on the Rhinns of Islay. This unit is assumed to make up the crust below the Dalradian schists immediately to the north of the Highland Boundary Fault. Isotopic data for these rocks is presented in Marcantonio et al. (1988). Trace element data is taken from the Rhinns Complex syenites, as published in Muir et al. (1994).

The surface of the Midland Valley Terrane is entirely made up of Palaeozoic sedimentary rocks. The basement is not exposed anywhere, but lower crustal xenoliths have been recovered from numerous Permian and Carboniferous dykes and sills across the region. Their trace element and isotopic geochemistry is presented by Halliday et al. (1993).

The Lewisian gneisses of the Hebridean Terrane are not thought to exist south of the Great Glen Fault (Fig. 1.1), and are not exposed closer than the island of Iona, 100 km from Arran. However, average trace element profiles for Lewisian amphibolite and granulite gneisses from Weaver and Tarney (1981) are shown for comparison. This may be useful as the Lewisian gneisses are an important source of crustal melts in similar studies of the other Hebridean centres (e.g. Gibson, 1990; Kerr et al., 1995; Troll et al., 2004), although it is unlikely to have had a real influence on the genesis of the Arran magmas.

5.4.1 Trace Elements

The trace element patterns of the analysed Arran rocks (discussed in Section 4.1.3) are plotted on primitive mantle normalised (Sun and McDonough, 1989) trace element diagrams along with published trace element data for the various crustal units that could be the source of contamination of these magmas (Figs. 5.21 – 5.32). It should be stressed that trace element signatures can be greatly altered by post-melt

generation processes; for example, Sr and Ti are largely influenced by the behaviours of plagioclase and Fe-Ti oxides, respectively, in the magma. With these processes in mind, these graphs can still provide insight into the input of crustal material into the Arran magmas.

Mafic units

The trace element profiles of the mafic rocks analysed in this study are shown in Figs. 5.21 – 5.24. These include the mafic dykes that intrude the CAIC and the North Arran Granite, the dolerite sill that intrudes the pyroclastic rocks of the Arran Volcanic Formation, and the gabbros associated with the Glenloig Hybrids in the CAIC. The magmas that formed the mafic intrusions cannot contain large amounts of melt derived from any of the crustal units discussed, and any partial melts would be silicic in composition. However, it is possible that relatively minor contamination could be the source of certain trace element signatures.

The mafic dykes that intrude the CAIC have flat trace element profiles in elements more compatible than Nb. The high La/Sm group is enriched in Rb and Ba and depleted in Nb, while the low La/Sm group shows very slight Ba enrichment and Nb depletion, but no Rb enrichment.

The Dalradian leucogranites are the most likely unit to have influenced the enrichment of both Rb and Ba in the high La/Sm group, although a Lewisian-like source could also have caused this. The low Rb/Ba ratio of the low La/Sm dykes is more akin to the trace element pattern of the Midland Valley crust. The Midland Valley samples have the closest overall shape to the CAIC dykes – this may be expected, as the CAIC lies south of the Highland Boundary Fault, *i.e.*, in the Midland Valley Terrane. The Rhinns Complex syenites have the most pronounced negative Nb anomaly. This may have influenced the Nb concentrations of some of the high La/Sm dykes.

The dykes which intrude the North Arran Granite show the same general trends as those in the CAIC. The high La/Sm group is highly enriched in Rb and Ba, with a negative Nb anomaly. The low La/Sm group does not show these trends, and has a slightly more incompatible-element-depleted general pattern. The high La/Sm group has higher incompatible element concentrations than the high La/Sm dykes in the CAIC. This may be due to their slightly more evolved overall compositions.

Much like the CAIC dykes, the Rb and Ba enrichment of the high La/Sm group could have been formed by interaction with Dalradian-derived melts (again, to be expected as these dykes were emplaced into the Grampian Terrane), while the

low La/Sm group has flatter patterns more similar to the Midland Valley basement xenoliths.

The high La/Sm North Arran Granite dykes show similar trace element patterns to the Lewisian gneisses. This source of contamination cannot be ruled out, as magma is known to travel laterally for large distances in the form of dykes, but Lewisian crust is not thought to be a realistic contaminant of the Arran magmas.

The dolerite sill that intrudes the pyroclastic rocks of the Arran Volcanic Formation has a convex-up trace element pattern with an apex at Sr, that mirrors its REE profile. It has significant Ba enrichment and Nb depletion, with variable Rb – although most samples have greatly depleted Rb relative to Ba. This pattern of extreme Rb and Nb depletion and Ba enrichment suggests interaction with Rhinns Complex material. The overall shape, especially in the most incompatible elements also closely matches the Midland Valley xenoliths' trace element pattern.

The enriched Rb and Ba, and depleted Nb signatures of the gabbros are more similar to the Dalradian leucogranites, but also closely match the pattern of the Midland Valley xenoliths.

Certain trace element ratios can be used to study contamination relationships in more detail. The La/Nb ratio of the mafic rocks is plotted against chondrite-normalised (McDonough and Sun, 1995) La/Nd in Fig. 5.25, along with the possible crustal contaminants discussed in this section. The same information is presented in Fig. 5.26, with the ratios rearranged to have La in the denominator of both – this makes any binary mixing lines straight.

Both of these diagrams show that all of the mafic dykes and the gabbros define a trend from the average N-MORB composition towards the Midland Valley and Dalradian crust. The low La/Sm dykes (of both the CAIC and North Arran Granite) show significantly less contaminated compositions on these graphs.

The dolerite sill that intrudes the CAIC has restricted range of chondrite normalised La/Nd, but forms a clear trend towards high La/Nb (low Nb/La) values. The only crustal rocks with sufficiently high La/Nb are the Rhinns Complex syenites. However, Fig. 5.26 suggests that the sill magma was contaminated by a unit with higher chondrite normalised Nd/La than the Rhinns syenites.

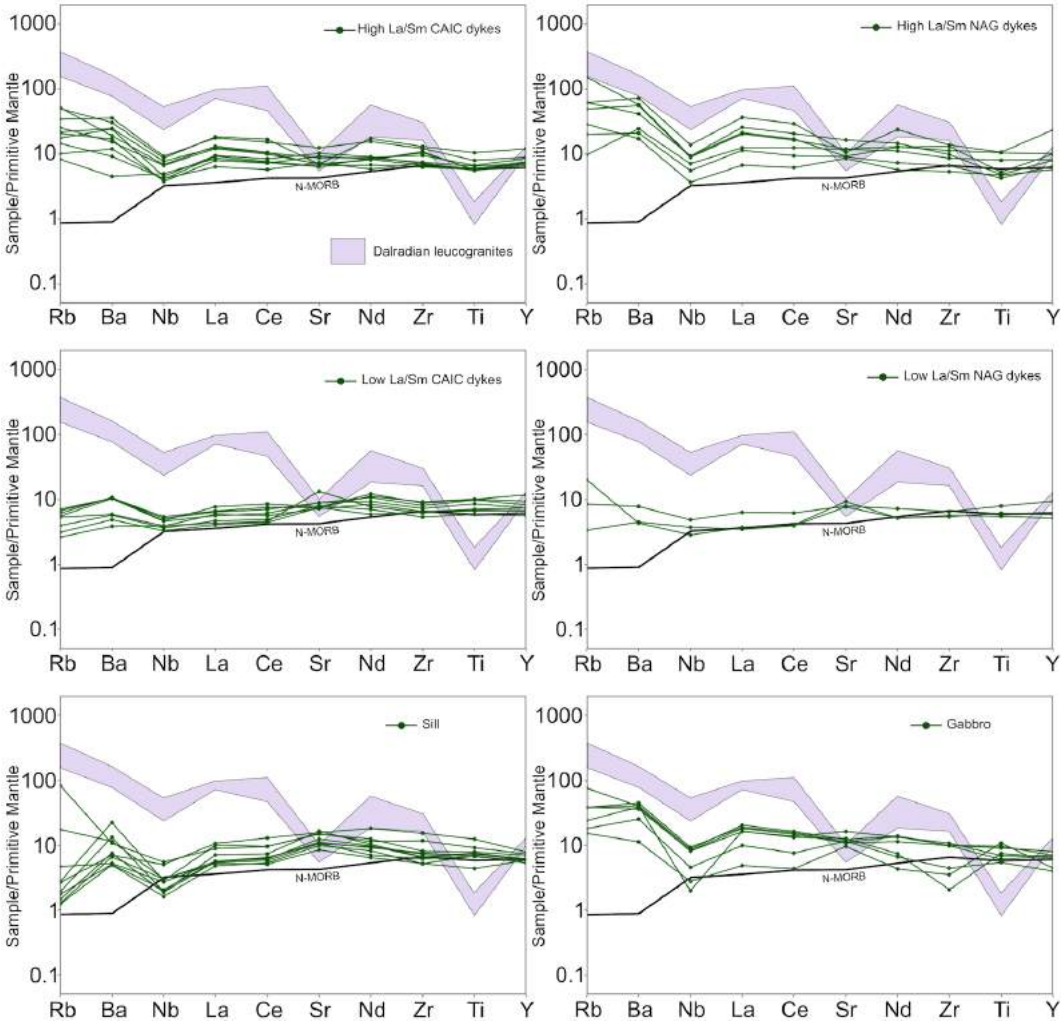

Fig. 5.21 – Primitive mantle normalised (Sun and McDonough, 1989) trace element diagrams for the mafic Arran rocks analysed in this study, along with data for Dalradian-derived leucogranites from Johnson et al. (2003).

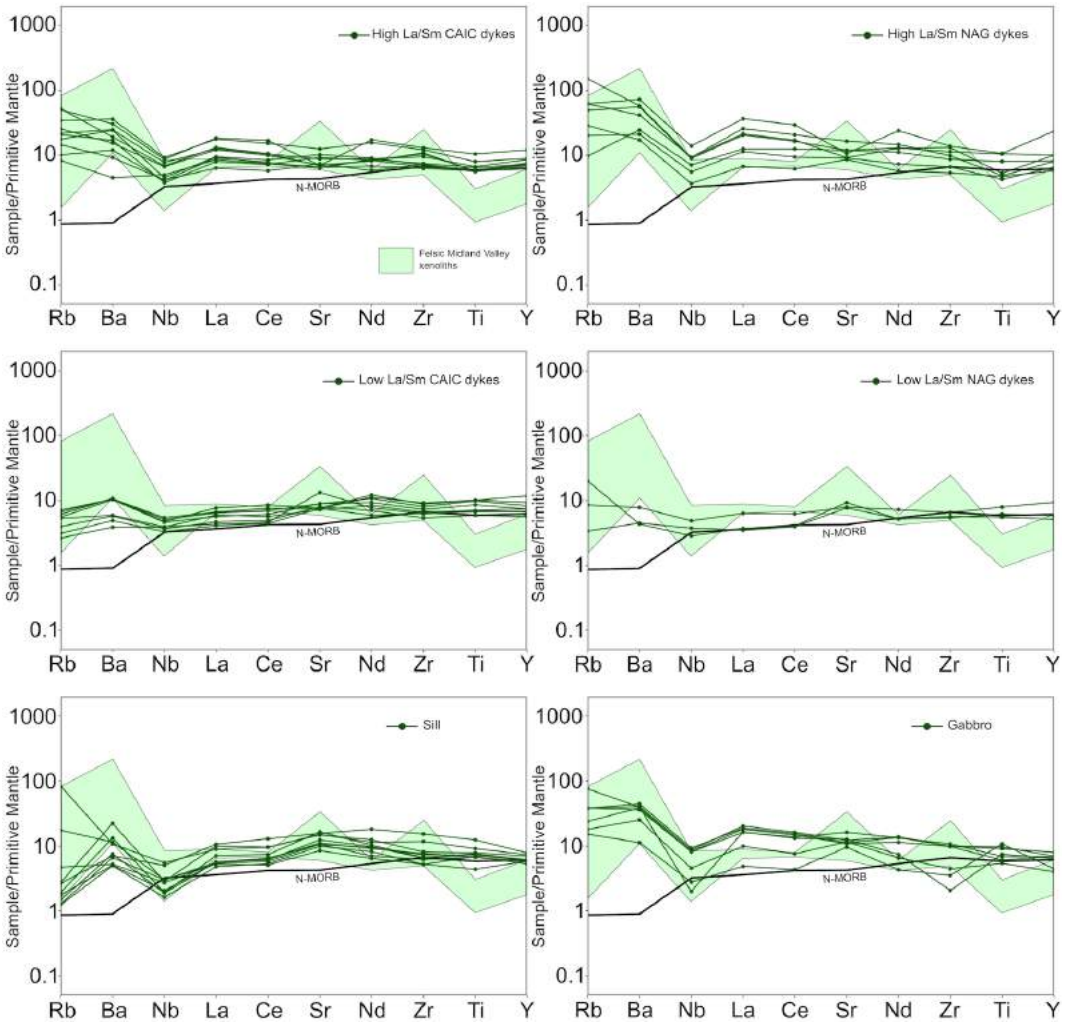

Fig. 5.22 – Primitive mantle normalised (Sun and McDonough, 1989) trace element diagrams for the mafic Arran rocks analysed in this study, along with data for the felsic Midland Valley xenoliths presented in Halliday et al. (1993).

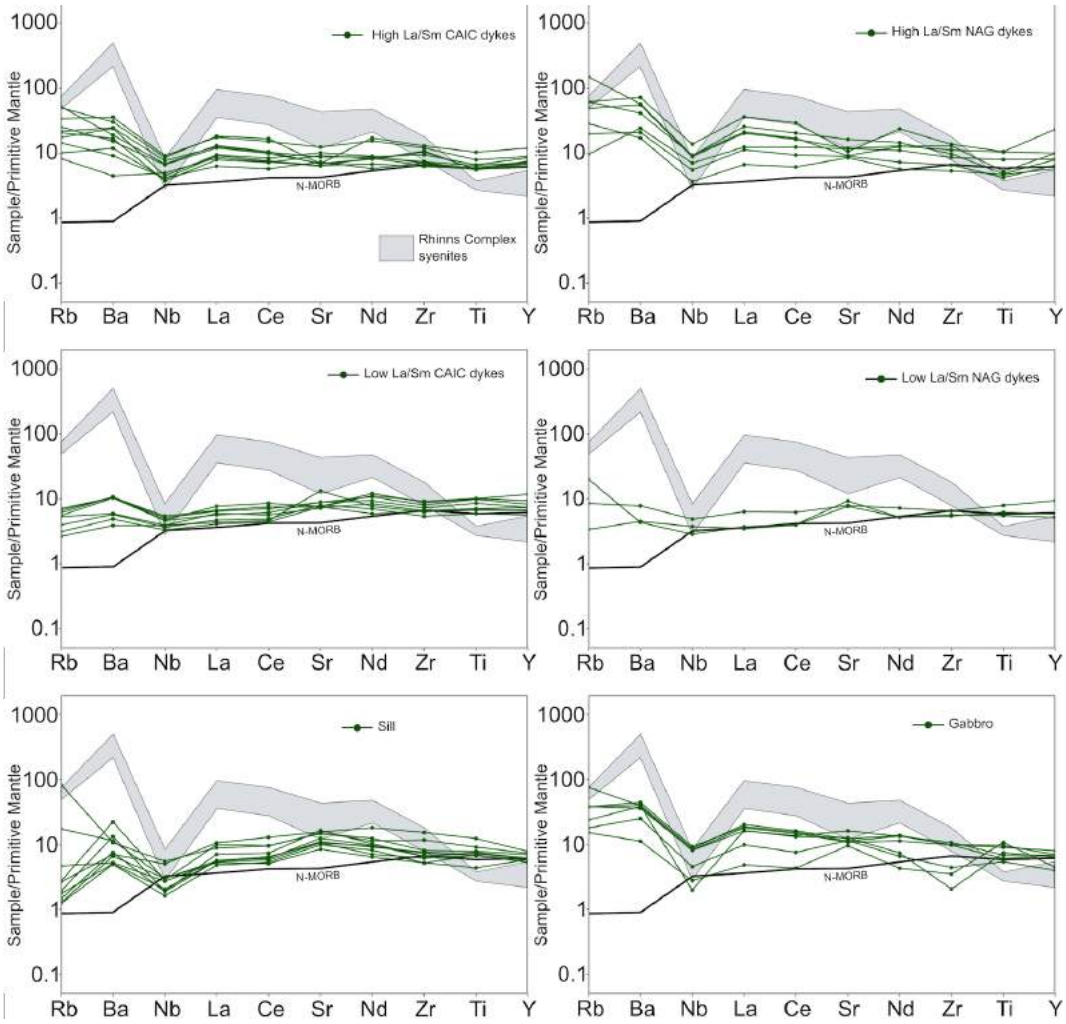

Fig. 5.23 – Primitive mantle normalised (Sun and McDonough, 1989) trace element diagrams for the mafic Arran rocks analysed in this study, along with data for the Rhinns Complex syenites from Muir et al. (1994).

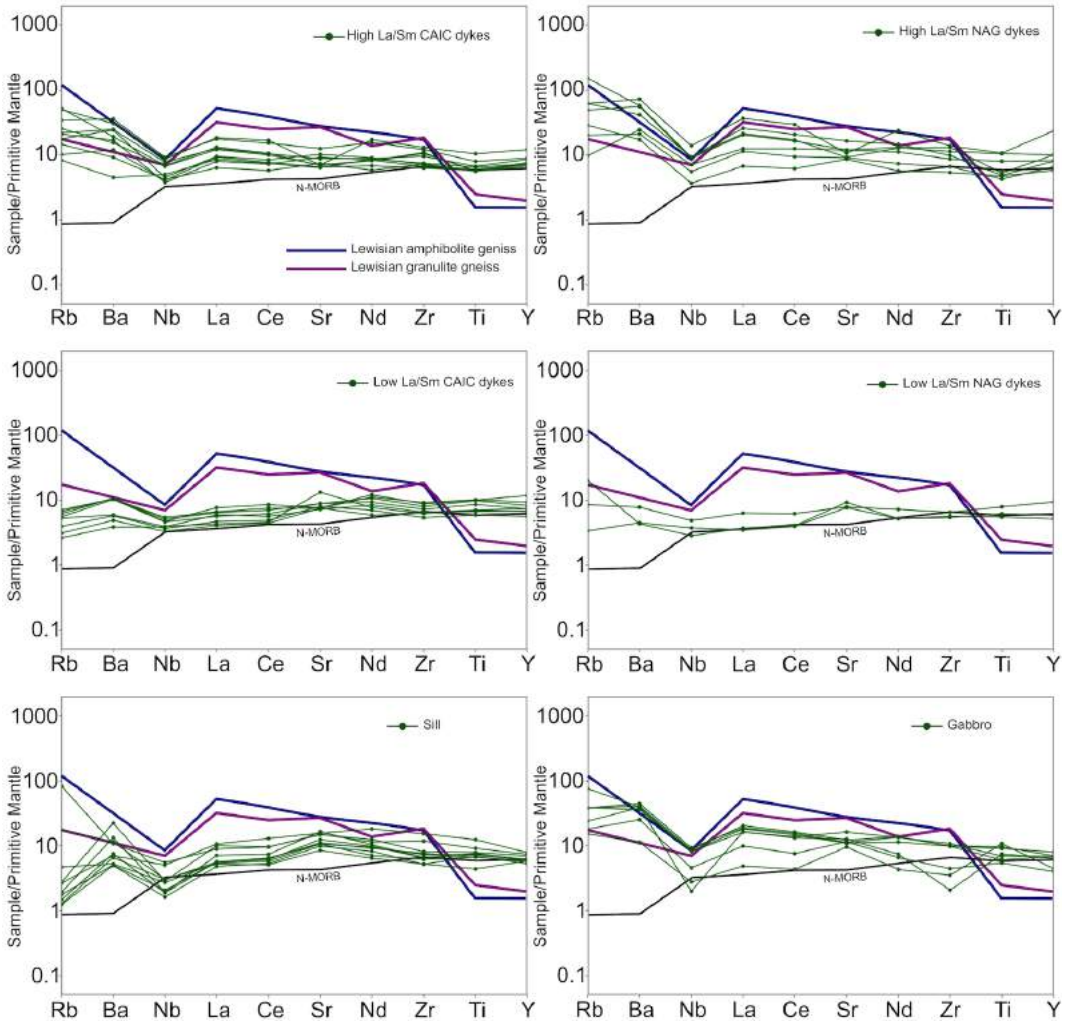

Fig. 5.24 – Primitive mantle normalised (Sun and McDonough, 1989) trace element diagrams for the mafic Arran rocks analysed in this study, along with data for average Lewisian amphibolite- and granulite-grade gneisses from Weaver and Tarney (1981).

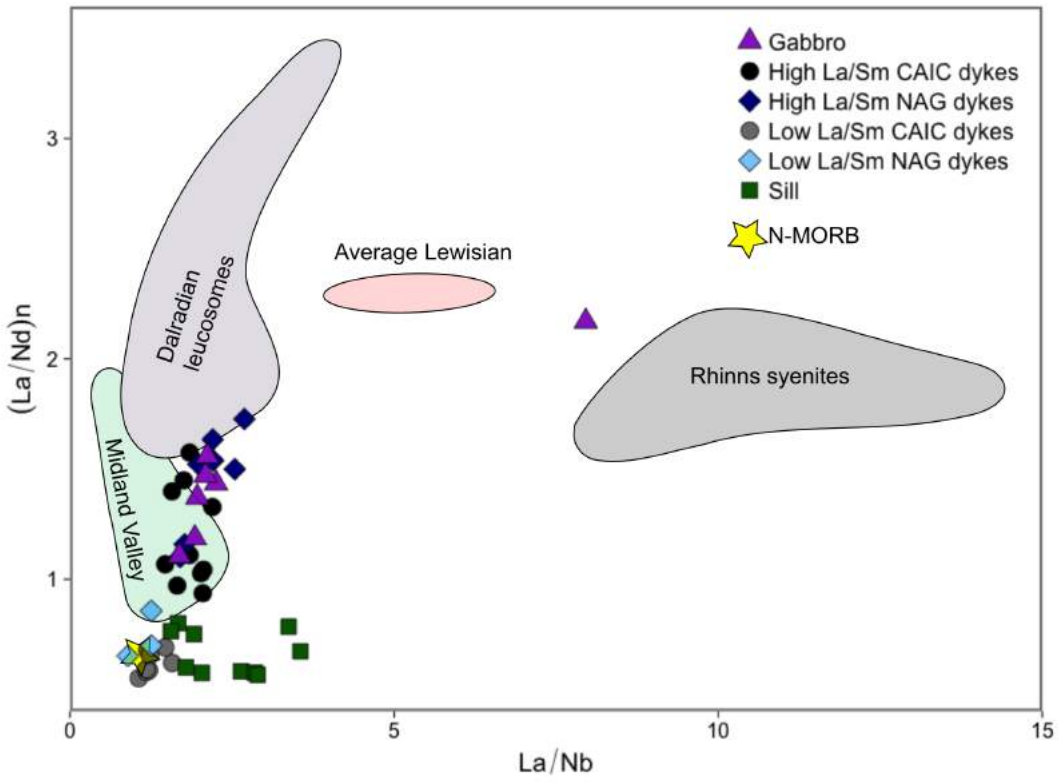

Fig. 5.25 – La/Nb ratio vs. chondrite-normalised (McDonough and Sun, 1995) La/Nd for the mafic Arran rocks, as well as various crustal units.

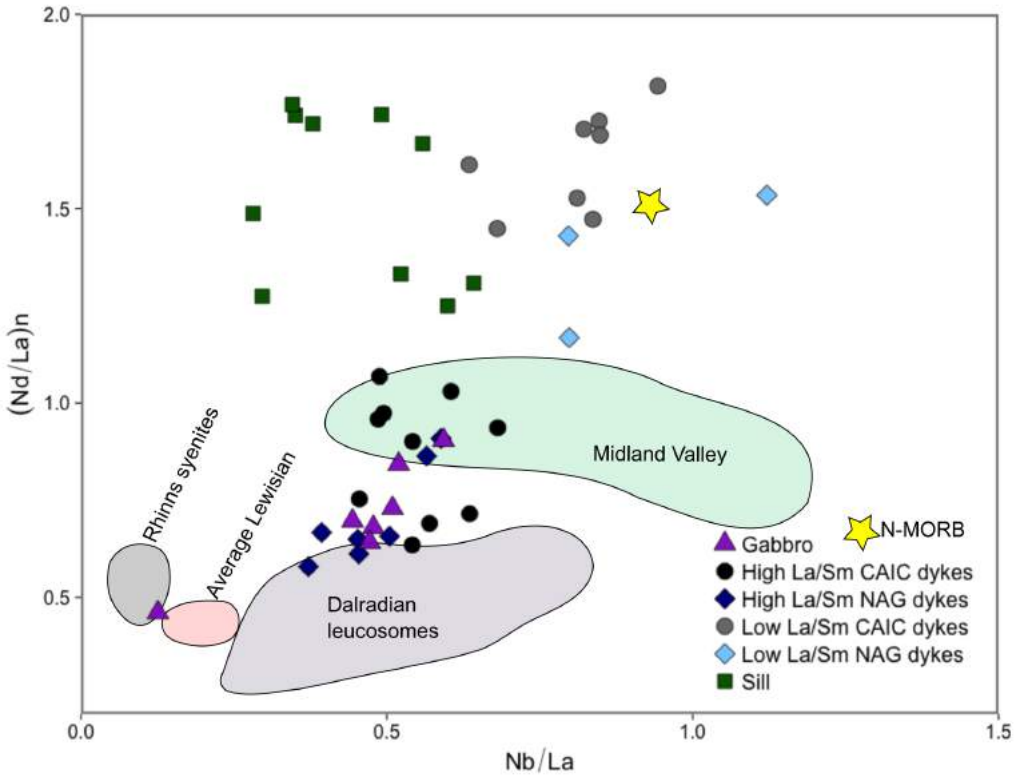

Fig. 5.26 – Nb/La ratio vs. chondrite-normalised (McDonough and Sun, 1995) Nd/La for the mafic Arran rocks, as well as various crustal units. Note that this is the same information as presented in Fig. 5.25 with La in the denominator, to display straight mixing lines.

Silicic units

The trace element profiles of the silicic rocks analysed in this study are shown in Figs. 5.27 – 5.30. These include the Glen Craigag and Satellite Granites of the CAIC, the North Arran Granite, the granite clasts in the ignimbrites of the AVF, the pitchstone dyke intruding the AVF, and the rhyolitic lava-like ignimbrites of the AVF.

It should be noted that these rocks are all rhyolitic and granitic in composition. The only crustal unit in this discussion that is also granitic is the Dalradian-derived leucogranite. This may be the reason that most trace element profiles are closest in fit to the Dalradian, rather than any of the other crustal units. It should also be pointed out that negative Ba, Sr, and Ti anomalies in granites are most often due to fractional crystallisation of K-feldspar, plagioclase, and Fe-Ti oxides. For these reasons, interpretations on the input of crustal melts are best left until the discussion of radiogenic isotopes and mixing modelling (Section 5.4.2).

Taking these issues into account, the trace element pattern of the pitchstone dyke is a near-exact match for the Dalradian-derived leucosomes (Fig. 5.27). In the absence of isotopic information for this dyke, it can be inferred that this magma was formed at least in part from partial melting of the Dalradian schists to the north of the Highland Boundary Fault.

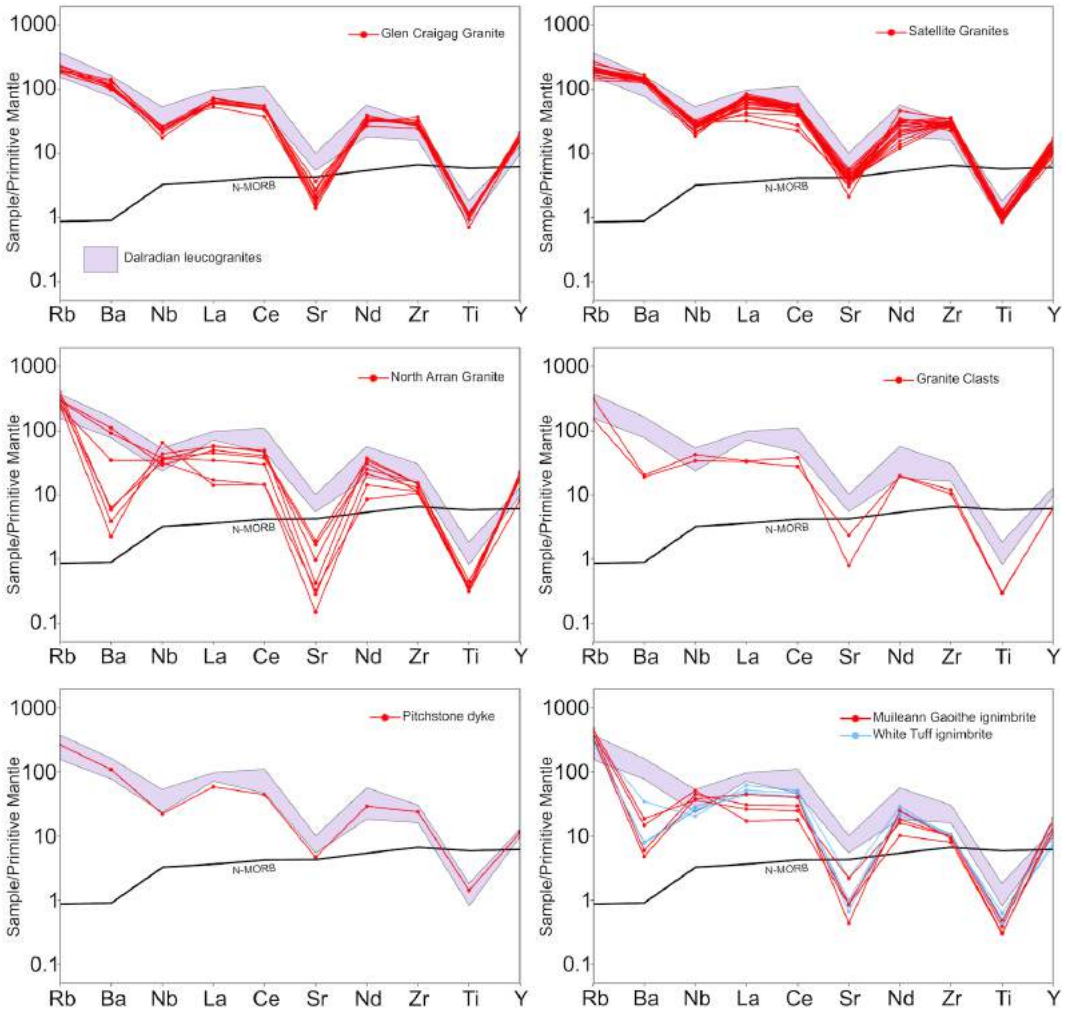

Fig. 5.27 – Primitive mantle normalised (Sun and McDonough, 1989) trace element diagrams for the silicic Arran rocks analysed in this study, along with data for Dalradian-derived leucogranites from Johnson et al. (2003).

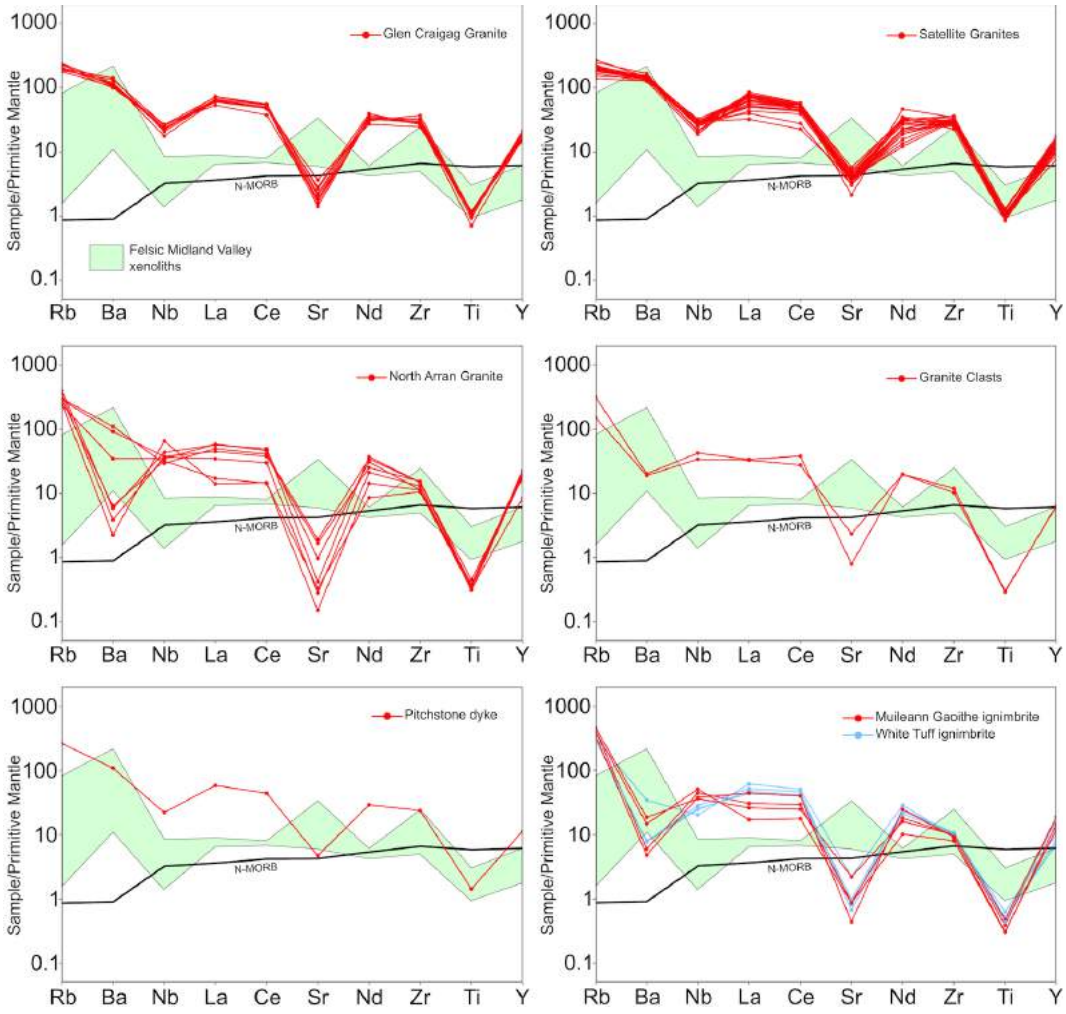

Fig. 5.28 – Primitive mantle normalised (Sun and McDonough, 1989) trace element diagrams for the silicic Arran rocks analysed in this study, along with data for the felsic Midland Valley xenoliths presented in Halliday et al. (1993).

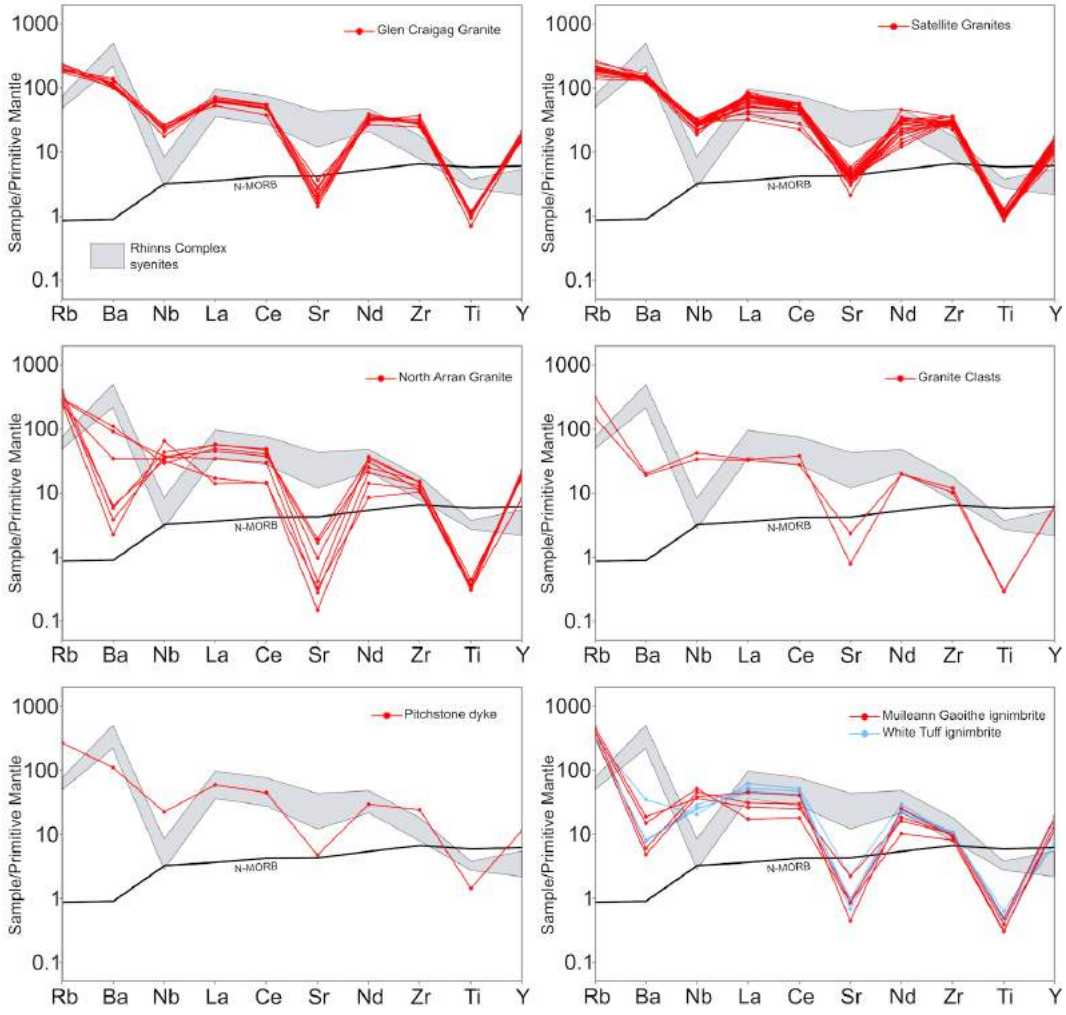

Fig. 5.29 – Primitive mantle normalised (Sun and McDonough, 1989) trace element diagrams for the silicic Arran rocks analysed in this study, along with data for the Rhinns Complex syenites from Muir et al. (1994).

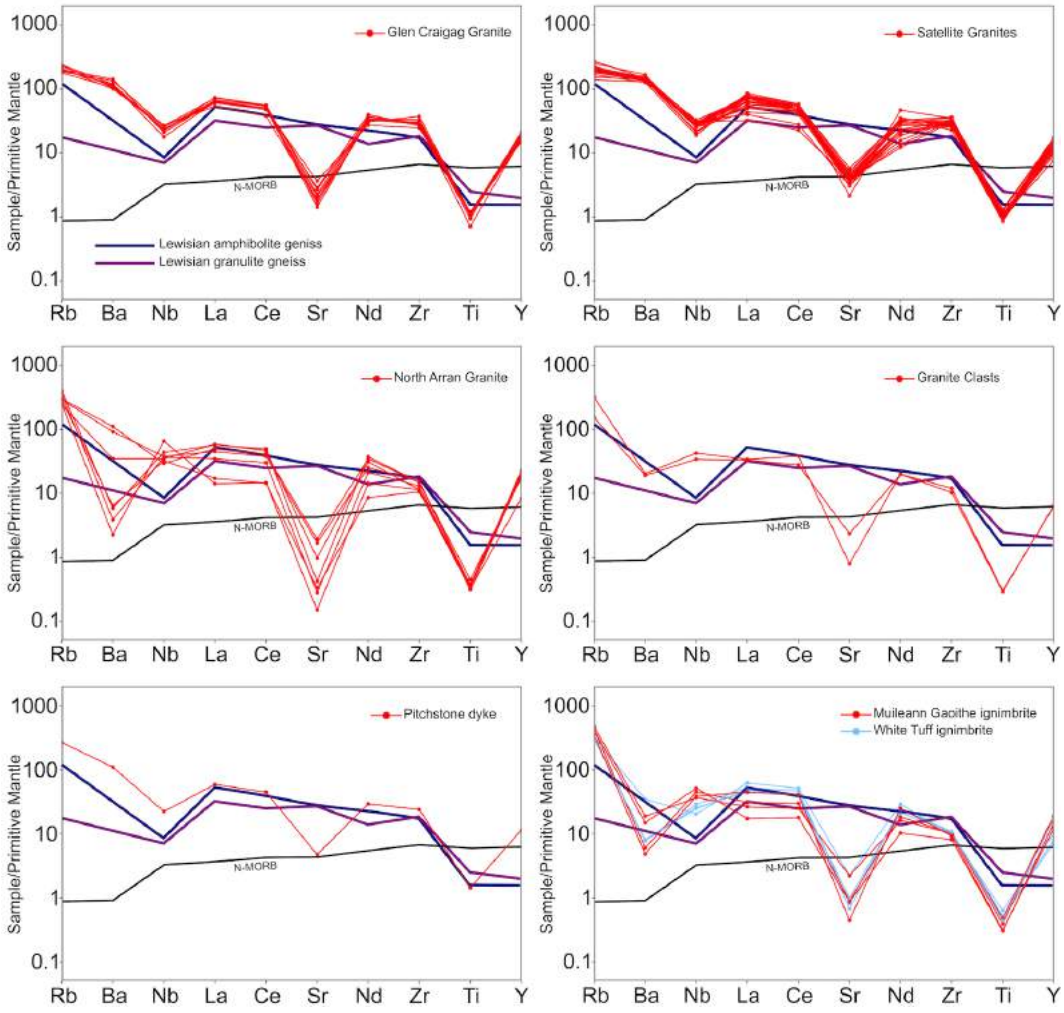

Fig. 5.30 – Primitive mantle normalised (Sun and McDonough, 1989) trace element diagrams for the silicic Arran rocks analysed in this study, along with data for average Lewisian amphibolite- and granulite-grade gneisses from Weaver and Tarney (1981).

Intermediate and hybrid units

The trace element profiles of the intermediate and hybrid rocks analysed in this study are shown in Figs. 5.31 and 5.32. These include the Glenloig Hybrids of intermediate and silicic composition, as well as the intrusive rocks of the Sheans and Tighvein.

The graphs of silicic Glenloig Hybrids should be treated with care in much the same way as those for the granites (above), in that these rocks have granitic compositions, meaning they are likely to have similar trace element patterns to the Dalradian leucogranites – the only crustal unit of granitic composition discussed here.

No isotopic data are available for the Sheans and Tighvein units. The Tighvein magmas are more enriched in incompatible elements, with a prominent relative Nb depletion, making the overall profile very similar to that of the Dalradian leucogranites. The Sheans samples have flatter overall trace element profiles with a less pronounced Nb anomaly, making them appear more similar to the Midland Valley xenoliths.

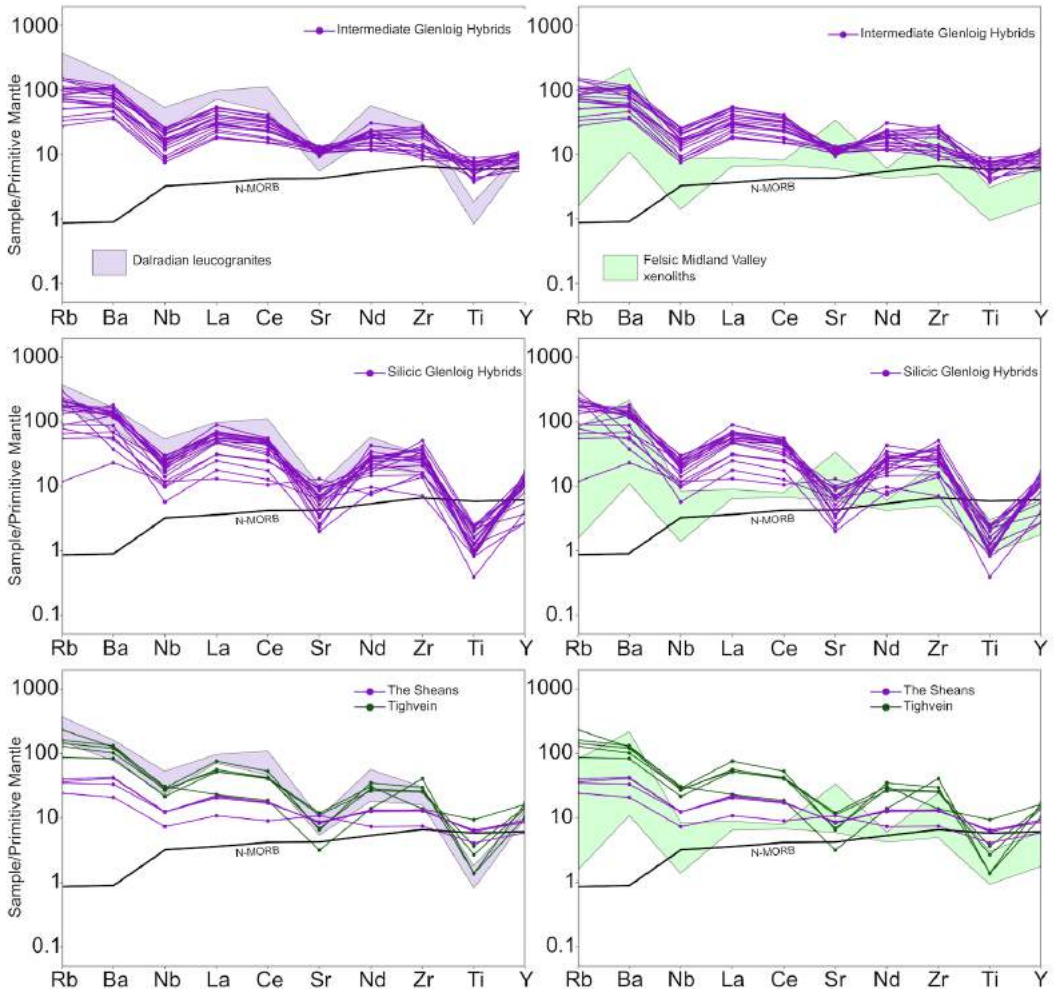

Fig. 5.31 – Primitive mantle normalised (Sun and McDonough, 1989) trace element diagrams for the intermediate Arran rocks analysed in this study, along with data for Dalradian-derived leucogranites from Johnson et al. (2003) on the left and the felsic Midland Valley xenoliths presented in Halliday et al. (1993) on the right.

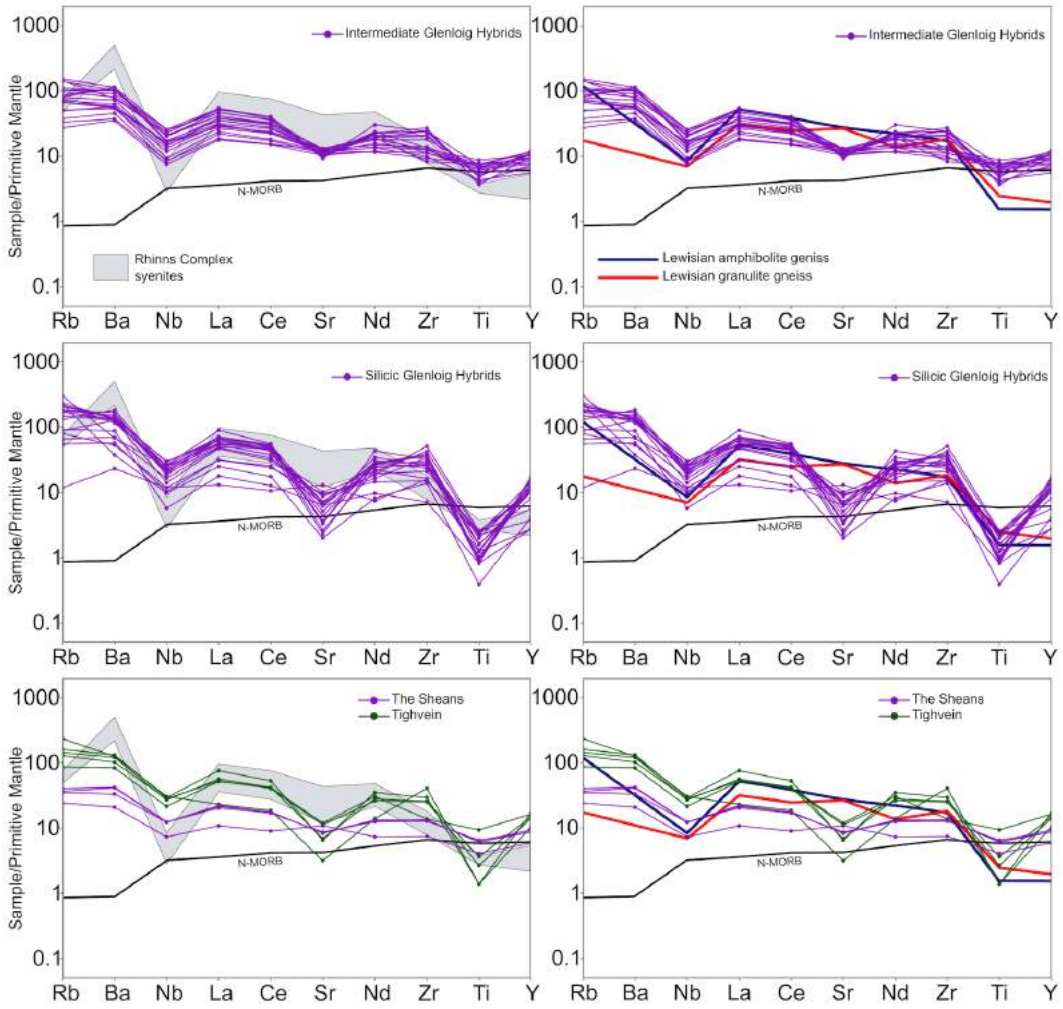

Fig. 5.32 – Primitive mantle normalised (Sun and McDonough, 1989) trace element diagrams for the intermediate Arran rocks analysed in this study, along with data for the Rhinns Complex syenites from Muir et al. (1994) on the left and average Lewisian amphibolite- and granulite-grade gneisses from Weaver and Tarney (1981). on the right.

Summary

Trace element diagrams can provide insights into the geochemistry of the crustal units that analysed magmas interacted with (or formed from), but must be used with caution as post-melt generation processes account for much of the shape of a sample's trace-element profile – particularly in more evolved rocks.

By comparing trace element ratios of the mafic Arran rocks with various crustal units, it can be suggested that most were contaminated by the Dalradian crust, the Midland Valley basement, or both. The sill that intrudes the CAIC appears to have been contaminated by a crustal unit geochemically resembling the syenites of the Rhinns Complex on Islay – thought to be the basement to the Dalradian schists.

For those units for which isotopic data are available, discussion about crustal contamination is best saved for the next section. However, for the other units, useful inferences can be made based on trace element data. It is tentatively suggested that the pitchstone dyke which intrudes the pyroclastic rocks of the AVF was sourced partly or entirely from crustal anatexis of the Dalradian schists, and must therefore have moved laterally for at least 3 km from a source north of the Highland Boundary Fault.

The intrusions of the Tighvein Intrusion Complex also show geochemical similarities with leucogranites derived from the Dalradian schists, implying even greater lateral magma transport of at least 10 km to the south. The petrographically similar rocks of the Sheans, immediately to the east of the CAIC, have a trace element signature which implies at least partial involvement of silicic Midland Valley crust, suggesting these magmas could have been sourced directly below their site of intrusion.

5.4.2 Mixing Modelling

Binary mixing between two isotopically distinct end-members can be modelled using mass-balance equations. The isotopic composition of a mixture M of end-member components A and B is given by the following equation:

$$R_{\mathrm{M}} = \frac{R_{\mathrm{A}} \cdot C_{\mathrm{A}} F + R_{\mathrm{B}} \cdot C_{\mathrm{B}}(1-F)}{C_{\mathrm{A}} F + C_{\mathrm{B}}(1-F)}$$

where R is the isotopic ratio of interest, C is the concentration of that element, and F is the weight fraction of A in the mixture (making (1-F) the weight fraction of B).

Mixing lines have been constructed between possible primary magma compositions and possible crustal contaminants. The possible primary magma compositions

Table 5.3 – Mean isotopic and trace element data for the end-members used in mixing calculations.

	DMM[a]	Iceland[b]	Picrite[c]	Dalradian[d]	MV Mafic[e]	MV Felsic[e]	Rhinns[f]
$^{143}Nd/^{144}Nd$	0.51303	0.51299	0.51261	0.51137	0.51254	0.51223	0.51165
$^{87}Sr/^{86}Sr$	0.70261	0.70307	0.70457	0.74490	0.70456	0.71012	0.71015
$^{177}Hf/^{176}Hf$	0.28320	0.28317	0.28312	–	–	–	–
$^{206}Pb/^{204}Pb$	18.172	18.411	18.428	17.564	18.549	18.276	17.494
$^{207}Pb/^{204}Pb$	15.481	15.470	15.495	15.402	15.558	15.528	15.415
$^{208}Pb/^{204}Pb$	37.917	38.022	38.288	38.156	38.544	38.637	36.143
Nd (ppm)	0.58	12.25	3.35	23.70	14.55	18.28	55.14
Sr (ppm)	7.66	173.60	141.4	94.00	647.02	345.73	869.80
Hf (ppm)	0.16	2.05	1.02	–	–	–	–
Pb (ppm)	0.02	0.96	4.18	12.14	3.71	4.92	4.00

[a]Workman and Hart (2005), [b]Kempton et al. (2000), [c]sample 338 - this study, [d]Dickin (1994); Dickin et al. (1981), [e]Halliday et al. (1993), [f]Marcantonio et al. (1988). Note that the Pb concentration of the Rhinns complex is not known; 4.00 ppm is an arbitrary number required to make the calculations work.

are average Depleted MORB Mantle (DMM; Workman and Hart, 2005), average Icelandic basalt (Kempton et al., 2000), and an Arran picrite dyke (sample 338, this study). The possible crustal contaminants are the Dalradian schists (Dickin, 1994; Dickin et al., 1981), the unexposed basement to the Midland Valley Terrane (Halliday et al., 1993), and the Proterozoic Rhinns Complex of Islay, thought to represent the basement to the Dalradian succession (Marcantonio et al., 1988). The average isotopic and trace element compositions of these units is given in Table 5.3. In most graphs, mixing of primary magmas with mafic Midland Valley basement is not included, as this is less likely to melt than the silicic rocks of the same crustal unit.

The results of mixing calculations are shown in Figs. 5.33 – 5.35. It must be stressed that condensing entire primary sources and volumetrically vast crustal units into single average compositions is a major caveat. All of these crustal units have provided highly varied isotopic compositions, and these represent a small number of analyses. The geochemical variation within these units is likely to be much greater than currently understood, but these models can still provide useful insight.

Of the three possible primary magma compositions, DMM seems to provide the best fitting mixing lines for most Arran samples (Fig. 5.33). Using DMM as a source also requires much less input of crustal material to achieve the isotopic compositions seen on Arran (this is because of the much lower incompatible trace element concentrations in DMM relative to the crustal units). When Icelandic basalts are used as a primary magma composition (Fig. 5.34), many of the Arran samples can still be modelled by binary mixing, but in many cases the fit is not as good, and

much greater addition of crust is required. Some Arran samples fit onto mixing lines when the Arran picrite is used as a primary magma composition, but this is less convincing. This source cannot explain the isotopic composition of those samples with more radiogenic Nd and less radiogenic Sr compositions than sample BJG/15/338.

North Arran Granite

It is clear that the North Arran Granite magma was formed from interaction of a primary magma with the Dalradian crust. When using DMM as a source, the first three graphs in Fig. 5.33 suggest input of 3–5% Dalradian crust. The $^{206}Pb/^{204}Pb$ vs. $^{208}Pb/^{204}Pb$ graph also shows North Arran Granite magmas forming as a mixture of DMM and Dalradian crust, but requiring <0.5% crustal input.

The North Arran Granite samples also lie on the Iceland–Dalradian mixing line, but the first three graphs in Fig. 5.34 show at least 40% of crustal material, while the $^{206}Pb/^{204}Pb$ vs. $^{208}Pb/^{204}Pb$ graph shows 10–20% crustal input.

Using the Arran picrite as a primary composition does not result well-fitting mixing lines (Fig. 5.35).

Satellite Granites

The Satellite Granites of the CAIC plot in most cases along mixing lines between primary sources and the silicic Midland Valley basement. In the first three graphs in Fig. 5.33 the isotopic compositions of the Satellite Granites are consistent with mixing between a DMM source and around 20% silicic Midland Valley crust. It is interesting to note that on the $^{206}Pb/^{204}Pb$ vs. $^{208}Pb/^{204}Pb$ graph the Satellite Granites, along with the other CAIC granites and hybrids, form a clear linear trend between DMM and the more radiogenic mafic Midland Valley samples. This trend, however, extends beyond the 100% crustal input point; this is presumably due to the problem of condensing all mafic Midland Valley samples into one mean value.

The Satellite Granites can also be explained by well-fitting mixing lines between an Icelandic source and the silicic Midland Valley basement. However this model requires input of around 80% of crustal material – much more than is needed for the DMM models. This is probably an unfeasibly high amount of crustal melting in the context of the BPIP. Again, the $^{206}Pb/^{204}Pb$ vs. $^{208}Pb/^{204}Pb$ graph suggests mixing between an Icelandic source and the mafic Midland Valley crust.

Unlike the North Arran Granite, it is possible to model the isotopic compositions of the Satellite Granites using picrite sample 338 as a primary magma. This would require 40–60% crustal input from the silicic Midland Valley crust.

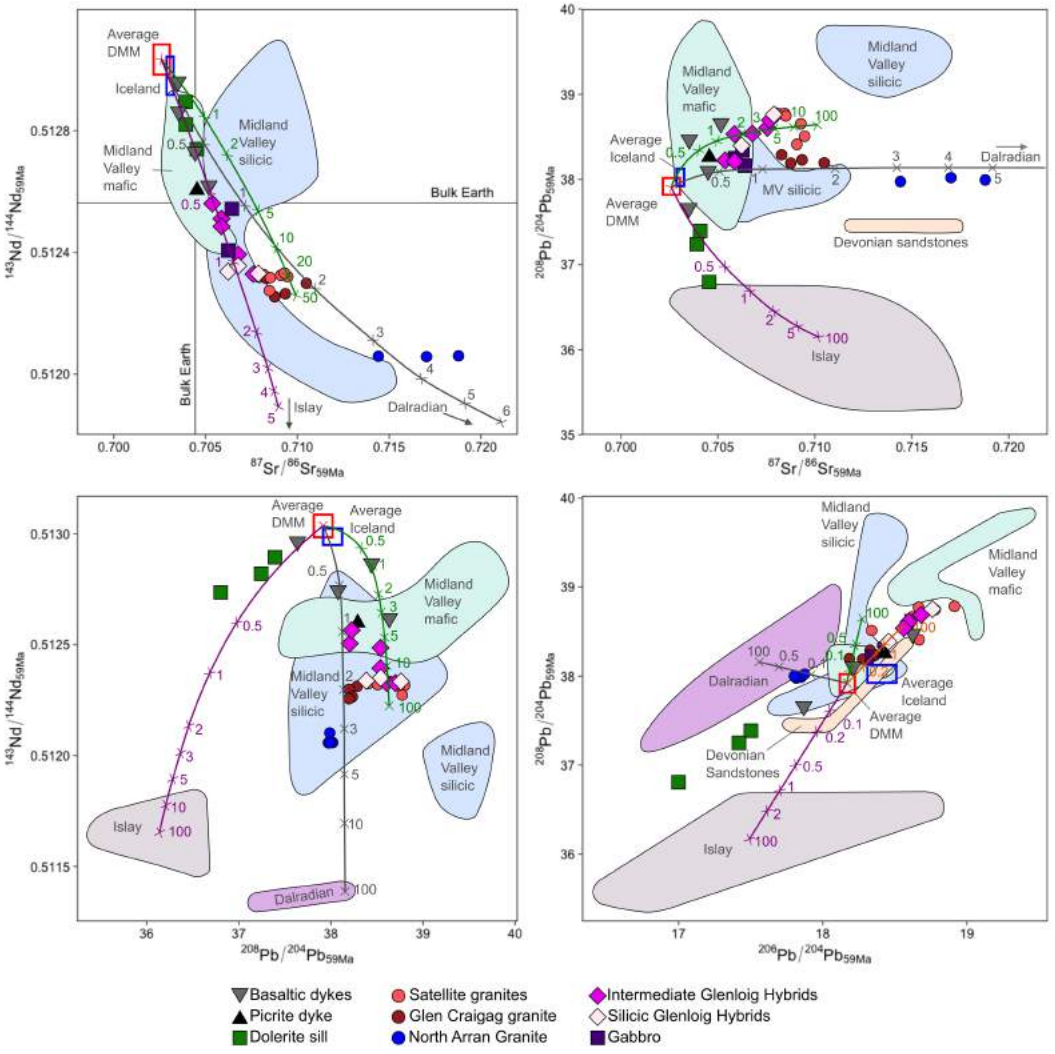

Fig. 5.33 – Selected isotopic ratio-ratio diagrams as seen in Section 4.2. Lines show mixing models between the average DMM composition and various crustal units. Crosses show percentage of crustal material in the mixture. Grey = Dalradian, Green = Felsic Midland Valley, Orange = Mafic Midland Valley, Purple = Rhinns Complex.

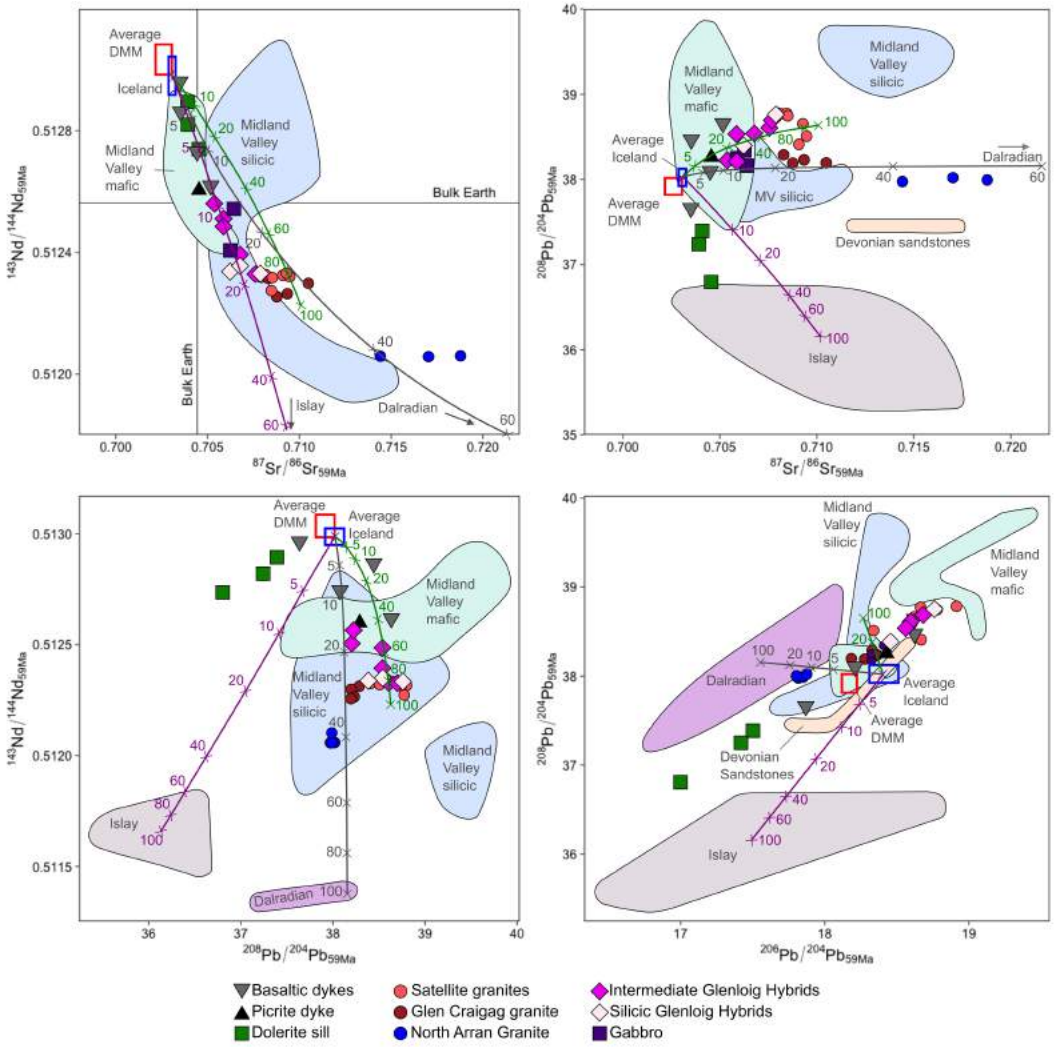

Fig. 5.34 – Selected isotopic ratio-ratio diagrams as seen in Section 4.2. Lines show mixing models between the average Icelandic composition and various crustal units. Crosses show percentage of crustal material in the mixture. Grey = Dalradian, Green = Felsic Midland Valley, Purple = Rhinns Complex.

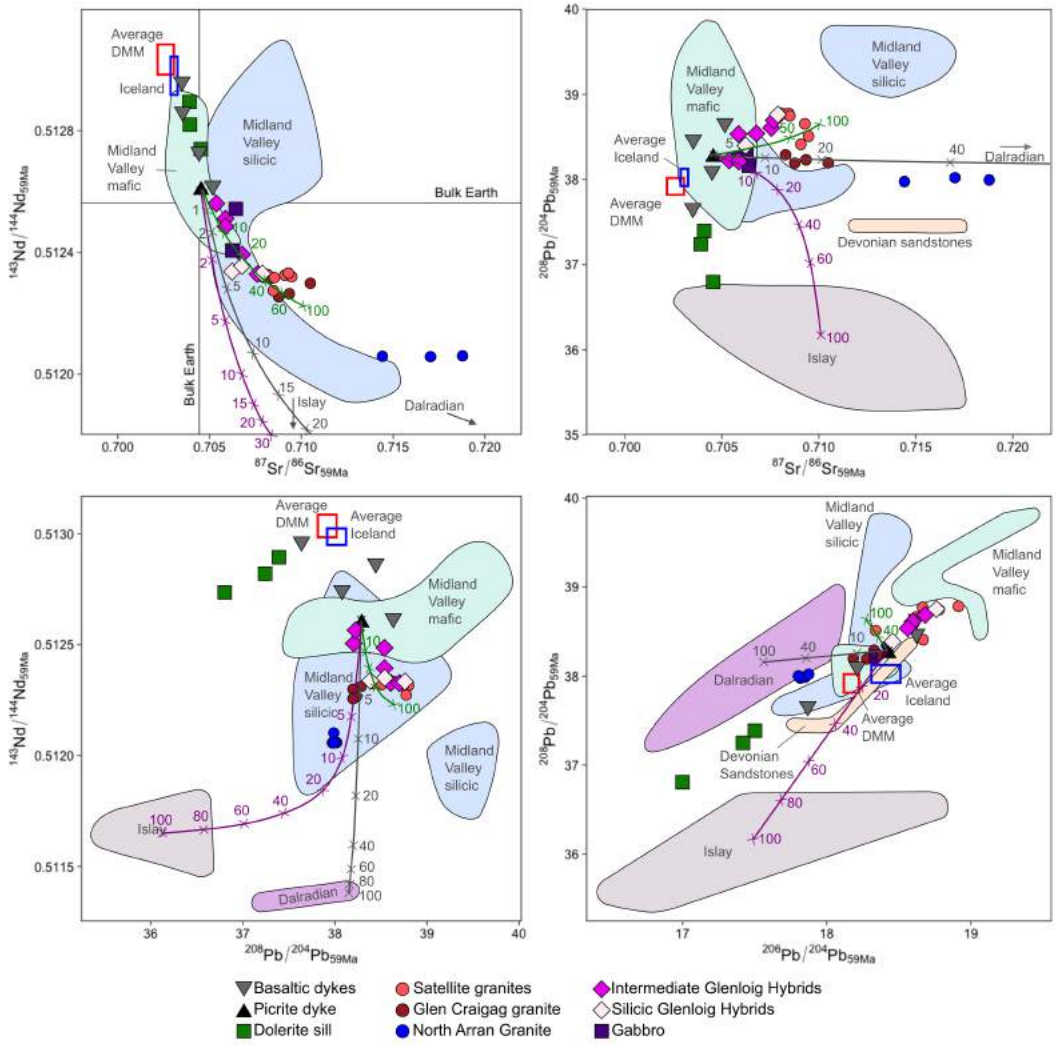

Fig. 5.35 – Selected isotopic ratio-ratio diagrams as seen in Section 4.2. Lines show mixing models between composition of picrite sample #338 and various crustal units. Crosses show percentage of crustal material in the mixture. Grey = Dalradian, Green = Felsic Midland Valley, Purple = Rhinns Complex.

Glen Craigag Granite

The origin of the Glen Craigag granite in these models is slightly more ambiguous. Although these samples plot close to the Satellite Granites in isotopic space, they could be explained by crustal contamination from either a Midland Valley or Dalradian source. The first three graphs in Fig. 5.33 consistently show a good fit for contamination of a DMM source with 2% input of Dalradian crust. These graphs could also show a mixture of DMM with around 20% silicic Midland Valley crust, although this fit is not as convincing. On the $^{206}Pb/^{204}Pb$ vs. $^{208}Pb/^{204}Pb$ graph in Fig. 5.33 the Glen Craigag granite samples largely plot between the mixing lines from DMM to silicic Midland Valley crust and DMM to mafic Midland Valley crust, requiring addition of 0.2–0.5% of either.

As with the North Arran Granite and Satellite Granites, using Iceland as a source rather than DMM shows very similar trends, but requires a much greater input of crustal material. A good approximation of the analysed samples can be modelled with input of 20–30% Dalradian material or 80–90% silicic Midland Valley material. The $^{206}Pb/^{204}Pb$ vs. $^{208}Pb/^{204}Pb$ graph in Fig. 5.34 shows the Glen Craigag granite samples plotting between 10% input of silicic Midland Valley crust and <5% input of Dalradian crust.

The Glen Craigag granite can be modelled using the picrite as a primary source, although the models do not agree on the crustal contaminant (Fig. 5.35). The $^{87}Sr/^{86}Sr$ vs. $^{143}Nd/^{144}Nd$ graph suggests a mixture of picrite magma with 40–80% silicic Midland Valley crust. The $^{87}Sr/^{86}Sr$ vs. $^{208}Pb/^{204}Pb$ graph suggests a mixture of picrite magma with 10–20% Dalradian crust. The $^{208}Pb/^{204}Pb$ vs. $^{143}Nd/^{144}Nd$ graph suggests a mixture of picrite magma with 5% Dalradian crust. The $^{206}Pb/^{204}Pb$ vs. $^{208}Pb/^{204}Pb$ graph suggests a mixture of picrite magma with 5–10% Dalradian crust.

Glenloig Hybrids

The intermediate and silicic Glenloig Hybrids display a relatively large spread in isotopic compositions, and as such fit along various mixing lines, at various degrees of crustal input. The mixing lines along which they most consistently fit are those between the various primary sources and the Midland Valley basement. Although they seem to plot along a mixing line towards the Rhinns complex on the $^{87}Sr/^{86}Sr$ vs. $^{143}Nd/^{144}Nd$ graph in Fig. 5.33 and Fig. 5.34, this relationship is not seen in any other models, suggesting it is an illusion related to the two-dimensional plane of this graph.

The first three graphs in Fig. 5.33 suggest that the Glenloig Hybrids could be formed from a DMM source with an input of high amounts (~50%) silicic Midland Valley material. Much like the Satellite Granites, the $^{206}Pb/^{204}Pb$ vs. $^{208}Pb/^{204}Pb$ graph suggests a mixture between DMM and mafic Midland Valley crust, but to an extent greater than 100% in this model.

Fig. 5.34 shows that the Glenloig Hybrids could also be formed by mixing of an Iceland source with <80% silicic Midland Valley crust.

The first three graphs in Fig. 5.35 show relatively good fits of the Glenloig Hybrids samples along the silicic Midland Valley mixing lines, but with a large range of required crustal input.

Basaltic dykes

The basaltic dykes have a wide range in isotopic compositions, as could be expected from a series of disconnected and possibly laterally extensive intrusions in a region of complex crustal architecture. They are generally less contaminated than the more evolved units. On the $^{87}Sr/^{86}Sr$ vs. $^{143}Nd/^{144}Nd$ graphs in Fig. 5.33 and Fig. 5.34, the mixing lines are too close in the upper left corner to distinguish which provides a closer fit to the analysed basaltic dykes. The compositions of the dykes cannot be modelled using the picrite as a source, as they have lower radiogenic Sr and higher radiogenic Nd (Fig. 5.35).

The $^{87}Sr/^{86}Sr$ vs. $^{208}Pb/^{204}Pb$ and $^{208}Pb/^{204}Pb$ vs. $^{143}Nd/^{144}Nd$ graphs in Fig. 5.33 both suggest that two dykes were formed from mixing of DMM with <5% silicic Midland Valley crust, one shows a mixture of DMM and 0.5% Dalradian crust, and one shows a mixture of DMM and 0.1% Rhinns Complex material. These general relationships are echoed in the $^{206}Pb/^{204}Pb$ vs. $^{208}Pb/^{204}Pb$ graph, although the sample that is otherwise suggested to lie on a Dalradian mixing line is less clear.

The $^{87}Sr/^{86}Sr$ vs. $^{208}Pb/^{204}Pb$ and $^{208}Pb/^{204}Pb$ vs. $^{143}Nd/^{144}Nd$ graphs in Fig. 5.34 also show two dykes being formed by contamination by a Midland Valley source, but this is not as good a fit than when DMM is used as the source. The sample contaminated by the Rhinns Complex also shows a worse mixing line fit than when DMM is the source. However, the sample that lies on the Dalradian mixing line shows a much better fit on the $^{87}Sr/^{86}Sr$ vs. $^{208}Pb/^{204}Pb$ and $^{208}Pb/^{204}Pb$ vs. $^{143}Nd/^{144}Nd$ graphs, as well as the $^{206}Pb/^{204}Pb$ vs. $^{208}Pb/^{204}Pb$ graph, all of which suggest that this dyke is the result of mixing between Icelandic basalt and <10% Dalradian crust.

Dolerite sill

The three analysed samples of the dolerite sill have varying isotopic compositions, but these are roughly collinear suggesting that they formed from different degrees of mixing between the same two sources. Much like the basaltic dykes, they can not be explained by mixing of a picrite source as they have lower radiogenic Sr and higher radiogenic Nd (Fig. 5.35).

All graphs in Fig. 5.33 and Fig. 5.34 suggest that the dolerite sill formed from contamination of a primary magma with Rhinns Complex material. The mixing lines using DMM as a source form the best fit, and suggest mixing with <0.5% of Rhinns-like crust (Fig. 5.33). When Icelandic basalts are used as a source, the lines do not fit as well, but could explain the composition of the dolerite sill with addition of up to around 20% Rhinns Complex crust.

Summary

The main caveat with binary mixing modelling done in this way is the need to condense end-members into single 'representative' compositions. The issues involved with doing this with the depleted upper mantle are discussed in Workman and Hart (2005). For the other units (other than the picrite dyke which has a single composition), this has been attempted by simply taking mean values from the published literature for isotopic ratios and trace element compositions. In many cases these datasets are very limited and cannot possibly provide true representations of extensive crustal units. However, they are still useful and have allowed the construction of mixing models which appear to explain the isotopic compositions of most of the magmas analysed in this study.

These highly simplified mixing models suggest the following origins of the measured isotopic compositions in the Arran intrusions:

- The North Arran Granite magma formed from a DMM source with 3–5% Dalradian crust.
- The Satellite Granites magma formed from a DMM source with 20% silicic Midland Valley crust, with some input from mafic Midland Valley crust.
- The Glen Craigag granite magma formed from contamination of a DMM-derived melt by 2–3% Dalradian crust with some contamination from a silicic Midland Valley crustal source. This magma could also have formed from a greater degree of contamination of an Icelandic-like source.

- The Glenloig Hybrids magmas formed from either a DMM or Icelandic source, with up to 80% silicic Midland Valley crust, with some input from mafic Midland Valley crust.
- Two mafic CAIC dykes were formed from a DMM source with <5% silicic Midland Valley crust.
- One mafic CAIC dyke formed from a DMM source with 0.1% Rhinns Complex crust.
- One mafic CAIC dyke formed from an Icelandic source mixed with up to 10% Dalradian crust.
- The dolerite sill magma formed from a DMM source with <0.5% Rhinns complex crust.

Although these specific results must be treated with caution, due to the restrictions of the model described above, some general broad conclusions can be confidently drawn:

- The North Arran Granite was contaminated by Dalradian crust.
- The CAIC hybrids and the majority of the CAIC granites were contaminated by the Midland Valley crust.
- The Glen Craigag Granite magma may have been contaminated by the Dalradian schists, the Midland Valley, or both.
- The dolerite sill in the CAIC was contaminated by some other unit entirely, as suggested in Section 5.4.1. This could be the the Proterozoic gneisses exposed on the Rhinns of Islay.
- The basaltic dykes that intrude the CAIC were contaminated to a minor extent by a variety of different crustal sources.

5.4.3 Further Work

The contamination trends shown in this section are convincing, however they have been analysed with rather basic comparison and modelling methods. Binary mixing is an idealised process that does not take into account certain magmatic processes that are known to occur in the real world, for example fractional crystallisation or exhaustion of fertile material in the crust. Binary mixing and comparison of trace element profiles have been used due to a lack of complete datasets for the

various crustal units. The crustal blocks studied as possible contaminants here are volumetrically vast and lithologically complex, and many previous studies have only produced data for certain units within those blocks or focus on a certain aspect of the geochemistry. For this reason, many crustal lithologies only have data for trace elements without isotopes, or *vice versa*. For a full account of crustal contamination of Palaeogene magmas in the vicinity of the Highland Boundary Fault, a complete dataset of trace element and isotope geochemistry of the Dalradian, the Midland Valley basement and sedimentary cover, and the Rhinns Complex would first need to be compiled.

Once such a dataset is available, it would be possible to utilise models that take into account more than just simple binary mixing. Assimilation of crustal material during fractional crystallisation of the magma (AFC) can be modelled based on the equations of DePaolo (1981). AFC modelling has recently been shown to explain the compositions of magmatic rocks on Arran, as well as elsewhere in the BPIP (e.g. Meade et al., 2014, 2009), so it is likely that it could better explain the data presented here.

A major limitation on the discussion of crustal contamination presented here is the nature of the lithologies that have been considered as possible contaminants, and their potential fertility. Crustal rocks do not melt and assimilate uniformly, and it is only the partial melts that contribute a geochemical signature to the final melt composition. For example, the Dalradian leucogranites presented by Johnson et al. (2003) are themselves the products of partial melting, whereas the Midland Valley basement may have experienced partial melt extraction prior to Palaeogene magmatism. These two scenarios are likely to have greatly different effects on the final magma composition. Indeed, studies from the BPIP (Kerr et al., 1995; Meade et al., 2014) have shown that the fertility of crustal units may have changed throughout the evolution of local igneous systems. Ideally, more products of crustal anatexis from the relevant crustal blocks will be geochemically analysed and allow for more realistic contamination models to be constructed in the future.

To account for factors such as the ability of a crustal unit to produce partial melts, and the ability of a body of magma to sufficiently heat that crust, the Energy-Constrained Assimilation-Fractional Crystallization (EC-AFC) model was proposed by Spera and Bohrson (2001) and Bohrson and Spera (2001). This would require a more complete dataset of crustal lithologies than is currently available, but would certainly provide a better explanation of crustal contamination of the Arran magmas than binary mixing or AFC modelling.

Table 5.4 – Key geochemical characteristics of the Palaeogene magma types in the Hebrides, from Kent and Fitton (2000)

Magma type	Local name (Mull, Skye)	Classification	Y/Zr	Ti/Zr	Ce/Y
M1	Mull Plateau Group, Skye Main Lava Series	Transitional (tholeiitic–alkalic)	0.1–0.3	43–93	0.4–4.8
M2	Coire Gorm Fairy Bridge	Transitional (tholeiitic–alkalic)	0.2–0.4	84–143	0.3–1.2
M3	Central Mull Tholeiites Preshal More	Tholeiitic	0.2–1	82–139	0.01–1.6
M4	Late Mull Type Beinn Dearg More	Transitional (tholeiitic–mildly alkalic)	0.3–0.4	80–119	0.1–0.4

5.5 Comparison with Other BPIP Units

5.5.1 Magma Types

The Hebrides of Scotland are famous among igneous petrologists as the area in which Bailey et al. (1924) developed the idea of 'magma types', based around his petrographic and geochemical observations of lavas on the Isle of Mull. His two recognised magma types – the 'Plateau Magma Type' and the 'Non-porphyritic Central Type' – have since been named the Mull Plateau Group and the Central Mull Tholeiites (Kerr, 1995; Morrison et al., 1980), and correspond to the globally abundant alkaline series and tholeiitic series, respectively. Later extensive geochemical studies of lavas and intrusions on Mull identified two other magma types (Kerr, 1995; Kerr et al., 1999). The lava flows at the summit of Ben More – the highest point on the island – belong to the Coire Gorm type, while a series of late-stage intrusions belong to the Late Mull type. Geochemical correlatives of these magma types are found on Skye, and in both locations they display a chronostratigraphic evolution. The similar magma types on Mull and Skye were grouped together by Kent and Fitton (2000), and the key characteristics of each are shown in Table 5.4

The changes in trace element geochemistry observed between the four Hebridean magma types are thought to reflect temporal changes in the depth of melting, the depth of crustal contamination, and the input of an Iceland-plume source relative to an N-MORB source (Kent and Fitton, 2000; Kerr, 1995; Kerr et al., 1999).

The lavas of Antrim also show evidence of distinct magma types, although these are different from those seen in the Hebrides, and not stratigraphically sequential. The first magma type is seen in the Lower Basalt Formation and Upper Basalt Formation of the Antrim lavas. The second comprises the Causeway Tholeiite Member, which

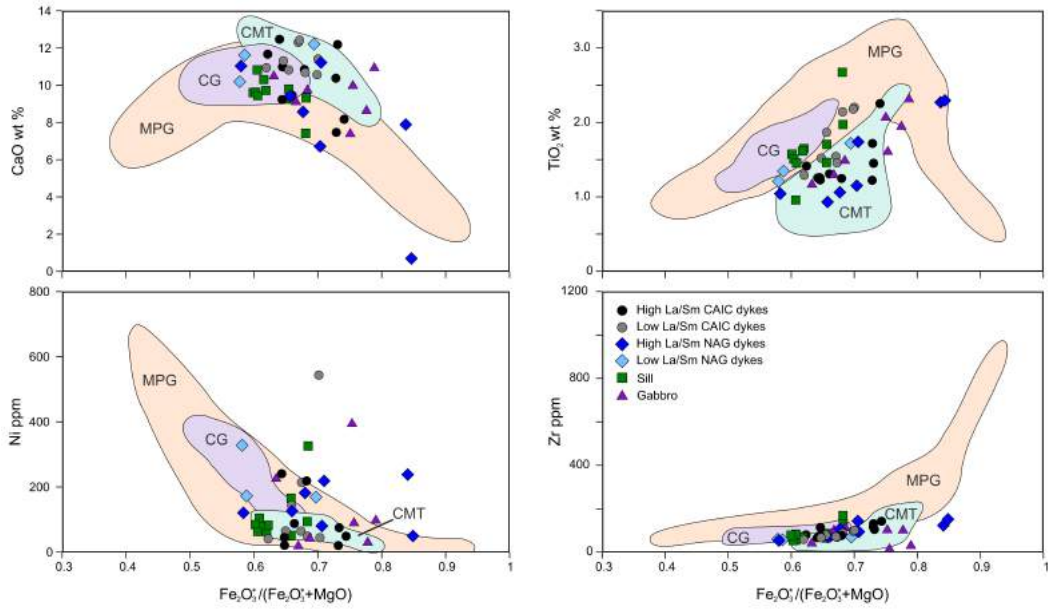

Fig. 5.36 – Binary plots of selected major and trace elements for the basaltic groups of the CAIC, as well as the dykes that intrude the North Arran Granite, plotted with fields showing the composition of the three magma types seen in the lava sequence on Mull. Adapted, with new data, from Kerr et al. (1999).

lies stratigraphically between the Lower and Upper Basalt Formations. Some lavas within the Causeway Tholeiite Member are distinctly LREE depleted. These are discussed here as the Depleted Causeway Tholeiite. As Arran lies half-way between Mull and Antrim it is possible that the basaltic intrusions on Arran are formed from magmas belonging to the Hebridean types, the Antrim types, or both.

Major and Trace Elements

Kerr et al. (1999) differentiated between the Mull magma types using various major and trace elements, as well as the ratio Fe_2O_3*/(Fe_2O_3*+MgO), as shown as fields in Fig. 5.36. It is clear that the samples from this study have a more restricted range in these compositions than the Mull lavas (it should be noted that the two North Arran Granite dykes with high Fe_2O_3*/(Fe_2O_3*+MgO) values are andesitic in composition and are therefore not directly comparable with basaltic lavas). The main cluster of Arran samples plots broadly in the field of the Coire Gorm and Central Mull Tholeiites compositions, with generally higher CaO, lower TiO_2 and Zr, and more restricted Fe_2O_3*/(Fe_2O_3*+MgO) than the Mull Plateau Group lavas. On some of these diagrams the CAIC dolerite sill appears to have slightly more Coire Gorm-like compositions, while the gabbro and dykes have slightly more Central Mull Tholeiite-like compositions. On the Fe_2O_3*/(Fe_2O_3*+MgO) vs. TiO_2 graph,

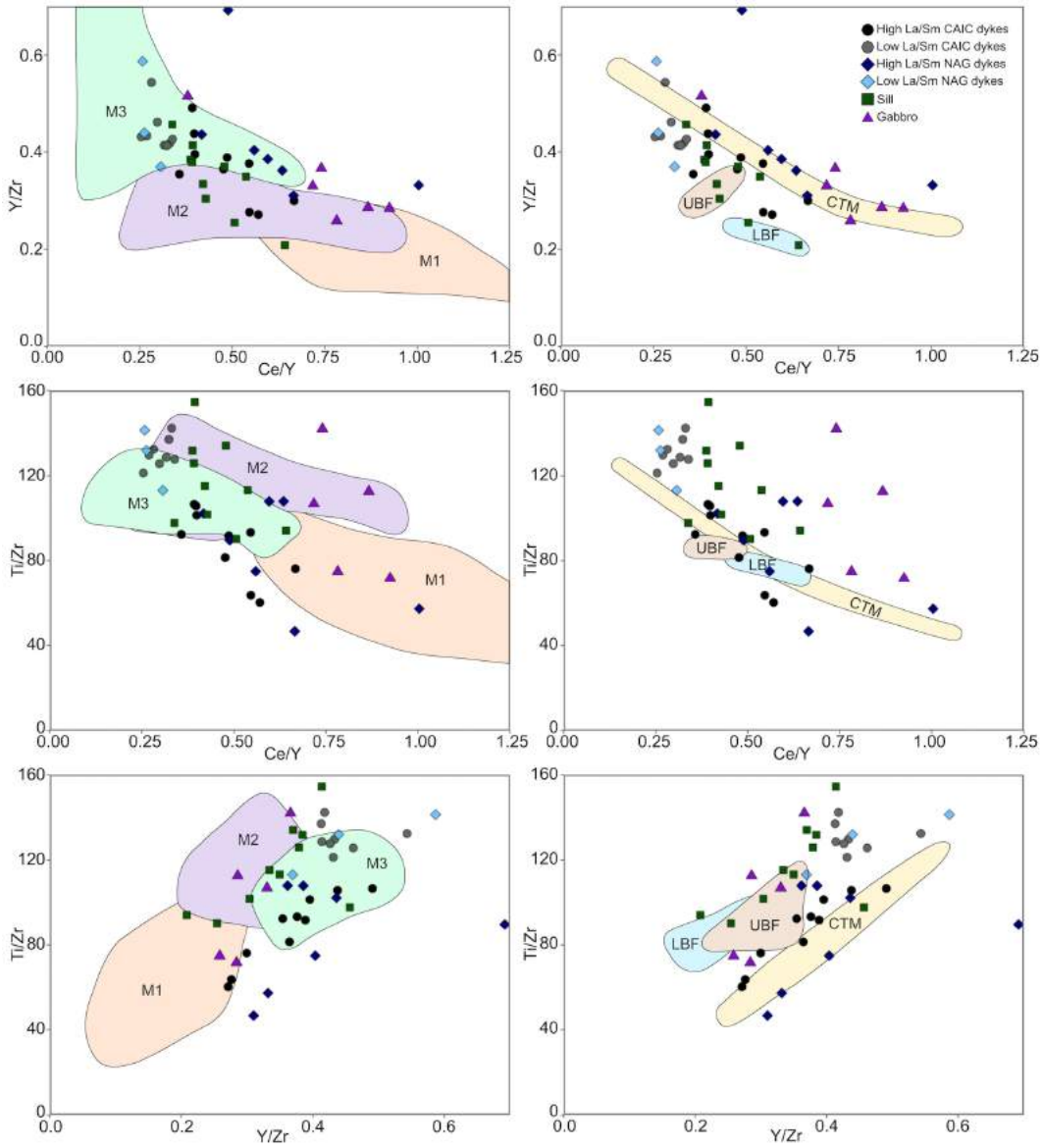

Fig. 5.37 – Trace element ratio-ratio plots, using the ratios shown in Table 5.4 (Kent and Fitton, 2000) for the basaltic groups of the CAIC, as well as the dykes that intrude the North Arran Granite. The coloured fields in the left-hand column show the compositions of dykes belonging to the different magma types of the Hebrides (data from Kerr et al. (1999) and Kent and Fitton (2000)). The coloured fields in the right-hand column show the compositions of lava flows belonging to the different stratigraphic units of the lava succession in Antrim (data from Barrat and Nesbitt (1996)). LBF - Lower Basalt Formation, UBF - Upper Basalt Formation, CTM - Causeway Tholeiite Member. Note that these fields contain a small number of data points.

it appears as though the low La/Sm dykes (of both the CAIC and the North Arran Granite) lie in a parallel array higher than the high La/Sm dykes, and closer to the Coire Gorm type Mull lavas.

The trace element ratios shown in Table 5.4 are displayed graphically in Fig. 5.37. This shows the Hebrides and Antrim lava types as fields, along with the data from this study. (Note that the Hebrides magma types closely correlate with the Mull magma types – see Table 5.4) Much like in Fig. 5.36, the Arran samples generally cluster around the M2 and M3 types, and have higher Y/Zr and generally lower Ce/Y than the M1 type. Again, the sill plots more in the M2 type field than either of the others. The low La/Sm CAIC and North Arran Granite dykes have lower Ce/Y and higher Y/Zr and Ti/Zr than their high La/Sm counterparts, which on the Ce/Y vs. Y/Zr suggests they are closer in composition to the M3 type than the M2 type, contrary to what is suggested by Fig. 5.36.

The only Antrim magma type which has as large a compositional range on Fig. 5.37 as the Arran samples is the Causeway Tholeiite Member, which forms a linear array parallel to that of the Arran samples. None of the Arran groups convincingly cluster around either the Upper or Lower Basalt Formation types.

Rare-earth Element Patterns

The different magma types of the Hebrides and Antrim have distinct REE patterns, derived from differences in melting conditions (Barrat and Nesbitt, 1996; Kent and Fitton, 2000; Kerr, 1995; Kerr et al., 1999). The Hebridean M1 type is relatively enriched in light rare-earth elements (LREE) with heavy rare-earth element (HREE)-depleted patterns, giving this type an overall steep REE pattern (Fig. 5.38). This HREE depletion relative to chondritic profiles is ascribed to melting of a mantle source region containing garnet (Ellam, 1992; Kerr, 1995), and modelling suggests the M1 magmas were formed by 6–10% melting (Kerr, 1995).

Type M2 has much flatter REE patterns, with slight relative depletion of LREEs. These magmas are suggested to have formed from 8–12% melting of a mantle lherzolite source at a depth in which spinel is stable. The M2 magmas described in Kent and Fitton (2000) show a slight convex-up pattern centred on Nd and Sm (Fig. 5.39), which could be explained by some amount of garnet in the melting source (Barrat and Nesbitt, 1996).

Type M3 has flat HREE patterns, and is significantly depleted in LREEs (Fig. 5.40). Kerr (1995) suggests that this pattern forms from high-degree melting (12-17%) of a depleted spinel lherzolite source.

The Upper Basalt Formation (UBF) and Lower Basalt Formation (LBF) magma type of the Antrim lavas (Fig. 5.41) has a noticeably convex-up (centred on Nd) REE pattern, as discussed by Barrat and Nesbitt (1996), who suggest this shape occurs when an N-MORB mantle source melts in the garnet stability field.

The majority of Causeway Tholeiite lavas are enriched in LREEs, with flat HREE patterns (Fig. 5.42), although some are significantly LREE-depleted – more similar to MORB. Barrat and Nesbitt (1996) suggest that all of the Causeway Tholeiite magmas formed from melting of a, N-MORB mantle source in the spinel lherzolite stability field, but were contaminated by varying degrees of crustal (Dalradian?) material, which had the effect of enriching these magmas in LREEs.

The relationship between magma type and stratigraphy in both the Scottish Hebrides and the Antrim lava pile shows shallowing of the site of magma formation from the garnet stability field (M1, LBF) into the spinel stability field (M2, M3, Causeway Theoleiite Member), with a later deepening back into the garnet stability field, possibly due to re-thickening of the lithosphere due to magmatic underplating or sill intrusion (Barrat and Nesbitt, 1996; Kent and Fitton, 2000; Kerr, 1995; Kerr et al., 1999).

Figs 5.38 – 5.40 show the REE patterns of the basaltic groups from the CAIC and the North Arran Granite dykes, plotted against REE patterns for intrusions of the different Hebridean magma types. Figs 5.41 and 5.42 show the REE patterns for the same Arran rocks plotted against the REE patterns for volcanic rocks of the Antrim magma types.

These comparisons are summarised in Fig. 5.43, which shows the LREE ratios (chondrite-normalised La/Sm) and the HREE ratios (chondrite-normalised Gd/Yb) for the Arran samples as well as the different BPIP magma types.

Fig. 5.43 convincingly shows that none of the igneous rocks sampled from Arran belong to the M1 magma type. The only Arran rocks with sufficiently high LREE ratios are the gabbros and some of the mafic dykes, but these do not have depleted HREE values (high (Gd/Yb)n ratios). These patterns are reflected in Fig. 5.38.

The similarities between the dolerite sill's REE pattern and those of the M2 magma type are shown in Figs. 5.39 and 5.43. Both are characterised by depleted LREE patterns (chondrite-normalised La/Sm <1) and moderately depleted HREE patterns (chondrite-normalised Gd/Yb 1–1.7). This could suggest that garnet was present in the melting mantle, although Kerr (1995) modelled the M2 magmas by melting purely spinel lherzolite. This dichotomy could be explained by melting in the garnet-spinel transition zone, as suggested by modelling in this study (Fig. 5.7). No other Arran units have the moderately depleted HREE patterns characteristic of magma type M2.

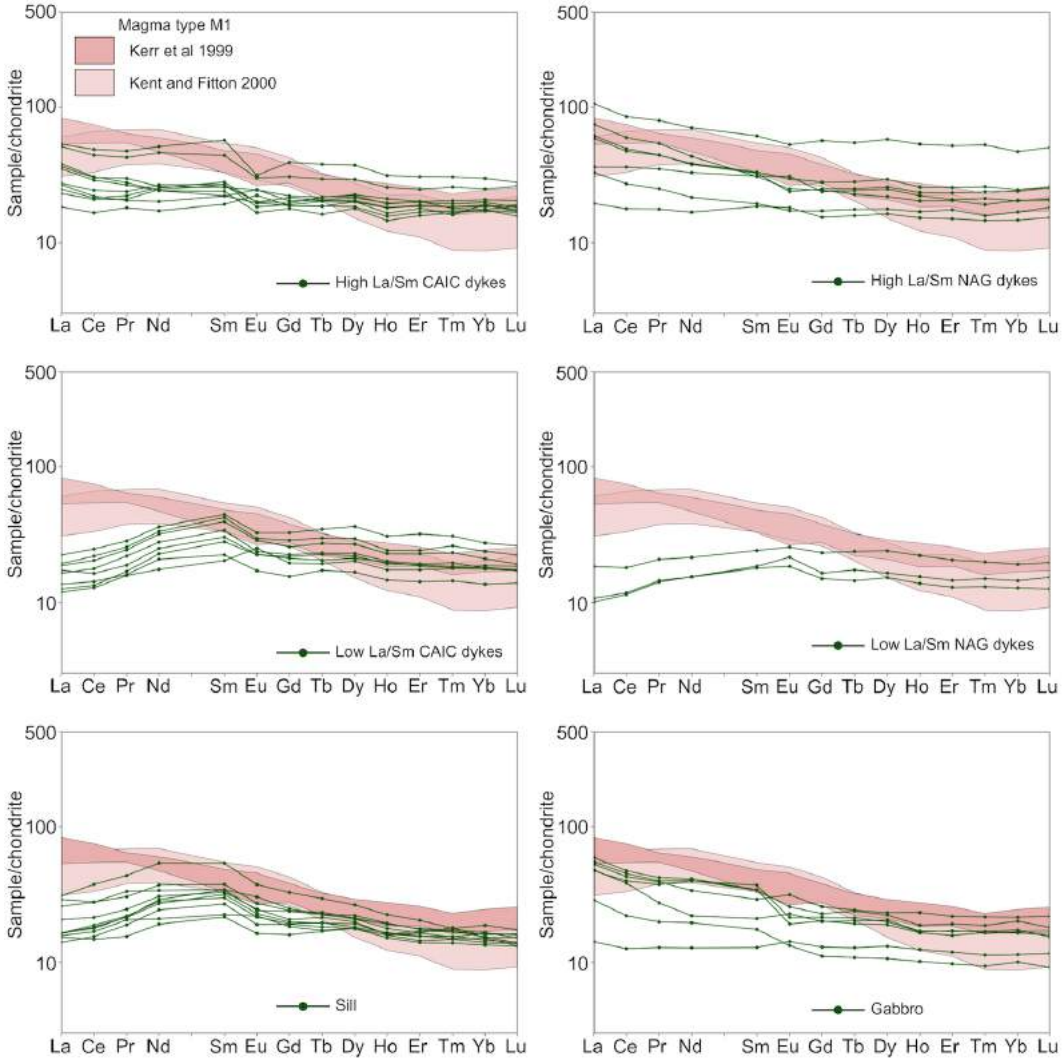

Fig. 5.38 – Chondrite-normalised (McDonough and Sun, 1995) REE plots for the basaltic rocks of the CAIC, as well as the dykes that intrude the North Arran Granite, plotted with fields showing the composition of M1 dykes from the Hebrides, from Kerr et al. (1999) and Kent and Fitton (2000).

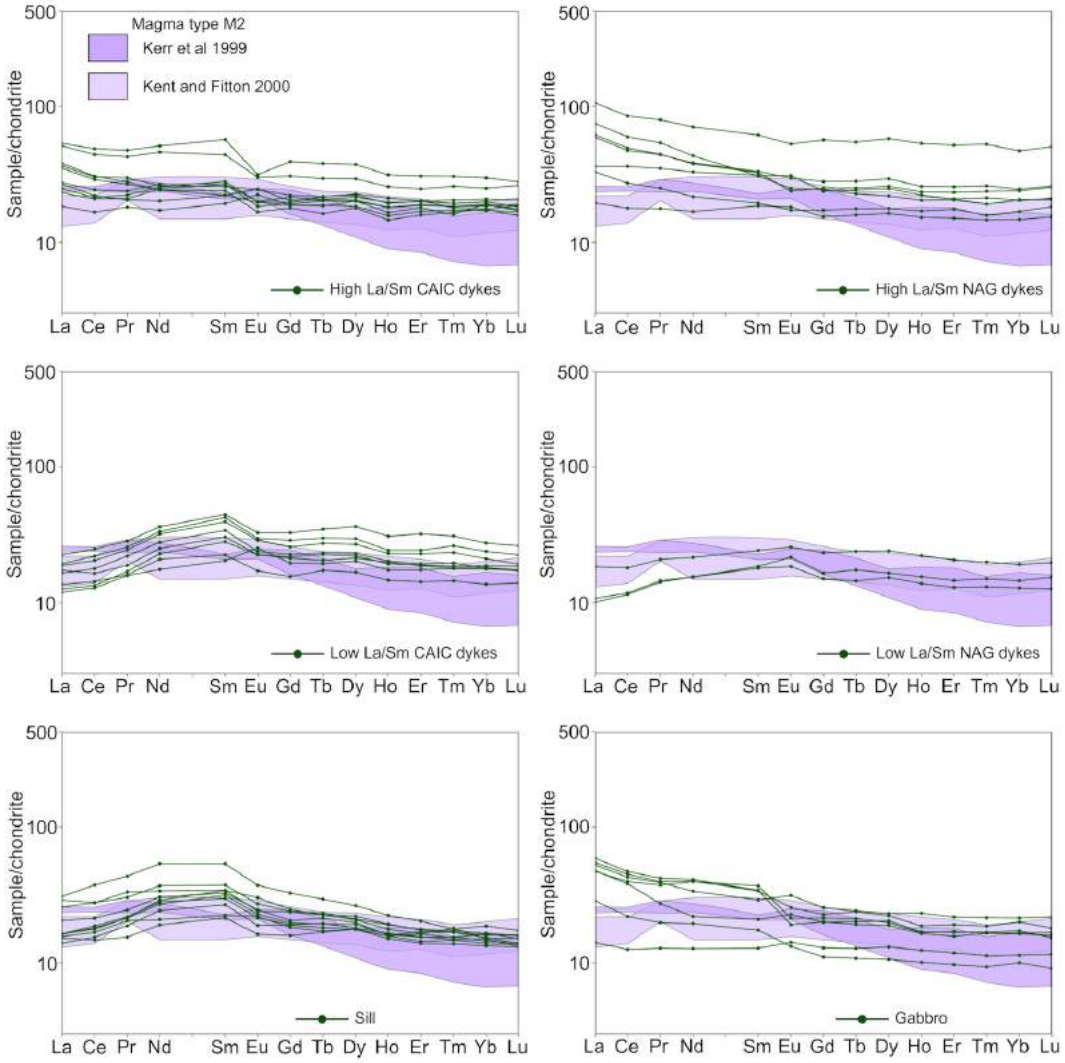

Fig. 5.39 – Chondrite-normalised (McDonough and Sun, 1995) REE plots for the basaltic rocks of the CAIC, as well as the dykes that intrude the North Arran Granite, plotted with fields showing the composition of M2 dykes from the Hebrides, from Kerr et al. (1999) and Kent and Fitton (2000).

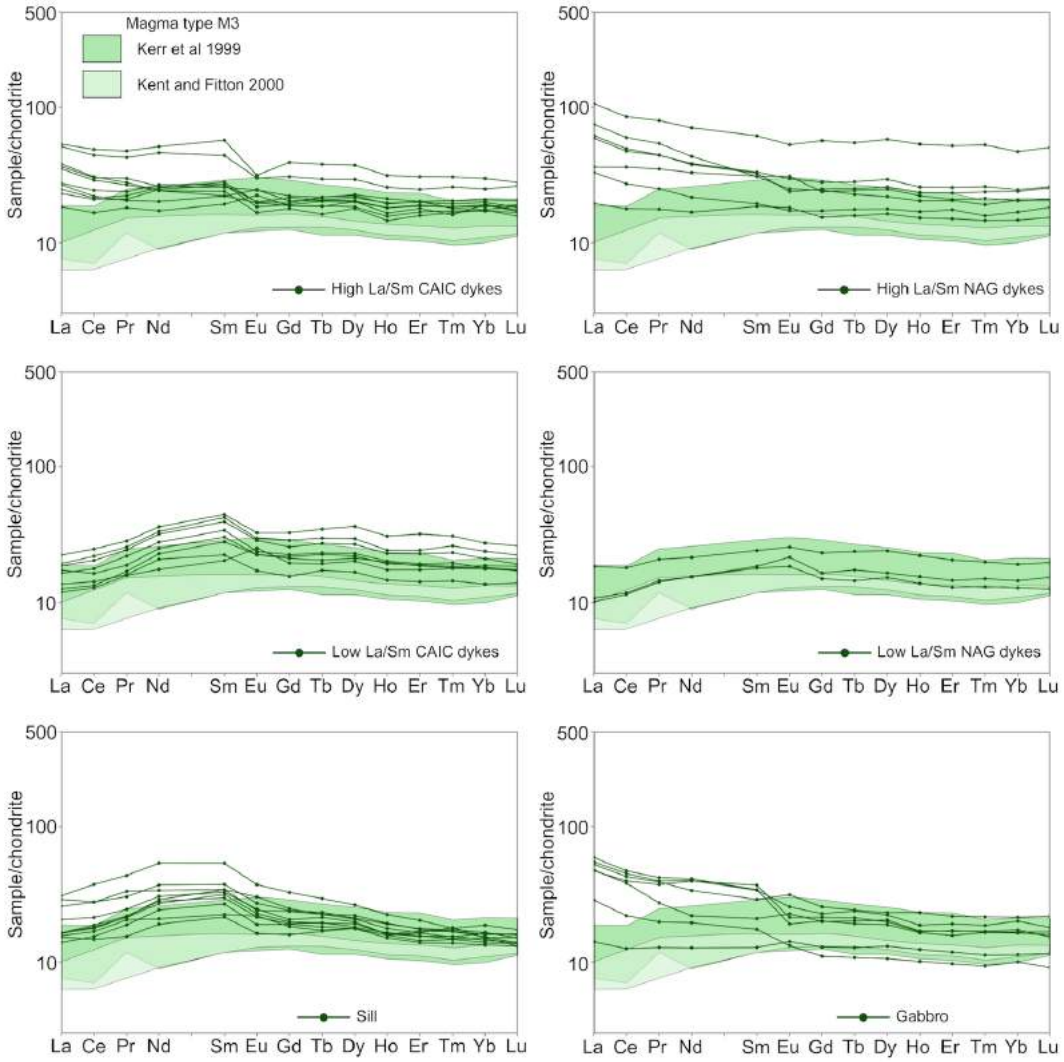

Fig. 5.40 – Chondrite-normalised (McDonough and Sun, 1995) REE plots for the basaltic rocks of the CAIC, as well as the dykes that intrude the North Arran Granite, plotted with fields showing the composition of M3 dykes from the Hebrides, from Kerr et al. (1999) and Kent and Fitton (2000).

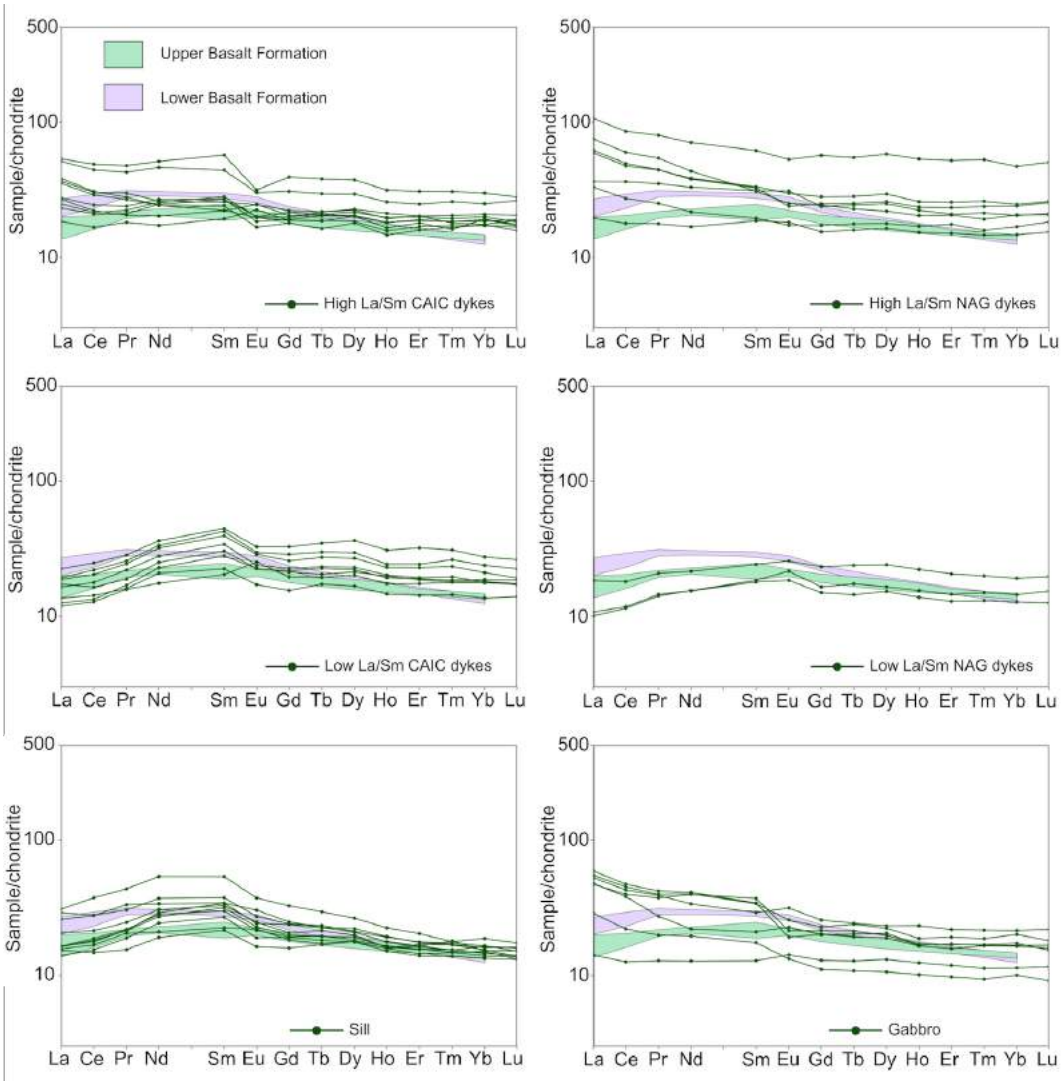

Fig. 5.41 – Chondrite-normalised (McDonough and Sun, 1995) REE plots for the basaltic rocks of the CAIC, as well as the dykes that intrude the North Arran Granite, plotted with fields showing the composition of Lower Basalt Formation and Upper Basalt Formation lavas from Antrim, from Barrat and Nesbitt (1996).

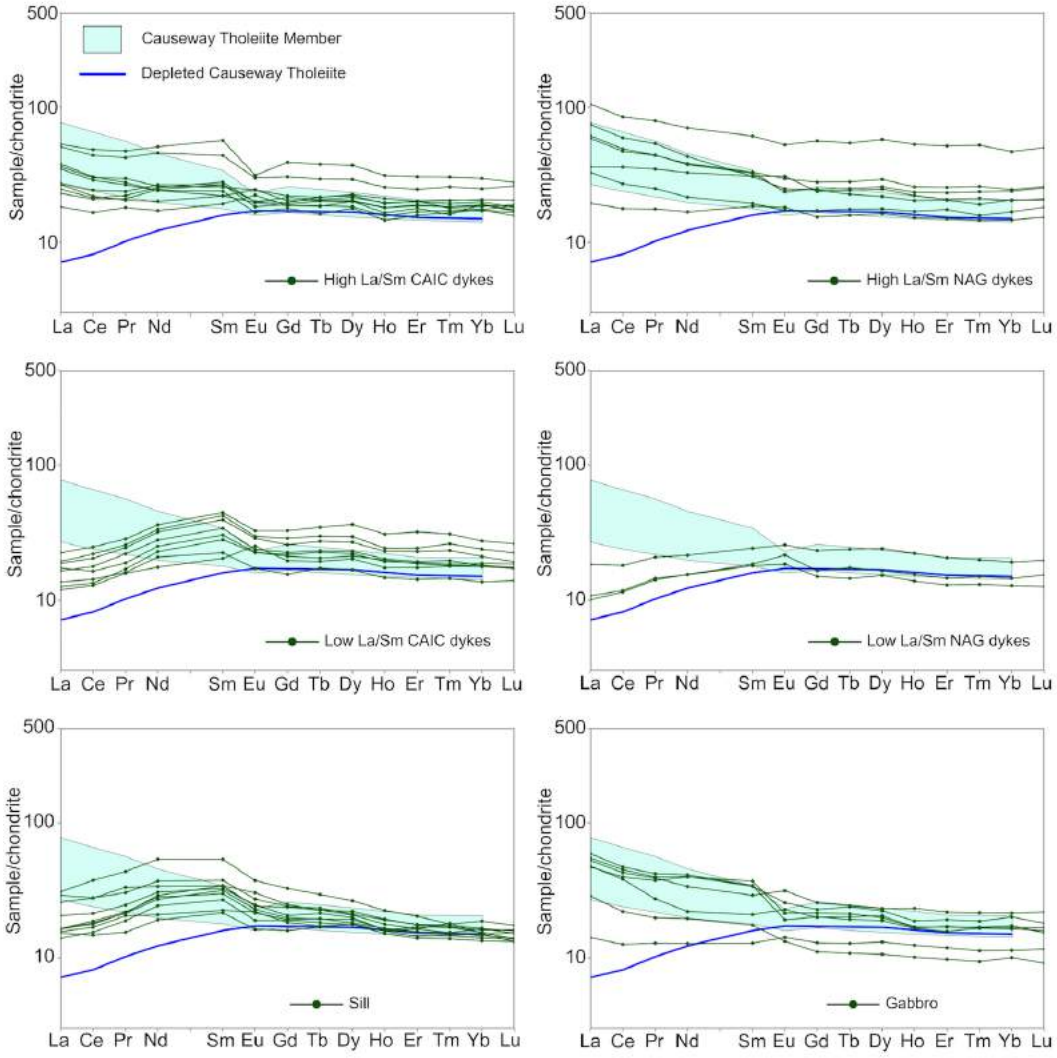

Fig. 5.42 – Chondrite-normalised (McDonough and Sun, 1995) REE plots for the basaltic rocks of the CAIC, as well as the dykes that intrude the North Arran Granite, plotted with fields showing the composition of Causeway Tholeiite Member lava flows from Antrim, from Barrat and Nesbitt (1996).

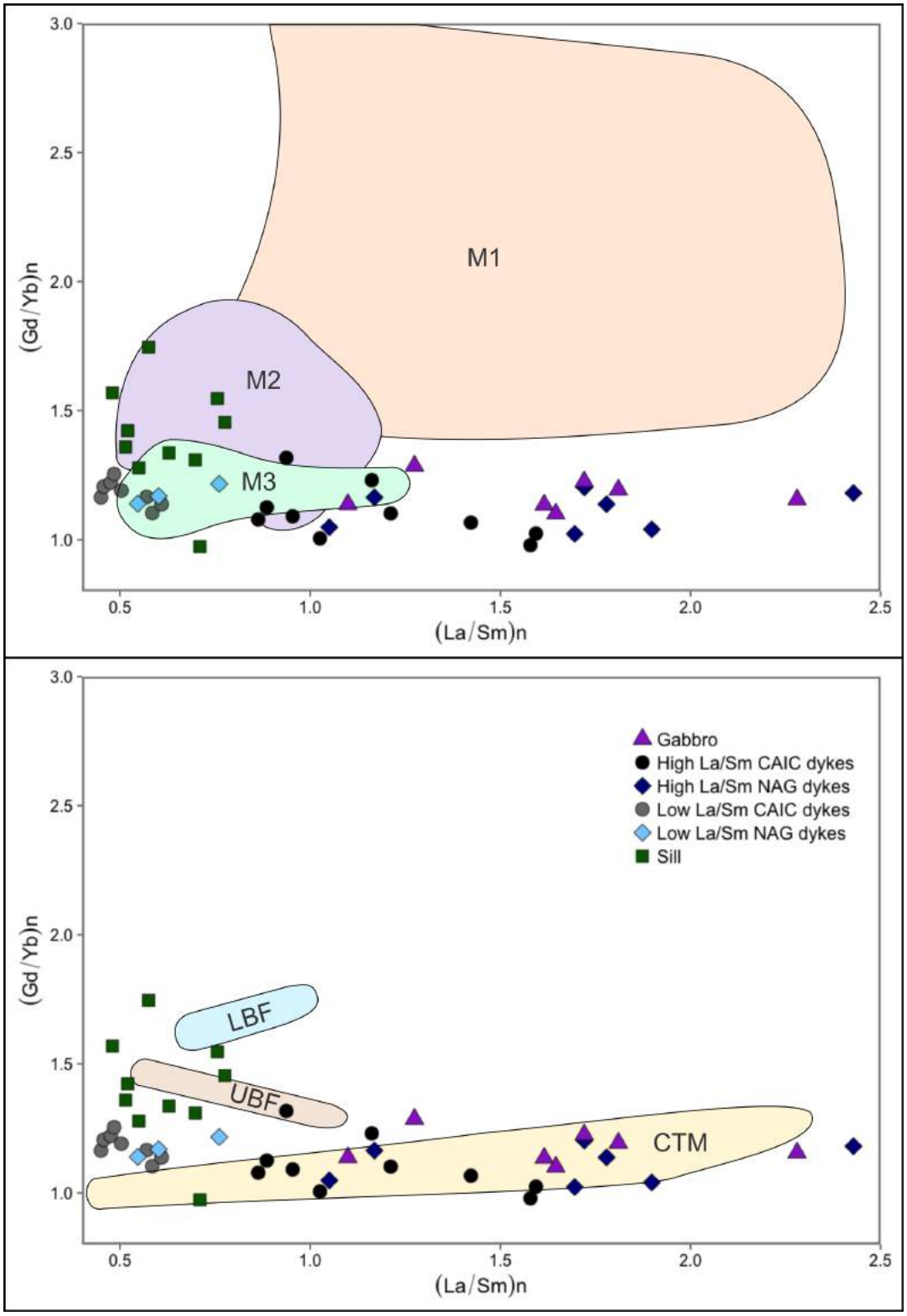

Fig. 5.43 – Chondrite-normalised (McDonough and Sun, 1995) La/Sm ratios against Gd/Yb ratios for the mafic units of the CAIC and the dykes that intrude the North Arran Granite, plotted with fields showing the compositions of the Mull and Antrim magma types. LBF - Lower Basalt Formation, UBF - Upper Basalt Formation, CTM - Causeway Tholeiite Member.

The flat HREE and depleted LREE patterns of the M3 magma type are a close match for the low La/Sm dykes from the CAIC and the North Arran Granite (Figs. 5.40, 5.43). By comparison with previous models (Kerr, 1995) this suggests formation from high degree melting of a spinel lherzolite source. This is consistent with the modelling in this thesis (Figs. 5.3, 5.6). The majority of the high La/Sm dykes and gabbros are too LREE-enriched to belong to this magma type, but there is some overlap.

As discussed in Barrat and Nesbitt (1996), the Lower Basalt Formation (LBF) and Upper Basalt Formation (UBF) of the Antrim lavas belong to a magma type with a distinctly convex-up REE pattern. The only Arran unit which is sufficiently depleted in both LREEs and HREEs relative to medium REEs is the dolerite sill which intrudes the ignimbrites of the AVF (Figs. 5.41, 5.43). Although the M2 and LBF/UBF are suggested to have formed in different melting environments, their shared geochemical similarity to the dolerite sill of the CAIC shows they must come from a similar source. It is therefore likely that the LBF/UBF magma type, the M2 magma type, and the dolerite sill magma had both spinel and garnet in their mantle source region.

The LREE-enriched Causeway Tholeiite Member lavas have REE patterns which are similar to the high La/Sm dykes of the CAIC and the North Arran Granite, as well as the CAIC gabbros (Figs. 5.42, 5.43). The Causeway Tholeiite Member REE patterns reflect both the LREE-enriched profiles of these units, and the large spread of (La/Sm)n values (within a restricted range of (Gd/Yb)n values). The depleted Causeway Tholeiite has a normalised REE element pattern that is similar to the low La/Sm CAIC and North Arran Granite dykes (Fig. 5.42). As the spread of LREE ratios in the Causeway Tholeiite Member is explained by varying levels of crustal contamination, it is suggested that the high La/Sm dykes and the CAIC gabbros were contaminated by continental crust to varying extents. This is consistent with isotopic data and binary mixing modelling discussed in Section 5.4.2.

Summary

The mafic rocks from central Arran analysed in this study show similar major element, trace element, and REE trends to various magma types previously described from the Hebrides and Antrim (Barrat and Nesbitt, 1996; Kent and Fitton, 2000; Kerr, 1995; Kerr et al., 1999). These similarities can be explained by similar proposed melting environments, and are broadly consistent with the results of modelling in this study (Section 5.2.1).

None of the Arran rocks show much geochemical similarity with the M1 magma type of the Hebrides. This suggests that this early episode of melt generation in the history of the BPIP, involving small-to-moderate-degree melting of a depleted garnet lherzolite source, did not supply magmas to central Arran or the dykes intruding the North Arran Granite. (A study on whether or not this magma type is evident in the numerous dykes exposed along Arran's south coast would make for an interesting future project).

The high La/Sm dykes which intrude both the CAIC and the North Arran Granite share some major and trace element similarities with the M3 magma type, with occasional overlap with the M2 field. However, the REE profiles show that these dykes are more enriched in LREE than either of these magma types. They show the best geochemical fit with the Causeway Tholeiite Member magma type, in terms of trace elements and REE. However, it has been proposed that the elevated LREE profiles of the Causeway Tholeiite Member basalts could be a result of significant crustal contamination (Barrat and Nesbitt, 1996). It is therefore suggested that the high La/Sm dykes from this study are of the M2 magma type, but show varying amounts of crustal contamination – making them similar to the Causeway Tholeiite Member type. Formation of the high La/Sm dykes in a melting environment similar to that of the M2 magma type, *i.e.*, small-degree melting of a depleted spinel lherzolite source (Kerr, 1995), is confirmed by modelling.

The low La/Sm dykes of the CAIC and North Arran Granite show major, trace, and rare-earth element similarities to the M3 magma type of the Hebrides. Once again, the proposed M3 melting environment, *i.e.*, larger-degree melting of a depleted spinel lherzolite source (Kerr, 1995), is confirmed by our modelling.

The dolerite sill which intrudes the ignimbrites of the Arran Volcanic Formation shows major and trace element similarities with the M2 and M3 Hebridean magma types. However, its REE profile suggests similarities with both M2 and the LBF/UBF magma type of Antrim. These magma types are proposed to have formed from different mantle source regions (depleted spinel and garnet lherzolite, respectively) as discussed in Kerr (1995) and Barrat and Nesbitt (1996). Modelling of the sill in this study suggests that the magma formed from mantle melting in the garnet-spinel transition zone, so can therefore be partly reconciled with both pre-described magma types.

The CAIC gabbros have highly variable major and trace element concentrations, but their REE profiles show similarities to the Causeway Tholeiite Member. Again, they could therefore be explained by varying contamination of an M2-like magma.

5.5.2 Granitic rocks

The petrogenesis of the silicic rocks from Arran can be put in context by comparison to other granitic and rhyolitic intrusions in the BPIP, which have varying proposed models of formation. Not all BPIP granitic centres have been subjected to complete geochemical study, but what information is available provides useful and important comparison.

The Mull granites belong to two broad geochemical groups, corresponding to the magmatic centre with which they are associated. The first group (Early granites associated with Centre 1) formed by fractional crystallisation of magma similar in composition to the Early Cone-sheets with a significant input of partially melted Lewisian crustal material (Kerr et al., 1999; Walsh et al., 1979). The second group (Late granites associated with Centres 2 and 3) also formed from fractional crystallisation of a magma similar to the associated Late cone-sheets, with a relatively minor input from partially melted crustal material (Kerr et al., 1999; Walsh et al., 1979).

The Skye granites have varied REE compositions, but generally define a profile with a steep LREE-enriched section, a flat to slightly-depleted HREE profile, and a moderate negative Eu anomaly. It has been suggested that these granitic magmas could largely have been formed from fractional crystallisation of the basaltic magma preserved as lavas and dykes on Skye, possibly contaminated by a relatively small amount of crustal material (Meighan, 1979; Thompson, 1982a).

The silicic rocks of the Rùm igneous centre have very steep LREE-enriched and HREE-depleted REE profiles. Crucially, they show very little evidence of negative Eu anomalies, showing that fractionation of plagioclase did not play a significant part in the petrogenesis of these magmas (Meyer et al., 2009; Troll et al., 2004). Their REE patterns are instead suggested to show formation from anatexis of Lewisian amphibolite gneiss (Meyer et al., 2009).

Major and trace elements

Fig. 5.44a shows total-alkali vs. silica (TAS) plots for the silicic Arran rocks analysed in this study, as well as the granites of Mull and Skye. This shows that, in general, the Arran granitic rocks have higher SiO_2 concentrations than the Mull and Skye granites, with lower total alkali concentrations than all but Mull's Centre 1 granites. The Arran samples are also generally more tholeiitic (higher SiO_2 and lower alkalis) than the Ailsa Craig, Rockall, Raasay, Slieve Gullion, and Ardnamurchan granites (Fig. 5.44b). The granitic BPIP rocks with the most similar compositions to the granite samples are St Kilda, Lundy, the Mourne Mountains, and Carlingford. These

magmatic centres are all peripheral to the BPIP, away from the high-density of magmatic centres around the Inner Hebrides.

A plot of SiO_2 against Zr for the silicic Arran rocks and the Mull granites is shown in Fig. 5.45. The Satellite Granites, Glen Craigag Granite, the pitchstone dyke, and the majority of the silicic Glenloig Hybrids have lower Zr than the Centre 2 and Centre 3 Mull granites, but similar Zr to the Centre 1 granites (but with significantly higher SiO_2 concentrations). The North Arran Granite, the granite clasts from the AVF, and the lava-like ignimbrites of the AVF have lower Zr concentrations than any of the Mull granites.

The Mull granites, Skye granites, Glen Craigag Granite, Satellite Granites, CAIC pitchstone dyke, and Glenloig Hybrids all lie on the same positive trend on a Nb vs Zr graph (Fig. 5.46). This is the trend shown by a fractionating magma in which both Nb and Zr are incompatible in the crystallising assemblage. The North Arran Granite, the granite clasts found in the ignimbrites of the AVF, and the two lava-like ignimbrite units of the AVF (the Muileann Gaoithe Member and the White Tuff Member) form a clear flat trend on this graph (Fig. 5.46) suggesting fractionation of zircon in these evolving magmas (Section 5.3). This diagram shows that fractionation of zircon in granitic melts has not happened to nearly the same extent on Mull and Skye.

In fact, when the Zr concentrations of these units are compared with the other granitic rocks of the BPIP, it is apparent that very few magmatic centres have comparably low Zr concentrations (Fig. 5.47). This suggests that fractionation of zircon in evolving granitic melts was not a common process in the BPIP, restricted to Arran and possibly Lundy and the Mourne Mountains.

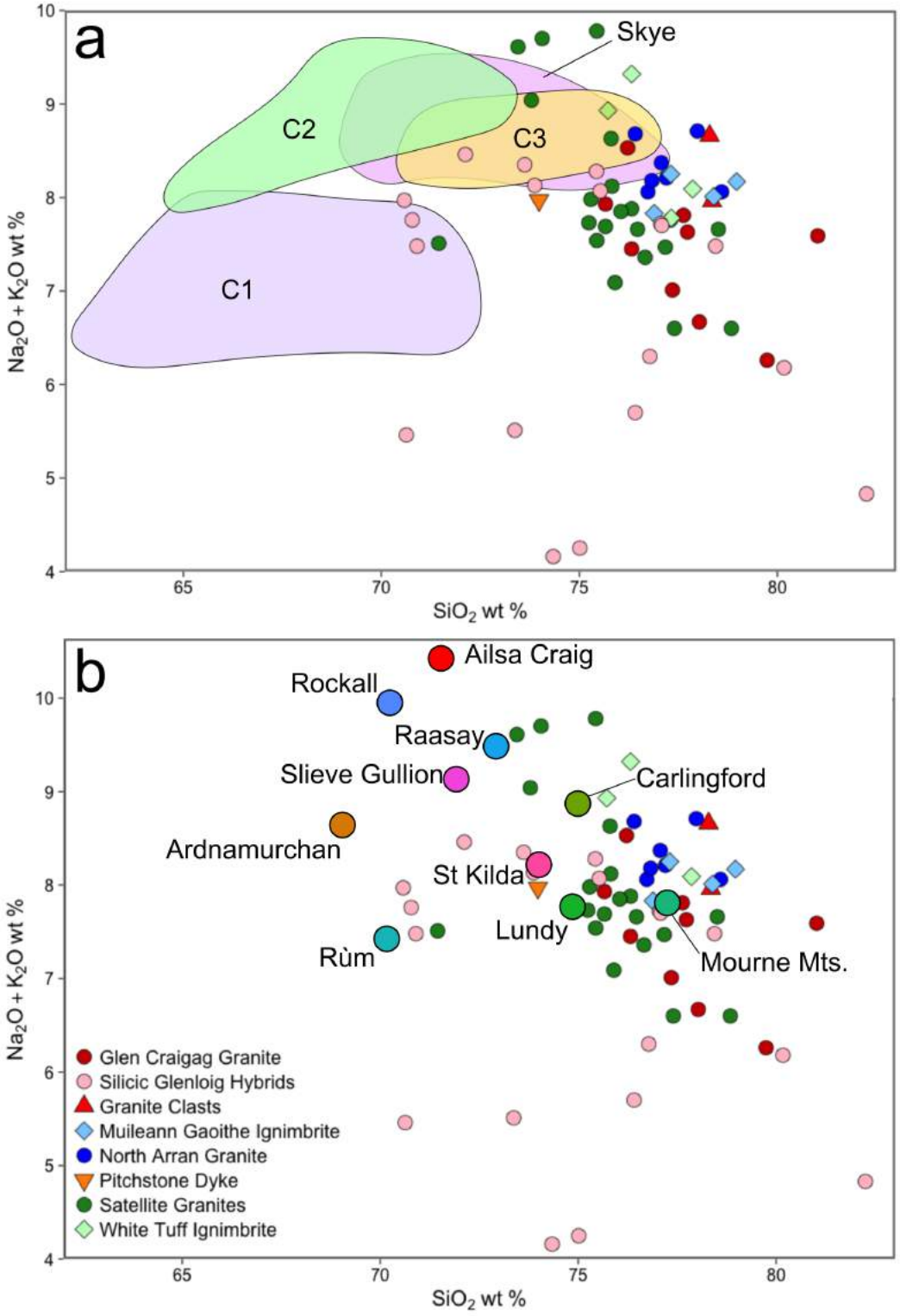

Fig. 5.44 – a) Total alkalis vs. silica (TAS) plot of the silicic rocks of the CAIC, as well as the North Arran Granite, with fields for the Centre 1, Centre 2, and Centre 3 granites from Mull (Walsh et al., 1979) and the granitic rocks of Skye (Sutherland, 1982; Thompson, 1968). b) TAS plot of the silicic rocks of the CAIC, as well as the North Arran Granite, with compositions for other granitic rocks of the BPIP (Sutherland, 1982).

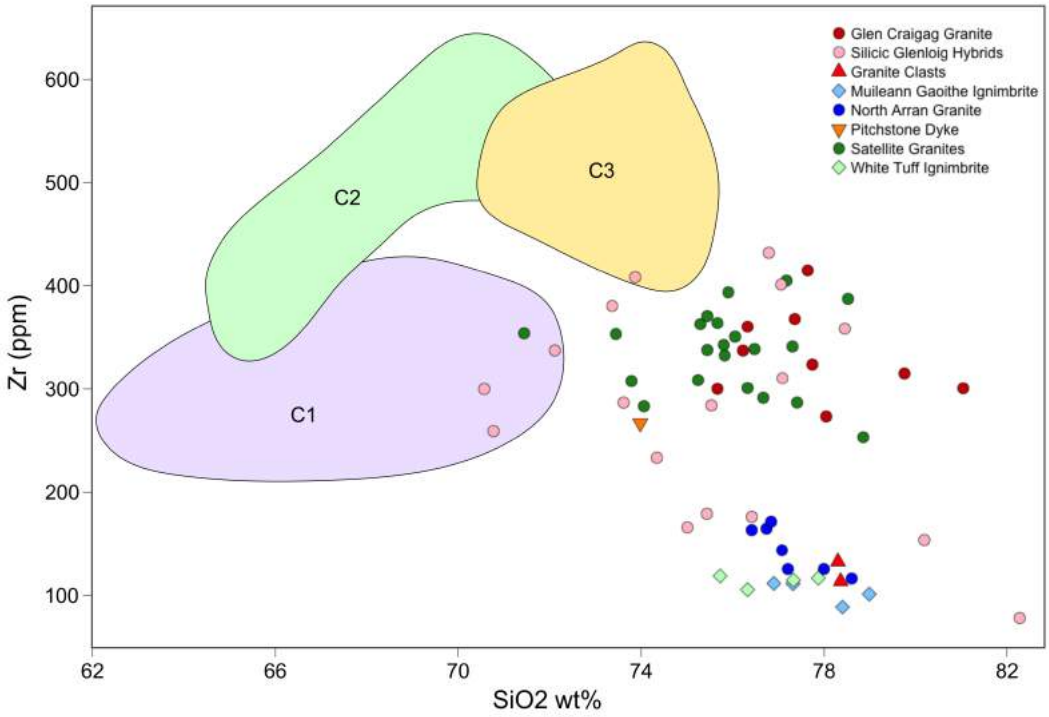

Fig. 5.45 – Plot of SiO_2 against Zr for the silicic rocks of the CAIC, as well as the North Arran Granite, with fields for the Centre 1, Centre 2, and Centre 3 granites from Mull (Walsh et al., 1979).

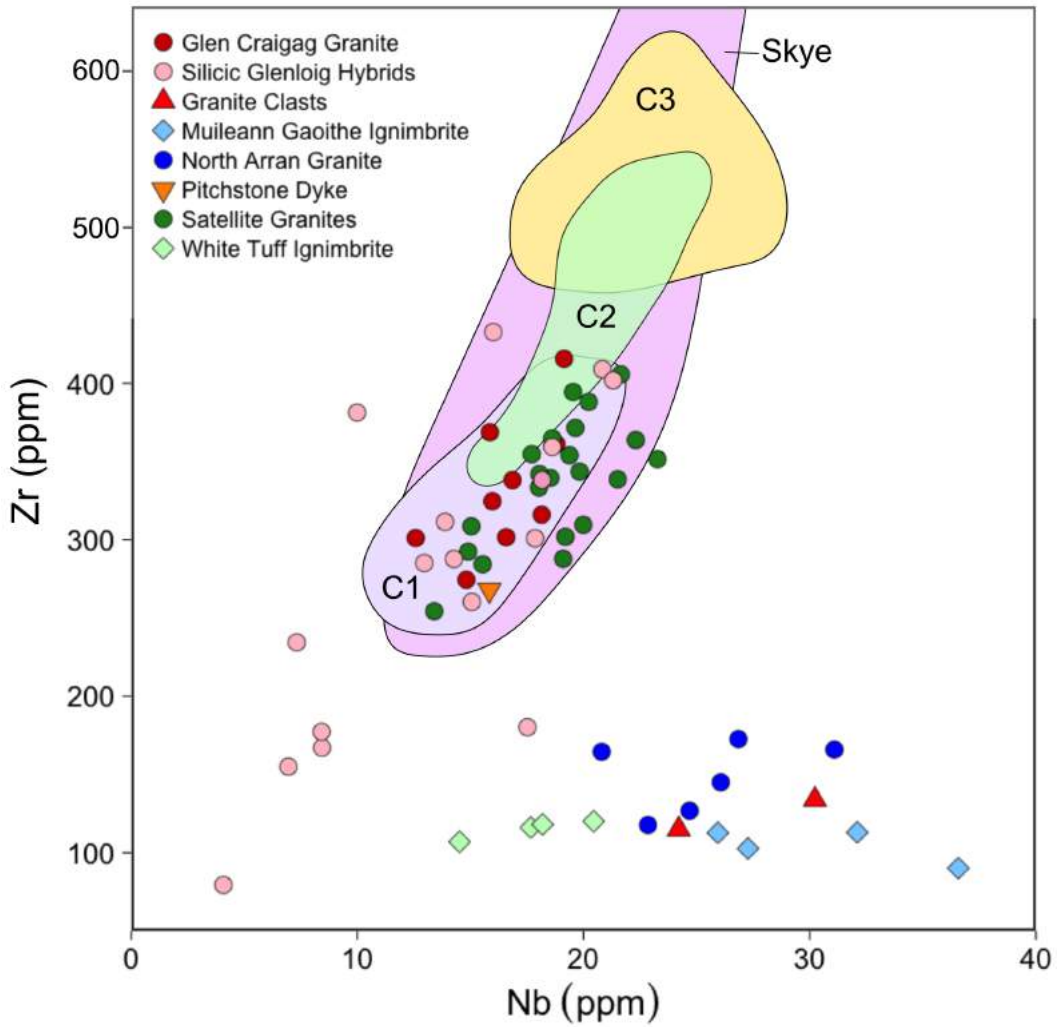

Fig. 5.46 – Plot of Nb against Zr for the silicic rocks of the CAIC, as well as the North Arran Granite with fields for the Centre 1, Centre 2, and Centre 3 granites from Mull (Walsh et al., 1979) and the granites of Skye (Thompson, 1982b).

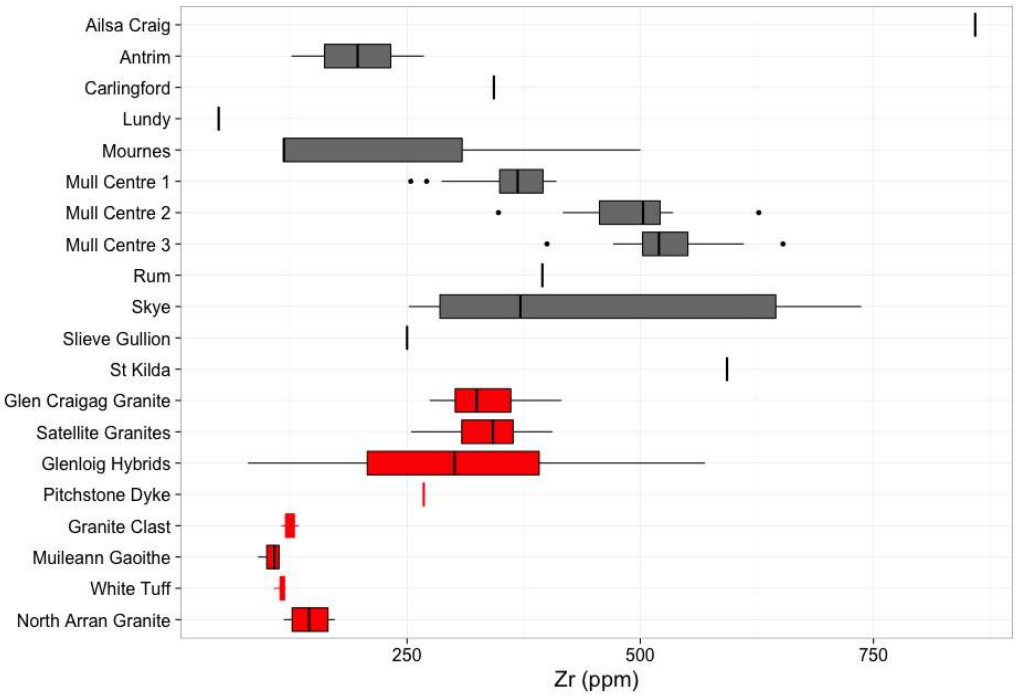

Fig. 5.47 – Boxplot of Zr concentrations for the granitic rocks of the BPIP (grey) along with the silicic rocks of Arran from this study (red). Data from Meighan (1979); Thompson (1982b); Walsh et al. (1979).

Rare-earth Elements

Chondrite normalised (McDonough and Sun, 1995) rare-earth element diagrams comparing the Arran rocks to granites and rhyolites from the Mull, Rùm, and Skye centres are shown in Figs. 5.48 – 5.50. REE profiles for various other silicic rocks from elsewhere in the BPIP are shown in Fig. 5.51 for comparison.

The Mull granites have similar REE profiles to several of the Arran units Fig. 5.48. The Centre 1 Mull granites have gently downward-sloping HREE profiles which is not reflected in any of the Arran groups, except some of the silicic Glenloig Hybrids. The flat HREE profiles and relatively steep LREE profiles of the Centre 2 and 3 granites are similar to the Glen Craigag Granite, the CAIC pitchstone dyke, and the White Tuff Member lava-like ignimbrite. None of these Arran units, other than the White Tuff, have as pronounced negative Eu anomalies as the Centre 3 granite.

Almost all Arran samples show flatter HREE patterns, and much higher overall HREE abundances than the Rùm units (Fig. 5.49). The Satellite Granites, the pitchstone dyke, and the White Tuff ignimbrites have similar LREE profiles, but flat HREE patterns and significant Eu anomalies. The closest matches for the Rùm granitic rocks are found in certain samples of the silicic Glenloig Hybrids. These have steep LREE-enriched profiles, HREE depletions, and small to non-existent negative Eu anomalies. The main cluster of silicic Glenloig Hybrid samples however have more elevated HREEs and negative Eu anomalies. This suggests that these rocks come from a range of sources, which would explain their wide compositional spread. By comparison with the Rùm REE patterns, it could be concluded that crustal anatexis plays a large role in the petrogenesis of the hybrid rocks with the lowest total REE concentrations.

The general REE profile of the Skye granites is similar to those of the Satellite Granites and some of the silicic Glenloig Hybrids (Fig. 5.50). The REE profiles for the Glen Craigag Granites and the pitchstone dyke also almost completely overlap the Skye granites field.

Summary

The silicic rocks from Arran analysed in this study generally have higher SiO_2 and lower $Na_2O + K_2O$ (total alkalis) than the granitic rocks from Mull Centres 2 and 3, Skye, and the rest of the BPIP. They have similar total alkalis to the Mull Centre 1 granites and the Western Granophyre of Rùm, but with higher SiO_2. This suggests that the Arran rocks are even more evolved, and may define a trend of greater SiO_2 saturation than the majority of the BPIP. Some of the granitic rocks

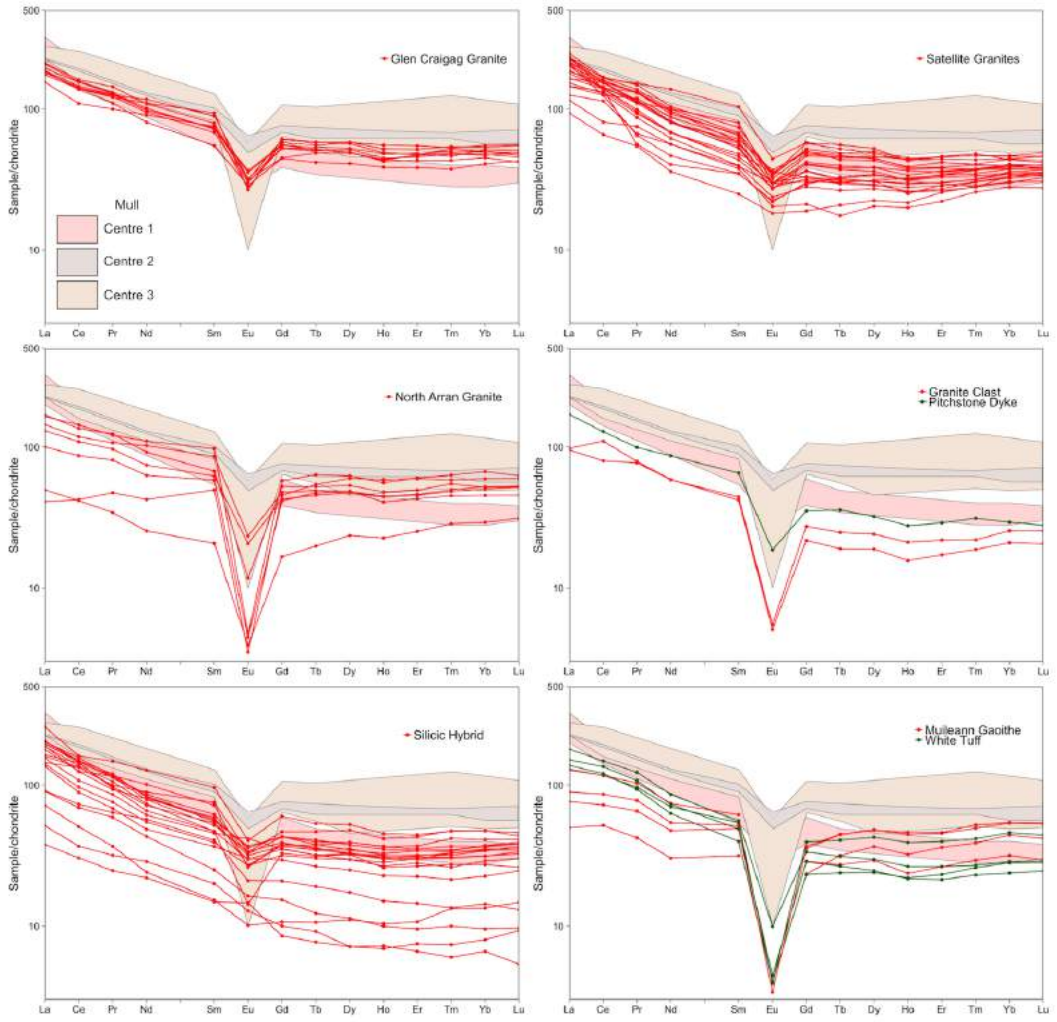

Fig. 5.48 – Chondrite normalised (McDonough and Sun, 1995) rare-earth element diagrams of silicic Arran rocks, with fields for the Centre 1, Centre 2, and Centre 3 granites from Mull (Walsh et al., 1979).

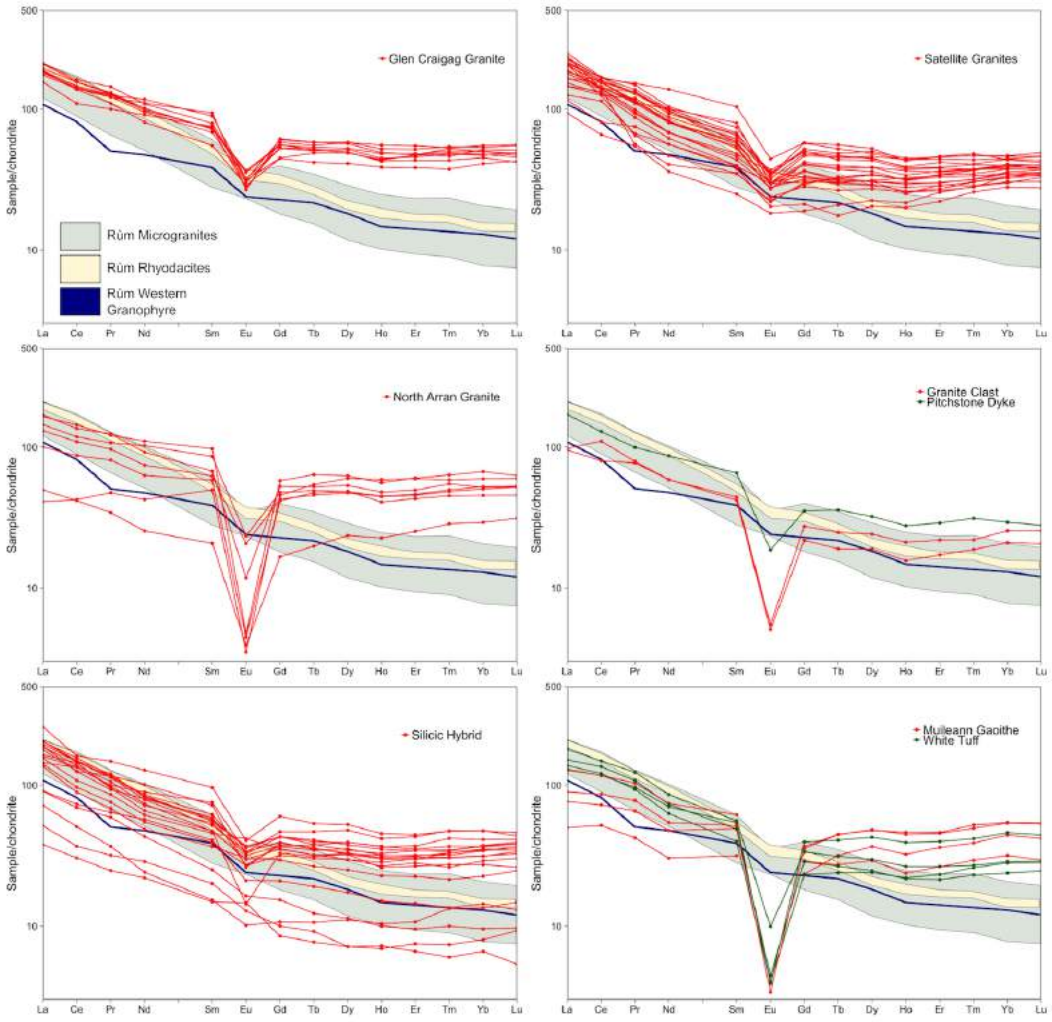

Fig. 5.49 – Chondrite normalised (McDonough and Sun, 1995) rare-earth element diagrams of silicic Arran rocks, with fields for the microgranites, rhyodacites, and Western Granophyre of Rùm (Meighan, 1979; Meyer et al., 2009).

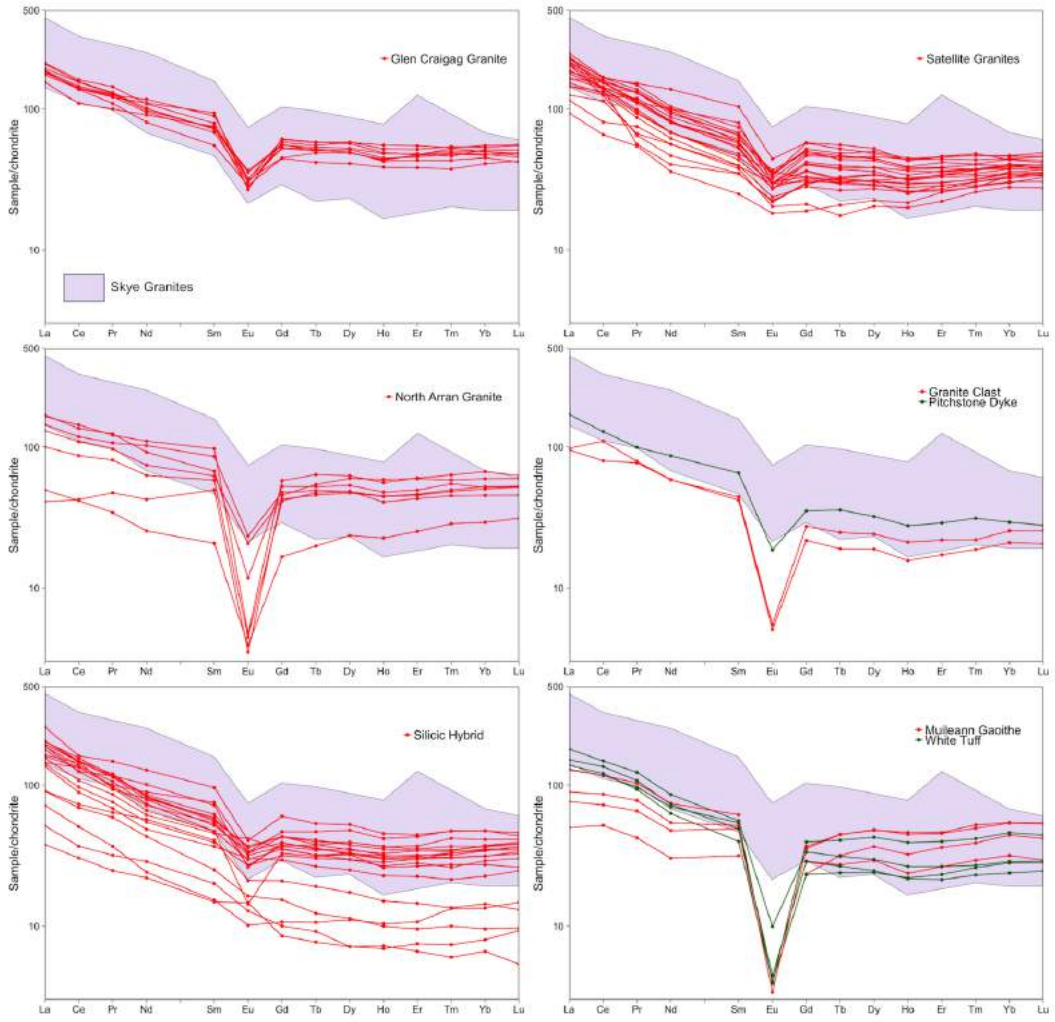

Fig. 5.50 – Chondrite normalised (McDonough and Sun, 1995) rare-earth element diagrams of silicic Arran rocks, with a field for the Skye granites (Meighan, 1979; Thompson, 1982b).

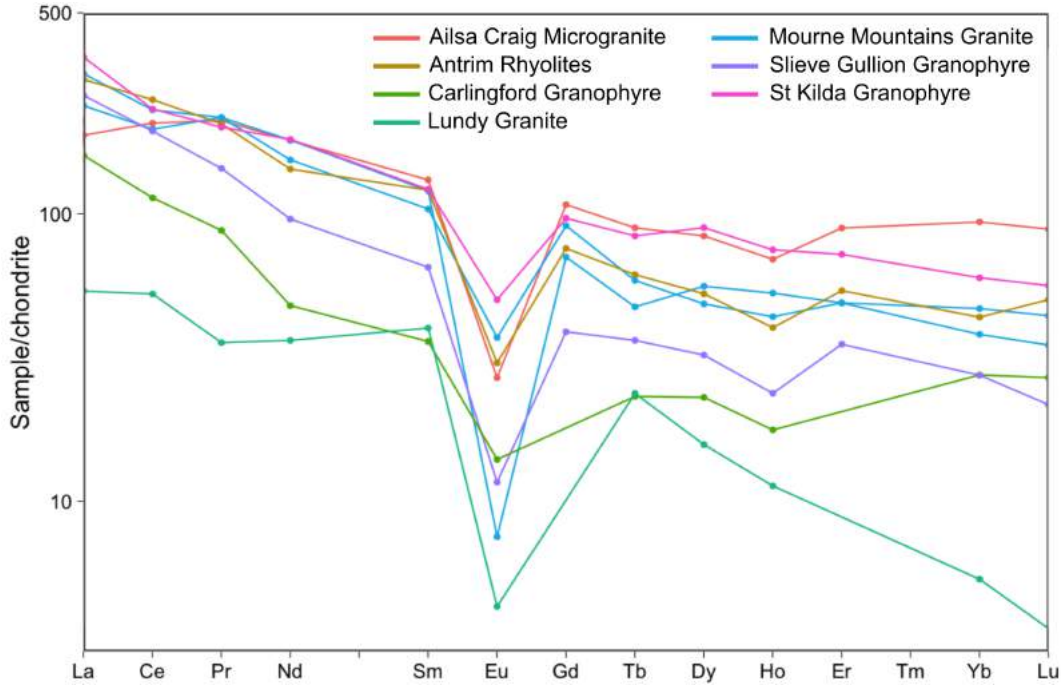

Fig. 5.51 – Chondrite normalised (McDonough and Sun, 1995) rare-earth element diagrams for other granitic and rhyolitic rocks of the BPIP (Meighan, 1979).

from the periphery of the BPIP (St Kilda, Lundy, Carlingford, Mourne Mountains) have similar SiO_2 and total alkali concentrations.

The Arran rocks can be divided into two groups based on Zr content. The first includes the Satellite Granites, the Glen Craigag Granites, the silicic Glenloig Hybrids, and the pitchstone dyke. These have Zr contents which are around the low end for the Mull and Skye granites, but lie on the same trend as the Mull and Skye granites when plotted against Nb, showing the same incompatible nature of Zr in the evolving granitic magma.

The second group contains the North Arran Granite, the granite clasts found in the ignimbrites of the Arran Volcanic Formation, and both lava-like ignimbrites of the Arran Volcanic Formation. These units all have much lower Zr than the Mull and Skye granites, and are amongst the lowest in the BPIP. These rocks formed from magmas in which zircon was a fractionating phase. Fractional crystallisation of zircon is not seen anywhere else in the BPIP, other than perhaps Lundy and the Mourne Mountains, but it has been reported from elsewhere in Arran, with a drop in Zr concentrations with high SiO_2 values in the An Cumhann rhyolite (Meade et al., 2009).

The Glen Craigag Granite, the pitchstone dyke that intrudes the CAIC, and the White Tuff lava-like ignimbrite have REE profiles similar to those of the Mull Centre 2 and 3 granites, pointing towards an origin comprising fractional crystallisation of

basaltic magmas, with a minor input from partial melting of crustal material. The Satellite Granites and the majority of the silicic Glenloig Hybrids have REE profiles similar to the Skye granites, which have a similar proposed mode of formation. Some of the silicic Glenloig Hybrids have REE patterns that match the Rùm microgranites and rhyodacites, suggesting formation of the magmas almost entirely by melting of crustal material.

5.5.3 Isotopes

Radiogenic isotopes have been used to determine the petrogenetic histories of igneous rocks throughout the BPIP. As these studies all show some degree of crustal contamination of the BPIP magmas, isotopic data also provide information on the nature of the crust through which the magmas ascended. As the crustal architecture of Scotland and the northern part of Ireland (Fig. 1.1) is known to be complex (e.g. Bluck et al., 1992), the isotopic signatures of magmatic rocks can be used to show the arrangement of isotopically-distinct crustal blocks at depth.

A summary of Sr and Nd isotope data for the BPIP is shown in Fig. 5.52, along with certain major crustal units, and the Arran data from this study. Pb isotope studies of certain BPIP centres have been carried out, but this is a much less complete data set.

In general, magmas from each central complex generally show contamination by the crustal block (terrane) they ascended through and into which they were emplaced. The Skye lavas, cone sheets, and granites show evidence of varying degrees of contamination by amphibolite- and granulite facies Lewisian gneiss (Fig. 5.52), which are considered to be representative of the variation in crustal material within the Hebridean Terrane (Bell et al., 1994; Carter et al., 1978; Dickin, 1981). This has been interpreted as showing assimilation of material at different levels within the crust. Rùm is the other onshore BPIP central complex that was emplaced into (and erupted onto) the Hebridean Terrane (Fig. 1.1). Although some basic magmas retain primary mantle-like compositions (Geldmacher et al., 2002; Upton et al., 2002), all silicic and many mafic rocks analysed from the island show formation partly or wholly from anatexis of Lewisian amphibolite gneiss (Geldmacher et al., 2002; Meyer et al., 2009).

The central complexes of Ardnamurchan and Mull were emplaced into the Northern Highland Terrane (Fig. 1.1), characterised by outcrop of the Moine schists at the surface. However the ‘terrane boundary’ separating this crustal block from the Hebridean Terrane to the north west is a shallowly dipping reverse fault (the Moine Thrust), and the Moine schists are known to be underlain by Lewisian-like gneisses,

probably as far south east as the Great Glen Fault (Hall, 1987; Park et al., 2002). The isotopic composition of the Ardnamurchan cone sheets reflect this crustal structure, showing evidence of contamination by Lewisian gneisses in the lower crust, and then assimilation of upper crustal material that isotopically resembles the Moine metasedimentary rocks (Geldmacher et al., 2002). The Mull lavas show a much steeper trend on Fig. 5.52, suggesting contamination by only Lewisian gneiss in the lower crust (Kerr et al., 1995), with no clear interaction with Moine schists onto which they were erupted.

The Antrim plateau basalts straddle the Highland Boundary Fault and the Southern Upland Fault (Fig. 1.1). The Upper and Lower Basalt Formations, and the intrusions, show slight isotopic contamination by a high $^{87}Sr/^{86}Sr$, low $^{143}Nd/^{144}Nd$ crustal component. The more contaminated Causeway Tholeiite Member lavas have much more radiogenic Sr and less radiogenic Nd, which has been interpreted as showing assimilation of Dalradian schists (Barrat and Nesbitt, 1996).

The Slieve Gullion central complex lies on the southern edge of the Southern Upland Terrane (Fig. 1.1). The flat isotopic profile, at around $^{143}Nd/^{144}Nd = 0.5124$ on Fig. 5.52 has been interpreted by Troll et al. (2005) as deriving from varying degrees of assimilation of lower Palaeozoic Southern Uplands sedimentary rocks, and the Caledonian Newry Granodiorite.

Isotopic values for various mafic lavas and dykes of Arran, as well as the BPIP, are shown in Fig. 5.53. Of the BPIP units, the Mull and Skye lavas show a clear trend towards the Lewisian granulite gneiss. The Antrim lavas trend towards a Dalradian (or possibly Midland Valley) contaminant. The dykes of the Jura-Islay-Gigha (JIG) swarm (Hole et al., 2015) define a trend between the Lewisian and Dalradian mixing trends. It therefore appears that these dykes were formed by crustal contamination of mantle-derived melt with Rhinns like crust, which is to be expected given their proximity to the exposed Rhinns Complex.

The samples from the Arran CAIC sill all lie entirely within the field of the JIG dykes. This reinforces the suggestion that the magma that formed this sill was contaminated by Rhinns-like crustal material, possibly within the Islay Block.

The CAIC dykes form a trend parallel to the Upper Basalt Formation lavas of Antrim on the $^{87}Sr/^{86}Sr$ vs. $^{143}Nd/^{144}Nd$ plot (Fig. 5.53). Three of the CAIC mafic dykes (not including the sample that isotopically similar to the dolerite sill) and the CAIC picrite define a trend further to the right of the Mull lavas or JIG dykes on the $^{208}Pb/^{204}Pb$ vs. $^{143}Nd/^{144}Nd$ plot, showing that their crustal contaminant was isotopically different. These trends suggest that the CAIC dykes (and possibly some Antrim lavas) were contaminated by a high $^{87}Sr/^{86}Sr$, high $^{208}Pb/^{204}Pb$ unit, such as the Midland Valley basement.

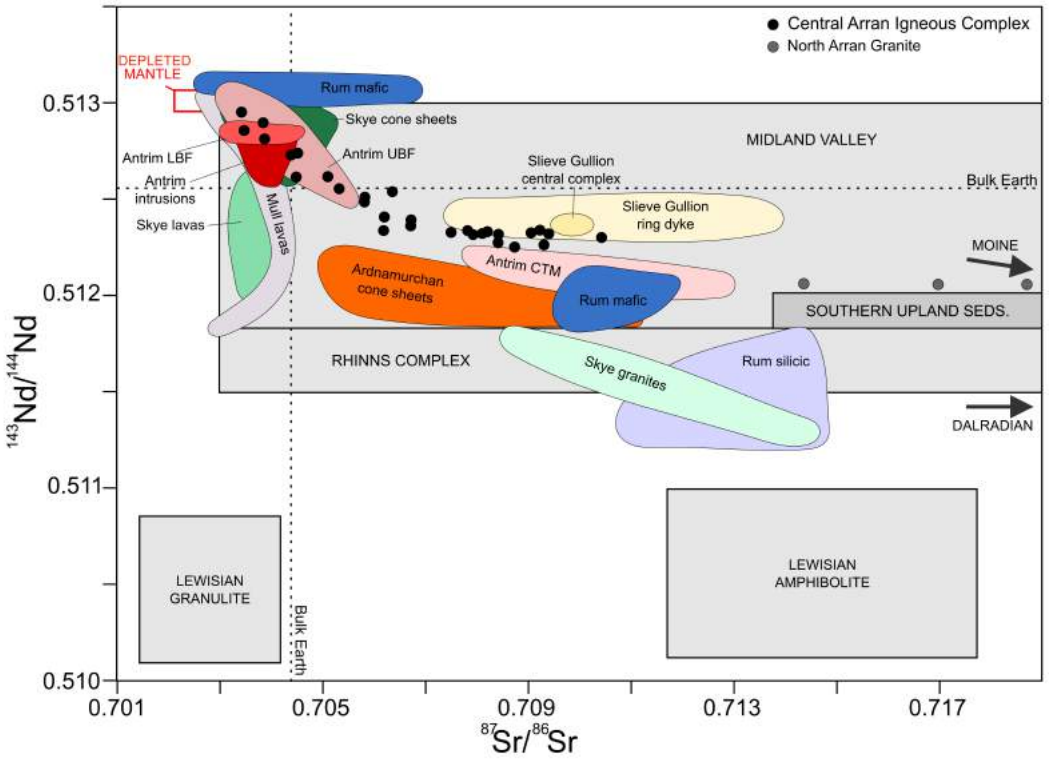

Fig. 5.52 – Age-corrected (59 Ma) $^{87}Sr/^{86}Sr$ vs. $^{143}Nd/^{144}Nd$ plot for the igneous rocks of the BPIP, along with the data from Arran (this study) plotted as circles, and the major crustal units of western Scotland shown as grey fields. Data from Barrat and Nesbitt (1996); Bell et al. (1994); Carter et al. (1978); Dickin (1981); Gamble et al. (1992); Geldmacher et al. (1998); Kerr et al. (1995); Meyer et al. (2009); Troll et al. (2005).

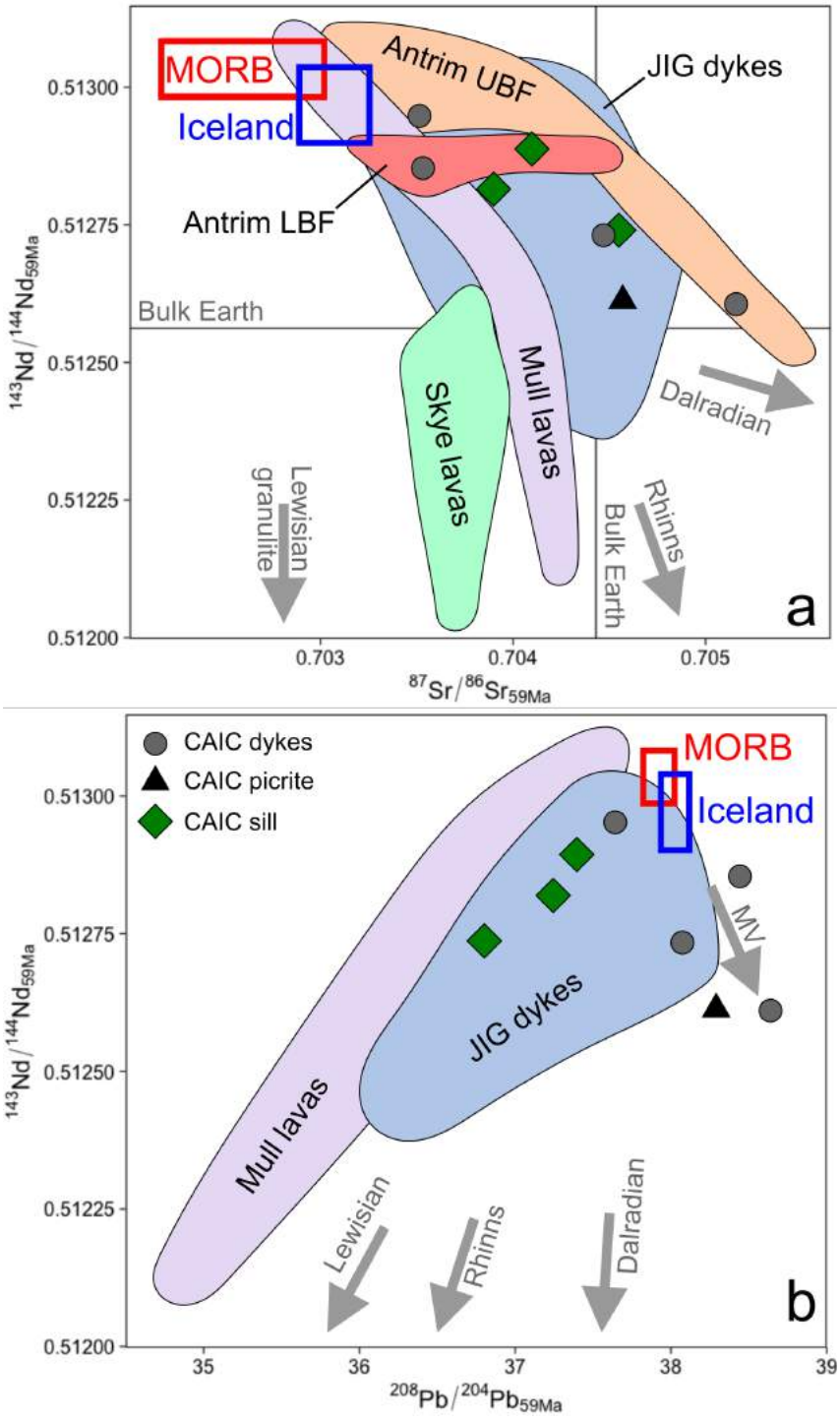

Fig. 5.53 – Age-corrected (59 Ma) $^{87}Sr/^{86}Sr$ vs. $^{143}Nd/^{144}Nd$ plot **(a)** and $^{208}Pb/^{204}Pb$ vs. $^{143}Nd/^{144}Nd$ plot **(b)** for the mafic lavas and dykes of the BPIP, along with the data from Arran (this study) plotted as points. *JIG – Jura, Islay, Gigha*. Grey arrows show general mixing trends between mantle and crustal end members. Data from Barrat and Nesbitt (1996); Carter et al. (1978); Hole et al. (2015); Kerr et al. (1995).

Overall, it is clear that those lavas and central complexes to the north west of the Great Glen Fault (Fig. 1.1) show steeper trends on Fig. 5.52, derived from their interaction with the relatively unradiogenic Lewisian crust. Those centres south of the Great Glen (Arran, Antrim, Slieve Gullion) have flatter profiles, with Nd isotope ratios that are not particularly low, but very high radiogenic Sr levels. These patterns are derived from contamination by the high $^{87}Sr/^{86}Sr$, low $^{143}Nd/^{144}Nd$ crustal units of the Dalradian schists, Midland Valley, Islay Block (Rhinns Complex), and the Palaeozoic rocks of the Southern Upland Terrane.

The North Arran Granite has the highest $^{87}Sr/^{86}Sr$ ratio of any igneous rock sampled from the BPIP. This is consistent with a relatively high degree of contamination by Dalradian crust.

5.5.4 Other Palaeogene Arran rocks

Several previous studies have looked at the geochemistry and petrogenesis of the Palaeogene intrusions on Arran. Dickin et al. (1981) concluded that both the mafic and silicic Arran intrusions formed from fractional crystallisation of mantle derived melts that experienced varying degrees of crustal contamination. Dickin (1994) refined this model, using isotopic data to show that the North Arran Granite had been contaminated by crustal units north of the Highland Boundary Fault, while the granites of the CAIC were contaminated by the crust south of the Highland Boundary Fault. This is to be expected as the fault is thought to run between these two igneous systems at depth. However, he showed that certain intrusions in the south of the island (south of the Highland Boundary Fault) showed isotopic evidence of being contaminated by crustal material north of the fault before being intruded laterally towards the south.

This process was also noted more recently by Meade et al. (2009), who confirmed that the magmas that formed the Drumadoon intrusive complex (south of the Highland Boundary Fault) were contaminated by Grampian Terrane crust prior to emplacement. They noted that the basaltic magma that formed the edges of the composite Doon sill and An Cumhann dyke was contaminated by a unit isotopically resembling the Rhinns complex on Islay. The rhyolitic magma found throughout the Drumadoon complex has a much higher radiogenic Sr isotope signature, and the authors interpreted this as showing contamination by a Rhinns-like unit in the lower crust, and then by a unit similar to the Dalradian schists at shallower levels.

Isotopic data for the Arran intrusions presented in these previous studies are shown in Fig. 5.54. The first thing that should be noted is that the data for the North Arran Granite and the CAIC granites from Dickin (1994); Dickin et al. (1981)

are very similar to the results from this study. The same conclusions about the contamination histories of these units (by the Dalradian schists and the Midland Valley basement, respectively) have been found both in this thesis and the previous studies.

The minor silicic intrusions (Dickin, 1994; Dickin et al., 1981) have a spread isotopic values greater than the CAIC granites (this study), and overlap with the least contaminated North Arran Granite samples (Fig. 5.54). It is clear from the Pb isotope plot that this group contains magmas that were contaminated by both the Midland Valley crust and the Dalradian schists, as suggested by Dickin (1994).

The data for the minor basic intrusions from the same works have a similar wide range of isotope values (Fig. 5.54). Again, the Pb isotope plot shows that they have been contaminated by the Midland Valley crust, as well as either the Dalradian schists, the Rhinns of Islay gneisses, or both. The same is true of the mafic dykes that intrude the CAIC (this study), which collectively show contamination by all of these crustal units. The previously published data therefore back up the conclusions from this thesis that mafic rocks in central (/southern) Arran have magmatic ascent histories involving different crustal depths on either side of the Highland Boundary Fault.

Meade et al. (2009) determined, using modelling, that the Drumadoon complex mafic magmas formed from a mantle-derived melt with the addition of around 10% Rhinns complex gneiss. This crustal input of Rhinns-like material is an order of magnitude greater than that modelled for the dolerite sill that intrudes the CAIC (this study). This fits the trend seen on the $^{87}Sr/^{86}Sr$ vs. $^{143}Nd/^{144}Nd$ graph (Fig. 5.54), in which the Drumadoon mafic samples lie on the same mantle–Islay mixing line as the CAIC dolerite sill, but show significantly more contaminated compositions.

The Drumadoon rhyolites are proposed to have formed from 7.5% addition of Rhinns-like gneiss, then a further 40% addition of Dalradian schist. This model seems to be in agreement with its position at lower radiogenic Sr values on Fig. 5.54, as these rhyolites would lie to the left of the mantle–Dalradian mixing line (this study) presented in Figs. 5.33 and 5.34. Only Sr and Nd values are presented in Meade et al. (2009) – analysis of the Pb isotope geochemistry of the Drumadoon complex would allow a multi-dimensional mixing model to be constructed, which may confirm or refute the double-contamination theory.

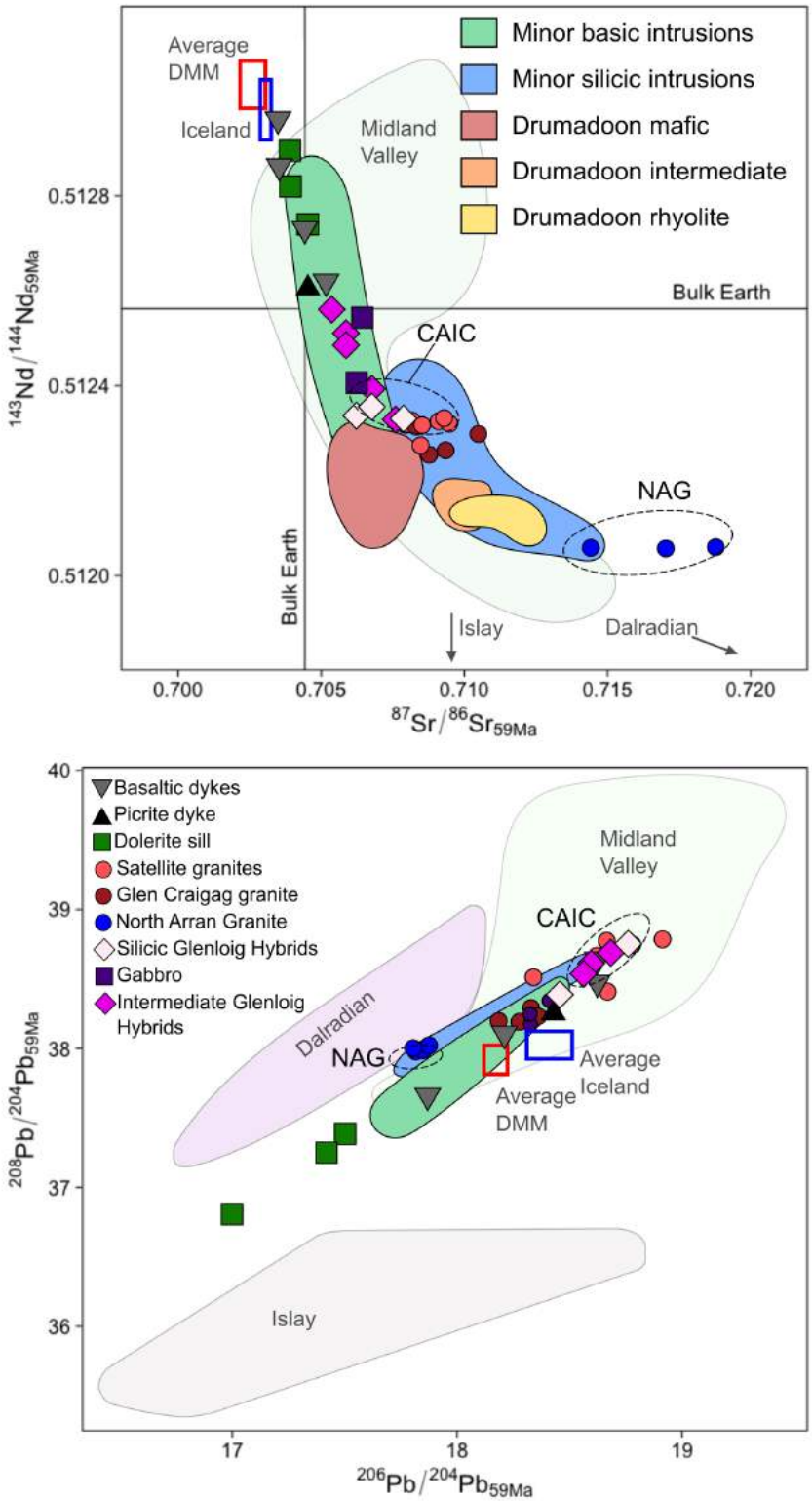

Fig. 5.54 – Binary plots of age-corrected (59 Ma) isotopes for samples analysed in this study, with coloured fields showing data for other Palaeogene intrusions on Arran, from Dickin (1994); Dickin et al. (1981); Meade et al. (2009). Also shown are previous analyses of the North Arran Granite and the granites of the CAIC (circled) from Dickin (1994); Dickin et al. (1981). Pale fields show the crustal units.

5.6 Summary

In this section, the petrogenesis of the different units in the CAIC, as well as the North Arran Granite and the dykes which intrude it, will be summarised in terms of mantle melting, fractional crystallisation, crustal contamination, and comparison with other rocks throughout the BPIP.

5.6.1 Mafic Dykes

The dyke with the most primitive composition found in the CAIC is the olivine picrite dyke that intrudes the Glen Craigag Granite in Ballymichael Glen, which has an MgO concentration of 19.59 wt.% and Mg# 79.32. The Mg contents of the olivine crystals (the only preserved olivines in the CAIC) suggest that this dyke formed from a picritic magma that had accumulated at least 15% olivine. The calculated primary melt with which these olivines would have been in equilibrium has MgO = 14.41 wt.% and Mg# 73.91. This is still significantly less Mg-rich than the M9 picrite from the isle of Rùm (Upton et al., 2002) which has an MgO concentration of 34.61 wt.%. REE concentrations suggest that the Arran picrite formed from 2% melting of a spinel lherzolite source. Isotopic data suggest that it was contaminated to some degree by crustal material resembling the Midland Valley basement.

The mafic dykes can be divided into two distinct geochemical groups, based on their La/Sm ratios (Section 4.1.4). This geochemical distinction seems to have its origin in the melting environments of these magmas. The low La/Sm dykes which intrude the CAIC and the North Arran Granite are proposed to have formed from relatively high-degree (5-10%) melting of a spinel lherzolite source, while the high La/Sm dykes are suggested to have formed from up to 4% melting of a similar spinel lherzolite source. All mafic dykes formed from melting of a mantle source that was made up of both N-MORB and Icelandic plume-like end-members.

The near-primary magmas that intruded to form these dykes underwent fractional crystallisation, with some crustal contamination from a variety of isotopically distinct sources. Fractional (or near-fractional) crystallisation of olivine, plagioclase, and magnetite from picritic melts resembling either the M9 Rùm picrite or the calculated primary Arran picritic melt could have formed the mafic dyke magmas. The fractionation of olivine$\pm$plagioclase$\pm$magnetite can explain most of the major element variation seen among the mafic dykes that intrude the CAIC and the North Arran Granite.

The mafic dyke magmas were contaminated to a relatively small degree (<5%) by crustal units that isotopically resemble the Midland Valley basement, the Rhinns

Complex of Islay, and the Dalradian schists of the Grampian Terrane. The high La/Sm dykes are geochemically similar to the M2 magma type of the Hebrides, with contamination causing the resemblance to the Causeway Tholeiite Member from Antrim. This similarity is due to a similar melting regime. The low La/Sm dykes are more similar to the M3 magma type of the Hebrides, again due to a similar proposed melting environment.

5.6.2 Dolerite Sill

The dolerite sill that intrudes the CAIC has a distinct convex-up REE pattern, and is suggested to have formed from 5–8% melting of an N-MORB transitional garnet-spinel lherzolite source. Both fractional crystallisation and crustal contamination were significant processes in the petrogenesis of the sill magma. Modelling shows that the magma could have formed from fractional crystallisation of olivine, plagioclase, and magnetite from the calculated primary Arran picrite, or from fractional crystallisation of olivine from a primary melt with the composition of the M9 Rùm picrite.

The isotopic composition of the sill shows that the MORB-derived magma was contaminated by up to 0.5% additional crustal material which geochemically resembles the Rhinns Complex of Islay. The dolerite sill shares some geochemical similarities with the M2 and M3 Hebridean magma types, and the Lower/Upper Basalt Formations magma type of Antrim.

5.6.3 Glenloig Hybrids

The intermediate Glenloig Hybrids are petrographically varied, and this variation is reflected in the spread of isotopic data. However, they have remarkably consistent REE profiles (Section 4.1.4), suggesting they all share an ultimate origin. Their isotopic compositions suggest that these magmas represented a MORB-derived melt contaminated by varying amounts of crustal material resembling the Midland Valley basement.

The silicic Glenloig Hybrids do not show evidence of fractionation of significant amounts of plagioclase, and have more contaminated isotopic compositions, suggesting crustal anatexis was a major process in their petrogenesis. The isotopic data suggest up to 80% contamination by Midland Valley crust. Their highly variable REE profiles and trace element compositions suggest they come from a range of sources.

The silicic Glenloig Hybrids display a wider range of major element compositions that most other granitic units in the BPIP. The REE profiles of the samples with no negative Eu anomalies are very similar to those of the granitic rocks on Rùm, suggesting an origin by crustal anatexis.

5.6.4 The Sheans and Tighvein

The Tighvein samples closely resemble the trace element patterns of the Dalradian-derived leucogranites, suggesting a possible anatexis source from north of the Highland Boundary Fault. Depleted Sr and Ti could also indicate fractionation of plagioclase and Fe-Ti oxides during evolution. The petrographically similar samples from the Sheans do not show any evidence for plagioclase of Fe-Ti oxide fractionation, indicating that they may have formed by crustal anatexis. The most likely crustal source, based on trace element profiles, is the Midland Valley basement.

5.6.5 Granites

The Satellite Granites show evidence of some fractional crystallisation of plagioclase, but this is not extensive. They also have highly contaminated isotopic signatures, indicating up to 50% addition of Midland Valley crustal material. The major and trace elements are somewhat similar to the Mull and Skye granites. The REE profiles are similar to Skye and Mull Centre 3, suggesting formation by a combination of fractional crystallisation and crustal anatexis.

The Glen Craigag Granite samples have moderate negative Eu anomalies implying significant fractionation of plagioclase during evolution. A greater degree of fractional crystallisation than the Satellite Granites is confirmed by mixing modelling, implying a lesser, but still significant, crustal input. The models suggest contamination by up to 30% Dalradian crust, likely with some input from Midland Valley material as well. The Glen Craigag Granite has major and trace chemistry similar to the Skye and Mull Centre 1 granites, with REE profiles more similar to the Mull Centre 2 and 3 granites, confirming a petrogenetic model involving both fractional crystallisation and crustal anatexis.

The North Arran Granite shows evidence of significant fractionation of plagioclase, K-feldspar, zircon, and apatite during magmatic evolution. The isotopic data clearly show minor contamination from the Dalradian schists – around 3% if a DMM source is assumed. Because of the fractionation of zircon, the North Arran Granite is geochemically distinct from all other granitic rocks in the BPIP other than the An Cumhann dyke (Arran), and possibly Lundy and the Mourne Mountains.

The granite clasts found in the ignimbrites of the CAIC have very similar geochemistry to the North Arran Granite, including evidence for the same degree of fractionation of plagioclase, K-feldspar, and zircon. The only way their petrogenesis differs is less evidence for fractionation of apatite. Nevertheless, they are likely derived from the same magma as the North Arran Granite, possibly the North Arran Granite intrusion itself.

5.6.6 Other Silicic Rocks

The pitchstone dyke that intrudes the ignimbrites of the CAIC in Glen Craigag has a significant negative Eu anomaly, suggesting fractional crystallisation of plagioclase during evolution of the magma. Its trace element compositions are very similar to those of Dalradian-derived leucogranites, suggesting a possible crustal source north of the Highland Boundary Fault. A similar REE profile to the Mull Centre 2 and 3 granites confirms an origin involving both fractional crystallisation of basaltic magma and partial melting of crustal material.

The Muileann Gaoithe Member and White Tuff Member rhyolitic lava-like ignimbrites from the CAIC show evidence of significant fractionation of plagioclase, K-feldspar, and zircon, much like the North Arran Granite. They also show evidence for similarly moderate amounts of apatite fractionation. Nb concentrations suggest that the Muileann Gaoithe ignimbrite is slightly more evolved than the White Tuff Member, but this is not reflected in SiO_2 concentrations. Again, REE similarities to the Mull Centre 2 and 3 granites suggest both fractional crystallisation and crustal contamination played a role in the generation of these magmas.

Chapter 6

Synthesis and Conclusions

6.1 Summary of CAIC Lithologies

A summary of the ages and magmatic sources of the igneous rocks of the CAIC and other localities discussed in this study is shown in Table 6.1.

6.1.1 Mafic Units

The mafic rocks analysed in this study are derived from a number of distinct magma sources, and have undergone various post-melt generation processes. The magmas that formed the basalt and dolerite dykes that intrude the CAIC and most that intrude the North Arran Granite were generated from a source geochemically transitional between the Iceland plume and N-MORB. The dolerite sill that intrudes the ignimbrites of the Arran Volcanic Formation was derived from a distinctly N-MORB source, while the picrite dyke that intrudes the CAIC, and two dykes that intrude the North Arran Granite were source from Iceland plume-like mantle (Fig. 5.9). As Chambers and Fitton (2000) showed that the relative influence of the Iceland plume (relative to N-MORB) changed throughout the development of the BPIP, these differences could suggest melt generation at different times. However, this Icelandic component is thought to have increased and the decreased again throughout the period 61–58 Ma, so it cannot be said in which temporal order the magmas that make up the Arran dykes and CAIC sill formed.

The REE concentrations and chondrite-normalised REE profiles of these mafic units can be used to approximate melting conditions. The fertile upper mantle is mineralogically stratified, with garnet lherzolite existing, in plume environments, below 95 km depth, spinel lherzolite shallower than 85 km, and the region at 85–95 km depth represented by transitional garnet-spinel lherzolite (Watson, 1993). By

Table 6.1 – A summary of the ages and origins of the units that make up the Central Arran Igneous Complex, as well as the other igneous rocks on Arran described in this study.

Unit	Age (Ma)	Relative age	Magma source	Crustal contamination
CAIC mafic dykes		Younger than Glen Craigag Granite, Glenloig Hybrids, Muileann Gaoithe Member	Varying degrees of melting of transitional Icelandic/MORB spinel lherzolite	Midland Valley, Rhinns Complex, and Dalradian crust
CAIC picrite dyke		Younger than Glen Craigag Granite	Low degree melting of an Iceland-like spinel lherzolite source. 15% accumulation of olivine.	Midland Valley basement
CAIC pitchstone dyke		Younger than Allt Ruadh Member	Crustal anatexis of Dalradian schists?	
CAIC dolerite sill		Younger than Pigeon Cave Member. Older than Ard Bheinn Member?	Moderate degree melting of transitional garnet-spinel lherzolite N-MORB source	Rhinns Complex
CAIC gabbros		Older than Glenloig Hybrids rhyolites	Transitional Icelandic/ MORB	Midland Valley basement. Possible Dalradian?
Intermediate Glenloig Hybrids		Older than mafic dykes, some silicic Glenloig Hybrids	Mantle derived melts	Varying amounts of Midland Valley basement
Silicic Glenloig Hybrids	58.71 ± 0.07	Some younger than intermediate Glenloig Hybrids, gabbro. Some older than Allt Ruadh Member	Significant crustal anatexis. More than one source?	Significant amounts of Midland Valley crust
Glen Craigag Granite	58.74 ± 0.06	Field evidence suggests older than Allt Ruadh Member – see discussion	Mantle derived melts	Both Dalradian and Midland Valley crust
Satellite Granites	58.78 ± 0.11 – 58.74 ± 0.06	Younger than Arran Volcanic Formation. Younger than mafic dykes?	Mantle derived melts	Significant amounts of Midland Valley crust
Arran Volcanic Formation	58.92 ± 0.19 – 58.79 ± 0.04	Older than Silicic Glenloig Hybrids. Younger than Satellite Granites. Younger than CAIC dykes?	Rhyolitic lava-like ignimbrites similar to North Arran Granite	
North Arran Granite	58.98 ± 0.06 – 58.86 ± 0.07	Older than CAIC (King, 1954)	Mantle derived melts	Significant amounts of Dalradian schists
NAG mafic dykes		Younger than North Arran Granite	Varying degrees of melting of transitional Icelandic/MORB spinel lherzolite	
Sheans			Crustal anatexis of Midland Valley crust?	
Tighvein			Fractional crystallisation of Glenloig Hybrids	Dalradian ?

modelling the partial melting of these mantle lithologies, and comparing the results with measured values, depth estimations can be made regarding the formation of the mafic Arran magmas.

The mafic dykes that intrude the CAIC and the North Arran Granite belong to two geochemically distinct groups (Fig. 4.24). This difference appears to reflect different degrees of melting of a spinel lherzolite source, suggesting melting depths of <85 km. The dolerite sill in the CAIC has a convex-up REE pattern, and modelling suggests this magma was sourced from a melting region containing some garnet. This suggests a deeper source than that of the magma which formed the dykes, around 85–95 km. This difference could also be temporally controlled, as the depth of melting below the BPIP is known to have changed through time (Ellam, 1992; Kerr, 1994; Kerr et al., 1999). However, melting is thought to have begun at depths at which garnet is stable, then shallowed to spinel lherzolite depths, then returned to the garnet-spinel transition zone (Kerr et al., 1999). The differences observed in the Arran magmas therefore cannot be used to suggest a chronological order.

The primary mantle melts that eventually became the mafic intrusions underwent fractional crystallisation of olivine, plagioclase, and magnetite, and experienced minor amounts of crustal contamination. Two of the analysed CAIC dykes were contaminated by a crustal unit that isotopically resembles xenoliths from the unexposed Midland Valley crystalline basement (Halliday et al., 1993), suggesting these magmas ascended through the crust south of the Highland Boundary Fault. One of the dykes in the CAIC has an isotopic composition that suggests contamination by a crustal unit geochemically resembling the Dalradian schists. This suggests the magma ascended north of the Highland Boundary Fault. The dolerite sill that intrudes the CAIC, and one of the dykes, show evidence of crustal contamination by a unit that isotopically resembles the Rhinns Complex of Islay. This unit has been suggested to represent the basement upon which the Dalradian metasediments were deposited (Stephenson et al., 2013, and references therein). These magmas could therefore have ascended through the crust north of the Highland Boundary Fault, and been contaminated at a deeper level than the magmas contaminated by Dalradian schists (but see Section 6.4 for a discussion of crustal architecture).

6.1.2 Intermediate and Hybrid Units

A large proportion of the CAIC, and the surrounding igneous rocks in central Arran are made up of amphibole-bearing intermediate and silicic intrusions. ‘The Glenloig Hybrids’ is an umbrella term for an extensive group of diorites and microgranites that exist in a continuous body in the north and east of the CAIC. They are petrographi-

cally and geochemically diverse (Section 2.1, Chapter 4), and display a diverse range of intrusion and mingling textures. They have been somewhat arbitrarily classified into two geochemical groups: the intermediate Glenloig Hybrids (SiO_2<70 wt.%) and the silicic Glenloig Hybrids (SiO_2>70 wt.%).

The intermediate Glenloig Hybrids show clear linear evolution-related trends in their trace element compositions (Fig. 4.15, and consistent REE concentrations (Fig. 4.27). This suggests that they derive from a common magmatic source and are related by fractional crystallisation. The silicic Glenloig Hybrids, however, do not show clear evolution-related trends, and display a wide range of trace element concentrations at high levels of SiO_2 and Zr (Figs. 4.15 and 4.17). They also have highly variable REE concentrations and chondrite-normalised REE patterns (Fig. 4.27). This suggests that they are derived from a number of magmatic sources. This is consistent with field and petrographic observations, as several kinds of silicic intrusion are seen within the Glenloig Hybrids unit, and show evidence of formation at different times.

It is possible that one group of the silicic Glenloig Hybrids formed from fractional crystallisation of the intermediate Glenloig Hybrids. These are the samples that lie on the evolution trend of the intermediate hybrids (high incompatible element concentrations at high levels of SiO_2 and Zr; Figs. 4.15 and 4.17). This group also has higher REE concentrations than the intermediate Glenloig Hybrids, steeper LREE profiles, and slight negative Eu anomalies (Figs. 4.27, 5.18). The other group (very depleted in HREE) have REE profiles similar to other rocks from the BPIP that are known to have formed largely by crustal anatexis (Fig. 5.49), implying that this was a major source of these magmas.

All samples of the Glenloig Hybrids analysed for isotopes show evidence for significant crustal contamination by the Midland Valley basement. Modelling suggests that in some cases, the amount of crustal material was >50%, showing that crustal anatexis was a significant process in the genesis of these magmas. The Glenloig Hybrids do not show any evidence of contamination by Grampian Terrane lithologies, so these magmas must have ascended through the crust south of the Highland Boundary Fault.

The intermediate and hybrid rocks of the Sheans and Tighvein appear very similar to the Glenloig Hybrids, with amphibole-bearing diorites, silicic dykelets, and magma mingling textures (Sections 2.7.2, 2.7.3), but they are petrographically distinct. All samples from the Sheans are less evolved than those from Tighvein, which has major and trace element compositions similar to those of the more evolved Glenloig Hybrids that lie on the evolution trend from the intermediate hybrids (Figs. 4.15). This could be the source of the Tighvein intrusions, although their

trace element profiles could also have been formed by partial melting of Dalradian crust. The trace elements profiles of the Sheans show that relatively little fractional crystallisation has occurred, and these magmas may have been formed by anatexis of Midland Valley crust.

6.1.3 Granites

The granites of the CAIC and the North Arran Granite have trace element and isotopic compositions consistent with fractional crystallisation of mantle-derived melts, as well as some degree of crustal contamination. The Satellite Granite magmas have been significantly contaminated by Midland Valley crustal material, with crustal anatexis possibly accounting for >50% of the source of the magma. The Glen Craigag Granite magma was also ultimately mantle-derived, and isotope binary-mixing modelling shows that it was contaminated by crustal material from both the Midland Valley basement and the Dalradian schists, meaning that it interacted with the crust on both sides of the Highland Boundary Fault. The North Arran Granite also formed from fractional crystallisation of mantle-derived melt along with significant crustal contamination. The contaminant in this case was clearly the Dalradian schists (Fig. 5.33) into which the North Arran Granite was emplaced.

All granites show evidence of fractionation of plagioclase (Fig. 5.18), although this is relatively minor in the Satellite Granites. The Glen Craigag Granite shows a similar fractional crystallisation history to the Satellite Granites, but with more pronounced negative Eu anomalies (Figs. 5.18, 4.29). The North Arran Granite, however, has much more pronounced negative Eu anomalies showing fractionation of large amounts of plagioclase. It and also shows evidence for significant fractional crystallisation of zircon, K-feldspar, Ti- or Fe-Ti oxides, and apatite during its evolution. Fractionation of zircon is uncommon in the granites of the BPIP.

6.1.4 Ignimbrites

The ignimbrites of the Arran Volcanic Formation are highly diverse, and are discussed fully in Chapter 3. Most of the ignimbrites contain lithic and/crystal fragments inherited from elsewhere in the system, so whole-rock geochemical techniques are of limited use for studying magmatic processes. However, the homogenous rhyolitic lava-like ignimbrites of the Muileann Gaoithe and White Tuff Members are thought to be near-magmatic, and so have been analysed for whole-rock elemental data.

The trace element concentrations in these ignimbrites make it clear that both units are geochemically (as well as petrographically) similar, and have a very similar

fractional crystallisation history to the North Arran Granite (Figs. 5.18, 5.19). They have similar negative Eu anomalies, and similar levels of Zr, Ba, and TiO_2, suggesting fractional crystallisation of plagioclase, zircon, K-feldspar, and Fe-Ti oxides in similar proportions to the NAG. The only major geochemical difference between the CAIC rhyolitic ignimbrites and the NAG is the apparent lack of apatite fractionation in the ignimbrite magma. Apart from this, it seems likely that both the North Arran Granite and the CAIC rhyolitic ignimbrites were sourced from the same magmatic system.

This observation has some interesting consequences. If the CAIC lava-like ignimbrites originate from the same magma chamber as the North Arran Granite, it suggests that this source was capable of providing magma to a large laccolith north of the Highland Boundary Fault, as well as to a volcanic system south of the Highland Boundary Fault. The fact that the $\pm 2\sigma$ values for the interpreted $^{206}Pb/^{238}U$ ages of the outer part of the North Arran Granite and the White Tuff ignimbrite overlap significantly further suggests that both may have been tapped from the same magma reservoir.

Another link between the North Arran Granite and the ignimbrites of the CAIC comes from the granite clasts found in the mLT of the Allt Ruadh Member ignimbrites. These clasts have trace element compositions that places them in the same group as the North Arran Granite and the rhyolitic lava-like ignimbrites, *i.e.*, evidence of plagioclase, K-feldspar, zircon, and Fe-Ti oxide fractionation (Figs. 5.18, 5.19). They are geochemically distinct from any of the granites of the CAIC. The simplest explanation for their inclusion in the CAIC ignimbrites is that there was a granite body, similar to the North Arran Granite and derived from the same magma reservoir, below the developing CAIC caldera, that was eroded from vent walls during eruption of the Allt Ruadh ignimbrites, or from the substrate across which the PDCs travelled.

6.2 Evolution of the Caldera

Volcanism at the CAIC was a relatively short-lived affair (Sections, 4.3, 6.3.4), with the time from caldera collapse to the eruption of the youngest ignimbrites lasting a maximum of 360 kyr. However, the pyroclastic rocks of the Arran Volcanic Formation make up the majority of exposures in central Arran. Despite this short duration of caldera formation, a complex history of eruptive, erosional, fluvial, and structural processes can be determined (Chapter 3). A timeline of volcanism and caldera processes is given below, and is summarised in Fig. 6.1:

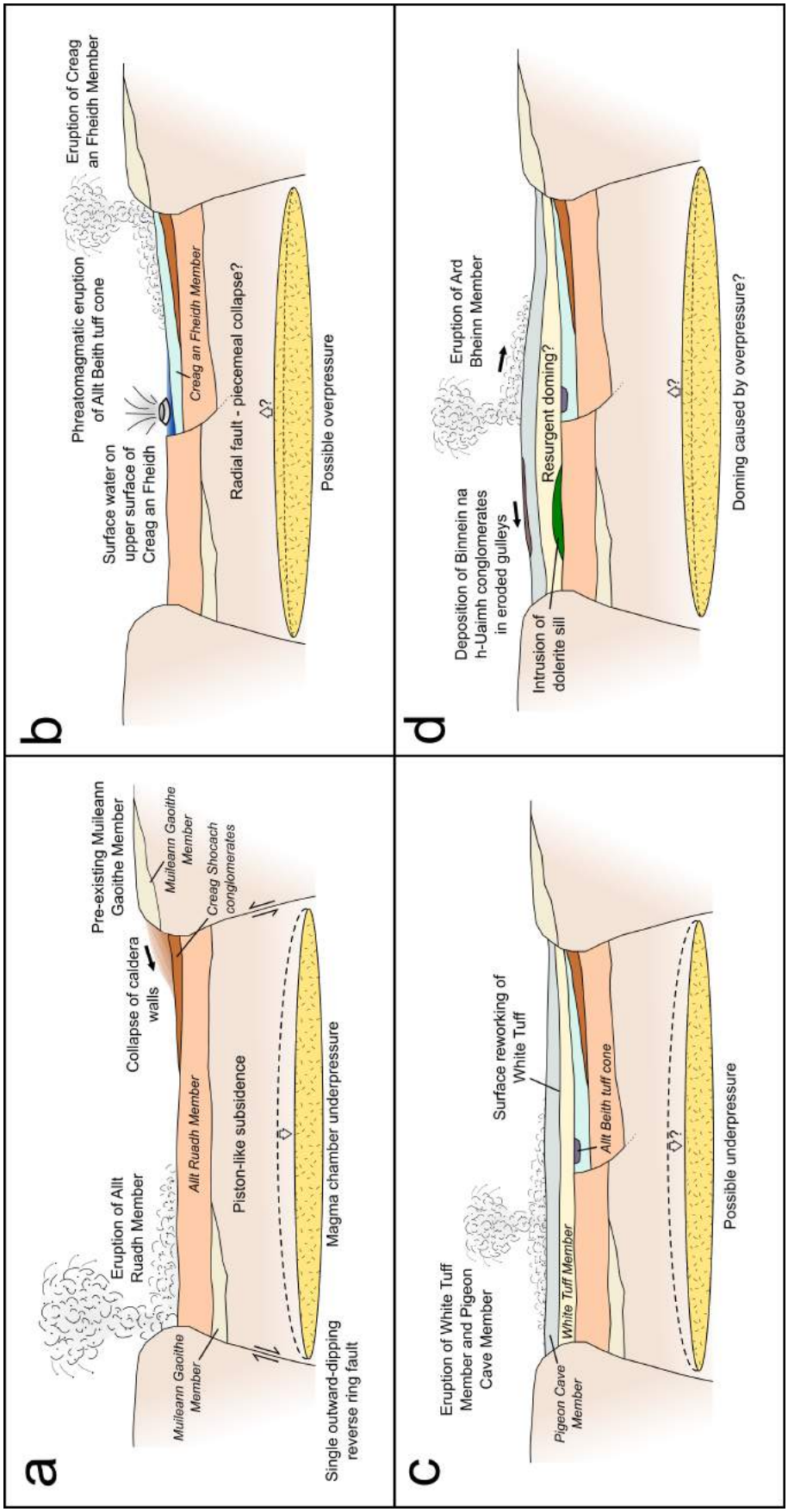

Fig. 6.1 – A series of generalised cross sections through the Arran Volcanic Formation showing the history of eruption and caldera collapse. Lithologies other than the caldera-fill succession have been omitted for clarity.

1. The lava-like ignimbrites of the Muileann Gaoithe Member are preserved *in situ* and as clasts within the later ignimbrite units. As the base is not seen within the caldera, it cannot be confirmed whether this was the first stage of volcanism in the area. It is possible that it overlies the erupted products of earlier volcanism that are now buried.

2. A period of highly explosive eruptions formed the Allt Ruadh Member (Fig. 6.1a). This blanket of mLT covers the entire area of the caldera (Fig. 3.1).

3. This evacuation of magma caused underpressure in the underlying magma chamber and caused the caldera to collapse. Collapse at this stage was piston-like, with a coherent caldera floor moving along a single ring fault, although an element of trapdoor subsidence with thickening to the west may have occurred (see Acocella, 2007). The steep caldera walls left by the outward-dipping reverse ring fault collapsed, forming the Creag Shocach conglomerates (Fig. 6.1a).

4. The Creag an Fheidh Member was erupted in the eastern part of the caldera (Fig. 3.1) and ponded against a radial fault (Fig. 6.1b). The presence of this fault could be due to some degree of resurgent doming (see Troll et al., 2002).

5. The upper part of the Creag an Fheidh Member was fluvially reworked in a period of volcanic quiescence. A small pulse of mafic magmatism interacted with this surface water and/or groundwater, and the resulting phreatomagmatic eruption built the Allt Beith tuff cone (Fig. 6.1b).

6. The rhyolitic lava-like ignimbrites of the White Tuff Member were erupted (Fig. 6.1c). These ignimbrites are lithologically and petrographically almost identical to the Muileann Gaoithe Member ignimbrites, but were erupted after a significant period of non-homogeneous lower-grade volcanism. This stratigraphy, of variable pyroclastic rocks stratigraphically 'sandwiched' between two thick rhyolite units is very similar to that observed at Sabaloka, Sudan (Almond, 1971). This eruption was followed by a period of volcanic quiescence in which the upper surface was reworked.

7. The Pigeon Cave Member was erupted (Fig. 6.1c), and intruded by a dolerite sill (Figs. 3.3, 3.32). The nature of the pre-Palaeogene sedimentary rocks (Cretaceous chalk and possibly Cretaceous sandstone) preserved within this unit is unclear as contacts are not exposed, but work on Rùm suggests that supposed intra-caldera 'megablocks' may in fact be broadly coherent pieces of caldera floor (Holohan et al., 2009; Lipman, 1976). If this is the case on Arran,

these caldera floor segments may have been exposed by subsidence-related faulting and/or resurgent doming (see below).

8. The intrusion of a dolerite sill, or overpressure from the underlying magma chamber, or both, caused resurgent doming to form a palaeo-topographic high (Fig. 6.1d) in the vicinity of the modern Ard Bheinn summit.

9. Debris flows comprising material from outside the caldera flowed away from this palaeo-high and were deposited as the Binnein na h-Uaimh conglomerates in steep-sided canyons eroded into the upper surface of the Pigeon Cave Member (Fig. 6.1d).

10. The heterogeneous high-grade ignimbrites of the Ard Bheinn Member were erupted (Fig. 6.1d). The lowest of these – coarse crystal tuffs – flowed away from the palaeo-high and were deposited in valleys eroded into the underlying members (Fig. 3.1).

11. An unknown thickness of the Ard Bheinn Member and any overlying units were lost to erosion.

6.2.1 Summary

The main episode of piston-like caldera collapse at the CAIC, represented by the Allt Ruadh Member mLT, was followed by erosion of the steep caldera walls and deposition of this material within the caldera. By the time of the eruption of the Creag an Fheidh Member, radial faults were present at the surface, suggesting some degree of piecemeal subsidence. Water on the caldera floor, on the upper surface of the Creag an Fheidh Member, is indicated by the occurrence of conglomerates, and the presence of the phreatomagmatic Allt Beith tuff cone. After eruption of the White Tuff and Pigeon Cave ignimbrites, and intrusion of a dolerite sill, a palaeo-high was present in the approximate centre of the caldera. This may have been as a result of resurgent doming caused by magma chamber overpressure, or could be a result of sill emplacement. Debris flows travelled away from this intra-caldera topographic high in steep-sided canyons, forming the Binnein na h-Uaimh conglomerates. The Ard Bheinn Member ignimbrites are the youngest preserved evidence of volcanism, with any younger volcanic rocks being eroded away.

6.3 Discussion of Chronology

This section will discuss the age relationships between the units of the CAIC, as well as the North Arran Granite. These are often complicated by disagreement between zircon ages and field relationships. Such problems are exacerbated by the incredibly short timescales involved (resulting in overlapping radiometric dates) and the poor exposure of vital contacts and field relationships in general.

6.3.1 The North Arran Granite

It has been previously suggested (King, 1954) that the formation of the CAIC post-dates the emplacement of the North Arran Granite, as its bounding structures cross-cut the regional doming that formed during the North Arran Granite's intrusion. Radiometric U-Pb zircon dates from this study indicate that this is likely, with the inner fine-grained unit of the North Arran Granite showing the oldest interpreted $^{206}Pb/^{238}U$ age of any analysed in this study (Fig. 4.69). It is possible the outer coarse-grained unit of the North Arran Granite is also older than the first activity at the CAIC, but its interpreted $^{206}Pb/^{238}U$ date ($\pm 2\sigma$) overlaps with those from the volcanic rocks of the Arran Volcanic Formation, at around 58.9 – 58.8 Ma. The interpreted age of the Allt Ruadh Member mLTs is older than the coarse North Arran Granite, but the Allt Ruadh date has the largest 2σ of any unit studied, so this older age may reflect inherited xenocrystic zircons from a magma body active at the time of North Arran Granite formation. It is therefore reasonable to retain the suggestion that the North Arran Granite is older than the CAIC, but only by (at most) 200 kyr.

The interpreted ages for the North Arran Granite are younger than the (recalculated) ages for the Drumadoon Sill porphyritic rhyolite, reported by Meade et al. (2009) of 59.425±0.14 Ma and 59.546±0.17 Ma.

6.3.2 Pre-volcanic Intrusions?

Of the CAIC rocks dated by U-Pb zircon geochronology in this study, the ignimbrites of the AVF give the oldest interpreted ages. However, field relationships suggest that explosive volcanism was not the first stage in the development of the CAIC. At Glenloig, it appears that mLT of the Allt Ruadh Member (related to the main episode of caldera collapse) overlies diorites of the Glenloig Hybrids. This has been interpreted as a depositional, rather than intrusive, contact – although this is not conclusive. If the mLT of the Allt Ruadh Member was deposited on top of diorites of the Glenloig Hybrids, it suggests that at least some of the hybrids had been intruded,

cooled, and unroofed before eruption of the Allt Ruadh Member ignimbrites. They could therefore also pre-date the North Arran Granite.

In Ballymichael Burn (Fig. 1.9) the contact between the Allt Ruadh Member ignimbrites and the Glen Craigag Granite can be observed. This was interpreted during initial fieldwork as a depositional contact, due to its approximately horizontal, locally planar nature. Again, this is not conclusive, and the contact itself is wet, mossy, and very weathered. If this is a depositional contact it would suggest that the Glen Craigag Granite had been intruded and exposed before the commencement of explosive volcanic activity, along with (part of) the Glenloig Hybrids.

However, U-Pb dating of zircons from the Glen Craigag Granite and the Glenloig Hybrids suggests that both intrusive units are *younger* than the ignimbrites of the AVF (Fig. 4.69). This disagreement is easy to explain for the Glenloig Hybrids; the dated sample was from a granitic vein that clearly intruded the dioritic rocks and was therefore younger. This suggests that the rocks considered together as the 'Glenloig Hybrids' had a protracted magmatic history, involving intrusions of magma both before and after explosive volcanism and formation of the caldera. Such a situation is to be expected based on field observations, but exposure is not good enough to allow identification of different events in the formation of the Glenloig Hybrids using contact relationships alone.

The disagreement between field relationships and interpreted $^{206}Pb/^{238}U$ dates is harder to explain for the Glen Craigag Granite. It should be noted that the $\pm 2\sigma$ dates of the AVF ignimbrites and the Glen Craigag Granite overlap at 58.8 Ma (Fig. 4.69). However, the interpreted age for the Glen Craigag Granite is younger than that of the ignimbrites, suggesting that the contact between the two is in fact intrusive, or the U-Pb data have been interpreted incorrectly. It is not clear which scenario is more likely.

Lithic-clast-bearing ignimbrites from several units contain fragments of basalt and dolerite. This indicates there must have been at least some (presumably Palaeogene) mafic magmatism in central Arran prior to the onset of explosive volcanism.

6.3.3 Mafic Dykes

The timing of the intrusion of mafic dykes is potentially an important marker event in the timeline of the CAIC. Mafic dykes are seen to intrude the Glen Craigag Granite, the Glenloig Hybrids, and the extra-caldera ignimbrites of the Muileann Gaoithe Member and the Banded Tuffs (Fig. 1.9). They are not observed intruding the Satellite Granites or the intra-caldera ignimbrites of the AVF. Of course, absence of evidence does not equal evidence of absence, but this is an interesting observation.

The general density of mafic dykes on Arran suggests that if they intruded all units uniformly, it's likely they would be observed in the intra-caldera AVF and the Satellite Granites, even when accounting for poor exposure. Critically, even at Dereneneach Quarry and along the Creag Mhor ridge, where exposure of the Satellite Granites is 100%, no mafic dykes are observed. The same is true of the Ard Bheinn–Binnein na h-Uaimh summit region, where exposure of ignimbrites if good but no dykes are observed.

Treating intrusion of mafic dykes as a single event is probably a gross oversimplification, but the above relationships suggest that a period of mafic magmatism occurred after formation of the Glenloig Hybrids and the Glen Craigag Granite, but before the formation of the intra-caldera ignimbrites and intrusion of the Satellite Granites. This provides further evidence that the Glenloig Hybrids and the Glen Craigag Granite predated explosive volcanism.

Given that dykes are seen to intrude the extra-caldera ignimbrites of the Muileann Gaoithe Member, but not the Allt Ruadh Member in the caldera, it could be tentatively speculated that a mafic dyke intrusion event occurred between eruption of the Muileann Gaoithe and Allt Ruadh Members, *i.e.*, immediately prior to the main caldera collapse event.

The lack of mafic dykes within the caldera could be due to the likelihood that basaltic magma injected into the unconsolidated caldera-fill succession would form sills. Sill formation within the caldera-fill succession is known, and peperitic textures suggest that this occurred while the volcaniclastic rocks were still largely unconsolidated.

6.3.4 Explosive volcanism

The chronology of volcanic and sedimentary events recorded in the Arran Volcanic Formation is discussed in Chapter 3, and summarised in Section 6.2. Zircon U-Pb dating suggests that explosive volcanism was the earliest phase of magmatism at the CAIC, occurring shortly after the emplacement of the North Arran Granite, although field relationships do not necessarily agree (see above).

The three ignimbrite units subjected to radiometric dating give interpreted $^{206}Pb/^{238}U$ ages that agree with their positions in the stratigraphy (Allt Ruadh Member 58.92 Ma, White Tuff Member 58.81 Ma, Ard Bheinn Member 58.79 Ma), but with overlapping $\pm 2\sigma$ values (Fig. 4.69). These dates suggest that the whole process, from caldera collapse to the eruption of the Ard Bheinn Member ignimbrites (the youngest preserved volcanic unit), took place within 360 kyr. This is very rapid, especially considering the erosional processes that are known to have created

high-relief palaeo-surfaces in times of quiescence between eruption of the different members.

This period of surface magmatism is important for the wider story of Arran's igneous rocks, as it seemingly commenced during cooling of the (pre-caldera) North Arran Granite, and was still occurring during emplacement of the (post-caldera) Bridge Farm Granite. The geochemical similarities between the North Arran Granite and the rhyolitic lava-like ignimbrites of the AVF indicate that the same active magma system was supplying both at approximately the same time. This suggests that volcanism was happening at the (pre-caldera subsidence) surface in central Arran at the same time that the North Arran Granite laccolith was still deeply buried, several kilometres to the north. Likewise, the products of explosive eruptions sampled in this study must have been buried, presumably by later pyroclastic layers, incredibly rapidly before emplacement of the Bridge Farm Granite, and the other Satellite Granites.

6.3.5 The Dolerite Sill

As discussed in Chapter 3, the dolerite sill exposed on the western slopes of Ard Bheinn is thought to have been intruded after eruption of the Pigeon Cave Member ignimbrites, but before the eruption of the Ard Bheinn Member ignimbrites. This is because fingers of the dolerite sill intrude the Pigeon Cave ignimbrites on Binnein na h-Uaimh, but the lower tuffs of the Ard Bheinn Member seems to occupy a valley eroded into the upper surface of the dolerite sill in Ballymichael Glen. This dates the intrusion of the sill to between 58.81 Ma and 58.79 Ma (the interpreted ages of the White Tuff and Ard Bheinn Member ignimbrites, respectively). It is possible that many of the mafic dykes found within the complex intruded at the same time as the dolerite sill. However, the mafic dykes (both groups) are geochemically distinct from the sill, so this is not necessarily the case.

6.3.6 Post-volcanic intrusions

The Satellite Granites are younger than the ignimbrites of the AVF, as confirmed by both field relationships and U-Pb zircon dating (Fig. 4.69). The Creag Mhor granite can be seen intruding the Allt Ruadh Member ignimbrites as a shallowly-dipping sheet, and the northern margin of the Bridge Farm Granite is irregular and sub-vertical in places, suggesting intrusive contacts. Interpreted $^{206}Pb/^{238}U$ ages for the Bridge Farm and Creag Mhor granites are 58.78 Ma and 58.74 Ma, respectively

(Table 4.3). The position of the Satellite Granites around the periphery of the complex suggest their magmatic ascent may have been controlled by the caldera ring fault.

The youngest interpreted $^{206}Pb/^{238}U$ date from the CAIC comes from a granitic vein intruding the dioritic Glenloig Hybrids on Cnoc Dubh in the north east of the complex. As the diorites at Glenloig are thought to be older than the Allt Ruadh Member ignimbrites, this age is taken to represent a granitic intrusion event that is not related to the main emplacement of the Glenloig Hybrids, and may instead be associated with the intrusion of the Satellite Granites.

6.4 Magma Pathways and Crustal Architecture

The fact that all of the onshore centres of Palaeogene magmatic activity in Scotland lie on or close to major crustal lineaments (Fig. 1.1) led Emeleus (1991) to suggest that large-scale faults could have acted as the conduits for the ascending magmas in the BPIP. It has also been proposed that the site of magma ascent is marked by the prominent, steep-sided positive gravity anomalies that are centred on each of the BPIP's central complexes (e.g. Bott and Tuson, 1973).

Arran has both of these features. The Highland Boundary Fault is known to cross Arran in some form (although it is not well-exposed, if at all, at the surface – see below), and a positive gravity anomaly is focussed on the centre of the island – below the CAIC (Fig. 1.4). Arran's gravity anomaly is not as large or as steep-sided as those of Mull, Rùm, and Skye, but is distinct and comparable in size to that of Ardnamurchan (Fig. 1.2; BGS, 2007), and suggests the presence of a large volume of high-density mafic or ultramafic rocks – possibly cumulates – at depth below the CAIC.

In an area with geochemically distinct crustal units either side of a major fault, magma ascent pathways can be traced using radiogenic isotope ratios. However, the three-dimensional structure of the crust in this part of western Scotland is very poorly known. In this situation, this isotopic information can be used to provide insight on both magma pathways *and* crustal architecture.

6.4.1 Crustal Structure of SW Scotland

To the north of the Highland Boundary Fault, the surface geology of Arran is dominated by the Southern Highland Group of the Dalradian Supergroup. These schists, phyllites, and slates were deposited as turbidite sequences on the Laurentian passive margin in the latest Neoproterozoic to Cambrian, and deformed and metamorphosed to greenschist facies in the Ordovician Grampian Orogeny, the earlier phase of the

larger Caledonian Orogeny (Stephenson et al., 2013). The crustal basement upon which these passive margin sediments were deposited is poorly understood. It is thought to be represented by Proterozoic gneisses exposed on Islay, Colonsay, and the Irish island of Inishtrahull, together known as the Rhinns Complex (Bentley, 1988; Daly et al., 1991; Marcantonio et al., 1988; Muir et al., 1994), shown as the Islay Block on Fig. 1.1. Although undeformed contacts between the Rhinns Complex and the Dalradian succession are not exposed, Rhinns-like crust is thought to underlie at least part of the Grampian Terrane, as its isotopic signature can be seen in some Caledonian granites in the region (Dickin and Bowes, 1991).

The Midland Valley comprises, at the surface, mostly Upper Palaeozoic sedimentary and volcanic rocks, with a series of Lower Palaeozoic sedimentary inliers. Its basement is not exposed (Bamford, 1979), and is only known from a handful of deep crustal xenoliths brought up by Permian and Carboniferous volcanic and intrusive rocks (Halliday et al., 1993; Upton et al., 1976).

Even the nature of the boundary between these two terranes, the Highland Boundary Fault, is still a subject of considerable debate (Bluck, 2010; Tanner and Sutherland, 2007; Tanner et al., 2013; Young and Caldwell, 2012). Whether the Ordovician oceanic rocks of the Highland Border Complex (HBC) stratigraphically overlie the Dalradian (e.g. Tanner and Sutherland, 2007) or are separated from the Dalradian by a crustal-scale fracture (e.g. Bluck, 2010) has huge implications for the crustal architecture of the region, and the orientation of the Highland Boundary Fault itself (Bluck, 2002). Using gravity data, Dentith et al. (1992) suggested that the contact between HBC and the Lower Old Red Sandstones of the Midland Valley is vertical, while the contact between the HBC and the Dalradian dips 20° to the north west.

6.4.2 Proposed Crustal Models

In this section, two scenarios will be discussed in relation to the isotopic evidence presented in Section 4.2. Fig. 6.2 shows perhaps the simplest possible structure of the Arran crust, involving Dalradian schists underlain by Proterozoic basement, separated from the Midland Valley sedimentary rocks (underlain by an unexposed crystalline basement) by a vertical Highland Boundary Fault. The dense cumulates below the CAIC are inferred from the positive gravity anomaly centred on central Arran (Fig. 1.4). This model would show similar results if re-drawn with a northerly-dipping Highland Boundary Fault, as suggested by Dentith et al. (1992)

This model allows vertical (diapiric?) ascent of the North Arran Granite magma through the Grampian Terrane, with crustal contamination by the Dalradian schists

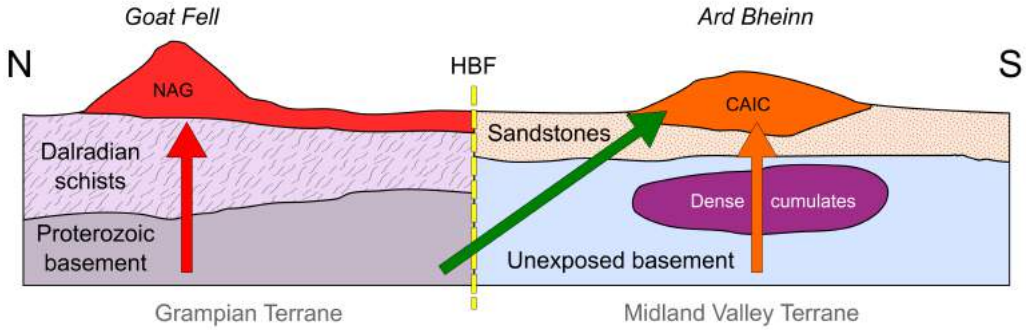

Fig. 6.2 – Schematic crustal cross section through Arran, showing a vertical Highland Boundary Fault (HBF) between the CAIC and the North Arran Granite. The red arrow represents North Arran Granite magma, the orange arrow represents CAIC magmas, and the green arrow represents CAIC dolerite sill magma.

(as shown by isotopes; Section 4.2) at shallow levels in the crust (*i.e.*, above Proterozoic basement levels). This model would also allow for vertical ascent of CAIC magmas through the Midland Valley crust (again, suggested by isotopes) without interaction with the Grampian Terrane crust.

The basaltic magma that was intruded as the CAIC dolerite sill requires a more complex explanation. This magma is known to have been contaminated by crust resembling the Rhinns Complex (Section 4.2) north of the Highland Boundary Fault, yet it has been emplaced into the Midland Valley Terrane. This requires lateral transport of this magma towards the south at some level within the crust. This has previously been documented from quartz-feldspar-phyric rhyolite intrusions in the south of the island, which also show evidence of contamination by Grampian Terrane lithologies (Dickin, 1994; Meade et al., 2009). Magma is known to have travelled huge distances as dykes during the development of the BPIP; the Mull dyke swarm is known to reach the southern North Sea, and may even extend into Dutch international waters (MacDonald et al., 2015; Underhill, 2009). Lateral magma movement has been also documented from more recent systems, including ~10 km transport of rhyolitic magma during the 1912 Katmai-Novarupta eruption in Alaska, USA (Hildreth and Fierstein, 2012) and >45 km transport of basaltic magma during the 2014-15 Bárðarbunga eruption, Iceland (Sigmundsson et al., 2015).

In this (admittedly very simple) model, the Highland Boundary Fault does not appear to have much physical control on magma ascent. Also, the positive gravity anomaly is related to the site of only some of the magmas that formed the granitic and intermediate rocks of the CAIC.

An alternative model of crustal architecture, including a southerly dipping Highland Boundary Fault which underlies the CAIC at depth, is shown in Fig. 6.3. This

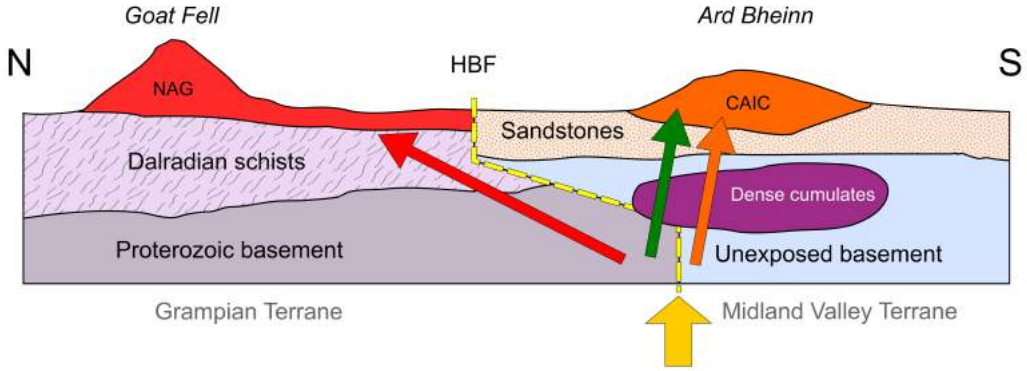

Fig. 6.3 – Schematic crustal cross section through Arran, showing a S-dipping Highland Boundary Fault (HBF) that underlies the CAIC at depth. The red arrow represents North Arran Granite magma, the orange arrow represents CAIC magmas, and the green arrow represents CAIC dolerite sill magma. The yellow arrow shows the general path of magma ascent from depth along the Highland Boundary Fault.

model is also consistent with isotopic analyses (Section 4.2). There are certain observations, from this study and previous work, which are better explained by this model than the vertical Highland Boundary Fault model. Firstly, it allows for a single site of magma ascent at depth, along the Highland Boundary Fault, as proposed by Emeleus (1991). Secondly, it allows this site of fault-controlled magma ascent to be located at the focus Arran's positive gravity anomaly (represented in Fig. 6.3 by dense cumulates), as suggested by Bott and Tuson (1973).

This model removes the need for lateral transport of the CAIC dolerite sill magmas, as it allows for the presence of Rhinns-like Proterozoic basement gneiss at depth below the CAIC Fig. 6.3. However, lateral movement of magmas at shallow levels in the crust is known to be a viable process, as described above, so this is merely an observation rather than a requirement.

Stevenson and Grove (2014) showed that the laccolithic North Arran Granite was likely emplaced from the south, and suggested that this may show a relationship with the positive gravity anomaly centred on the CAIC. A southerly-dipping Highland Boundary Fault allows for emplacement of the North Arran Granite from the south without interaction of the magma with Midland Valley crustal units. A similar arrangement of granitic magma moving laterally through the crust, from a site of high gravity to its site of emplacement, has been previously documented in the BPIP at the Western Mourne Mountains centre (Stevenson and Bennett, 2011).

This model (Fig. 6.3) may also provide a better explanation of the isotopic composition of the Glen Craigag Granite (Section 4.2), which shows evidence of contamination by both Grampian Terrane and Midland Valley crust.

6.4.3 Summary

Two models of crustal structure below Arran are proposed. Field observations are of little use in constructing these models, as basement lithologies are not exposed in the region, and the nature of the Highland Boundary Fault (and indeed, its precise location) across Arran is not known and is the subject of ongoing debate (e.g. Bluck, 2010; Tanner and Sutherland, 2007; Young and Caldwell, 2012).

The model involving a vertical (or northerly dipping) Highland Boundary Fault allows for vertical ascent of the North Arran Granite magma and the majority of CAC magmas, leading to contamination by the crustal units through which they rose (Fig. 6.2). This model requires significant lateral movement of basaltic magma from the Grampian Terrane by which it was contaminated, to the CAIC where it was emplaced as a dolerite sill. Such lateral transport of magma within the crust is known from Arran and the BPIP, as well as from historical eruptions (Hildreth and Fierstein, 2012; MacDonald et al., 2015; Meade et al., 2009; Sigmundsson et al., 2015).

An alternative model involves a southerly-dipping Highland Boundary Fault which underlies the CAIC (and positive gravity anomaly) at depth (Fig. 6.3). This allows for all magmas to make their way through the crust along the Highland Boundary Fault, at a site centred on the positive gravity anomaly that is presumably caused by the presence of mafic/ultramafic cumulates. It also allows for the presence of Rhinns-like Proterozoic basement at depth below the CAIC, removing the need for significant lateral transport of the CAIC dolerite sill magma. This model does, however, require that the North Arran Granite was intruded from the south, as previously suggested by Stevenson and Grove (2014). The isotopic signature of the Glen Craigag Granite (showing input of both Grampian and Midland Valley Terran material) can be more satisfactorily explained by this model.

Whether or not this model can explain the Drumadoon intrusions and other quartz porphyries described by Dickin (1994); Meade et al. (2009) without invoking lateral transport depends on whether it allows for Dalradian schists (as well as Rhinns-like gneisses) to exist at depth below southern Arran. These rhyolites and quartz porphyries show contamination by Dalradian schists, while the Drumadoon mafic lithologies show contamination with the Rhinns Complex gneisses. If both Rhinns-like gneisses *and* Dalradian schists are present below central/southern Arran, then all igneous units, other than the North Arran Granite, could be explained with only near-vertical magma transport. As previously mentioned, significant lateral magma transport within the crust has been documented numerous times, so removing the need for lateral movement isn't necessarily required, but this model provides a situation in which it may not have occurred.

It is tentatively suggested that the second of these two models provides a more adequate explanation for the isotopic data from this study, the positive gravity anomaly centred on the CAIC (BGS, 2007; Bott and Tuson, 1973), the suggestion of Stevenson and Grove (2014) that the North Arran Granite was intruded from the south, and the Highland Boundary Fault as a locus of crustal-scale magma ascent (Emeleus, 1991).

6.5 Arran's Place in the BPIP

A summary of radiometric ages (both U-Pb and Ar-Ar) from the onshore BPIP is shown in Fig. 6.4. U-Pb data are from Emeleus and Bell (2005), and references therein, recalculated Ar-Ar data are from Wilkinson et al. (2016), and references therein, and data for Lundy are from Charles et al. (2018). Compared to the spread of ages from the BPIP, from almost 64 Ma to younger than 56 Ma, magmatic activity on Arran (the North Arran Granite, the CAIC, and the Drumadoon complex) was very short lived. It took place mid-way through the evolution of the BPIP. The other igneous activity occurring at approximately 59 Ma was taking place at Ardnamurchan and Lundy, as well as early activity on Skye and the later activity on Mull (Fig. 6.4).

Arran is curious among the Hebridean central complexes in that it does not appear to have been preceded by eruption of a significant lava-pile. It is possible that plateau lavas were erupted on Arran, as numerous mafic dykes are preserved all over the island, but any evidence of lava flows has been eroded away. The outcrop of basaltic material on the western slopes of Ard Bheinn was originally thought to be the only preserved fragment of a pre-caldera lava-pile that had subsided into the volcanic system (King, 1954; Tyrell, 1928). However, the conclusion of this study is that this basaltic material is in fact a dolerite sill. Another line of evidence that there was no pre-caldera lava-pile is found on Muileann Gaoithe and Tir Dhubh, where extra-caldera ignimbrites are exposed very close to the pre-Palaeogene sandstones upon which they were apparently deposited (Fig. 1.9). If this is indeed a depositional contact, there must have been no lava deposited on the landscape prior to the onset of explosive volcanism, or it must have been completely eroded away. Given the thicknesses of the lava-piles on Mull, Skye, and Antrim, the former seems more likely. A possible reason for this lack of a lava-pile, seemingly at odds with the density of basaltic dykes, is that the surface geology in the southern part of Arran is dominated by shallowly-dipping sedimentary layers. This type of geology would be susceptible to sill formation, and mafic sills are indeed common in southern Arran. This hypothesis – that Arran's 'missing' lava-pile was instead intruded below the

surface – could easily be tested by a rigorous geochemical study of the Arran dyke swarm and Arran sills.

Another feature that makes Arran seemingly unique in the BPIP is the huge volume of diorites and other amphibole-bearing rocks. The Glenloig Hybrids are the most extensive unit of the CAIC, and almost all exposures contain amphibole as a major rock-forming constituent. The reason that central Arran contains so many amphibole-bearing rocks, which are sparse throughout the rest of the complex, is unknown. There was presumably some source of wet magmas that was unique to Arran that caused so much amphibole to crystallise in these intrusions.

The similarities and differences between Arran and the rest of the BPIP regarding petrogenetic processes is discussed in Section 5.5. Much like the most other igneous rocks from the BPIP, Arran's magmas are ultimately derived from a mantle source with characteristics of both the Iceland Plume and N-MORB, and result from melting of a lherzolite source containing spinel $\pm$ garnet. Unlike on Mull, Skye, and Antrim, Arran's lack of a lava-pile means that a stratigraphy of basaltic rocks cannot be determined. This means that changes in the mantle source or melting depth through time cannot be explored. Nevertheless, comparisons to magma types throughout the BPIP can be made. The high La/Sm dykes that intrude the CAIC and the North Arran Granite are geochemically similar to the M2 magma type from the Hebrides, with similarities to the Causeway Tholeiite Member of Antrim explained by varying degrees of crustal contamination. The low La/Sm dykes on Arran are more geochemically similar to the M3 Hebridean magma type, possibly suggesting that they are younger, as seen on Mull and Skye (Kent and Fitton, 2000; Kerr et al., 1999). The dolerite sill that intruded the caldera-fill succession of the CAIC shows similarities with both Hebridean and Antrim basalts

All rocks from Arran show evidence of crustal contamination, with evolved rocks being more contaminated than mafic rocks, consistent with what is observed throughout the BPIP. Whether or not the location or depth of crustal contamination changed through time is impossible to say, due to the poorly understood crustal architecture of the region (Section 6.4) and the difficult-to-constrain chronological sequence of magmatic events at the CAIC (Section 6.3). The granitic rocks are geochemically similar to the other granites of the BPIP, most of which are also suggested to have derived from fractional crystallisation of mantle-derived melts with moderate contamination from crustal anatexis. However, the North Arran Granite is unique among the Hebridean granites in that it shows evidence of fractional crystallisation of zircon during evolution.

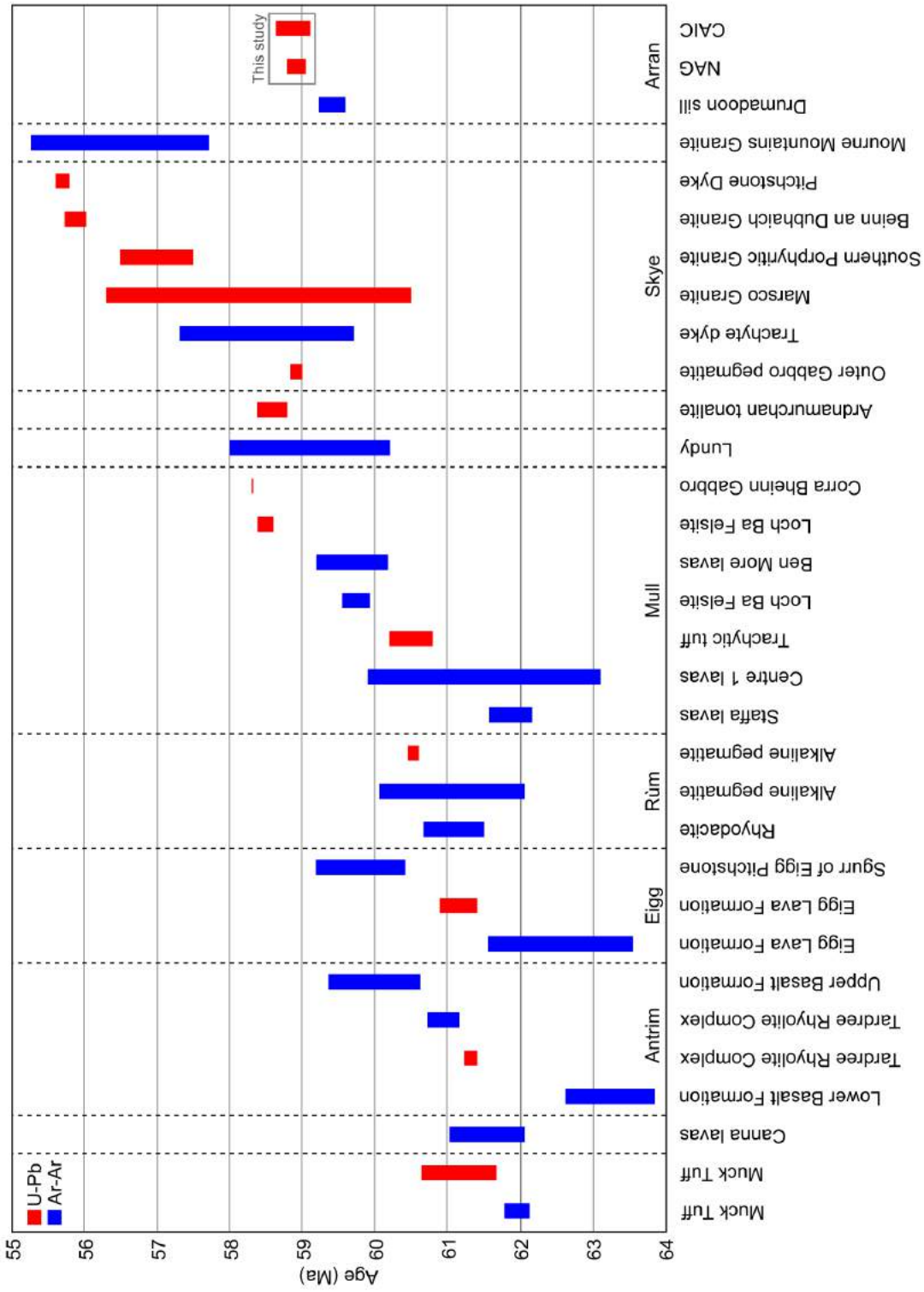

Fig. 6.4 – A summary of radiometric dates from the BPIP (bars show reported error, which is $\pm 1\sigma$ in some cases, and $\pm 2\sigma$ in others (see sources for details). Data from Charles et al. (2018); Emeleus and Bell (2005); Wilkinson et al. (2016), and references therein. Data from Arran from this study (NAG and CAIC) and Meade et al. (2009) (Drumadoon Sill).

6.6 Unanswered Questions and Further Work

The Central Arran Igneous Complex is a poorly exposed, highly weathered, intensely complex system of intrusive and volcanic rocks. Many of the structural and temporal relationships discussed in this thesis are based on contacts and field evidence that are only exposed in a small number of stream beds or mossy crags, if at all. Any future geologists doing fieldwork on this complex will no doubt find key exposures that we did not, or will form different interpretations regarding those we did. In particular, more field work is needed to better constrain the age relationships between the pyroclastic rocks and the intrusions. Another puzzle that was not adequately addressed in this study is the nature of the pre-Palaeogene sedimentary rocks in the caldera, and their relationship to the surrounding ignimbrite facies. I am also certain that a dedicated field-based study of the Glenloig Hybrids will yield a complex history of numerous phases of intrusion and magma mingling/mixing.

With regard to geochemistry, this project has looked at a tiny fraction of the Palaeogene igneous rocks on Arran. Any geochemical study of the mafic dykes that intrude only the CAIC and North Arran Granite is woefully incomplete without expanding to include the dykes that are spectacularly exposed along the south coast of the island. The same is true of the poorly exposed sills and sheets that make up around half of southern Arran's geology. The Central Arran Igneous Complex has proved to a fascinating igneous system, but it must not be viewed in isolation.

References

Acocella, V. (2007). Understanding caldera structure and development: An overview of analogue models compared to natural calderas. *Earth-Science Reviews*, 85(3-4):125–160.

Acocella, V., Di Lorenzo, R., Newhall, C., and Scandone, R. (2015). An overview of recent (1988 to 2014) caldera unrest: Knowledge and perspectives. *Reviews of Geophysics*, 53(3):896–955.

Almond, D. (1971). Ignimbrite vents in the Sabaloka cauldron, Sudan. *Geological Magazine*, 108(2):159–176.

Anderton, R. (2009). Tertiary events: the North Atlantic plume and Alpine pulses. In Woodcock, N. and Strachan, R., editors, *Geological history of Britain and Ireland*, pages 374–391. John Wiley & Sons.

Andrews, G. D. and Branney, M. J. (2011). Emplacement and rheomorphic deformation of a large, lava-like rhyolitic ignimbrite: Grey's Landing, southern Idaho. *Geological Society of America Bulletin*, 123(3-4):725–743.

Bailey, E. B., Clough, C. T., Wright, W. B., Richey, J. E., and Wilson, G. V. (1924). *Tertiary and Post-Tertiary Geology of Mull, Loch Aline, and Oban: A Description of Parts of Sheets 43, 44, 51, and 52 of the Geological Map*, volume 43. HM Stationery Office.

Bamford, D. (1979). Seismic constraints on the deep geology of the Caledonides of northern Britain. In Harris, A. L., Holland, C. H., and Leake, B. E., editors, *The Caledonides of the British Isles – reviewed*, volume 8, pages 93–96. Geological Society of London.

Barrat, J. and Nesbitt, R. (1996). Geochemistry of the Tertiary volcanism of Northern Ireland. *Chemical Geology*, 129(1-2):15–38.

Bell, B. and Emeleus, C. (1988). A review of silicic pyroclastic rocks of the British Tertiary Volcanic Province. *Geological Society, London, Special Publications*, 39(1):365–379.

Bell, B. and Williamson, I. (2002). Tertiary igneous activity. In Trewin, N. H., editor, *The Geology of Scotland*, pages 371–407. The Geological Society, London.

Bell, B. R., Claydon, R. V., and Rogers, G. (1994). The petrology and geochemistry of cone-sheets from the Cuillin Igneous Complex, Isle of Skye: evidence for combined assimilation and fractional crystallization during lithospheric extension. *Journal of Petrology*, 35(4):1055–1094.

Bentley, M. (1988). The Colonsay Group. In Winchester, J., editor, *Later Proterozoic stratigraphy of the northern Atlantic regions*, pages 119–130. Blackie and Son Ltd.

BGS (1987). *Arran, Scotland Special Sheet; 1:50 000 Series; Third Solid Edition.* British Geological Survey.

BGS (2007). *Gravity anomaly UK North. 1:625 000 scale. Onshore areas: Bouguer anomaly. Offshore areas: Free-air anomaly.* British Geological Survey.

Bluck, B., Gibbons, W., and Ingham, J. (1992). Terranes. *Geological Society, London, Memoirs*, 13(1):1–4.

Bluck, B. J. (2002). The Midland Valley terrane. In Trewin, N. H., editor, *The Geology of Scotland*, pages 149–66. The Geological Society, London.

Bluck, B. J. (2010). The Highland Boundary Fault and the Highland Border Complex. *Scottish Journal of Geology*, 46(2):113–124.

Bohrson, W. A. and Spera, F. J. (2001). Energy-constrained open-system magmatic processes II: application of energy-constrained assimilation-fractional crystallization (EC-AFC) model to magmatic systems. *Journal of Petrology*, 42(5):1019–1041.

Bott, M. and Tantrigoda, D. (1987). Interpretation of the gravity and magnetic anomalies over the Mull Tertiary intrusive complex, NW Scotland. *Journal of the Geological Society*, 144(1):17–28.

Bott, M. and Tuson, J. (1973). Deep structure beneath the Tertiary volcanic regions of Skye, Mull and Ardnamurchan, north-west Scotland. *Nature Physical Science*, 242:114–116.

Branney, M., Bonnichsen, B., Andrews, G., Ellis, B., Barry, T., and McCurry, M. (2008). 'snake River (SR)-type' volcanism at the Yellowstone hotspot track: distinctive products from unusual, high-temperature silicic super-eruptions. *Bulletin of Volcanology*, 70(3):293–314.

Branney, M. J. and Kokelaar, B. P. (2002). *Pyroclastic density currents and the sedimentation of ignimbrites: Geological Society Memoir no. 27.* The Geological Society, London.

Branney, M. J., Kokelaar, B. P., and McConnell, B. J. (1992). The Bad Step Tuff: a lava-like rheomorphic ignimbrite in a calc-alkaline piecemeal caldera, English Lake District. *Bulletin of Volcanology*, 54(3):187–199.

Brown, D. J. and Bell, B. R. (2013). The emplacement of a large, chemically zoned, rheomorphic, lava-like ignimbrite: the Sgurr of Eigg Pitchstone, NW Scotland. *Journal of the Geological Society*, 170(5):753–767.

Brown, D. J., Holohan, E. P., and Bell, B. R. (2009). Sedimentary and volcano-tectonic processes in the British Paleocene Igneous Province: a review. *Geological Magazine*, 146(03):326–352.

Brown, R., Kokelaar, B., and Branney, M. (2007). Widespread transport of pyroclastic density currents from a large silicic tuff ring: the Glaramara tuff, Scafell caldera, English Lake District, UK. *Sedimentology*, 54(5):1163–1190.

Brown, R. J., Orsi, G., and de Vita, S. (2008). New insights into Late Pleistocene explosive volcanic activity and caldera formation on Ischia (southern Italy). *Bulletin of Volcanology*, 70(5):583–603.

Bucher, W. H. (1936). Cryptovolcanic structures in the United States. *Inter. Geol. Congr., Rep. Sessions, 16th*, 2:1055–1084.

Carter, S., Evensen, N., Hamilton, P., and O'Nions, R. (1978). Neodymium and strontium isotope evidence for crustal contamination of continental volcanics. *Science*, 202(4369):743–747.

Cashman, K. V. and Giordano, G. (2014). Calderas and magma reservoirs. *Journal of Volcanology and Geothermal Research*, 288:28–45.

Cawood, P. A., Nemchin, A. A., Smith, M., and Loewy, S. (2003). Source of the Dalradian Supergroup constrained by U–Pb dating of detrital zircon and implications for the East Laurentian margin. *Journal of the Geological Society*, 160(2):231–246.

Chambers, L. and Fitton, J. (2000). Geochemical transitions in the ancestral Iceland plume: evidence from the Isle of Mull Tertiary volcano, Scotland. *Journal of the Geological Society*, 157(2):261–263.

Chambers, L., Pringle, M., and Parrish, R. R. (2005). Rapid formation of the Small Isles Tertiary centre constrained by precise 40Ar/39Ar and U–Pb ages. *Lithos*, 79(3):367–384.

Chambers, L. M. (2000). *Age and duration of the British Tertiary Igneous Province: implications for the development of the ancestral Iceland plume.* PhD thesis, University of Edinburgh.

Charles, J.-H., Whitehouse, M., Andersen, J. Ø., Shail, R., and Searle, M. (2018). Age and petrogenesis of the Lundy granite: Paleocene intraplate peraluminous magmatism in the Bristol Channel, UK. *Journal of the Geological Society*, 175(1):44–59.

Cole, J., Milner, D., and Spinks, K. (2005). Calderas and caldera structures: a review. *Earth-Science Reviews*, 69(1-2):1–26.

Condon, D., Schoene, B., McLean, N., Bowring, S., and Parrish, R. (2015). Metrology and traceability of U–Pb isotope dilution geochronology (EARTHTIME Tracer Calibration Part I). *Geochimica et Cosmochimica Acta*, 164:464–480.

Cox, K. G., Bell, J. D., and Pankhurst, R. J. (1979). *The interpretation of igneous rocks*. G. Allen & Unwin London.

Daly, J., Muir, R., and Cliff, R. (1991). A precise U-Pb zircon age for the Inishtrahull syenitic gneiss, County Donegal, Ireland. *Journal of the Geological Society*, 148(4):639–642.

Danyushevsky, L. V. and Plechov, P. (2011). Petrolog3: Integrated software for modeling crystallization processes. *Geochemistry, Geophysics, Geosystems*, 12(7).

Dentith, M., Trench, A., and Bluck, B. (1992). Geophysical constraints on the nature of the Highland Boundary Fault Zone in western Scotland. *Geological Magazine*, 129(4):411–419.

DePaolo, D. J. (1981). Trace element and isotopic effects of combined wallrock assimilation and fractional crystallization. *Earth and planetary science letters*, 53(2):189–202.

Di Giuseppe, M. G., Troiano, A., and Carlino, S. (2017). Magnetotelluric imaging of the resurgent caldera on the island of Ischia (southern Italy): inferences for its structure and activity. *Bulletin of Volcanology*, 79(12):85.

Dickin, A. (1994). Nd isotope chemistry of Tertiary igneous rocks from Arran, Scotland: Implications for magma evolution and crustal structure. *Geological Magazine*, 131(03):329–333.

Dickin, A. and Bowes, D. (1991). Isotopic evidence for the extent of early Proterozoic basement in Scotland and northwest Ireland. *Geological Magazine*, 128(4):385–388.

Dickin, A., Moorbath, S., and Welke, H. (1981). Isotope, trace element and major element geochemistry of Tertiary igneous rocks, Isle of Arran, Scotland. *Earth and Environmental Science Transactions of The Royal Society of Edinburgh*, 72(3):159–170.

Dickin, A. P. (1981). Isotope geochemistry of Tertiary igneous rocks from the Isle of Skye, NW Scotland. *Journal of Petrology*, 22(2):155–189.

Druitt, T., Mellors, R., Pyle, D., and Sparks, R. (1989). Explosive volcanism on Santorini, Greece. *Geological Magazine*, 126(2):95–126.

Druitt, T. and Sparks, R. (1984). On the formation of calderas during ignimbrite eruptions. *Nature*, 310(5979):679.

Ellam, R. (1992). Lithospheric thickness as a control on basalt geochemistry. *Geology*, 20(2):153–156.

Emeleus, C. (1982). The central complexes. In Sutherland, D. S., editor, *Igneous rocks of the British Isles*, pages 369–414. Wiley-Blackwell.

Emeleus, C. (1991). Tertiary igneous activity. In Craig, G. Y., editor, *Geology of Scotland*, volume 3, pages 455–502. Geological Society London.

Emeleus, C. and Troll, V. (2014). The Rum Igneous Centre, Scotland. *Mineralogical Magazine*, 78(4):805–839.

Emeleus, C. H. and Bell, B. R. (2005). *The Palaeogene volcanic districts of Scotland*, volume 3. British Geological Survey.

England, R. W. (1992). The genesis, ascent, and emplacement of the Northern Arran Granite, Scotland: Implications for granitic diapirism. *Geological Society of America Bulletin*, 104(5):606–614.

Evans, A. L., Fitch, F. J., and Miller, J. A. (1973). Potassium-argon age determinations on some British Tertiary igneous rocks. *Journal of the Geological Society*, 129(4):419–438.

Fitton, J., Saunders, A., Norry, M., Hardarson, B., and Taylor, R. (1997). Thermal and chemical structure of the Iceland plume. *Earth and Planetary Science Letters*, 153(3-4):197–208.

Fyfe, J. (1993). *The geology of the Malin-Hebrides sea area*. Stationery Office/Tso.

Gamble, J., Meighan, I., and McCormick, A. (1992). The petrogenesis of Tertiary microgranites and granophyres from the Slieve Gullion Central Complex, NE Ireland. *Journal of the Geological Society*, 149(1):93–106.

Ganerød, M., Smethurst, M., Torsvik, T., Prestvik, T., Rousse, S., McKenna, C., Van Hinsbergen, D., and Hendriks, B. (2010). The North Atlantic Igneous Province reconstructed and its relation to the plume generation zone: the Antrim lava group revisited. *Geophysical Journal International*, 182(1):183–202.

Geldmacher, J., Haase, K. M., Devey, C. W., and Garbe-Schönberg, C. D. (1998). The petrogenesis of Tertiary cone-sheets in Ardnamurchan, NW Scotland: petrological and geochemical constraints on crustal contamination and partial melting. *Contributions to Mineralogy and Petrology*, 131(2-3):196–209.

Geldmacher, J., Troll, V. R., Emeleus, C., and Donaldson, C. (2002). Pb-isotope evidence for contrasting crustal contamination of primitive to evolved magmas from Ardnamurchan and Rum: implications for the structure of the underlying crust. *Scottish Journal of Geology*, 38(1):55–61.

Geshi, N., Acocella, V., and Ruch, J. (2012). From structure-to erosion-controlled subsiding calderas: evidence thresholds and mechanics. *Bulletin of volcanology*, 74(6):1553–1567.

Geshi, N. and Miyabuchi, Y. (2016). Conduit enlargement during the precursory Plinian eruption of Aira Caldera, Japan. *Bulletin of Volcanology*, 78(9):63.

Gibb, F. and Henderson, C. (1978). The petrology of the Dippin sill, Isle of Arran. *Scottish Journal of Geology*, 14(1):1–27.

Gibson, S. A. (1990). The geochemistry of the Trotternish sills, Isle of Skye: crustal contamination in the British Tertiary Volcanic Province. *Journal of the Geological Society*, 147(6):1071–1081.

Gooday, R. J., Brown, D. J., Goodenough, K. M., and Kerr, A. C. (2018). A proximal record of caldera-forming eruptions: the stratigraphy, eruptive history and collapse of the Palaeogene Arran caldera, western Scotland. *Bulletin of Volcanology*, 80(9):70.

Green, T., Blundy, J., Adam, J., and Yaxley, G. (2000). SIMS determination of trace element partition coefficients between garnet, clinopyroxene and hydrous basaltic liquids at 2–7.5 GPa and 1080–1200 C. *Lithos*, 53(3):165–187.

Gregory, J. and Tyrell, G. (1924). Excursion to Arran: July 27th to August 3rd, 1923. *Proceedings of the Geologists' Association*, 35(4):401.

Gudmundsson, A. (1988). Formation of collapse calderas. *Geology*, 16(9):808–810.

Gudmundsson, A. (1998). Formation and development of normal-fault calderas and the initiation of large explosive eruptions. *Bulletin of Volcanology*, 60(3):160–170.

Gunn, W., Geikie, A., Peach, B. N., and Harker, A. (1903). *The geology of North Arran, South Bute, and the Cumbraes, with parts of Ayrshire and Kintyre,(Sheet 21, Scotland).: The description on North Arran, South Bute, and the Cumbraes*, volume 21. Printed for HM Stationery Office, by J. Hedderwick & Sons.

Gunn, W., Peach, B. N., and Newton, E. T. (1901). On a remarkable volcanic vent of Tertiary age in the Island of Arran, enclosing Mesozoic fossiliferous rocks. *Quarterly Journal of the Geological Society*, 57(1-4):226–243.

Hall, J. (1987). Physical properties of Lewisian rocks: implications for deep crustal structure. *Geological Society, London, Special Publications*, 27(1):185–192.

Halliday, A. N., Dickin, A. P., Hunter, R. N., Davies, G. R., Dempster, T. J., Hamilton, P. J., and Upton, B. G. (1993). Formation and composition of the lower continental crust: evidence from Scottish xenolith suites. *Journal of Geophysical Research: Solid Earth (1978–2012)*, 98(B1):581–607.

Hamilton, P., O'Nions, R., Evensen, N., Bridgwater, D., and Allaart, J. H. (1978). Sm–Nd isotopic investigations of Isua supracrustals and implications for mantle evolution. *Nature*, 272(5648):41.

Harker, A. and Barrow, G. (1908). *The geology of the small isles of Inverness-shire:(Rum, Canna, Eigg, Muck, etc.) – Sheet 60, Scotland.*, volume 60. Printed for HM Stationery Off., by J. Hedderwick & Sons, Ltd.

Harker, A. and Clough, C. T. (1904). *The Tertiary igneous rocks of Skye*. HM Stationery Office.

Harland, W. B., Cox, A. V., Craig, L. E., Smith, A. G., and Smith, D. G. (1989). *A geologic time scale*. Cambridge University Press.

Herriot, A. (1975). Observations of the Tighvein 'Complex', Arran. *Proceedings of the Geological Society of Glasgow, for the years 1972-1974*, pages 7–11.

Hiess, J., Condon, D. J., McLean, N., and Noble, S. R. (2012). $^{238}U/^{235}U$ systematics in terrestrial uranium-bearing minerals. *Science*, 335(6076):1610–1614.

Hildreth, W. and Fierstein, J. (2012). *The Novarupta-Katmai eruption of 1912: largest eruption of the twentieth century: centennial perspectives*, volume 1791. Geological Survey (USGS).

Hodgson, B., Dagley, P., and Mussett, A. (1990). Magnetostratigraphy of the Tertiary igneous rocks of Arran. *Scottish Journal of Geology*, 26(2):99–118.

Hole, M., Millett, J., Rogers, N., and Jolley, D. (2015). Rifting and mafic magmatism in the Hebridean basins. *Journal of the Geological Society*, 172(2):218–236.

Holohan, E., Troll, V. R., Errington, M., Donaldson, C., Nicoll, G., and Emeleus, C. (2009). The Southern Mountains Zone, Isle of Rum, Scotland: volcanic and sedimentary processes upon an uplifted and subsided magma chamber roof. *Geological Magazine*, 146(03):400–418.

Hudson, J. and Trewin, N. (2002). Jurassic. In Trewin, N., editor, *The Geology of Scotland*, pages 323—350. Geological Society of London, London.

Hyslop, E., Gillanders, R., Hill, P., and Fakes, R. (1999). Rare-earth-bearing minerals fergusonite and gadolinite from the Arran granite. *Scottish Journal of Geology*, 35(1):65–69.

Johnson, T., Hudson, N., and Droop, G. (2003). Evidence for a genetic granite–migmatite link in the Dalradian of NE Scotland. *Journal of the Geological Society*, 160(3):447–457.

Jordan, N. J., Rotolo, S. G., Williams, R., Speranza, F., McIntosh, W. C., Branney, M. J., and Scaillet, S. (2018). Explosive eruptive history of Pantelleria, Italy: Repeated caldera collapse and ignimbrite emplacement at a peralkaline volcano. *Journal of Volcanology and Geothermal Research*, 349:47–73.

Kempton, P., Fitton, J., Saunders, A., Nowell, G., Taylor, R., Hardarson, B., and Pearson, G. (2000). The Iceland plume in space and time: a Sr–Nd–Pb–Hf study of the North Atlantic rifted margin. *Earth and Planetary Science Letters*, 177(3):255–271.

Kent, R. W. and Fitton, J. G. (2000). Mantle sources and melting dynamics in the British Palaeogene Igneous Province. *Journal of Petrology*, 41(7):1023–1040.

Kerr, A. C. (1993). *The geochemistry and petrogenesis of the Mull and Morvern Tertiary lava succession, Argyll, Scotland.* PhD thesis, Durham University.

Kerr, A. C. (1994). Lithospheric thinning during the evolution of continental large igneous provinces: A case study from the North Atlantic Tertiary province. *Geology*, 22(11):1027–1030.

Kerr, A. C. (1995). The geochemistry of the Mull-Morvern Tertiary lava succession, NW Scotland: an assessment of mantle sources during plume-related volcanism. *Chemical Geology*, 122(1):43–58.

Kerr, A. C., Kempton, P. D., and Thompson, R. N. (1995). Crustal assimilation during turbulent magma ascent (ATA); new isotopic evidence from the Mull Tertiary lava succession, NW Scotland. *Contributions to Mineralogy and Petrology*, 119(2-3):142–154.

Kerr, A. C., Kent, R. W., Thomson, B. A., Seedhouse, J. K., and Donaldson, C. H. (1999). Geochemical evolution of the Tertiary Mull volcano, western Scotland. *Journal of Petrology*, 40(6):873–908.

King, B. C. (1954). The Ard Bheinn area of the central igneous complex of Arran. *Quarterly Journal of the Geological Society*, 110(1-4):323–355.

Kostopoulos, D. K. and James, S. D. (1992). Parameterization of the melting regime of the shallow upper mantle and the effects of variable lithospheric stretching on mantle modal stratification and trace-element concentrations in magmas. *Journal of Petrology*, 33(3):665–691.

Lanphere, M. and Dalrymple, G. (1978). The use of ^{40}Ar/^{39}Ar data in evaluation of disturbed K-Ar systems. *US Geological Survey Open-File Report*, 13:241–243.

Lapen, T. J., Mahlen, N. J., Johnson, C. M., and Beard, B. L. (2004). High precision Lu and Hf isotope analyses of both spiked and unspiked samples: a new approach. *Geochemistry, Geophysics, Geosystems*, 5(1).

Le Bas, M., Maitre, R. L., Streckeisen, A., Zanettin, B., and on the Systematics of Igneous Rocks, I. S. (1986). A chemical classification of volcanic rocks based on the total alkali-silica diagram. *Journal of petrology*, 27(3):745–750.

Le Maitre, R. W., Streckeisen, A., Zanettin, B., Le Bas, M., Bonin, B., and Bateman, P. (2002). *Igneous rocks: a classification and glossary of terms: recommendations of the International Union of Geological Sciences Subcommission on the Systematics of Igneous Rocks*. Cambridge University Press.

Lee, G. W. and Bailey, S. E. (1925). *The Pre-Tertiary Geology of Mull, Loch Aline and Oban: (being a Description of Sheets 35, 43, 44, 45 and 52)*. HM Stationery Office.

Lipman, P. W. (1976). Caldera-collapse breccias in the western San Juan Mountains, Colorado. *Geological Society of America Bulletin*, 87(10):1397–1410.

Lipman, P. W. (1997). Subsidence of ash-flow calderas: relation to caldera size and magma-chamber geometry. *Bulletin of volcanology*, 59(3):198–218.

MacDonald, J., Macgregor, M., and Herriot, A. (1983). *Macgregor's excursion guide to the geology of Arran*. Geological Society of Glasgow.

MacDonald, R., Fettes, D., and Bagiński, B. (2015). The Mull Paleocene dykes: some insights into the nature of major dyke swarms. *Scottish Journal of Geology*, pages 2014–016.

Marcantonio, F., Dickin, A., McNutt, R., and Heaman, L. (1988). A 1,800-million-year-old Proterozoic gneiss terrane in Islay with implications for the crustal structure and evolution of Britain. *Nature*, 335(6185):62.

McDonald, I. and Viljoen, K. (2006). Platinum-group element geochemistry of mantle eclogites: a reconnaissance study of xenoliths from the Orapa kimberlite, Botswana. *Applied Earth Science*, 115(3):81–93.

McDonough, W. F. and Sun, S.-S. (1995). The composition of the Earth. *Chemical geology*, 120(3):223–253.

McKenzie, D. and O'Nions, R. (1991). Partial melt distributions from inversion of rare earth element concentrations. *Journal of Petrology*, 32(5):1021–1091.

McLean, N. M., Condon, D. J., Schoene, B., and Bowring, S. A. (2015). Evaluating uncertainties in the calibration of isotopic reference materials and multi-element isotopic tracers (EARTHTIME Tracer Calibration Part II). *Geochimica et Cosmochimica Acta*, 164:481–501.

Meade, F., Troll, V., Ellam, R., Freda, C., Font, L., Donaldson, C., and Klonowska, I. (2014). Bimodal magmatism produced by progressively inhibited crustal assimilation. *Nature communications*, 5:4199.

Meade, F. C., Chew, D. M., Troll, V. R., Ellam, R. M., and Page, L. (2009). Magma Ascent along a major terrane boundary: crustal contamination and Magma mixing at the Drumadoon Intrusive complex, Isle of Arran, Scotland. *Journal of Petrology*, 50(12):2345–2374.

Meighan, I. (1979). The acid igneous rocks of the British Tertiary Province. *Bulletin of the Geological Survey of Great Britain*, 70:7–8.

Mellors, R. and Sparks, R. (1991). Spatter-rich pyroclastic flow deposits on Santorini, Greece. *Bulletin of Volcanology*, 53(5):327–342.

Meyer, R., Nicoll, G. R., Hertogen, J., Troll, V. R., Ellam, R. M., and Emeleus, C. H. (2009). Trace element and isotope constraints on crustal anatexis by upwelling mantle melts in the North Atlantic Igneous Province: an example from the Isle of Rum, NW Scotland. *Geological Magazine*, 146(3):382–399.

Miller, J. and Harland, W. (1963). Ages of some Tertiary intrusive rocks in Arran. *Mineralogical Magazine*, 33(261):521–523.

Moore, I. and Kokelaar, P. (1998). Tectonically controlled piecemeal caldera collapse: A case study of Glencoe volcano, Scotland. *Geological Society of America Bulletin*, 110(11):1448–1466.

Mori, J. and McKee, C. (1987). Outward-dipping ring-fault structure at Rabaul caldera as shown by earthquake locations. *Science*, 235(4785):193–195.

Morrison, M. A., Thompson, R., Gibson, I., and Marriner, G. (1980). Lateral chemical heterogeneity in the Palaeocene upper mantle beneath the Scottish Hebrides. *Phil. Trans. R. Soc. Lond. A*, 297(1431):229–244.

Muir, R., Fitches, W., and Maltman, A. (1994). The Rhinns Complex: Proterozoic basement on Islay and Colonsay, Inner Hebrides, Scotland, and on Inishtrahull, NW Ireland. *Earth and Environmental Science Transactions of The Royal Society of Edinburgh*, 85(1):77–90.

Münker, C., Weyer, S., Scherer, E., and Mezger, K. (2001). Separation of high field strength elements (Nb, Ta, Zr, Hf) and Lu from rock samples for MC-ICPMS measurements. *Geochemistry, Geophysics, Geosystems*, 2(12).

Mussett, A., Dagley, P., Hodgson, B., and Skelhorn, R. (1987). Palaeomagnetism and age of the quartz-porphyry intrusions, Isle of Arran. *Scottish Journal of Geology*, 23(1):9–22.

Mussett, A., Dagley, P., and Skelhorn, R. (1989). Further evidence for a single polarity and a common source for the quartz-porphyry intrusions of the Arran area. *Scottish Journal of Geology*, 25(3):353–359.

Newhall, C. G. and Dzurisin, D. (1988). *Historical unrest at the large calderas of the world*, volume 2. Department of the Interior, US Geological Survey.

Nobile, A., Acocella, V., Ruch, J., Aoki, Y., Borgstrom, S., Siniscalchi, V., and Geshi, N. (2017). Steady subsidence of a repeatedly erupting caldera through inSAR observations: Aso, Japan. *Bulletin of Volcanology*, 79(5):32.

Noble, S., Hyslop, E., and Highton, A. (1996). High-precision U–Pb monazite geochronology of the c. 806 Ma Grampian Shear Zone and the implications for the evolution of the Central Highlands of Scotland. *Journal of the Geological Society*, 153(4):511–514.

Nowell, G. and Parrish, R. (2001). Simultaneous acquisition of isotope compositions and parent/daughter ratios by non-isotope dilution-mode Plasma Ionisation Multi-collector Mass Spectrometry (PIMMS). In Holland, G. and Tanner, S., editors, *Plasma Source Mass Spectrometry: The New Millenium*, volume 267, pages 298–310. Royal Society of Chemistry.

Oliver, G., Stone, P., and Bluck, B. (2002). The Ballantrae Complex and Southern Uplands terrane. In Trewin, N. H., editor, *The Geology of Scotland*, volume 4, pages 167–200. The Geological Society, London.

Park, R., Stewart, A., and Wright, D. (2002). The Hebridean terrane. In Trewin, N. H., editor, *The Geology of Scotland*, pages 45–80. The Geological Society, London.

Pearce, J. A. (1996). A user's guide to basalt discrimination diagrams. *Trace element geochemistry of volcanic rocks: applications for massive sulphide exploration. Geological Association of Canada, Short Course Notes*, 12(79):113.

Plank, T. and Langmuir, C. H. (1992). Effects of the melting regime on the composition of the oceanic crust. *Journal of Geophysical Research: Solid Earth*, 97(B13):19749–19770.

Preston, J. (2009). Tertiary igneous activity. In Holland, C. H. and Saunders, I. S., editors, *The Geology of Ireland*, pages 333–354. Dunedin Academic Press, Edinburgh.

Putirka, K. D. (2008). Thermometers and barometers for volcanic systems. *Reviews in Mineralogy and Geochemistry*, 69(1):61–120.

Rhodes, J., Dungan, M., Blanchard, D., and Long, P. (1979). Magma mixing at mid-ocean ridges: evidence from basalts drilled near 22 °N on the Mid-Atlantic Ridge. *Tectonophysics*, 55(1-2):35–61.

Roeder, P. and Emslie, R. (1970). Olivine-liquid equilibrium. *Contributions to mineralogy and petrology*, 29(4):275–289.

Rogers, N. and Gibson, I. (1977). The petrology and geochemistry of the Creag Dubh composite sill, Whiting Bay, Arran, Scotland. *Geological Magazine*, 114(01):1–8.

Sahy, D., Condon, D. J., Hilgen, F. J., and Kuiper, K. F. (2017). Reducing Disparity in Radio-Isotopic and Astrochronology-Based Time Scales of the Late Eocene and Oligocene. *Paleoceanography*, 32(10):1018–1035.

Saunders, A., Fitton, J., Kerr, A., Norry, M., and Kent, R. (1997). The North Atlantic Igneous Province. *Large igneous provinces: Continental, oceanic, and planetary flood volcanism*, pages 45–93.

Saunders, S. J. (2001). The shallow plumbing system of Rabaul caldera: a partially intruded ring fault? *Bulletin of volcanology*, 63(6):406–420.

Self, S., Rampino, M., Newton, M., and Wolff, J. (1984). Volcanological study of the great Tambora eruption of 1815. *Geology*, 12(11):659–663.

Self, S. and Rampino, M. R. (1981). The 1883 eruption of Krakatau. *Nature*, 294(5843):699.

Sguigna, A., Larabee, A., and Waddington, J. (1982). The half-life of ^{176}Lu by a γ–γ coincidence measurement. *Canadian Journal of Physics*, 60(3):361–364.

Sigmundsson, F., Hooper, A., Hreinsdóttir, S., Vogfjörd, K. S., Ófeigsson, B. G., Heimisson, E. R., Dumont, S., Parks, M., Spaans, K., Gudmundsson, G. B., et al. (2015). Segmented lateral dyke growth in a rifting event at Bárðarbunga volcanic system, Iceland. *Nature*, 517(7533):191.

Smith, N. J. and Kokelaar, B. P. (2013). Proximal record of the 273 ka Poris caldera-forming eruption, Las Cañadas, Tenerife. *Bulletin of volcanology*, 75(11):768.

Speight, J., Skelhorn, R., Sloan, T., and Knaap, R. (1982). The dyke swarms of Scotland. *Igneous rocks of the British Isles*, pages 449–459.

Spera, F. J. and Bohrson, W. A. (2001). Energy-constrained open-system magmatic processes I: General model and energy-constrained assimilation and fractional crystallization (EC-AFC) formulation. *Journal of Petrology*, 42(5):999–1018.

Steiger, R. and Jager, E. (1977). Subcommission on geochronology-convention on use of decay constants in geochronology and cosmochronology. *Earth and Planetary Science Letters*, 36(3):359–362.

Stephenson, D., Mendum, J. R., Fettes, D. J., and Leslie, A. G. (2013). The Dalradian rocks of Scotland: an introduction. *Proceedings of the Geologists' Association*, 124(1):3–82.

Stevenson, C. and Bennett, N. (2011). The emplacement of the palaeogene mourne granite centres, Northern Ireland: New results from the Western Mourne Centre. *Journal of the Geological Society*, 168(4):831–836.

Stevenson, C. and Grove, C. (2014). Laccolithic Emplacement of the Northern Arran Granite, Scotland, Based on Magnetic Fabric Data. In Németh, K., editor, *Advances in Volcanology*. Springer.

Storey, M., Duncan, R. A., and Tegner, C. (2007). Timing and duration of volcanism in the North Atlantic Igneous Province: Implications for geodynamics and links to the Iceland hotspot. *Chemical Geology*, 241(3):264–281.

Strachan, R., Smith, M., Harris, A., and Fettes, D. (2002). The Northern Highland and Grampian terranes. In Trewin, N. H., editor, *The Geology of Scotland*, pages 81–147. The Geological Society, London.

Sun, S.-S. and McDonough, W. F. (1989). Chemical and isotopic systematics of oceanic basalts: implications for mantle composition and processes. *Geological Society, London, Special Publications*, 42(1):313–345.

Sutherland, D. S. (1982). *Igneous rocks of the British Isles*. John Wiley & Sons Incorporated.

Tanner, P. and Evans, J. (2003). Late Precambrian U–Pb titanite age for peak regional metamorphism and deformation (Knoydartian orogeny) in the western Moine, Scotland. *Journal of the Geological Society*, 160(4):555–564.

Tanner, P. G. and Sutherland, S. (2007). The Highland Border Complex, Scotland: a paradox resolved. *Journal of the Geological Society*, 164(1):111–116.

Tanner, P. G., Thomas, C. W., Harris, A. L., Gould, D., Harte, B., Treagus, J. E., and Stephenson, D. (2013). The Dalradian rocks of the Highland Border region of Scotland. *Proceedings of the Geologists' Association*, 124(1-2):215–262.

Taylor, H. P. and Forester, R. W. (1971). Low-^{18}O igneous rocks from the intrusive complexes of Skye, Mull, and Ardnamurchan, Western Scotland. *Journal of Petrology*, 12(3):465–497.

Thirlwall, M. (2002). Multicollector ICP-MS analysis of Pb isotopes using a ^{207}Pb-^{204}Pb double spike demonstrates up to 400 ppm/amu systematic errors in Tl-normalization. *Chemical Geology*, 184(3-4):255–279.

Thompson, R, N. (1968). Tertiary granites and associated rocks of the Marsco area, Isle of Skye. *Quarterly Journal of the Geological Society*, 124(1-4):349–380.

Thompson, R. (1982a). Geochemistry and magma genesis. In Sutherland, D. S., editor, *Igneous rocks of the British Isles*. John Wiley and Sons.

Thompson, R. (1982b). Magmatism of the British Tertiary Volcanic Province. *Scottish Journal of Geology*, 18(1):49–107.

Thompson, R., Esson, J., and Dunham, A. (1972). Major element chemical variation in the Eocene lavas of the Isle of Skye, Scotland. *Journal of Petrology*, 13(2):219–253.

Thompson, R., Gibson, I., Marriner, G., Mattey, D., and Morrison, M. A. (1980). Trace-element evidence of multistage mantle fusion and polybaric fractional crystallization in the Palaeocene lavas of Skye, NW Scotland. *Journal of Petrology*, 21(2):265–293.

Thompson, R. and Gibson, S. A. (1991). Subcontinental mantle plumes, hotspots and pre-existing thinspots. *Journal of the Geological Society*, 148(6):973–977.

Trewin, N. and Thirlwall, M. (2002). Old red sandstone. In Trewin, N., editor, *The Geology of Scotland*, pages 213–249. The Geological Society, London.

Troll, V., Walter, T. R., and Schmincke, H.-U. (2002). Cyclic caldera collapse: Piston or piecemeal subsidence? Field and experimental evidence. *Geology*, 30(2):135–138.

Troll, V. R., Chadwick, J. P., Ellam, R. M., Mc Donnell, S., Emeleus, C. H., and Meighan, I. G. (2005). Sr and Nd isotope evidence for successive crustal contamination of Slieve Gullion ring-dyke magmas, Co. Armagh, Ireland. *Geological Magazine*, 142(6):659–668.

Troll, V. R., Donaldson, C. H., and Emeleus, C. H. (2004). Pre-eruptive magma mixing in ash-flow deposits of the Tertiary Rum Igneous Centre, Scotland. *Contributions to Mineralogy and Petrology*, 147(6):722–739.

Troll, V. R., Emeleus, C. H., and Donaldson, C. H. (2000). Caldera formation in the Rum central igneous complex, Scotland. *Bulletin of Volcanology*, 62(4-5):301–317.

Troll, V. R., Nicoll, G. R., Donaldson, C. H., and Emeleus, H. C. (2008). Dating the onset of volcanism at the Rum Igneous Centre, NW Scotland. *Journal of the Geological Society*, 165(3):651–659.

Tyrell, G. W. (1928). *The geology of Arran*. Printed under the authority of HM Stationery Office.

Underhill, J. R. (2009). Role of intrusion-induced salt mobility in controlling the formation of the enigmatic 'Silverpit Crater', UK Southern North Sea. *Petroleum Geoscience*, 15(3):197–216.

Upton, B., Aspen, P., Graham, A., and Chapman, N. (1976). Pre-palaeozoic basement of the Scottish Midland Valley. *Nature*, 260(5551):517.

Upton, B., Aspen, P., Rex, D., Melcher, F., and Kinny, P. (1998). Lower crustal and possible shallow mantle samples from beneath the Hebrides: evidence from a xenolithic dyke at Gribun, western Mull. *Journal of the Geological Society*, 155(5):813–828.

Upton, B., Skovgaard, A. C., McClurg, J., Kirstein, L., Cheadle, M., Emeleus, C., Wadsworth, W., and Fallick, A. (2002). Picritic magmas and the Rum ultramafic complex, Scotland. *Geological Magazine*, 139(4):437–452.

Walker, G. P. (1970). *The distribution of amygdale minerals in Mull and Morvern (Western Scotland)*. The University of Saugar, India.

Walsh, J., Beckinsale, R., Skelhorn, R., and Thorpe, R. (1979). Geochemistry and petrogenesis of Tertiary granitic rocks from the Island of Mull, Northwest Scotland. *Contributions to Mineralogy and Petrology*, 71(2):99–116.

Watson, E. B. (1979). Zircon saturation in felsic liquids: experimental results and applications to trace element geochemistry. *Contributions to Mineralogy and Petrology*, 70(4):407–419.

Watson, S. (1993). Rare earth element inversions and percolation models for Hawaii. *Journal of Petrology*, 34(4):763–783.

Weaver, B. L. and Tarney, J. (1981). Lewisian gneiss geochemistry and Archaean crustal development models. *Earth and Planetary Science Letters*, 55(1):171–180.

Wetherill, G. W. (1956). Discordant uranium-lead ages I. *Eos, Transactions American Geophysical Union*, 37(3):320–326.

Wilkinson, C. M., Ganerød, M., Hendriks, B. W., and Eide, E. A. (2016). Compilation and appraisal of geochronological data from the North Atlantic Igneous Province (NAIP). *Geological Society, London, Special Publications*, 447:SP447–10.

Workman, R. K. and Hart, S. R. (2005). Major and trace element composition of the depleted MORB mantle (DMM). *Earth and Planetary Science Letters*, 231(1):53–72.

Young, G. and Caldwell, W. (2012). The Northeast Arran Trough, the Corrie conundrum and the Highland Boundary Fault in the Firth of Clyde, SW Scotland. *Geological Magazine*, 149(4):578.

A – Laboratory Methods

A.1 Preparation of rock powders

Rock powders were produced using the rock preparation facilities at Cardiff University. Weathered surfaces were removed from the rock samples using a diamond-bladed rock saw. Samples were then crushed to a coarse grit by a Mn-steel jaw crusher. The resulting rock chips were reduced to a fine powder in either an agate ball mill or an agate ring-and-puck mill. Agate was used in preference to WC to minimise Nb and Ta contamination. Approximately 2 g of each powdered sample was ignited for two hours in a furnace at 900°C to drive off volatiles and determine loss on ignition (LOI) values. The LOI of a sample was calculated using the following equation:

$$LOI\ (wt.\%) = \frac{Mass\ of\ wet\ powder - Mass\ of\ ignited\ powder}{Mass\ of\ wet\ powder}$$

These ignited powders were then used for solution preparation for whole-rock geochemistry methods..

A.2 Whole-rock Major and Trace Element Analysis

A.2.1 Preparation of solutions for ICP-OES and ICP-MS

Solutions for inductively-coupled plasma (ICP) elemental analysis were prepared using the lithium metaborate fusion method. To prepare the samples, 0.1 ± 0.001 g of each ignited powder was mixed with 0.6 ± 0.004 g of lithium metaborate flux in a platinum crucible. Six drops of lithium iodide wetting agent were added to each mixture which was then fused using the Claisse Fluxy automated fusion system. The mixture was then dissolved in a solution of 20 ml of 10% HNO_3 and 30 ml of 18.2 Ω deionised water. After the mixture had fully dissolved, 1 ml of 100 ppm Rh spike was added to the solution, which was then made up to 100 ml with 18.2 Ω deionised

water. Approximately 20 ml of each solution was run on ICP-OES to obtain major element and some trace element abundances. Another 1 ml of each solution was added to 1 ml of In and Tl and 8 ml of 2% HNO_3 and run on the ICP-MS to obtain trace element abundances. The samples were run on a Jobin Yvon Horiba Ultima 2 ICP-OES and a Thermo Elemental X7 series ICP-MS at Cardiff University by Dr. Iain McDonald. This is the same analytical process as described in McDonald and Viljoen (2006). Four batches of solutions were prepared and analysed between May 2015 and September 2017.

A.2.2 Evaluation of the accuracy and precision of elemental data

Standards

In order to assess the accuracy and precision of the whole rock elemental data obtained by ICP-OES and ICP-MS, external and internal standards were analysed. The external standards used were JB1-A, BIR-1, JG-3, JP1, SDO1, JG1a and MRG1. BIR-1 and JG-3 were run in every batch of samples analysed to assess the accuracy of the results, and also to help determine the precision of the results. Three internal standards were also run in every sample batch.

Accuracy

Results from the different runs of standards are given in Appendix E4 along with percentage errors of the measured values compared to certified values. The % errors for all elements in the standards are calculated using the following equation:

$$\%Error = 100 - \left(\frac{Certified\ value}{Measured\ value} \right) \times 100$$

Precision

The precision of the elemental data can be determined by examining the multiple analyses of the external and internal standards. The precision of a standard sample with respect to each element is represented by the relative standard deviation (RSD). The RSD for all the elements in the standards are given in Appendix E4, and is calculated for each element using the following equations:

$$x_a = \frac{\Sigma x}{n}$$

where x_a is the average element concentration, x is the element concentration and n is the number of measurements

$$S = \frac{\sqrt{\Sigma(x - x_a)^2}}{n-1}$$

where S is the standard deviation

$$RSD(\%) = \frac{100S}{x_a}$$

A.3 Whole-rock Radiogenic Tracer Isotope Analysis

Samples were prepared and analysed at the National Isotope Geoscience Laboratories (NIGL) at the British Geological Survey, Keyworth, England. Column chemistry was done by Robert Gooday and Dr. Ian Millar. Analyses were done by Dr. Ian Millar.

A.3.1 Dissolution and column chemistry

150–200 mg of sample was weighed into 15 ml Savillex teflon beakers and leached in 5 ml of 6 M HCl at 60°C for 2 hours. After discarding the leachate, the samples were washed and centrifuged twice in mQ water, dried and reweighed. Mixed ^{149}Sm-150Nd and ^{176}Lu-^{177}Hf isotope tracers were weighed and added to the samples. 1–2 ml of 2× quartz-distilled 16 M HNO_3 and 5–6 ml of 29 M HF were added, and the sample beakers were left closed on a hotplate at 140°C overnight. After evaporating to dryness, a further 1–2 ml of HNO_3 were added, and the samples were left on the hotplate closed overnight. The samples were then converted to chloride form using 10 ml of 2× quartz-distilled HCl. The samples were then dissolved in 2 ml of 1 M HCl + 0.1 M HF in preparation for column chemistry, and centrifuged. A second aliquot of sample was weighed into 15 ml Savillex beakers, leached and dissolved as above prior to Pb separation and analysis.

Primary column separation

Primary columns consisting of 2 ml of Eichrom AG50x8 cation exchange resin in 10 ml Biorad Poly-Prep columns were used to separate bulk high field strength elements (HFSE: Ti, Hf, Zr), a fraction containing Sr, Ca and Rb, and a bulk rare-earth element (REE) fraction. Samples were loaded onto the columns in 1.5 ml of 1 M HCl + 0.1 M HF, and the HFSE were immediately eluted in 10 ml of 1 M HCl + 0.1 M HF. This fraction was evaporated to dryness in preparation for separation of Hf (below). Sr, Ca and Rb were eluted in 30 ml of 1.5 M HCl, and evaporated to dryness in preparation for separation of Rb and Sr (below). Finally, the REE were

eluted in 10 ml of 6 M HCl and evaporated to dryness in preparation for separation of Sm, Nd and Lu (below).

Separation of Hf

Hafnium separation followed a procedure adapted from Münker et al. (2001). HFSE concentrates from the primary columns were dissolved in 2 ml of 6 M HCl and loaded onto columns packed with 1 ml of EICHROM LN-SPEC ion exchange resin packed into 10 ml Biorad Poly-Prep columns. Matrix elements were eluted in 10–20 ml of 6 M HCl, and 2× 2 ml of milliQ water was then passed through the column to remove HCl from the columns prior to subsequent elution steps involving peroxide (mixing of HCl and peroxide would result in immediate elution of HFSE from the columns). The columns were then washed with several 10 ml column volumes of a solution containing citric acid, nitric acid and peroxide. In this medium, titanium citrate complexes show a distinctive bright orange colour, allowing Ti to be quantitatively removed from the column by repeated washing. Once all traces of Ti were removed from the columns, 5 ml of peroxide-free citric acid + nitric acid solution were eluted, again in order to avoid mixing of peroxide with HCl solutions. Zr was then washed from the columns using 50–80 ml of 6 M HCl + 0.06 M HF. Finally, Hf was collected in 10 ml of 6 M HCl + 0.2 M HCl.

Separation of Sr

Samples from the primary column separation were dried down and taken up in 2 ml of 2.5 M HCl and pipetted onto quartz-glass columns containing 4 ml of AG50x8 cation exchange resin. Matrix elements were washed off the column using 48 ml of calibrated 2.5 M HCl, and discarded. Sr was collected in 12 ml of 2.5 M HCl, and evaporated to dryness.

Separation of Sm, Nd and Lu from the bulk REE fraction

Sm and Nd were separated using 2 ml of EICHROM LN-SPEC ion exchange resin packed into 10 ml Biorad Poly-Prep columns. The bulk REE fraction was dissolved in 200 µl of 0.2 M HCl and loaded onto the columns. La, Ce, and Pr were eluted using a total of 14 ml of 0.2 M HCl. Nd was collected in 3 ml of 0.3 M HCl and Sm was collected in 3.5 mls of 0.6 M HCl. The middle rare-earth elements were eluted in 50 ml of 2.5 M HCl, and finally Lu (+ some residual Yb) was collected in 10 ml of 6 M HCl. Sm, Nd and Lu fractions were evaporated to dryness in preparation for mass spectrometry.

Separation of Pb

Dissolved samples for Pb were converted to bromide form using 2 ml of concentrated HBr. Pb was separated using using columns containing 100 µl of Dowex AG1x8 anion exchange resin using standard bromide separation methods.

A.3.2 Mass spectrometry

Lu analysis

Lu fractions were dissolved in 1 ml of 2% HNO_3 prior to analysis on a Thermo-Electron Neptune mass spectrometer, using a Cetac Aridus II desolvating nebulizer. 0.006 l/min of nitrogen were introduced via the nebulizer in addition to Ar in order to minimise oxide formation. The instrument was operated in static multicollection mode, with cups set to monitor ^{176}Er, ^{177}Er, ^{172}Yb, ^{173}Yb, ^{175}Lu, ^{176}Lu+Hf+Yb, ^{177}Hf and ^{179}Hf. Standard sample cones and X-skimmer cones were used, giving a typical signal of c. 600 V/ppm Lu. 1% dilutions of each sample were tested prior to analysis, and samples diluted to 20 ppb prior to the addition of 20 ppb of Er. Data reduction followed Lapen et al. (2004), using a ratio of 0.6841 for ^{167}Er/^{166}Er to correct ^{176}Lu/^{175}Lu for mass fractionation using an exponential law. ^{176}Yb and ^{176}Hf interferences on ^{176}Lu were monitored using ^{173}Yb and ^{177}Hf respectively; ^{176}Yb/^{173}Yb and ^{176}Hf/^{177}Hf were corrected for mass bias using ^{167}Er/^{166}Er = 0.6841 before interference corrections were made. During the period of analysis, Ames Lu gave a value for ^{176}Lu/^{175}Lu of 0.02658 $\pm$ 0.00002 (2σ, n=59), which lies within analytical uncertainty of the value obtained by Lapen et al. (0.02656 $\pm$ 0.00003, 2σ).

Hf analysis

Hf fractions were dissolved in 1 ml of 2% HNO_3 + 0.1 M HF, prior to analysis on a Thermo-Electron Neptune mass spectrometer, using A Cetac Aridus II desolvating nebulizer. 0.006 l/min of nitrogen were introduced via the nebulizer in addition to Ar in order to minimise oxide formation. The instrument was operated in static multicollection mode, with cups set to monitor ^{172}Yb, ^{173}Yb, ^{175}Lu, ^{176}Lu+Hf+Yb, ^{177}Hf, ^{178}Hf, ^{179}Hf and ^{180}Hf. 1% dilutions of each sample were tested prior to analysis, and samples diluted to 20 ppb. Standard sample cones and X-skimmer cones were used, giving a typical signal of 800–1000 V/ppm Hf. Correction for ^{176}Yb on the ^{176}Hf peak was made using reverse-mass-bias correction of the ^{176}Yb/^{173}Yb ratio empirically derived using Hf mass-bias corrected Yb-doped JMC475 solutions (Nowell and Parrish, 2001). ^{176}Lu interference on the ^{176}Hf peak was corrected by

using the measured ^{175}Lu and assuming ^{176}Lu/^{175}Lu = 0.02653. The column procedure used to separate Hf effectively removes most Yb and Lu, so these corrections are minimal. Spike-stripping was carried out using an iterative algorithm. Data are reported relative to ^{179}Hf/^{177}Hf = 0.7325.

The Hf standard solution JMC475 was analyzed during each analytical session and sample ^{176}Hf/^{177}Hf ratios are reported relative to a value of 0.282160 for this standard (Nowell and Parrish, 2001). Eleven analyses of JMC475 gave a mean ^{176}Hf/^{177}Hf value of 0.282141 $\pm$ 0.000004 (1σ). Data are reported relative to a value of 0.282160 for this standard. Typical external precision for a single day's analysis was in the range between 13–22 ppm.

Sm analysis

Sm fractions were loaded onto one side of an outgassed double Re filament assembly using dilute (0.6 M) HCl, and analysed in a Thermo Scientific Triton mass spectrometer in static collection mode. Replicate analysis of the BCR-2 rock standard across the time of analysis gave a mean Sm concentration of 6.27 $\pm$ 0.11 ppm (1σ, n=2)

Nd analysis

Nd fractions were loaded onto one side of an outgassed double Re filament assembly using dilute HCl, and analysed in a Thermo Scientific Triton mass spectrometer in multi-dynamic mode. Data are normalised to ^{146}Nd/^{144}Nd = 0.7219. 17 analyses of the JND-i standard gave a value of 0.512102 $\pm$ 0.000013 (25 ppm, 1σ). All other standard and sample data is quoted relative to a value of 0.512115 for this standard. One analysis of the BCR-2 rock standard gave ^{143}Nd/^{144}Nd = 0.512634 $\pm$ 0.000004 (1σ).

Sr analysis

Sr fractions were loaded onto outgassed single Re filaments using a TaO activator solution, and analysed in a Thermo-Electron Triton mass spectrometer in multi-dynamic mode. Data are normalised to ^{86}Sr/^{88}Sr = 0.1194. 16 analyses of the NBS987 standard gave a value of 0.710259 $\pm$ 0.000006 (7.8 ppm, 1σ). Sample data is normalised using a preferred value of 0.710250 for this standard.

Pb analysis

Prior to Pb isotope analysis each sample was spiked with a Tl solution, which was added to allow for the correction of instrument-induced mass bias. Samples

were then introduced into a Thermo Scientific Neptune Plus multicollector ICP-MS using an Aridus II desolvating nebulizer. For each sample, five ratios were simultaneously measured ($^{206}Pb/^{204}Pb$, $^{207}Pb/^{204}Pb$, $^{208}Pb/^{204}Pb$, $^{207}Pb/^{206}Pb$ and $^{208}Pb/^{206}Pb$). Each individual acquisition consisted of 75 sets of ratios, collected at 5-second integrations, following a 60 second de-focused baseline. The precision and accuracy of the method was assessed through repeat analysis of an NBS 981 Pb reference solution (also spiked with Tl). The average values obtained for each of the measured NBS 981 ratios were then compared to the known values for this reference material (Thirlwall, 2002). All sample data were subsequently normalised, according to the relative daily deviation of the measured reference value from the true, with the aim of cancelling out the slight daily variations in instrumental accuracy, allowing the direct comparison of the data obtained during different analytical sessions. Internal uncertainties (the reproducibility of the measured ratio) were propagated relative to the external uncertainty.

A.4 U-Pb dating of Zircons

Zircons were separated and analysed at NIGL. Zircon separation was done by Robert Gooday and Dr. Ian Millar. Crystal selection (picking) was done by Robert Gooday and Dr. Dan Condon. Analyses were done by Dr. Dan Condon.

A.4.1 Sample preparation and zircon separation

Samples were crushed using a steel jaw crusher and disk mill. The <500 µm fraction was processed using a Haultain Superpanner in order to extract a heavy mineral concentrate, which was further purified by passing through di-iodomethane with a specific gravity of 3.3. The most magnetic material was extracted using a hand magnet and a Frantz magnetic separator.

A.4.2 Isotope Dilution Thermal Ionisation Mass Spectrometry (ID-TIMS) methodology

Zircons selected for analysis were chemically abraded following a modified procedure to remove damaged parts of the crystal that were likely to have experienced open-system behaviour. Firstly, the zircons were thermally annealed at 900°C for 60 hours in quartz crucibles before being individually selected, photographed and loaded into FEP Teflon beakers. Single zircon crystals, or fragments, were selected

for dissolution using transmitted light microscopy. Zircons were selected based upon their external morphology and observation of internal features (*i.e.*, visible cores).

Zircons were then refluxed in 4 M HNO_3 on a hotplate at 120°C for > 2 hours, followed by ultrasonic cleaning for at least 20 minutes. The zircon crystals were rinsed with acetone and 4 M HNO_3 and loaded into individual 300 µl FEP Teflon microcapsules and leached in 29 M HF inside a Parr vessel (a self-sealing stainless-steel jacket) for 12 hours at 180°C. The zircons were rinsed with 4 M HNO_3 and refluxed in 6 M HCl at 120°C for 2-5 hours, before a final rinsing with 4 M HNO_3 several times.

The leached zircons and all total procedural blanks were spiked with mixed ^{205}Pb-^{233}U-^{235}U (ET535) EARTHTIME tracer solution and dissolved in ~150 µl 29 M HF and trace HNO_3 in a Parr vessel at 220°C for at least 60 hours. Complete dissolution was checked by visual inspection of some larger crystals and assumed for smaller grains, following standard protocol for dissolution at NIGL. The solutions were dried down as fluorides and re-dissolved in 3 M HCl in a Parr vessel overnight at 180°C. U and Pb fractions were isolated by HCl-based anion exchange procedure using Bio-Rad AG-1 resin in Teflon columns. Pb and U fractions were then recombined and dried down with ~10 µl of H_3PO_4. The dried samples were then loaded onto zone-refined Re filaments in a silica gel matrix to enhance ionisation.

Isotope ratios were measured on a Thermo-Electron Triton thermal ionisation mass spectrometer (TIMS). Pb was measured in dynamic mode on a MassCom secondary electron multiplier; Pb mass bias corrections were made using a fractionation factor of 0.14±0.02 % /amu (1σ) for samples spiked using ET535. Dead-time and linearity of the secondary electron multiplier were monitored using repeated analyses of the standards NBS 982, NBS 981 and U 500. U oxide (UO_2) was measured, and corrected for isobaric interferences using a ^{18}O/^{16}O value of 0.00205 (IUPAC value and measured in-house at NIGL). U was measured in dynamic mode and a mass bias fractionation correction calculated in real-time using the ^{233}U-^{235}U ratio of the ET535 tracer solutions. Corrections for the addition of Pb and U during the procedure (*i.e.*, laboratory contamination) were made using the long-term measured isotopic composition and variability of blanks using an amount that is based upon contemporary total procedural blanks. The U/Pb ratio for each analyses was determined via isotope dilution principles and the ET535 mixed ^{205}Pb-^{233}U-^{235}U tracer (Condon et al., 2015; McLean et al., 2015). A ^{238}U/^{235}U value of 137.818 was assumed (Hiess et al., 2012) and used in the data reduction algorithm.

Due to the slightly larger ionic radius of Th the intermediate daughter ^{230}Th is excluded during zircon crystallisation such that a correction is required to account for ^{230}Th disequilibrium and resulting in deficit ^{206}Pb. This disequilibrium

correction requires a priori knowledge of the Th/U of the magma coexisting with the crystal during growth. A sensitivity analysis of the choice of Th/U ratio in the Th-correction shows an inverse exponential relationship between the magnitude of the Th-correction and Th/U ratio that plateaus between Th/U = 3-4. A value of Th/U = 3.5 was selected for the Th-correction in this study.

See Sahy et al. (2017) for full ID-TIMS methods, references and discussion of age interpretation.

A.5 Energy-Dispersive X-ray Spectrometry

Mineral chemistry data and major element maps of polished thin sections were produced at the Electron Microbeam Facility in the School of Earth and Ocean Sciences at Cardiff University by Robert Gooday and Dr Duncan Muir.

This laboratory uses a Zeiss Sigma HD Field Emission Gun Analytical Scanning Electron Microscope (SEM) equipped with two Oxford Instruments 150 mm^2 EDS detectors. Operating conditions were set at 20 kV and aperture size to 120 µm, with a nominal beam current of 4–5 nA and working distance of 8.9 mm. Using Aztec software, maps were acquired with pixel sizes ranging from 10 to 36.5 µm, depending on the resolution of acquired spectral images. A process time of 1 µs was used in conjunction with a pixel dwell time of 2,500–14.000 µs.

B – List of Electronic Appendices

Electronic Appendices can be found on the CD included with this (hard copy) thesis. Alternatively, they are available at https://www.researchgate.net/profile/Robert_Gooday or by contacting the author.

Appendix E1 - Sample Locations

Excel spreadsheet listing all samples taken during this project, along with British National Grid references for each one. Also shows which samples were made into thin sections or polished thin sections, and which samples were analysed for whole-rock geochemistry, mineral geochemistry, isotope geochemistry, and zircon ages.

Appendix E2 - Mineral compositions

Excel spreadsheet containing EDS data, presented as oxide wt.%, for pyroxenes, olivines, and feldspars analysed in this study.

Appendix E3 - ICP whole-rock data

Excel spreadsheet containing raw ICP-OES and ICP-MS data for all samples analysed as part of this study. Also contains major element data recalculated to anhydrous values for both FeO and Fe_2O_3, trace element data used in the thesis, and chondrite-normalised (McDonough and Sun, 1995) REE values.

Appendix E4 - ICP Accuracy and Precision

Excel spreadsheet showing accuracy and precision calculations, as described in Appendix A, for the ICP-OES and ICP-MS data used in this thesis.

Appendix E5 - Radiogenic isotope data

Excel spreadsheet showing the results of Sr, Nd, Pb, and Hf isotope analyses, as well as age-correction calculations (59 Ma) and ε values.

Appendix E6 - Zircon U-Pb data

Excel spreadsheet showing results of U-Pb ID-TIMS analyses for the nine samples subjected to zircon dating.

Appendix E7 - Map of the Central Arran Igneous Complex

PNG file showing the geological map of the CAIC (Fig. 1.9) for easier electronic viewing.